

World Renewable Energy Congress – Sweden

8–13 May, 2011
Linköping, Sweden

Editor

Professor Bahram Moshfegh

Copyright

The publishers will keep this document online on the Internet – or its possible replacement – from the date of publication barring exceptional circumstances.

The online availability of the document implies permanent permission for anyone to read, to download, or to print out single copies for his/her own use and to use it unchanged for non-commercial research and educational purposes. Subsequent transfers of copyright cannot revoke this permission. All other uses of the document are conditional upon the consent of the copyright owner. The publisher has taken technical and administrative measures to assure authenticity, security and accessibility.

According to intellectual property law, the author has the right to be mentioned when his/her work is accessed as described above and to be protected against infringement.

For additional information about Linköping University Electronic Press and its procedures for publication and for assurance of document integrity, please refer to its www home page: <http://www.ep.liu.se/>.

Linköping Electronic Conference Proceedings, 57
Linköping University Electronic Press
Linköping, Sweden, 2011

http://www.ep.liu.se/ecp_home/index.en.aspx?issue=057
ISBN: 978-91-7393-070-3
ISSN 1650-3740 (online)
ISSN 1650-3686 (print)

© The Authors

Volume 14

Solar Thermal Applications

Table of Contents

Environmental Regulation, Solar Energy Technology Components and International Trade - An Empirical Analysis of Structure and Drivers <i>Felix Groba</i>	3670
Environmental Impacts of Solar Thermal Systems with Life Cycle Assessment <i>Alexis de Laborderie, Clément Puech, Nadine Adra, Isabelle Blanc, Didier Beloin-Saint-Pierre, Pierryves Padey, Jérôme Payet, Marion Sie and Philippe Jacquin</i>	3678
Solar Energy Measurement on the South African East Coast <i>E. Zawilska¹ and M.J. Brooks</i>	3686
Investigation of Solar Collector Systems Use in Latvia <i>P. Shipkova, K. Lebedeva, G. Kashkarova, L. Migla and M. Pankars</i>	3694
New Method for Predicting the Performance of Solar Pond in any Sunny Part of the World <i>Adel O. Sharif, Hazim Al-Hussaini and Ibrahim A. Alenezi</i>	3702
Choice of Solar Share of a Hybrid Power Plant of a Central Receiver System and a Biogas Plant in Dependency of the Geographical Latitude <i>Spiros Alexopoulos, Bernhard Hoffschmidt, Christoph Rau and Johannes Sattler</i>	3710
Building-integrated Solar Collector (BISC) <i>Bin-Juine Huang, Yu-Hsing Lin, Wei-Zhe Ton, Tung-Fu Hou and Yi-Hung Chuang</i>	3718
Passive Solar Design in Schools for the Protection of the Environment Greece: A Case Study <i>Agisilaos Agisilaos Economou</i>	3726
Modeling of the Seawater Greenhouse Systems <i>G.R. Salehi, M. Ahmadpour and H. Khoshnazar</i>	3733
An Exergy Based Unified Test Protocol for Solar Cookers of Different Geometries <i>Naveen Kumar, G. Vishwanath and Anurag Gupta</i>	3741
Evaluation of an Integrated Photovoltaic Thermal Solar (IPVTS) Water Heating System for Various Configurations at Constant Collection Temperature <i>Rajeev Kumar Mishra and G.N. Tiwari</i>	3749
Design of a Latent Heat Energy Storage System Coupled with a Domestic Hot Water Solar Thermal System <i>Robynne Murray, Louis Desgrosseilliers, Jeremy Stewart, Nick Osbourne, Gina Marin, Alex Safatli, Dominic Groulx and Mary Anne White</i>	3757
Retrofitting Domestic Hot Water Tanks for Solar Thermal Collectors. A Theoretical Analysis <i>Luís Ricardo Bernardo, Henrik Davidsson and Björn Karlsson</i>	3765
Travelling Energy Collectors <i>Ernst Kussul, Tatiana Baidyk, José Saniger, Felipe Lara and Neil Bruce</i>	3773
Configuration of Daylighting System via Fibers and Experiments of Concentrated Sunlight Transmission <i>JF Song, YP Yang, HJ Hou and MX Zhang</i>	3781

Type12 and Type56: a Load Structure Comparison in TRNSYS <i>Helena Persson, Bengt Perers and Bo Carlsson</i>	3789
Reducing Energy Consumption in Natural Gas Pressure Drop Stations by Employing Solar Heat <i>Mohammad Rezaei, Mahmood Farzaneh-Gord, Ahmad Arabkoohsar and Mahdi Deymi Dasht-bayaz</i>	3797
Performance of Hybrid Photovoltaic Thermal (HPVT) Biogas Plant <i>Prabhakant, Rajeev Kumar Mishra and G. N.Tiwari</i>	3805
Air Bottoming Cycle for Hybrid Solar-Gas Power Plants <i>Fouad Khaldi</i>	3813
Economic Implications of Thermal Energy Storage for Concentrated Solar Thermal Power <i>Sharon J. Wagner and Edward S. Rubin</i>	3821
Social and Technical Aspects in Solar System Design <i>Dorota Wójcicka-Migasiuk and Andrzej Chochowski</i>	3830
On the Significance of Concentrated Solar Power R&D in Sweden <i>Torsten Strand, James Spelling, Björn Laumert and Torsten Fransson</i>	3836
Experimental Heat Transfer Research in Enhanced Flat-Plate Solar Collectors <i>R. Herrero Martín, A. García Pinar and J. Pérez García</i>	3844
Closed Environment Design of Solar Collector Trough using Lenses and Reflectors <i>Kazy Fayeen Shariar, Enaiyat Ghani Ovy and Tabassum Aziz Hossainy</i>	3852
Optimum Integration of a Large Size Collector to a Solar Thermal Power Plant <i>M. Yaghoubi S. Zarrini and S. Mirhadi</i>	3859
Theoretical Modelling of a Dynamic Solar Thermal Desalination Unit with a Fluid Piston Engine <i>B. Belgasim and K. Mahkamov</i>	3866
Theoretical Study of the Aspect Ratio of a Solar Still with Double Slopes <i>A. Madhlopa and J. A. Clarke</i>	3873
Concentrating Solar Power Plants for Electricity and Desalinated Water Production <i>Soteris A. Kalogirou</i>	3881
Analysis of Solar Lithium Bromide-Water Absorption Cooling System with Heat Pipe Solar Collector <i>Amir Falahatkar and M. Khalaji Assadi</i>	3889
Design Analysis for Expansion of Shiraz Solar Power Plant to 500 kW Power Generation Capacity <i>K. Azizian, M. Yaghoubi, R. Hesami and P. Kanan</i>	3897
Thermal Regimes in Solar-Thermal Linear Collectors <i>Javier Muñoz, José M. Martínez-Val and Rubén Abbas</i>	3905
Surface Temperature Distribution and Energy Gain from Semi-Spherical Solar Collector <i>Ilze Pelece, Imants Ziemelis and Uldis Iljins</i>	3913

The Effectivity of a Hybrid Solar Distillator Directly Combined with a Solar Cell	
<i>Kazuo Murase, Tin Yao, Toki Aoyagi and Keishi Okuyama</i>	3921
Comparative Energy and Exergy Analysis of Various Passive Solar Distillation Systems	
<i>Raghendra Singh, Rahul Dev, M. M. Hasan and G. N. Tiwari</i>	3929
Simulation of a Solar Assisted Combined Heat Pump-Organic Rankine Cycle-System	
<i>Stefan Schimpf, Karsten Uitz and Roland Span</i>	3937
Optimisation of Low Temperature Difference Solar Stirling Engines using Genetic Algorithm	
<i>Kwanchai Kraitong and Khamid Mahkamov</i>	3945
Performance Prediction and Experimental Analysis of a Solar Liquid Desiccant Air Conditioner	
<i>S. Alizadeh and H. R. Haghgou</i>	3953
Investigation on Radiative Load Ratio of Chilled Beams on Performances of Solar Hybrid Adsorption Refrigeration System for Radiant Cooling in Subtropical City	
<i>K. F. Fong, C.K. Lee and T. T. Chow</i>	3961
A Hybrid Solar-Gas Air Conditioning System Based on Adsorption and Chilled Water Storage	
<i>Antonio P. F. Leite, Douglas B. Riffel, Celina M.C. Ribeiro, Francisco A. Belo, Paulo V.S.R. Domingos, Daniel Sarmento, Manoel B. Soares and Leonaldo J. L. Nascimento</i> ...	3969
Performance Analysis of the Solar-Thermal Assisted Air-Conditioning System Installed in an Office Building	
<i>Masaya Okumiya, Takuya Shinoda, Makiko Ukai, Hideki Tanaka, Mika Yoshinaga, Kazuyuki Kato and Toshiharu Shimizu</i>	3977
Characterization of Nanostructure Black Nickel Coatings for Solar Collectors	
<i>Z. Ghasempour and S. M. Rozati</i>	3985
Investigations of Heating Process and Absorber Materials in Air Heating Collector	
<i>Aivars Aboltins and Janis Palabinskis</i>	3991
Characterization of Black Chrome Films Prepared by Electroplating Technique	
<i>S. Jafari and S. M. Rozati</i>	3999
Selective Solar Absorber Coating Research at the CSIR (South Africa)	
<i>K.T. Roro, N. Tile, B. Yalisi, M. De Gama, T. Wittes, T. Roberts and A. Forbes</i>	4006
Steel-Tinplate as a Solar Wall Panel and Its Effectiveness	
<i>G. Ruskis, A. Aboltins and J. Palabinskis</i>	4014
Nano Structure Black Cobalt Coating for Solar Absorber	
<i>G. Toghdori, S.M. Rozati, N. Memarian, M. Arvand and M.H. Bina</i>	4021
Combining the Radiative, Conductive and Convective Heat Flows in and Around a Skylight	
<i>Martin Fält and Ron Zevenhoven</i>	4027

Development of a Aolar Intermittent Refrigeration System for Ice Production <i>G. Moreno-Quintanar, W. Rivera and R. Best</i>	4033
Development of Model Solar Kitchen with Green Energy for Demonstration and Application in Rural Areas <i>Sanjib Kumar Rout</i>	4041

Environmental Regulation, Solar Energy Technology Components and International Trade - An Empirical Analysis of Structure and Drivers

Felix Groba^{1,*}

¹ German Institute of Economic Research, Berlin, Germany

* Corresponding author. Tel: +49 30 89789681, Fax: +49 30 89789113, E-mail: F.Groba@diw.de

Abstract: Dynamics of the global renewable energy market are mostly described in terms of investment and added capacity. The role and characteristics of cross border trade flows with renewable energy system components, however, remains blurred. While national environmental regulation and innovative capacity is important for the promotion of renewable energies the effect of regulation and innovative efforts on export dynamics remains ambiguous as empirical studies on the pollution haven and the Porter hypothesis reach diverging conclusions and rarely focus on the renewable energy sector. This paper closes the gap by: First, focusing on solar energy technology components, structure and development of international trade since 1996 is analyzed. Second, determinants of OECD exports are identified in an econometric panel study estimating a gravity trade model. The results unveil a highly dynamic global market for solar energy technology components since 2002, with Europe as dominant market and increasingly strong exports from China. Additionally, the analysis supports the Porter hypothesis as countries with a strong framework supporting renewable energies have gained a comparative advantage in exporting solar technology goods. Analyzing the importer side shows that tariff reduction and FDI inflows have increased imports.

Keywords: Renewable Energies, International Trade, Trade Barriers, Regulation

1. Introduction

Diffusion and transfer of climate friendly energy technologies remain decisive topics in international climate negotiations as they play an important role in the nexus of economic development and a sustainable energy system transformation. Therefore, the development of the global renewable energy market is monitored in numerous studies. These studies commonly either refer to added capacity or investments into renewable energy projects to describe growth, structure and market development [1]. Although international trade has been identified as a decisive channel for technological change the role of the manufacturing sector, producing necessary components, and the international trade system in this production process is mostly neglected. While the interaction between trade flows and environmental regulation and the issue of clean technology transfer have become prominent literature strands, little effort has been put into accessing drivers and dynamics of global trade with specific renewable energy components. Additionally, current negotiation obstacles in WTO talks on environmental goods liberalization unveil that the relationship between trade, technology transfer and clean energy technologies are relevant.

The objective of this paper is to analyze the structure and identify drivers of clean energy technology trade with a specific focus on solar energy technology components. This step is necessary before trade effects such as technology diffusion and sustainable development can be studied in later research. After outlining the methodology, this paper describes structure and development of the international market for solar energy technology components. Subsequently, potential drivers of these specific technology exports from OECD countries to the world are characterized in a panel study estimating a standard gravity model. Three hypotheses are empirically tested: First, as components for solar energy systems are research intensive, the innovative capacity in exporting countries affects the export performance with respective goods. Second, following the Porter hypothesis, countries with a strong policy

framework of supporting renewable energies have gained a comparative world market advantage as such a framework is likely to support a national renewable energy industry that is a striving for export markets. Third, barriers to trade and an unreliable policy environment in receiving countries are obstacles to clean technology trade as additional costs to exporters are imposed.

2. Data description and methodology

Numerous empirical studies adopted the gravity model to explain the relationship between international trade flows and environmental regulation with respect to various goods and sectors. Introduced by Tinbergen [2] the model became the workhorse of trade relation analysis. The popularity can be explained by its successful empirical performance and by strong theoretical foundations outlined in the literature [3]. The general formulation of the gravity model (1) describes trade flows (F) from exporting country i to destination country j at time t as a function of economic masses (M), distances (D) and an error term (η). It furthermore takes a gravitational constant (G) into account depending on the units of measurement for F_{ijt} , $M_{it,jt}$.

$$(1) \quad F_{ijt} = G \frac{M_{it}^{\beta_1} M_{jt}^{\beta_2}}{D_{ij}^{\beta_3} \eta_{ijt}}$$

As the aim of the study is to determine the drivers of international trade with solar energy technologies, the dependent panel variable is the bilateral export flow (EXP_{ijt}) from i to j at time t . The i -exporting countries are Australia, Austria, Belgium, Canada, Czech Republic, Denmark, Finland, France, Germany, Greece, Ireland, Italy, Japan, Korea, Netherlands, Norway, Portugal, Spain, Sweden, Switzerland, the United Kingdom and the United States. An analysis of developing country exports such as Chinese exports is excluded due to a lack of data on control variables. Nevertheless, the sample represents approximately 80 % of global exports in 2008. The sample of j -importing countries includes 129 states, including OECD countries. The time period analyzed with the balanced panel goes from 2000 to 2007. Empirical computation requires the gravity model to be transformed into logs, establishing a linear relationship between variables. This also allows interpreting the percentage change in the dependent variable due to a change in explanatory variables. Based on the explanatory variables, as explained in the subsequent sections, the exact gravity model applied has the following from:

$$(2) \quad \ln SolarEXP_{ijt} = \beta_0 + \beta_1 \ln(GDP_{it}GDP_{jt}) + \beta_2 \ln(POP_{it}) + \beta_3 \ln(POP_{jt}) + \beta_4 \ln(Dist_{ij}) \\ + \beta_5 Border_{ij} + \beta_6 Language_{ij} + \beta_7 Contig_{ij} + \beta_8 Import_Tariff_{ijt} \\ + \beta_9 \ln(FDI_{jt}) + \beta_{10} RoL_{jt} + \beta_{11} \ln(Envirregulation_{jt}) \\ + \beta_{12} \ln(EnergyIntensity_{it}) + \beta_{13} \ln(Envirregulation_{jt}) + \beta_{14} \ln(RDBSolar_{it-1}) \\ + \beta_{15} \ln(PatentStock_{it}) + \alpha_i + \varepsilon_{ijt}$$

2.1.1. Development of solar energy technology component exports

Solar energy technology components are defined as investment goods and associated products needed in solar energy systems. This includes solar thermal and photovoltaic components. Reliable cross country data on trade flows with renewable energies are hardly available. National industry polls, commonly asking for sales as well as imports and exports, are likely to be biased as the number of companies active in the renewable energy market is unclear and poll return might be interest driven. Therefore, the representativeness of these polls is limited and can only be used as a rough indicator for national branch development. Furthermore,

industry polls do not guarantee data comparability. Therefore, international trade data based on the Harmonized Commodity Description and Coding Systems (HS 1996) using the UNCTAD COMTRADE database serves as the source of the dependent variable.

The classification with respect to environmental goods and energy technologies has been well defined by the OECD [4]. Nevertheless, the aspired solar energy technology differentiation requires addressing data validity. A product group based on 6-digit HS 1996 codes, under which solar system components are traded, has been generated (Table 1). The problem is that data might be inflated as the products environmental end use cannot be monitored, i.e. goods that are used for renewable energy systems and goods that might be used otherwise are traded under a common HS code and the renewable energy goods share under one HS code might vary between countries. However, the method used constructs the best available proxy for cross time cross country analysis as data is available on an international common methodology. Furthermore, contrary to industry polls, imports of inputs are likely to be captured allowing a more comprehensive picture of the market. Finally, product similarity can be assumed making the actual end use irrelevant.

Table 1. Nomenclature of solar energy technologies, HS 1996.

HS Code	Explanation
Solar Thermal	
841911	Instantaneous gas water heaters.
841919	Other instantaneous or storage water heaters, non-electric.
840219(ex)	Steam or other vapor generating boilers [Other vapor generating boilers, including hybrid boilers].
841950(ex)	Heat exchange units [Heat-exchange units for solar thermal or geothermal applications].
900290	Concentrator systems to intensify solar power in solar energy systems, other optical elements of any material mounted
Solar Photovoltaic	
850440(ex)	Static converters [Inverters (for converting DC power to AC power)] - change solar energy into electricity.
850720(ex)	Other lead-acid accumulators [solar batteries], i.e batteries for energy storage in off-grid photovoltaic systems.
854140(ex)	Photosensitive semiconductor devices, including photovoltaic cells whether or not assembled in modules or made up into panels; light emitting diodes.

The data show that exports have grown considerably from 1996 to 2008, whereas the largest growth occurred since 2002. Figure 1 supports the finding that the production of clean technology goods is highly skewed towards high income countries [5]. However, East Asian Pacific countries (LDCEAP), mainly China, have gained considerable market share. Interestingly, the data also show that the share of solar energy technology components in trade with industrial goods has been increasing since 1996. Although still low between 0,5 and 1,5% this indicates a quite dynamic market as the solar component trade growth rate has been larger than industrial goods trade growth rates. Another insight is that although the OECD countries are major exporters, the group runs an increasing net trade deficit hinting to the dominance of only some countries. An analysis of the trade direction between regions underlines that main import markets are in high income OECD countries with most of the trade occurring between OECD countries. Another important trade direction is from developing countries to developed countries. Trade between developing country regions remains marginal. Overall, it becomes obvious that the international market for solar energy

technology components is dominated by Europe and China as the main exporting players. Europe furthermore is the dominating importer with most of the global trade occurring within Europe itself.

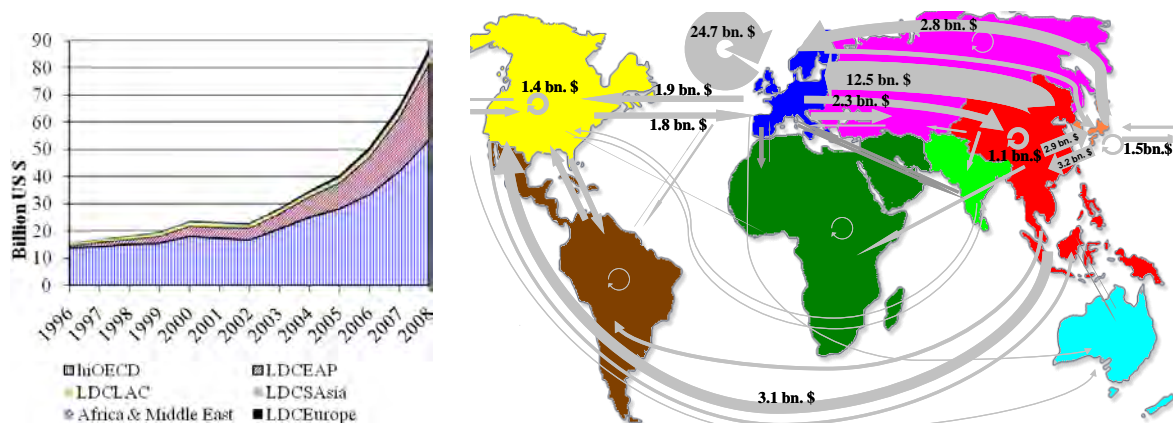


Figure 1. Development of Solar energy technology component exports by country group 1996-2008 and market structure 2008 (Source: UNCOMTRADE)

The analysis of country specific export flows and market shares underlines the dynamics and outlines the dominance of only some countries as well as the increasing importance of developing countries. Although, with a high increase in market volume the development of market export shares over time indicates a crowding out of some OECD exporters mainly due to strong export growth of China.

2.1.2. General parameter of trade analysis

The gravity model predicts that the bilateral trade volume is positively related to a countries' income ($GDP_{it}GDP_{jt}$) [6]. A counter force in this respect is population size as countries with a larger population (POP_{it} , POP_{jt}) are expected to trade less. The reason is that available resources and the domestic market size are expected to be positively correlated with the population size. The anticipated sign is thus negative as the market is able to rather produce goods itself. Theoretically, with increasing distance ($DIST_{ij}$), trade and transportation cost increase, reducing trade volume and causing the expected sign to be negative. Further determinants of bilateral trade flows that are empirically justified are included. Sharing an official language ($LANG$) and having a common border (ADJ_{ij}) is expected to increase bilateral trade flows as goods can be transported at lower costs. Data for these variables have been retrieved from the World Bank World Development Indicators (2009) and from the CEPII's Gravity Dataset (2010).

2.1.3. The role of environmental regulation

The empirical literature on the interaction between trade and environmental regulation remains ambiguous regarding the support of either the polluter haven or the Porter hypothesis [7]. According to the Porter hypothesis, shocks produced by new, stricter regulation creates external pressure on the firms which are subsequently fostered to create new products and processes that positively affect the dynamic behaviour of that economy and hence its international competitiveness. Thus, countries with a stringent environmental regulation may become net exporters of clean technology. The lead market literature, which supports the Porter hypothesis, indicates that an early introduction of adequate technology support policies can create an industry with a competitive world market advantage. A contrary theoretical effect of introducing environmental regulation is that specific clean technology demand is

generated causing additional imports as, in an open economy, foreign producers may provide technology either better or cheaper.

This studies' focus is on the effects of regulation on specific trade flows rather than on overall trade flows. Numerous policy instruments that increase the demand and supply of renewable energy technologies have been identified. The IEA report on 'Renewable energy market and policy trends' provides an overview of policies and time of introduction. Due to the heterogeneous character of these policies across countries the database does not facilitate an evaluation of regulatory stringency or renewable energy supportiveness in a panel context. Therefore, different measures of environmental stringency or renewable energy supportiveness, respectively, are used. In their study on export dynamics of energy technologies, Constantini and Crespil (2008) point out that an indirect measure of environmental stringency, such as CO₂ emissions per unit of GDP is adequate to investigate the Porter hypothesis as well as the political importance of energy saving strategies [7]. The variables *EnergInt_{it}* and *EnvirREG_{it}* give the relative environmental strictness in exporting countries. The underlying assumption is that countries implementing stricter environmental regulation exhibit a positive effect on export dynamics of solar energy technology components. The measures are based on the following environmental indicators:

- Level of Energy intensity 1996 – 2008 in tons of oil equivalent per thousand units of purchasing power parity GDP extracted from the IEA Energy Balance database;
- Level of Carbon intensity 1996 – 2008 in kg per thousand units of purchasing power parity GDP extracted from the Carbon Dioxide Information Analysis Center database.

Subsequently, following the literature, sample countries have been ranked on these relative and dynamic measures (1990 =100) assigning the lowest rank to the worst performer. In the given panel structure this ranking method better allows for a comparison of relative environmental strictness than a comparison of levels of energy use and emissions.

The introduction of further variables controlling for environmental regulation and thus a renewable energy friendly policy environment is neglected. Although statistics suggest that the Kyoto Protocol induced more innovation there seems to be no significant effect of the Protocol on technology transfer and thus trade.⁵ In addition, other proxies of environmental regulation such as environmental private and public expenditures, environmental tax revenues and public environmental protection expenditures are likely to be captured by applied controls. The same is true for expected returns on energy investment, which is generally best reflected by electricity price trends. But, as total primary energy supply and therefore the energy market size of a country, is included in the estimation, incentives to invest in renewable energies are respected to some extent.

2.1.4. The role of the innovation system in exporting countries

In general, innovation is assumed to be a product of knowledge generating inputs [8]. As this study focuses on highly innovative technology goods, two variables controlling for the role of the innovation system in exporting countries are included.

First, a variable measuring a countries public technology specific research and development spending (*RDBsolar_{it}*) is introduced. In theory, research and development increases exports as new technology might be developed which, in an open economy, is available to the world market as well. The variable enters the analysis lagged by one period assuming that the process of technology development takes some time until a new product is ready for market entry. Data is obtained from the IEA (2010) Energy Technology Research, Development and

Demonstration database. The data show that combined OECD public spending on solar energy has been constant since 1990 and is decreasing since 2006. Yet, there is substantial country level variation leaving the actual effect on export performance unclear.

Second, productivity of new knowledge is assumed to depend on the existing stock of ideas [8]. The patent stock of a country is the best proxy for knowledge stock in this respect. Therefore, patent counts for renewable energy have been extracted from the OECD (2010) Science, Technology and R&D Statistics database. Aiming at comparability and an unbiased estimation, only patent applications by inventor country issued under the international patent cooperation treaty have been included (Figure 2).

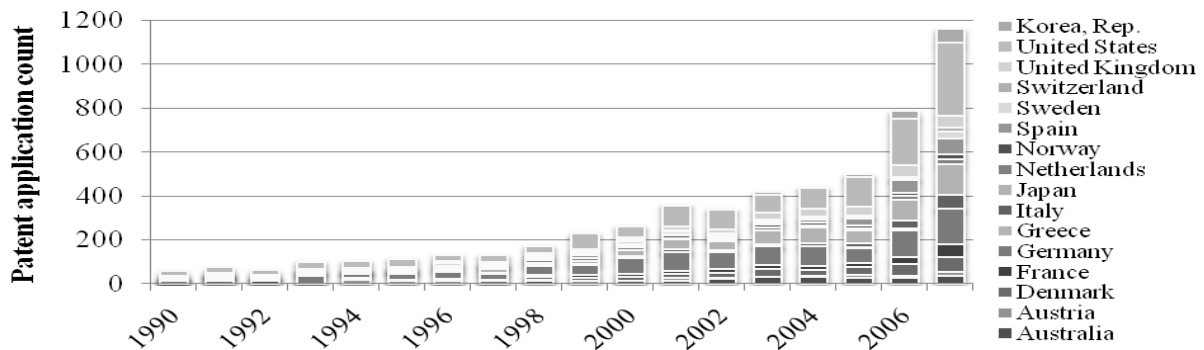


Figure 2: Renewable Energy Patent applications by country of origin 1990 – 2007

Based on the patent counts the countries' patent stock has been calculated with depreciation rate α of 15% as is commonly done in the literature⁸:

$$(3) \quad PatStock_{i,t} = (1 - \alpha)PatStock_{i,t-1} + Patents_{i,t}$$

Naturally, the stock of knowledge with respect to renewable energies differs substantially between countries. Therefore, the assumption to be tested empirically is that countries with a higher renewable energy knowledge stock export more to the world market.

2.1.5. The role of barriers to trade and regulation in importing countries

A general assumption is that tariff and non-tariff barriers inhibit trade while a positive general policy environment as well as environmental friendly regulation in importing states supports cross border flows of the specific high technology goods which are the focus of this study. Hence, import tariffs ($Import_Tariff_{ji}$) applied to the compounded product group of solar goods are introduced as an explanatory variable. Data on the effectively ad valorem tariff applied by the importing country j to solar technology component exports from i in percent of the import value is obtained from the UNCTAD TRAINS database. The indicator serves as control for the potential impact of a liberalization of environmental goods as discussed in the WTO Doha negotiations and denounces the reduction of additional trade cost over time. The expected coefficient sign is negative as bilateral trade flows are high with lower tariffs as exporters face reduced trade costs. The development of tariffs over time seems to support the theoretical underpinning. While solar energy technology component exports of OECD countries increased significantly, the mean tariff applied by the samples importing countries decreased substantially from 10% in 1996 to 5% in 2008.

Environmental regulation and renewable supportiveness in receiving countries potentially plays a role as demand for clean technologies can be satisfied through the world market.

Hence, the environmental stringency variable $EnergREG_{jt}$ is introduced as control for such regulation using the same method as for exporting countries described above. The study also includes the World Bank's rule of law indicator (ROL_j) as a proxy for the quality of institutions and the capacity to respect legal rules which might be relevant for exporters.

As currently the solar energy market development is often described in terms of investments, controlling for such investments to explain technology component export flows is necessary. Adequate solar technology specific investment data on a cross time cross country level is not yet available. Therefore, the best proxy in this respect is net foreign direct investment inflow in importing countries (FDI_{jt}). Trade flows are tightly linked to foreign direct investments flows [9]. Following the literature on trade flows and foreign direct investments the coefficient should be positive as a higher attractiveness of a county for FDI also exhibits a higher attractiveness for exports.

3. Results

The gravity model as stated in equation (2) has been estimated using random and fixed effects in order to control for country heterogeneity with robust standard errors clustered on country level. However, the significance of the Hausman test clearly indicates that exporting country individual effect (α) and the repressors are correlated. Thus, only the consistent fixed effect estimation coefficients on the repressors are reported in Table 2. Adequate tests for the robustness of the results have been conducted.

Table 2. Gravity model and the role of environmental regulation, innovation and trade parameters

	(1)	(2)	(3)	(4)	(5)	(6)	(7)	(8)
$\ln GDP_{ijt}$	1,57***	1,58***	1,18***	1,59***	1,55***	1,55***	1,65***	1,53***
$\ln POP_{it}$	-6,81*	-7,19*	-6,49*	-6,89*	-8,31*	-6,81	-5,02	-11,63**
$\ln POP_{jt}$	-0,42***	-0,44***	-0,06	-0,45***	-0,43***	-0,43***	-0,46***	-0,41***
$\ln DIST_{ij}$	-1,01***	-0,98***	-0,99***	-1,00***	-1,01***	-1,00***	-0,99***	-0,93***
ADJ_{ij}	0,01	0,06	-0,05	-0,01	0,15	0,16	-0,22	0,038
$LANG_{ij}$	1,15***	1,19***	1,01***	1,13***	1,11***	1,10***	1,19***	1,06***
Import Tariff _{ijt}	-0,01***							
$\ln FDI_{jt}$		0,17***						
RoL_{jt}			0,02***					
$\ln EnvirREG_{jt}$				0,11*				
$\ln EnergInt_{it}$					0,24*			
$\ln EnvirREG_{it}$						0,15*		
$\ln RDBsolar_{it-1}$							0,03*	
$\ln PatStock_{it}$								0,03
Time dummies	yes							
N	22382	21630	22550	22550	21793	19475	21263	36092
R ²	0,68	0,69	0,70	0,68	0,67	0,67	0,70	0,64

note: significance level *** p<0.01, ** p<0.05, * p<0.1

The results show that standard control coefficients of trade flow analysis such as income, population and distance have the expected impact. Thus, this set of controls is taken as basis for the analysis of the remaining control variables. These specific control variables also

behave as expected. A one unit increase in tariffs decreases imports by 0.01 units. Thus, Higher tariffs significantly decrease import flows while the relationship between investment inflows and the institutional quality in receiving countries is positive. The impact of environmental regulation in importing countries on trade flows is weak but positive. The role of the innovation system in exporting countries remains ambiguous. On the one hand public spending in solar energy technology has a positive significant impact on export flows. On the other hand the renewable energy patent stock has no significant impact. The results of the study support the Porter Hypothesis as countries with a more stringent environmental regulation and a better energy intensive score export more solar energy technology components to the world market and thus seem to have gained a competitive advantage.

4. Discussion and Conclusion

This study applies an empirical gravity model to identify the main drivers of trade with solar energy technology components. Finding evidence for the Porter hypothesis and the importance of the innovations system the results are in line with findings of related work on environmental regulation and trade as well as with the OECD's strategy on environmental regulation, innovation and green growth. Yet, besides the issues related to a potential dual use of products under one HS-code the effects might be biased by the use of rather broad control variable specifications such as general renewable energy patents instead of solar specific patents to construct the knowledge stock. Nevertheless, the results are interesting from a global climate negotiation perspective as it is shown that the regulatory context in receiving countries is decisive for clean technology imports and thus potential technology transfer.

Consequently, the remaining research agenda should focus on technology transfer in trade with these clean energy technologies as well as the study of potential trade effects. Within this context the construction of regulation measures capturing renewable energy supportiveness of a country more directly should be developed.

References

- [1] REN 21, 2009. Renewables Global Status Report: 2009 Update, 2009, Paris.
- [2] Tinbergen, J., 1962. Shaping the World Economy, Twentieth Century Fund, New York.
- [3] Jug, J.; Mirza, D., 2005. Environmental regulations in gravity equations: evidence from Europe, *World Economics* 28(11), pp.1591-1615.
- [4] OECD, 1999. The environmental goods and services industry manual for data collection and analysis, Paris.
- [5] Dechezleprêtre, A.; Hascic, I., 2008. Invention and Transfer of Climate Change Technology on a Global Scale: A Study Drawing on Panel Data, Paris, 2008.
- [6] Harris, M.; et al., 2002. Modeling the Impact of Environmental Regulation on Bilateral Trade Flows: OECD, 1990 -1996, in: *The World Economy*, vol.25 (3), 2002, pp.387-407.
- [7] Constantini, V.; Crespi, F., 2008. Environmental regulation and the export dynamics of energy technologies, in: *Ecological Economics* 66(2008), pp. 447-460.
- [8] Braun, F.; et.al., 2010. Innovative Activity in wind and solar technology: empirical evidence on knowledge spillovers using patent data, DIW Discussion Paper XI992/2010, Berlin.
- [9] Makki, S., 2007. Impact of Foreign Direct Investment and Trade on Economic Growth, Washington.

Environmental Impacts of Solar Thermal Systems with Life Cycle Assessment

Alexis de Laborderie^{1*}, Clément Puech¹, Nadine Adra¹, Isabelle Blanc², Didier Beloin-Saint-Pierre², Pierryves Padey², Jérôme Payet³, Marion Sie³, Philippe Jacquin⁴

¹ Transénergie, Ecully, France

² MINES ParisTech, Sophia Antipolis, France

³ Cycleco, Ambérieu, France

⁴ PHK Consultants, Ecully, France

* Corresponding author. Tel: +33 472860407, Fax: +33 472860400, E-mail: a.delaborderie@transenergie.eu

Abstract: Solar thermal systems are an ecological way of providing domestic hot water. They are experiencing a rapid growth since the beginning of the last decade. This study characterizes the environmental performances of such installations with a life-cycle approach. The methodology is based on the application of the international standards of Life Cycle Assessment. Two types of systems are presented. Firstly a temperate-climate system, with solar thermal collectors and a backup energy as heat sources. Secondly, a tropical system, with thermosiphonic solar thermal system and no backup energy. For temperate-climate systems, two alternatives are presented: the first one with gas backup energy, and the second one with electric backup energy. These two scenarios are compared to two conventional scenarios providing the same service, but without solar thermal systems. Life cycle inventories are based on manufacturer data combined with additional calculations and assumptions. The fabrication of the components for temperate-climate systems has a minor influence on overall impacts. The environmental impacts are mostly explained by the additional energy consumed and therefore depend on the type of energy backup that is used. The study shows that the energy pay-back time of solar systems is lower than 2 years considering gas or electric energy when compared to 100% gas or electric systems.

Keywords: Environmental impact, LCA, Solar thermal systems

1. Introduction

Solar thermal systems have encountered a high interest over the last ten years in many locations worldwide [1,2]. Indeed, it is a robust, efficient and simple technology to implement for individual households: solar thermal relies on well known process and materials. Its capacity in reducing energy load for domestic hot water (DHW) is significant in locations with high irradiation level.

Some studies have been carried out on thermosiphon solar water heaters in different countries [3-6] but none was focused on solar thermal systems with auxiliary energy source. This study is focused on this second type of installation since they often are preferred for Northern-European countries (collector and storage with integrated backup).

The main purpose of the work is to characterize the environmental impacts of solar domestic hot water systems, or solar water heaters (SWH), integrating auxiliary heating (electric or gas heaters). Furthermore, this study also aims at identifying the most discriminating parameters to support implementation solutions. These systems' performances are analyzed as case-studies both for temperate climates (typically in France) and for tropical climates (typically in the Caribbean).

Life Cycle Assessment (LCA) methodology is used for this environmental evaluation. Among several LCA impact indicators, this study focuses on primary energy consumption, global warming potential, effect on ecosystem quality and human health issues. Greenhouse gas emissions (expressed in CO₂ equivalent) and non-renewable energy consumption are considered here as key LCA outputs.

Environmental performances of the different SWH with gas-backup, electrical-backup or no backup (for tropical zone's systems) are compared with standard hot water systems without any solar contribution.

2. Methodology

This Life Cycle Assessment (LCA) study was performed in compliance with the ISO standards 14040 and 14044 [7,8].

2.1. Scope of the study

This study has been carried out on individual solar thermal systems applied in the case of temperate and tropical climates. For temperate locations, four systems have been studied, namely two traditional systems without solar systems considering only electricity or gas heater, and two systems with solar system and integrated backup energy (electricity backup see Fig. 1 or gas backup). Due to the irregular solar irradiation all over the year, this kind of solar thermal system requires a backup system to reach the target temperature. For tropical climates, one thermosiphonic solar system (without backup energy) has been analyzed (Fig. 2).

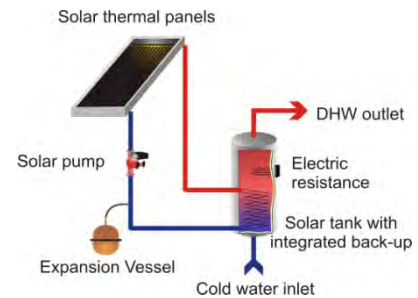


Fig. 1. Sketch-plan of temperate-type solar water heaters (electric backup)

To study both temperate and tropical systems, two climatologically average located places have been determined, namely Lyon (continental France) for temperate climate and Le Lamentin (Martinique, overseas France) for tropical climate.

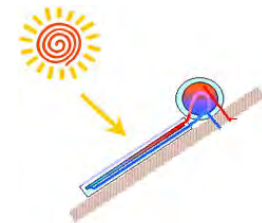


Fig. 2. Sketch-plan of tropical-type solar water heaters

The solar systems configuration and backup energy uses are different according to the climatic conditions. Therefore, two different Functional Units have been defined:

The temperate climate Functional Unit: Production of DHW for a four-person household, (assessed to be 140 litres of 60°C) in temperate climate and 20 years of life expectancy.

The tropical climate Functional Unit: Production of DHW for a four-person household, (assessed to be 200 litres of 50°C) in tropical climate and 20 years of life expectancy.

Given that tropical-type SWH does not include backup energy, the target temperature (50°C) is an indicator required to calculate solar energy but it does not represent the real outlet water temperature.

Corresponding irradiation levels and electricity mixes have been considered.

2.2. Inventory

2.2.1. Inventory building strategy and sources

Many hypotheses are necessary to evaluate the life cycle environmental impacts of DHW production. These hypothesis have been defined with the expertise of the consulting and

engineering partner¹ as well as technical data collected from public industrial actors. Thus, the different systems' component has been determined and sized. On the second hand, inventories for the electricity mix have been determined for the temperate-climate system.

For this study, the ecoinvent 2.0 LCI database [9] was used. Ecoinvent 2.0 contains international industrial life cycle inventory data on a various range of activities (energy supply, resource extraction, transport services,...). However, most of the SWH components are not defined exactly in the existing database. Thus, it has been necessary to modify or create new processes. When components' inventories were available in the database they were assessed in order to determine the validity of this inventory regarding the components' origin and main characteristics (materials used, manufacturing process and weight). When necessary, some inventories were modified by applying a weight or size ratio. Some inventories have also been completed by specific technical data collected within this project. When no inventory was available for a component, a new inventory has been built by the project team to estimate the required data.

As for the construction of the inventory, the composition of each component comes from different sources, which are described in Table 1.

Table 1. Data collection for infrastructures in scenarios

Component	Sources
Solar panel	Ecoinvent modified (to match with the surface defined for the scenarios)
Water Pump	Ecoinvent modified (estimates, from the mass of material)
Expansion Vessel	Ecoinvent (slightly oversized compared to usual design, but minor impact)
Hot water tank	Ecoinvent modified (from a 2000 l tank)
Solar regulation	Rough estimate (from the mass of the material, mostly electronics)
Mounting support	Datasheets from manufacturers, completed by estimates when necessary
Plumbing	Experience and estimates from the consulting and engineering partner
Electrical backup	Ecoinvent (slightly oversized, but minor impact)
Gas backup	Ecoinvent modified (to exclude the impacts related to domestic heating)

2.2.2. System boundaries

The system boundaries are described in Fig. 3. They include the solar panels manufacturing (panels, mounting systems), water tanks, internal heat exchanger, pipes, hydraulic components (pumps, valves, expansion vessel), regulation, cabling and solar fluid. In addition, they also include the use phase (backup energy consumption for temperate-climate SWH) and the recycling of components.

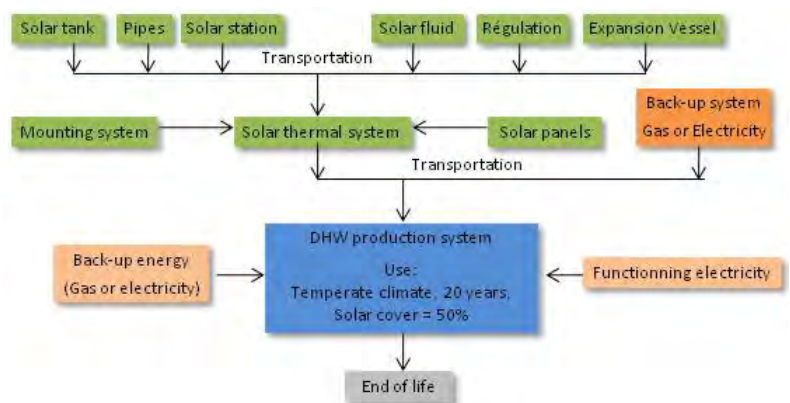


Fig. 3. Scheme of system boundaries

¹ Transénergie, <http://www.transenergie.eu>

2.2.3. Scenarios

Table 2 describes the four scenarios (scenarios 1-4) built for this study used for temperate climate systems. Scenario 5, standing as a reference for other scenarios results, comes from the ecoinvent 2.0 database.

Table 2. Scenarios for temperate climates

Temperate climate Scenarios					
	Scenario 1	Scenario 2	Scenario 3	Scenario 4	Scenario 5
<i>System</i>	Solar Thermal + Gas	Solar Thermal + Electricity	Gas heater	Electric heater	Solar Thermal + Gas
<i>Solar Panels</i>	Flat plate collectors ²				Flat plate collectors ³
<i>Water tank</i>	300 litres vertical tank	300 litres vertical tank			400 litres vertical tank
<i>Backup system</i>	Individual gas heater and heat exchanger ⁴	Electric resistance ⁵	Individual gas heater	Electric heater tank	Individual gas heater and heat exchanger ⁵
<i>Other components</i>	Mounting system, pipes, regulation and solar station			Pipes	Mounting system, pipes, regulation and solar station
<i>Overall lifetime energy consumption</i>			205 000 MJ		~330 000 MJ
<i>Solar coverage</i>		50%		None	58,4%
<i>Life expectancy</i>			20 years		25 years

Table 3. Scenarios for tropical climate systems

Table 3 describes the scenario built for this study for tropical SWH which is based on a thermosiphonic solar system. Flat plate collectors inventory is an average of the three main products that exists on the Caribbean market.

Tropical climate Scenarios	
<i>System</i>	Thermosiphon
<i>Solar Panels</i>	Flat plate collectors ⁵
<i>Solar tank</i>	200 l horizontal tank
<i>Other components</i>	Mounting system, pipes
<i>Overall lifetime energy consumption</i>	147 000 MJ
<i>Life expectancy</i>	20 years

2.3. Payback time indicator

Energy Payback Time (EBPT) has been calculated with the following definition:

$$EPBT = \frac{E_p^{fabrication} + E_p^{backup}}{avoidedE_p^{production}} \quad (1)$$

² Collector Area = 4,4 m² with solar panel coefficients : B=0,75 ; K=4,5 W/(m².K)

³ Collector Area = 4 m² with unknown solar panel coefficients

⁴ Integrated in the upper part of the tank

⁵ Collector Area = 2 m² with solar panel coefficients : B=0,75 ; K=4,5 W/(m².K)

$E_p^{fabrication}$: Non-renewable primary energy used for the fabrication of the installation.

E_p^{backup} : Non-renewable primary energy used for the backup system.

$avoidedE_p^{production}$: Non-renewable primary energy avoided (thanks to the backup energy used, in case of electric backup, specific electricity mix of the country avoided where the SWH is installed).

In the case of electric backup or the comparison with the full electric system, this method of calculating EPBT gives results only valid for the country where the solar panels are installed.

3. Results and analysis

Results have been calculated according to the impact 2002+ (v2.04) [10] method available in SimaPro 7.1 PhD and the database ecoinvent 2.0.

3.1. Temperate climate-type systems

3.1.1. Overall environmental impacts

Scenarios are compared among all impact categories in figure 4. Figures 5 and 6 present the results for the most significant impact categories with the details of their origin.

It strikes that the necessary water auxiliary heating has a strong influence on the overall impact indicators. In the case of a SWH with electric backup (scenario 2), CO₂ equivalent emissions are significantly cut down compared to a SWH with gas backup (scenario 1).

However, considering the other three impact categories, SWH with gas backup appears as the best impact reduction potential option compared to “traditional systems” (scenarios 3 and 4: respectively gas only or electricity only) as well as SWH with electric backup.

It is important here to point out that the electricity mix chosen here influences thoroughly the environmental performances of the ST installation, as well as the comparison with the electricity only scenario. Indeed, according to ecoinvent 2.0, the French electricity mix has particularly low carbon content: 103g/kWh. Thus, the energy backup’s choice is critical according to the environmental impact reduction targeted.

3.1.2. Distribution of environmental impacts

The graphs below presents the climate change and non-renewable primary energy impacts. They show the distribution of the impacts of each scenario for the different main life cycle components.

In each of the five scenarios, transports (of materials to the manufacturing plant, as well as of the products to the installation location) play a minor role in non-renewable primary energy consumption. The electricity consumed for the operation of the SWH accounts for a smaller amount of non-renewable primary energy too. Backup energy consumptions stand by far

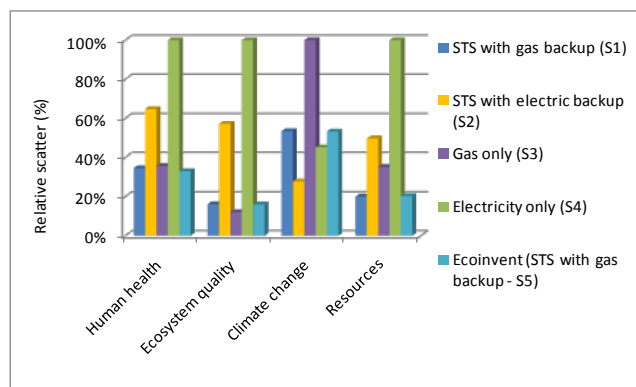


Fig. 4. Comparison of the temperate-climate-type scenarios on the complete lifetime

(>80-90%) for the most important part of for the climate change and non-renewable primary energy consumption impacts. Components of the solar thermal systems (solar thermal panels, pumps, solar tank and regulation system) finally make up for a lesser part of overall impacts, and once produced, consume very little electricity in the operating phase while providing 50% of DHW energetic demand.

In the case of electric backup, CO₂ equivalent emissions are low because the electricity mix chosen is mainly based on nuclear energy (France) and has particularly low CO₂ emissions. On the other hand, the French electricity mix has an important primary energy use (13.6 MJ of primary energy per kWh, according to ecoinvent 2.0), which is why, in this precise configuration (scenario 2), electric backup stands for 91% of non-renewable primary energy (see Fig. 5).

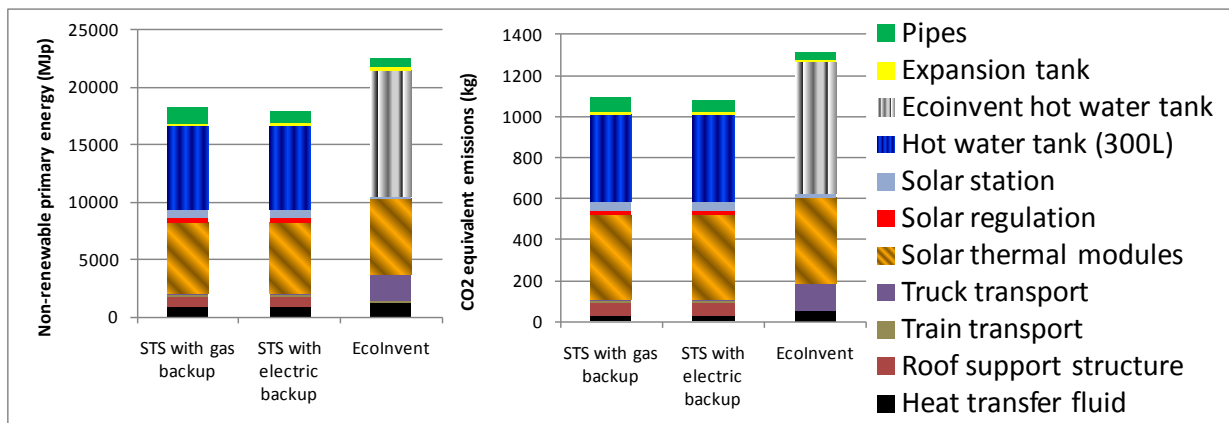
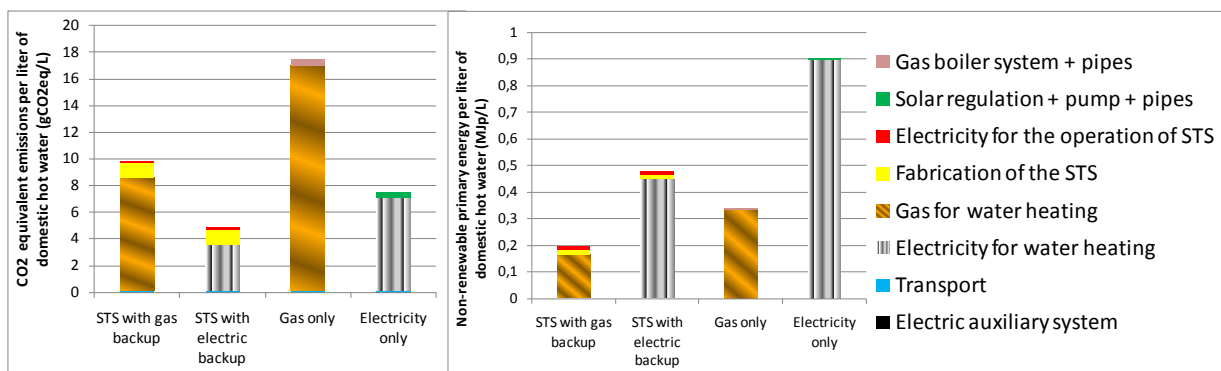


Fig. 5. Distribution of environmental impacts on climate change and non-renewable primary resources for the first four scenarios for temperate-climate-type SWH

Figure 6 shows the impacts of the fabrication of the solar thermal systems' components for the three scenarios with SWH. The results for those three scenarios show the same trend: solar thermal panels and the hot water tank are the major contributor to the environmental impacts of the two analyzed impact categories. Going further into details, it shows that the use of a large amount of steel stands for the most important part of the impacts of the hot water tank. As for solar thermal panels, it is aluminum (mainly for the frame) that causes most of the



impacts. The major differences between the two SWH scenarios come from the fitting between the hot water tank and the boiler for the gas backup (fitting that is not necessary in the case of electric backup, which is integrated in the hot water tank).

Fig. 6. Detailed environmental impact potential of temperate-climate solar thermal system on climate change and non-renewable primary resources

3.1.3. Comparison with ecoinvent 2.0

Scenario 5 (the ecoinvent scenario) shows significant different results compared to the first two scenarios. This is due to the water tank used which is 1/3 larger in scenario 5 (400 l instead of 300 l). Besides, the transports hypotheses are much less favorable in scenario 5 compared to the first two. On the other hand, the supposed solar coverage ratio (SCR) is noticeably higher in the ecoinvent scenario while the solar thermal panels surface is lower: respectively 58.5% instead of 50% for the SCR, and 4 m² instead of 4.4 m². A further examination indicates that the main differences of results between the two sets of scenarios comes from hypotheses and choice of study parameters (lifetime, SCR, annual energy demand), and therefore shows the coherence between scenarios 1 (gas backup) and 2 (electrical backup) and the ecoinvent scenario (scenario 5).

3.1.4. Energy payback time

Energy payback time (cf. its definition in paragraph 1.3) has been studied in order to compare the energy required for the fabrication of SWH, to the energy avoided thanks to these systems while providing the same service (cf. functional unit). For the sake of clarity, only SWH with gas backup (scenario 1) has been compared to “traditional systems” (scenarios 3 and 4). Energy payback time is 1.5 years when comparing SWH with gas backup to gas only (scenario 1 to scenario 3), and less than 1 year when comparing SWH with gas backup to electricity only (scenario 4).

3.2. Tropical-type scenario

3.2.1. Environmental impacts and distribution

As detailed in Table 2, the solar thermal systems studied here as the tropical-type scenario shows specific differences with the systems used in temperate-climate conditions. Considering that the impact of gas or electricity consumption makes up the major part of overall impacts in the previous scenarios, the impacts of this scenario are significantly different from the previous in terms of distribution.

Fig. 7 shows the distribution of the impacts for each category. The water tank strikes as the major contributor to the impacts of the SWH, between 31% and 60% of each impact.

The other significant contributions are made by the solar thermal panels (about 20% of the impacts), the pipes (mostly because of the copper used), 23% and 31% respectively for human health and quality of ecosystems. The support structure accounts for 7% to 11% according to the impact category.

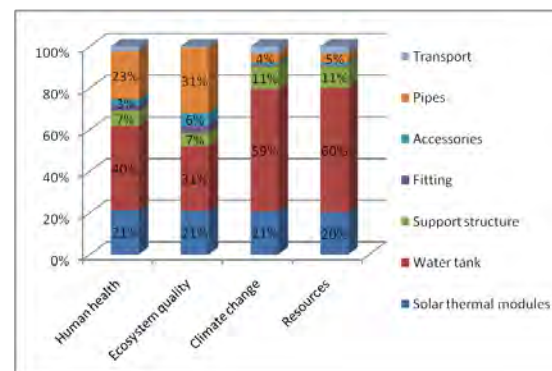


Fig. 7. Distribution of environmental impacts of the tropical-type SWH for each category of impact

3.2.2. Energy Payback Time

Payback time of tropical SWH (with no auxiliary energy) ranges between 5 and 6 months.

4. Conclusions, recommendations and perspectives

This study clearly shows that solar thermal systems are a very interesting solution to reduce the environmental impacts of domestic hot water production.

The impact assessment results for temperate climate systems highlight the backup energy as the major factor on environmental impacts. However, this study does not end with a clear-cut

environmental hierarchy among the different SWH systems: electricity or gas as a backup energy. This is mainly due to characteristics of the French electricity mix that has a low CO₂ content but an important primary energy ratio.

For all SWH, regardless of backup energy, solar panels, water tank and pipes emerge as the key environmental components.

Therefore, considering those results, technical improvement related to the main impacting components can be realized to lower the environmental impacts of the solar thermal part of SWH.

This project has been followed by a LCA on larger solar thermal installations to determine their related environmental impacts and compare with domestic solar systems⁶.

Acknowledgments

ADEME (French Environment and Energy Management Agency) is co-financing this project which brings together different French specialists from the solar thermal industry and LCA fields.

References

- [1] Eurobserv'er, Solar thermal Barometer, SYSTÈMES SOLAIRES - le journal des énergies renouvelables N° 191, June 2009
- [2] Solar Thermal Markets in Europe Trends and Market Statistics 2009, ESTIF, 2010
- [3] Soteris Kalogirou, Thermal performance, economic and environmental life cycle analysis of thermosiphon solar water heaters, *Solar Energy* 83, 2009, pp. 39–48
- [4] Fulvio Ardente, Life cycle assessment of a solar thermal collector: sensitivity analysis, energy and environmental balances, *Renewable Energy* 30, 2005, pp. 109–130
- [5] Crawford, R. H., Net energy analysis of solar and conventional domestic hot water systems in Melbourne, Australia, *Solar Energy* 76, 2004, pp. 159-163
- [6] Soteris Kalogirou, Environmental benefits of domestic solar energy systems, *Energy Conversion and Management* 45, 2004, pp. 3075-3092
- [7] International Standard Organization. ISO 14040. Environmental management – Life Cycle Assessment – principles and framework. 2006
- [8] International Standard Organization. ISO 14044. Environmental management – Life Cycle Assessment – requirements and guidelines. 2006.
- [9] Swiss Center for Life Cycle Inventories. The life cycle inventory data version 2.0. <http://www.ecoinvent.ch>. 2008.
- [10] O. Jolliet, M. Margni, R. Charles, S. Humbert, J. Payet, G. Rebitzer, R. Rosenbaum. Impact 2002+: A new life cycle impact assessment methodology, *International Journal of Life Cycle Assessment*. 2003. Volume: 8, Issue: 6, Pages: 324-330

⁶ More information are available on <http://www.esthace.eu>

Solar energy measurement on the South African east coast

E. Zawilska^{1*}, M.J. Brooks²

¹ Department of Mechanical Engineering, Mangosuthu University of Technology, Durban, South Africa

² Sustainable Energy Research Group, School of Mechanical Engineering, University of KwaZulu-Natal, Durban, South Africa

* Corresponding author: Email: ewa@mut.ac.za, Tel: +27 319077233, Mobile: +27 825864123

Abstract: This study presents the record and analysis of solar radiometry and selected meteorological parameters for Durban, South Africa over a full one-year period from January to December 2007. The results comprise of the key components essential in an assessment of the solar energy resource including global horizontal irradiance, global irradiance on a north-pointing tilted plane at 30° latitude angle, direct normal irradiance and diffuse horizontal irradiance. In addition, the ambient air temperature, humidity and rainfall records are presented and discussed. Selected solar radiometry variables obtained from the STARlab study were compared with data available from various sources including the HelioClim dataset, the NASA SSE database and the literature. The ongoing aim of this study is to build a reliable record of the solar resource for planning, engineering design and effective operation of solar energy systems and applications.

Keywords: Solar energy potential, Radiometry data, Meteorological data, Renewable energy

1. Introduction

The development and deployment of sustainable energy technologies across the globe continues at a growing pace, and of the various options available, solar energy remains among the most promising. As a developing nation, South Africa possesses an abundant solar resource, yet the country has traditionally been a carbon-intensive economy. For example, coal provided 70% of its primary energy in 2004, and 90% of the country's electricity [1]. In 2003, a government White Paper on Renewable Energy (WPRE) addressed future energy needs by committing the nation to achieving 4% of its anticipated power requirements from renewable sources by 2013 [2]. This target includes the deployment of end-use technologies such as solar powered water heaters, which South African power utility Eskom estimates could contribute 23% of the target. Eskom has since rolled out a large-scale solar water heating program, offering an incentive to consumers to replace existing electric geysers with the solar alternative [3]. In all these cases, however, an accurate and reliable understanding of the solar resource at the chosen geographic location is essential. Obtaining high-quality irradiation measurements poses a challenge due to the high cost of setting up and maintaining ground-based solar monitoring stations. As a consequence, only a limited number of solar resource assessment studies have been carried out in South Africa in recent years, which either possess inadequate resolution for use in coastal areas, or which have focused on sparsely populated desert regions in the Northern Cape province where concentrating solar power potential is greatest [3-5]. Densely populated urban areas on the east coast have largely been overlooked, yet this is where demand-side reduction programs could contribute greatly to lessening the country's reliance on grid electricity.

Durban is the largest city on the east coast of South Africa and in the province of KwaZulu-Natal (KZN). Despite high population density, growth and energy consumption few comprehensive studies have been done to characterize Durban's solar resource [6,7]. Lefevre et al. [8] compared

satellite-derived data with ground-based irradiance data using 35 ground stations in Africa but only Pretoria and Cape Town are included.

This study is part of a broader radiometric research program at Mangosuthu University of Technology, Durban, South Africa. Data were measured at a ground station located 3 km inland of the Indian Ocean coastline and is considered to be representative of the South Africa east coast region. This paper presents the record and analysis of the solar resource along with meteorological parameters for the period of January to December, 2007. In addition, the ambient air temperature, humidity, wind and rainfall records are presented and discussed. Selected solar radiometry variables obtained from the study are compared with the Meteosat-derived HelioClim dataset, NASA's SSE resource, as well as the literature. The ongoing aim of this study is to build a reliable record of the solar resource for planning, engineering design and effective operation of solar energy systems and applications. The database is also intended to support research in radiometric modeling. We anticipate expanding the database to geographic areas beyond Durban to cover more of the South African eastern coastal region. These efforts are intended to support the deployment of renewable energy resources and reduce the burden on the South African electrical grid.

2. Methodology

The data were recorded at the Solar Thermal Applications Research Laboratory (STARlab) which is an outdoor solar energy research centre in Durban, South Africa (29°58'N; 30°55'E). The station is at 105.5 m above sea level. STARlab is equipped with instrumentation for solar and meteorological monitoring, including thermopile radiometers and a weather station. The serial numbers, mounting and parameters of the radiometry instrumentation are listed in Table 1. The STARlab control room houses solar radiometry and meteorology data logging instrumentation. This includes two Agilent Technologies 34970A data acquisition units (one as back-up) with 34901A 20-channel multiplex modules connected to a desktop computer. Monitoring equipment is connected via an uninterruptible power supply unit. Data logging is controlled by custom-developed LabVIEW application that records point values at 30 sec intervals, with each set of values written to a spreadsheet file that is date- and time-stamped with day, month, year as well as local clock time and a corresponding solar time. In this study the PSA Algorithm was used for locating the solar vector [9] and generating key information such as declination, azimuth, zenith and hour angles. The radiometry data are recorded in terms of solar time, with solar noon occurring when the zenith angle is at a minimum. To obtain irradiation values, the irradiances are integrated over time. Weather variables such as temperature, wind speed and direction, rainfall, humidity and atmospheric pressure are recorded at 30 minute intervals for each 24-hour daily period. STARlab instrumentation is subject to a daily maintenance routine. For the period of this study less than 4% of data were missing due to unavoidable equipment malfunctions. A simple linear interpolation technique, similar to that reported in [6,10] was employed to replace missing information. A flowchart of the solar data monitoring system used in this study is given in Fig. 1.

The results of this study comprise key components essential to an assessment of the solar energy resource including global horizontal irradiance (G_t) global irradiance on a north-pointing tilted plane at 30° latitude angle (G_{tS}), direct normal irradiance (G_{DN}) and diffuse horizontal irradiance (G_d).

Table 1. Specification of STARlab radiometric instrumentation

Instrument	Serial number	Mounting	Parameter
Eppley PSP	# 34332F3	Horizontal plane, unshaded	Total global irradiance (G_t) in the wavelength range 285 nm to 2800 nm
Eppley PSP	#33583F3	Inclined at 30° slope to the horizontal, aligned true north, unshaded	Total global irradiance in the wavelength range at a 30° tilt angle (G_{tS})
Eppley NIP	#31955E6	Mounted on a ST-1 motorised solar tracker	Direct normal irradiance in the visible wavelength range (G_{DN})
Eppley TUVR	#34623	Horizontal plane	Ultra violet irradiance in the range 295 nm to 385 nm

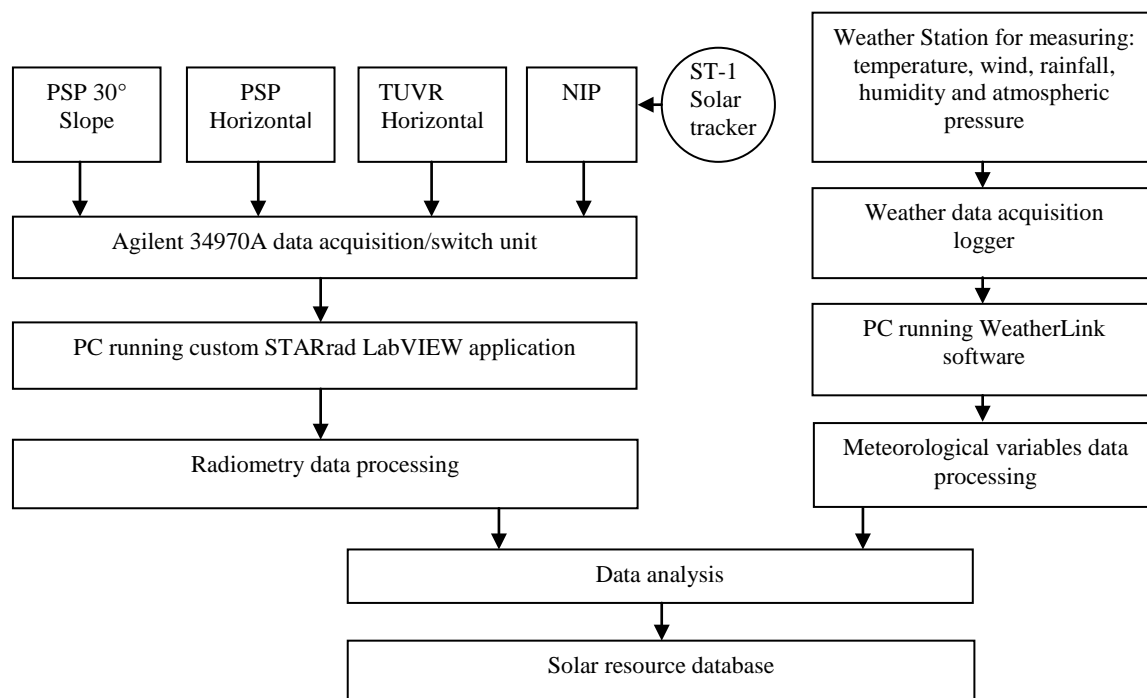


Fig. 1. Flow chart of the method applied in generating the STARlab solar resource database

In addition, the air ambient temperature, humidity, wind and rainfall records are discussed. Selected solar radiometry variables obtained from the STARlab ground-based records are compared with corresponding data available from HelioClim [11], NASA SSE [12] and sources in the literature. Data derived from Meteosat satellites have been used for comparison in a number of studies [8,13] and are currently in use by South African practitioners.

3. Results and Discussion

3.1. Radiometric analysis

Records of global horizontal irradiance G_t (W/m^2), global irradiance on a north-pointing tilted plane at 30° G_{tS} (W/m^2) and direct normal irradiance G_{DN} (W/m^2) were acquired from STARlab radiometers between January and December of 2007. The diffuse solar irradiance G_d (W/m^2) is calculated using the closure equation [14].

$$G_d = G_t - G_{DN} \cos \theta_z \quad (1)$$

where θ_z is the solar zenith angle. Daily cumulative irradiance values for G_t , G_{DN} , G_{tS} , and G_d are obtained by numerical summation of point values, to give H_t , H_{DN} , H_{tS} , and H_d , each representing a measure of energy per square meter (J/m^2). Daily values are averaged for each calendar month in the study to yield monthly average daily irradiation per square meter. Monthly average daily irradiation is often quoted as an indicator of energy availability for renewable energy activities. As a southern hemisphere country, South Africa's daily global horizontal irradiation trends higher between November and March. The winter period between April and October is characterized by clearer skies, but lower solar radiation intensity. The selected Durban results obtained from STARlab are compared with HelioClim-3 database values and NASA SSE datasets using the mean bias error (MBE) and root mean square (RMSE) approach to quantify difference. The MBE and RMSE are defined as follows:

$$MBE = [\sum(H_{sat} - H_{meas})]/n \quad (2)$$

$$RMSE = \{[\sum(H_{sat} - H_{meas})^2]/n\}^{1/2} \quad (3)$$

where H_{sat} is the predicted monthly average daily irradiation value for Durban from either HelioClim dataset or the SSE, H_{meas} is the measured monthly value from STARlab and n is the number of calendar months. The MBE and RMSE percentage values are calculated using the measured annual averages for each irradiation component for Durban. It should be noted that MBE and RMSE represent differences between the measured and modeled values, and not fundamental measurement uncertainty of the instrumentation.

The results show a typical trend for the southern hemisphere. For the eastern coastal region around Durban, two broad seasons can be identified: summer from November through March and winter from April through October. The monthly average of the daily global irradiation on the horizontal surface for summer and winter periods recorded at STARlab for 2007 were $5.62 \text{ kWh}/\text{m}^2$ and $3.6 \text{ kWh}/\text{m}^2$ respectively with the annual average value of $4.45 \text{ kWh}/\text{m}^2$. The highest value of $6.39 \text{ kWh}/\text{m}^2$ was recorded in January while the lowest value of $2.81 \text{ kWh}/\text{m}^2$ was measured in June. Similarly, the monthly average daily direct normal irradiation for summer and winter periods were measured as $5.25 \text{ kWh}/\text{m}^2$ and $4.94 \text{ kWh}/\text{m}^2$ respectively, with the maximum value of $5.90 \text{ kWh}/\text{m}^2$ recorded in February. The values of irradiation measured on the 30° incline are higher than those on the horizontal from March through October. Between November and February, the values on the horizontal exceed those on the incline. For example, the monthly average daily of the global irradiation on the 30° incline for May, June and July was 5.48 , 4.30 and $4.89 \text{ kWh}/\text{m}^2$, with an annual average of $5.04 \text{ kWh}/\text{m}^2$. The corresponding values on the horizontal were 3.64 , 2.81 and $3.17 \text{ kWh}/\text{m}^2$ respectively. The annual averages of daily

global irradiation components recorded at STARlab are found to be in reasonably close agreement with values obtained from HelioClim-3 and the NASA SSE datasets. The MBE and RMSE statistics are given in Table 2 and Table 3.

Table 2. Mean bias error and root mean square error for recorded data versus HelioClim data (Durban, 2007)

Solar radiation component	MBE kWh/m ²	MBE %	RMSE kWh/m ²	RMSE %
H _t	0.6	13.4	0.7	15.1
H _{DN}	-0.4	-9.1	0.6	15.6
H _d	0.2	9.0	0.3	17.1

Table 3. Mean bias error and root mean square error for recorded data versus NASA SSE data (Durban, 2007)

Solar radiation component	MBE kWh/m ²	MBE %	RMSE kWh/m ²	RMSE %
H _t	0.3	5.6	0.6	12.5
H _{tS}	0.1	2.4	0.5	10.1

Solar energy availability is often characterized by the diffuse fraction which provides a useful statistical distribution of the global irradiation at a location [6,14]. The diffuse fraction is particularly helpful in evaluating performance of systems such as flat-plate collectors. The monthly average diffuse fraction K_d is the ratio of monthly average daily diffuse irradiation on a horizontal surface (H_d) to the monthly average daily global total irradiation on a horizontal surface (H_t), as given in equation (4) [14], where H_d and H_t are measured in (kJ/m²).

$$K_d = \frac{H_d}{H_t} \quad (4)$$

The ratio of monthly average daily diffuse to global irradiation is presented in Fig. 2. This shows the expected seasonal trend for the Durban coastal region, with the diffuse fraction decreasing over the dry winter season, then increasing towards the humid summer season.

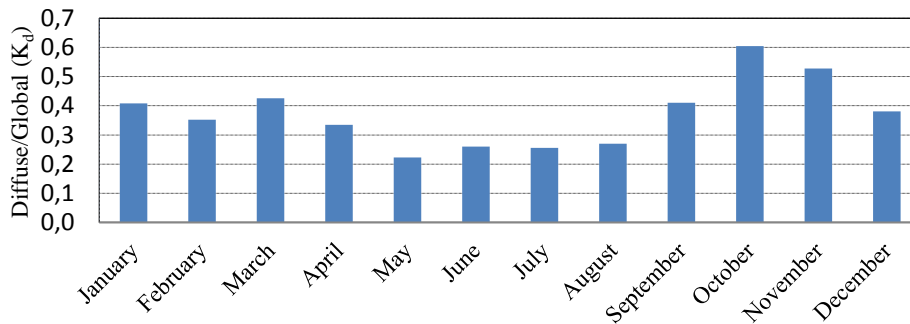


Fig. 2. Monthly average daily diffuse fraction values at STARlab

The measured annual average diffuse fraction for Durban in 2007 was 0.38. The annual cumulative values of solar energy measured in the year under consideration were 5881.85 MJ/m² for total global irradiance on a horizontal surface and 6592.09 MJ/m² for total global irradiance on a northward pointing 30° incline. The latter represents a 13% increase in energy availability, confirming the value of tilting flat-plate collectors in Durban at an angle equal to the latitude. For this assessment of solar resource potential it is useful to do a comparison with other areas around the world. Table 4 includes measured cumulative total global irradiation in the horizontal plane for 10 global cities, against which the Durban results are compared. It should be noted that not all values in Table 4 for other locations were obtained in 2007. The comparison is nevertheless indicative of Durban's relative solar potential. Arizona's desert is often considered as a benchmark when evaluating a location's solar resource and offers some of the highest solar potential in the world. Although this location has a significantly higher resource compared with Durban, the South African city exhibits similar solar energy potential to Sanary in France, Singapore and Miami (USA). Results suggest that Durban's solar potential is considerably higher than those of Seattle and Coeur d'Alene (USA), as well as Melbourne, Australia.

Table 4. Comparison of Durban measured annual total global irradiation in the horizontal plane with selected other locations

Location	Latitude	Reference	Year	Annual totals [MJ/m ²]	Relative solar resource
<i>Durban, South Africa</i>	29°58'S	STARlab data	2007	5881.9	100%
Coeur d'Alene, Idaho	47°72'N	[15]	1982-86	4485.6	76%
Eugene, Oregon	44°05'N	[15]	1975-97	4791.6	81%
Hermiston, Oregon	45°82'N	[15]	1979-97	5396.4	92%
Ely, Nevada	39°15'N	[16]	1961-90	6462.0	110%
Phoenix, Arizona	33°32'N	[16]	1961-90	7545.6	128%
Seattle, Washington	47°68'N	[16]	1961-90	4392.0	75%
Miami, Florida	25°34'N	[17]	2007	6242.0	104%
Sanary, France	43°08'N	[17]	2007	5996.1	104%
Singapore	01°22'N	[17]	2007	6030.0	103%
Melbourne, Australia	37°49'S	[17]	2007	5385.0	93%

3.2. Meteorological parameters

The meteorological parameters recorded and analyzed in this study were temperature, humidity, wind speed and direction as well as rainfall. Data were collected at 30 minute intervals over each 24 hour daily period. Fig. 3 shows the maximum, minimum and average daily ambient air temperature while Fig. 4 shows maximum, minimum and average daily humidity throughout the year under study. Durban has a subtropical climate with hot and humid summer and mild winter. Maximum monthly average daily temperatures of 24.0 °C, 24.9 °C and 23.4 °C were recorded in January, February and March respectively. The lowest monthly average daily temperatures were recorded in June and July at 18.5 °C and 18.2 °C respectively. Humidity remains high for most of the year due to the influence of the warm Mozambique current flowing along KwaZulu-Natal's coast. The annual average monthly daily humidity recorded is 74.9%. Total rainfall recorded for

the year was 972 mm with a maximum value of 231.2 mm recorded in November and minimum of 1.4 mm measured in May.

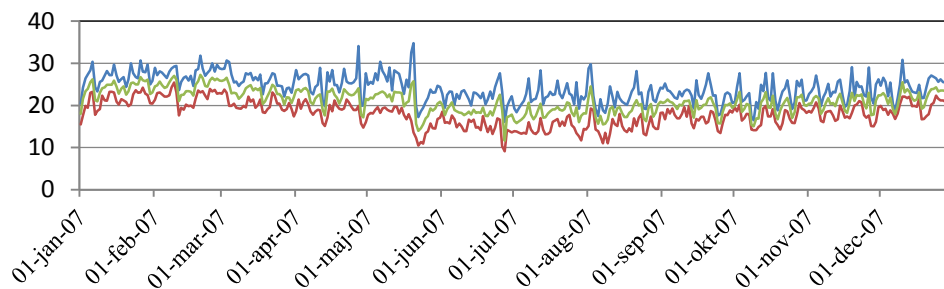


Fig. 3. Durban's daily average, minimum and maximum temperatures throughout the year

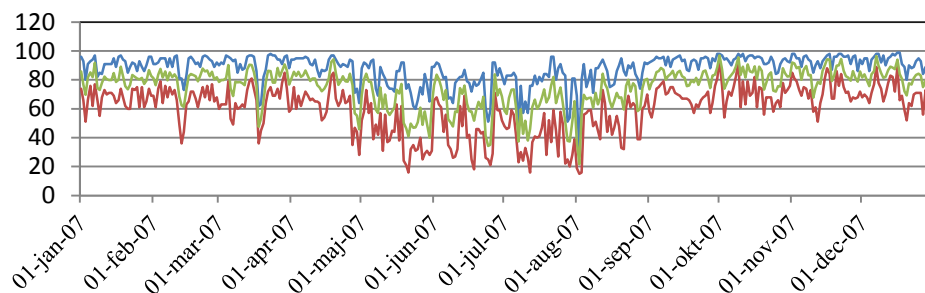


Fig. 4. Durban's daily average, minimum and maximum relative humidity throughout the year

4. Conclusions

With a population density exceeding the national average, the east coast of South Africa around the city of Durban offers good potential for reducing demand on the electricity grid by switching to sustainable technologies like domestic solar water heaters and energy-efficient architecture. For urban planners, engineers and equipment suppliers there is a growing need for reliable solar radiation data on which to base technical and economic projections. In this study we show that two satellite-based software tools, HelioClim and NASA SSE offer reasonable estimates of the solar resource and each might be considered a good 'first step' for estimating available energy. For 2007, mean bias differences in the satellite-based data versus measured values for annual average daily global irradiation were 13.4% for HelioClim and 5.6% for SSE. Random mean square differences were 15.1% and 12.5% respectively, suggesting that the SSE database is slightly more accurate. The HelioClim database tended to underestimate direct normal irradiation by 9.1% with random mean square difference of 15.6%. SSE is also able to predict annual irradiation on a tilted surface. The bias and random errors for the NASA database versus measured readings from a sloping pyranometer at 30° latitude tilt were 2.4% and 10.1% respectively. The measured annual average of daily global horizontal irradiance for 2007 was 4.45 kW/m² while the annual cumulative value was 5881.85 MJ/m². Overall, the solar resource for Durban is comparable to that of Singapore and Miami, marginally better than Melbourne's and about 28% weaker than that of Phoenix, Arizona. We anticipate expanding measurement activities to cover more of South Africa's eastern seaboard, via the recently established

GRADRAD network. These efforts are intended to aid radiometric research and reduce South Africa's dependence on fossil fuels for power generation.

Acknowledgements

The authors thank Dr. A. Mienie of Mangosuthu University of Technology and the University of Stellenbosch's Centre for Renewable and Sustainable Energy Studies for their assistance.

References:

- [1] <http://www.dme.gov.za/energy> [accessed 5 October 2010]
- [2] Whitepaper on Renewable Energy, Department of Minerals and Energy of South Africa, November 2003, <http://unfccc.int/files> [accessed 5 October 2010]
- [3] <http://www.eskom.co.za> [accessed 5 October 2010]
- [4] Munzhedi, R., Sebitosi, A.B., Redrawing the solar map of South Africa for photovoltaic applications, *Renewable Energy* 34: 165-169, 2009
- [5] Fluri, T.P., The potential of concentrating solar power in South Africa, *Energy Policy* 37: 5075-5080, 2009
- [6] Lysko, M., Measurement and Models of Solar Irradiance. Norwegian University of Science and Technology, PhD Thesis, 2006
- [7] <http://www.weathersa.co.za>, South African Weather Service
- [8] Lefevre, M., Wald, L., Diabate, L., Using reduced data sets ISCCP-B2 from the Meteosat satellites to assess surface solar irradiance, *Solar Energy* 81: 240-253, 2007
- [9] Blanco-Muriel, M., Alarcon-Padilla, D.C., Lopez-Moratalla, T., Lara-Coira, M., Computing the solar vector, *Solar Energy* 70: 432-441, 2001
- [10] Muzathik, A.M., Wan Nik, W.N.M., Samo, K., Ibrahim, M.Z., Reference Solar Radiation Year and Some Climatology Aspects of East Coast of West Malaysia, *American J. of Engineering and Applied Sciences*, 3 (2): 293-299, 2010
- [11] <http://www.sodais.com/> [accessed 1 November 2010]
- [12] <http://eosweb.larc.nasa.gov/sse> [accessed 2 September 2010]
- [13] Cros, S., Albuisson, M., Lefevre, M., Rigollier, C., Wald, L., HelioClim: a long-term database on solar radiation for Europe and Africa, *Proceedings of Eurosun 2004*, published by PSE GmbH, Freiburg, Germany, pp. (3) 916-920, 2004
- [14] Iqbal, M., *An Introduction to Solar Radiation*, Academic, Toronto, 1983
- [15] <http://solardat.uoregon.edu/> [accessed 1 November 2010]
- [16] http://rredc.nrel.gov/solar/old_data/nsrdb/ [accessed 1 November 2010]
- [17] <http://www.atlaswsg.com> [accessed 1 November 2010]

Investigation of Solar Collector systems use in Latvia

P. Shipkovs^{1,*}, K. Lebedeva¹, G. Kashkarova¹, L. Migla², M. Pankars²

¹ Institute of Physical Energetic, Energy Resources Laboratory, Riga, Latvia

² Riga Technical University, Riga, Latvia

* Corresponding author: Tel: +371 67553537, Fax: +371 67553537, shipkovs@edi.lv

Abstract: Solar energy is the biggest energy resource on the earth. Latvia environment is very potential for solar usage, but there are many reasons why consumers have skepticism and a perception that the environment in this region is not suitable for solar energy usage.

To have broken this stereotype, this study is conducted. The aim of this program is to explore the suitability of Latvian environment with the use of solar collector. For the attainment of objective monotype house will be modeled, the house will be equipped with the combined solar heat system, which will be placed in different regions. There are various amounts of sunny days in different regions, as well as diverse average temperature, wherewith the amount of heat differs. For the modeling of building, modeling program model of solar collectors will be used, which is provided for several solar heat systems, inter alias for the calculation of combined solar heat supply system and for the solving of several relevant tasks. Program is simulation program for the thermal solar energy systems. It suits both for determination of hot water use and heating system use.

There are countries which are located in sunny regions and which history of solar energy usage is very longstanding, wherewith also technological achievements are high. Yet our contemporary rapid technology development enables to use ever more solar energy in the regions which are not so rich with the solar radiance, for example in Latvia. Interest about the usage of solar energy in Latvia increase – partly it is explicable to unpredictable and essential price rise of fossil firing resources and partly to the desire to invest in technologies which could reduce this rise in price in the future.

Keywords: Modeling, Simulation, Solar Energy, Renewable Sources, Combined systems

1. Introduction

During last few years significance of environmental problems increase. Wherewith, activation of environmental problems increases humans' interest about different environmentally friendly technologies. One of the biggest air polluters are fallouts resulted from burning of fossil firing. That is why urgent becomes utilizations of renewable resources for the energy obtaining, which are less nocuous to environment. Latvia's total final energy consumption is secured from local energy resources and the flow of primary resources from Russia, the CIS countries, the Baltic countries, EU and other countries. Currently, three types of energy resource making up approximately equal proportions dominate in the delivery of Latvia's primary resources – oil products, natural gas and wood-fuel. Like many other European Union countries, Latvia is dependent on imports of primary resources. The share of RES has traditionally been significant in Latvia's energy supply and in 2008 it comprised 29.9% of the total final energy consumption. Interest about the usage of solar energy in Latvia increase – partly it is explicable to unpredictable and essential price rise of fossil firing resources and partly to the desire to invest in technologies which could reduce this rise in price in the future. That is the reason why is it necessary to investigate solar energy potential in Latvian conditions.

Global radiance consists of direct and diffused radiance. Direct radiance is connected with the direction of sunbeams. Diffused radiance develops when molecule and particles in atmosphere disperse sunbeams in all directions. The duration and intensity of solar radiance depends on season, climatic conditions and geographical location. Global radiance of the earth on the horizontal area in the regions of solar zone may reach 2200 kWh/m². Maximal volume of solar radiance in North Europe is 1100 kWh/m². We can conclude that even in such

small country as Latvia are several different solar sliding duration zones. In the zone along the Baltic Sea is the longest solar sliding duration – more than 1900 hours, in its turn in Vidzeme heights it is the least – less than 1700 hours. Volume of Solar radiance is the main factor of solar energy usage in Latvia. [2]

2. Methodology

In order to define, how great volume of heat from building total use of the heat is possible to secure using solar heat energy, the model of the building will be created using modeling program. With the help of this program it is possible to carry out research, the modeling, the calculation of heat supply solar systems. Simulation of all type heating supply solar system is based on independent meteorological data. Time step of simulation is possible starting with one second even until one hour, it depends on situation, in its turn, there are a lot of versions of model simulation time periods – starting from one day until several years. The calculation basis in program has been integrated from subprogram Meteonorm. Using preferences of simulation program have been cleared up most effective location for solar collector in Latvian conditions. Comparatively, effective solar radiation may catch solar collector that is placed 55° anent to horizon or slope and 0° anent to the South or orientation and which has clean horizon, nothing puts a slur and otherwise do not affect the activity of collector, that is why received amount of solar heat takes as average from all models that are placed in corresponding place and location. However first of all foreseeable tables has been made. Data about the volume of receivable heat from 1 m² solar collector that depends from location, to be more precise in what angle as to the ground it has been put and in what orientation as to the South solar collector will catch the greatest volume of heat, has been put in the table.

Table 1. Percipient heat volume from 1 m² of solar collector in Riga dependence of location, kWh/m².

Orient. \slope	0°	15°	30°	45°	55°	60°	75°	90°
0°	259	325	382	417	426	425	401	348
15°	259	320	376	412	422	423	406	359
30°	259	325	380	412	417	414	385	324
45°	259	310	362	396	407	408	395	357
60°	259	322	370	396	397	393	358	294
75°	259	297	341	370	380	381	370	335
90°	259	314	355	373	369	363	325	262

Such location is the most effective and in the table 1 there are the same data, then we can conclude that program is comparatively precise for the calculation in the Latvia conditions. The least received heat volume is when the solar collector is located 0° anent to the Earth horizon. This location is the most inappropriate for the detection of solar radiance. To 0° anent to horizon at any orientation, the volume of received heat is constant, because ray angle falling form the Sun anent to the area is constant at any orientation of solar collector. In the Table 1 it is clearly seen how volume of received heat change and its changes are twice as much bigger. Therefore the precise setting up of solar collector has significant meaning. Although this calculation was done only for one type collectors, though the calculation corresponds to previously defined, we can conclude that in wholesale it is similar to all collectors.

The collector efficiency mainly depends on the difference between the mean collector temperature and the ambient temperature $T_m - T_a$. If this difference is high then the heat radiation and the convection losses are high. At small temperature differences the efficiency can reach 90%. If the mean collector temperature drops below ambient temperature because of a cold heat transfer medium then the efficiency can exceed even 100%. In this case the heat transfer medium is not only heated by the sun, it's also heated by the ambient air. [1] The efficiency is described by the efficiency curve. The temperature difference ($T_m - T_a$) divided by the irradiation normal to the collector (G_k) is the variable (x).

$$x = \frac{T_m - T_a}{G_k} \quad (1.)$$

Following a typical efficiency curve of a regular glazed flat collector:

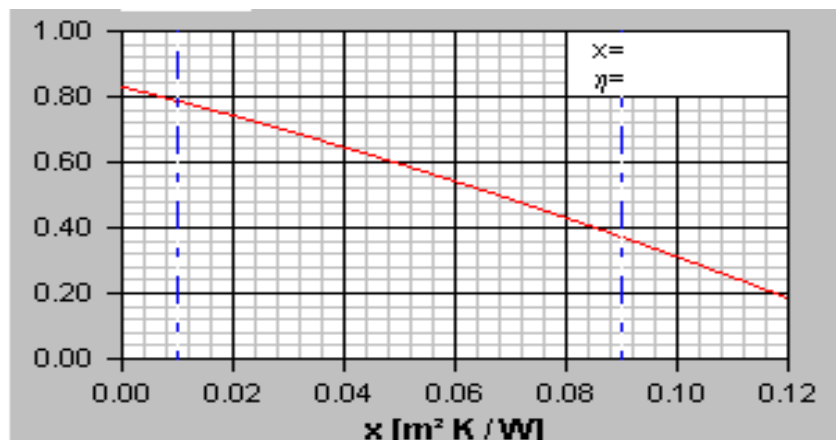


Fig. 1. Efficiency curve of a glazed flat collector.

The higher the mean collector temperature lowers the efficiency. The irradiation is $800 \text{ W} \cdot \text{m}^{-2}$. This curve is described by a 2nd order Polynom with sufficient accuracy. This Polynom is clearly defined by three parameters, c_0, c_1, c_2 (or a_0, a_1, a_2 ; values measured under wind speed of $2-4 \text{ m} \cdot \text{s}^{-1}$):

$$\eta = c_0 - c_1 x - c_2 G_k x^2 \quad (2.)$$

where η – efficiency of collector; c_0, c_1, c_2 – coefficient of polynomial set in model; G_k – tightness of solar radiation, that falls athwart to the surface of collector,

The efficiency value amounts to c_0 , if the mean collector temperature and the ambient temperature are equal. This value should be high. c_1 and c_2 describe a combination of different loss factors. These values are low if a collector is well insulated. It is worth to mention that such polynomial is used in modeling program for the calculation of efficiency. [1]

3. Results

Since program isn't potted to the conditions of Latvia, there isn't meteorological data, which are necessary for activity simulating of the combined heat supply of solar system in the Latvian conditions in its data basis. Since this program contains meteorological data from all world, in order to get this necessary information, accurate coordinates from different towns of Latvia, which are located in different zones of sun shining: Riga, Liepaja, Daugavpils has been entered. For the more visible efficiency determination of heat supply solar system, also

coordinates of typical sunny south city Bremen (Germany) and cool northern city Boden (Sweden). Wherewith, computer models will be created for different climatic zones and conditions in the European Union countries.

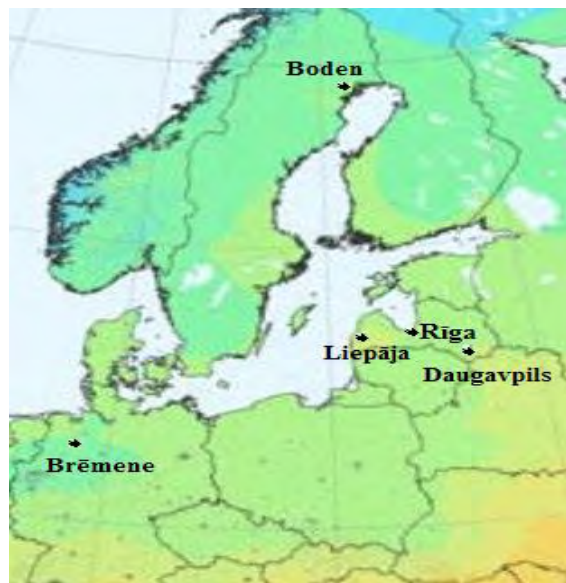


Fig. 2. Locations of cities that are used for modeling

Those data of communities that are used for the modeling of combined solar heat supply system are shown in table 2.

Table 2. Meteorological data for Meteororm

Place of location	Latitude	Degrees of longitude	Elevation above sea level, m
Riga, Latvia	56,88°	24,13°	14
Liepāja, Latvia	56,49°	21,02°	1
Daugavpils, Latvia	55,87°	26,52°	105
Boden, Sweden	72,80°	12,58°	121
Bremen, Germany	65,78°	21,67°	31

Initially model one family building with the floor space 150 m², 4 persons will live in that building. Heat loss through demarcation constructions of building (external walls, roof, windows etc.) makes essential part form total use of heat energy. Power efficiency of demarcation constructions is able to evaluate when thermal coefficient of given construction is U (W/m²·K). Because in Latvia there is relatively cool climatic conditions, than building must be well isolated with heavy constructions. Walls are made from bricks and from outside they have 0.2 m heavy insulation. Air exchange 0.6 l/h, and radiant 400W. Require heating capacity 6.1 kW at -8°C. Looking closely at balance sheet of used and acquired heat of each place we can conclude that in all chosen places development of heat use during year is similar, only volume of heat differs.

Table 3. Heat energy consumption for space heating depending from location, kWh/m² per year.

Place of location	Common use of heat energy for room heating (kWh per year)	Use of heat energy for room heating on 1 m ² (kWh/m ² per year)
Riga, Latvia	12 650	85
Liepaja, Latvia	12 500	80
Daugavpils, Latvia	13 615	92
Bremen, Germany	9 652	65
Boden, Sweden	27 342	182

In warmer climatic zone use of thermal energy reduces. Because Bremen is located closer to equator and its average temperature is superlative for all viewed cities, for that reason required volume of thermal energy is the least. Yet looking closely at Boden, which is located close to the North, it is contrary. Distinction among Riga, Liepaja and Daugavpils brings about location of those towns' towards the sea. Temperature at the sea in winter is warmer wherewith volume of thermal energy for room heating is different, yet towns are located relatively close to each other, wherewith volume of thermal energy is not very different. As in the building lives 4 persons and it is known that on one person provides 2 m² solar collectors, than for the building model use 8 m² flat area collectors. Previously we found out that solar collector works most effective when its slope angle is 55° anent to horizon and 0° anent to the South. We estimate position along vertical of solar collector modules. Wherewith, we can define thermal conductivity and thermal capacity of pipes, as well as the stream speed in pipes. Pump and system described values are calculated automatic after input of necessary data. In this case inputted values are the following: flow of pump, flow speed of their process 120 l·h⁻¹ and back process 0,06 m ·s⁻¹. Also one more important parameter of efficiency determination of combined solar heat supply system is heat carrier data of used solar collector. Usually water is used like heat carrier, due to its availability, low price and suitable physical qualities. In combined heat supply solar systems, water can be used only in the inner supply of heat and water. For the very reason in Latvia conditions pipes are excluded as heat carrier in exterior contour. Therefore glycol solutions must be chosen as the heat carrier in pretence model. Necessary volume of heat for the preparation of hot water in all climatic conditions is nearly identical 4069 kWh in a year. In some places suspended volume of solar heat is different.

Table 5. Perceptive solar heat volume, kWh/in a year.

Place of location	Common use of heat energy for room heating (kWh per year)	Use of heat energy for room heating on 1 m ² (kWh·m ⁻² per year)
Riga, Latvia	3 200	400
Liepaja, Latvia	3 345	418
Daugavpils, Latvia	3165	395
Bremen, Germany	2930	366
Boden, Sweden	2890	360

It is not possible to unequivocal assert that solar collectors works more effective closer to the South and to the North they do not work effective. The most effective works solar collector that is located in Riga and not the solar collector in Bremen that is closer to the South. It is explained by the less requirement of system for heating, because during the year in all models the volume of warm water for the preparation of hot water and containers heat loss is equal. In a period when heating is necessary but available volume of solar heat

energy is sufficient not only for the preparation of hot water but also for the room heating, combined solar system has been used valuable. In the Northern models such periods are longer, wherewith the volume of used solar energy is greater. Riga’s model in comparison with Bremen model volume of used solar energy is greater, because the air temperature in Bremen at the beginning and at the end of the year is a bit lower, but available solar heat is greater, wherewith the volume of used solar thermal energy increase. In all versions the volume of produced heat in auxiliary boiler is greater than necessary for the building. It is explained by the extra load of auxiliary boiler for the production of hot water. Because several simulations with different combinations has been carried out with different capacity auxiliary boilers and electricity, then average result has been accepted as the volume of produced heat of auxiliary boiler.

Table 6. Heat volume from auxiliary boiler, kWh/year.

Place of location	Heat volume from auxiliary boiler (kWh in a year)
Riga	15 400
Liepaja	14 800
Daugavpils	16 080
Boden	11980
Bremen	27120

In existing versions of auxiliary boilers more to the North, the volume of produced heat increase on the count of necessary volume of the heat for the production of hot water. At the beginning of colder season auxiliary boiler has been started later, because sufficient volume of the heat is stocked up in the container, which ensures room heating and preparation of hot water for the short period. In that way heat has been stocked up for the later use, which is one of the formation preconditions of the combined heat supply solar system. It is not important to evaluate the productivity of solar collector but the relations of produced capacity in the power balance of the building. As models of Riga, Daugavpils and Liepajas is relatively similar and let the chart is more obvious only Riga, Bremen and Boden will be compared.

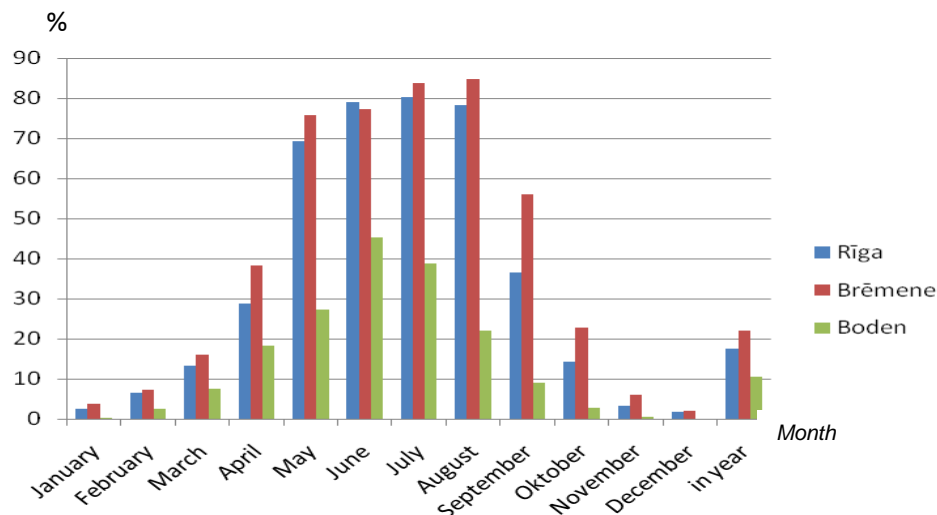


Fig.3. Percentage of produced heat from solar collector, %

Solar collectors may cover the necessary volume of heat during the summer month. Capacity of heat is not necessary for the room heating during the summer month, capacity of heat is necessary only for the preparation of hot water. It is important that solar collectors of Riga’s

model produce practically the same volume of heat energy from building heat balance as it is in Bremen. To be more precise solar collectors in Riga's model produce more heat energy than Bremen model but heat loss of building is greater in Riga. The decrease of heat volume necessary for room heating reflects not only in the volume of used heat but also partly in not received volume of solar heat. In its turn, the volume of solar heat that is used in the preparation of hot water is growing, because the volume of solar heat is available. For that reason the bigger part of the solar heat energy is observed in used volume of heat. Important conclusion in that during the winter month volume of received heat is minimal and very similar to all viewed models. Consequently during those months combined solar heat supply system has reduction of usefulness. Probable it is worth to consider on solar collector unlock during the cooler season, in such a way raising its usefulness. Though already in early spring solar collectors may provide 30% from the use of building heat for the room heating and hot water. The volume of suspended solar heat do not show real possible volume of solar heat energy that may be used, because conveying of solar heat energy to the storing container happens during almost all light period of day, only disconnecting circulation pumps of model in short periods.

The Developed models were viewed on the other side. Heat exchanger effect on System efficiency was determinate. The system affects the handling characteristics, such as heat exchangers. They fulfill the important function as a heat-transfer. The resulting solar collector heat storage tank is given by the mixing of heat already is there or whether the fluid is more effective when the heat from the solar collector storage tank into the system through a heat exchanger. The heat storage tank heat loss is smallest when the system has been equipped with heat exchanger for Domestic hot water. Previously was found how to place the solar collectors to receive the maximum amount of solar radiation.

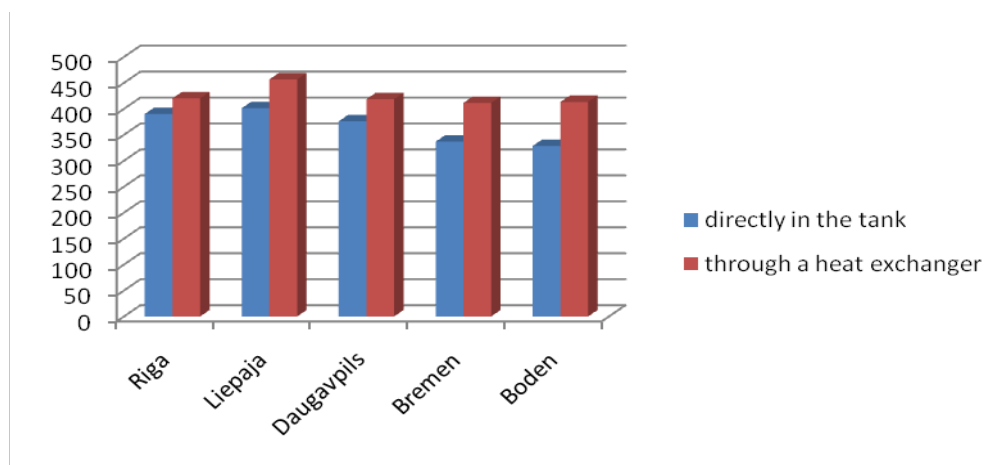


Fig. 4. Heat quantity W/m^2 depending of heat transforms type in system

The heat transfer from the solar collector system to the heat storage tank through a heat exchanger is about 14% efficiently than in cases where heat transfer occurs mixing of solar collector fluid transforms the heat in the tank. This is explained by the fact that the liquid flowing through the heat exchanger is less than the local losses. As well as more efficient heat exchange takes place.

4. Conclusions

The activity of the system depends on the weather conditions of particular place, which have an impact of the geographical fix, available volume of solar heat. It depends also on the individualities of particular place: the hills, the sea, the wind direction etc. In addition, the

great importance has the users of combined solar heat supply system, their way of life. Wherewith, comparing of simulation models located in different places is conventional.

The greatest volume of perceived solar heat in Riga is in the situation when solar collector is placed 55° against horizon and 0° orientation against the South

The combined solar heating system provides for constant domestic hot water and seasonally variable space heating demand ensuring in annual terms. As well as changing hot water and constant heating demand ensuring in daily. Combined solar heating system operation depends on various technical specifications and performance characteristics of system components, such as the installed area of solar collectors, size of thermal storage tank, heat conductivity, as well as other parameters of system. During the winter months such a system is not useful, but it pays off in the summer months, producing enough heat for domestic hot water and pre warming for space heating. Effect on system's efficiency gives availability and location of heat exchanger. The heat transfer from the solar collector system to the heat storage tank through a heat exchanger is about 14% efficiently than in cases where heat transfer occurs mixing of solar collector fluid transforms the heat in the tank.

Difference between accumulated solar collector's heat of the Latvian, Sweden (Boden) and Germany (Bremen) models are not significant. But Consumed heat for space heating and domestic hot water is drastically different. Hence contribution varies of solar thermal system in consumer balance sheets. As the building model of Boden has the highest heat consumption, than solar collector contribution in balance sheet are relative the smallest.

References

- [1] Polysun 3.3. Documentation 2003. Solar Energy Laboratory SPF;
- [2] P. Shipkovs, *Atjaunojamo energoresursu izmantošana Latvijas apstākļos*, RTU, Rīga, P. 2007, pp. 67;

New Method for Predicting the Performance of Solar Pond in any Sunny Part of the World

Adel O. Sharif*, Hazim Al-Hussaini, Ibrahim A. Alenezi

Centre for Osmosis Research & Applications, Chemical & Process Engineering Department, Faculty of Engineering & Physical Sciences, Surrey University, UK.

* Corresponding author: Tel: +44(0)1483 686584; F: +44(0)1483 686584; email: a.sharif@surrey.ac.uk

Abstract: The solar pond is considered one of the most reliable and economic solar systems. The collecting and storing of the solar energy is in one system, so the heat in summer can be utilised in winter in the same system. To predict the potential of solar pond at any part of the world a mathematical model is established to calculate the parameters affecting the performance of the solar pond through a computer programme. The solar radiation input to the pond is calculated using the daily monthly average method. One dimensional steady state and transient assumptions in the gradient zone are used to predict the effect of any parameter on the solar pond performance. The results show excellent agreement with the experimental data under the steady state assumption. Many parameters affecting the performance of the solar pond such as shading effect, depths of the upper, gradient and storage zones, ground temperature and covered insulation for different climates and different latitudes have been studied. The results show that the solar pond has high potential even for colder climates such as that of the UK, where the heat could be used for a number of applications including domestic and industrial.

Keywords: Solar Pond, Solar Energy, Modelling

Nomenclature

N	the number of the day in the year	T	temperature.. °C
φ	latitude of the location.....degree	Q_{sru}	absorbed heat of solar radiation in the upper zone..... $W.m^{-2}$
θ	the Incident angle degree	Q_{uw}	heat loss from the sides in the upper zone..... $W.m^{-2}$
I_{sc}	Solar constant $W.m^{-2}$	Q_{ub}	heat gained from the bottom in the upper zone..... $W.m^{-2}$
I_o	the average daily extraterrestrial solar irradiance $W.m^{-2}$	Q_{uc}	heat loss by convection in the upper zone..... $W.m^{-2}$
δ	the declination angle degree	Q_{ur}	heat loss by radiation in the upper zone..... $W.m^{-2}$
ω_s	hour angle degree	Q_{ue}	heat loss by evaporation in the upper zone..... $W.m^{-2}$
I_{od}	is daily total direct normal extraterrestrial radiation..... $W.m^{-2}$	Q_{srs}	absorbed heat of solar radiation in the storage zone..... $W.m^{-2}$
IBF	the fraction of the extraterrestrial radiation	Q_{sw}	heat loss from the sides in the storage zone..... $W.m^{-2}$
F_c	the monthly correction factor	Q_{sb}	heat loss from the bottom in the storage zone..... $W.m^{-2}$
\bar{H}_T	the monthly daily- average total irradiation on a horizontal surface $W.m^{-2}$	Q_{st}	heat loss from the top in the storage zone..... $W.m^{-2}$
H_{oT}	the total extraterrestrial radiation on a horizontal surface $W.m^{-2}$	Q_{se}	heat loss by heat extraction in the storage zone..... $W.m^{-2}$
ρ	water density..... $kg.m^{-3}$		
C_p	specific heat $J.kg^{-1}.^{\circ}C^{-1}$		
A	Area m^2		
x	the depthm		

1. Introduction

Natural water temperature gradients was observed and reported first time by Kalecsinsky in the Medve Lake in Transylvania in 1902 [1,2]. This observation suggested the possibility of constructing and using the ponds as solar energy collectors and storage areas. Tabor (1964), Weinberger (1964), and Tabor and Matz (1965) reported a series of theoretical and experimental studies of these salt gradient ponds [3].

The solar pond is one of the simplest methods that can directly collect and convert solar energy to thermal power. Moreover, it is a solar power collector and a thermal storage unit at the same time. All Ponds convert solar radiation to heat although most of them lose that heat as a result of convection and evaporation. In nature when the sun's rays fall on the lake or the pond, the temperature of water increases gradually towards the bottom of the pond. Therefore, the water in the bottom becomes warmer then it rises to the surface and loses its heat to the atmosphere, a phenomenon called convection. However, the solar pond technology inhibits this phenomenon by dissolving salt into the bottom layer of this pond, making the fluid too heavy to rise to the surface, even when being hot. This idea can increase the temperature of the bottom layer up to more than 100 oC [4]. Once a high temperature is obtained, the bottom layer can be used as a heat source to provide continuous heat through a heat exchanger at any time. The solar pond principle is to prevent vertical convection and/or evaporation according to the type of the solar ponds [5].

A typical salinity-gradient solar pond consists of three main zones as shown in Fig. 1:

- The Upper Convecting Zone (UCZ) which has the least cost, salinity, temperature, and is close to ambient temperature. The thickness of this zone is typically 0.3 m and it should be kept as thin as possible. The cost of constructing the UCZ is usually reasonable.
- The Non-Convecting Zone (NCZ) which is located between the upper and the lower zones of the pond. Since the temperature and salinity increase with depth, this layer is not homogeneous. If the salinity gradient is large enough, the NCZ inhibits a convection phenomenon even when the lower zone is hotter.
- The Lower Convecting Zone (LCZ), which is a homogenous layer and has a relatively high salinity and high temperature. Heat is stored in this zone and can be exchanged in or out of the pond. As the LCZ's depth increases, the heat capacity increases and the temperature variation decreases.

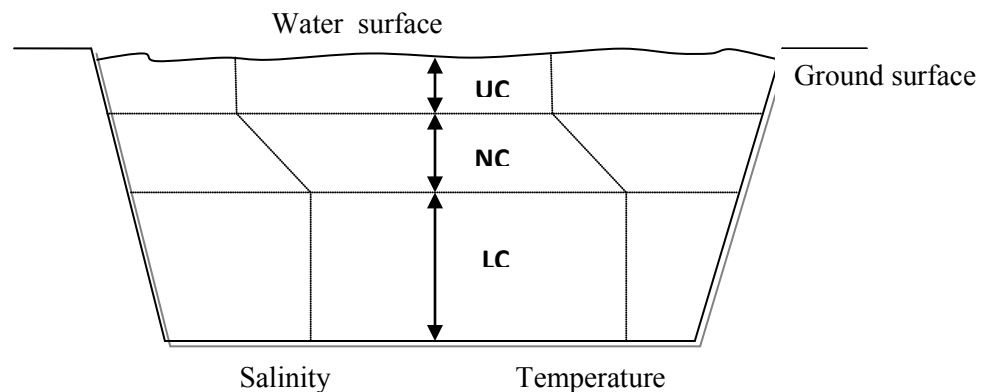


Fig. 1. Salinity and temperature profiles through the salinity gradient solar pond zones.

Non-convective solar ponds can provide heat for domestic, agricultural, industrial, power generation and desalination purposes. More details about solar pond construction and limitation can be obtained from [1], [2] and [4].

2. Methodology

Solar irradiation data have been widely measured and recorded for almost every region in each country in the world for many years. Nevertheless, the predictions and calculations of the irradiation are sometimes required to obtain a good approximation of the irradiation.

According to a solar pond location, the sun path in the sky is changed seasonally thus the sun's altitude and azimuth angle and the daily sunshine period are varied and cause a great effect on the amount of the incident solar radiation and then on the performance of the solar collector.

It is found that monthly averaged data are the most effective for representing the climate changes and calculations, since hourly and daily calculations and measurements are changed from year to another and are quite short to represent a general impression about the climate. In addition to this, seasonal and yearly readings cannot accurately represent the climate computations. Thus, averaged monthly measurements or computations have been adapted in this study.

Matlab computer software has been used to build a multi-scripts programme to solve ordinary differential equations by finite difference method for steady state models. This programme takes into account the changes of boundary conditions and surround factors with time.

This solar radiation computation program requires only a latitude value to predict sunrise, sunset and sunshine period to compute the solar radiation equations. A new predicted empirical equation has been added to this script to give a good agreement and it has been tested for three different locations in the middle east which are Kuwait, Riyadh and Jerusalem. The incident solar radiation values, based on monthly average daily amounts can be obtained from the available references or the 22 years average values which are recorded in NASA website [6].

Since the earth-sun distance varies each season, the apparent extraterrestrial solar irradiation changes during the year. Therefore, the solar irradiation intensity depends on the number of the day in the year. The average daily extraterrestrial solar irradiance is given by

$$I_o = I_{sc} \left[1 + 0.0033 \cos \left(\frac{360N}{370} \right) \right] \quad (1)$$

Solar constant (I_{sc}) value has been measured by many researchers since the beginning of the 20th century. Abbot [7] and his team in Smithsonian Institute after many research proposed the value of 1353 W/m^2 to be the value of the solar constant. Many further investigations were made on ground-base and high altitude measurements and eventually 1353 W/m^2 has been accepted to be the standard for the solar constant. NASA, after many measurements on the space, has recommended this value as well [8]. It has very recently been published in NASA's

website that the generally accepted value of the solar constant is 1368 W/m^2 as a satellite measured yearly average, which is close to the standard value.

The total daily extraterrestrial radiation on a horizontal surface can be computed by

$$H_{oT} = \frac{I_{od}}{\pi} \left[\cos \theta \cos \delta \sin \omega_s + \frac{2\pi\omega_s}{360} \sin \varphi \sin \delta \right] \quad (2)$$

Where I_{od} is daily total direct normal extraterrestrial radiation and can be obtained by yielding the value of extraterrestrial radiation solar irradiation throughout the day as the following

$$I_{od} = 24I_o \quad (3)$$

To use these equations for computation of the monthly daily-average total extraterrestrial radiation on a horizontal surface \bar{H}_{oT} , the month representative-day is needed and given by lunde[9] in addition to other useful equations in solar radiation calculations. The new empirical equation which works with available solar radiation equations to estimate the solar radiation based on a single input parameter is

$$IBF = \frac{1.5\varphi - 14.25}{\varphi} Fc \quad (4)$$

Where Fc is a predicted monthly correction factor validated accurately for the Middle East with NASA published data and the above equation can be utilized in the following formula;

$$\bar{H}_T = IBF(\bar{H}_{oT}) \quad (5)$$

Eq(5) is a well known formula in the solar radiation equations which are expansively explained in [9] based on the cloudiness (or clearness) index, however, the index here is substituted by the predicted factor ,IBF, which is obtained by linking the field solar radiation data with longitudes in a special computer programme.

The steady state model for a solar pond has been widely adopted by the most famous researchers in the SGSP field such as Weinberger [10], Rabl and Nielsen [11], Kooi [12], Ali [13], Wang and Akbarzadeh [14] and many of other researchers. A downward one-dimensional flux model is often used for simplification purposes. The convective zones (upper and storage layers) are assumed to be well thermally mixed i.e. lumped systems. The upper layer steady state equation is:

$$\rho_u C_{pu} A x_u \frac{dT_u}{dt} = Q_{sru} + Q_{ub} - Q_{uc} - Q_{ur} - Q_{ue} \quad (6)$$

The gradient layer is considered as a conduction slab and all absorbed solar radiation is consumed in building and maintaining the temperature profile in this layer. The storage zone steady state correlation will be

$$\rho_s C_{ps} A x_s \frac{dT_s}{dt} = Q_{srs} - Q_{st} - Q_{sb} - Q_{sw} - Q_{se} \quad (7)$$

More details about each parameter in Eq(6) and Eq(7) are given by Lunde[9], Rable and Nielson[11] and Ali[13]. Model validation is possibly the most essential step in the model building stages. In this study, the model validation is applied to Ali's study in Kuwait [13].

3. Results

The single input program is used to calculate the solar radiation in Kuwait, Riyadh and Jerusalem. The output of this script is compared with NASA average 22 year measurements data and the results are really good and shown in Fig. 2 for Kuwait, Fig. 3 for Riyadh and Fig. 4 for Jerusalem solar radiations.

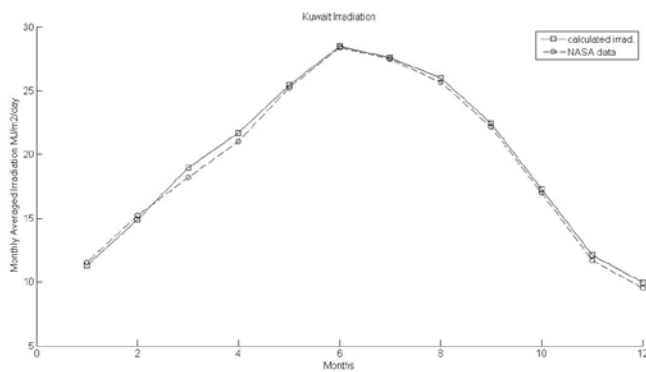


Fig. 2. NASA data and calculated solar irradiation for Kuwait.

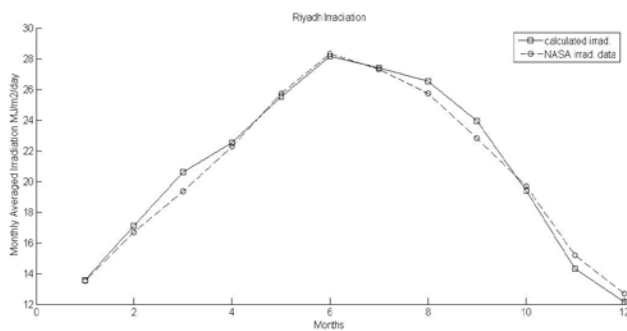


Fig. 3. NASA data and calculated solar irradiation for Saudi Arabia, Riyadh.

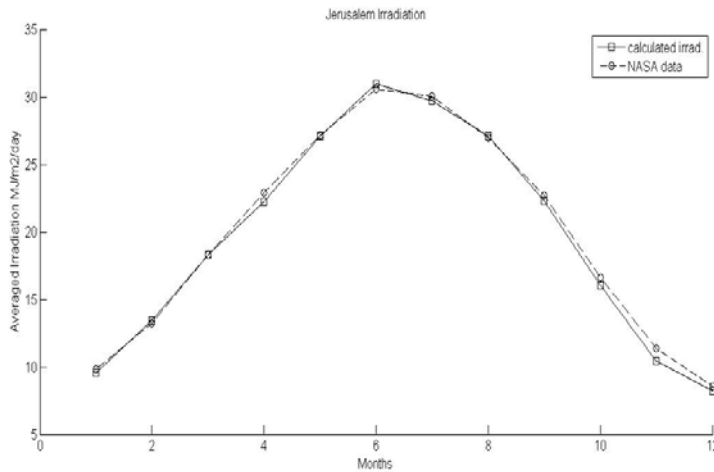


Fig. 4. NASA data and calculated solar irradiation for Jerusalem.

The obtained solar radiation data is used for one-dimensional time-dependent steady state program to predict the solar pond temperature behaviour in the storage zone during a year and an excellent agreement is obtained comparing with real temperature measurements by Ali [13] and this output and measured data are illustrated in Fig. 5.

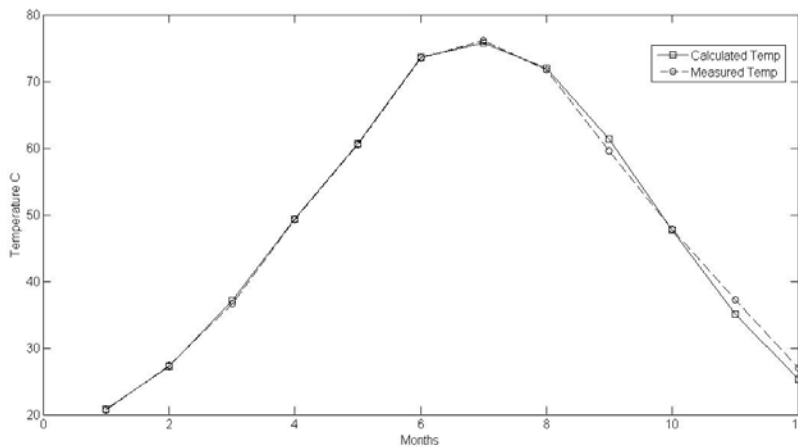


Fig. 5. Measured and calculated storage zone temperature in Kuwait solar pond.

The program can predict the performance of a solar pond in a cold climate location and for this purpose the University of Surrey in the UK has been chosen. The result is plotted in Fig. 6 and the storage zone temperature behaviour can be improved by changing the depth of the solar pond layers to reach 80 °C .

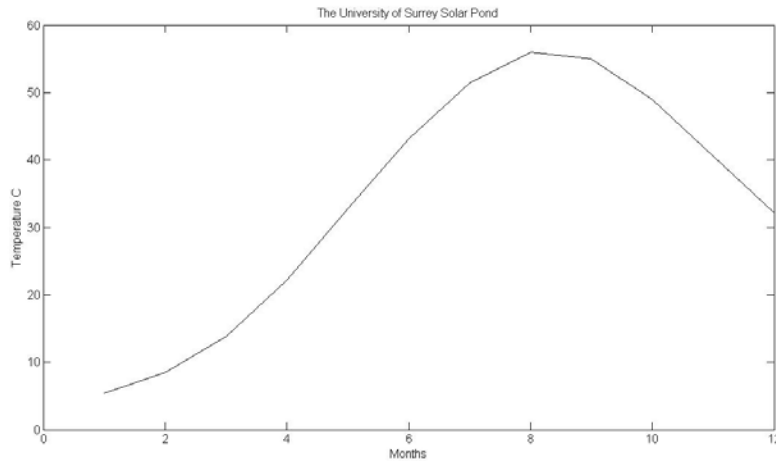


Fig. 6. Surrey storage zone(1m) temperature at 1m depth of gradient zone.

4. Conclusions

The proposed method provides an accurate prediction of the solar radiation based on a single input data which is the location latitude. The predicted results are validated by comparison with NASA 22 years averaged data in three various locations in the Middle East, where very close agreement has been obtained. The one-dimensional time-dependant steady state model has shown excellent agreement with Kuwait solar pond measurement data. The transient model was investigated as well. However, it was found that the steady state model provided more realistic results. The solar pond performance in cold climate locations such as the UK has been studied and the pond temperature can reach 80 °C levels using some designs.

References

- [1] W. C. Dickinson and P. N. Cheremisinoff, "Solar Energy Technology Handbook" Marcel Dekker, New York, (1980) 374.
- [2] J. F. Kreider and F. Kreith "Solar Energy Handbook" McGraw-Hill, New York (1981) 10-2
- [3] J. A. Duffie, and W. A. Beckman "Solar Engineering of Thermal Processes" 3rd Ed. , John Wiley & Sons (2006) 652.
- [4] H. M. Lu, A. H. P. Swift, H. D. Hein and J. C. Walton, "Advancements in salinity gradient solar-pond technology based on sixteen years of operational experience" J. Sol. EnergyTrans. ASME 126 (2004) 759-767.
- [5] J. F. Kreider and F. Kreith "Solar heating and Cooling Active and Passive Design" (1982) 284.
- [6] NASA's Website http://www.eoearth.org/article/Solar_radiation
- [7] C.G. Abbot "The Solar Constant" Solar Energy 9(2) (1965) 166-167.
- [8] H. P. Garg "Treatise on Solar Energy" V1, John Wiley & Sons (1982).
- [9] P. J. Lunde "Solar Thermal Engineering" John W New York (1980).
- [10] H. Weinberger, "The physics of solar ponds", Solar Energy 8 (1964) 45.
- [11] A. Rabl and C. E. Nielsen, "Solar Ponds for Space Heating" Solar Energy 17 (1975) 1-12.

- [12] C. F. Kooi, "The steady state salt gradient solar pond" *Solar Energy* 23 (1979) 37-45.
- [13] H. M. Ali "Mathematical modeling of salt gradient solar pond performance" *Energy Research* 10 (1986) 377-384.
- [14] Y. F. Wang and A. A. Akbarzadeh, "A parametric study on solar ponds" *Solar Energy* 30 (1983) 555-562.

Choice of solar share of a hybrid power plant of a central receiver system and a biogas plant in dependency of the geographical latitude

Spiros Alexopoulos^{1,*}, Bernhard Hoffschmidt¹, Christoph Rau¹, Johannes Sattler¹

¹ Solar-Institut Jülich, University of Applied Sciences Aachen, Jülich, Germany

* Tel: +49 241600953551, Fax: +49 241600953570, E-mail: alexopoulos@sij.fh-aachen.de

Abstract: The potential of renewable energies varies significantly from North to South Europe. Southern Europe has a high solar potential and is ideal for the implementation of solar concentrated power plants. To this group of solar thermal power systems belong the solar tower, parabolic trough, solar dish and linear Fresnel systems. North European countries, especially the Scandinavian countries, have a high biomass and hydropower potential. This paper focuses on calculation of the power production for hybrid systems of solar tower with gas turbine in Southern Europe and biogas-only operation in Northern Europe.

The solar tower system consists of a heliostat field, which concentrates direct solar irradiation on an open volumetric central receiver. The receiver heats up ambient air to temperatures of around 700°C. The hot air's heat energy is transferred to a steam Rankine cycle in a heat recovery steam generator (HRSG). The steam drives a steam turbine, which in turn drives a generator for producing electricity. In order to increase the operational hours of a solar tower power plant, a heat storage system and/ or hybridization may be considered.

The advantage of solar-fossil hybrid power plants, compared to solar-only systems, lies in low additional investment costs due to an adaptable solar share and reduced technical and economical risks. On sunny days the hybrid system operates in a solar-only mode with the central receiver and on cloudy days and at night with the gas turbine only. As an alternative to methane gas, environmentally neutral biogas can be used for operating the gas turbine. Hence, the hybrid system is operated to 100% from renewable energy sources.

An advanced software tool library has been developed for modelling such solar hybrid power plants. This library includes the components of the solar-heated hot gas cycle and the steam cycle. Moreover, a choice of different gas turbine and duct burner components is given. When developing a simulation model for the calculation of a small hybrid power plant, components from the library are inserted into the model. The software tool features the possibility of either calculating the energy output of individual operating points or of time intervals in the range of days up to an entire year.

With this simulation tool, hybrid solar tower systems are calculated for various locations with high solar potential within Europe. In addition, locations in North Scandinavian countries with high biomass potential are investigated and power plants with biogas as fuel without solar input are calculated.

Keywords: solar tower, central receiver, hybridization, biogas, renewable energy

1. Introduction

The potential of renewable energies varies significantly from North to South Europe. Southern Europe has a high solar potential and is ideal for the implementation of solar concentrated power plants. North European countries, especially the Scandinavian countries, have a high biomass and hydropower potential.

Since 1980s, power production with solar thermal power plants and the increasing use of biogas has been a promising option for reducing the consumption of fossil fuels.

The development of solar thermal technologies has gone into many directions, which can be exemplified with the various heat transfer media that are deployed in existing systems. Many solar thermal power plants contribute to the electricity generation in various European countries. To this group of solar thermal power plants belong the solar tower, parabolic trough, solar dish and linear Fresnel systems. Parabolic trough and solar tower systems are the most developed technologies as well as the most economical solar thermal plants at this moment of time.

A solar tower consists mainly of a heliostat field, a central receiver and a conventional steam Rankine cycle. Various central receiver technologies have been developed throughout the world. The software tool described in this paper models a solar tower with an open volumetric receiver. This type of receiver has been deployed in the Solar Tower Jülich (STJ), Germany, since its completion in 2008. The subsequent explanations are valid for this type of receiver only. At the STJ, the heliostat field, a field of sun-tracking mirrors, reflects and concentrates the direct solar irradiation onto the open volumetric receiver. This receiver consists of porous ceramic absorber modules. Incident sun rays enter the porous receiver, are absorbed inside and heat it up. To remove the heat, ambient air is continuously sucked through the porous receiver and is heated up to almost 700°C. The hot air is passed through a heat recovery steam generator (HRSG) in which it passes its heat to a water-steam cycle. The steam is expanded in a steam turbine and the rotation of the turbine's shaft drives a generator to produce electricity. Utilization of air as a heat transfer fluid (HTF) secures a high plant efficiency due to the reason that air can be heated to very high temperatures, which in turn enables higher steam temperatures in the Rankine cycle and thus a better Carnot efficiency. Moreover, it allows a fast start-up to operating conditions; it is non-toxic and is available at no cost in unlimited amounts.

In order to increase the operational hours of a solar tower power plant, a heat storage system and/or hybridization e.g. with biofuels must be considered.

As an alternative to methane gas, environmentally neutral biogas can be used as fuel for operating a gas turbine. Hence, the hybrid system is operated to 100% from renewable energy sources. The gas turbine not only delivers electricity but also heat in the waste gas, which can be reused.

2. Methodology

This paper focuses on the calculation of different important characteristic quantities, which include the annular power production, the solar share and the annual fuel consumption. The combination of two renewable technologies, namely biogas and solar concentrated energy, is investigated. Therefore the operation of a hybrid system consisting of a solar tower power plant and biogas-fuelled gas turbine is investigated.

2.1. Considered technologies

2.1.1. Solar tower plant

Germany's first solar tower power plant, which has a rated power output of 1.5 MW_e, was constructed and completed in 2008 in the town of Jülich [1]. It commenced solar operation in spring of 2009. The plant was built by the general contractor Kraftanlagen München and is operated by the local utility Stadtwerke Jülich. The Solar-Institut Jülich (SIJ) and the German Aerospace Center (DLR) conduct the accompanying research. The project is funded by the economic ministries of the German states of Northrhine-Westphalia and Bavaria, as well as by the German Federal Ministry for the Environment, Nature Conservation and Nuclear Safety.

The objective of the power tower project in Jülich is to demonstrate the entire system in commercial-like operation over a longer period of time, to develop control and plant management strategies and to further improve performance and reliability of the key components. Jülich was chosen as the favoured location because it is situated close to the involved research institutions and due to its fluctuating direct solar irradiation conditions. The latter reason has the advantage that it allows and requires the investigation into the system

operation strategy under transient conditions, especially with regard to optimizing the charging and discharging process of the thermal storage [2].

2.1.2. Biogas

Biogas is produced by the biological breakdown of organic matter in the absence of oxygen. It can be produced by anaerobic digestion or the fermentation of biodegradable materials such as biomass, manure or sewage, municipal waste, green waste and energy crops. Biogas is composed of 45-85% methane and 15-45% carbon dioxide, depending on the conditions during production. Moreover, biogas comprises small amounts of hydrogen sulphide, ammonia and nitrogen. Its field of application includes combustion engines, burners as well as gas turbines for electricity generation and co-generation of heat and power. Biogas can be further enhanced from low-quality to natural gas quality before it is fed in the public gas grid. This article considers biogas-fuelled gas turbines only.

2.1.3. Biogas potential

In all Scandinavian countries, biomass has a high potential. In the TRANS-CSP study [3] the theoretical potential of biomass is estimated for Norway at 26 TWh/a, for Sweden at 80 TWh/a and for Finland at 54 TWh/a.

Taking Sweden as an example, the country has approximately 233 biogas facilities with a total biogas production of 1.3 TWh/a [4]. Biogas can be produced at large-scale centralized plants, where different feed stocks materials are digested, and at small farm-based plants, which use and digest mainly agricultural feed stocks.

The theoretical potential of biogas production in Sweden lies at around 14-17 TWh/a, which is more than 10 times that of the present annual production [5]. From the feed stocks materials 70% is manure and farm waste, 13% is industrial waste, 9% is household waste and the remainder is garden waste and sewage sludge.

For Italy, the best biogas performance is recorded in the northern part of the country especially in the regions of Lombardy, Emilia Romagna, Trentino A.A, Veneto and Piedmont. With a share of 23.8%, the region of Lombardy is the biggest producer of biogas in Italy and dominates the biogas market. Moreover, Lombardy has the biggest biogas potential, which is estimated at 4,643 GW. As for the production of biogas from manure, 3,800,000 pigs and 1,600,000 heads of cattle were counted for the region of Lombardy in the ISTAT census in 2001. Together this amounts to 44% of the total domestic animal breed in Italy [6].

2.1.4. Hybrid system

To improve the availability and the capacity factor of a solar tower power plant, a hybridization of the plant is considered. In regions with very high irradiation, solar thermal power plants with heat storage facilities can reach a maximum of 3,000 to 4,000 nominal load hours per year. Hybridization, for example with the combustion of biogas, enables the operator to produce electricity day and night for up to 8,600 hours per year. It is expected that such hybrid power plants will have a high potential for the market introduction in the next decade.

The upgrade of a solar tower power with air receiver technology to a hybrid system by combining it with a gas turbine is shown in Fig. 1.

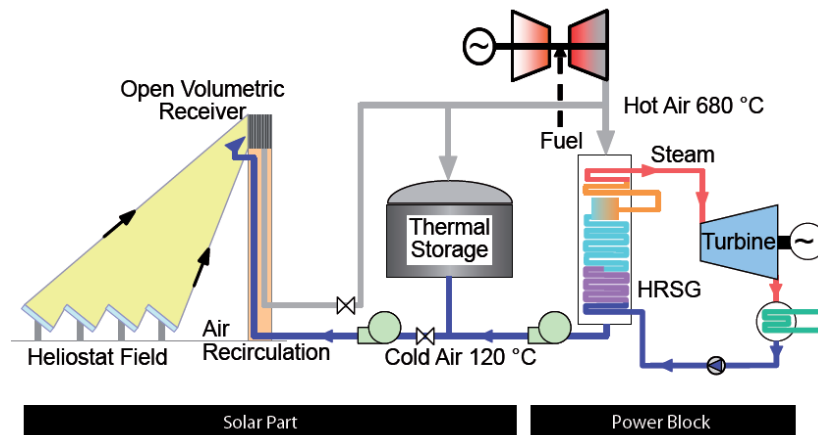


Fig. 1: Schematic diagram of a solar tower demonstration plant hybridised with a gas turbine

The operating strategy for the hybrid plant involves an alternating operation of the gas turbine and the air receiver. On sunny days the air receiver is operated in a solar-only mode. On days with very low direct solar irradiation (very cloudy conditions) the thermal energy provided by the heliostat field is not sufficient for operating the plant. On those days the gas turbine must be operated. The hot exhaust gas from the gas turbine is directed through the heat recovery steam generator (HRSG) for steam generation [7]. Throughout the nights, solely the gas turbine is operated.

2.2. Simulation

2.2.1. Implementation of the model

The implementation of the solar tower power plant model has been realised in the MATLAB/Simulink environment. MATLAB is a high-performance language for technical computing. It integrates computation, visualization, and programming in an easy-to-use environment, where problems and solutions are expressed in familiar mathematical notation. Simulink is a toolbox in MATLAB that provides an environment for modelling, simulating, and analyzing dynamic systems. It supports linear and nonlinear systems, modelled in continuous time or a sampled time. The implementation of systems can also occur at a multi-rate, i.e. have different parts that are sampled or updated at different rates [8].

2.2.2. Model library

The simulation models are based on thermodynamic theory using assumptions for simplification in order to maintain a fast simulation time while retaining good accuracy. Several components like the steam turbine, generator, burner, solar receiver, heliostat field, etc. are included in the model library. They include mostly energy and mass balance equations as well as additional algebraic equations. Most components models are optimized for steady-state operation. However, components with high thermal inertia, such as a part of the HRSG, are implemented as dynamic models.

The model library (Fig. 2) was developed with consideration of the following characteristics [9]:

- compatibility of the components related to the connection of one to the other
- possibility of choosing different geographical locations for performing the calculations
- applicability for different power plant sizes
- adjustability to different transport media: e.g. air, gas, exhaust gas

- ease of modification
- usability for short time intervals (minutes)

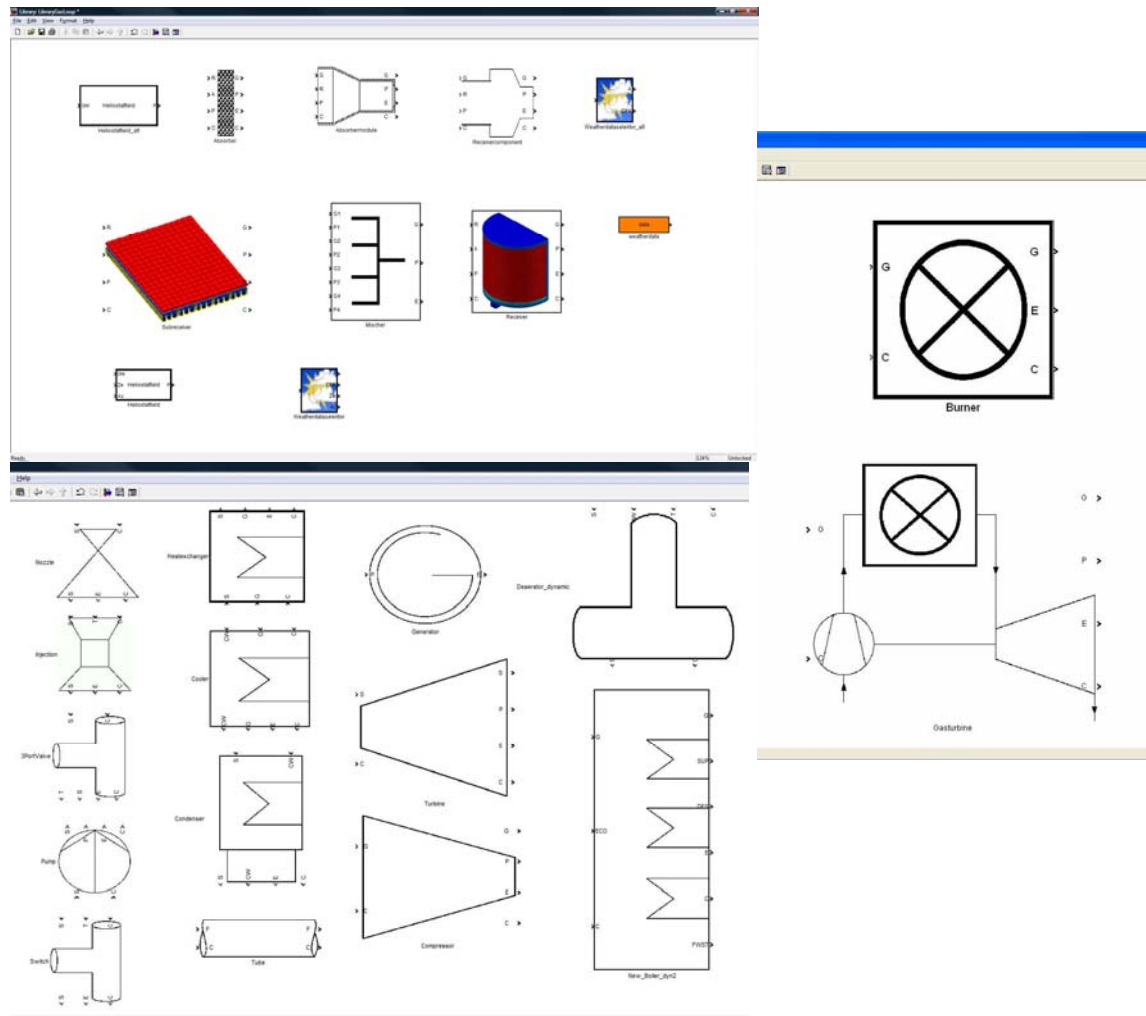


Fig. 2: Model libraries for the steam cycle, the solar and hybridization components

Gas and steam properties can be integrated in each model. The various state variables for water and steam are computed with polynomials taken from the industry standard IAPWS-IF97. For calculating the state variables for different gas mixtures, algorithms stated in the VDI (Verein Deutscher Ingenieure - engl.: Association of German Engineers) guideline 4670 [10] and provided by NASA Technical Memorandum 4513 [11] are integrated.

With the developed software, the annual performance and the electrical power output of small solar hybrid tower plants, combined cycle with gas turbine and solar-only operated solar tower with or without storage can be calculated.

2.2.3. Validation of library components

The components of the model library were validated mainly with calculation results of other simulation software [12]. They were also verified with results from different design points. The three thermodynamic cycles, namely the steam, air and water cooling cycle, were tested separately before they were combined to a complete power plant system.

3. Results

A comparison of energy production and fuel consumption was made for a combined-cycle plant in Sweden and a hybrid solar tower power plant located both in Jülich and North Italy. The combined-cycle plant in Sweden was taken as reference. It operates with a gas turbine, which utilizes biogas as fuel. The selected gas turbine is a Centrax 501-KB3 [13], which generates a nominal power of 2.68 MW_e. The hot exhaust gases are directed through a boiler for steam generation. In the steam cycle, the steam is expanded in a steam turbine. The generator, which is driven by the steam turbine, produces an additional 1.34 MW_e.

For all states and power plants, the biogas is composed of 56% methane, 40% carbon dioxide and other constituents. The configurations and main simulation parameters are shown in Table 1.

Table 1. Main simulation parameters

Place	Scandinavia	Jülich	Northern Italy
Nominal Power GT [MW _e]	2.68	2.68	2.68
Nominal Power ST [MW _e]	1.34	1.50	1.50
Heliostats [-]	0	2,150	2,150
Mirror area [m ²]	-	8	8
Maximum air/flue gas temperature [°C]	571	680	680

Original weather data has been used for the locations Jülich and Milano (Italy). For Jülich, data from the year 2007 in a time resolution of 15 min was integrated. For Milano, data of the year 2006 in a one hour resolution has been used. The quasi-steady-state simulations are computed in time steps of maximum 60 seconds. The steam turbine and generator of the steam cycle for both locations have a generation capacity of about 1.5 MW_e. For the hybrid mode, the same gas turbine as simulated for the combined-cycle plant in Sweden (2.68 MW_e) was integrated.

The calculation for the location in Scandinavia (Sweden) was performed for a nominal plant operation with 8,760 hours of gas turbine operation. For the hybrid solar tower power plants, the calculation was realized with alternating operating mode. Hence, in the solar-only mode, nominal parameters could not always be reached. The results presented in Table 2 have an estimated error of about ±10%.

Table 2. Simulation results for the three sites.

Place	Energy Production [GWh]	Fuel Consumption [t]
Scandinavia	35.21	20,385
Jülich	25.17	14,004
Northern Italy	21.30	11,761

The results show that a Conventional Combined Power Plant in Scandinavia generates the estimated energy of 35.21 GWh at a fuel consumption of 20,385 t. The hybrid solar tower power plants instead produce less electrical energy, because only the steam turbine generates energy in daytime. Thus again means, that also less fuel is consumed. The difference between the two locations Jülich and Italy reflects this coherence. Locations with high insolation are associated with the less fuel consumption and less electricity production. This effect occurs if an alternate hybrid operation is considered.

In Fig. 3, which shows a good day regarding solar radiation (DNI), a typical operation of the hybrid plant in alternate mode is illustrated. The specific electrical (index EL) power of the steam turbine resp. gas turbine are shown. Furthermore, the thermal (index TH) power of the receiver (index Rec) and the heat input at the HRSG (index HRSG).

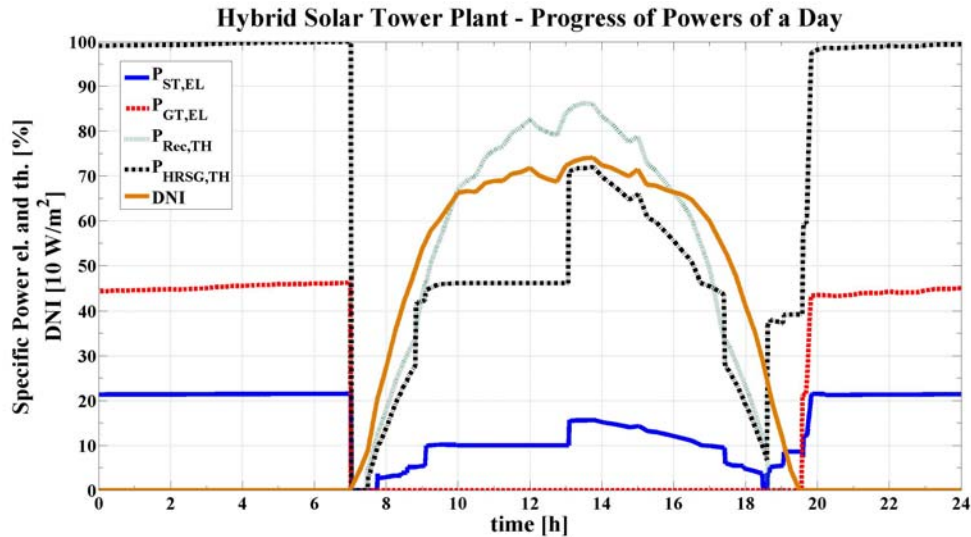


Fig. 3: Hybrid solar power tower plant operation for the 27th March 2007

At night the gas turbine provides continuous electricity and heat to the HRSG, so that a combined-cycle operation is conducted. When solar irradiation increases the gas turbine is shut down. Because of the clear switch to solar operation the electricity generation by the steam turbine may diminish. When solar radiation increases the electricity production increases, too. At a certain stage, by the receiver produced heat is send to the storage. The heat input to the HRSG is kept constant. When the storage is charged to a certain level, the charging is terminated and the full heat input is provided by the receiver (cf. fig 3. Jump at 13 h). When the sunset starts the storage is discharged slowly and the heat for the HRSG is supplied by the storage. In the evening the shift from storage operation to gas turbine operation is executed. This demonstrated operation strategy needs still optimization to ensure a maximum yield of power production and a continuous operation. Therefore weather dependent operation strategies and controlling has to be developed.

4. Discussion and Conclusions

Numerical procedures should be applied for the calculation of the annual energy yield of solar tower power plants. With the simulation tool, hybrid solar towers at different locations with high solar potential in Europe are calculated. Moreover, locations with high biogas potential in North Scandinavian countries are considered and power plants with biogas as fuel without solar input are investigated. The results of the simulation analysis show that the created model library is a solid basis for the simulation of hybrid concepts for solar tower systems.

In next steps a detailed investigation and analysis of the simulation results is planed. The simulation models and especially the operation strategies will be optimized in order to get even more accurate results.

In further steps an additional site in South Europe, for example in South Italy on the island of Sicily, will be investigated. For that reason weather data will be selected and a solar-only operation of a solar tower power plant will be regarded.

Acknowledgments

The authors gratefully acknowledge the financial support of the German Federal Ministry for the Environment, Nature Conservation and Nuclear Safety (BMU), the ministries of economic affairs of the German states of North Rhine-Westphalia (NRW) and Bavaria in the solar tower demonstration project. The research into hybridization is supported by the German Federal Ministry of Education and Research (BMBF).

References

- [1] K. Hennecke, P. Schwarzbözl, S. Alexopoulos, J. Götsche, B. Hoffschmidt, M. Beuter, G. Koll, T. Hartz: SOLAR POWER TOWER JÜLICH The first test and demonstration plant for open volumetric receiver technology in Germany, Proceedings of the 14th Biennial CSP SolarPACES Symposium, Las Vegas, Nevada, 4-7 March 2008, London.
- [2] Alexopoulos, S., Goettsche, J., Hoffschmidt, B., Rau, C., Sattler, J., Schmitz, M., Warkerkar, Sh., Hennecke, K., Schwarzboezl, P., Beuter, M., Koll, G., Hartz Th. (2009): SOLAR TOWER POWER PLANT JUELICH First experience with an open volumetric receiver plant and presentation of future enhancements, Proceedings Renewable Energy World Europe Conference, Cologne, Germany.
- [3] Trans-Mediterranean Interconnection for Concentrating Solar Power, DLR, 2006
- [4] Swedish energy agency. Production and use of biogas, 2005.
- [5] Lantz, M., Svensson, M., Björnsson, L., Börjesson, P.: The prospects for an expansion of biogas systems in Sweden: Incentives, barriers and potential, Energy policy, 35:1830-1843, 2007
- [6] Ceriani, A.: “Le energie alternative e rinnovabili in Lombardia nell’ambito delle attività produttive”, Istituto Regionale di Ricerca Della Lombardia, Milan, January, 2010
- [7] S. Alexopoulos, B. Hoffschmidt, C. Rau, P. Schwarzbözl: Simulation results for a hybridization concept of a small solar tower power plant, SolarPACES Symposium, Berlin, 15-18 September 2009
- [8] MATLAB/Simulink Manual, <http://www.mathworks.com>, 2010
- [9] S. Alexopoulos, B. Hoffschmidt, C. Rau, M. Schmitz, P. Schwarzbözl, S. Pomp: Simulation results for a hybridised operation of a gas turbine or a burner for a small solar tower power plant, SolarPACES Symposium, Perpignan, France, 21-24 September 2010
- [10] McBride, B. J., Gordon, S., Reno, M. A.: Coefficients for calculating thermodynamic and transport properties of individual species, Nasa Technical Memorandum 4513, 1993
- [11] VDI: Thermodynamische Stoffwerte von feuchter Luft und Verbrennungsgasen - VDI 4670, 2003
- [12] S. Alexopoulos, B. Hoffschmidt, J. Götsche, C. Rau, P. Schwarzbözl: First simulation results for the hybridization of small solar power tower plants, 1st International Conference on Solar Heating, Cooling and Buildings, Lisboa, Portugal, 7-10 October 2008
- [13] ASUE - Arbeitsgemeinschaft für sparsamen und umweltfreundlichen Energieverbrauch E.V.: Gasturbinen-Kenndaten-Referenzen, 2006

Building-integrated Solar Collector (BISC)

Bin-Juine Huang^{1,*}, Yu-Hsing Lin¹, Wei-Zhe Ton¹, Tung-Fu Hou¹, Yi-Hung Chuang¹

¹ New Energy Center, Department of Mechanical Engineering National Taiwan University, Taipei, Taiwan

* Corresponding author. Tel: +886 2 2363-6576, Fax: +886 2 2363-6576, E-mail: bjhuang@seed.net.tw

Abstract: The present study intends to develop building-integrated solar collector (BISC). The storage tank inside is designed in multi-function. BISC combines the solar collector and the water storage tank together with one face acting as the solar absorber. A double-glazing design is adopted to reduce the heat loss. A PC-based automatic operating system is designed and built to monitor the long-term performance of the BISC system with 8 collector units. Hot water discharge is controlled from 18:00 until 22:00 to simulate the hot water load of a family. The discharge rate is at 60 L/hr. A 30 L backup electric water heater was connected to the BISC system. The long-term test results in winter season show that about 50 % energy saving was achieved in clear days. The monitored results have also shown that the daily-total solar irradiation on a 75° tilted surface (the BISC installed angle) is higher than the horizontal surface, about 40-50 % higher at $H_t > 10 \text{ MJ/m}^2\text{day}$. This assures that BISC will produce more hot water in winter. This proves that the use of BISC as parapet or sun-shading canopy of a building (installation angle $> 75^\circ$) is technically feasible. The characteristic efficiency of the installed BISC with different colors is 0.34-0.39.

Keywords: Solar thermal, Building-integrated collector, Solar collector.

Nomenclature

η	the daily-total thermal efficiency of BISC ..	η_{dc}	the heat removal efficiency.....
η^*	the characteristic daily thermal efficiency of BISC.....	τ_f	spent time when heat removal second
α_o	solar collecting efficiency (when $T_i=T_a$)....	m_e	the heat removal flow rate..... $\text{kg}\cdot\text{s}^{-1}$
U_s	the heat loss coefficient $\text{MJ/m}^2\text{C}\cdot\text{day}$	C_p	specific heat of water..... $\text{MJ/kg}\cdot^\circ\text{C}$
T_i	initial temperature when collect heat $^\circ\text{C}$	T_e	water outlet temperature $^\circ\text{C}$
T_a	average ambient temperature $^\circ\text{C}$	T_{wi}	water inlet temperature $^\circ\text{C}$
H_T	the daily-total solar irradiation $\text{MJ/m}^2\cdot\text{Day}$	M_t	total mass of water storage kg
		$T_{initial}$	initial temperature of water storage tank

1. Introduction

The solar building involves advanced solar collector technology for heating and hot water supply. Our research intends to develop a building-integrated solar collector (BISC) as parapet or sun-shading canopy of a building, Figure 1.1. BISC has a dual function of solar utilization and building constructing material, which can greatly reduce the cost.

As part of the building constructing material, the design of BISC needs to consider the thermal performance, the mechanical strength, installation method on building, and outlook. We focus on the research of the thermal performance including heat utilization efficiency of hot water and the heat insulation of the front side.

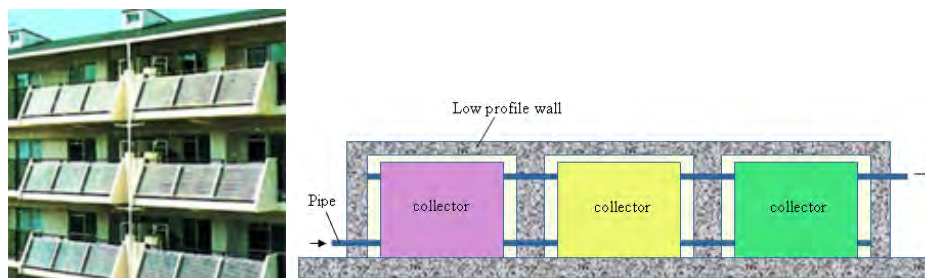


Fig. 1.1 BISC for parapet or sun canopy of a building

We have developed the first generation product of BISC. The special design features of BISC include:

- 1) Color glass cover: BISC uses the color glass cover in order to be compatible with building. It will match the architecture appearance by choosing the glass color.
- 2) Modular design: The solar water heater is designed as a module and easy to install. It only needs to fix on the wall or the ground and connect the water supply lines.
- 3) Multi-function water storage tank: The BISC combines the solar collector and the water storage tank together. It combines the solar collector and the water storage tank together. One surface of the water storage tank is the solar absorber which absorbs solar energy and directly conducts to the water inside the storage tank.
- 4) Double air-layer insulation: The BISC has a double-layer insulation, with two air gaps in front of the collector. This can reduce the heat loss.

2. Methodology

Design of BISC

The design specification of the BISC unit is as follows:

- outside dimension: 100cm x 70cm x 20cm
- solar absorber dimension: 90cm x 60cm
- storage tank: 90cm x 60cm x 7.5cm
- water storage: 40 liter
- glazing: 2 layers, 4mm color glass + 6mm PC
- glass color: clear, ocean blue, French green
- front double air layer insulation: 3cm/3cm
- heat exchanger: PC 6mm, 60cm x 90cm, 3 rows, 3.2m²

There were 8 units of BISC were installed in the building for demonstration and field test. Figure 2.1 is the 3D drawings of BISC. Figure 2.2 is the real BISC. Figure 2.3 is the building installation of BISC.

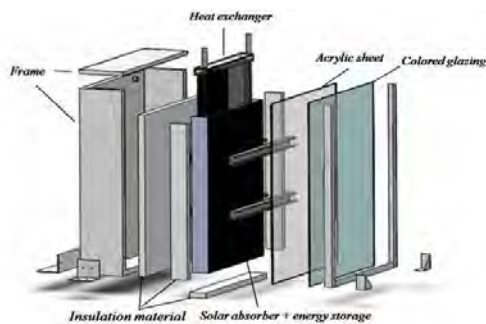


Fig. 2.1 3D drawings of BISC.



Fig.2.2 Color glass: clear, green, blue.

Equations (1) and (2) are used to determine the daily-total thermal efficiency of BISC (equation 1) and heat removal efficiency (equation 2):

$$\eta = \alpha_o - U_s \frac{T_i - T_a}{H_T} \quad (1)$$

$$\eta_{dc} = \frac{\int_0^{T_f} m_e C_p [T_e(t) - T_{wi}] dt}{M_t C_p (T_{initial} - T_{wi})} \quad (2)$$

The heat removal efficiency η_{dc} is defined as the ratio of the withdraw of total amount of useful heat compared to the total heat stored at sunset. Testing equipment for the measurement of daily-total thermal efficiency of BISC was designed and built in the research.

The equipment setups are shown in Figure 2.4. This testing equipment is automatic from early in the morning to sunset.

Design of a BISC system for a family

Figure 2.5 is the BISC system design to supply hot water for a family.



Fig. 2.3 BISC installation

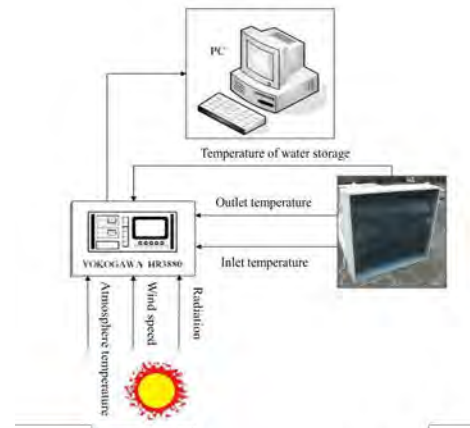


Fig. 2.4 BISC test equipments

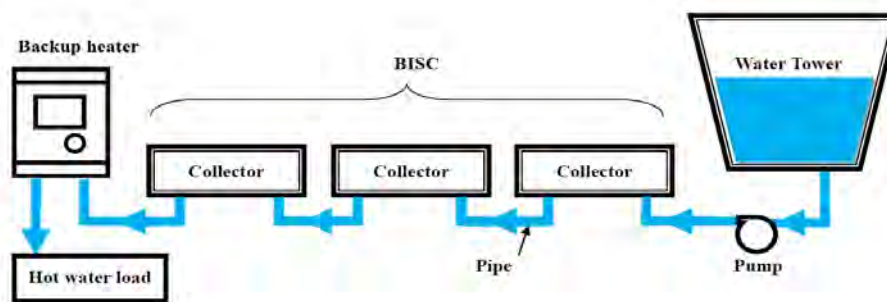


Fig. 2.5 BISC system.

Design of BISC system automatic monitoring system

A PC-based automatic operating and control system is designed and built to monitor the long-term performance of the BISC system built in the research. The operating system (Figure 2.6) monitors the instantaneous performance of the BISC system all day. Hot water discharge is controlled from 18:00 to simulate the hot water load of a family. The discharge rate is 30 L at every 15 minutes with 15 minutes stop after each discharge until 22:00. That is, the discharge rate is at 60 L/hr. A 30 L backup electric water heater was connected to the BISC system. The temperature setting of the backup heater is 55 °C.

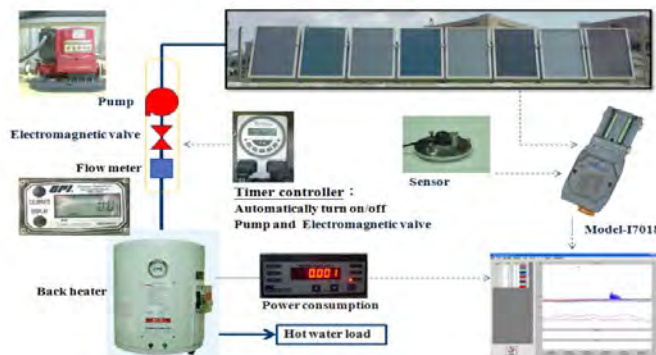


Fig. 2.6 Automatic monitor and control system

Figure 2.7 shows the water outlet temperature from BISC system. Figure 2.8 shows the electric consumption of the backup water heater. Figure 2.9 shows the daily performance pattern.

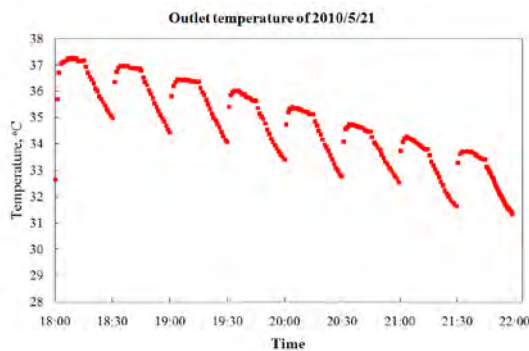


Fig. 2.7 BISC system outlet temperature

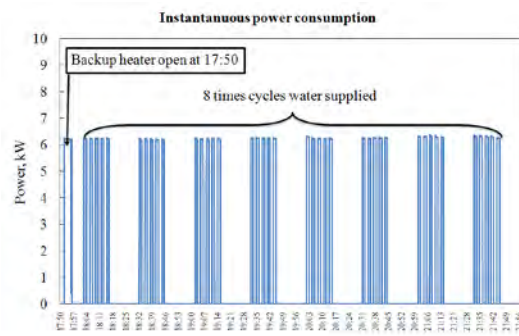


Fig. 2.8 Backup heater power consumption

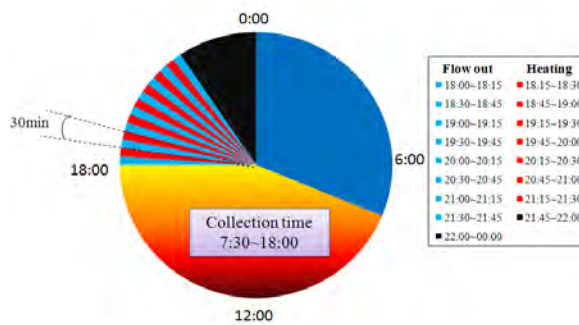


Fig. 2.9 Daily operation of BISC system.

3. Results

3.1. Measurement of daily thermal performance of BISC installed in building

Daily-total thermal efficiency test at 75° tilt

The data collected from the BISC system installed in building can be used to analyze the thermal performance of BISC at the installed tilt angle (75°), using the testing standard CNS B7277 developed by Huang [1-5]. The daily-total thermal efficiency tests were performed for BISC installed at 75° tilted angle with different color glazing, all facing south.

The daily-total efficiency is calculated using the measurement of daily-total energy stored in the storage tank and the total solar irradiation. Figure 3.1-1~Figure 3.1-5 and Table 3.1-1 present the daily-total thermal efficiency of BISC. The test results show that the characteristic efficiency of BISC with different colors which are installed in building with 75° tilt angle is 0.34-0.39 which is lower than the conventional solar water heater (0.50) with clear glass and tilted at lower angle (25°).

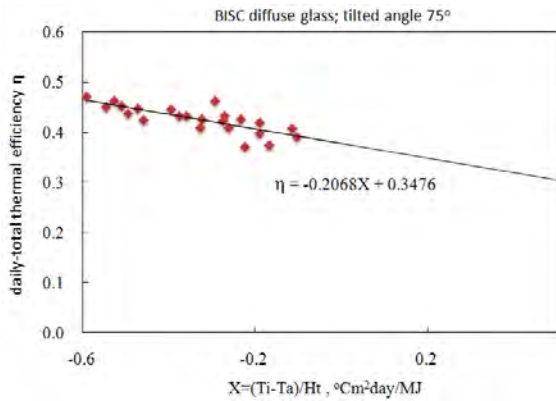


Fig. 3.1-1 Daily-total efficiency of BISC (diffuse glass).

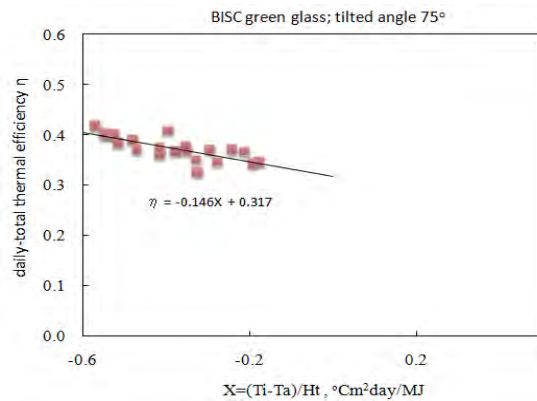


Fig. 3.1-2 Daily-total efficiency of BISC (green glass).

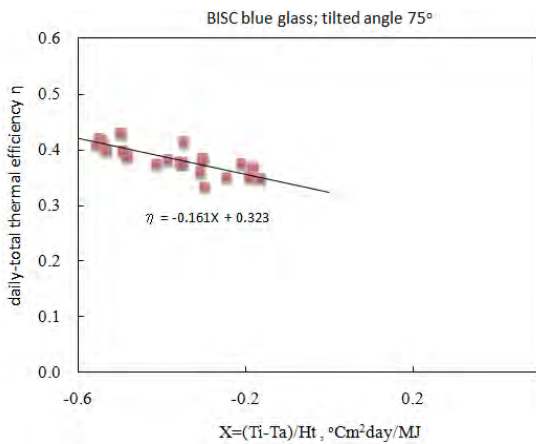


Fig. 3.1-3 Daily-total efficiency of BISC (blue glass).

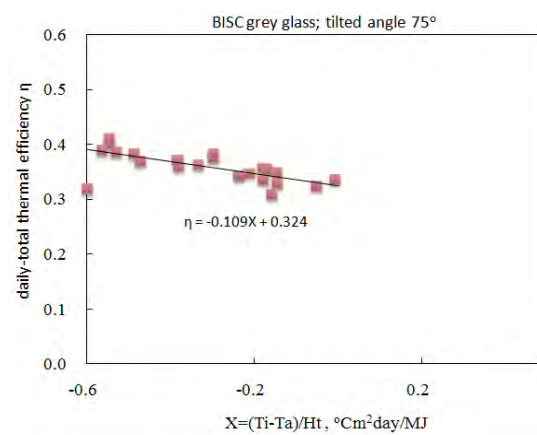


Fig. 3.1-4 Daily-total efficiency of BISC (grey glass).

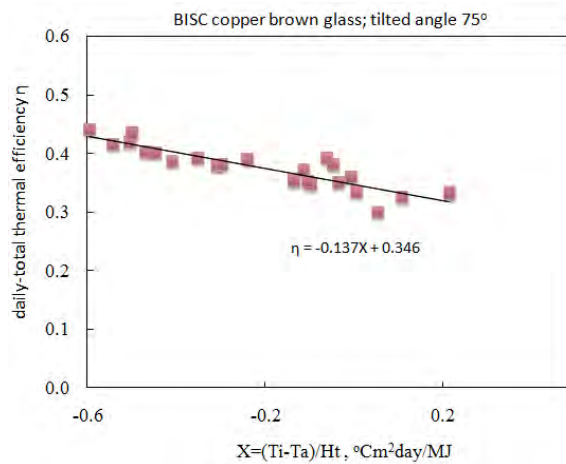


Fig. 3.1-5 Daily-total efficiency of BISC (brown glass).

Table 3.1-1 Test results of daily-total efficiency of BISC.

BISC facing South	U_s	α_o	η^*
Diffuse glass, tilted 75°	0.207	0.348	0.39
Green glass, tilted 75°	0.147	0.318	0.35
Blue glass, tilted 75°	0.161	0.323	0.35
Grey glass, tilted 75°	0.109	0.325	0.34
Copper-brown glass, tilted 75°	0.137	0.346	0.36

3.2. Long-term thermal performance test of BISC

The BISC system installed in building is tested by simulating the daily operation for a family. To estimate the energy saving of the backup electric heater, a baseline test was carried out to measure the daily energy consumption of the electric heater without using BISC. At daily solar irradiation 0.62 MJ/m² which is assumed as no solar radiation (rainy, the daily electricity consumption is 11.1 kWh. At daily solar irradiation 21.7 MJ/m² (the best weather), the daily electricity consumption is 4.0 kWh.

The first long-term performance monitoring is in winter season. Figure 3.2-1 shows the long-term monitoring results of BISC. It is shown that BISC can save 40 % to 50 % of electricity per day in winter. Figure 3.2-2 shows the variation of daily energy consumption and collected water temperature with solar irradiation in winter season. In spring season, the test results are shown in Figure 3.2-3 and Figure 3.2-4.

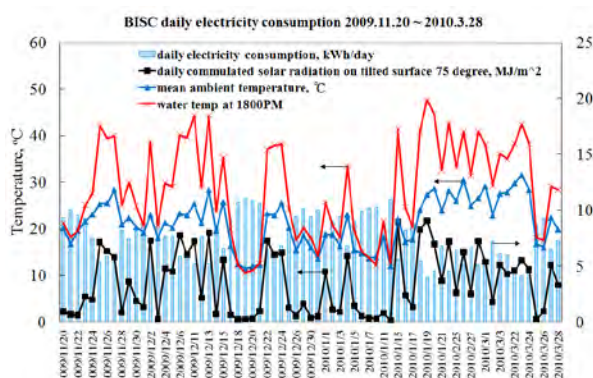


Fig. 3.2-1 Long-term monitoring results of BISC at Taipei 2009.11.20~2010.3.28.

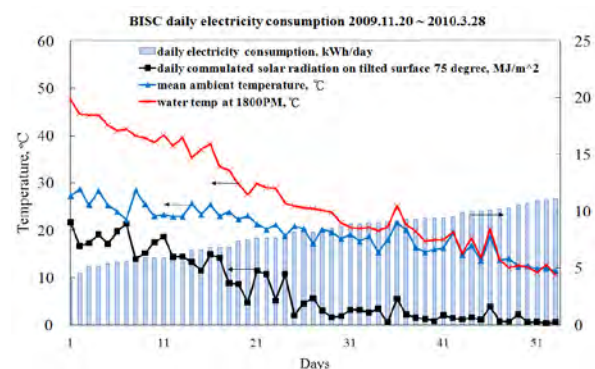


Fig. 3.2-2 Variation of daily energy consumption and collected water temperature with solar irradiation at Taipei 2009.11.20~2010.3.28

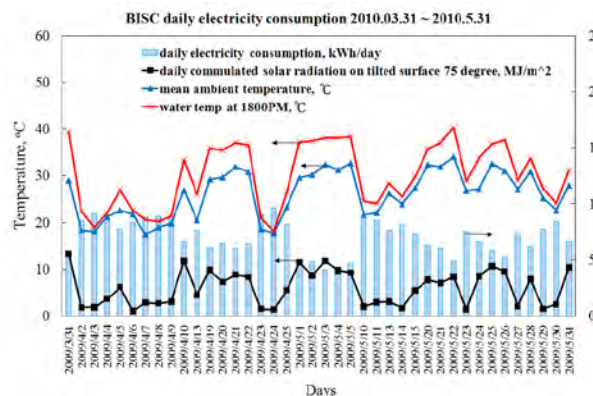


Fig. 3.2-3 Long-term monitoring results of BISC at Taipei 2010.3.31~2010.5.31

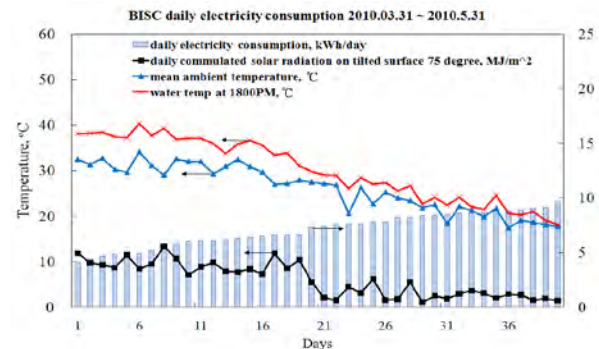


Fig. 3.2-4 Variation of daily energy consumption and collected water temperature with solar irradiation at Taipei 2010.3.31~2010.5.31

Figure 3.2-5 and Figure 3.2-6 shows the variation of daily-total solar irradiation on 75° and horizontal surfaces. The monitored results have also shown that the daily-total solar irradiation on a 75° tilted surface (the BISC installed angle in building) is higher than the horizontal surface, about 40-50 % higher at $H_t > 10 \text{ MJ/m}^2\text{day}$. This verifies that the use of BISC for parapet or sun-shading canopy of a building (installation angle $> 75^\circ$) is feasible. In summer, it is expected that the solar irradiation on 75° surface will be less than the horizontal one and the heat collection efficiency will be lower. However, the hot water load in summer decreases about 50 % in summer. Therefore, the use of BISC as parapet or sun-shading canopy of a building is feasible.

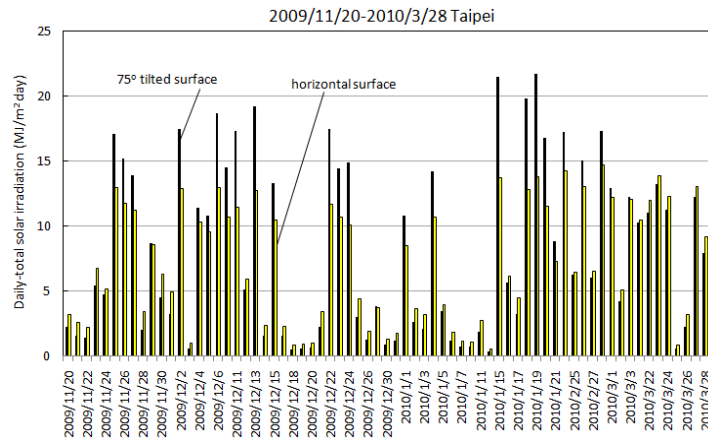


Fig. 3.2-5 Variation of daily-total solar irradiation 75° and horizontal surfaces.

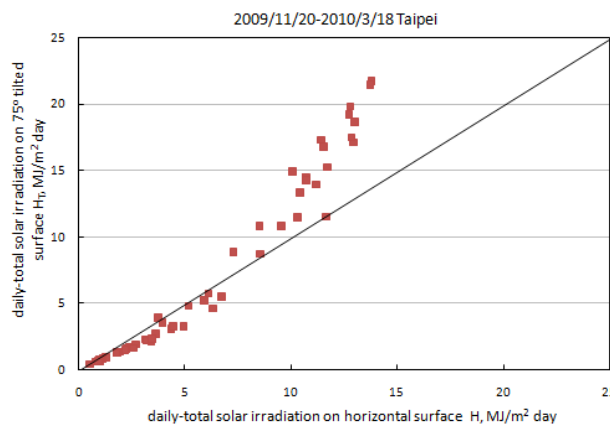


Fig. 3.2-6 Variation of daily-total solar irradiation on 75° and horizontal surfaces.

3.3. Heat removal efficiency test

The heat removal efficiency test is carried out to determine how much energy can be extracted from the tank rated at the total water extraction identical with the storage volume. With the Figure 3.4-1 By the equation (2), we can see the numerator is the real instantaneous removal heat (similar a trapezoid area), and the denominator is the total storage heat (rectangle area), then the heat removal efficiency calculate about 0.72.

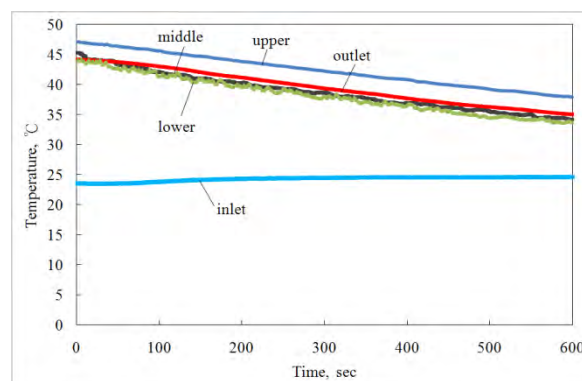


Fig. 3.4-1 Heat removal efficiency test.

4. Discussion and Conclusions

Our research intends to develop building-integrated solar collector (BISC). The BISC is designed to be part of construction material of a building. The storage tank inside is designed

in multi-function. BISC combines the solar collector and the water storage tank together with one face acting as the solar absorber which absorbs solar energy and directly conducts to the water inside the storage tank. A double-glazing design is adopted to reduce the heat loss. The outer transparent cover (glass) is made of color glass for architecture requirement. 8 units were installed on the roof of the lab at the Innovation and Incubation Center of NTU for field demonstration and test.

A PC-based automatic operating and control system is designed and built to monitor the long-term performance of the BISC system installed in the research. The system monitors the instantaneous performance of the BISC system all days. Hot water discharge is controlled from 18:00 to simulate the hot water load of a family. The discharge rate is 30 L at every 15 minutes with 15 minutes stop after each discharge until 22:00. That is, the discharge rate is at 60 L/hr. A 30 L backup electric water heater was connected to the BISC system. The temperature setting of the backup heater is at 55 °C which is fixed. The long-term test results in winter season show that about 50 % energy saving was achieved in clear days. The monitored results have also shown that the daily-total solar irradiation on a 75° tilted surface (the BISC installed angle in building) is higher than the horizontal surface, about 40-50 % higher at $H_t > 10 \text{ MJ/m}^2\text{day}$. This assures that BISC will produce more hot water in winter. This proves that the use of BISC as parapet or sun-shading canopy of a building (installation angle $> 75^\circ$) is technically feasible. The test results show that the characteristic efficiency of BISC with different colors which are installed in building with 75° tilt angle is 0.34-0.39, lower than the conventional solar water heater (0.50).

The monitoring of long-term performance will be continued to find out the defects and efficiency of the system. Since BISC is part of the building, it needs a BISC with high quality in art design, high thermal performance, good manufacturing technique, and long service life (reliability). The reliability issue will be the focus of forthcoming research.

Acknowledgment

This publication is based on work supported by Award No. KUK-C1-014-12, made by King Abdullah University of Science and Technology (KAUST), Saudi Arabia

References

- [1] B. J. Huang and S. C. Du, "A performance test method of solar thermosyphon system", ASME Journal of Solar Energy Engineering, Vol.113, pp.172-179.(1991)
- [2] Test Standard CNS B7277, Method of Test for Solar Water Heater System, 1988. Taiwan.
- [3] B. J. Huang, "Performance rating method of thermosyphon solar water heaters". Solar Energy, Vol.50, No5, pp.435-440.(1993).
- [4] J. M. Chang, "A Proposed Modified Efficiency for Thermosyphon Solar Heating Systems", Solar Energy, Vol. 76, No. 6, pp.693-701. (2004)
- [5] J. M. Chang, "A Criterion Study of Solar Irradiation Patterns for the Performance Testing of Thermosyphon Solar Water Heaters," Solar Energy, Vol. 73, No. 4, pp.287-292.(2002)
- [6] B. J. Huang, "Development of Long-Term Performance Correlation for Solar Thermosyphon Water Heater". ASME Journal of Solar Energy Engineering, Vol.111, pp.124-131. (May 1989)

Passive solar design in schools for the protection of the environment Greece: a case study

Agisilaos Economou^{1,*}

¹ National Technical University of Athens, Athens, Greece

* Corresponding author. Tel: +03 9345386, Fax: +039345386, E-mail: aghs@mail.ntua.gr

Abstract: The survey focuses on the passive solar schools units that have been built to date in Greece. It investigates on the one hand the bioclimatic principles applied to several school units with regard both to the building shell and the layout of the schoolyard area, and on the other hand the energy saving schemes that have been introduced to reduce energy consumption. This investigation is followed by a comparison with conventional schools in order to assess the economic and environmental benefits that the implementation of passive solar design bring to Greek schools.

The present survey relies on statistical data collected from passive solar design and conventional school buildings taking into account, among others, energy consumption, school building plots and implemented bioclimatic principles. Furthermore, in order to collect information about various issues and the cost of these new school units, the survey relies on personal interviews with staff members of the School Building Organization which is responsible for the construction of these schools.

The survey has shown that passive solar design used in the building of schools in conjunction with the installation of electronic control equipment to reduce consumption and the use of renewable energy, achieves a larger degree of environmental protection.

Keywords: *Passive solar design in schools, Save energy.*

1. Introduction

In Greece, school buildings, according to past interventions for energy saving and protection are divided into neoclassical buildings of the interwar period until 1950, school buildings built prior to the application of the General Building Rules (GBR)(1950-1980), school buildings constructed under the new implementation of the (GBR) (1979) [1] until 1998 when new measures were taken and terms were set to improve energy efficiency of buildings [2]. After Directive 2002/91/EC [3] of the European Union for the energy performance of buildings new measures were taken to reduce energy consumption in buildings, more specifically law 3661 [4], the Regulation of Energy Efficiency of Buildings [5] and law 3855 [6] in accordance with the directives of the European Union for energy saving.

Initially, the proposals for interventions in school buildings (from 1950 to 1980) refer to the closure of open corridors, to the insulation of the roof, replacement of window and door frames, the addition of RES, ventilation cooling and shading. Thermal bridges reduction was added to school buildings from 1980 to 1998 [7]. The bioclimatic design in school buildings was implemented on a pilot basis. Generally, the measures applied were thermal insulation, green roofs, and minimization of northern openings exposure during the winter,. On the other hand, during the summer, the measures applied were the minimization of western openings, shading and cross ventilation. Other passive systems such as solar atriums, skylights, cooling chimneys and soil pipes, were implemented [8].

Take into account that most schools have been built before the year 2000, it is shown that heat losses are much larger than those of school buildings constructed after 2000, which have implemented more stringent requirements for insulation and appropriate choice of materials.

Especially from 2007 and onwards, all schools in Greece are built in accordance with the principles of bioclimatic design related to both the architectural design and the choice of

location of the school. Also the extension of bioclimatic design in courtyards contributes more to the improvement of environmental conditions in schools and the better use of space and climate conditions.

In addition, the pilot application for the introduction of technology on energy saving systems in schools such as BMS systems, opens new horizons in energy saving.

Generally, the new design of schools, taking into account the bioclimatic principles both in the building shell and in the exterior space as well as energy-saving technologies in conjunction with the strictest standards for heat insulation, will contribute to good weather conditions with the minimum of energy consumption. The degree to which this new way of designing schools unit contributes to energy saving, will be analyzed below.

We note that the new standards for energy conservation should not be in conflict with bioclimatic design principles, but to complement them.

2. Methodology

First a reference to the policies implemented so far for the construction of schools in Greece is made. Next, the survey compares the fuel consumption between conventional schools and new schools with passive systems. Taking into account the thermal and climatic conditions in the region, the implementation or not of bioclimatic principles, an effort to estimate to which degree the use of passive solar systems can contribute to saving energy and protect the environment is made.

Thus, statistical data on the area and fuel consumption in selected schools are used in the survey. Also, the survey was supplemented with new data on the current policy for the construction of schools units. This information have been obtained through personal interviews of the directors of the School Building Organization, which is responsible for the construction of schools in Greece. The creation of maps is achieved by using data from Geographic Information Systems (GIS).

3. Results

The survey focused on schools units which are built according to the principles of bioclimatic design, as well as on conventional schools. Specifically, the research focused on the energy consumption for heating, taking into account the thermal, climatic conditions in the area and the buildings were designed.

From a survey made to the staff of the School Building Organization which are responsible for the construction of schools in Greece it is found that:

- Nowadays, the lack of suitable land in areas with increased urbanization, creates problems in the design of schools according to the principles of bioclimatic design.
- The old schools units need both maintenance and upgrading of heat insulation and sun protection.
- All schools built since 2007, and onwards follow the bioclimatic design principles, taking into account the location and orientation of the building. Techniques for sun protection, natural lighting, shading, natural ventilation (ventilation, traction phenomenon, solar chimney and cooling tower) and thermal insulation are applied. Green materials, wooden structures as well as green roofs and high planting are used (Fig. 1).
- Introduction of new insulating materials and automation programs for saving energy.

- Expansion of the use of natural gas in schools units in order to save energy and reduce emission of pollutants.
- Exploitation of strong sunlight via the use of photovoltaic systems. Due to good weather conditions and sunshine, in Greece, the design of school buildings different from those of northern European Union countries with different climatic conditions.
- Introduction of geothermal energy for heating and cooling in special school units, which are constructed for children with special needs, requiring greater energy consumption.
- Introduction of the new regulation on the energy performance of buildings in school buildings in order to obtain an energy building certification.

3.1. Schools units in Greece

New passive solar building constructed from 2007 onwards in Greece are presented in the following map (Fig. 1).

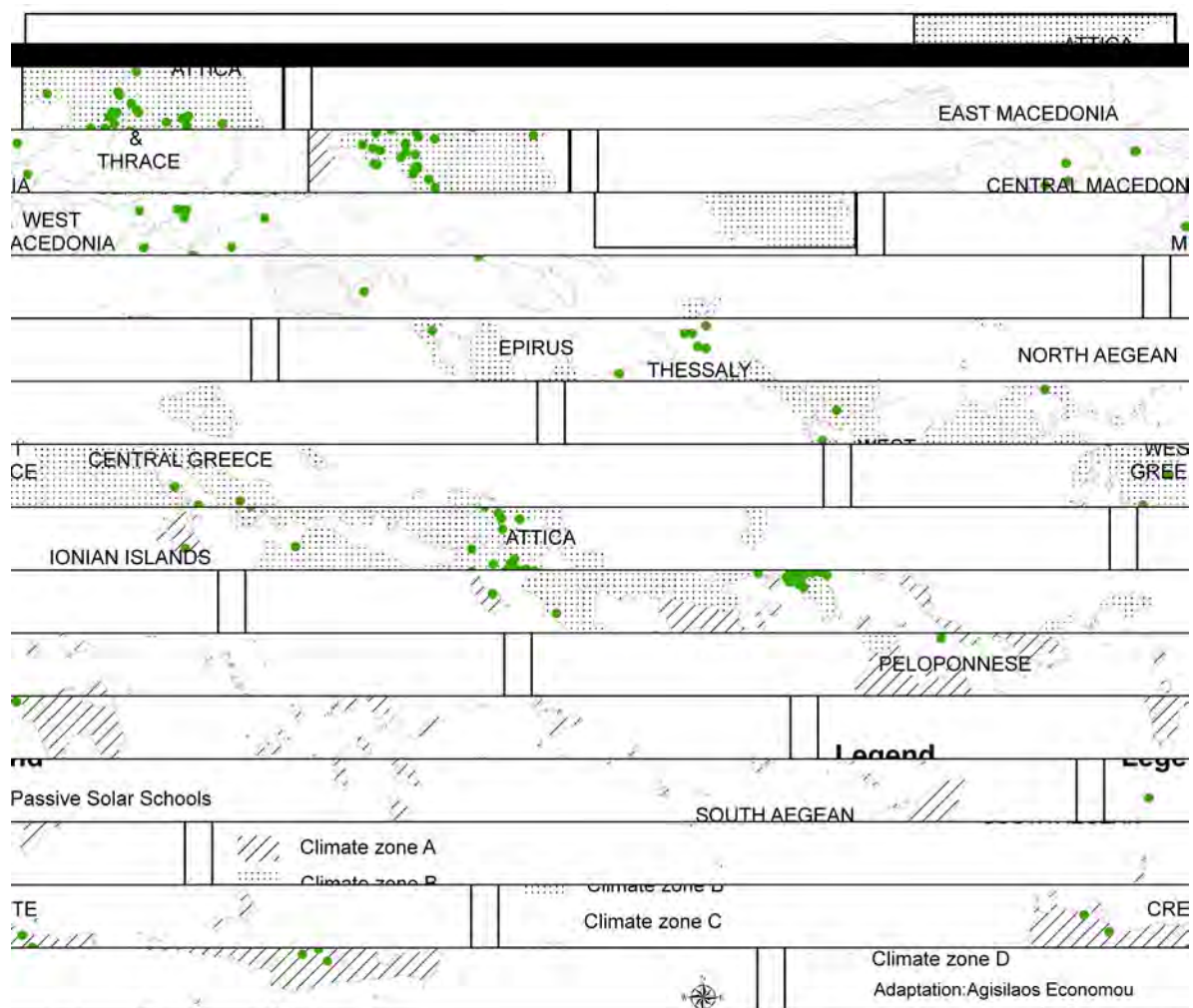


Fig. 1. Passive solar schools in Greece from 2007 up-today.

3.2. Schools units in Athens

As conventional schools, schools in Athens which are listed in the table below have been selected (Fig. 2), (Table 1). On the other hand, from the new modern schools the 6th Nursery school in Paleo Faliro, which is the first school designed with passive systems was selected. It features specific provisions for sun protection, shading, ventilation with carbon dioxide sensors to upgrade and clean the air, greenhouse and two green roofs. Also, it has lighting

control systems which take into account the sunshine outside and for heating, natural gas is used. Also a photovoltaic systems has been installed on the school for electricity production.

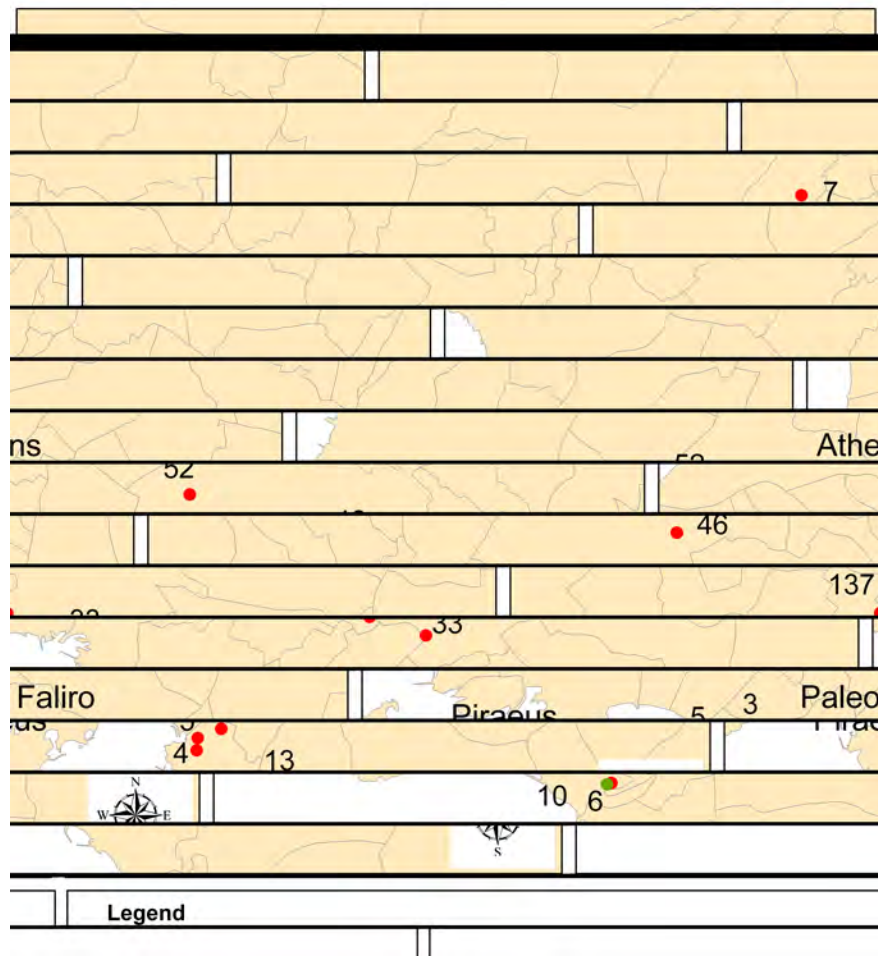


Fig. 2. Schools units in Athens

The survey found that in conventional school units there are different levels of consumption, depending on heat insulation and on the time period during which the boiler is operating for heating purposes.

In contrast in the 6st nursery school of Paleo Faliro (passive solar) a significant decrease in fuel consumption, compared to other schools in the same period was found.

Similar reductions were made to other schools in the past. For example, in the school unit of A. Kapon in Andros in 1989, which has an area of 513.5 m² with Tromble walls and 10 cm polystyrene insulation, the consumption was 12.36 Kwh/m². While in the school unit of I. Kalligeris in Rethymno in 1987, which has an area of 893.7m², through the use of greenhouses and shading, the consumption was at 6.73 Kwh/m². [8]. In other school units systems for solar gain, solar terraces, double glazing and others have been implemented.

Table 1. Use of natural gas for heating in school units in Athens during the period time 9/2009-8/2010 [9,10]

Schools units	Year of construction	Total floor area (m ²)	Total volume of building	Consumption of natural gas (Kwh)	(Kwh/ m ²)
46 High School of Athens	1917	2698.00	9421.00	70990.85	26.31
52 High School of Athens	1970	2714.45	9734.35	50091.29	18.45
7 Secondary of Metamorfosi	1980	1244.00	4552.00	62691.07	50.39
33 High School of Athens	1984	2451.07	12429.12	42235.80	17.23
5 High School of Paleo Faliro	1986	3835.80	7448.85	42012.18	10.95
13 Secondary of Paleo Faliro	1992	1896.24	7600.00	48663.39	25.66
3 Nursery of Paleo Faliro	1993	210.50	800.00	5444.56	25.86
137 Secondary of Athens	1993	1626.00	5962.00	36700.86	22.57
10 Secondary of Paleo Faliro	1995	1700.00	6652.00	38724.61	22.77
4 High School of Paleo Faliro	2000	3835.80	7448.85	21728.73	5.66
6 Nursery of Paleo Faliro	2005	600.20	2640.90	3063.00	5.10

Also, the use of natural gas in the schools units has further reduced the emissions of CO₂ in contrast to oil (Table 2)

Emission of CO₂, natural gas 0.20 kg/kWh, diesel fuel oil 0.26 kg/kWh) [11]

4. Discussion

Fuel consumption for heating of school grounds, varies depending on:

The climatic conditions of each region: Based on heating degree days and altitude, we have four climatic zones. From the hottest to the coolest (Fig. 1).

Heating time: The duration of the heating season ranged from 60 days to the region of Crete and reaches 210 days in the areas of Macedonia and Thrace [5].

Heat insulation: The heat insulation of buildings and the way of construction such as the orientation of the building, insulation of walls, floors and roofs, thermal insulation materials used and the use of openings.

Also, many schools and big complexes are attached to the operation of one boiler, which means that the above operation of a school or a department requires the operation of the boiler for more time as a result of which school units are heated unnecessarily.

Nowadays, in conventional schools interventions are made in order to increase the insulation during the winter and to ensure sun protection, ventilation and cooling during the summer months.

Table 2. Consumption in school units and emission of CO₂

Schools units	Consumption of natural gas[10] (Kwh)	Emission of CO ₂ (ton) (if we used natural gas) (ton)	Emission of CO ₂ (if we used oil) (ton)
46 High School of Athens	70990.85	14.19	18.45
5 High School of Paleo Faliro	50091.29	10.01	13.02
7 Secondary of Metamorfofi	62691.07	12.53	16.30
33 High School of Athens	42235.8	8.44	10.98
5 High School of Paleo Faliro	42012.18	8.40	10.92
13 Secondary of Paleo Faliro	48663.39	9.73	12.65
3 Nursery of Paleo Faliro	5444.56	1.08	1.41
137 Secondary of Athens	36700.86	7.34	9.54
10 Secondary of Paleo Faliro	38724.61	7.74	10.06
4 High School of Paleo Faliro	21728.73	4.34	5.64
6 Nursery of Paleo Faliro	3063	0.61	0.79

The above data shows (Table 1) that new schools planned in accordance with the principles of bioclimatic design and new energy saving measures, require less energy to operate than conventional schools.

In addition, the use of natural gas has reduced energy consumption due to the higher calorific value of gas compared to oil. Even the use of renewable energy sources in new school units it will contribute more to the protection of the environment.

5. Conclusions

New school units require less energy than conventional schools. An important role in energy consumption is played by the location of the school unit, thermal insulation as well as the use of passive solar systems. As it turned out, the implementation of new laws on heat insulation has increased significantly the reduction of energy consumption.

The survey showed that the existing conventional schools who consume large amounts of energy, are in need of improvement.

Also, the use of renewable energy sources such as photovoltaic systems, saves important natural resources, while the introduction of geothermal energy to schools, will reduce energy consumption even further.

Conclusively, not only do passive solar schools contribute to energy consumption reduction, but they also contribute to the conservation of natural resources and the reduction greenhouse gases emissions to the atmosphere. Nowadays, new techniques applied in schools and new energy-saving systems create a new field of research in the forthcoming years.

References

- [1] Official Journal of the Hellenic Republic, 362/D/07.04.1979, pp.3960-4035
http://www.et.gr/search_publication
- [2] Official Journal of the Hellenic Republic, 880/B/19.08.1998, pp.10071-10077
http://www.et.gr/search_publication
- [3] Commission of the European Communities, Directive 2002/91/EC of the European Parliament and of the Council of 16 December on the energy performance of buildings, OJ, L1/65, Brussels, 2003, pp. 1-7.
- [4] Official Journal of the Hellenic Republic, 89/19.05.2008, pp.1371-1377
http://www.et.gr/search_publication
- [5] Official Journal of the Hellenic Republic, 407/B/09.04.2010, pp.5333-5346
http://www.et.gr/search_publication
- [6] Official Journal of the Hellenic Republic. 95/A/23.06.2010, pp.1955-1964
http://www.et.gr/search_publication
- [7] Ministry of Environment Energy & Climate Change/ Directorate of Urban Affairs and Housing – Center for Renewable Energy Sources (CRES), Action Plan for energy saving in residential sector "Energy 2001", 1995.
- [8] E. Lazari, Center for Renewable Energy Sources (CRES), Bioclimatic Design in Greece: Energy efficiency and guidelines for implementation, Pikermi, 2002, pp.1-40.
- [9] SBO (School Building Organization S.A.), Statistics Data Units 2007-2010, Athens, 2010.
- [10] EPA, Provider of natural gas, Statistical Data on natural gas consumption in Attica buildings during the year 2009, Athens, 2009.
- [11] Papanikas D., Natural Gas Technology, Media Guru, M.&Fr. Papanika Editions, Vol I, 2nd edition, Athens, Greece 2007, pp.156-157.

Modeling of the Seawater Greenhouse Systems

G.R. Salehi^{1,*}, M. Ahmadpour², H. Khoshnazar³

¹Islamic Azad University Nowshahr Branch, Nowshahr, Iran

²Islamic Azad University Takestan Branch, Takestan, Iran

³Shiraz university, Shiraz, Iran

* Corresponding author. Tel: +989122031671, E-mail: rezasalehi20@gmail.com

Abstract: The Seawater Greenhouse system uses sunlight, seawater and air to provide freshwater and cooled and humid air, so that in addition to provide the water required for greenhouse, supply more sustainable environmental condition from cultivation of crops in arid coastal regions. In this system ambient air is passed through the two evaporative cooling pads, which plant growth area is placed between those pads, by fans that placed end of the building, and then returned taking humidity on the tube-and-fin condenser. In order to decrease the entrance heating load to the plants, use pipe arrays to provide shade. This paper tries to describe simulation the Seawater Greenhouse considering condition of the Bandar Abbas City in IRAN. it shows that by increasing entrance air relative humidity, the water production and floor temperature increases and the differential temperature decreases. Also with increasing seawater flow rate, the water production increases and differential temperature and floor temperature decreases. With increasing entrance air flow rate, the water production water production and floor temperature decreases and differential temperature increases. Different cycle is developed and investigate in this paper and shows that in cycle that is water exist from first evaporator is passed under the greenhouse floor, is the effective cycle and produces more water than other cycle.

Keywords: Seawater greenhouse, cycle design, condenser

Nomenclature

D	Pipe diameter.....	m	1	Entering air to first evaporator.....
E	Pipe thickness.....	m	2	Entering Water to first evaporator.....
F	Seeing surface.....		3	Water out from first evaporator.....
g	Acceleration due to gravity.....	$m \cdot s^{-2}$	4	Air out from first evaporator.....
h	enthalpy.....	$kJ \cdot kg^{-1}$	5	Entering Water to pipes array.....
h	heat transfer coefficient.....	$W \cdot m^{-2} \cdot K^{-1}$	7	Entering air to growing space.....
I	solar radiation intensity.....	$W \cdot m^{-2}$	8	Air out from roof space.....
k	Thermal conductivity.....	$W \cdot m^{-1} \cdot K^{-1}$	9	Air out from growing space.....
M	mass.....	kg	10	Entering water to second evaporator.....
M^0	flow rate.....	$lits^{-1}$	11	Entering air to second evaporator.....
Nu	Nusselt number.....		12	Water out from second evaporator.....
p	pressure.....	pa	13	Air out from second evaporator.....
pr	Prandtl number.....		14	Entering water to condenser.....
Q	Heat transfer.....	kJ	15	Water out from condenser.....
Re	Reynolds number.....		16	water production.....
T	Temperature.....	K	17	Air out from condenser.....
U	Specific energy.....	$kJ \cdot kg^{-1}$	α	absorptance.....
V	velocity.....	$m \cdot s^{-1}$	ε	Emittance.....
V	viscosity.....	$m \cdot s^{-1}$	φ	Relative humidity.....
V	transmittance.....	$m \cdot s^{-1}$	ω	Water content.....
ω	stefan-boltzmann constant.....	$W \cdot m^{-2} \cdot K^4$		

1. Introduction

The earliest solar distillation plant on record was designed and built in 1872 by Charles Wilson in Chile [1]. It was further developed at the University of Arizona in 1961 in cooperation with the Georgia Institute of Technology and the University of Sonora, Mexico at Puerto Peñasco, New Mexico. A well detailed study about sun fresh water making plans and

policies was investigated [2, 3, 5, 6]. But, the seawater Greenhouse history returned to 1991. The first experimental project started in Tenerife in 1994. This prototype Seawater Greenhouse was planned in England and constructed in Tenerife[7].

The increasing water requesting growth and water providing resources shortage are two certain and predictable problems in 21 century. Now, the great areas in the world suffer from drought. The deserts are developing and in comparison, raining has a fixed movement. While water requesting have been two times in present 20 years, request forwarding from refreshing resources amount is following at the same way. About 70% total water uses are in farming and then water crisis can be review in so close relationship with food materials producing and economy development and creating. Custom and traditional farming which just need few hundred liters water just produces one kg output and it is because of this farming style inefficiency in water management. The farming and its increasing water requesting will be an important pressure point in which seawater Greenhouse will help using and incorporating natural processes in order to provide low-cost resolution for presenting permanent and similar model in arid coastal regions to decrease this pressure. Seawater Greenhouse provides an ambient in which plants sweating is as low as possible. So, Greenhouse produces its needed sufficient water during sun distillation operation.

2. Seawater greenhouse process description

The greenhouse seawater system uses the sun, the sea and the atmosphere to produce fresh water and cooled air to the growth of crops in the greenhouse. The idea of its operation depends on creating the natural water cycle in controlled environment. First seawater pumped into a cold seawater tank after filtration. The seawater pumped to the condenser before reaching the first cooling pad evaporator at the front side of the greenhouse. The seawater greenhouse consist of two evaporator that planting area is located between them. The seawater passes through first evaporator from top to bottom, while air passes perpendicular direction to the flow of water. This evaporator faces the prevailing wind. Also fan assist and control air movement. The humidified and cooled air passes through planting area and combined with hot dry air from the cavity under the roof. The mixture passes through a second evaporator and creating hot saturated air which then flows through the condenser. The seawater is pumped to a pipe array which is installed in the cavity below the plastic cover and warmed up by solar energy and passes through second evaporator from top to bottom. It noted that only small fraction of solar radiation involved in photosynthesis since the roof traps infrared heat while allowing light through to promote photosynthesis. The saturated humid air from second evaporator passes through the condenser which is cooled by seawater flow. The temperature difference creates fresh water to condense out of air stream. The resulting condensate collected for using in irrigation of crops.

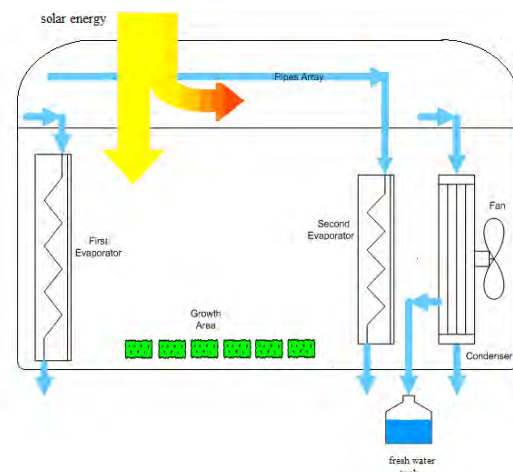


Fig1. Seawater greenhouse process schematic diagram

3. Modelling and Optimisation

Seawater greenhouse is consist of two evaporator, which is planting area located between them, condenser, and pipe array, which is feed the second evaporative pad through water which heated by the sun, is located in cavity under the greenhouse plastic cover. In analyzing the green house all of these parts must be modeling.

The first evaporator:

Energy and mass balance for evaporator cooling pad in the front of greenhouse gives:

$$\dot{m}_1 h_1 + \dot{m}_2 h_2 = \dot{m}_3 h_3 + \dot{m}_4 h_4 \quad (1)$$

$$\dot{m}_1 + \dot{m}_2 = \dot{m}_3 + \dot{m}_4 \quad (2)$$

The entrance air mass obtained with equation 3:

$$\dot{m}_{Air} = \frac{\dot{m}_1}{1 + \omega_1} \quad (3)$$

The evaporative water amount will take from:

$$\dot{m}_4 - \dot{m}_1 = \dot{m}_{Air} (\omega_4 - \omega_1) \quad (4)$$

$$h_1 = f(T_1, P_{Ambient}, \omega_1) \quad (5)$$

$$\omega_1 = f(T_1, P_{Ambient}, \varphi_1) \quad (6)$$

$$h_2 = f(T_2, P_{Ambient}) \quad (7)$$

$$h_3 = f(T_3, P_{Ambient}) \quad (8)$$

$$T_4 = f(h_4, P_{Ambient}, \varphi_4) \quad (9)$$

$$\omega_4 = f(T_4, P_{Ambient}, \varphi_4) \quad (10)$$

The growth area:

Air after passing through the evaporator enters the growth space. Before air entering in plants growth space, part of it directs to the space in up. This part has an important role in freshwater production and simulate as follow:

The roof:

$$\alpha_{Body} I - h_{Out} (T_{Roof} - T_1) - h_{Up} (T_{Roof} - T_{Up}) - F_{Roof.Pipe} \cdot \sigma \cdot \varepsilon_{Body} (T_{Roof}^4 - T_{Pipe}^4) - F_{Roof.Sky} \cdot \sigma \cdot \varepsilon_{Body} (T_{Roof}^4 - T_{Sky}^4) = 0 \quad (11)$$

The left:

$$\alpha_{Body} I - h_{Out} (T_{Left} - T_1) - h_{Down} (T_{Left} - T_{Down}) - F_{Left.Pipe} \cdot \sigma \cdot \varepsilon_{Body} (T_{Left}^4 - T_{Pipe}^4) - F_{Left.Sky} \cdot \sigma \cdot \varepsilon_{Body} (T_{Left}^4 - T_{Sky}^4) - F_{Left.Floor} \cdot \sigma \cdot \varepsilon_{Body} (T_{Left}^4 - T_{Floor}^4) = 0 \quad (12)$$

The right:

$$\alpha_{Body} I - h_{Out} (T_{Right} - T_1) - h_{Down} (T_{Right} - T_{Down}) - F_{Right.Pipe} \cdot \sigma \cdot \varepsilon_{Body} (T_{Right}^4 - T_{Pipe}^4) - F_{Right.Sky} \cdot \sigma \cdot \varepsilon_{Body} (T_{Right}^4 - T_{Sky}^4) - F_{Right.Floor} \cdot \sigma \cdot \varepsilon_{Body} (T_{Right}^4 - T_{Floor}^4) = 0 \quad (13)$$

Pipes carrying seawater:

$$\alpha_{Pipe} \cdot \rho_{Body} \cdot I - h_{Pipe} (2T_{Pipe} - T_{Up} - T_{Down}) - F_{Pipe,Left} \cdot \sigma \cdot \varepsilon_{Pipe} (T_{Pipe}^4 - T_{Left}^4) - F_{Pipe,Right} \cdot \sigma \cdot \varepsilon_{Pipe} (T_{Pipe}^4 - T_{Right}^4) - F_{Pipe,Floor} \cdot \sigma \cdot \varepsilon_{Pipe} (T_{Pipe}^4 - T_{Floor}^4) - F_{Pipe,Roof} \cdot \sigma \cdot \varepsilon_{Pipe} (T_{Pipe}^4 - T_{Roof}^4) - \frac{2T_{Water} - T_{Up} - T_{Down}}{\frac{1}{h_{Water}} + \frac{e}{k}} = 0 \quad (14)$$

The Floor:

$$\alpha_{Floor} \cdot (\rho_{Body} \cdot \rho_{Pipe} + 2\rho_{Body}) I - h_{Down} (T_{Floor} - T_{Down}) - F_{Floor,Left} \cdot \sigma \cdot \varepsilon_{Floor} (T_{Floor}^4 - T_{Left}^4) - F_{Floor,Right} \cdot \sigma \cdot \varepsilon_{Floor} (T_{Floor}^4 - T_{Right}^4) - F_{Floor,Pipe} \cdot \sigma \cdot \varepsilon_{Floor} (T_{Floor}^4 - T_{Pipe}^4) = 0 \quad (15)$$

The Greenhouse out air h:

$$h_{Out} = \frac{Nu_{Out} \cdot k_{Out}}{L} \quad (16)$$

$$Nu_{Out} = (0.037 Re_{L,Out}^{4/5} - 871) Pr_{Out}^{1/3} \quad (17)$$

$$Pr_{Out} = f(T_1) \quad (18)$$

$$Re_{L,Out} = \frac{V_{Out} \cdot L}{\mu_{Out}} \quad (19)$$

$$\mu_{Out} = f(T_1, P_{Ambient}, \omega_1) \quad (20)$$

$$V_{Out} = \rho_1 \dot{m}_1 \quad (21)$$

$$\rho_1 = f(T_1, P_{Ambient}, \omega_1) \quad (22)$$

$$k_{Out} = f(T_1, P_{Ambient}, \omega_1) \quad (23)$$

The passing water h from the pipes:

$$h_{Water} = \frac{Nu_{Water} k_{Water}}{D_{Pipe}} \quad (24)$$

$$Nu_{Water} = 3.66 + \frac{0.0668 \frac{D_{Pipe}}{L} Pr_{Water} Re_D}{1 + 0.04 (D_{Pipe} Pr_{Water} \frac{Re_D}{L})^{1/4}} \quad (25)$$

$$Pr_{Water} = f(T_{Water}, P_{Ambient}) \quad (26)$$

$$Re_D = \frac{4\dot{m}_{10}}{\pi D_{Pipe} \mu_{Water}} \quad (27)$$

$$\mu_{Water} = f(T_{Water}, P_{Ambient}) \quad (28)$$

$$k_{Water} = f(T_{Water}, P_{Ambient}) \quad (29)$$

In this stage, by taking two control volumes around the Greenhouse up and down space that separating by the pipes carrying seawater, we have the following equations.

$$\dot{m}_6 h_6 + h_{Up}(T_{Roof} - T_{Up}) + h_{Pipe}(T_{Pipe} - T_{Up}) - \dot{m}_8 h_8 = 0 \quad (30)$$

$$\dot{m}_7 h_7 + h_{Down}(T_{Floor} + T_{Left} + T_{Right} - 3T_{Down}) + h_{Pipe}(T_{Pipe} - T_{Down}) - \dot{m}_9 h_9 = 0 \quad (31)$$

$$T_8 = f(h_8, P_{Ambient}, \omega_8) \quad (32)$$

$$T_9 = f(h_9, P_{Ambient}, \omega_9) \quad (33)$$

$$T_{Up} = \frac{1}{2}(T_6 + T_8) \quad (34)$$

$$T_{Down} = \frac{1}{2}(T_7 + T_9) \quad (35)$$

$$T_{Water} = \frac{1}{2}(T_5 + T_{10}) \quad (36)$$

The entering air divided into two branches that flowing down branch has the duty of humidification and cooling of the ambient and the up branch has the duty of by removing the heat gained from sun by pipe arrays and applying it increasing humidity capacity of air in exit. These two branches were mixed by near the second evaporator and caused increasing air temperature and moisture capacity. These combinations write as follow:

$$\phi_{11} = f(T_{11}, P_{Ambient}, \omega_{11}) \quad (37)$$

$$h_{11} = f(T_{11}, P_{Ambient}, \omega_{11}) \quad (38)$$

The second evaporator:

This evaporator analyzes such as the first one

Condenser:

According figure 3, the governing equations are as following:

$$\dot{m}_{13}h_{13} + \dot{m}_{14}h_{14} = \dot{m}_{15}h_{15} + \dot{m}_{16}h_{16} + \dot{m}_{17}h_{17} \quad (39)$$

$$\dot{m}_{13} - \dot{m}_{17} = \dot{m}_{Air}(\omega_{13} - \omega_{17}) \quad (40)$$

$$\dot{m}_{13} = \dot{m}_{16} + \dot{m}_{17} \quad (41)$$

$$h_{14} = f(T_{14}, P_{Ambient}) \quad (42)$$

$$T_{15} = f(h_{15}, P_{Ambient}) \quad (43)$$

$$h_{16} = f(T_{16}, P_{Ambient}) \quad (44)$$

$$\omega_{17} = f(T_{17}, P_{Ambient}, \phi_{17}) \quad (45)$$

$$h_{17} = f(T_{17}, P_{Ambient}, \omega_{17}) \quad (46)$$

Finally, all of these equations stimulate and solved by EES program.

4. Result and conclusion

Bandar Abbas have chosen as stimulation reference, and was simulated based on the following the following conditions[8]:

$$P_{Ambient} = 100KPa, V_{Out} = 10m/s, I = 250W/m^2, L = 42m, \phi = 0.64, \dot{m}_1 = 20kg/s, \dot{m}_2 = 3Lit/s$$

Figure 2 shows the difference temperature between the inlet and outlet of the first evaporator as function of the mass flow rate and relative humidity of entrance air. With increasing mass flow rate, Re and h was increased and it caused more evaporation and the temperature of air was decreased.

Figure 3 shows the difference temperature between the inlet and outlet of the first evaporator as function of the mass flow rate of sea water and the relative humidity of entrance air. As shown in the figure, the more increasing mass flow is lead to the more decreasing temperature drop. Furthermore, the more increasing humid, the more decreasing temperature difference. Figure 4 shows water producing according to entrance air mass flow and various air humid. As you see in this figure, entrance air increasing has affected water producing tendency increasingly and has had an important step toward its decrease.

Figure 5 shows water producing mass flow based on seawater mass flow and various airs humidity. As have shown seawater mass flow increasing causes differential temperature dropping, then more warm air goes to the roof and its entrance will be warmer and caused the exit water will be warmer, this increases water inclination to evaporation and humid absorbing more. These events in addition to warmer air gets condense better in condenser will increase producing water in it and also we see clearly increasing in seawater mass flow will increase the producing water.

Figure 6 shows the temperature of Greenhouse floor as a function of seawater mass flow and various airs humid. It is cleared that the increasing water producing mass flow has increased soil temperature. It happens more in much humid

Figure 7 shows Greenhouse floor temperature based on entering air mass flow and various air humid. As have considered, increasing entrance air mass flow will decrease the outlet temperature of the first evaporator, and it results in more heat transfer to greenhouse floor and

decrease its temperature. In addition, entrance air mass flow increase affects Re and Nu and increasing h and absorbs multiple heat, so we can say the higher humid will be as the same as more soil temperature. As we see in this figure, entrance mass flow increasing has decrease heat, and more humid, will increase Greenhouse floor in a certain air mass flow.

The difference cycles was simulated here to find the optimum cycles in this Greenhouse. The stimulations were done according the Bandar Abbas conditions. The first cycle which has shown by C1 in the figures, is the simplest one and the other plan is based on changes changes in this plan. C2 is a plan for decreasing the greenhouse floor temperature. The air which exits the condenser will be passed the under of the growth space in order to decrease Greenhouse floor temperature. C3 is a similar plan with the same goal by another approach. In this cycle, the water which exit the first evaporator is passed the under of Greenhouse floor space, like previous plan, for decreasing the temperature. C4, C5 and C6 have considered in order to low cost and each of them includes these changes: condenser feeding from the first evaporator exit water, pipes array feeding through condenser exit and finally pipes array feeding by the second evaporator exit. Now, we study these graphs in detail: Considering present cycles we can see with increasing humidity the water producing was increased. Another important result will obtain from this graph is $C3 > C2 > C6 > C5 > C4 > C1$

Figure 8 shows water producing in different cycles according to various air humid, and describe cycle 3 is the best in water production and providing pleasure heat for greenhouse floor (in this way and through thermal transmitting increasing to the air produces water) and also says condenser feeding through exit water from operator just low cost and hasn't so profits in water producing. Figure 9 shows water producing in different cycles based on various entrance air mass flow rate. This graph interpretation is like graph 8 and the alone point which isn't mentioned is in all cycles increasing entrance air mass flow water producing is decreased. Figure 10 shows the location of different places in basic cycle.

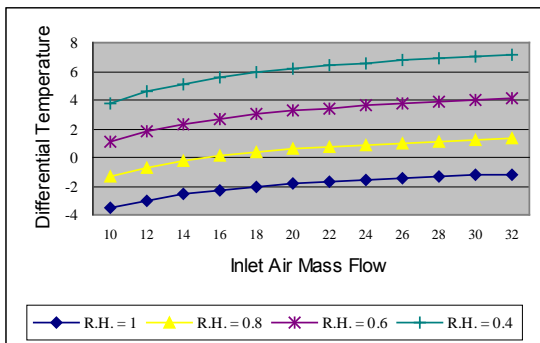


Fig 2- effect of heat inlet mass flow in Diff. T.

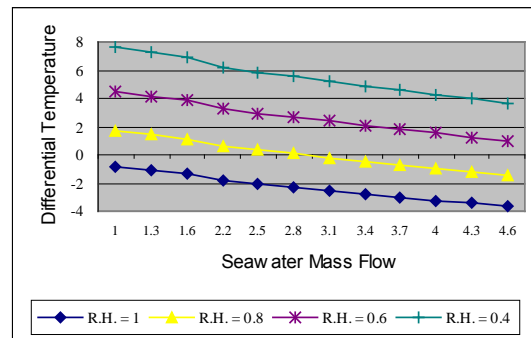


Fig 3- effect of sea water mass flow in Diff. T

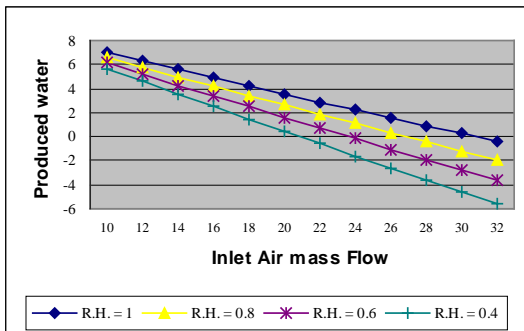


Fig 4- effect of inlet mass flow in produced water

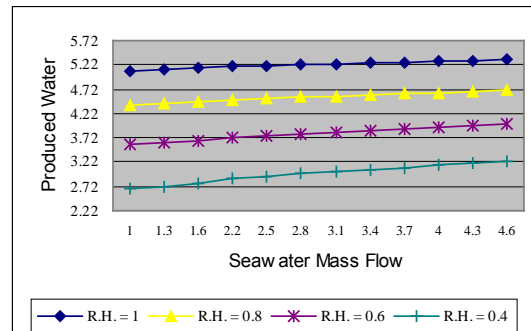


Fig 5- effect of sea water mass flow in produced water

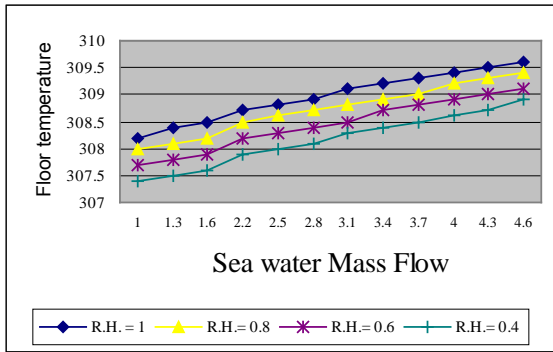


Fig 6-effect of sea water mass flow on floor temp.

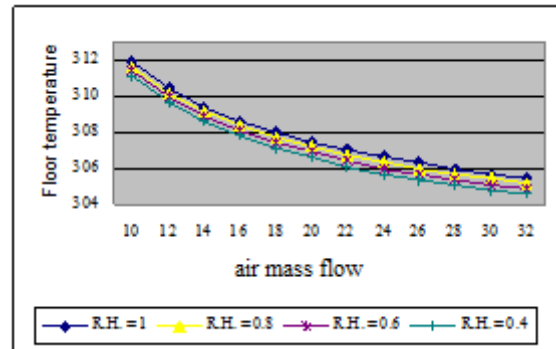


Fig 7-effect of air mass flow on Floor Temperature

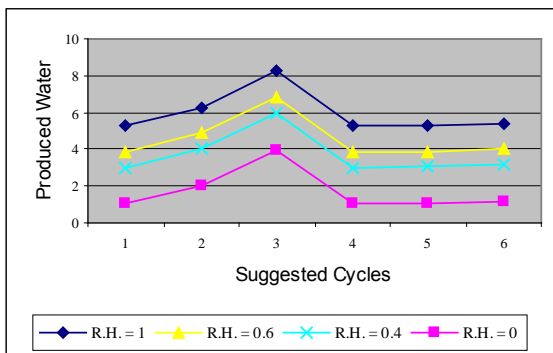


Fig 8- effect of suggested cycles in produced water

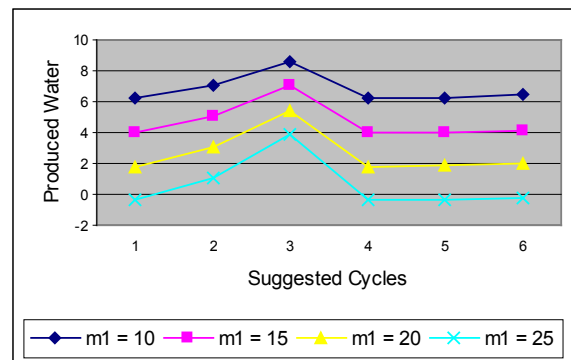


Fig 9- effect of suggested cycles in produced water in mass

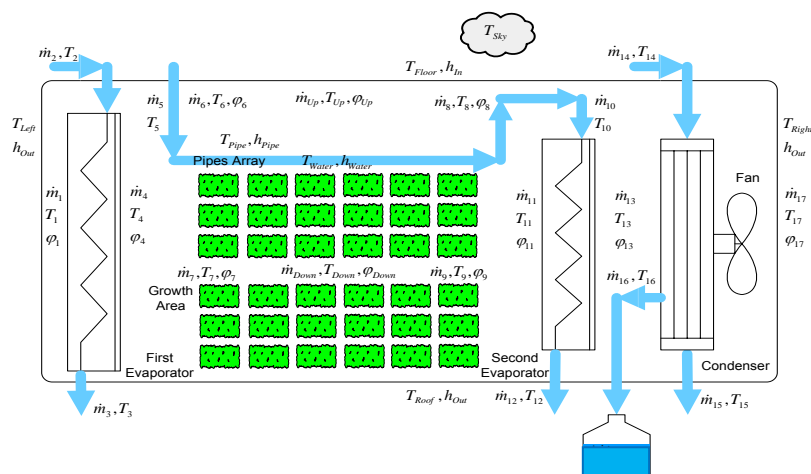


Fig 10. Location of basic cycle

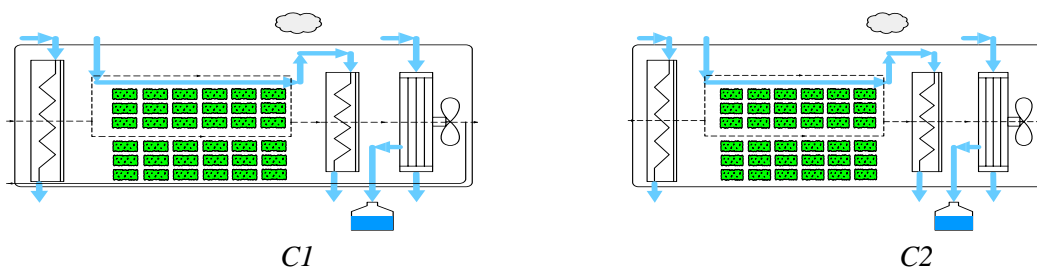


Fig 11. Location of different places in basic cycle

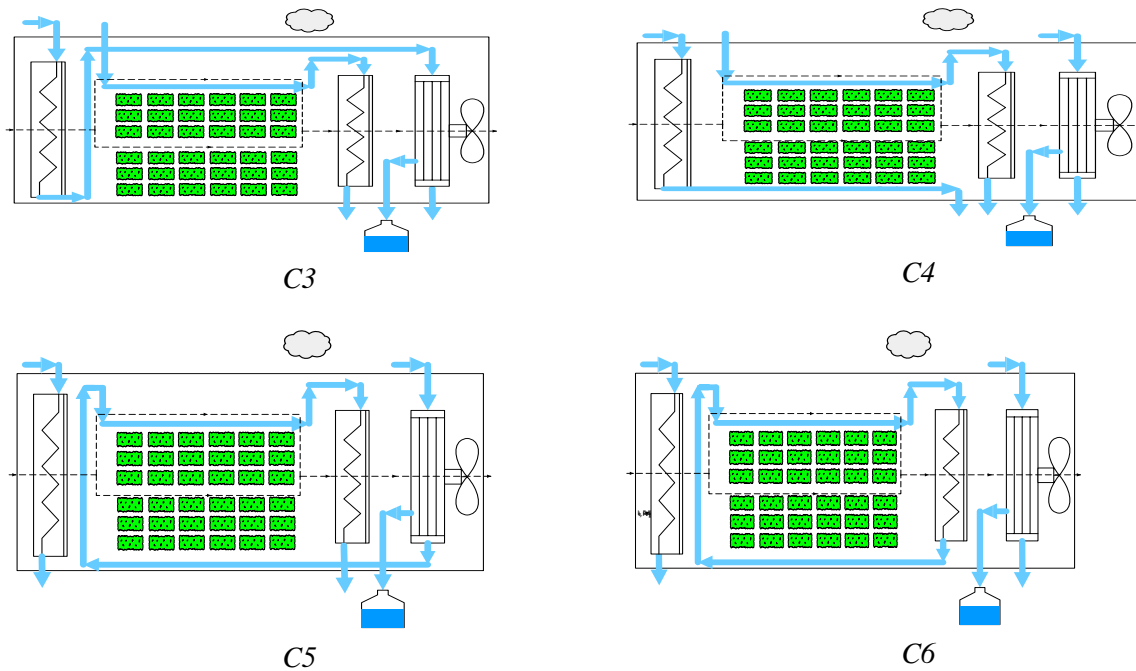


Fig 11. continue

5. Conclusion

The seawater greenhouse was investigated in the Bandar Abass wether conditions.it shows that by increasing entrance air relative humidity, the water production and floor temperature increases and the differential temperature decreases. Also with increasing seawater flow rate, the water production increases and differential temperature and floor temperature decreases. With increasing entrance air flow rate, the water production water production and floor temperature decreases and differential temperature increases. Also different cycle is developed and investigates in this paper and shows that in cycle C3 which is water exist from first evaporator is passed under the greenhouse floor, is the effective cycle and produces more water than other cycle.

References

- [1] Talbert, S. G., Lof, C-M Wong and E. N. Sieder, 1970. Manual on solar
- [2] Yadav. Y. P. and L. K. Jha, 1989. A double-basin solar still coupled to a collector and operating in the thermo siphon mode. *Energy*, 14(10): 653–659.
- [3] Hamed, O. A., E. I. Eisa and W. E. Abdullah, 1993.Overview of solar desalination. *Desalination*, 93: 563–579.
- [4] Farid, M. M. 1999.Recent developments in solar desalination. In: *Water Management, Purification and Conservation in Arid Climates. Vol. II. Water Purification.* M. F. A.
- [5] Goosen and W. H. Shayya. Technomic Publishing Co., Lancaster, PA, pp. 277–296.
- [6] Goosen, M. F. A., S. S. Sablani, W. H. Shayya, C. Paton, and H. Al-Hinai, 2000.Thermodynamic and Economic considerations in solar desalination. *Desalination*, 129: 63–89.
- [7] Paton, A. C. and P. A. Davis, 1996. International Engineering Conference (IEC) “Mutah 2004”, Mutah University, JORDAN, April 26-28. Pages 523-540.
- [8] Data Processing Center, Annual Weather Report of the Year 2000

An exergy based unified test protocol for solar cookers of different geometries

Naveen Kumar^{1*}, G. Vishwanath¹, Anurag Gupta¹

¹ IITD&M Kancheepuram, IIT Madras Campus, Chennai-600036, Tamil Nadu, India.

* Corresponding author. Tel: +914422578555, Fax: +914422578555, E-mail: nkumar@iitdm.ac.in

Abstract: It is good for the consumer to have solar cookers of various varieties in terms of geometrical designs, performance and price but it is a challenge to develop a uniform test standard for evaluating the thermal performance of the cookers irrespective of their geometrical construction. Due to the lack of uniform test protocol, consumer cannot compare the quantitative performance of the cookers of different configuration and become confused. For this end, we plotted graphs between exergy output and temperature difference, for solar cookers of different designs and it resembled a parabolic curve for each design. The peak exergy (vertex of the parabola), can be accepted as a measure of devices' fuel ratings. The ratio of the peak exergy gained to the exergy lost at that instant of time can be considered as the quality factor of the solar cooker. Besides, the exergy lost is found to vary linearly with temperature difference irrespective of the topology of the device and the slope of the straight line obtained through curve fitting represents the heat loss coefficient of the cooker. The proposed parameters can lead to development of unified test protocol for solar cookers of diversified designs.

Keywords: Solar Cookers, Test Protocol, Exergy Analysis

Nomenclature

A	gross area of glazing surface..... m^2	G	instantaneous solar insolation..... W/m^2
c	specific heat capacity of water $J/kg K$	m	mass of water..... kg
E_o	output energy J	T_{am}	instantaneous ambient temperature K
E_{Xi}	input exergy kJ	T_f	final water temperature..... K
E_{Xo}	output exergy kJ	T_i	initial water temperature..... K
F_1	first figure of merit..... $m^2 K/W$	T_s	surface temperature of sun..... K
F_2	second figure of merit	Δt	time interval..... s

1. Introduction

Solar cookers are a very useful and popular thermal device which is available throughout the world. It is one of the few renewable energy thermal gadgets which are portable, user friendly, easily operable, meant to fulfil the very basic need and economically competitive. Its affordable price makes it very attractive commercially, especially among the rural populace in the developing countries. In order to meet the demands of broad spectrum of the society and penetrate the market, different novel varieties of solar cookers have become available in accordance with peoples' need and purchasing capacity. Solar box type cookers (SBC) are available for domestic as well as community based applications. Similarly, SK-14, SK-10 and Scheffler paraboloid type concentrating cooker are also present in the market for fast cooking for domestic/community and industrial applications. In addition parabolic trough type concentrating cookers are being reported in recent studies for both domestic as well as community type applications. Depending on the topology of the cooker construction, different test procedures and thermal indicators have been established, which act as benchmark thermal performance evaluators for various geometrical varieties of the cooker. On one hand it is good for the customer to have solar cookers of diversified designs in terms of geometry, performance and price but on the other hand it is a challenge to develop a uniform test standard for evaluating the thermal performance of the cookers irrespective of their geometrical construction. In the absence of such unified test/standard protocol, it is very confusing for the customer to compare the performance of these devices. In addition, to

promote renewable energy technologies (RETs), many governments throughout the world, are adopting environment friendly policies. This includes the provision of providing direct/indirect subsidies and other benefits to the user on the usage of the RETs. Many a times, manufacturers are not able to receive the subsidy benefits because the parameters set for eligibility criterion matches one design of solar cooker and not the others. Through the present manuscript, we propose an exergy based unified test protocol for solar cookers of different geometries. In this protocol, the test methodology for conducting full load test for solar cookers remains the same but the analyzing procedure has been altered so as to fulfill the above necessities. In order to develop a realistic and unified test protocol, we utilize the reported data from different well known published manuscripts and analyze it comprehensively to cater to the above mentioned needs.

2. Methodology

In order to test the performance of the solar box type cooker, two figures of merit (FOM) viz. F_1 and F_2 are generally calculated, as given by Mullick [1]. The first FOM, F_1 is defined as the ratio of optical efficiency to the heat loss factor by bottom absorbing plate and is a measure of the differential temperature gained by the absorbing plate at a particular level of solar insolation. The second FOM, F_2 is more or less independent of climatic conditions and gives an indication of heat transfer from absorbing plate to the water in the containers placed on the plate. Bureau of Indian standards have also accepted these parameters as performance indicators for SBC [2]. However, as per international test protocol for solar box cookers, the performance should be estimated in terms of its standardized cooking power as given by Funk [3], which is calculated through extrapolation of the curve/data. The value of the cooking power determined through this procedure comes out to be high and does not represent the actual cooking potential of the cooker. Internationally, the procedure for measuring the efficacy of cooking of solar cookers based on parabolic trough and Scheffler concentrating type topology is not very well known, nevertheless Scheffler concentrators are generally employed for very large scale cooking/industrial operations. As per Ministry of New and Renewable Energy (India), thermal performance of SK-14/SK-10 type cookers should be determined by its heat loss factor, optical efficiency and cooking power [4]. In all above mentioned thermal performance evaluation processes, energy based approach is employed. But, the benchmark parameters derived from the energy based method does not provide complete information and are inadequate performance indicators because their values can be misleadingly high or low depending on the temperature difference between source and sink, even though input energy condition may remain same. Exergy is a measure of the potential of the system to extract heat from the surroundings, as the system moves closer to the equilibrium with its environment [5]. After the system and the surroundings reach equilibrium, the exergy becomes zero. In the present manuscript, we would take the case of each of the different solar cookers of the above mentioned geometries and apply the exergy based approach so as to reach a holistic/uniform approach for deciding the common thermal indicators irrespective of the cooker design topology. The exergy of solar radiation, as the exergy input E_{Xi} to the solar cooker, can be calculated using the available solar energy flux (GAt) and is expressible through Eq. (1) which has the widest acceptability [5, 6].

$$E_{Xi} = G \left[1 + \frac{1}{3} \left(\frac{T_{am}}{T_s} \right)^4 - \frac{4T_{am}}{3T_s} \right] A \Delta t \quad (1)$$

where T_{am} is instantaneous ambient temperature, T_s is surface temperature of sun, G is instantaneous solar insolation, A is aperture area of cooker, and Δt is time interval. The sun's black body temperature of 5762 K results in a solar spectrum concentrated primarily in the 0.3–3.0 μm wavelength band [5, 7, 8]. Although the surface temperature of the sun (T_s) varies due to the spectral distribution of sunlight on the earth's surface, the value of 5800 K has been considered for the T_s . The energy gained by water in the vessel, kept inside the cooker, due to rise in temperature can be considered as the output energy (E_o) of the system and is mathematically given as

$$E_o = mc(T_f - T_i) \quad (2)$$

In the expression above, the output energy depends only on the difference in initial and final values of temperatures ($T_f - T_i$) but in actual practice, ambient temperature as well as the initial and final temperature values also play the role in deciding the efficiency of the system, and this kind of qualitative effect can not be accommodated in the energy based approach. The exergy gained by water in the vessel kept inside the cooker due to rise in temperature can be considered as the output exergy (E_{x0}) [5, 6, 7, 9] of the system and is expressible through

$$E_{x0} = E_o - mcT_{am} \ln \frac{T_f}{T_i} \quad (3)$$

The beauty of the exergy analysis/approach is self evident in the expression above as it considers the effect of ambient temperature as well as the absolute values of initial and final temperature in addition to ($T_f - T_i$). The second term on the right hand side of this expression signifies the exergy losses elucidating the true potential of the system in converting the input energy. Thus, exergy analysis is a more complete synthesis tool because it accounts for the temperatures associated with energy transfers to and from the cooker, as well as the quantities of energy transferred, and consequently provides a measure of how nearly the cooker approaches ideal efficiency. Here, we propose to plot a graph between output exergy power and temperature difference and fit the data points with second order polynomial; temperature difference is the difference in the instantaneous water temperature and ambient temperature. From the fitted curve, it is easier to obtain the peak value of exergy, which is very near to the actual value of the peak exergy. The temperature difference gap corresponding to the half exergy points of the curve can be determined. The exergy lost during the test period can also be plotted against temperature difference so as to estimate the overall heat loss coefficient of the cooker. In order to determine the above mentioned parameters, we are taking the data from various manuscripts for each of the different solar cookers geometries.

3. Results and Discussion

Four different geometries of solar cookers are considered for depicting their thermal performance on the basis of exergy based parameters. These geometries are domestic box type cooker, domestic SK-14 type cooker, Scheffler community type cooker, parabolic trough type cooker. The proposed four exergy based parameters, which can be considered as the benchmark indicators of the performance of the cookers are as follows, (i) Peak Exergy, (ii) Quality factor, (iii) Exergy temperature difference gap product, (iv) Heat loss coefficient. Peak exergy is the highest/maximum exergy output power obtained through curve fitting by plotting the graph between exergy output power and temperature difference. This can be realistically considered as a measure of its fuel ratings. The ratio of the peak exergy gained to the exergy lost at that instant of time can be considered as the quality factor of the solar cooker. A higher quality factor is always desirable. The product of the temperature

difference gap corresponding to the half power points and the peak exergy power can also be considered to be another benchmark indicator in this kind of analysis. Higher temperature difference gap means the lesser heat losses from the cooker. This kind of scheme is generally considered in electronics for expressing the performance of a BJT amplifier, as gain bandwidth product and also a quality factor in case of a notch/band pass filter. The heat loss coefficient of the device can be calculated by dividing the value of the slope of the line, obtained through linear curve fitting of exergy lost variations with temperature difference, by the value of glazing/focal area. In this approach, we are not dependent much on extrapolation and all the parameters were realistically calculated from the graphs/data. Calculations of the above mentioned topologies of the solar cooker are described in the subsequent sub-sections.

3.1. Domestic solar box type cooker

The variation in the exergy output as a function of temperature difference for domestic SBC of aperture area 0.25 m^2 is presented in Fig. 1, which depicts the case when the amount of water inside the cooking vessels/pots is 2.5 Kg. The maximum exergy power obtained through curve fitting is 6.46 W and the temperature difference gap corresponding to the half power points is 46.2 K. The peak exergy and temperature difference gap product for this case is found to be 298.5 WK. The experimental data, for performing calculation and obtaining the thermal parameters, is taken from Kumar [11].

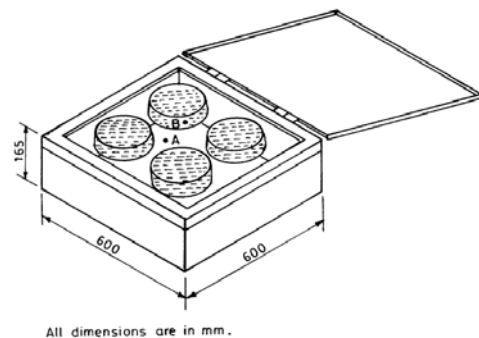
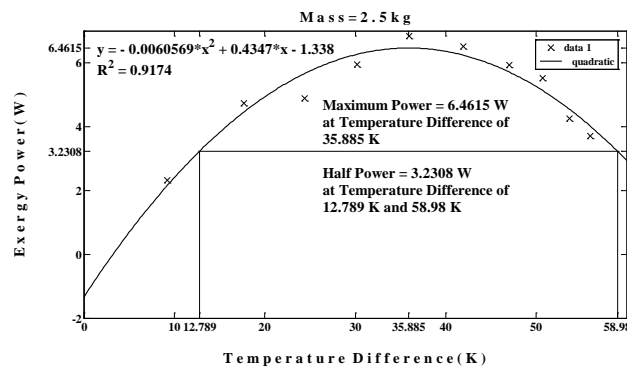


Fig. 1. Variation of Exergy output power with Temperature Difference for Domestic SBC with its schematics.

The curve between the exergy lost v/s temperature difference is plotted in Fig. 2. Heat loss coefficient is obtained by dividing the slope of the curve (which depicts the exergy lost per change in temperature, i.e., W/K), by the gross aperture area. The heat loss coefficient and quality factor, for 2.5 kg mass of water, are found to be 5.24 W/K m^2 and 0.123, respectively. The specific heat loss coefficient for this cooker is found to be $2.096 \text{ W/K m}^2 \text{ kg}$.

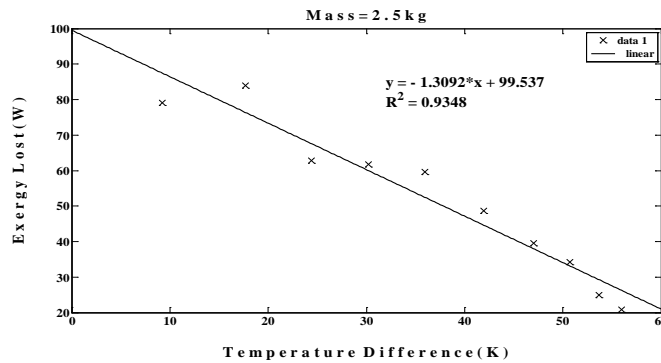


Fig. 2. Variation of Exergy power lost with Temperature Difference for Domestic SBC.

3.2. SK-14 type cooker

The variation in the exergy output as a function of temperature difference for domestic SK - 14 type of gross aperture area 1.47 m^2 and a focal area of 0.134 m^2 is presented in Fig. 3, which depicts the case when the amount of water inside the cooking vessels/pots is 5 Kg. The reflective area of the cooker is 1.47 m^2 with its focal length equal to 0.28 m. The maximum exergy power obtained through curve fitting is 18.21 W and the temperature difference gap corresponding to the half power points is 40.374 K. The peak exergy and temperature difference gap product for the two cases is found to be 735.3 WK. The experimental data, for performing calculation and obtaining the thermal parameters, is taken from Kaushik [7]. The curve between the exergy lost v/s temperature difference is plotted in Fig. 4. The heat loss coefficient and quality factor, for 5 kg mass of water, are found to be 40.35 W/K m^2 and 0.106, respectively. The specific heat loss coefficient for this cooker is found to be $8.07 \text{ W/K m}^2 \text{ kg}$.

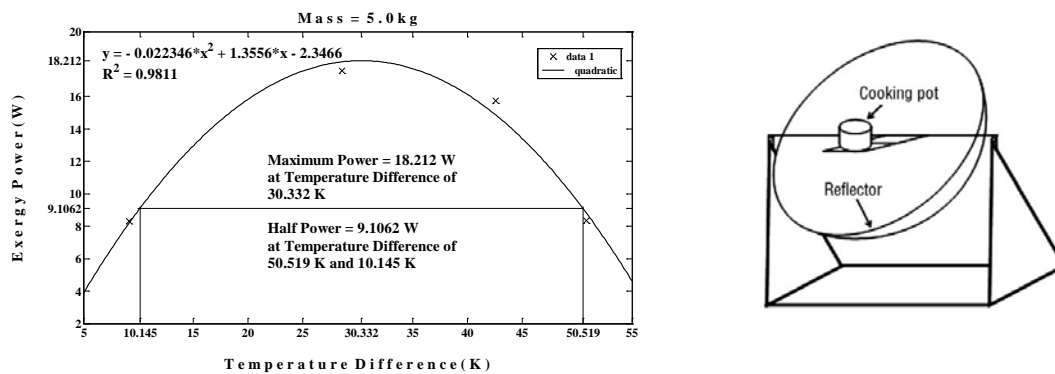


Fig. 3. Variation of Exergy output power with Temperature Difference for SK-14 type cooker with its schematics.

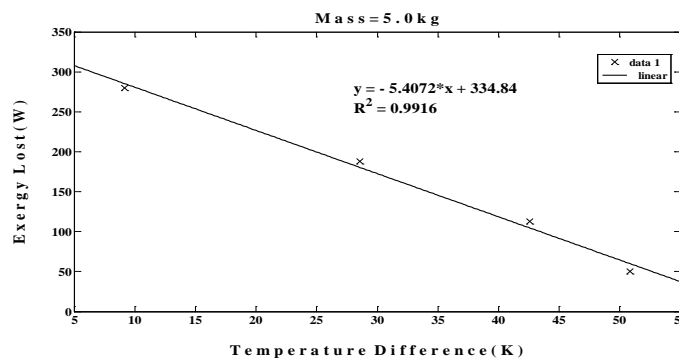


Fig. 4. Variation of Exergy power lost with Temperature Difference for SK-14 type cooker.

3.3. Scheffler Community type cooker

The variation in the exergy output as a function of temperature difference for Scheffler community type of gross aperture area 8.21 m^2 and a secondary focal area of 0.36 m^2 is presented in Fig. 5, which depicts the case when the amount of water inside the cooking vessels/pots is 20 Kg. The primary reflector area of the concentrator is 7.3 m^2 with aperture diameters of 3.8 m lengthwise and 2.75 m widthwise and has depth of 0.3 m. The reflective area of secondary reflector is 0.36 m^2 . The maximum exergy power obtained through curve fitting is 55.75 W and the temperature difference gap corresponding to the half power points is 39.62 K. The peak exergy and temperature difference gap product for the two cases is found to be 2208.815 WK. The experimental data, for performing calculation and obtaining the thermal parameters, is taken from Kaushik [7]. The curve between the exergy lost v/s temperature difference is plotted in Fig. 6. The heat loss coefficient and quality factor, for 20 kg mass of water, are found to be 54.125 W/K m^2 and 0.099, respectively. The specific heat loss coefficient for this cooker is found to be $2.706 \text{ W/K m}^2 \text{ kg}$.

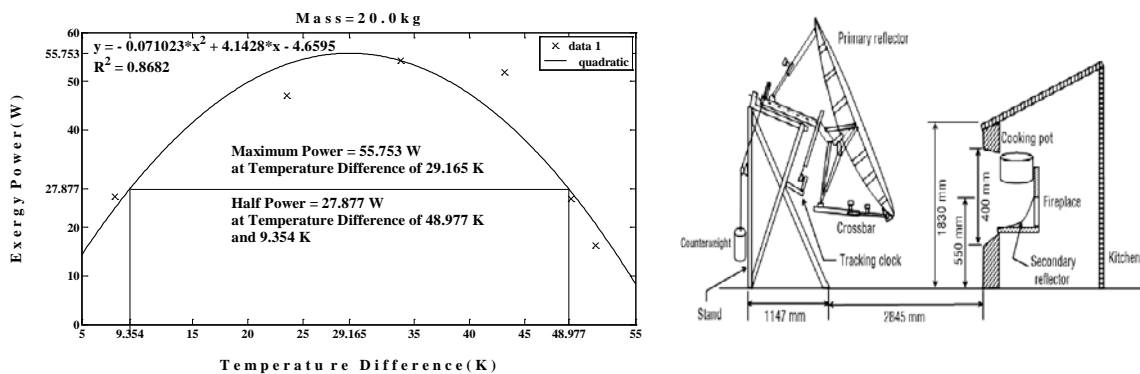


Fig. 5. Variation of Exergy output power with Temperature Difference for Scheffler type cooker with its schematics.

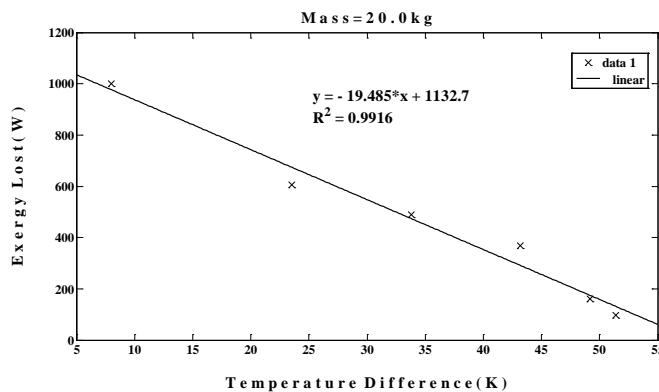


Fig. 6. Variation of Exergy power lost with Temperature Difference for Scheffler type cooker.

3.4. Parabolic trough type concentrating cookers

The variation in the exergy output as a function of temperature difference for parabolic trough type concentrating cooker of aperture area 0.9 m^2 and focal area of 0.088 m^2 is presented in Fig. 7, which depicts the case when the amount of water inside the cooking vessels/pots is 6.3 Kg . The maximum exergy power obtained through curve fitting is 6.92 W and the temperature difference gap corresponding to the half power points is 23.15 K . The peak exergy and temperature difference gap product for the two cases is found to be 160.198 WK . The experimental data, for performing calculation and obtaining the thermal parameters, is taken from Ozturk [8]. The curve between the exergy lost v/s temperature difference is plotted in Fig. 8. The heat loss coefficient and quality factor, for 6.3 kg mass of water, are found to be 47.73 W/K m^2 and 0.087 , respectively. The specific heat loss coefficient for this cooker is found to be $7.58 \text{ W/K m}^2 \text{ kg}$.

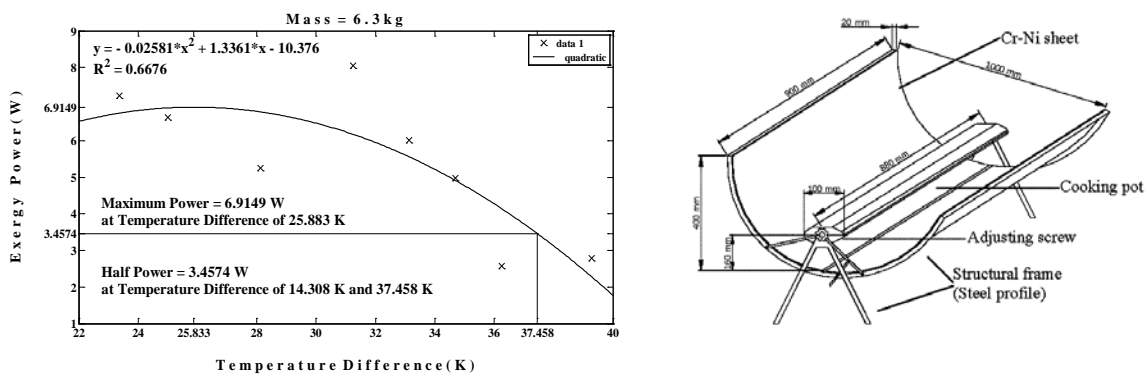


Fig. 7. Variation of Exergy output power with Temperature Difference for parabolic trough cooker with its schematics.

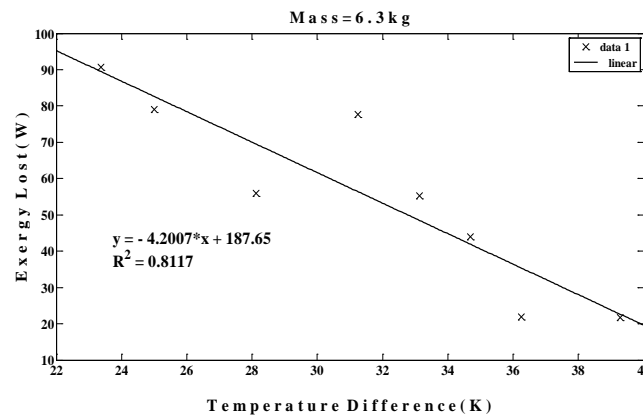


Fig. 8. Variation of Exergy power lost with Temperature Difference for parabolic trough cooker.

The cooker which attains higher exergy at higher temperature difference is the better one. It has been also noticed that the variation in the exergy lost with temperature difference is more linear when temperature of water varies in the range of 60°C to 95°C (see Fig. 2, 4, 6, 8). This range of temperature is also generally used in calculation/determination of F_2 (second figure of merit), which is an important and well known performance indicator for SBC [1, 12]. The amount of heat energy at higher temperature is more valuable than the same amount of heat energy at lower temperature and in energy analysis it is not possible to take into account such qualitative difference. The exergy analysis is a more complete synthesis tool because it

account for the temperatures associated with energy transfers to and from the cooker, as well as the quantities of energy transferred, and consequently provides a measure of how nearly the cooker approaches ideal efficiency.

4. Conclusion

An exergy based analysis is applied to solar cookers of different designs. Variations in exergy output and exergy lost with respect to temperature difference are studied and four thermal performance indicators, viz. peak exergy, quality factor, exergy temperature difference gap product and heat loss coefficient, are proposed. The approach presented through this manuscript is comprehensive, realistic and flexible for it can easily accommodate the effect of variations in solar insolation (peak to valley) which can be greater than 300 W/m^2 . The exergy output power, if required, can be converted into standardized exergy power on par with standardized cooking power. To establish a test standard for different types of solar cookers, one may require more comprehensive testing and data analysis. However, the proposed parameters may stimulate the discussion and strengthen the case for exergy based test standards.

References

- [1] Mullick, S.C., Kandpal, T. C., Subodh Kumar, 1996. Testing of box-type solar cookers: second figure of merit F_2 and its variation with load and number of pots. *Solar Energy* 57(5), 409-413.
- [2] BIS 2000. IS 13429 (part 3): 2000. Indian Standards Solar – Box Type- Specification Part 3 Test Method (First Revision) New Delhi: Bureau of Indian Standards.
- [3] Funk, P. A., 2000. Evaluating the international standard procedure for testing solar cookers and reporting performance, *Solar Energy*. 68(1), 1-7.
- [4] S.C. Mullick, T. C. Kandpal and Subodh Kumar, 'Thermal test procedure for a paraboloid concentrator solar cooker', *Solar Energy*, 46(3), 139- 144, 199.
- [5] Petela, R., 2003. Exergy of undiluted thermal radiation. *Solar Energy*, 74, 469-488.
- [6] Petela, R., 2010. *Engineering Thermodynamics of Thermal Radiation for Solar Power Utilization*, McGraw-Hill, New York.
- [7] Kaushik, S.C., Gupta, M. K., 2008. Energy and exergy efficiency comparison of community-size and domestic-size paraboloidal solar cooker performance, *Energy for Sustainable Development*. 3, 60-64.
- [8] Ozturk, H.H., 2004. Experimental determination of energy and exergy efficiency of solar parabolic-cooker. *Solar Energy*, 77, 67-71.
- [9] Ozturk, H.H., 2007. Comparison of energy and exergy efficiency for solar box and parabolic cookers. *J. Energy Engg.*, 133(1), 53-62.
- [10] <http://www.mnre.gov.in/pdf/test-proc-dish-cooker.pdf>
- [11] Subodh Kumar, 2004. Thermal performance study of box type solar cooker from heating characteristic curves. *Energy Conversion and Management*, 45, 127-139..
- [12] Mullick, S.C., Kandpal, T. C., Saxena, A. K., 1987. Thermal test procedure for box-type solar cookers. *Solar Energy* 39(4), 353-360.

Evaluation of an integrated photovoltaic thermal solar (IPVTS) water heating system for various configurations at constant collection temperature

Rajeev Kumar Mishra^{1,*}, G.N.Tiwari¹

¹ Centre for Energy Studies, Indian Institute of Technology Delhi, New Delhi, India

* Corresponding author. Tel: +91 9717720464, Fax: +91 1126591251, E-mail: bhu.rajeev@gmail.com

Abstract: Photovoltaic thermal (PVT) technology refers to the integration of a PV and a conventional solar thermal collector in a single piece of equipment. In this paper, an integrated photovoltaic thermal solar (IPVTS) water heating system for various configurations has been evaluated for constant collection temperature. Analysis is based on basic energy balance for hybrid flat plate collector in terms of design parameters for a solar water heater installed at Solar Energy Park, IIT Delhi, India and climatic parameters provided by India Meteorological Department Pune, India. It is observed that the daily thermal energy gain of IPVTS system decreases with increasing the constant collection temperature. It is also observed that for collectors partially covered by PV modules, daily thermal energy increases with decrease of collector area covered by PV module. The exergy analysis of IPVTS system has also been carried out.

Keywords: Hybrid PV thermal, Thermal energy, Exergy.

Nomenclature

<p>A Area.....m^2</p> <p>C Specific heat..... $J/kg\ K$</p> <p>F' Flat plate collector efficiency factor.....<i>dimensionless</i></p> <p>F_R Flow rate factor.....<i>dimensionless</i></p> <p>h Heat transfer coefficient.....W/m^2</p> <p>PF_1 Penalty factor first.....<i>dimensionless</i></p> <p>PF_2 Penalty factor second.....<i>dimensionless</i></p> <p>$I(t)$ Incident solar intensity.....W/m^2</p> <p>K Thermal conductivity.....$W/m\ K$</p> <p>\dot{m}_w Rate of flow of water mass in collector.....kg/sec</p> <p>\dot{Q}_u Rate of useful energy transfer.....kW</p> <p>T Temperature.....$^{\circ}C$</p> <p>$U_{t,c,a}$ Total heat transfer coefficient from solar cell to ambient through glass cover.....$W/m^2\ K$</p> <p>$U_{L,m}$ An overall heat transfer coefficient from blacken surface to ambient.....$W/m^2\ K$</p> <p>V Air velocity.....m/s</p>	<p><i>Subscripts</i></p> <p>A ambient.....</p> <p>c solar cell</p> <p>f fluid.....</p> <p>f_i inlet fluid.....</p> <p>f_o outlet fluid</p> <p>g glass.....</p> <p>m module</p> <p>N number of collectors.....</p> <p><i>Greek letters</i></p> <p>α absorptivity..-.....</p> <p>$(\alpha\tau)_{eff}$ product of effective.....</p> <p>β packing factor.....</p> <p>η_i an instantaneous</p> <p>τ transmittivity</p>
--	--

1. Introduction

Photovoltaic thermal (PVT) technology refers to the integration of a photovoltaic (PV) module and a conventional solar thermal collector in a single piece of equipment. The reason behind the hybrid concept is that more than 80% of the solar radiation falling on PV cells is either reflected or converted to thermal energy. This leads to an increase in the PV cell's

working temperature as much as 40-50° C above the ambient temperature. Because of this temperature increase there can be two undesirable consequences: (i) 0.3% to 0.6 % of efficiency loss per degree C rise in PV cell temperature and (ii) a permanent damage in the structure of PV module if the thermal stress remains for a long period of time. In applications of PVT system, the production of electricity is the main priority, and therefore, it is necessary to operate the PV modules at low temperature in order to keep the PV cell electrical efficiency at a sufficient level. The temperature of the PV module in the hybrid PVT system can be reduced by cooling the base of PV module by allowing water/air to flow below it (Prakash [1], Tripanagnostopoulos et al. [2], Zondag et al. [3], Jones and Underwood [4], Chow [5], and Infield et al. [6]). Thermal energy available from PV module can be used for many applications namely water and air heating for domestic, agricultural sectors and buildings for thermal heating/cooling.

In this paper, the performance of the N collectors connected in series is evaluated by considering the three different cases, namely: Case A: All the collectors are fully covered by glass and connected in series. Case B: All collectors are partially covered by PV modules and connected in series and Case C: All the collectors are fully covered by PV module (glass to glass) and connected in series.

2. Methodology

For the present study conventional tube-in-plate-type collector of area of 2m² is considered. The design parameters of photovoltaic thermal (PVT) collectors are shown in Table 1. The glazing surface of the collector is either glass or PV module depending upon the requirement of the user. To increase the absorption of solar radiation the absorber plate of collector is blackened by black paint.

Energy balance equations:

In order to write the energy balance equation of PVT solar water collectors connected in series, the following assumptions have been made:

- One dimensional heat conduction is good approximation for the present study.
- The specific heat of water remains constant. It does not change with rise in temperature of water.
- The system is in quasi-steady state.
- The ohmic losses in the solar cell and PV module are negligible.

Energy balance for solar cells of PV module (glass-glass),

$$\alpha_c \tau_g \beta_c I(t) W dx = \left[U_{tc,a} (T_c - T_a) + h_{c,p} (T_c - T_p) \right] W dx + \eta_c \beta_c I(t) \cdot W dx \quad (1)$$

From Eq.(1) the expression fro cell temperature is

$$T_c = \frac{(\alpha \tau)_{1,eff} I(t) + U_{tc,a} T_a + h_{c,p} T_p}{U_{tc,a} + h_{c,p}} \quad (2)$$

Energy balance for blackened absorber plate below the PV module,

$$\alpha_p (1 - \beta_c) \tau_g^2 I(t) W dx + h_{c,p} (T_c - T_p) W dx = h_{p,f} (T_p - T_f) W dx \quad (3)$$

From Eq. (3), the expression for plate temperature is

$$T_p = \frac{(\alpha \tau)_{2,eff} I(t) + PF_1 (\alpha \tau)_{1,eff} I(t) + U_{L1} T_a + h_{p,f} T_f}{U_{L1} + h_{p,f}} \quad (4)$$

Energy balance for water flowing through an absorber pipe below the PV module,

$$\dot{m}_f C_f \frac{dT_f}{dx} = F' h_{p,f} (T_p - T_f) W dx \quad (5)$$

In the present study three different configurations of PVT solar water collectors have been considered

Case A: All collectors are fully covered by glass and connected in series:

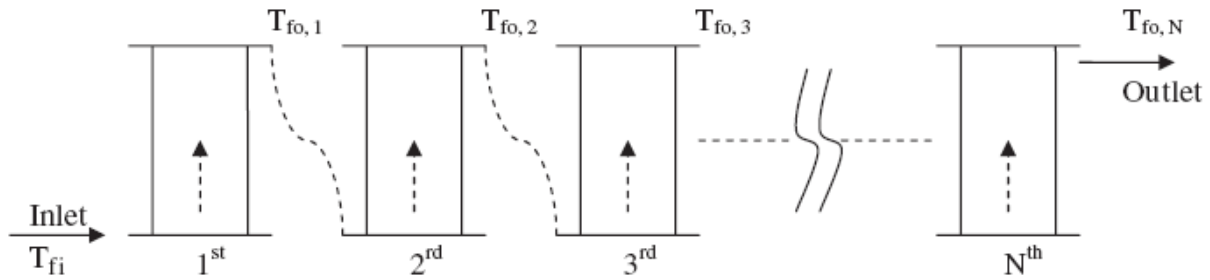


Fig. 1. Collectors fully covered by glass and connection in series.

Following Duffie and Beckman [7] and Tiwari [8] the mass flow rate for N collectors connected in series can be obtained as:

$$\dot{m}_f = \frac{F' N A_c U_{L,c}}{C_f \left[\log \left\{ T_{fi} - \left(\frac{(\alpha\tau)_{c,eff} I(t)}{U_{L,c}} + T_a \right) \right\} - \log \left\{ T_{foN} - \left(\frac{(\alpha\tau)_{c,eff} I(t)}{U_{L,c}} + T_a \right) \right\} \right]} \quad (6)$$

Case B: The collectors are partially covered by PV modules and connected in series

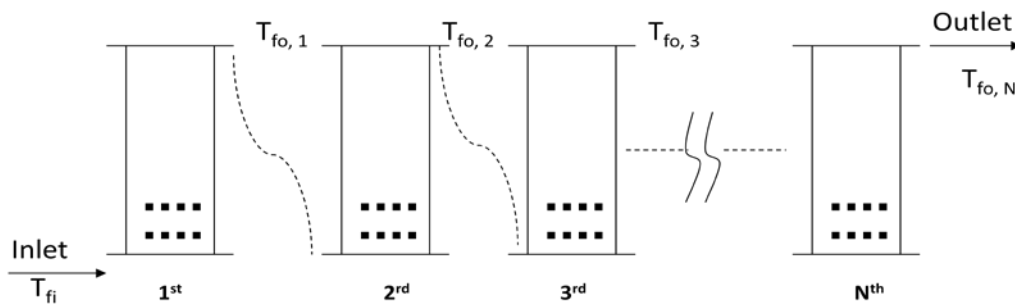


Fig. 2. Collectors partially covered by PV module and connected in series.

Following Dubey and Tiwari [9] the outlet water from N such collectors connected in series can be given as:

$$T_{foN} = \frac{(AF_R(\alpha\tau))_1}{\dot{m}_f C_f} \left(\frac{1 - K_K^N}{1 - K_K} \right) I(t) + \frac{(AF_R U_L)_1}{\dot{m}_f C_f} \left(\frac{1 - K_K^N}{1 - K_K} \right) T_a + T_{fi} K_K^N \quad (7)$$

where,

$$K_K = \left[1 - \frac{(AF_R U_L)_1}{\dot{m}_f C_f} \right]$$

$$(AF_R (\alpha\tau))_1 = \left[A_m F_{Rm} P F_2 (\alpha\tau)_{m,eff} \left(1 - \frac{A_c F_{Rc} U_{L,c}}{\dot{m}_f C_f} \right) + A_c F_{Rc} (\alpha\tau)_{c,eff} \right]$$

and

$$(AF_R U_L)_1 = \left[A_m F_{Rm} U_{L,m} \left(1 - \frac{A_c F_{Rc} U_{L,c}}{\dot{m}_f C_f} \right) + A_c F_{Rc} U_{L,c} \right]$$

Case C: All the collectors are fully covered by glass to glass type PV module and connected in series

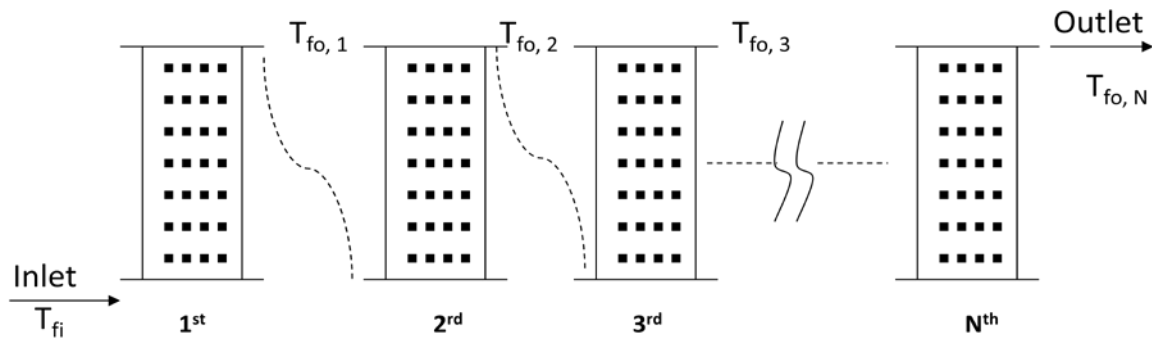


Fig.3. Collectors fully covered by PV modules and connected in series.

Following Dubey and Tiwari [9] Mass flow rate for N collectors partially covered with PV modules connected in series can be obtained as,

$$\dot{m}_f = \frac{N F' A_m U_{L,m}}{C_f \left[\log \left\{ T_{fi} - \left(\frac{P F_2 (\alpha\tau)_{m,eff} I(t)}{U_{L,m}} + T_a \right) \right\} - \log \left\{ T_{foN} - \left(\frac{P F_2 (\alpha\tau)_{m,eff} I(t)}{U_{L,m}} + T_a \right) \right\} \right]} \quad (8)$$

The rate of useful thermal energy obtained from N identical collectors connected in series can be given as

$$\dot{Q}_u = \dot{m}_f C_f (T_{foN} - T_a) \quad (9)$$

Electrical Efficiency of solar cell depends on solar cell temperature and can be given by Evans [10] and Schott [11]

$$\eta_c = \eta_o \left[1 - \beta_o (\bar{T}_c - T_o) \right] \quad (11)$$

Table 1. Design parameters of photovoltaic thermal (PV/T) collector

Parameters	Values	Parameters	Values
A_C	2.0m^2	U_{LC}	$3.0\text{ W/m}^2\text{°C}$
A_m	0.605m^2	U_{Lm}	3.44 W/
C_f	4190 J/kgK	$U_{t,c,a}$	$9.5\text{ W/m}^2\text{°C}$
F'	0.968	V	1.0 m/s
F_{Rc1}	0.95	W	0.125 m
F_{Rc2}	0.94	α_c	0.90
F_{Rm}	0.96	τ_c	0.95
$h_{c,p}$	5.7 W/m^2	β_c	0.89
$h_{p,f}$	100 W/m^2	η_o	0.12
PF_1	0.357	α_p	0.80
PF_2	0.965	τ_g	0.95
K	$204\text{ W/m}^2\text{°C}$		
\dot{m}	0.06 kg.sec		

3. Result and Discussions

The variation of solar intensity and ambient temperature for a typical day in the summer month (January) is shown in Figure 4. The values of design parameters of flat plate collector are given in Table 1. Here, the results of the three cases, case A (fully covered by glass) and case B (partially covered by PV modules) and case C (fully covered by PV modules) are discussed in detail. Equations 6, 7 and 8 have been computed using MATLAB software for evaluating the mass flow rate at different outlet water temperatures for a typical day during the month of January for a given design and climatic parameters (Table 1). Figures 5a and 5b represent the hourly variation of mass flow rate for case A and case B respectively at various constant outlet temperatures. The result shows that for constant collection temperatures 30-60°C the mass flow rate of water in tubes decreases from 0.1 - 0.01 kg/s in case A, 0.08-0.01 kg/s in case B. Figure 5c gives the hourly variation of mass flow rate for case C. Figure shows that in this case one cannot get the outlet water temperature more than 40°C in January month and the mass flow rate decreases from 0.04 to 0.01 kg/s for case C.

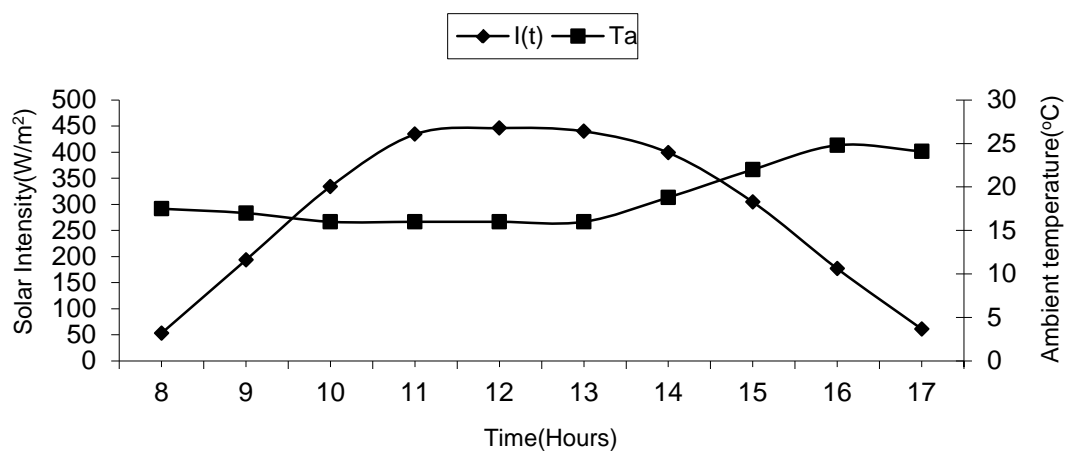


Fig. 4. Hourly variation of solar intensity and ambient temperature of a typical day in the month of January.

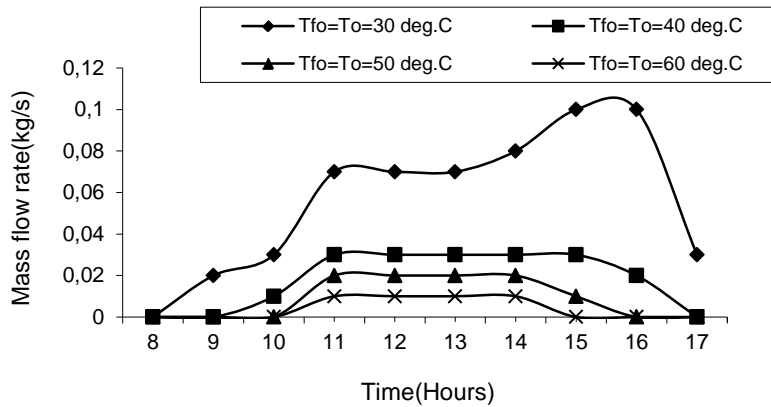


Fig. 5a. Hourly variation of mass flow rate at different outlet temperature for case A.

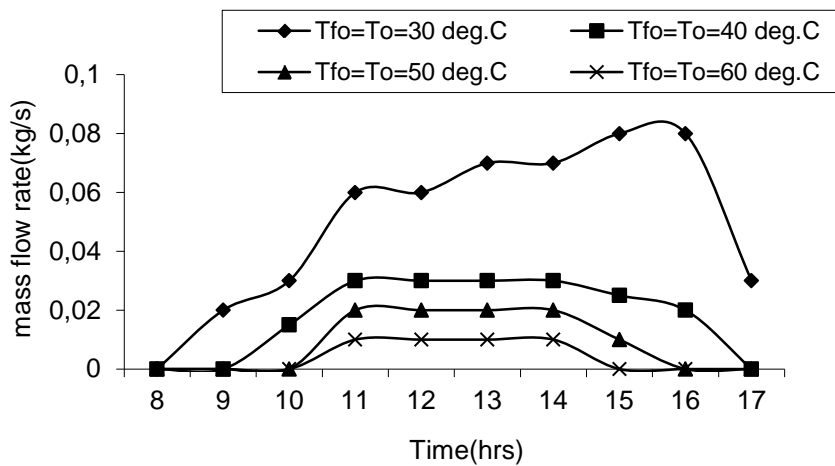


Fig. 5b. Hourly variation of mass flow rate at different outlet temperature for case B.

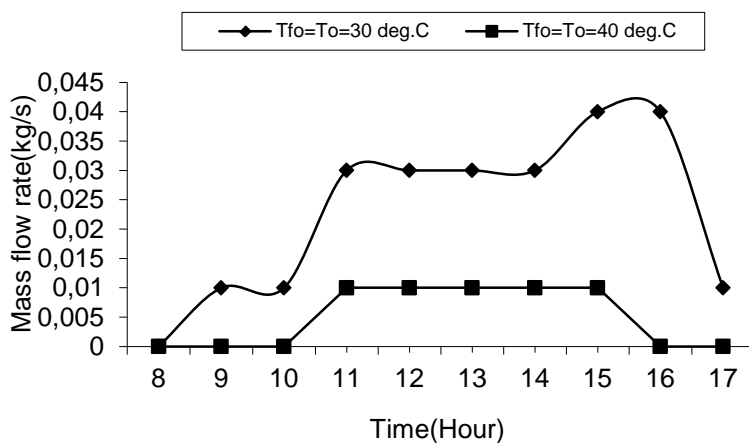


Fig. 5c. Hourly variation of mass flow rate at different outlet temperature for case C.

Fig. 6a and 6b represent the hourly variation of thermal energy gain and electrical energy gain respectively for various configurations of PVT collectors. The figures show that as the

collector area covered by PV modules increases the thermal energy gain decreases whereas the electrical energy gain increases as the collector area covered by PV modules increases.

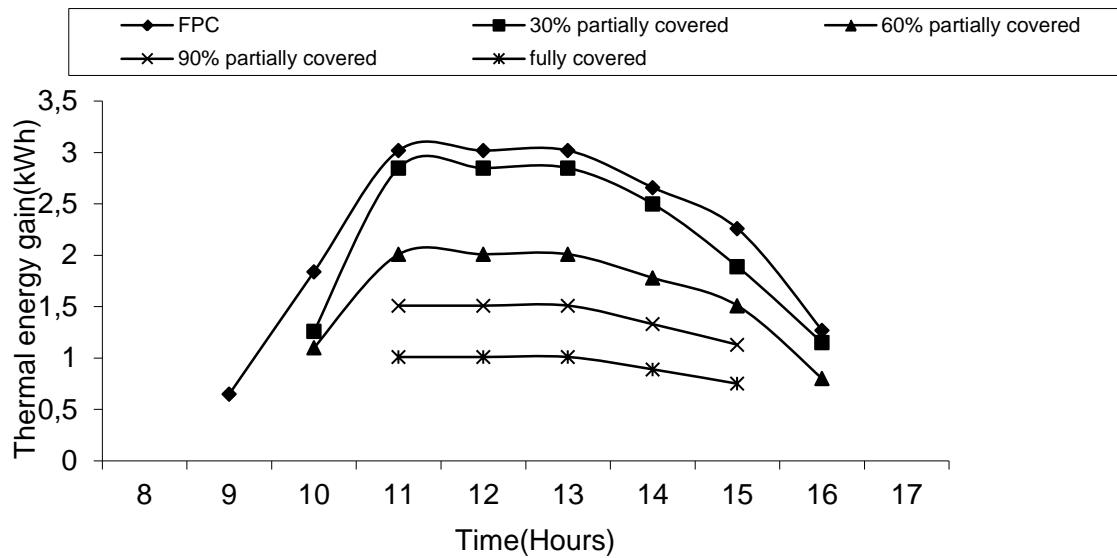


Fig. 6a. Hourly variation of thermal energy gain for different configuration.

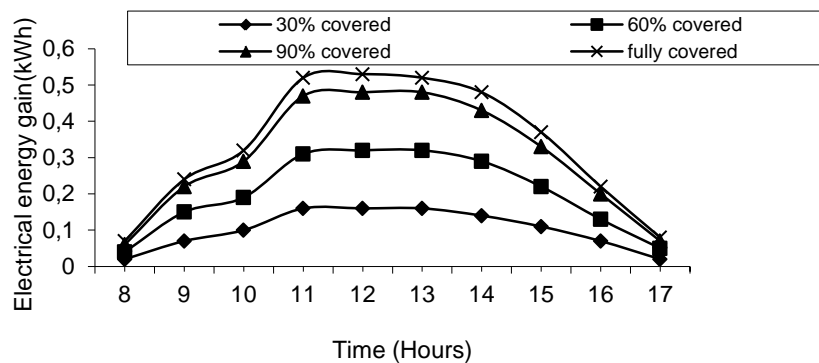


Fig. 6b. Hourly variation of electrical energy gain for different configurations.

4. Conclusion

The maximum thermal energy gain is obtained when collectors fully covered by glass cover; however maximum electrical energy gain is obtained when collectors are fully covered by PV modules.

References

- [1] Prakash, J., Transient analysis of a photovoltaic-thermal solar collector for co-generation of electricity and hot air/water. Energy Conversion and Management. 35, 1994 pp. 967 - 972.
- [2] Tripanagnostopoulos, Y., Hybrid photovoltaic/thermal solar system, Solar Energy 72(3), 2002, pp. 217-234.
- [3] Zondag, H.A., de Vries, D.W. de, van Helden, W.G.J., van Zolengen, R.J.C., Steenhoven, A.A., The thermal and electrical yield of a PV-thermal collector. Solar Energy 72 (2), 2002, pp. 113-128.

- [4] Jones, A.D., Underwood, C.P., A thermal model for photovoltaic systems. *Solar Energy* 70 (4), 2001, pp. 349-359.
- [5] Chow, T.T., Performance analysis of photovoltaic-thermal collector by explicit dynamic model. *Solar Energy* 75, 2003, pp.143-152.
- [6] Infield, D., Mei, L., Eicker, U., Thermal performance estimation of ventilated PV facades, *Solar Energy*, 76(1-3), 2004, pp. 93-98.
- [7] Duffie, J.A., Beckman, W.A., 1991. *Solar Engineering of Thermal Processes*. John Wiley and Sons, New York.
- [8] Tiwari, G.N., *Solar Energy: Fundamentals, Design, Modeling and Applications*. Narosa Publishing House, New Delhi, 2004.
- [9] Dubey, S. and Tiwari, G.N., Analysis of different configurations of flat plate collectors connected in series, *International Journal of Energy Research*, 32, 2008, pp. 1362-1372.
- [10] Evans, D.L., Simplified method for predicting PV array output. *Solar Energy* 27, 1981, pp. 555-560.
- [11] Schott, T., Operational temperatures of PV modules. In: *Proceedings of 6th PV Solar Energy Conference*, 1985, pp. 392-396.

Design of a Latent Heat Energy Storage System Coupled with a Domestic Hot Water Solar Thermal System

Robynne Murray^{1,3}, Louis Desgrosseilliers^{1,2,3}, Jeremy Stewart¹, Nick Osbourne¹,
Gina Marin¹, Alex Safatli², Dominic Groulx^{1,3*}, Mary Anne White^{2,3}

¹ Department of Mechanical Engineering, Dalhousie University, Halifax, Canada

² Department of Chemistry, Dalhousie University, Halifax, Canada

³ Institute for Research in Materials, Dalhousie University, Halifax, Canada

* Corresponding author. Tel: +1 902 494-8835, Fax: +1 902 423-6711, E-mail: dominic.groulx@dal.ca

Abstract: Solar domestic hot water (SDHW) can be used to reduce energy bills and greenhouse gas emissions associated with heating domestic water. However, one of the most significant barriers to further deployment of solar thermal applications is the space and weight required for storage of the energy collected. Phase change materials (PCMs) are advantageous for daily energy storage with SDHW due to their high storage density and isothermal operation during phase transitions, and would overcome these obstacles.

The aim of this paper is to outline the initial steps in the development of a SDHW energy storage system using PCMs, with emphasis on the numerical and experimental studies used to access the phase change and thermal behaviour of the selected PCM. Lauric acid was selected as the PCM based on the melting temperature range which was targeted by studying solar data from an existing solar hot water system in Halifax, Nova Scotia, Canada. Due to the low thermal conductivity of PCMs, additional work is required to develop and validate a design to enhance heat transfer to the storage material using fins. The selected design will be built and installed in an existing large scale solar thermal system on an apartment building in Halifax. The system will be instrumented in order to acquire continuous data (temperatures, flow rates, pressures, etc.) to fully characterize the system.

Keywords: Latent heat storage, Solar domestic hot water, Phase change materials, Heat transfer enhancement

1. Introduction

Solar thermal energy for domestic hot water heating is one of the most cost effective and efficient areas of alternative energy exploitation [1]. The use of phase change materials (PCMs) in latent heat energy storage systems (LHESS) can reduce the volume and weight of storage due to their high storage density, and overcome major obstacles in the further deployment of solar thermal energy [1]. LHESS have high energy densities compared with sensible heat storage systems [2], and have been shown to store up to 14 times more heat per unit volume than sensible heat storage materials [3]. Fig. 1 shows a simple schematic of a SDHW system with PCM energy storage.

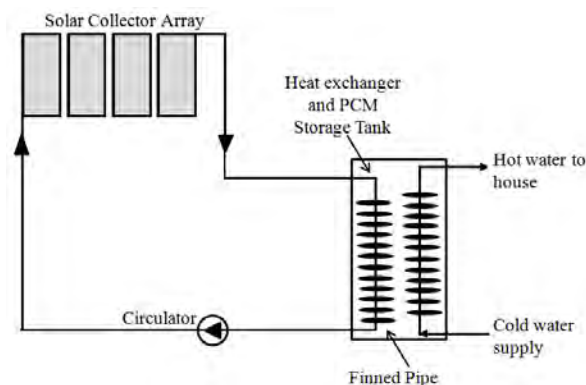


Fig. 1. Schematic of a LHESS for SDHW.

Energy storage using PCMs in combination with solar collectors has been studied mathematically [4] and experimentally [5] and shown to be advantageous. However, missing from previous works is a working prototype of a SDHW system for a large scale application [6].

This paper presents a phase change heat transfer study performed using a PCM, lauric acid, in a small-scale experimental LHESS using fins to enhance the overall heat transfer process. A numerical model was also created and its results are compared and validated with experimental results. Results of this study are to be used in the design of a SDHW system, with the numerical model to be used further in design optimization, mainly for fin configurations, of the LHESS. The resulting LHESS design will be built and installed in an existing large scale solar thermal system on an apartment building in Halifax by Scotian Windfield Inc.

2. Phase Change Material Selection

The PCM is selected based on its phase change temperature range and the operating temperatures of the SDHW system. A melting temperature range of 42 to 48°C and solidification temperature range of 35 to 40°C were targeted by studying the solar data from an existing SDHW system in Halifax, Canada. Several PCMs were considered based on their appropriate melting temperatures, low toxicities, and cost. The most promising materials were tested using a differential scanning calorimeter (DSC) to study their melting and solidification temperature ranges. Salt hydrates (e.g. Glauber's salt and sodium acetate) tested in the DSC showed significant supercooling, which is a common and undesirable phenomenon for these materials [7].

The DSC curve for lauric acid (dodecanoic acid; $\text{CH}_3(\text{CH}_2)_{10}\text{COOH}$; crude [$< 80\%$ pure], Fisher Scientific), presented in Fig. 2, shows a melting temperature range of 43.3 to 45.7 °C and solidification temperature range of 38.8 to 35 °C. The DSC curve for this lower purity sample compared well with literature curves for pure lauric acid [8]. Other fatty acids that were tested had either incompatible phase transition regions or toxicities and cost that were undesirable.

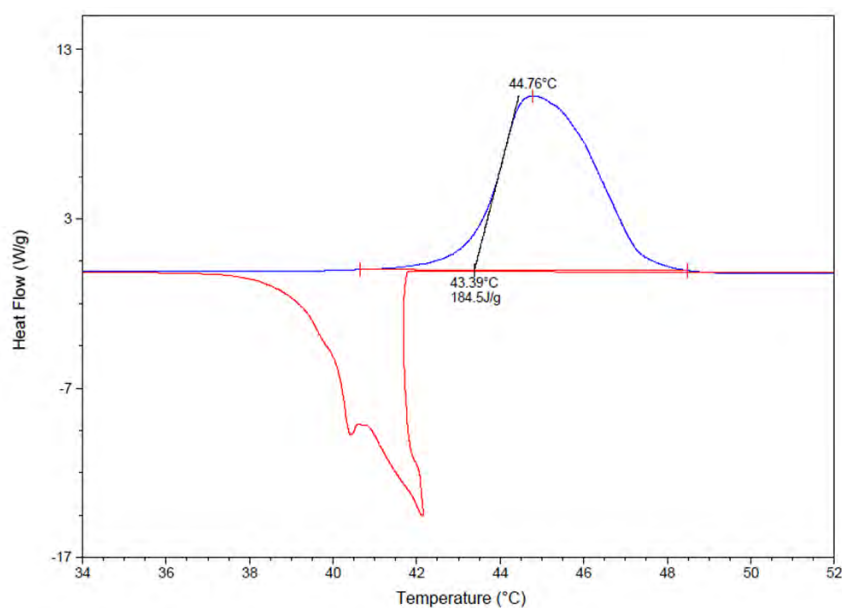


Fig. 2. DSC Curve for Lauric Acid (80% purity) measured at 10 K/min.

Lauric acid was selected based on its melting temperature range, high heat of fusion, minimal supercooling and safety. The material properties are displayed in Table 1.

Table 1. Thermal and Physical Properties of Lauric Acid [8,9].

Molecular Weight	200.31 (kg/kmol)
Density of Powder at 20°C / Liquid at 45°C §	869 / 873 (kg/m ³)
Fusion Temperature	42 (°C)
Latent Heat of Fusion	182 (kJ/kg)
Heat Capacities Solid/Liquid †	2.4/2.0 (kJ/kg·K)
Thermal Conductivities Solid/Liquid †	0.150*/0.148 (W/m·K)
Viscosity †	0.008 (Pa·s)

* Value obtained from present experiments.

† Nominal properties calculated near the melting point.

§ Density used in the numerical model presented = 880 kg/m³.

To insure stable properties after many melting/solidification cycles, lauric acid was thermally cycled from 37 to 63 °C. After 800 cycles, there were no obvious signs of degradation. Lauric acid is also safe to use in conjunction with a SDHW system because it is a food grade substance and only a mild irritant [9].

3. Experimental Setup

The experimental setup used to study the melting and solidification behavior of lauric acid in a cylindrical container with horizontal copper fins is shown schematically in Fig. 3a. A Solidworks 3D rendering of the container is shown in Fig. 3b. Eight type T probe thermocouples are connected to a National Instruments 16-channel thermocouple module (NI9213) CompactDAQ data acquisition system. Temperatures are recorded using LabView. Thermocouples are located inside the lauric acid (T2 to T7) as well as on the inlet and outlet (T1 and T8), as seen in Fig. 3a. A pulse counter flowmeter from Omega is connected to a counter/pulse generation module (NI9435) on the DAQ system and read by LabView. The container is made of ¼-inch acrylic plastic and is un-insulated to allow visual study of the system.

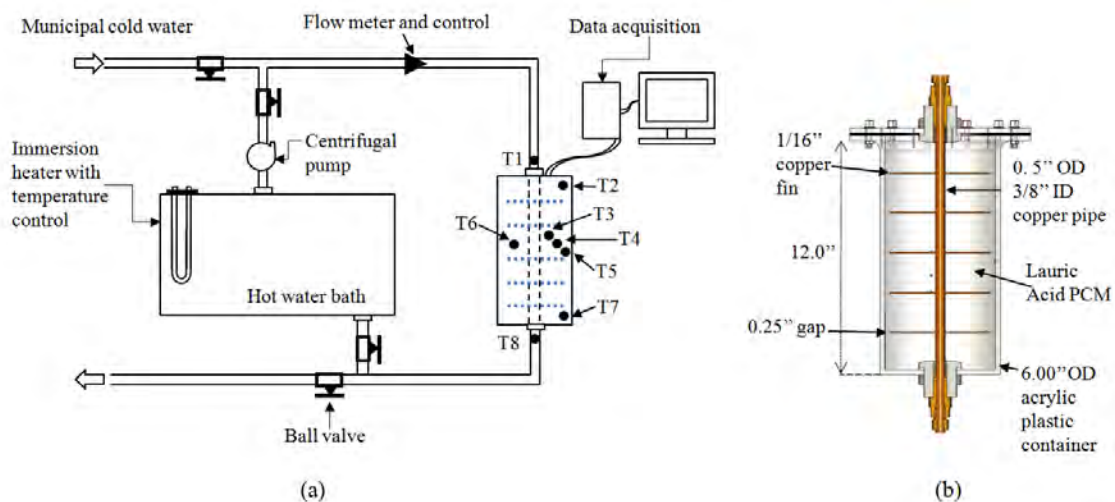


Fig. 3. (a) Schematic of the experimental setup and (b) PCM container.

The conditions under which the experiments were performed are summarized in Table 2.

Table 2. Experimental parameters.

Hot Water Inlet Velocity	1.5 (m/s)
Cold Water Inlet Velocity	3.5 (m/s)
Hot Inlet Temperature	55 ± 1 ($^{\circ}\text{C}$)
Cold Inlet Temperature	12 ($^{\circ}\text{C}$)

At the beginning of the experiment, lauric acid was solid in the container at room temperature. Hot water from the constant temperature water bath was pumped through the finned copper pipe, eventually melting the lauric acid. The charging portion of the experiment was completed when the system reached steady state. At this point, cold water from the municipal water supply was pumped through the system to solidify the lauric acid and recover the stored thermal energy. The experiment concluded when the lauric acid was at room temperature. The results obtained with this setup were compared to results of numerical simulations.

4. Numerical Study

COMSOL Multiphysics (version 4.0a) was used to build a 2D axisymmetric numerical model of the experiment using the *Heat Transfer in Solids* physics to model the copper and lauric acid, and the *Laminar Flow* and *Heat Transfer in Liquids* physics to model the flowing water. The thermophysical properties of water and copper used in the model are those given by COMSOL. For lauric acid, the thermophysical properties used are those presented in Table 1. In this first numerical study, natural convection in the lauric acid was neglected to reduce computing time. An extremely fine mesh was used, with a maximum element size of 2.58×10^{-9} m². The following boundary and initial conditions were used:

- i. Initial temperature of 295 K;
- ii. All outside walls have radiation heat losses to the surroundings and natural convection losses are accounted for on the side wall;
- iii. No-slip condition on the inner pipe wall;
- iv. Inlet temperature and water velocity as in Table 2;
- v. No viscous stress and convective flux at the pipe outlet.

Groulx and Ogoh's method of numerically modeling the melting process was used [10]. The simulated time for melting was 11.5 hours, and 10 hours for cooling. Simulations took approximately 8 hours to run.

In the experimental setup, two thermocouples (T4 and T6) were placed symmetrically between horizontal fins at the same height but spaced 180° apart in order to confirm symmetry in the experiment. In the numerical model, a reference point was added to extract information at this location, as shown in Fig 5.

5. Results and Discussion

5.1. Charging Process (Melting)

Figure 4 presents the temperatures measured experimentally by thermocouples T1 to T8 during the charging process. Refer to Fig. 3 for thermocouple positions.

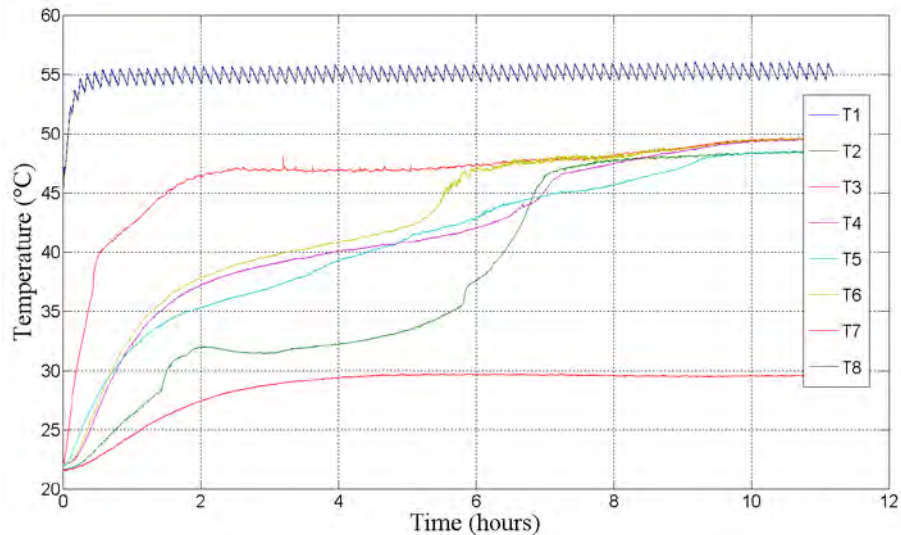


Fig. 4. Experimental temperatures during charging.

The inlet temperature (T1) fluctuates during the charging process due to the emersion heater on/off fluctuations, the outlet temperature (T8) logically follows the same trend. The temperature increases more rapidly close to the pipe and fins (T3), where it takes a longer time for the lauric acid to heat up and melt in regions farther from the pipe, T4 and T6, followed by T5. The region in the upper corner of the container experiences a fast increase in temperature (T2) after 6 hours, mainly due to the onset of natural convection in this region. The lauric acid does not reach the melting temperature in the bottom corner (T7).

Figure 5 shows the numerically obtained temperatures in the system during charging. The black contour line represents the melting interface.

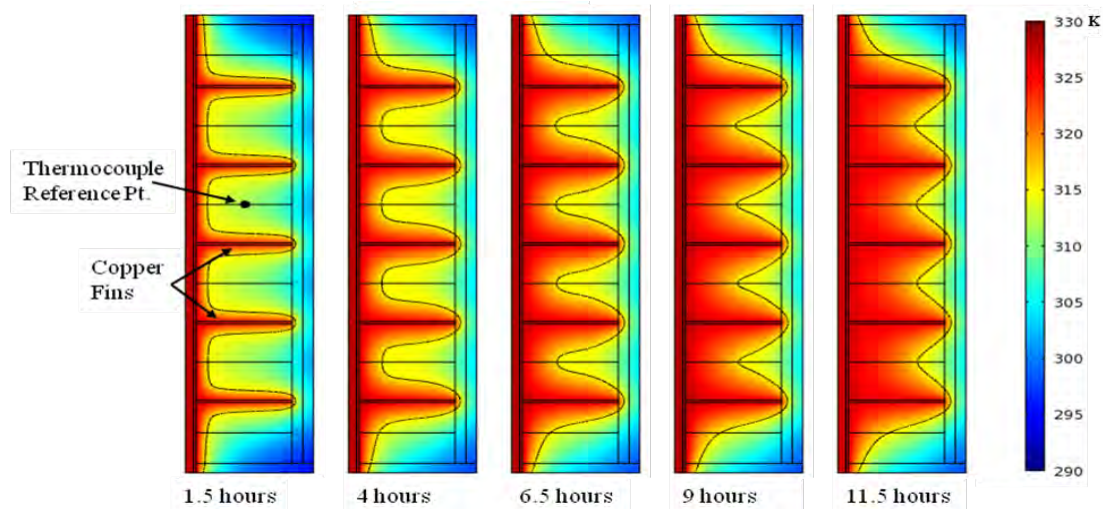


Fig. 5. Numerical temperature plots during charging after 1.5, 4, 6.5, 9 and 11.5 hours.

In Fig. 5, it can be observed that after 1.5 hours the melting process started near the pipe and fin surfaces first, with fairly small temperature increases everywhere else. The heat transfer has been enhanced by adding fins, which is clearly evident by looking at the overall temperature increases far from the pipe. After 11.5 hours of charging, solid lauric acid was still present around the inside wall of the container and in the corners. Experimentally, after 11.5 hours, solid lauric acid was only found in the bottom corners. This difference is thought

to be due to the effect of natural convection in the system, which increases the overall rate of heat transfer.

The experimentally measured (green and blue lines) and numerically calculated (red line) temperatures during the charging process are presented in Fig. 6.

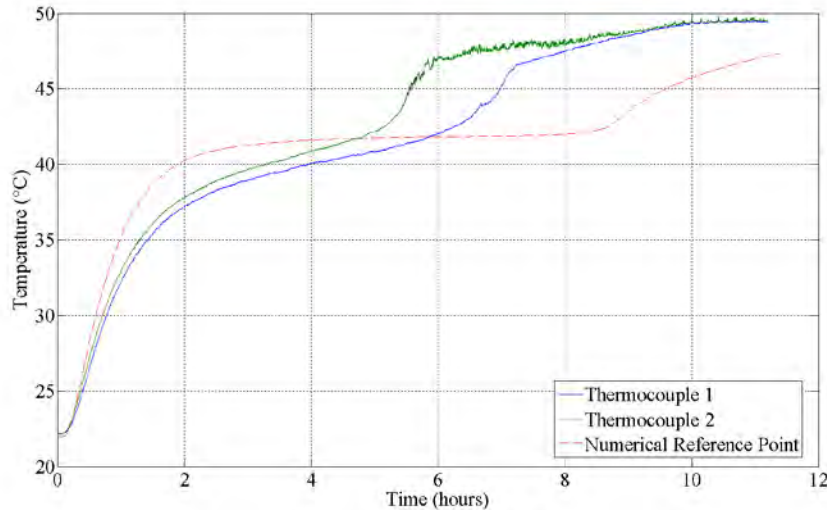


Fig. 6. Numerical validation of melting process in PCM container.

Thermocouples T4 and T6 showed slightly offset temperatures due to asymmetry in the fin assembly which caused one side of the container to heat up faster than the other. Melting occurred between 3 and 8.5 hours in the numerical model. The melting point was reached experimentally after 5 and 6 hours, with fairly constant temperature increases leading to this point; this is consistent with the formation of a mushy region around the thermocouple probes. Complete melting of the lauric acid numerically took longer, possibly due to the lack of natural convection in the model. Experimental results showed a sudden temperature increase in the liquid lauric acid just after melting; this rate of temperature increase in the liquid lauric acid was predicted well by the model.

The numerical model predicted higher effective heat transfer rates initially, leading to a faster temperature increase in the first 2 hours of charging; this is thought to be due to the ideal contact conduction between pipe, fins and lauric acid in the model. In the experimental setup, contact resistances between pipe and fins, as well as between copper surfaces and the solid lauric acid, may have resulted in decreased heat conduction rates at startup.

5.2. Discharging Process (Solidification)

Because of the higher flow rate of cold water used during the discharging process, solidification happened over a shorter period of time than melting: 3.5 hours compared to 11. Figure 7 shows the temperatures in the system during discharging, obtained numerically. The white contour line represents the solidification interface. Solidification of the lauric acid in the numerical model took 4 hours, as seen in Fig. 7.

Figure 8 shows the experimental (blue and green lines) and numerical (red line) cool down temperatures during discharging.

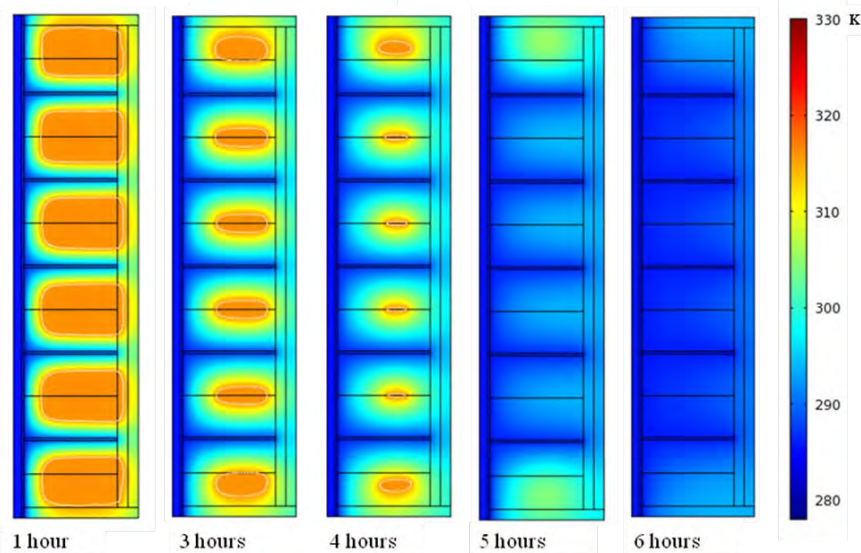


Fig. 7. Numerical temperature plots during discharging after 1, 3, 4, 5 and 6 hours.

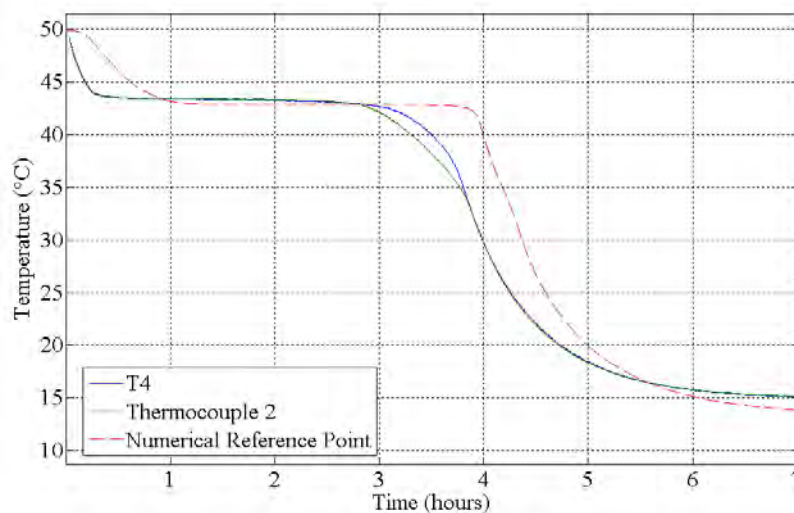


Fig. 8. Numerical validation of solidification process in PCM container.

Of importance to note, the lauric acid solidified at a temperature of 43°C , different from the predicted DSC measurements, which normally have a certain degree of supercooling. Nucleation happened in the first 15 minutes of cooling during the experiment, due to the presence of the thermocouple probes; this cannot be predicted numerically. However, the model does predict a solidification plateau similar to the one observed experimentally, and only slightly over predicts the time required for solidification at that point in the system.

Throughout the experiment, an insignificant amount of volume change from the solid to liquid phase was observed. Lauric acid did react weakly with copper, taking a bluish color in the liquid state; however this mild reaction does not lead to corrosion in any significant form [11].

6. Conclusion

The melting and solidification behavior of lauric acid inside a cylindrical container with a horizontal finned pipe was examined experimentally and numerically. Results for the charging experiment, when compared to the numerical simulations, clearly showed that a mushy region appeared in the system. The presence of natural convection in the liquid melt played a significant role in speeding up the heat transfer and melting process. During

discharging, the numerical results predicted fairly well the cooling and solidifying behavior observed in the experimental measurements; demonstrating that the effect of natural convection during solidification is for the most part negligible.

Acknowledgments

We thank Scotian Windfields for their support and expertise, as well as for funding for this project; Eco-Nova Scotia and the Natural Sciences and Engineering Research Council of Canada for their financial support; and the Dalhousie's Mechanical Engineering Department for research space and a flowmeter. The DSC is part of the Facilities for Materials Characterization managed by the Institute for Research in Materials at Dalhousie University.

References

- [1] F. Agyenim, N. Hewitt, P. Eames and M. Smyth, A review of materials, heat transfer and phase change problem formulation for LHTESS, *Renewable and Sustainable Energy Reviews* 14, 2010, pp.615–628
- [2] A.I. Fernandez, M. Martínez, M. Segarra, I. Martorell and L.F. Cabeza, Selection of materials with potential in sensible thermal energy storage, *Solar Energy Materials & Solar Cells* 94, 2010, pp. 1723-1729
- [3] A. Sharma, V.V. Tyagi, C.R. Chen and D. Buddhi, Review on thermal energy storage with phase change materials and applications, *Renewable and Sustainable Energy Reviews* 13, 2009, pp. 318–345
- [4] H. El Qarnia, Numerical analysis of a coupled solar collector latent heat storage unit using various phase change materials for heating the water, *Energy Conversion and Management* 50, 2009, pp. 247–254
- [5] A. Sari, and K. Kaygusuz, Thermal and heat transfer characteristics in a latent heat storage system using lauric acid, *Energy Conversion and Management* 43, 2002, pp. 2493–2507
- [6] A. Shukla, D. Buddhi and R.L. Sawhney, Solar water heaters with phase change material thermal energy storage medium: A review, *Renewable and Sustainable Energy Reviews* 13, 2009, pp. 2119–2125
- [7] Sandnes, B., and Rekstad, J., Supercooling Salt Hydrates: stored enthalpy as a function of temperature, *Solar Energy* 80, 2006, pp. 616-625
- [8] *Chemical Properties Handbook*, edited by C. L. Yaws, McGraw-Hill, 1999
- [9] A11672 – Dodecanoic Acid, Material Safety Data Sheet, Alfa Aesar, 2009, www.alfa.com/en
- [10] D. Groulx and W. Ogoh, Thermal behavior of phase change material during charging inside a finned cylindrical latent heat energy storage system: Effects of the arrangement and number of fins, *Proceedings of the International Heat Transfer Conference*, Washington, DC, USA, 2010
- [11] A. Sari and K. Kaygusuz, Some fatty acids used for latent heat storage: thermal stability and corrosion of metals with respect to thermal cycling, *Renewable Energy* 28, 2003, pp.939-948

Retrofitting Domestic Hot Water Tanks for Solar Thermal Collectors A theoretical analysis

Luís Ricardo Bernardo^{1,*}, Henrik Davidsson¹, Björn Karlsson²

¹ Energy and Building Design, Lund Technical University, Lund, Sweden

² Mälardalen University, Västerås, Sweden

* Corresponding author. Tel: +46 462227606, Fax: +46 462224719, E-mail: Ricardo.Bernardo@ebd.lth.se

Abstract: One of the most expensive components of a solar thermal system is the storage tank. Retrofitting conventional domestic hot water heaters when installing a new solar hot water system can decrease the total investment cost. In this study, retrofitting of existing water heaters using forced circulation flow was investigated. A comparison with a standard solar thermal system is also presented. Four simulation models of different system configurations were created and tested for the climate in Lund, Sweden. The results from the simulations indicate that the best configuration consists on connecting the collectors to the existing heater throughout an external heat exchanger and adding a small heater storage in series. For this retrofitted system, preliminary results show that an annual solar fraction of 53% is achieved. In addition, a conventional solar thermal system using a standard solar tank achieves a comparable performance for the same storage volume and collector area. Hence, it is worth to further investigate and test in practice this retrofitting. Furthermore, using the same system configuration, solar collectors can also be combined with new standard domestic hot water tanks at new installations, accessing a world-wide developed and spread industry.

Keywords: Solar thermal, Storage tank, Water heater, Retrofit, Domestic hot water

Nomenclature

T_{auxilia} Preset temperature of the auxiliary heater.....(°C)	T_{solar} Solar hot water temperature in the upper part of the retrofitted tank(°C)
T_{out} Collector outlet temperature.....(°C)	t Time during stagnation periods.....(h)

1. Introduction

Only in Sweden there exist more than half a million electrically heated single family houses that use conventional water heaters for domestic hot water production [1]. Since the solar tank is one of the most expensive components in a solar thermal system, retrofitting existing domestic water heaters when installing a new system can decrease its total investment cost. Previous research approached similar retrofitting using natural convection systems [2]. Thermosyphon systems became popular in several parts of the world such as Eastern Asia and Australia mainly due to its simplicity and reliability [3]. The thermosyphon driving force depends on the pressure difference and frictional losses between the heat exchanger side-arm and the tank. Hence, the generated flow will be complex function of the state of charge of the tank, the temperature profile along the heat exchanger and pipes, the height difference between the top of the heat exchanger and the top of the tank and the pressure drop in the heat exchanger, piping and connections [4].

Such dependence on the heat exchanger pressure drop and tank characteristics limits how the retrofit is carried out and which storage tanks can be used. Moreover, Liu and Davidson (1995) [5] showed that, when properly designed, forced circulation systems can generally achieve higher performances compared to natural convection driven systems.

In this research forced circulation was used to connect solar collectors to conventional domestic water heaters. This was carried out by means of two pumps, one in the tank loop and the other in the solar collector loop. Four different system configurations were simulated in TRNSYS [6]. Since forced circulation is used, almost any kind of storage tank can be retrofitted when installing a new solar thermal system. For a better understanding of the research contribution to the field and to increase the paper readability, the main objectives of the study are stated below:

- To compare the performance of different alternatives on retrofitting conventional domestic water heaters when installing a solar thermal system;
- To compare the performance of the retrofitted system with the performance of a standard solar thermal system.

2. Methodology

Four different simulation models of the retrofitted system were created in TRNSYS software [6] in order to estimate the configuration achieving the highest performance. A comparison with a conventional flat plate system was also performed. The retrofitted system models range from simple connections to more advanced configurations. However, the complexity was never raised up to a level that would be technically difficult to build such a system in practice. Also, it was avoided to design configurations that would predictably cause such a rise on the investment cost that would be hardly paid back by the increase in energy savings. Some of the systems' details are not revealed due to patent pending. Each system model is made up of a solar collector array, storage tank/s, auxiliary heater, heat exchanger between the collector and the tank loops, circulation pump/s, and radiation processor.

The main boundary of this investigation was to use the most common type of existing heater in single family houses in Sweden. This information is very important for the system design but also very hard to attain. To the best of our knowledge, there is no official data concerning the most common tank size in such houses. According to the Swedish domestic water heater manufacturers, installers and researchers in the field, the most common Swedish single family house tank size is 200-300 litres, depending on the family size. In any case, the tank volume tends to be proportional to the family size. Thus, the trend is that higher loads also correspond to higher available storage volumes and the system design strategy does not change. On the other hand, the average domestic hot water load in single family houses is documented. Preliminary results showed that retrofitting a 300 litre tank for such a domestic hot water load would achieve a higher annual solar fraction than using a 200 litre tank. Hence, to work on the safe side, it was decided to retrofit a 200 litre tank. If such a system achieves satisfactory performances the same should happen if a 300 litre tank is retrofitted instead.

An auxiliary heater power of 3 kW was used in all models since this is also the most common. The auxiliary heater keeps the top volume of the storage at 60°C. This is a recommendation of the Swedish building regulations to avoid legionella problems [7]. The same document legislate that it is mandatory that the hot water temperature available at the tap is not less than 50°C. As a design guideline it is recommended that the domestic hot water system can be able to deliver two times 140 litres of 40°C water in one hour [7]. If the temperature setting is increased, all the different simulated systems reach approximately this peak on consumption. In practice, the thermostat is set to 60°C which ensures that ordinary loads are fulfilled. In case of extraordinary large draw-offs, the user has the possibility to steer the set point temperature. This is also normally the case for stand-alone conventional heaters.

The domestic hot water load profile consists on seven different draw-offs during the day. It is a simplification of the hourly profile described by [8] but scaled down to the latest data on the Swedish average hot water consumption of 42 litres/person/day [9]. Simulation results show that using a detailed hour profile would have a minimum impact on the results and would only increase the simulation total time. The measured average cold water temperature in the taps was 8.5°C. The consumption variation during the year was also introduced [10]. The daily and yearly domestic hot water profiles used in the models are shown in Figure 1. The average number of inhabitants in Swedish single-family houses is three [11]. Hence, the domestic hot water annual consumption in these houses was estimated to be 2050 kWh/year.

Since long stagnation periods affect the system’s long-term reliability and can cause serious permanent damages on its components [12], the criteria used to design the collector array was based on the maximum solar fraction possible to be achieved under a certain overproduction limit. This deterioration factor was set to 5000 °C.h/year and integrates the number of hours which the collector was under stagnation and how much the collector outlet temperature raised over 100 °C during that period. This was calculated in the following way:

$$\Sigma (T_{out}-100) t \text{ (}^\circ\text{C.h) (during stagnation periods)} \quad (1)$$

Stagnation period was defined by the time period during which both the top of the storage tank and the outlet collector temperature was above 100°C. During this period the pump on the collector loop is stopped. As shown in equation 1, it was assumed that stagnation time and collector outlet temperatures above 100°C have a linear influence on this parameter. 5000°C.h/year was considered to represent a reasonable practical maximum overproduction. This corresponds to, for example, 100 hours at stagnation where the collector outlet temperature was 150°C. Hence, by means of simulation, the maximum collector area that ensures maximum solar fraction under the overproduction limit was determined for each system configuration at a 50° collector tilt from horizontal. This design criteria is further discussed in the “Results and Discussion” chapter.

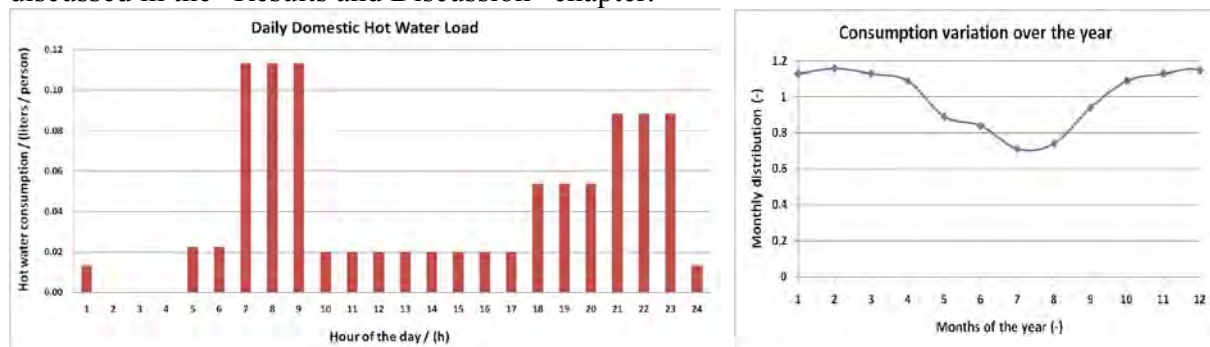


Fig. 1. Daily and yearly domestic hot water profile.

2.1. Standard system

A model of a standard solar thermal system was created and is described by the sketch in Figure 2. The figure illustrates a solar tank with an internal heat exchanger and auxiliary heater. The storage volume is 255 litres in order to match the volume of the retrofitted system that has the best performance (retrofitted system 4, Figure 6). There are three temperature sensors that control the pump, two placed on the tank’s surface and the other at the collector outlet.

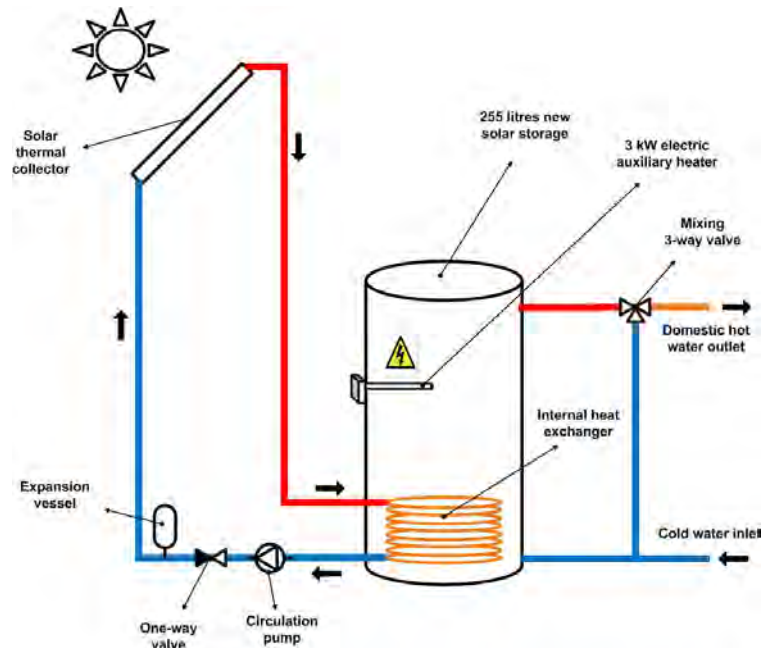


Fig. 2. Sketch of the standard solar thermal system.

2.2. Retrofitted system 1

Figure 3 describes one of the most simple and direct ways of assembling solar collectors to existing tank heaters. The connection is carried out by means of an external side-arm heat exchanger between the collector and the tank loops. Also, two temperature sensors are placed on the tank's surface in order to control both the collector and the tank pumps. As exemplified in Figure 2, solar storages are specially designed for solar thermal applications with, at least, two connections for the domestic hot water and two others for the solar collector loop. On the other hand, conventional tank heaters have only the two connections for domestic hot water (see Figure 3). In order to overcome this technical challenge, the working period of the pump placed on the tank loop must be controlled with the domestic hot water draw-offs so they do not coincide. When no hot water is required, the pump is able to charge the tank. When draw-offs take place, the pump is turned off and the incoming cold water is pressed in the bottom of the tank replacing the outgoing domestic hot water at the top.

2.3. Retrofitted system 2

In this system, a new 3 kW auxiliary water heater is added to the side-arm heat exchanger (Figure 4). Alternatively, if possible, the old auxiliary heater at the bottom of the existing tank can be used. The aim is to achieve stratification in the tank. The heater and the pump on the tank loop are turned on when the temperature in the sensor placed on the top of tank falls below the set point temperature minus the dead band. Consequently, the cold water in the tank bottom flows through the heat exchanger and is heated up in the side-arm heater before entering the top of the tank. The heater is turned off when the temperature on the upper sensor is higher than the set point temperature plus the dead band.

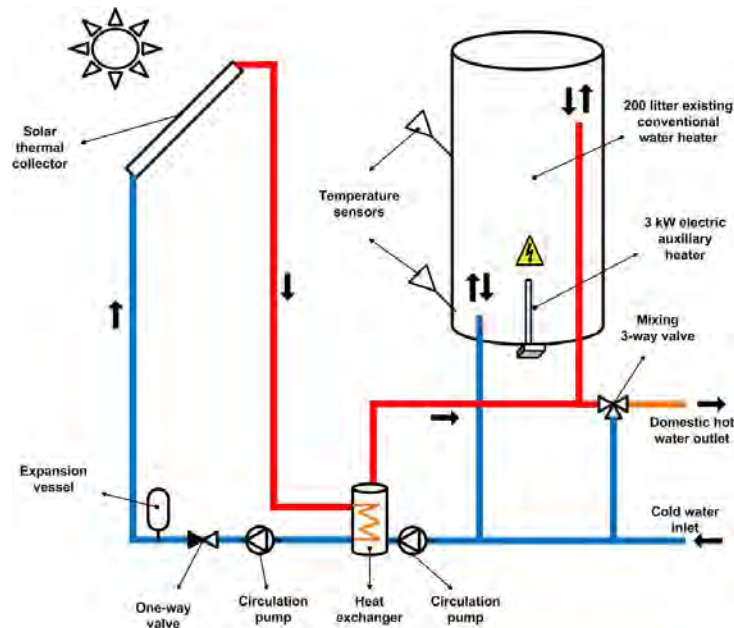


Fig. 3. Retrofitted system 1 - simple retrofitting of existing hot water heaters.

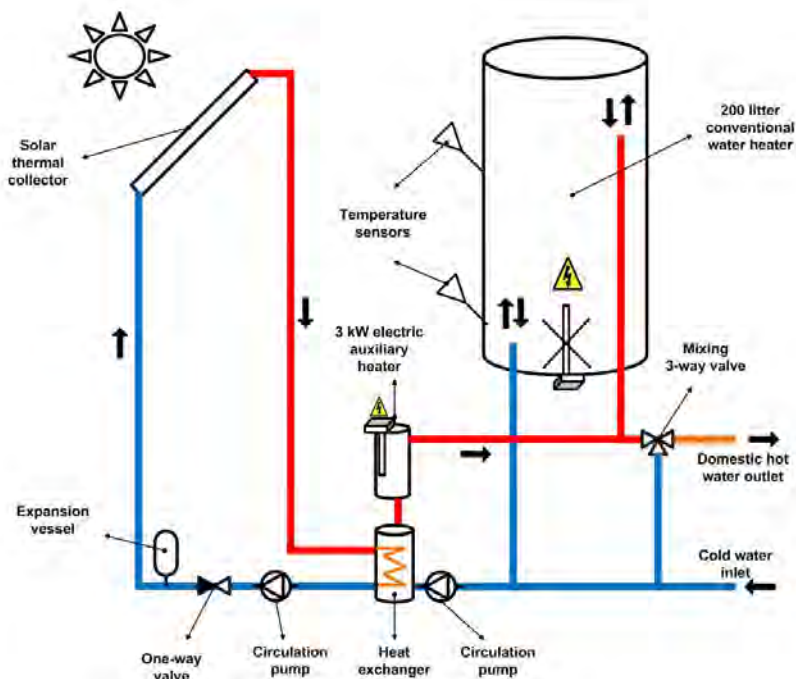


Fig. 4. Retrofitted system 2 - retrofitted system with auxiliary heater on the side-arm.

2.4. Retrofitted system 3

In retrofitted system 3, a small 55 litre auxiliary heater storage was added to the system (Figure 5). This means that the retrofitted storage is exclusively used for solar hot water. The volume of 55 litres was chosen based on design guideline for the domestic hot water load. The 4-way valve was modelled in TRNSYS using type 221 [13]. The valve has three inlets, two from hot sources and one from a cold source. It is programmed in order to use as much water volume as possible from the colder hot source which, in this case, corresponds to the solar storage. Hence, as long as there is available solar hot water in the retrofitted storage at the same temperature or above the domestic hot water load temperature, the water inside the auxiliary heater tank will not be used.

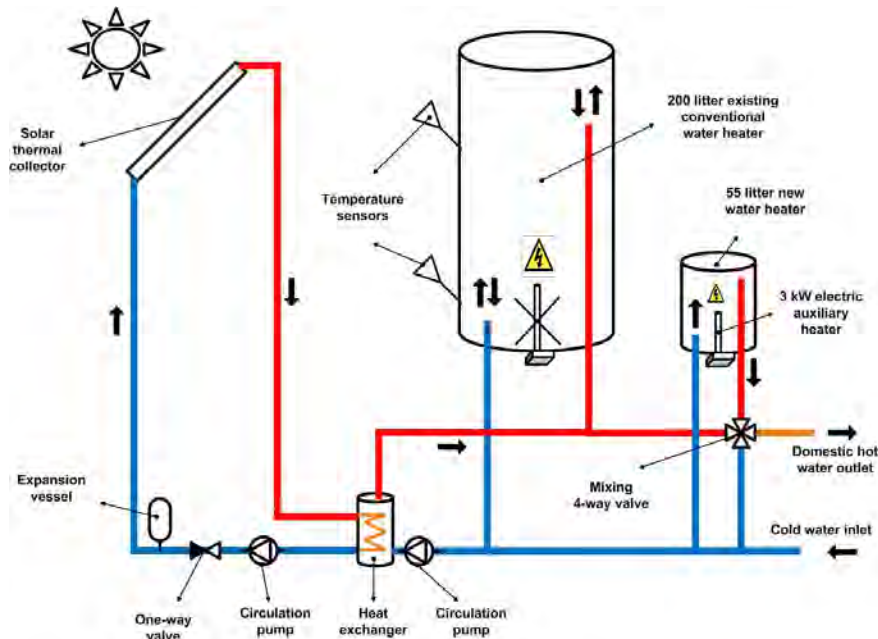


Fig. 5. Retrofitted system 3 - retrofitted system with an additional tank heater connected in parallel.

2.5. Retrofitted system 4

The last retrofitted system consists of connecting the small heater storage to the existing heater in series instead (Figure 6). Thus, when hot water is drawn off by the user, the water at the top of the solar storage is pushed to the bottom of the small heater.

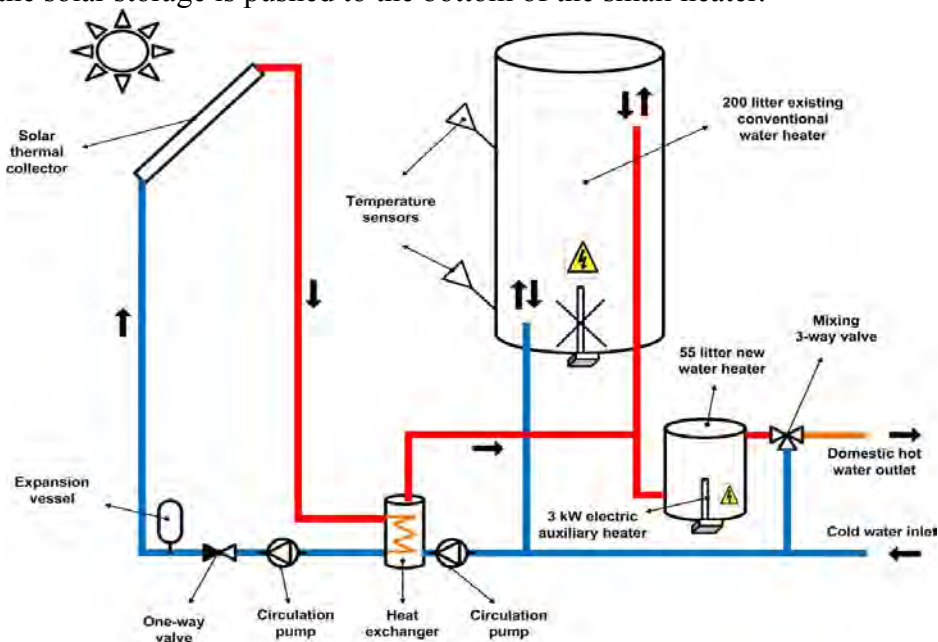


Fig. 6. Retrofitted system 4 - retrofitted system with an additional tank heater connected in series.

3. Results and Discussion

The assumed design criterion limiting the collector area takes into account not only the number of stagnation hours but also the collector outlet temperature. This deterioration factor was set to 5000 °C.h/year. Obviously, this design criterion can be questioned, especially when it comes to the particular chosen number of 5000 °C .h/year. Also, it is uncertain if temperature and time during stagnation periods should have equal weight on this factor.

Hence, further research is needed to understand how to quantify this factor and what should be its weight on the system design. However, the intention is to take into account a deterioration factor when designing a new solar thermal system. The assumed design guideline should be seen as a first iteration step in that direction. The important analysis at this stage is result comparison between these two different collector systems rather than conclude about the absolute value of the solar fraction results. As both systems were designed in the same way, inaccuracies that occur in one system will occur in the same way in the other one. This makes it significantly more reliable to take conclusions about the systems performances. In a future analysis the system should be design to minimize the costs per produced energy unit.

The simulation results of the annual solar fraction for every system are presented in Table 1.

Table 1. Annual solar fraction of the various retrofitted systems and the standard solar system.

System name	Annual solar fraction (%)
Standard system	52%
Retrofitted system 1	6%
Retrofitted system 2	15%
Retrofitted system 3	42%
Retrofitted system 4	53%

Retrofitted system 1 shows a very low annual solar fraction of 6%. This can be explained by the auxiliary heater placing at the bottom of tank which makes it impossible to establish any tank stratification. In addition, the cold water pushed in the bottom of the tank is directly heated to the set point temperature of 60°C demanding constantly auxiliary energy every time a draw-off takes place. Also, the inlet collector temperature is 60°C practically all year long which decreases the working hours and its efficiency.

In retrofitted system 2 the auxiliary heater is moved to the tank side-arm aiming to increase stratification. The results show that the annual solar fraction increases only to 15%. This is mainly explained by the small stratification increase. In this configuration, the upper volume of the tank is always at least at 60°C while the bottom is fairly cold most of the time. This is because hot water is extracted during the whole day and replaced by cold water at the bottom. Hence, the collector pump works many hours when the collector outlet temperature is higher than the tank bottom but lower than 60°C. Due to the inlets geometry of the retrofitted tank, water heated by the collector is placed at the very top of the tank. Consequently, the tank top temperature will decrease and destroy stratification making the auxiliary heater run during most of the year.

Simulation results of retrofitted system 3 show that the solar fraction increases to 42%. Since it is difficult to achieve stratification with the connections of the retrofitted tank it is more advantageous to place the heater in another tank. This prevents the heater to be turned on almost continuously when the collector is working at temperatures under 60°C. Hence, the retrofitted tank will work at lower temperatures increasing the collector working hours and efficiency. In addition, a new well insulated hot temperature tank provides the extra energy when solar energy is not available. Having the larger tank working at lower temperatures and the smaller tank at higher temperatures, decrease significantly the heat losses. One can say that the system “stratification” is achieved by two tanks with low stratification but working at different average temperatures.

The estimated annual solar fraction for retrofitted system 4 is 53%. The reason why the solar fraction of the series connected system is higher than the parallel connection is not obvious.

The main reason is that, during the summer period when solar hot water is available over 60°C, the total solar storage volume of the series connected system is increased to 255 litres, since both tanks are connected in series and no auxiliary energy is needed.

4. Conclusions

Four different system configurations on how to retrofit existing domestic hot water heaters were theoretically analysed. The simulation results show that the best configuration for the retrofitting consists on using the existing tank for solar hot water storage and connect it in series with a small auxiliary heater tank. The system annual performance was compared with that of a conventional solar thermal system. Preliminary results show that its annual solar fraction is 53% compared to 52% of a standard solar thermal system with the same storage volume. This means that both system performances are comparable. Hence, it is worth to further investigate and develop this retrofitting in practice. In the future, the model validation and an economical assessment will be performed. If it proves to be cost-effective, this solution can be very interesting since it can be applied not only in retrofitting existing tank heaters but also in combination with new heaters accessing a world-wide industry.

References

- [1] Swedish Energy Agency, Energy statistics for one- and two- dwelling buildings in 2008, 2009.
- [2] Cruickshank, C. and Harrison, S., Analysis of a Modular Thermal Storage for Solar Heating Systems, Proceedings of Canadian Solar Buildings Conference, 2004.
- [3] Lin, Q., Analysis, Modelling and Optimum Design of Solar Domestic Hot Water Systems, Ph.D. thesis, 1998, ISBN 87-7877-023-8.
- [4] Fraser, K. F., Hollands, K. G. T. And Brunger, A. P., An Empirical Model for Natural Convection Heat Exchangers in SDHW Systems, *Solar Energy* 55(2), 1995, pp. 75-84.
- [5] Liu, W. and Davidson, J., Comparison of Natural Convection Heat Exchangers for Solar Water Heating Systems, Proceedings of American Solar Energy Society Conference, 1995.
- [6] Klein, S. et al., TRNSYS, a Transient System Simulation Program, University of Wisconsin, Madison, 1999.
- [7] Swedish Building Regulation, Regelsamling för byggande, BBR 2008, ISBN 978-91-86045-03-6.
- [8] Widén, J., Lundh, M., Vassileva, I., Dahlquist, E., Ellegård, K. and Wäckelgård, E., Constructing load profiles for household electricity and hot water from time-use data— Modelling approach and validation, *Energy and Buildings* 41(7), 2009, pp. 753-768.
- [9] Stengård, L., Mätning av kall- och varmevattenanvändning i 44 hushåll, 2009.
- [10] Swedish Energy Agency, FEBY – Krav Specifikation för Minienergihus, 2009.
- [11] Statistics Sweden, Boende och boendeutgifter 2006, BO 23 SM 0801, 2006.
- [12] Hausner, R. and Fink, C., Stagnation behaviour of solar thermal systems, IEA SHC, task 26, 2002.
- [13] Nordlander S. and Bales C., TRNSYS type 221, distributed by the Solar Energy Research Centre, Sweden, 2007.

Travelling Energy Collectors

Ernst Kussul*, Tatiana Baidyk, José Saniger, Felipe Lara, Neil Bruce

CCADET, UNAM, Mexico city, Mexico

* Corresponding author. Tel: +52 55 56228602 ext.1204, Fax: +52 55 55500654, E-mail:
ekussul@servidor.unam.mx

Abstract: Almost all modern solar and wind energy plants can be used only as auxiliary energy sources because of their intermittent character. On the other hand, geothermal systems can produce energy continuously. However, geothermal power plants need expensive wells, and the well will not always give high temperature underground water. It is possible to improve the performance of the plant by combining the different features of these mentioned systems. It is possible to obtain hot water not from drills but by using solar and wind energy installations placed on mobile platforms (travelling energy collectors) that will transport hot water to the power plant, where it will be stored in special tanks. A similar procedure is possible for cold water. To transform thermal energy, stored in the hot water and cold water tanks to electric energy it is possible to use conventional equipment of geothermal power plants. In this paper we give estimations of some parameters of the proposed power generation system based on travelling energy collectors. The estimations show that the power plant based on travelling energy collectors can be considered as a base load source of electric energy.

Keywords: Solar energy, Wind energy, Travelling energy collector

1. Introduction

Solar energy and wind energy can be considered as complementary. Solar energy can be captured only during daytime. Wind energy at a height of more than 80 meters is more intensive at night time. In summer it is possible to obtain more solar energy than in winter, and in winter there is more wind energy. So, it is useful to make power plants based on both solar and wind energies.

If we want to create a base load power plant that uses solar and wind energy we also need to store energy for at least some days. The best type of energy storage for such a period is Thermal Energy Storage (TES). Many types of thermal energy storages have been proposed. In this article we will suppose that the TES is based on hot and cold water. Water is the cheapest material and it has high heat capacity.

The proposed solar-wind power plant will work as follows: solar concentrators will prepare hot water for TES, and wind powered refrigerators will produce cold water for TES. Sometimes wind powered heaters can be added to produce an additional amount of hot water. Hot water and cold water from the TES will be used to produce the electric energy with the same equipment that is used for geothermal power plants. The hot water from the TES can also be used for space heating and the cold water can be used for air conditioning purposes.

In principle, the solar concentrators can be placed in a compact area, but the wind power installations must be distributed in a relatively large region because of the turbulences that each installation produces. Moreover, wind speed is higher over the sea surface, and the power plant is to be located on the shore. For these reasons we propose Travelling Energy Collectors (TEC) that will collect solar and wind energy on the sea surface and transport this energy in the form of hot and cold water to the power plant. The distance of transportation (or service radius) will depend on economical considerations and can vary from some kilometers to many tenths of kilometers.

2. Methodology

2.1. Power plant based on travelling energy collectors

The scheme of the power plant based on travelling energy collectors (TEC power plant) is shown in Fig.1.

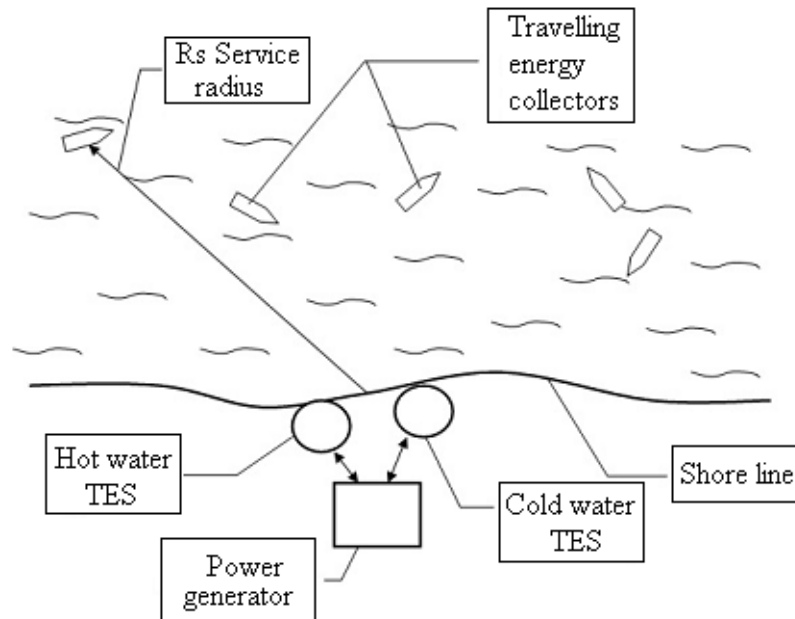


Fig. 1. Power plant based on travelling energy collectors.

It contains a power generator, hot water TES, cold water TES, and a multitude of thermal energy collectors (TECs). The TECs collect the solar and wind energy from the circular segment that has radius R_s , transform these energies to the hot water and cold water, and transport them to the hot water TES and cold water TES. The water from the hot water TES is supplied to the vapor generator that produces energy in the heat engine with the Organic Rankine Cycle (ORC). This type of engine is used for geothermal power plants. The water from the cold water TES is used for heat engine cooling. The Carnot efficiency of the power generator will be:

$$\eta_c = (T_h - T_c) / T_h \quad (1)$$

where T_h is the temperature of hot water and T_c is the temperature of cold water. The total efficiency of the power generator will be:

$$\eta = \eta_c \cdot \eta_r \quad (2)$$

where η_r is the relation of power generator efficiency to its Carnot efficiency. For ORC heat engines η_r usually has the values in the range of 0.5 – 0.67 [1]. In this article we will use a value $\eta_r = 0.55$.

If the temperature of the hot water is 90° C and the temperature of the cold water is 5° C, the efficiencies of the power generator will be:

$$\eta_c = 0.234, \quad \eta = 0.129 \quad (3)$$

If we put the hot water TES at a depth of 50 m below the sea surface to obtain overpressure of 5 bar, it will be possible to increase the hot water temperature up to 140° C. The temperature of the cold water can be decreased down to – 20° C, if we use an ice-water mixture of salted water. In this case the power generator efficiencies will be:

$$\eta_c = 0.387, \quad \eta = 0.21 \quad (4)$$

The efficiency 0.21 is at the level of the highest efficiencies of silicon photovoltaic panels, but in our case the power generator can supply the energy continuously.

2.2. Travelling energy collectors

A travelling energy collector (TEC) will be made as an unmanned sail catamaran. The scheme of the TEC is presented in Fig.2.

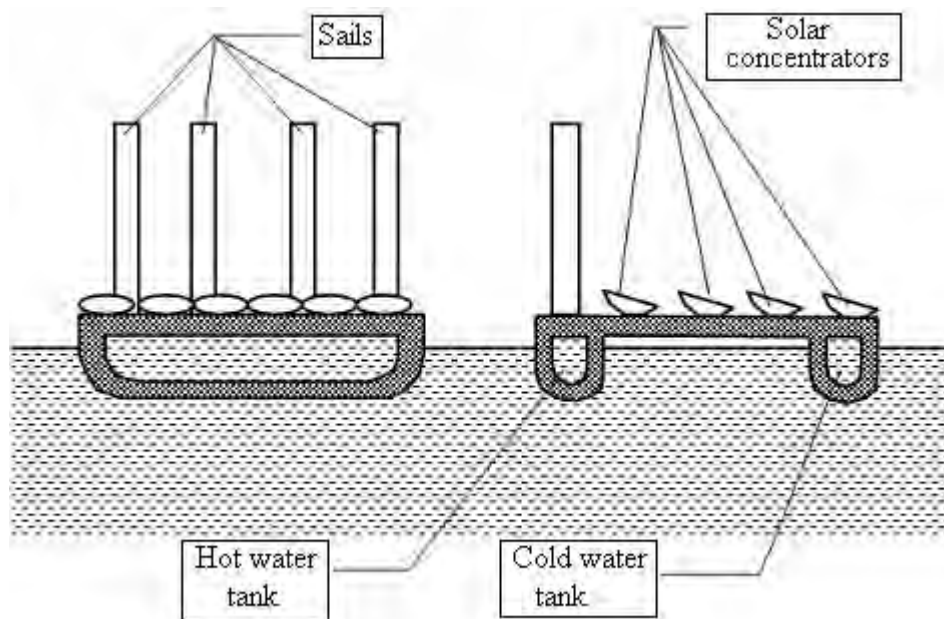


Fig.2. The scheme of the TEC.

The TEC contains sails, solar concentrators, small wind turbines, hot water tank and cold water tank. There are different types of maritime wind collectors. Some of them contain large wind turbines on the ship, others use the sails to move the ship, and submerged water turbine produce the electric energy [2]. We propose to use small wind turbines, because large wind turbines have large weight, and the scheme containing the submerged water turbine has low efficiency. Small wind turbines can be placed into the sails (Fig.3).

In this case the film roll and the rope roll will be placed in the leading edge of the sail. When the TEC is working in the mode of wind energy collection, the sail film is wound to the film roll and small wind turbines are open for the wind. If the sail is to be used to move the catamaran, the ropes will be wound to the rope roll. These ropes run around the rear roll and pull the film from the film roll to close the wind turbine space and to form the sail air foil. The TEC will work in solar energy mode in the presence of direct solar radiation; otherwise it will work in wind energy mode, in transport mode, or in discharge mode.

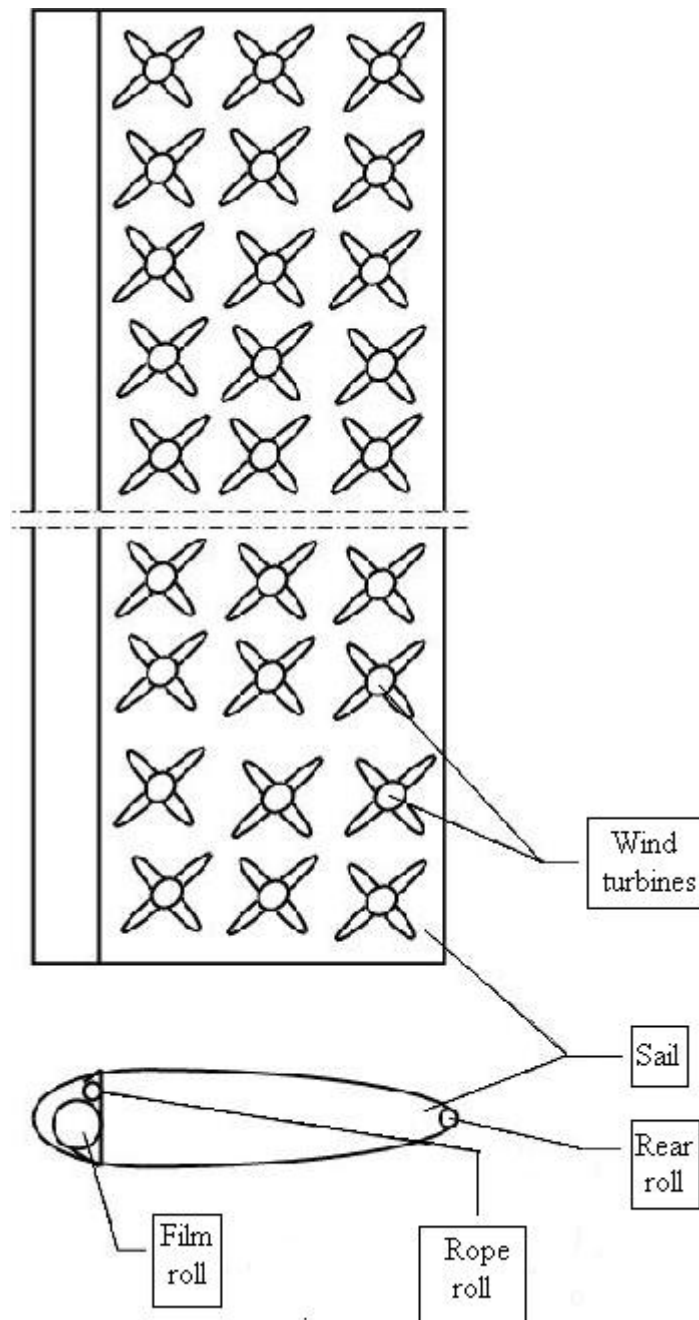


Fig.3. Small wind turbines.

In the solar energy mode the solar collectors will heat the water in the hot water tank. In the wind energy mode the energy from the wind turbines will feed the chiller to cool the ice-water mixture in the cold water tank and increase the amount of ice in the mixture. The approximate proportion of hot water energy to the cold water energy is:

$$E_h / E_c = T_h / T_c, \quad (5)$$

where E_h is the energy of the hot water stored in the hot water tank, E_c is the energy of the ice-water mixture stored in the cold water tank, T_h is mean temperature of the hot water tank, and T_c is the temperature of the cold water tank.

The hot-water energy can be calculated using the equation:

$$E_h = M_h \cdot C_w \cdot (T_{h1} - T_{h2}), \quad (6)$$

where E_h is the hot water energy, M_h is the hot water mass, C_w is specific heat capacity of the water, T_{h1} is the temperature of the hot water after the heating in the solar concentrators, T_{h2} is the temperature of the hot water before heating in the solar concentrators.

To calculate the cold water energy we will use the following equation:

$$E_c = M_i \cdot q_i, \quad (7)$$

where E_c is the cold water energy, M_i is the mass of the ice in the ice-water mixture, and q_i is the latent heat of ice melting.

3. Solar Concentrators

Low-cost light-weight solar concentrators are needed for travelling energy collectors to heat the water in the hot water tank. At present we are developing these concentrators [3]. Each concentrator will contain a multitude of flat triangular mirrors that approximate a parabolic surface. A prototype of the support frame for the mirrors is shown in Fig.4.

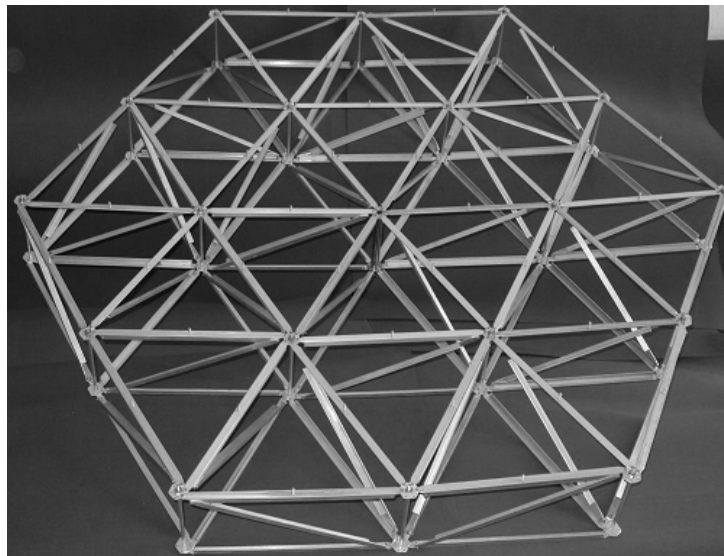


Fig.4. Support frame for the mirrors of solar concentrator.

The cost of mass production of these concentrators can be as low as 50 dollars for square meter of mirror surface [4].

3.1. Solar energy mode

The travelling energy collector will work in the solar energy mode in the presence of direct solar radiation. Let the TEC have a deck area of 1000 m². In this case the total area of solar concentrators can be approximately 500 m². Let us suppose that 1 m² of solar concentrator produces 700 Wt of heating power (concentrator efficiency is 0.7), and direct solar radiation is present during 4 hours per day. In this case the hot water will obtain the energy of

$$E_h = 504 \cdot 10^7 \text{ J/day.} \quad (8)$$

Let the initial temperature of hot water be $T_{h2} = 403^\circ \text{ K}$, the final temperature of hot water will be $T_{h1} = 423^\circ \text{ K}$. In this paper we will consider a TEC that discharges the hot and cold water each day. Using equation (6) it is possible to calculate the mass of hot water needed to store the heat energy in the hot water tank. In our case we will have:

$$M_h = 60000 \text{ kg} = 60 \text{ ton,} \quad (9)$$

3.2. Wind mode

In the nights and during cloudy days the TEC will work in the wind mode. For this purpose the TEC is to be oriented perpendicular to the wind speed, the sails are to be opened, and small wind turbines will produce the electrical energy for the ice machine. The ice machine will increase the amount of ice in the cold water tank. Using equations (5) and (8) we obtain:

$$E_c = E_h \cdot (T_c / T_h) = 504 \cdot 10^7 \cdot (253 / 413) = 308 \cdot 10^7 \text{ J/day} \quad (10)$$

Here we suppose that T_c equals -20° C and T_h equals 140° C .

The power of wind turbines can be evaluated using the equation:

$$P_t = \eta_t \cdot S_t \cdot (\rho \cdot u^3) / 2 \quad (11)$$

where η_t is turbine efficiency, S_t is the total area of the small wind turbines, ρ is the air density, and u is the wind speed. In this paper we will assume that $\eta_t = 0.3$, $S_t = 500 \text{ m}^2$, $\rho = 1.25 \text{ kg/m}^3$ and $u = 8 \text{ m/s}$. In this case we will have:

$$P_t = 48000 \text{ Wt,} \quad (12)$$

We will suppose that the transport and the discharge modes will take 3 hours per day. The solar mode takes 4 hours per day, so the wind mode will take 17 hours per day. Not all this time will be used for power generation, because the TEC has a drift that must be periodically compensated. For drift compensation the sails are to be closed as for transport mode and the TEC is to be moved against the wind. We will assume that drift compensation will take 30% of the total time in the wind mode. The power generation in the wind mode will take $t_g = 11.9$ hours per day. The energy generated by the wind turbines will be:

$$E_t = P_t \cdot t_g \cdot 3600 = 206 \cdot 10^7 \text{ J/day,} \quad (13)$$

If coefficient of performance of the ice machine is 1.5, the total cooling energy produced in the form of ice will be $E_c = 308 \cdot 10^7 \text{ J/day}$. This is sufficient to obtain the balance of heating and cooling energies in the power plant. To store this amount of energy it is necessary to produce the following mass of ice:

$$M_i = E_c / q_i, \quad (14)$$

where E_c is the cooling energy, q_i is the latent heat of water freezing. Water has the value of $q_i = 332$ kJ/kg. For our example M_i will be:

$$M_i = 9300 \text{ kg} . \quad (15)$$

We will assume that the mass of the ice-water mixture is:

$$M_{iw} = 40000 \text{ kg} = 40 \text{ ton}, \quad (16)$$

In this case the total weight of hot water and cold water in the tanks will be 100 ton. Different geographic areas have different relations between the amount of solar and wind energy, thus for each area different parameters of the power plant should be selected. The main parameter is the cold-water tank temperature. Increasing this temperature, it is possible to decrease the amount of wind energy to obtain good balance for example in tropical areas, where the wind energy can be relatively poor.

3.3. Transport and discharge modes

In transport mode the sails move the TEC from the power plant and after collection of energy return it to the power plant. The maximum distance of movement is:

$$R_s = t_{tr} \cdot u_{tr} / 2, \quad (17)$$

where R_s is the service radius of the power plant, t_{tr} is the time of the transportation mode, u_{tr} is the transportation speed. In our example $t_{tr} = 2$ hours. If the transportation speed is 10 km/h, the service radius will be:

$$R_s = 10 \text{ km}. \quad (18)$$

In the discharge mode the TEC discharges the hot water to the large hot-water tank of the power plant. The temperature of the discharged water is T_{h1} . After this the TEC loads its hot water tank from the large hot-water tank of the power plant with water that has the temperature T_{h2} . In parallel the ice-water mixture that contains M_{i1} kilograms of ice is discharged to the large cold-water tank of the power plant and a new ice-water mixture that contains M_{i2} kilograms of the ice is loaded to the small cold-water tank of the TEC.

3.4. TEC number

One TEC produces the energy of $504 \cdot 10^7$ J / day. This corresponds to a mean power $P_{TEC} = 58330$ Wt. If we want to create a power plant of power P_{pp} , we need the following number

N_{TEC} :

$$N_{TEC} = P_{pp} / (P_{TEC} \cdot \eta), \quad (19)$$

where P_{pp} is the output power of the power plant, P_{TEC} is the power of one TEC, η is the efficiency of the power plant. If $P_{pp} = 10$ MWt, $\eta = 0,21$, we need:

$$N_{TEC} = 816. \quad (20)$$

This calculation shows that each TEC cannot be driven by an operator. It must be made as an autonomous robot, and its cost is to be as low as possible.

4. Discussion

A power plant for continuous electrical energy supply is proposed. In this power plant the conventional equipment from geothermal power plants is used for electricity generation. Instead of drilling deep wells to obtain hot water we propose the use of moving platforms (TECs) that contain solar concentrators for hot water production and small wind turbines for cold water production. Moving platforms transport the hot and cold water to the power plant located on the sea shore. Approximate calculations show the feasibility of this system.

5. Conclusion

Travelling energy collectors will permit solar and wind energy collection from sea areas near the shore, transform it to heat energy and store in hot water and cold water thermal energy storages. These storages will permit continuous energy production using the equipment of geothermal power plants. The travelling energy collector will be implemented as a catamaran with sails that include a multitude of small wind turbines. The solar concentrators will be placed on the deck of the catamaran. The catamaran will contain a hot water tank and a cold water tank to transport the heat energy to the power plant. It is necessary to make a large number of travelling energy collectors for one power plant. For this reason the catamaran must have an autonomous control system that will allow operation without human interaction.

Acknowledgment

This work was supported partially by projects CONACYT50231, PAPIIT IN110510-3, PAPIIT IN119610 and the project ICyTDF 330/2009.

References

- [1] K. Rafferty, Geothermal power generation. A primer on low temperature, small-scale applications, <http://geoheat.oit.edu/pdf/powergen.pdf>.
- [2] Y.Terao, K. Watanabe, M. Wakita, A feasibility study of an ocean power plant using a mega yacht system, Proceedings of the Second International Conference on Marine Research and Transportation, 2007, pp. 55-62.
- [3] Kussul E., Baidyk T., Lara F., Saniger J., Bruce N., Estrada C., Micro facet solar concentrador, *International Journal of Sustainable Energy*, 2008, Vol.27, Issue 2, pp.61-71.
- [4] Kussul E., Baidyk T., Makeyev O., Lara-Rosano F., Saniger J.M., Bruce N., Flat facet parabolic solar concentrator, The 2nd WSEAS/IASME International Conference on Renewable Energy Sources (RES-08)-2008, October 26-28, 2008, Corfu, Greece, pp.46-51.

Configuration of daylighting system via fibers and experiments of concentrated sunlight transmission

Song JF^{1,*}, Yang YP¹, Hou HJ¹, Zhang MX¹

¹ The New and Renewable Energy of Beijing Key Laboratory, North China Electric Power University, Beijing, 102206, China

* Corresponding author. Tel: +86-10-61772816, Fax: +86-10-61772816, E-mail: songjifeng@ncepu.edu.cn

Abstract: A daylight concentrating and transmission system via plastic fibers based on dual axis sun tracker to lighting indoor has been built and investigated. The sunlight tracking and concentrating platform adopting horizontal coordinate system combined with photosensitive sensor can realize high position resolution. A sunlight concentrating and transmission experiment has been carried out using 6m long PMMA plastic fibers based on that platform. It is found that color temperature of light transmitted by fibers is 600K lower than that of nature light. The spectrum of light transmitted by fibers is similar to that of nature light. This similarity also exists in chromaticity coordinate, color rendering index, dominant wavelength between light transmitted by fibers and nature light. A quantitative determination of flux loss has been carried out and the results show that there is an attenuation about 2db existing on the interface of fiber.

Keywords: Sun tracking, Fibers, Concentrated, Transmission

Nomenclature (Optional)

NA numerical aperture.....	ψ longitude.....
α altitude angle.....	T colour temperature.....K
γ azimuth angle.....	λ intrinsic attenuation constant.....db/m
φ latitude.....	z length of fibres.....m
δ declination.....	γ loss coefficient on fibers' facet.....db
P_{out} output light flux.....lumen	η total loss coefficientdb
P_{in} input light flux..... lumen	I illumination..... lux
τ time adjustment.....s	D diameter of fibersm

1. Introduction

The daylighting system is an optic-mechanical-electric technology that collects day light outside to transmit into basement and room lacking nature light by fibers in high concentrated level [1-2]. The infrared portion of solar radiation has been separated and eliminated by lens and fibers so that the output flux is a cool light. There are two major benefits from daylighting. The first benefit is the reduction in purchased electricity needed to light the building, and the second benefit is a reduced cooling load due to the high efficiency of light. Another potential benefit of daylighting is the advantageous factors for healthy of natural lighting but this effect is difficult to quantify. The excellent color rendering properties of daylight and its close match to the photopic response of the human eye make it an ergonomic light source that is generally preferred for pleasant working conditions[3-4]. There are two types of daylighting systems including light guide pipe and fibers. The latter is the research hotspot at present due to its smaller and few penetrations on the roof which means saving on the building's heating, cooling, and maintenance bills. The purpose of this particular study is to evaluate the feasibility and performance of the technology. The day light concentrating and transmission system via fibers consists of a two-axis sun tracker and concentrating collector that gather direct normal solar radiation into the fibers. The key to realize stable flux output is high precision sun tracking which need a trade-off with fabrication cost[6]. And, at the present time, the optical parameters of sunlight transmission system via fibers have not get adequacy quantitative determination. Those problems provide the investigation motivation of this

research work. According to the structure forms, there are two ways of focalization including optical fiber bundle and single fiber. For the former, concentrator with large diameter is used to produce large focal spot, and so it can use optical fiber bundle to receive the concentrated radiation[7-9]. For the latter, the concentrator is lens with small diameter which produces small focal spot only suiting for single fiber. It is critical to obtain high accuracy position tracking in respect that small focus error will cause a large amplitude reduction of out flux due to single fiber's small diameter. Although much research has been devoted into sunlight concentrating and transmission system via fibers, there are still lots of problems and unknown characterizes awaiting solutions, such as quantitative study of the spectrum of output light. In order to try to answer above questions, a dual-axis sun tracking system has been investigated by the combined use of horizontal coordinate system and photosensitive sensor designed specially, based on that corresponding research has been done.

2. Dual axis sun tracking and concentrating system

2.1. Configuration of hardware

The system mainly is composed of support, reducing gears, motor, lens and control module. It must be emphasized that small deviation of focusing spot will lead to significant instability attributed to no light preserved module existing in the daylighting system. To satisfy above strict demand, orbit calculation method and optical sensing method are integrated into control flow. The prototype of the dual axis tracking and concentrating system is shown in Fig 1.

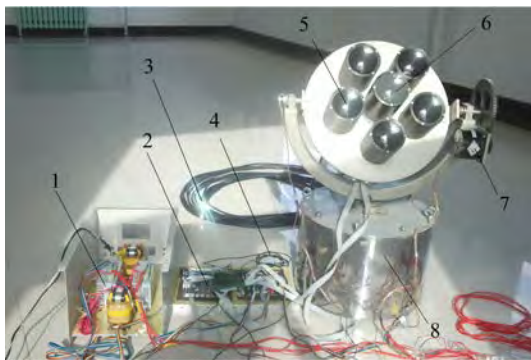


Fig. 1. Double-axis sun tracking system

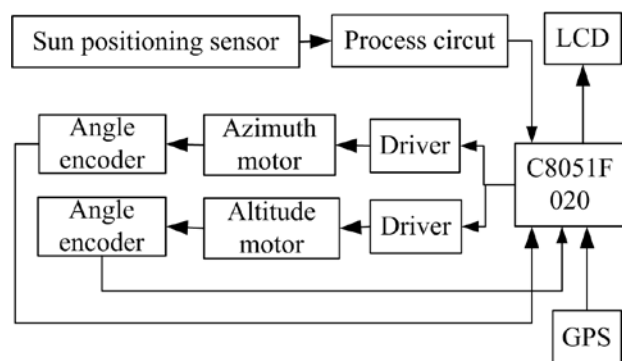


Fig. 2. Control system frame

In fig.1, the components numbered are step motor drivers, control board, plastic fibers, GPS module, lens, sun positioning sensor, altitude motor, substructure for installing azimuth motor successively. In practical, it is too difficult to realize accuracy positioning about 0.1° only depending on orbit calculation due to the varied limits, such as installation error and gravity deformation, et al, although it is possible in theory. The misalignment between geodetic coordinate and device coordinate led by installation error and gravity deformation will result in an inevitable calculation error in sun position[10]. So an optical sun positioning sensor is designed specially to eliminate the error accumulation and initial error, which uses photosensitive elements array to sensing the location of the focusing spot generated by lens. By comprehensive utilization of two methods, it is able to realize stability and high precision profit from orbit calculation method and sun optical positioning sensor respectively. The control system is designed to work automatically. Step motors are used to drive the tracking action and angle encoders are applied to feedback the real angle information of the mechanical components. Global positioning system module is adopted to provide exact time and latitude and longitude which are the parameters to calculate the sun position. With the help of GPS module, the tracking system can figure out the sunrise and sunset time to realize full automatic tracking without manual operation, meaning remarkable reduction of

maintenance. For convenience, a LCD display screen is installed to show real-time working state. Plano convex lenses made of K9 optical glass are adopted to concentrate sunlight which has a transmission coefficient that is no less than 0.9 at visible spectrum range. It is no cooling problem for lenses and fibers because there is nonexistence of hot spots due to their high transparency. Performance parameters of the hardware have been described in tab 1. To facilitate the precision drive, sinusoid subdivision drivers are used to improve step motors to achieve 12800 pulses per cycle, about 0.028° /pulse. In addition, gear pairs are applied to further improve the fine adjustment; however nonlinearity caused by gear clearance emerges isochronously. To ensure stable tracking, it is needed to introduce intelligent algorithm to compensate the nonlinearity. For instance, database is recorded in the program memory to distinguish different situations of nonlinearity. The concentrator is convex lens made of super white glass which transmittance is 0.92. According to the sun's

Table.1 Parameters of double-axis sun tracking and concentrating platform

Name	Unit	Amount	illustration
Torque of azimuth motor	N.m	3.6	Step motor
Torque of altitude motor	N.m	1.2	Step motor
Reduction ratio of azimuth		1:3	Straight gear
Reduction ratio of altitude		1:5	Straight gear
Tracking type			Orbit and optical sensor
Tracking accuracy	°	±0.15	
Range of altitude	°	0~90	
Range of azimuth	°	0~360	
Diameter of lens	m	Φ0.1	K9 material
Focal length	mm	180	Adjustable
Concentration ration		900-10000	Adjustable
Transmittance of lens		0.92	Visible band

2.2. Control method

As for the optical sun positioning sensor, it is used to detect detailed deviation and feedback the signal to microcontroller to realize exact tracking. The most important advantage of the optical sun positioning sensor is the ability to eliminate the error accumulation caused by errors from motor or reducing gears. The optical sun positioning sensor is good at dealing with error accumulation but bad at anti-climate impacts while the orbit calculation method is opposite. So it is wise to adopt combined utilization of both methods to obtain good tracking accuracy and anti-interference ability meanwhile. The flow chart of sun tracking process is shown in Fig 3. Because of complexity in practice, the flow chart has more fine regulation actions than that listed out in Fig 3.

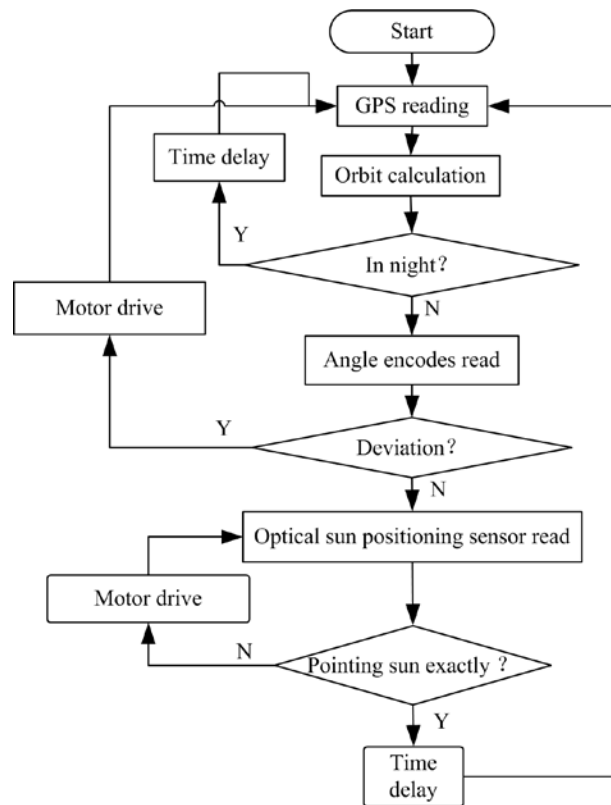


Fig.3. Control flow chart of sun tracking process

3. Plastic fibers

The diameter of fibers used for concentrated sunlight transmission is flexible and two orders of magnitude higher than that of fibers used for distant communication, whose range is 1-6mm generically. The materials of fibers include polymethyl methacrylate(PMMA), polystyrene and special quartz. Light attenuation is severe, about 0.25db/m, only suiting for close distance transmission not longer than 30m. Some parameters of the fibers tested in the work are described in Tab 2. The fiber tested in this research is made of PMMA, and has absorption peaks in 620nm and 705nm which is shown in Fig 4. The advantages of PMMA fibers are flexible and big numerical aperture which is very in favor for light focusing. Unfortunately, the upper limit for work temperature is only 70°C which restricts the upper limit of concentration ratio, about 2500 without water cooling. But this upper limit could be extended to 10000 for quartz fiber which is used in solar furnace.

Table.2 Parameters of PMMA fibers

Name	Unit	Amount	illustration
Diameter	mm	2.5	
Length	m	6	
Numerical aperture		0.5	Ranger of angle of incidence is ±30°
Average attenuation	db/m	0.25	380nm~760nm

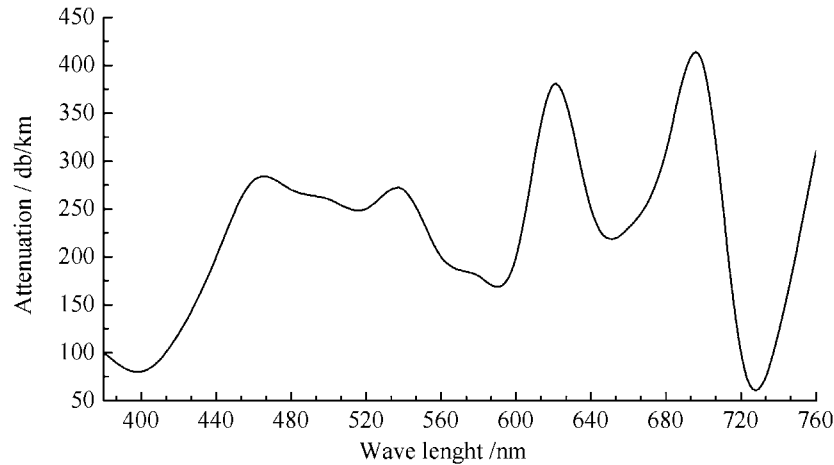


Fig.4. Curve of intrinsic attenuation of PMMA fibers

4. Results

The experimental system consists of the dual axis tracking and concentrating system, fibers, illuminometer and HAAS-2000 spectral radiometer, as in Fig 5. A sunlight concentrating and transmission experiment lasted for 9 hours has been carried out using 6m long PMMA fibers .

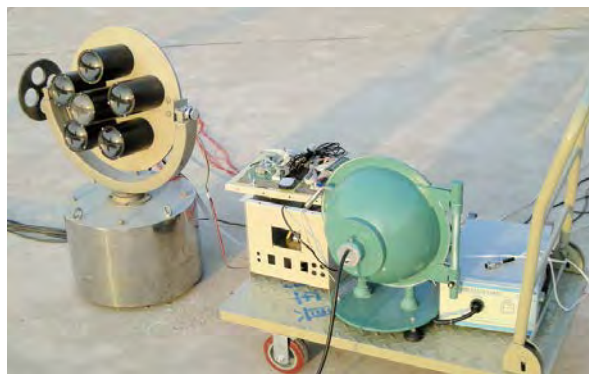


Fig.5 Optic testing system of concentrated sunlight transmission system

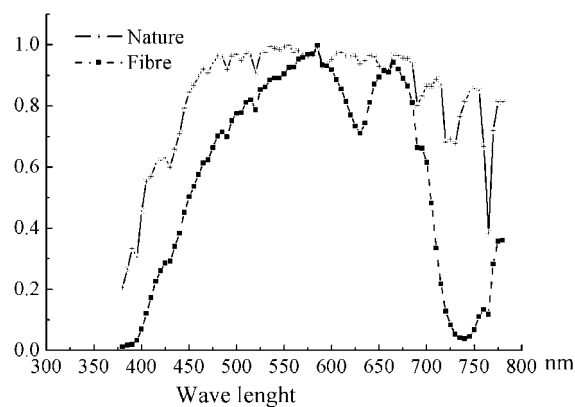


Fig.6 Spectrum comparison of nature light and light transmitted by fibers in visible band

The spectrum of light transmitted by fibers is similar to that of nature light, as shown in Fig 6. Although the deviation between two curves is evidence in 705nm led by absorption peaks of fibers, it influences the visual perception slightly because it is away from green band which is most sensitive for eyes. This similarity also exists in chromaticity coordinate, color rendering

index, dominant wavelength between light transmitted by fibers and nature light, as described in Tab 3.

Table.3 Parameters comparison between nature light and light transmitted by fibers

Parameters	Light out fibers	Daylight	Difference
Color temperature	4444K	5037K	-11.8%
Dominant wave length	571.6nm	569.4nm	+0.4%
Peak wavelength	585nm	538nm	+8.7%
Width of half wave	255.8nm	360.6nm	-29%
Color coordinate X	0.3688	0.3446	+7%
Color coordinate Y	0.3972	0.357	+11.2%
Color rendering index	88.9	99.3	-10.5%
Red light ratio	17.9	18.8	-4.8%

As identified in Tab 3, the flux transmitted through fibers is approximate to nature light, so it can satisfy the need of drawing office, indoor plant cultivation and shady bedroom.

As for the transmission loss, it consists of three parts which are intrinsic loss, loss on end faces of fibers and loss led by bend. Among them, the intrinsic loss is a constant while loss on face is a large variation, determined by roughness mainly. In fact, the loss on face takes an essential ratio of total loss. So it makes sense to make certain that how much loss on face is. A experiment for determining the value of loss on face is designed, which separates the intrinsic loss from total loss by a series calculations.

For fibers without bend, we have

$$P_{out}(z) = P_{in}(0)e^{-\lambda z} e^{-\gamma}$$

Here $z = 6m$. As for the total η , it can be described as followed

$$\eta = 10 \lg \frac{P_{out}(z)}{P_{in}(0)} = -10(\lambda z + \gamma) \lg e$$

Traditionally it is a custom to use decibel in attenuation analysis, so we have

$$\begin{cases} \bar{\lambda} = (10 \lg e) \cdot \lambda \\ \bar{\gamma} = (10 \lg e) \cdot \gamma \end{cases}$$

It is easy to get following conclusion after a further derivation

$$\begin{cases} \eta = -\bar{\lambda}z - \bar{\gamma} \\ \bar{\gamma} = -\eta - \bar{\lambda}z \end{cases}$$

$\bar{\lambda}$ is a constant known as 0.25 db/m and $P_{out}(z)$ can be measured by integrating sphere and spectroradiometer while $P_{in}(0)$ can be worked out by the following formula

$$P_{in}(0) = I \cdot \pi D^2 / 4$$

Measured data of luminance outdoor and output flux of fibers is shown in Fig 7. Two curves are anastomotic through one day.

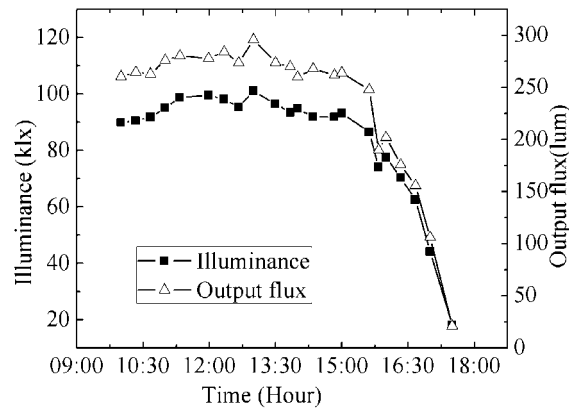


Fig.7 Corresponding relation of illumination outside and output flux of fibers

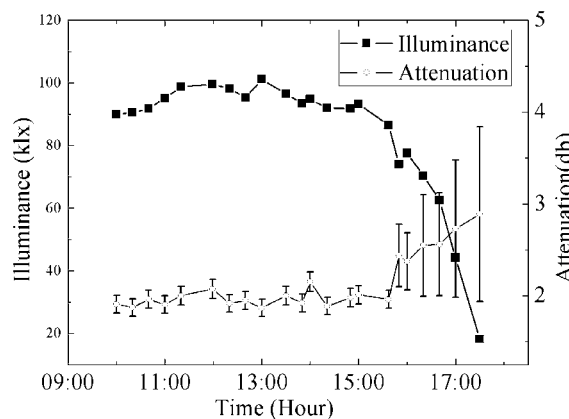


Fig.8 Corresponding relation of illumination outside and attenuation on interface

From measured data recorded in Fig7, the loss on face can be calculated out as shown in Fig 8. The loss on face can be regarded as a constant about 2db approximately which is accord with the optical principle. As to the increasing after 16:00pm, it can be explained that scattering radiation takes more and more proportion in total sunlight and this scattering radiation cannot be focusing onto the fibers, so above formulas in this situation produce large result.

5. Conclusions

Combination of orbit calculation method and sun optical positioning sensor poses accuracy and stability simultaneously in sun tracking which is the key to ensure the output flux of fibers stable. Different from solar thermal and photovoltaic application, there are no measures to storage nature light and so it is fatal when tracking error exceeds the allowable range. It must be pointed out that low speed drive is very beneficial to obtain high precision positioning in sun tracking which affords more time for the microcontroller to analyze the tracking status and implement compensation motions. This strategy makes full use of the feature of sun slow-moving. It is also relatively economic to adopt low power motors owe to the features of this strategy.

The spectrum of light transmitted by fibers is similar to that of nature light which make it favorable for places needing daylighting. Color temperature of the output light transmitted by fibres is about 600K lower than that of nature light which is caused by the selective absorption of plastic fibers. Fortunately, this selective absorption does not cause severe influence to the optical quality of sunlight transmission. The color rendering index still keeps a high value about 88.9 which is far better than those of incandescent lamp, fluorescent lamp and white LED. What's more, the loss on face of fibers cannot be neglected which is about 2db that is meaning 40% loss. The loss on face is relative to the roughness and incident angle. It requires precise measurement and mathematical modeling to establish the quantitative description of concentrated sunlight transmission.

Acknowledge

Financial support from National Natural Science Foundation of China (No.61004084) and Fundamental Research Funds for the Central Universities (09QG18) and State Key Development Program of (for) Basic Research of China (No. 2009CB219801) are appreciated.

References

- [1] C. Kandilli, K. Ulgen, Review and modelling the systems of transmission concentrated solar energy via optical fibres[J], Renewable and Sustainable Energy Reviews, Volume 13, Issue 1, January 2009, Pages 67-84.
- [2] Cemil Sungur, Multi-axes sun-tracking system with PLC control for photovoltaic panels in Turkey[J], Renewable Energy, Volume 34, Issue 4, April 2009, Pages 1119-1125.
- [3] Schlegel, G.O., et al., Analysis of a full spectrum hybrid lighting system[J]. Solar Energy, 2004. 76(4): p.359-368.
- [4] Tzempelikos, A., A.K. Athienitis, and P. Karava, Simulation of facade and envelope design options for a new institutional building[J]. Solar Energy, 2007. 81(9): p. 1088-1103.
- [5] Teolan Tomson. Discrete two-positional tracking of solar collec-tors Original Research Article, Renewable Energy, Volume 33, Issue 3, March 2008, Pages 400-405.
- [6] Tekelioglu, M. and B.D. Wood, Solar light transmission of po-lymer optical fibers. Solar Energy, 2009. 83(11): p. 2039-2049.
- [7] Tsangrassoulis, L. Doulos, M. Santamouris, et al, On the energy efficiency of a prototype hybrid daylighting system[J], Solar Energy, Volume 79, Issue 1, July 2005, Pages 56-64.
- [8] G. O. Schlegel, F. W. Burkholder, S. A. Klein, et al., Analysis of a full spectrum hybrid lighting system[J], Solar Energy, Volume 76, Issue 4, April 2004, Pages 359-368.
- [9] Earl, D.D., Maxey, C.L., Muhs, J.D., 2003. Performance of new hybrid solar lighting luminaire design[J]. In: International Solar Energy Conference, Kohala Coast, Hawaii Island, March 15–18.
- [10] H.Arbab, B.Jazi,M.Rezagholidzadeh, A computer tracking system of solar dish with two-axis degree freedoms based on picture processing of bar shadow[J], Renewable Energy, Vol34(2009) 1114-1118.

Type12 and Type56: a load structure comparison in TRNSYS

Helena Persson^{1,*}, Bengt Perers², Bo Carlsson¹

¹ School of Pure and Applied Natural Sciences, Linnaeus University, SE 39182 Kalmar, Sweden

² Department of Civil Engineering DTU, DK-2800 Kgs. Lyngby, Denmark

* Corresponding author. Tel: +46 731424645, E-mail: helena.persson@lnu.se

Abstract: An investigation of the accuracy, advantages and disadvantages of using the simpler degree day house load-model Type 12 as a replacement for the more complex multi-zone Type 56 has been made. Results show that Type 12 provides sufficient accuracy for all systems including a storage tank capable of holding at least one day load. A discussion whether Type 12 is an accurate model for other situations is made.

Keywords: TRNSYS, Renewable energy, Solar Combi, Programming, Type, 56

1. Introduction

The modeling of solar combisystems in the academic community is often done in a commercially available fortran based simulation environment named TRNSYS [1]. These systems often contain some form of heating system (heat pumps, solar collectors) and some form of load that uses the energy created (building, hot water load). The load is often connected to some form of weather data, deciding the ambient conditions. The interaction between the heat sources and loads form a TRNSYS deck, a series of component models connected to each other to provide information about a system. Here we seek to investigate the impact of the house load model that is chosen. The load structures that will be investigated are the two most common types of buildings used in TRNSYS: the very simple single-zone degree day model with internal gains described by Type 12, and the much more complex multi-zone model Type 56.

Previous work includes Olof Hallström [2], who in his thesis compared Type 12 to a much more complex model developed at Lund University. He found that even though Type 12 was surprisingly accurate for most conditions, especially during low indoor house temperatures, the drawbacks of the type made the choice between Type 12 and Type 56 hard to determine. He identified these drawbacks as the constant heat loss coefficient and the difficulty to include stored solar radiation. It can be noted however, that Type 56 also has a constant heat loss coefficient. Previous simplifications of TRNSYS models have among many others been performed by T. P. McDowell [3], completing a ground source model and by P. T. TSILINGIRIS [4] and his solar heating designs. In both cases a drastically decreased calculation time at low accuracy cost was reached.

Simplifying a deck has the advantage of a decreased calculation time, which can be a major problem in decks taking many hours or even days to complete, especially if a large amount of runs are desired for statistical or optimization purposes. A simpler deck is also highly advantageous for applications directed at the industry, installers and education, such as Climate Well [5] or Winsun Villa [6]. Winsun Villa contains a slightly modified version of Type 12. The conclusions of this publication will be used for the Flexi-Fuel project [7], which has strong connections to the industry and its installers and customers. The objective of the following paper is to determine the accuracy, calculation time and complexity of Type 56 and Type 12 under different conditions.

2. Methodology

2.1. TRNSYS

TRNSYS is a system simulation computational tool developed by Wisconsin University that allows for dynamic simulation of systems using variable time steps. It allows for systems, particularly heating systems, to be created by connecting several components, known as types. These types are mathematical subroutines, i.e. programs, which describe for example a pipe, a house or a heat pump. Apart from the possibility of self-made types, TRNSYS contains a large number of readymade types, and a large number of types are also developed by different institutes and available commercially or for free.

2.1.1. Available load-describing Types

There are several commercially available load models available, but we limit ourselves to observing those Types that are included in the basic TRNSYS package. These are: Type 12, the simplest model, Type 88, a version of Type 12 that also includes some internal gains, (It may be noted that these internal gains are being modeled directly in Type 12 under “misc heat gain”, for the investigations performed in this paper.) Type 56 which is a very complex and thorough multi-zone building model, and finally Type 19 a single zone building that is less complex than Type 56, but still requires the input of a large number of parameters. We choose to observe Type 12 and 56 since they are the source of the other models and represent the extremes in simplicity/speed and complexity/accuracy.

2.1.2. TYPE 56

Type 56 describes a building with multiple thermal zones, i.e. rooms. The model uses data from wall and window materials and thicknesses. Each room has a homogenous temperature, and radiation heat between the rooms is based on the room area. Heat addition from solar direct and diffuse radiation is calculated for each room depending on window and heat transfer properties.

2.1.3. TYPE 12

Type 12 is a simple degree-day, single-zone, single capacitance building model with internal gains. The model uses an effective heat capacity for the entire building together with the difference between indoor and outdoor climate to create a heating need. The load is corrected for internal gains. The use of a single heat capacity does not provide any information on solar radiation, which can have significant impact during summer. In this work the solar radiation is added to the internal gain, time step by time step. Duffie and Beckman reasons that since heat capacity effects are difficult to model with a single node when the outdoor temperature is fluctuating around the indoor temperature, Type 12 becomes less reliable for cooling loads. [8]. This has not been investigated here.

2.2. The House

As a reference building the IEA Task 32 building which is based on the IEA Task 26 reference building was used. [9] The reason for this choice is simply that it is a well defined and known building suitable for comparison purposes. Two levels of insulation are chosen to simulate an energy need of 60 or 100 kWh/m²a. The building consists of a two storey house with the specifications described in Table 1, 2 and 3.

Table 1. Building Properties.

		SFH60 SFH100				SFH60	SFH100	
		[m]	[m]	[kg/m ³]	[W/mK]	[kJ/kgK]	[W/m ² K]	[W/m ² K]
external wall	plaster inside	0.015	--	1200	0.600	1.00		
	Viertl brick	0.210	--	1380	0.700	1.00	0.154	0.491
	EPS	0.120	0.060	17	0.040	0.70		
	plaster outside	0.003	--	1800	0.700	1.00		
	Σ	0.468	0.288					
ground floor	Wood	0.015	--	600	0.150	2.50		
	plaster floor	0.060	--	2000	1.400	1.00	0.157	0.561
	XPS	0.120	0.060	38	0.037	1.45		
	Concrete	0.150	--	2000	1.330	1.08		
	Σ	0.445	0.285					
roof ceiling	Gypsumboard	0.025	--	900	0.211	1.00		
	Plywood	0.015	--	300	0.081	2.50	0.119	0.380
	Rockwool	0.200	0.060	60	0.036	1.03		
	Plywood	0.015	--	300	0.081	2.50		
	Σ	0.335	0.115					
internal wall	Clinker	0.200	--	650	0.230	0.92	0.962	0.962

Table 2. Window Area.

	window area [m ²]	window quotient [%]	total area [m ²]
South	12.0	24.0	50.0
East	4.0	9.9	40.5
West	4.0	9.9	40.5
North	3.0	6.0	50.0
Summary	23.0	12.7	181.0

Table 3. Window Properties

building	UWINDOW [W/m ² K]	g-Value [-]	UFRAME [W/m ² K]	construction [mm]	WindowID
SFH60	1.4	0.622	2.3	4/16/3	2004
SFH100	2.83	0.755	2.3	4/16/4	1202

A more detailed description on the house's architectural design, internal load and ventilation can be found in [9].

2.2.1. Estimating UA-values

Type 12 uses a single overall UA heat transfer value for the entire house. This value can be estimated by summarizing the U-values from all walls and windows in the building. An effective UA value for the ventilation can be added as this has the same temperature difference as the transmission losses.

$$UA = U_{WALL1} * A_{WALL1} + U_{WALL2} * A_{WALL2} + U_{WALL3} * A_{WALL3} + U_{WALL4} * A_{WALL4} + U_{WINDOWS} * A_{WINDOWS} + \\ + U_{Roof} * A_{Roof} + U_{Floor} * A_{Floor} + V_{house} * n * \frac{1}{3600} * (1 - \eta_{hx}) * \rho_{air} * c_{p_air} \quad (1)$$

2.2.2. Estimating solar radiation gain

In Type 12, Solar gains through windows can be estimated by adding the window area for each direction and multiply it with a transmission value (In this publication 0.6 has been used for all cases) as described in (2)

$$S = trm(WA_N + WA_E + WA_W + WA_S) \quad (2)$$

Where

trm = transmission constant

WA = Window area in the specified direction

This solar radiation gain value is then inserted into Type 12 through internal gains.

2.2.3 Effective thermal capacitance of the house

An effective thermal capacitance of the type 12 house can be estimated by adding up the thermal capacity for the individual parts of the house. Duffie and Beckman [8] give approximate values of 0.153 MJ/m²/K for a medium house and 0.415 MJ/m²/K for a heavy house and up to 0.810 for a very heavy building. This corresponds in this case (with 140 m² total floor area) to 21 MJ/K, 58 MJ/K and 113 MJ/K.

3. Measurements

Type 12 is deemed to be the less accurate model, and so when Type 56 and Type 12 are compared, any deviation from each other is considered to be due to an inaccuracy of Type 12.

3.1. The Timescale

Fig 1 shows the output of Type 12 and Type 56, as well as the difference between them. At first glance, the heating load required by Type 12 appears to be very inaccurate for both the well and the less insulated building as we see in the upper part of Fig.1. The whole line depicting the difference between the two types is in the order of 50% for most of the year.

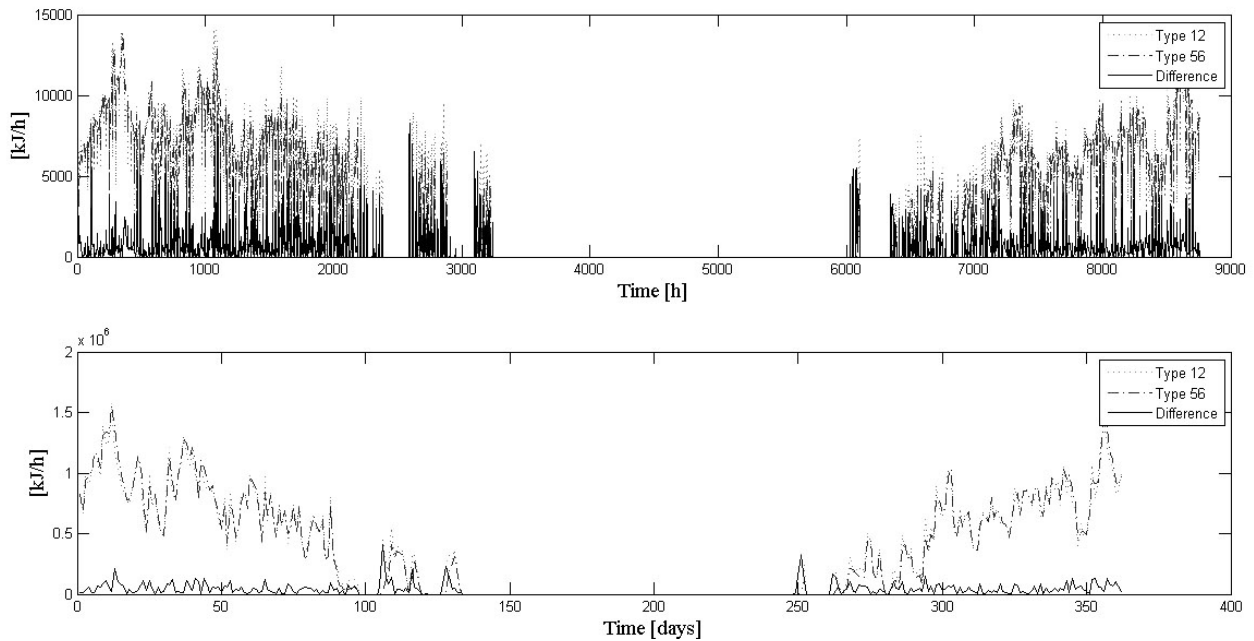


Fig.1 The output from Type12 and 56 with 12min time step (upper diagram) and 12h time step (lower diagram)

Possible heat pumps or solar collectors connected to a system are highly dependent on the temperature of the incoming flow. To gain sufficient accuracy for such heat sources a time step of a few minutes is required. The flow to such sources is often connected to some form of storage, such as a tank, between the load and the heat source. If for example a storage tank has the capacity of storing the energy required for heating a house for one day, a heat demand for one day is sufficient. When we integrate the output of both Type 56 and Type 12 over one day, we see a definite increase in agreement between the models as shown in the lower part of Fig.1.

3.2. The Accuracy of Type 12

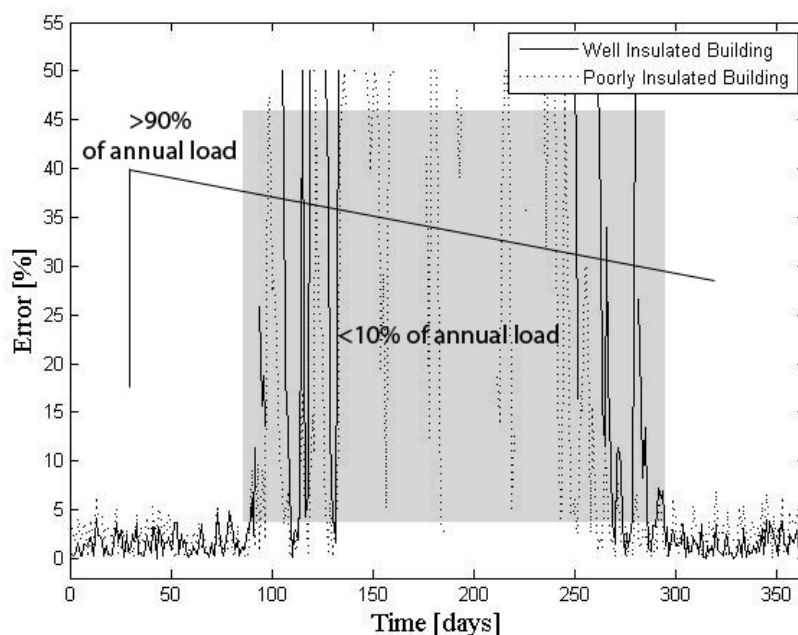


Fig. 2. The Difference in output for Type 12 and 56 for a poorly and a well insulated building

Fig.2 shows the error in percentage over one year. For the colder periods of the year the percentual error keeps below 7% for both levels of insulation. 7% is most likely a smaller error than those arising from building uncertainties such as cracks in the building shell or moisture in the isolation. Even though the error grows large in summertime, less than ten percent of the annual energy requirement occurs during this period. This means that for over 90% of the annual load, Type 12 performs acceptably. The yearly error becomes approximately 8%.

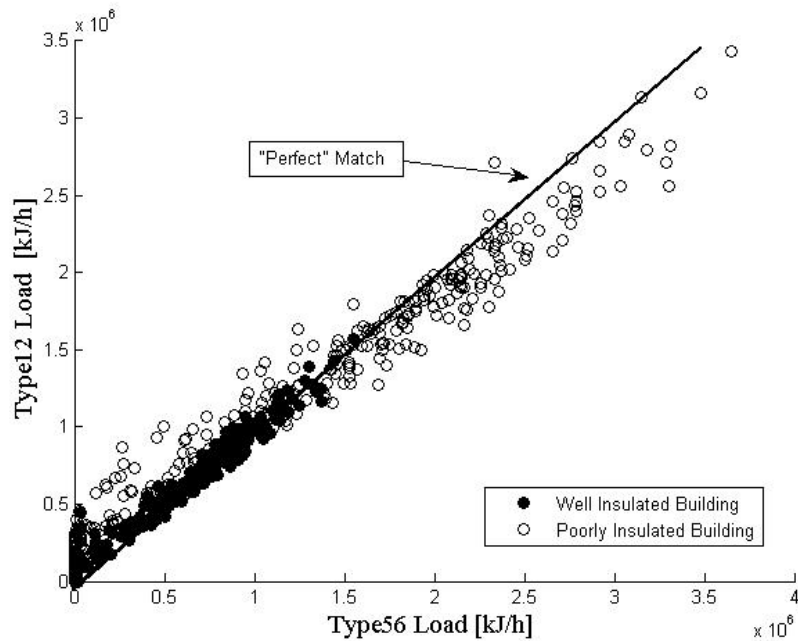


Fig. 2. Type 12 vs. Type 56 for a poorly and a well isolated building

Fig. 3 shows the output from the models plotted against each other. The error in output seems to be evenly distributed at the base of the line. The filled circles showing the well insulated building are closer to the line indicating that the overall UA value was a good guess for this case. At higher values we see a drift downwards, indicating that Type 12 underestimates the energy requirement for cold days, and overestimates it for warm days. This may be due to the fact that Type 12 does not store solar heat in the interior of the building.

3.3. The Phasing of Type 56

The difference in how the models react to outdoor temperatures is described in Fig. 4 and Fig. 5. Fig. 4 shows a zoomed in view of 3 days with the light gray line as outdoor temperature, the highly oscillating line as Type 12 and the less oscillating as Type 56. In this simulation, all windows, internal load and ventilation has been removed to get the crudest model possible. As seen in the image, Type 56 has a slight delay compared to the outdoor temperature, as might be expected by a more complex building model.

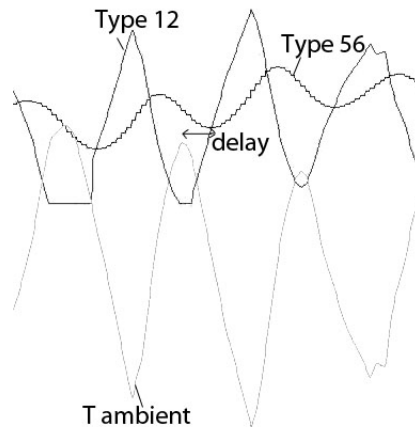


Fig. 4. The Delay of Type 56 when no windows are present

Fig. 5 shows two days but this time windows have been added to both models. Radiation coming through windows provides an instantaneous addition of heat, resulting in a model that responds much faster to outdoor weather. It could be argued that adding radiation through windows and ventilation provides a Type 56 that behaves more like Type 12.

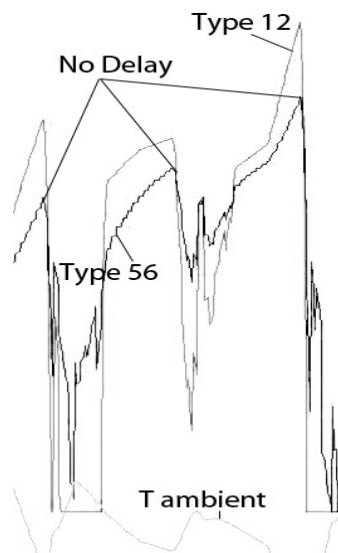


Fig. 5. No Delay of Type 56 when windows are present

3.4. Calculation Speed

Type 12 takes approximately half the simulation time for one year compared to Type 56 (23s against 42s). The time step was then rather long, 12minutes. In a full deck the tank may call the load several times before it converges, 10 times or more is not unusual. Also if a very short time step is used, this difference in calculation speed can have a significant impact on the usability of the deck.

4. Discussion

Considering the results presented above, Type 12 seems to be a good approximation under the right circumstances. It can be recommended for systems including a tank or other form of storage, or for systems that do not require high temporal resolution. The usage of Type 12 can not be recommended in applications consisting of heat sources without any storage. Type 12

only requires one UA parameter, which can be estimated as described above. In practical applications, the complete drawings of a building may not be easily accessible, or as in the case of the Flexi-Fuel project [7], it may prove very disadvantageous for a salesman to ask the client for every constructive layer in the wall before being able to demonstrate his/her products. In a real building the heat load will also be influenced by the wind dependent infiltration rate and quality of insulation work, as well as user behavior concerning choice of room temperature and for example open windows in some rooms periods of the day or night. The simulation model in the flexifuel project is aiming at fast but realistic system simulations and then type 12 may be the best choice.

References

- [1] Klein et al., 2000, <http://sel.me.wisc.edu/trnsys/>
- [2] O. Hallstrom, Solar Cooling Dimensioning, Modelling of Solar Cooling Installations Using a Thermal Chemical Accumulator from Climate Well AB, Thesis, 2008
- [3] T. P. McDowell, J. W. Thornton, and M. J. Duffy, Comparison of a Ground-Coupling Reference standard model to simplified approaches, Eleventh International IBPSA Conference Glasgow, Scotland July 27-30, 2009
- [4] P. T. Tsilingiris, Solar Water Design – A new simplified dynamic approach, Solar Energy Vol. 57, No. 1, pp. 19-28, 1996
- [5] ClimateWell AB. www.climatewell.com 20070121.
- [6] Winsun Villa, www.ebd.lth.se
- [7] H. Persson, B. Carlsson, B. Perers, P Olsson and Å. Hjort, Test Plant and Development of Tools for Design of Combi-Heating Systems for large building, Eurosun2010
- [8] Duffie, J. Beckman, W., Solar Engineering of Thermal Processes, John Wiley & Sons, Inc. 2006.
- [9] R. Heimrath, M. Haller, A Report of IEA SHC - Task 32, 2007

Reducing energy consumption in Natural Gas Pressure Drop Stations by Employing Solar Heat

Mohammad Rezaei¹, Mahmood Farzaneh-Gord^{2,*}, Ahmad Arabkoohsar², Mahdi Deymi Dasht-bayaz²

¹ Mazandaran Gas Company, Sari, Iran,

²The Faculty of Mechanical Engineering, Shahrood University of Technology, Shahrood, Iran

* Corresponding author. Tel-Fax: +98 2733395440, E-mail:mahmood.farzaneh@yahoo.co.uk

Abstract: In Iran (and probably in most countries) natural gas is transported through transmission pipeline at high pressures (5-7 Mpa) from production locations to consuming points. At consumption points, or when crossing into a lower pressure pipeline, the pressure of the gas must be reduced. This pressure reduction takes place in CGSs. At CGSs, the pressure is reduced from (5-7 Mpa) to (1.5-2.0 Mpa) (typically 1.7 Mpa) in high-pressure intrastate pipelines. Currently, gas pressure reduction is accomplished by using throttle-valves in all of Iran's CGSs, where the constant-enthalpy expansion takes place and a considerable amount of energy is wasted. The gas must be heated before it enters throttle valves to ensure that it remains above the hydrate-formation zone and dew point, so that no liquid or solid phase condenses at the station exit. The heaters are consuming a considerable amount of natural gas flowing through the CGS as fuel to provide the required heat for preheating the natural gas stream. As the low temperature heat is required for preheating the natural gas in a CGS, this makes a CGS as perfect place to utilize solar energy and to meet low temperature heat demand. As the low temperature heat is required for preheating the natural gas in a CGS, A solar collector array is proposed to be utilized in the CGS in order to displace heating duty of the heater and to reduce amount of fuel consumption. The proposition includes a modified design of an in-use CGS to take advantage of freely available solar heat. The proposed system has been applied to study the thermal behaviour of a CGS within Iran. The results show that the cost effectiveness of the proposed method with an array of 450 collector modules is resulted in fuel saving with variation between 0 to 20 USD/hr. The annual fuel saving is about 10678 USD and as the capital cost is about 76500 USD, the payback ratio is calculated to be around 9 years. The number of collector modules has been determined based on cost analysis.

Keywords: Natural gas pressure drop station, Line Heater, Solar energy, Solar thermal storage

Nomenclature

CGS	City Gate Stations,	h_{NG-1}	Enthalpy of Natural gas before heater W/kg
T_{NG-1}	Natural gas temperature before heater $^{\circ}C$	h_{NG-2}	Enthalpy of Natural gas after heater W/kg
T_{NG-2}	Natural gas temperature after heater.. $^{\circ}C$	T_w	Temperature of water in the tank..... $^{\circ}C$
T_{NG-2}	Natural gas temperature after valve. $^{\circ}C$	LHV	Lower heating value of fuel..... $kJ.kg^{-1}$
\dot{m}_{NG}	mass flow rate..... $kg.s^{-1}$	η_h	Heater efficiency
\dot{m}_{NG}	mass flow rate of fuel heater..... $kg.s^{-1}$	\dot{m}_f	mass flow rate consumed heater $kg.s^{-1}$
\dot{Q}_{solar}	Heat transfer rate produced by solar KW		
\dot{Q}_{heater}	Heat transfer rate produced by heater KW		

1. Introduction

Solar thermal technologies utilise the heat from the sun to offset the heating demand for many applications. The main component of any solar thermal technology is the solar collector. The device absorbs heat from solar radiation and transfers this heat to a circulating fluid (usually water). The heat absorbed by collectors then utilized in many applications. Kalogirou¹ presented a survey of the various types of solar thermal collectors and applications. These includes Solar water heating systems, Solar space heating and cooling, Solar refrigeration,

Industrial process heat, Solar desalination systems, Solar thermal power systems, Solar furnaces and Solar chemistry applications[1].

The utilization of solar energy for providing process heat in industrial applications is not common especially for low temperature cases and a few researches have been carried out in this subject. Norton [2] presented the most common applications of industrial process heat. The history of solar industrials and agricultural applications are presented and practical examples are explained. A system for solar process heat for decentralised applications in developing countries is presented by Spate et al. [3] The system is suitable for community kitchen, bakeries and post-harvest treatment.

In Iran (and probably in most countries) natural gas is transported through transmission pipeline at high pressures (5-7)MPa from production locations to consuming points. At consumption points, or when crossing into a lower pressure pipeline, the pressure of the gas must be reduced. This pressure reduction takes place in CGSs. At CGSs, the pressure is reduced from (5-7)MPa to 1.5-2.0 MPa (typically 1.7 MPa) in high-pressure intrastate pipelines. Currently, gas pressure reduction is accomplished by using throttle-valves in all of Iran's CGSs, where the constant-enthalpy expansion takes place and a considerable amount of energy is wasted (Farzaneh-Gord et al. [4]). The gas must be heated before it enters throttle valves to ensure that it remains above the hydrate-formation zone and dew point, so that no liquid or solid phase condenses at the station exit. Indirect Water Bath Gas Heaters (known as line heater) are employed in the CGS to preheat the natural gas. The heaters are consuming a considerable amount of natural gas flowing through the CGS as fuel to provide the required heat for preheating the natural gas stream. As the low temperature heat is required for preheating the natural gas in a CGS, this makes a CGS as a perfect place to utilize solar energy and to meet low temperature heat demand.

In this study, the objective is to reduce amount of the heater fuel consumption in the CGS by utilizing solar energy. A solar collector array is proposed to be utilized in order to displace heating duty of the line heater. The proposition includes a modified design of an in-use CGS to take advantage of freely available solar heat. The modification has been done in line to minimize the CGS design alteration and availability of the CGS to continue its tasks with or without additional solar system.

2. Methodology

When a natural gas pipeline approaches a city, the high-pressure gas has to be reduced to a distribution level. A city gate station (CGS) is a. Inlet Gas has a high temperature (T_{NG-1}) which is typically related to the ambient temperature (T_{am}). The gas must be heated before it passes through throttle valves to ensure that it remains above the hydrate-formation zone and dew point, so that no liquid or solid phase condenses at the output temperature (T_{NG-3}). The standard preheated gas temperature (T_{NG-2}) is in range of 30-55°C but its value highly depended on inlet pressure and temperature. The heaters are comprised of four basic components, the heater shell, the fire tube, the gas coil and the water expansion section.

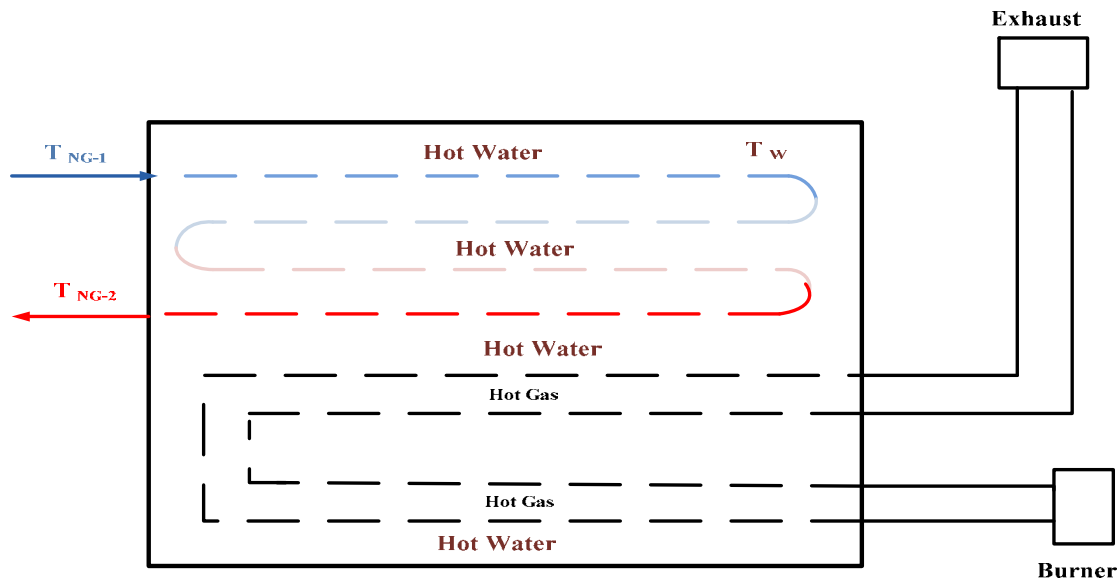


Fig. 1. A schematic diagram of an Indirect Water Bath Gas Heater (Line heater) employed in a CGS for preheating the gas

The heating duty of the heater and the water bath temperature could be estimated by knowing the station inlet and outlet gas temperature and pressure as discussed as follow.

Based on the standard outlet station gas pressure (250 psig or 17 barg) and the natural gas compositions, the hydrate gas temperature (T_{hyd}) could be calculated from thermodynamics models. The outlet station gas stream temperature (T_{NG-3}) is then selected 5 °C above the hydrate temperature [5]. By knowing the outlet station gas stream temperature, the gas temperature at the heater exit could be calculated as below:

$$T_{NG-2} = \overbrace{T_{hyd} + 5}^{T_{NG-3}} + \Delta T_{iv} \quad (1)$$

In which, $\Delta T_{iv}(=T_{NG-2}-T_{NG-3})$, is temperature drop due to pressure drop though the throttling valves. The amount of temperature drop is affected by the station inlet pressure and the natural gas compositions. Once, the gas temperature (and pressure) at the heater exit is known, the heater heating duty could be calculated as below:

$$\dot{Q}_{gh} = \dot{m}_{NG}(h_{NG-2} - h_{NG-1}) \quad (2)$$

As the gas travels a long distance before reaching to the station trough a buried pipeline at depth of 1.2 m, the gas temperature assumed to be equal to the surrounding soil temperature (Edalata and Mansoori,[6]). The soil temperature varies with environment temperature and locations. Najafi-mod et al.11 proposed an empirical correlation for a simple and rational relationship between ambient temperature and soil temperature at different depths. The soil temperature for depth higher than 1 m for Iran could be simplified as follow (Najafi-mod et al.[7]) :

$$T_{NG-1}(^{\circ}C) = T_{soil} = 0.0084T_{am}^2 + 0.3182T_{am} + 11.403 \quad (3)$$

The heating duty of the heater is provided by burning natural gas as fuel. Considering a value for thermal efficiency, η_h , of the heater, the fuel mass flow rate, \dot{m}_f , could be calculated as below:

$$\dot{m}_f = \dot{Q}_{gh} / (\eta_h LHV) \quad (4)$$

In which, LHV, is lowering heating value of the fuel (here Natural gas). It should be pointed out that the heater heat lost to ambient is considered through the heater thermal efficiency. The current thermal efficiency of conventional heaters are low and in range of 0.35 to 0.55. In this research, thermal efficiency of the heater is assumed to be 0.45.

As the water bath temperature wouldn't need to be higher than 70°C and the line heater are most needed during winter, in this study an array of flat plate solar collector are proposed to be installed parallel to the heater as shown in Fig.2. The solar flat plat collectors received the water, heated it up and finally returned it to the heater. As it could be realized, a current CGS could be easily modified to take advantages of solar thermal energy as proposed in the Fig.3. The heater is able to continue its normal take with or without solar collectors.

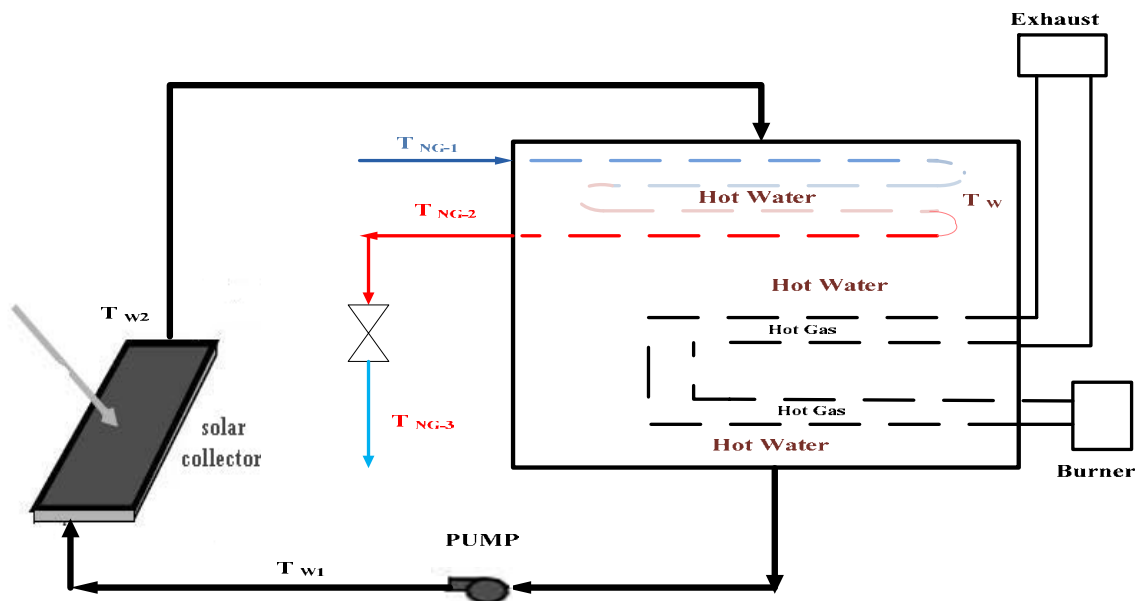


Fig. 2. A schematic diagram of the proposed system to utilize solar energy in the pressure drop stations

The governing equation for a perfectly mixed storage tank could be written as:

$$m_w C_{pw} \frac{dT_w}{dt} = \dot{Q}_{solar} + \underbrace{\dot{m}_f LHV \eta_h}_{\dot{Q}_{heater}} - \dot{Q}_{gh} \quad (5)$$

In which, $m_w C_{pw}$, is the system thermal capacity, T_w , is bath temperature and \dot{Q}_{solar} is rate of useful solar energy which is absorbed by the solar collector array and transferred into circulated water. \dot{Q}_{gh} is heating duty of the heater or solar load in the system.

\dot{Q}_{heater} is the rate of thermal energy provided by burning fuel. It should be noted that heat lost from the heater is considered in this term by introducing heater thermal efficiency. There are possibility of two scenarios at this point as a) a heater with automatic controllable \dot{Q}_{heater} b) a heater with fixed \dot{Q}_{heater} . It should be pointed out that although all line heaters (within Iran) could be controlled and the rate of \dot{Q}_{heater} could be varied, but these heaters are not equipped with automatic control unit. Here it is assumed that the heaters are equipped with automatic control unit and scenario a (a heater with automatic controllable \dot{Q}_{heater}) has been applied. In this scenario, the gas temperature at heater exit is fixed.

Fixed gas outlet temperature could be achieved by controlling rate of \dot{Q}_{heater} . \dot{Q}_{heater} could be estimated by making some simple assumptions and applying a “Euler” integration technique. For this, it will be assumed that the values of \dot{Q}_{gh} and \dot{Q}_{solar} are only a function of storage tank temperature at the start of the hour and that $(m_w C_{pw})$ of the storage is fixed. Therefore, assuming one hour time period (i.e. 3600 seconds), \dot{Q}_{heater} could be estimated by integrating both sides of equation(5). The final equation will be as below:

$$\dot{Q}_{heater} = m_w \cdot C_{pw} (T_{w(i+1)} - T_{w(i)}) / 3600 + (\dot{Q}_{gh} - \dot{Q}_{solar})_{(i)} \quad (6)$$

The above equation could be employed to find altered value of the heater fuel mass flow rate as below:

$$\dot{m}_f = (m_w \cdot C_{pw} (T_{w(i+1)} - T_{w(i)}) / 3600 + (\dot{Q}_{gh} - \dot{Q}_{solar})_{(i)}) / LHV \eta_h \quad (7)$$

Equation (6) or (7) could be rearranged to estimate the hourly variation in water bath temperature as below:

$$T_{w(i+1)} = T_{w(i)} + \frac{(\dot{Q}_{solar} + \dot{Q}_{heater} - \dot{Q}_{gh})_{(i)} \times 3600}{m_w \cdot C_{pw}} \quad (8)$$

3. Results

The heating duty should be supplied by heater either completely by fuel energy or by combination of solar and fuel energy. As discussed previously, the heater burns natural gas as fuel to preheat the gas. The rate of burning fuel would be useful for studying feasibility of the proposed solar system. Fig 3 shows the averagely daily rate of fuel (natural gas) burned in the heater for months of 2009.

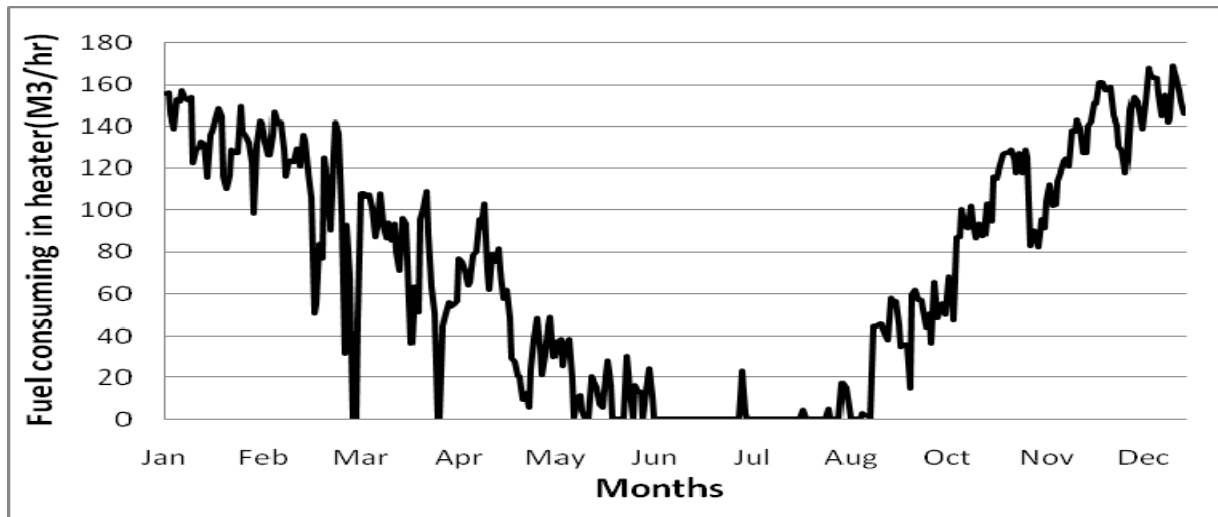


Fig. 3. The average daily rate of heater fuel (natural gas) consumption in 2009 ($m^3 \cdot hr^{-1}$)

As discussed previously, some part of required preheat energy in the heater is proposed to be replaced by energy gained in solar collector array. The average monthly of absorbed solar energy that gained in Akand Station area shown in Fig 4. It could be realized that the maximum absorbed solar energy is reached in Jun and The lowest value is in October.

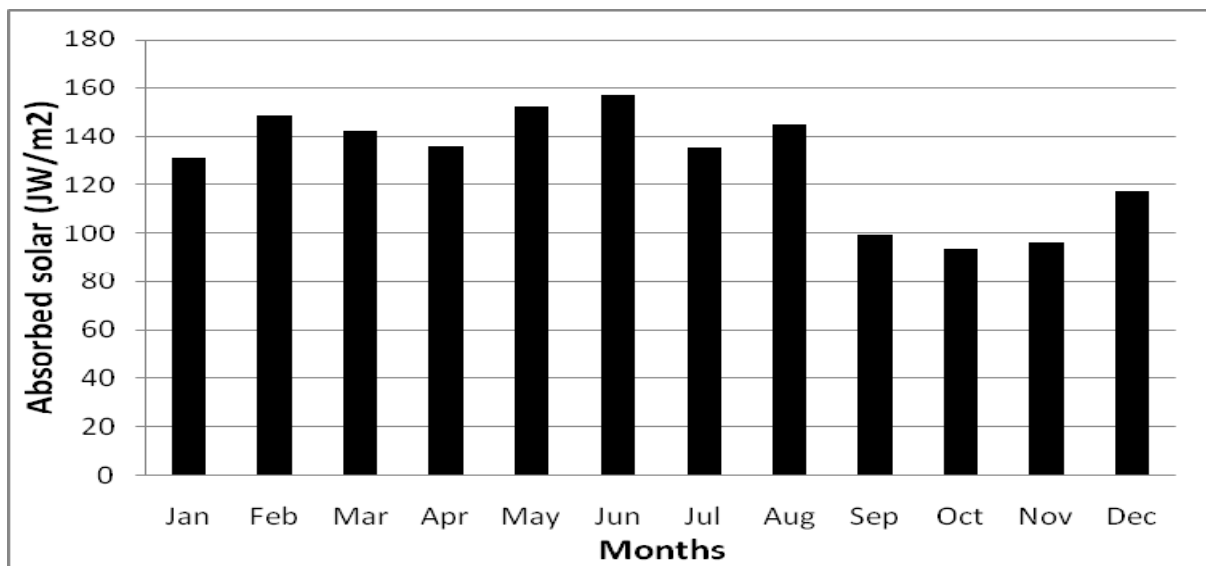


Fig. 4. Average monthly of absorbed solar energy in 2009

The capital cost of the proposed solar system or the array of collector modules could be actually calculated by multiplying the number of collector modules and cost of one module. The cost of one flat plate collector module is about 230 USD in Iran. As number of collector modules in the array increases, the capital cost increases but the heater fuel cost decreases. The variation of annual fuel cost of the heater and solar energy system capital cost against number of collectors modules are displayed in Fig.5. Considering the figure, one could select 450 as an optimum value for the number of collector modules.

It should be noted that the fuel cost calculation is based on current natural gas price which is 0.28 USD for each cubic meter.

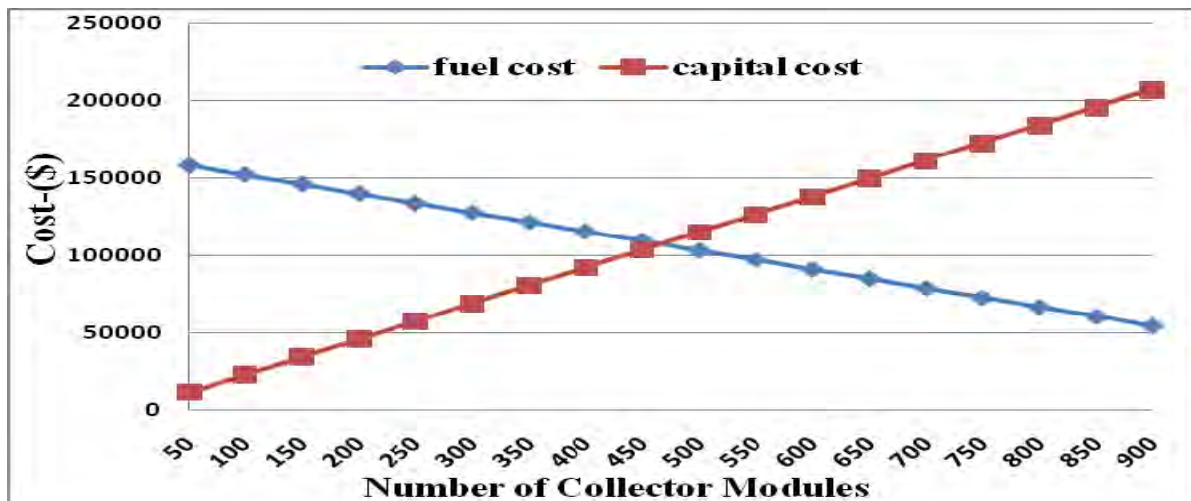


Fig. 5. Variation of solar system capital cost and fuel cost for against number of collector modules

To evaluate the desirability and to investigate the cost effectiveness of the proposed method with an array of 450 collector modules, Fig.6 shows the daily average heater fuel consumption required for preheating gas in 2009 in case of utilizing solar system or without solar system. The distinction between fuel consumptions, shows saving in fuel ($\text{m}^3 \cdot \text{hr}^{-1}$). Annually fuel cost saving can calculate by multiply this amount in 0.28 USD.

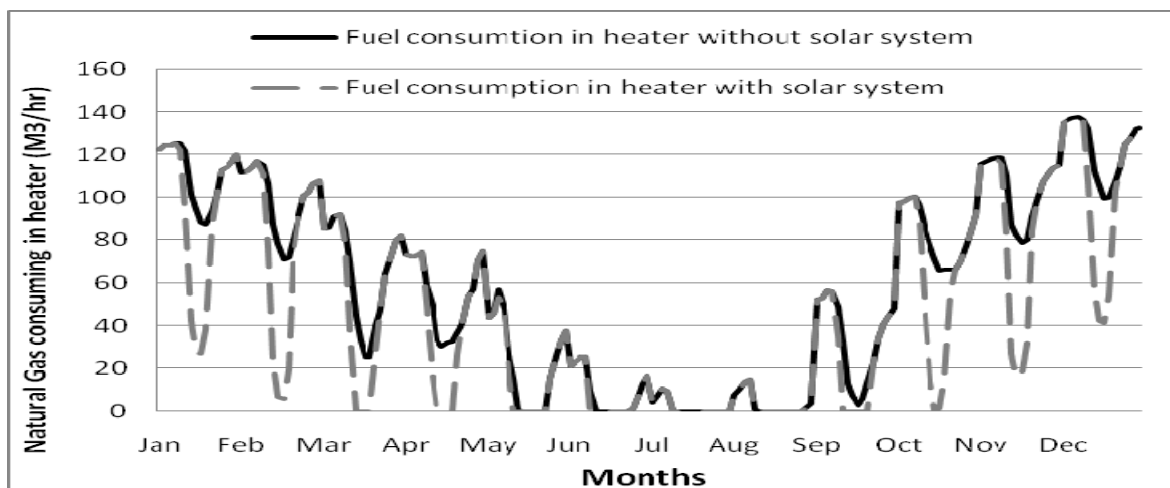


Fig. 6. The heater fuel (natural gas) consumption required for preheating gas in 2009

The annual fuel saving is about 10678 USD and as the capital cost is about 76500 USD, the payback ratio could be calculated as below:

$$\text{Payback Ratio} = (\text{Capital cost}) / (\text{Benefit}) = 9.2 \text{ years} \quad (9)$$

4. Discussion

The natural gas pressure must be reduced to distribution pressure when reaches its end users. The gas must be heated before it enters throttle valves to ensure that it remains above the hydrate-formation zone and dew point, so that no liquid or solid phase condenses at the station exit when pressure and temperature reduced. Currently in all Iran's CGSs, the gas is preheated through a bath type heat exchangers (known as line heater) which burns a portion of the gas for providing heating duty to warm up the natural gas. As the low temperature heat is required for preheating the natural gas in a CGS, A solar collector array is proposed to be

utilized in the CGS in order to displace heating duty of the heater and to reduce amount of fuel consumption. The proposition includes a modified design of an in-use CGS to take advantage of freely available solar heat. The proposed system has been applied to study the thermal behaviour of a CGS within Iran (Akand City Gate Station). The results show that the cost effectiveness of the proposed method with an array of 450 collector modules is resulted in fuel saving with variation between 0 to 20 USD.hr⁻¹. The annual fuel saving is about 10678 USD and as the capital cost is about 76500 USD, the payback ratio is calculated to be around 9 years. The number of collector modules has been determined based on cost analysis.

References

- [1] Soteris A. Kalogirou, Solar thermal collectors and applications, Progress in Energy and Combustion Science 30, 2004,231–295
- [2] Norton B. Solar process heat: distillation, drying, agricultural and industrial uses. Proceedings of ISES Solar World Congress, Jerusalem, Israel on CD-ROM, Jerusalem, Israel; 1999.
- [3] Spate F, Hafner B, Schwarzer K. A system for solar process heat for decentralised applications in developing countries. Proceedings of ISES Solar World Congress on CD-ROM, Jerusalem, Israel; 1999.
- [4] Farzaneh-Gord, M., Hashemi, S., Sadi, M., Energy destruction in Iran's Natural Gas Pipe Line Network, Energy Exploration and Exploitation, Volume 25, Issue 6, 2009.
- [5] Arnold, Ken; Stewart, Maurice, Surface Production Operations (2nd Edition) Volume 2 - Design of Gas-Handling Systems and Facilities, 1999 Elsevier.
- [6] Mohsen Edalata; G. Ali Mansoori, Buried Gas Transmission Pipelines: Temperature Profile Prediction through the Corresponding States Principle, Energy Sources, Part A: Recovery, Utilization, and Environmental Effects, Volume 10, Issue 4 1988 , pages 247 - 252
- [7] MH, Najafi-mod, Amin Alizadeh, Azadeh Mohamadian, Javad Mousavi, Investigation of relationship between air and soil temperature at different depths and estimation of the freezing depth (Case study: Khorasan Razavi), *Journal of water and soil of Ferdowsi University of Mashhad*, Vol. 22, No. 2, 2008

Performance of hybrid photovoltaic thermal (HPVT) biogas plant

Prabhakant^{1*}, Rajeev Kumar Mishra¹, G.N.Tiwari¹

¹Centre for Energy Studies, Indian Institute of Technology Delhi, New Delhi, India

* Corresponding author. Tel: +91 9810651484, Fax: +91 1126591251, E-mail: prabha.kant@nic.in

Abstract: In this paper, the energy balance equations for the different components of hybrid photovoltaic thermal (HPVT) biogas plant have been written for quasi - steady state conditions to develop a thermal model. An analytical expression for slurry temperature has been obtained as a function of design and climatic parameters namely mass of the slurry, mass flow rate of fluid in collector, number of collectors, solar intensity, ambient temperature etc. Numerical computations have been carried out for climatic conditions of Srinagar, India. Based on mathematical computations it has been observed that the optimum slurry temperature ($\sim 37^\circ\text{C}$) is achieved for a given set of design parameters of biogas plant and hybrid collectors ($M_s = 2000$, $\dot{m}_f = 0.05\text{kg/s}$, $L = 25\text{m}$). It has been observed that number of hybrid PVT collector has significant effect on slurry temperature.

Keywords: Hybrid PV thermal collector, Thermal modeling, Biogas plants.

Nomenclature

$I(t)$ Solar intensity at any time t Wm^{-2}
 T temperature..... $^\circ\text{C}$
 M mass..... Kg
 L length of the heat exchanger..... m
 N number of collectors..... dimensionless
 \dot{m}_f mass flow rate of water..... Kgs^{-1}
 r_1 Inner radius of the tube in heat exchanger..... m
 h heat transfer coefficient $\text{Wm}^{-2}\text{ }^\circ\text{C}^{-1}$
 α absorbitivity of the black absorber plate
 α' absorbitivity of the gas holder plate.....
 β temperature coefficient of efficiency
 τ transmittivity of the glass plate.....
 h_1 heat transfer coefficient from gas holde plate to gas..... $\text{Wm}^{-2}\text{ }^\circ\text{C}^{-1}$
 h_2 heat transfer coefficient from gas holder plate to ambient..... $\text{Wm}^{-2}\text{ }^\circ\text{C}^{-1}$
 h_3 heat transfer coefficient from gas to slurry $\text{Wm}^{-2}\text{ }^\circ\text{C}^{-1}$
 h_c heat transfer coefficient from gas holder to slurry $\text{Wm}^{-2}\text{ }^\circ\text{C}^{-1}$
 h_4 heat transfer coefficient from slurry to ground $\text{Wm}^{-2}\text{ }^\circ\text{C}^{-1}$
 hr_{ps} radiative heat transfer coefficient... $\text{Wm}^{-2}\text{ }^\circ\text{C}^{-1}$
 T_{so} slurry temp at time $t = 0$ $^\circ\text{C}$
 A_h horizontal area of the gas holder exposed to solar radiation..... m^2
 A_v veritcal area of the gas holder which is exposed to Solar radiation..... m^2
 A_h' vertical area of sulrry..... m^2
 A_v' submerged area of gas holder..... m^2

h_s heat transfer coefficient from tube to slurry $\text{Wm}^{-2}\text{ }^\circ\text{C}^{-1}$
 U_{lc} over all heat transfer coeff... $\text{Wm}^{-2}\text{ }^\circ\text{C}^{-1}$

Subscript

v vertical
 h horizontal
 o outlet
 i inlet
 s slurry
 a ambient
 c solar cell
 p plate
 f_i inlet fluid (water)
 f_o outlet fluid (water)
 m module
 g glass

1. Introduction

Biogas is the gas emitted from cow dung in its anaerobic decomposition. Biogas provides fuel for cooking, thus saves the forests and also women from fetching and carrying heavy loads of fuel wood. Biogas is also used for lighting and space heating purpose in rural villages. Thus improves the quality of life. Finally, anaerobic digestion also yields bio-slurry and bio-dregs rich in nutrients, minerals and biologically active compounds. This forms the excellent organic fertilizer for crops and fodder for pig and fish. Production of biogas is maximum when slurry temperature is between 32 to 37 °C.

In order to increase the slurry temperature in harsh cold climatic condition, the researchers have proposed the following techniques:

- (i) Erection of canopy green house over the biogas plant [1-6].
- (ii) Integration of solar water heater/ solar still with dome [7-10].
- (iii) Hot water charging the slurry before feeding into digester [11].
- (iv) Integration of flat plate collector to digester through heat exchanger inside slurry, generally referred as active heating [12-15].

In their study, either floating or fixed dome type biogas plant has been considered. On the basis of their finding, it has been concluded that active heating of slurry in digester is more effective in comparison with other heating methods [12-15]. The temperature of slurry can be increased upto optimum level (~ 37°C) by optimizing the area of flat plate collector for a given capacity of the slurry. It is further important to mention that only forced mode of operation for thermal heating is viable. Neto et al. [16] have suggested biogas/photovoltaic hybrid power system for decentralized energy supply of rural areas. Also, Dubey and Tiwari [17] have presented a hybrid photovoltaic flat plate collector (hybrid PV water collector) for forced mode to produce electrical as well as thermal energy. If such hybrid PV water is integrated to slurry through heat exchanger as shown in Figure 1a, then one can achieve the following:

- (i) Increase in slurry temperature for higher yield in harsh cold climatic condition.
- (ii) Hot water for domestic use.
- (iii) Electricity production for lighting.

In this case the proposed system can be proved to be more economical than single application in rural area in decentralised manner.

2. Design of hybrid photovoltaic thermal (HPVT)-biogas Plant:

There are two types of biogas plant namely floating gas holder type and fixed dome type. In this paper floating gas holder type biogas plant has been considered.

2.1. Hybrid floating type biogas plant:

Hybrid photolytic thermal (HPVT)-biogas plant has been shown in the Fig. 1. It consists of (i) a floating type biogas plant; (ii) partially PV covered solar collectors connected in series and (iii) a coil type heat exchanger. Heat exchanger is connected with partially PV covered solar collectors connected in series and is immersed in the slurry as shown in the Fig. 1a. The hot fluid (water) at outlet of hybrid collectors is allowed to flow through heat exchanger and then transferring the heat from heat exchanger to slurry and hence the slurry gets heated.

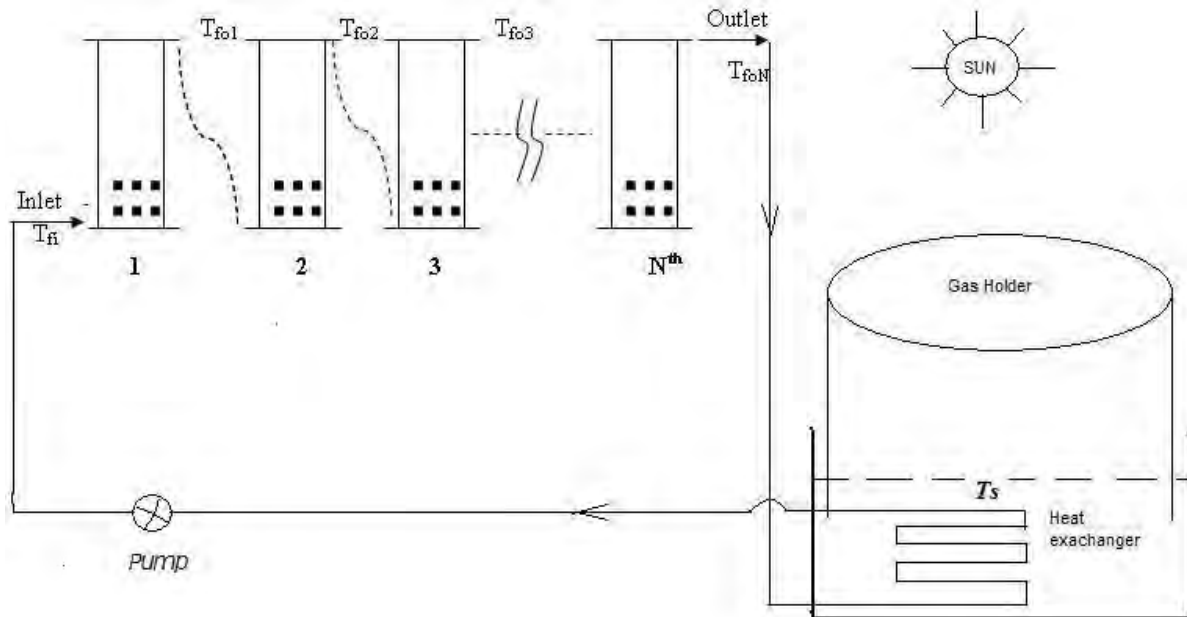


Fig.1 A conventional biogas plant integrated with hybrid PVT solar water collector.

3. Problem Identification

In this paper an attempt has been made to optimize the number of partially covered collectors, size of the heat exchanger and mass flow rate of the water in the heat exchanger for a given size of the biogas plant under a given climatic condition.

4. Thermal Modelling

4.1. Assumptions

In order to write the energy balance equation of hybrid photovoltaic thermal biogas plant, the following assumptions have been made:

- The biogas plant is of floating dome type
- Each component of the system is in quasi – steady state condition
- There is no stratification along the depth of the slurry and the gas column
- Thermal capacity digester and dome of the biogas plant has been neglected

4.2. Energy Balance Equations

The energy balance equations during sunshine hours have been formulated as follows.

For gas holder:

$$\alpha' \left[A_h I(t) + I(t) \frac{A_v}{2} \right] = h_1 A_t (T_p - T_g) + h_{rps} A_h (T_p - T_a) + A' v h_c (T_p - T_s) + h_2(t) A_t (T_p - T_a) \quad (1)$$

$$\text{For biogas:} \quad h_1 A_t (T_p - T_g) = h_3 A_h (T_g - T_s) \quad (2)$$

For slurry:

$$M_s C_s \frac{dT_s}{dt} = h_3 A_h (T_g - T_s) + A_h h_{rps} (T_p - T_s) + A'_v h_c (T_p - T_s) - h_4 A_h (T_s - T_\infty) - h_{sa} A'_h (T_s - T_a) - A'_h \dot{Q}_{es} + \dot{Q}_u \quad (3)$$

where,

$$\dot{Q}_{es} = h_{ew} (T_s - T_a) \quad (4)$$

and,

$$h_{ew} = \frac{0.016 h_{sa} \{P(\bar{T}_s) - \gamma P(\bar{T}_a)\}}{(\bar{T}_s - \bar{T}_a)}.$$

Now, the rate of heat transfer from flowing fluid in the heat exchanger to the slurry can be written as

$$\begin{aligned} \dot{Q}_u &= U 2\pi r_1 L (\bar{T}_w - T_s) \\ &= \dot{m}_f c_f \left(1 - \exp\left(-\frac{2\pi r_1 U}{\dot{m}_f c_f} L\right) \right) (T_{foN} - T_s) \end{aligned} \quad (5)$$

Following Dubey and Tiwari [4], for N identical collectors partially covered by PV modules connected in series, the outlet fluid temperature at the end of Nth collector can be given as,

$$T_{foN} = \frac{(AF_R(\alpha\tau))_1 \left(\frac{1-K_K^N}{1-K_K}\right) I(t) + (AF_R U_L)_1 \left(\frac{1-K_K^N}{1-K_K}\right) T_a + T_{fi} K_K^N}{\dot{m}_f c_f} \quad (6)$$

With the help of Eqs (4) & (5), Eq (3) can be solved for the slurry temperature

4.3. Electrical output:

The electrical output generated by proposed hybrid photovoltaic thermal biogas can be evaluated by the following expression

$$E_{daily} = \sum_{i=1}^n \eta_m \times I_i \times A_m \times N \quad (7)$$

where,

$$\eta_m = \eta_{mo} [1 - \beta (\bar{T}_f - T_a)], \quad \bar{T}_f = \frac{T_{foN} + T_{fi}}{2}, \quad \eta_{mo} = 0.12 \text{ and } \beta = 0.0045.$$

4.4. Thermal output:

The rate of thermal energy available from the proposed hybrid photovoltaic thermal biogas plant can be obtained as:

$$\dot{q}_u = \dot{m}_f \dot{c}_f (T_{foN} - T_{fi})$$

The daily thermal energy is given by

$$Q_u = \sum_{i=1}^n \dot{q}_{ui}; \quad n \text{ is sunshine hour.} \quad (8)$$

The daily exergy is given by

$$Ex_{daily} = Q_u \left[1 - \frac{\bar{T}_a + 273}{\bar{T}_{fON} + 273} \right] \quad (9)$$

For a set of design and climatic parameters, outlet temperature of n^{th} collector and Slurry temperature has been calculated using MATLAB software.

5. Results and discussions

Hourly variation of solar intensity on the horizontal and vertical walls of the dome has been calculated by using Liu and Jordan formula with the help MATLAB software. Fig. 2 shows the variation of solar intensity and ambient air temperature with time. Fig 3 gives the variation of outlet temperature from N^{th} collector and slurry temperature during 24 hours period of day and night. Figure shows that there is increase in slurry temperature (T_s) with time of the day as more thermal energy is available from hybrid PVT collectors. It attains maximum temperature (T_{smax}) of about 30°C at 4 pm due to heat capacity of the slurry. This temperature can be further increased by decreasing the mass of the slurry. Further, it is to be noted that the outlet fluid temperature is achieved upto about $80\text{-}90^{\circ}\text{C}$ at noon time as expected. Fig.4 shows the variation of peak slurry temperature (T_{smax}) with mass flow rate. The peak slurry temperature (T_{smax}) increases rapidly with increase of mass flow rate of the fluid due to fast transfer of heat into the slurry. It is observed that there is not much variation in peak slurry temperature (T_{smax}) after mass flow rate 0.05kg/s and hence one can conclude that the optimum mass flow rate is 0.05 kg/s for design parameters given in Table 1 and climatic parameters shown in Fig. 2. Fig.5 shows the variation of peak slurry temperature (T_{smax}) with the mass of the slurry (M_s). This figure shows that peak slurry temperature (T_{smax}) decreases with increase of the mass of the slurry (M_s). It is observed that for the given design and climatic parameters, the optimum mass of the slurry is 2000kg . The variation of peak slurry temperature (T_{smax}) with number of PV/T collectors N is shown in Fig.6. This figure shows that peak slurry temperature (T_{smax}) also increases with increase of number of collectors due to increase of thermal energy provided by PVT collectors to the slurry. It is observed that there is not much variation in peak slurry temperature (T_{smax}) after 50 numbers of collectors and hence the optimum number of collectors for a design and climatic parameters under consideration is about 50.

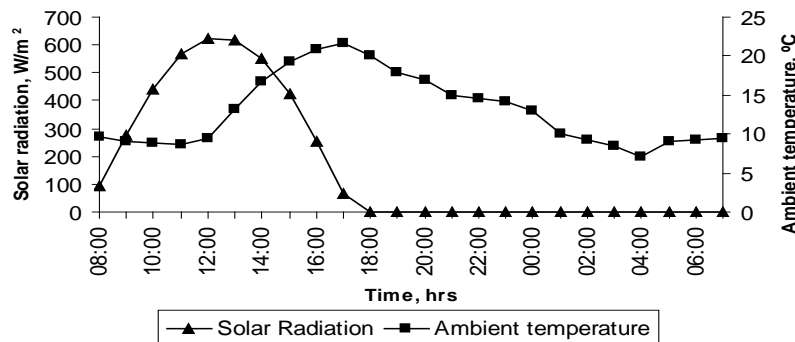


Fig.2. Variation of solar intensity and ambient temperature with time.

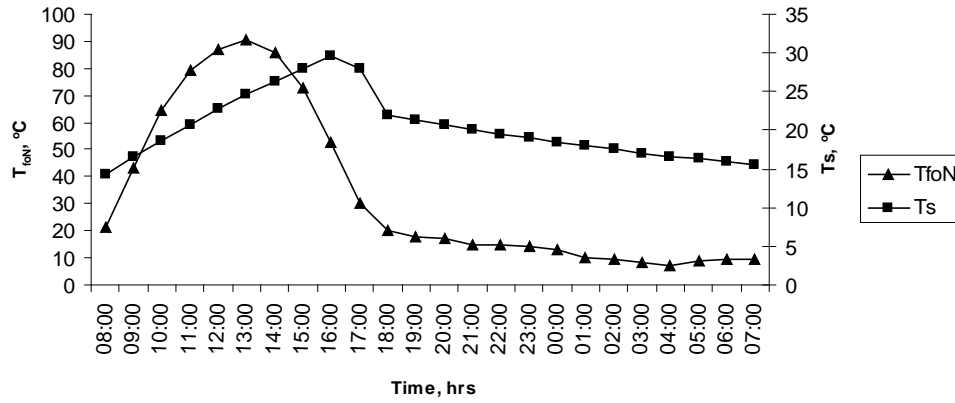


Fig.3. Variation of outlet water temperature (T_{foN}) and slurry temperature (T_s) with time ($M_S=2500$, $\dot{m}_f = 0.02\text{kg/s}$, $L = 25\text{m}$, $N=40$)

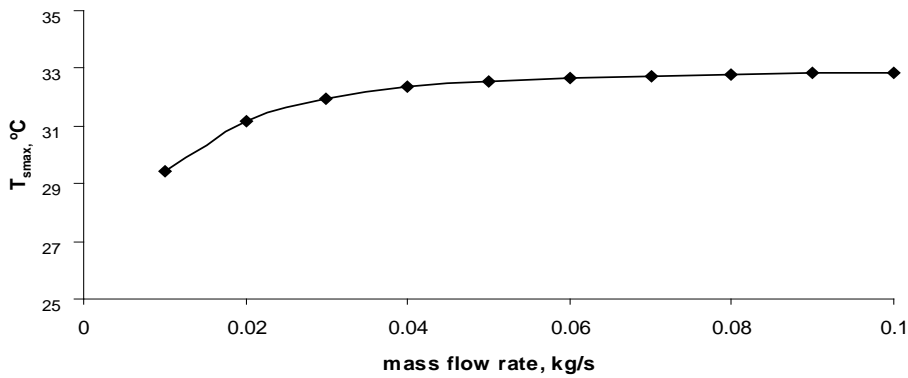


Fig.4. Variation of maximum slurry temperature with mass flow rate of the slurry.

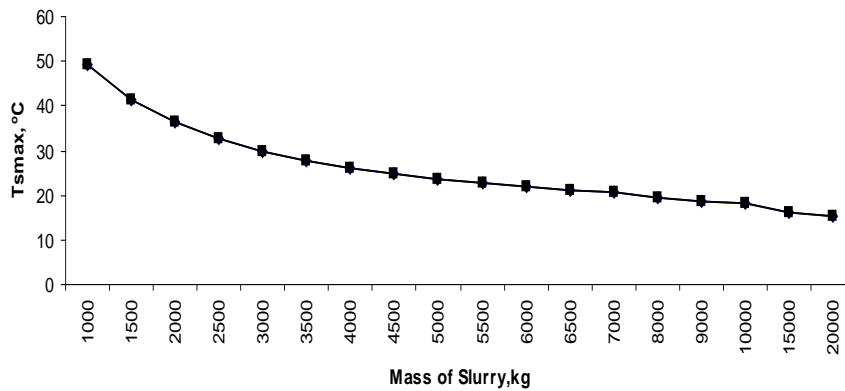


Fig.5: Variation of maximum slurry temperature with mass of slurry for $N=40$ and mass flow rate= 0.02 kg/s .

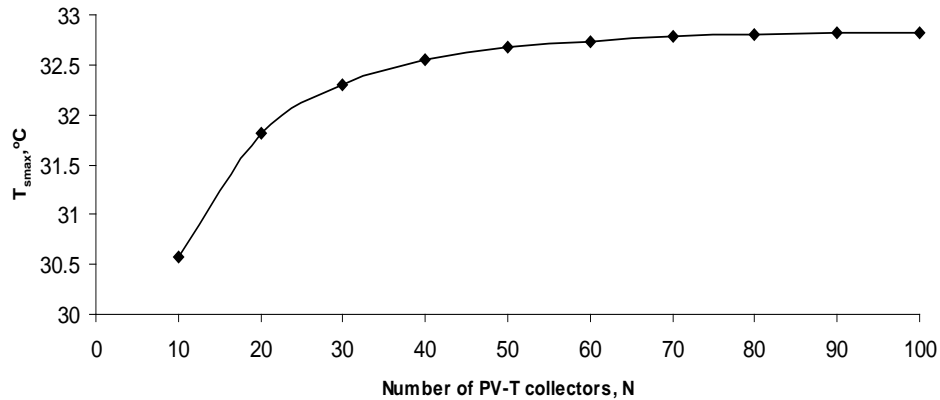


Fig.6. Variation of maximum slurry temperature with number of PV-T water collectors.

6. Conclusions

On the basis of present studies, one can conclude that:

- (i) The design parameter of PVT integrated biogas plant can be optimised for a given capacity by using the present thermal model.
- (ii) The present system is most suitable and self sustainable for cold climatic condition where ambient air temperature is much less than the optimum operating temperature ($\sim 37^{\circ}\text{C}$) of the biogas plant.

References

- [1] M.S. Sodha, S. Ram, N. K. Bansal and P. K. Bansal. Effect of PVC greenhouse in increasing the biogas production in temperate cold climatic conditions. *Energy Conversion and Management* 1987; 27 (1): 83–90.
- [2] K. Vinoth Kumar , R. Kasturi Bai Solar greenhouse assisted biogas plant in hilly region – A field study, *Solar Energy*. 2008; 82: 911–917.
- [3] N.K. Bansal, S.C. Bhand, S. Ram and K. K. Singh. A study of a greenhouse concept on conventional biogas systems for enhancing biogas yield in winter months. *International Journal Energy Resources*. 1985; 9: 119–128.
- [4] M. Dayal, K.K.Singh, P.K. Bansal and S. Ram Solar assisted biogas digesters I: thermal analysis. *International Journal Energy Resources* 1985; 9: 455–462.
- [5] K. Vinoth Kumar , R. Kasturi Bai Solar greenhouse assisted biogas plant in hilly region – A field study, *Solar Energy*. 2008; 82: 911–917.
- [6] J.A.Usmani, G.N.Tiwari and Avinash Chandra. Performance Characteristic of a greenhouse integrated biogas system. *Energy Conservation and Management* 1996; 37(9):1423-1433.
- [7] A. Kumar, N. Reddy, C.R. Prasad, P. Rajabapaiah, S.R.C. Satyanarayan.. Studies in biogas technology Part II – A novel biogas plant incorporating a solar water heater and solar water hater and solar still. *Proceedings of Indian Academy of Sciences C2 (Part-3)*. 1979; 387–393.

- [8] A.K.N. Reddy, C.R. Prasad, P. Rajabapaiah, S.R. Sathyanarayan. Studies in biogas technology, Part IV. A novel biogas plant incorporating solar water heater and solar still. *Proceedings of Indian Academic Science*. 1979;C2: 387–393.
- [9] D. Singh, K.K. Singh, N.K. Bansal. Heat loss reduction from the gas holder/fixed gas dome of a community-size biogas plant. *International Journal Energy Resources*. 1985; 9: 417–430.
- [10] G.N. Tiwari, A. Chandra. Solar assisted biogas systems: a new approach. *Energy Conversion and Management* 1986; 26 (2): 147–150.
- [11] D.J. Hills, J.R. Stephens. Solar energy heating of dairy-manure anaerobic digesters. *Agricultural Wastes*. 1980; 2 (2):103–118.
- [12] G. N. Tiwari, S. K. Singh and Kailash Thakur. Design criteria for an active biogas plant. *Energy* 1992; 17(10):955-958.
- [13] G.N. Tiwari. Enhancement in daily production of biogas systems. *Energy Conversion and Management*. 1986; 26 (3/4), 379–382.
- [14] G. N. Tiwari, S. B. Sharma and S. P. Gupta. Transient performance of a horizontal floating gas holder type biogas plant. *Energy Conversion and Management*. 1988; 28(3): 235-239.
- [15] A. Axaopoulos and P. Panagakis, Energy and Economics analysis of biogas heated livestock building, *Biomass and Bioenergy*, 2003,24,239-248.
- [16] M.R.Borges Neto, P.C.M. Carvalho, J.O.B. Carioca, F.J.F. Canafi's stula, Biogas/ Phtotvotaic hybrid power system for decentralized energy supply of rural areas, *Energy Policy* 2010; 38: 4497-4506.
- [17] Prabhakant and G. N. Tiwari. Analysis of Return on Capital for Bio Gas Plants with and without Embodied Energy. *Journal of Energy Storage and Conversion*, Jan-June. 2009; 1: 61-78.

Air bottoming cycle for hybrid solar-gas power plants

Fouad Khaldi*

Department of Physics, University of Batna, Batna, Algeria

* Corresponding author. Tel: +213 33819895, Fax: +213 33819895, E-mail: f.khaldi@univ-batna.dz

Abstract: Several solar-gas hybrid power plants based on the parabolic trough system are under construction in the MENA region and in Spain. The thermodynamic cycle of these plants is divided into topping cycle and bottoming cycle according to their temperature range. Since the solar collectors supply heat at a medium temperature level, up to 400°C, the existing technology uses a steam bottoming cycle (steam turbine). The present study aimed at investigating the thermodynamic feasibility of using air bottoming cycle (gas turbine) instead of the steam bottoming cycle. A thermodynamic scheme of solar air bottoming cycle was proposed. The case study considered an existing small size capacity gas turbine (<50 MW) as a topping cycle. The thermodynamic performance of the proposed solar air bottoming cycle was compared to two reference cases, without solar energy, a steam bottoming cycle and a conventional air bottoming cycle.

Keywords: Solar-gas hybrid power plant, Air bottoming cycle, Thermodynamic analysis.

Nomenclature

Acronyms

ABC	Air Bottoming Cycle	GR	Gas Recuperator
AC	Air Compressor	GT	Gas Turbine
ATC	Air Topping Cycle	GTC	Gas Topping Cycle
MENA	Middle East and North Africa	HRSG	Heat Recovery Steam Generator
C-ABC	Conventional Air Bottoming Cycle	IC	Intercooler
CC	Combined Cycle	PM	Pump
CD	Condenser	S-ABC	Solar Air Bottoming Cycle
CS	Combustion System	SBC	Steam Bottoming Cycle
DE	Deaerator	SGHPP	Solar-Gas Hybrid Power Plant
DR	Drum	SH	Superheater
EC	Economizer	SHX	Solar Heat Exchanger
EV	Evaporator	ST	Steam Turbine

1. Introduction

Algeria, located in the Middle East and North Africa (MENA) region, is counted among the best insolated areas. Over the country land, estimated at 2.4 millions Km², the Sahara represents 86%. It is exposed yearly to a direct sun irradiation higher than 2000 kWh/m² gain from 3500 hours of sunshine. These solar potential and land resources are optimal for the implementation of concentrating solar power plants (CSPPs) [1]. In 2009 the power generating capacity in Algeria was over 9 GW, 98% of this capacity is provided by gas-fired plants, guaranteed in 46% by gas turbine power plants [2]. In according to the Algerian energy policy fixing the share of renewable energy to 5% by 2010, augmented afterwards to 8% by 2020 [2], and since Algeria's natural gas resources are among the largest in the world, solar-gas hybrid power plant (SGHPP) is more suitable than solar-only power plant. The former technology allows for guaranteed power delivery to the grid without the thermal storage needed for compensating the solar energy intermittency day/night [3].

Currently, a 150 MW plant is expected to start run very soon in Algeria with about 25 MW from solar field. Similar power stations are under construction in other MENA region countries [4], Egypt [5], Morocco, whereas in Iran [6, 7] and Jordan [8] SGHPPs are under

consideration. The technology is based on the integrating of parabolic trough systems into combined cycles (CC) with gas topping cycle (GTC) and steam bottoming cycle (SBC). The parabolic trough systems represent the most mature solar thermal power technology, from both commercial and technical viewpoints, for mid-to-large scale grid connected power plants [9, 10]. The parabolic trough collectors can supply to the SBC a hot heat transfer fluid at medium temperature level of about 400 °C [11].

In recent years, intensive research works have been directed toward developing advanced bottoming thermodynamic cycles [12, 13]. The examined thermodynamic schemes were based on the combination of air cooling, intercooling, gas to gas recuperation and reheating [14-20]. For large-scale power generation, greater than 50 MW, it is proven that SBC is the most effective thermodynamic scheme than any other bottoming cycle [21-23]. However, for small-scale power gas turbines, generating less than 50 MW, suffering from limited efficiency, ABC can be competitive, thanks to size and economic constraints rendering unfavorable the use of SBC.

The present paper presents a conceptual analysis of SGHPP based on ABC. Air, instead of steam, is used in the bottoming cycle to recover both partially the energy supplied by the solar field and the energy from the gas turbine topping cycle exhaust. This plant will be dispensing with all the equipments related to steam power plant (high-pressure steam generator, steam turbine, condenser, pumps, water treatment plant, cooling towers, etc.). Hence, it is expected that the SGHPP based on ABC to be compact and less complex. In comparison to the steam turbine plant the gas turbine plant has some advantages: low capital investment cost and operating and maintenance cost, compact size, short delivery, high flexibility and reliability, fast starting and loading. In addition, gas turbines, free of water requirement, are more suitable to be implemented in high solar irradiation regions, limited in water resources.

A solar-air bottoming cycle (S-ABC) is proposed, analyzed and compared to two reference bottoming cycles (without solar energy), conventional air bottoming cycle (C-ABC) and steam bottoming cycle (SBC). The comparison is based on three main parameters, net output power, energy efficiency and exergy efficiency. For all scenarios, the same topping cycle was considered, an existing small size power turbine gas.

The thermodynamic simulations were performed by the flow-sheet program, “Cycle-Tempo”. This software is a freeware advanced tool for the analysis and optimization of energy systems, developed at the Delft University of Technology [24].

2. Thermodynamic simulations and evaluations

2.1. Thermodynamic bottoming cycles

In the evaluation, for the three considered bottoming cycles the same gas turbine topping cycle was used. The GE M&I LM5000-PC(1) gas turbine model was chosen [24], it is a simple open cycle composed of a compressor (AC), a gas turbine (GT), a generator (G); all linked by a shaft, and a combustion system (CS). The cycle generates 34.450 MW, at ISO conditions (1.013 bars, 15°C, RH 60%, and CH₄ as fuel), with exhaust temperature and mass flow, respectively, 432.22 °C and 124.738 Kg/s. The energy and exergy efficiencies are respectively, 36.57% and 34.86%.

2.1.1. Solar-air bottoming cycle

The schematic flow diagram of the cycle is shown in Fig. 1. To limiting the number of heat exchangers incorporated in the cycle, just one intercooler (IC) was applied between two

compressors, (AC1) and (AC2). The intercooler cooled the air exiting the first compressor (AC1) down to 40°C. After exiting the second compressor (AC2) the air was heated to 370°C in the solar heat exchanger (SHX). Afterwards, after expanding in the first gas turbine (GT1) the air penetrated into the recuperator (GR) for recovering some energy from the topping cycle flue gas before expanding in the second turbine (GT2). The effectiveness of the solar heat exchanger was set at 90%, whereas the air recuperator had the effectiveness of 85%. It assumed that the hot heat transfer fluid, coming from the solar collector, entered into the solar heat exchanger with about 395°C and then leaved with about 295°C. For the two compressors, the optimum pressure ration was 3.16 and 2.41, respectively. Both compressors and the turbine had an isentropic efficiency of 90%. The relevant air mass flow was estimated at 143 kg/s.

Heat delivered to the air in the solar heat exchanger is:

$$\dot{Q}_a = \dot{m}_a \Delta h, \quad (1)$$

where \dot{m}_a is the mass flow rate of air, and Δh is the specific enthalpy gain of the air across the SHX. The solar irradiation input to the solar collector is calculated as:

$$\dot{Q}_s = \frac{\dot{Q}_a}{\eta_{sf}}, \quad (2)$$

where η_{sf} denotes the efficiency of the global conversion of solar irradiation to heat. This includes both the optical efficiency of the solar collector and the thermal efficiency characterizing the heat transportation from the solar collector to the SHX. The value of η_{sf} is chosen to be 0.75, appropriate for the LS3 collector technology [25, 26].

The exergy input through the solar irradiation is determined by the formula [27, 28]:

$$\dot{E}x_s = \left[1 - \frac{4T_0}{3T_s} (1 - 0.28 \ln(f)) \right] \dot{Q}_s, \quad (3)$$

the symbols T_0 and T_s are, respectively, the ambient temperature and the temperature of the Sun (5777 K), and f is the dilution factor (1.3×10^{-5}).

The energy and exergy efficiencies of the cycle are defined, respectively, as follows:

$$\eta_e = \frac{P_{el}}{LHV\dot{m}_f + \dot{Q}_s}, \text{ and} \quad (4)$$

$$\eta_{ex} = \frac{P_{el}}{E\dot{x}_f + E\dot{x}_s}, \quad (5)$$

where P_{el} is the total net power delivered by the cycle, and LHV, $E\dot{x}_f$ and \dot{m}_s are, respectively, the lower heating value, the exergy rate and the mass flow rate of fuel.

2.1.2. Conventional air bottoming cycle

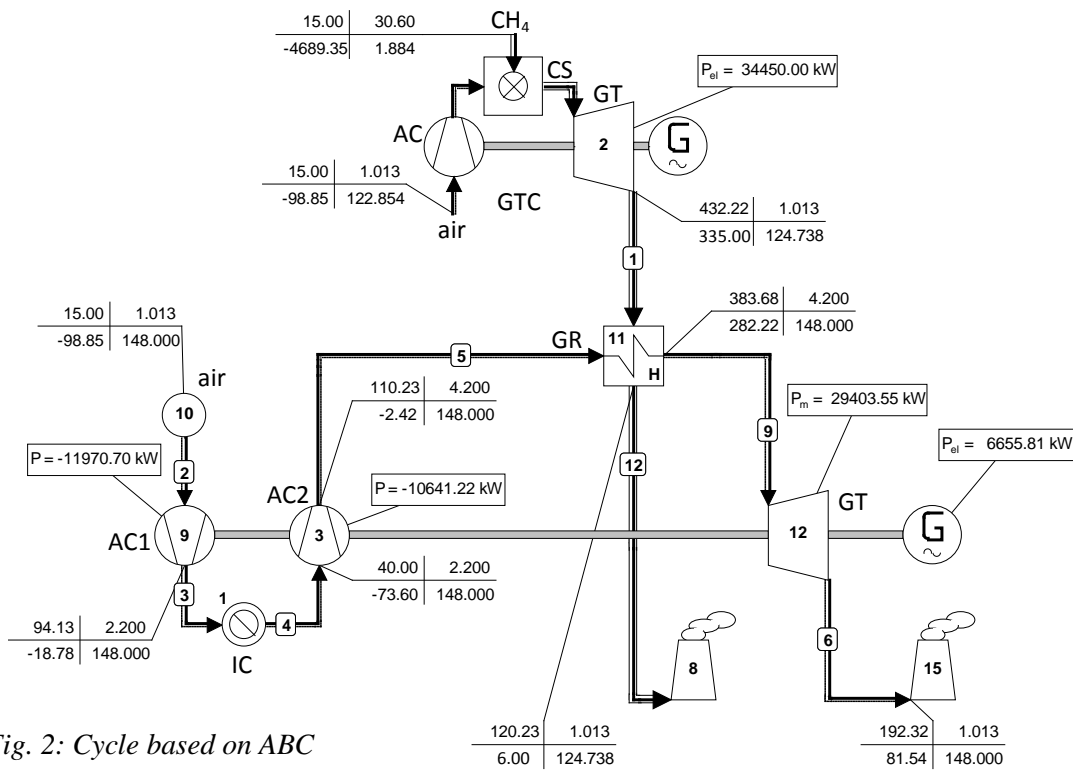


Fig. 2: Cycle based on ABC

As shown in Fig. 2, the air bottoming cycle without solar energy was examined. The C-ABC had the same characteristics as the S-ABC, except that the optimum pressure ration was 2.17 and 1.91, respectively. Also the air mass flow was fixed at 148 kg/s.

2.1.3. Steam bottoming cycle

Since the gas turbine topping cycle is of small size (<50 MW), a single-pressure HRSG was chosen. The HRSG was composed of an economizer (EC), an evaporator (EV), a superheater (SH) and a drum (DR). It had the pinch temperature of 20 °C and the approach temperature of 14°C. The superheater had the effectiveness of 87%. The superheated steam entered into the turbine (ST) at 404°C and 19 bars. The isentropic efficiency of the turbine was 85%. The pressure in the condenser (CD) was fixed at 0.074 bars, corresponding to saturation temperature of 40°C. Also, the deaerator (DE) pressure was set at 1.2 bars. More details about the cycle are presented in Fig. 3.

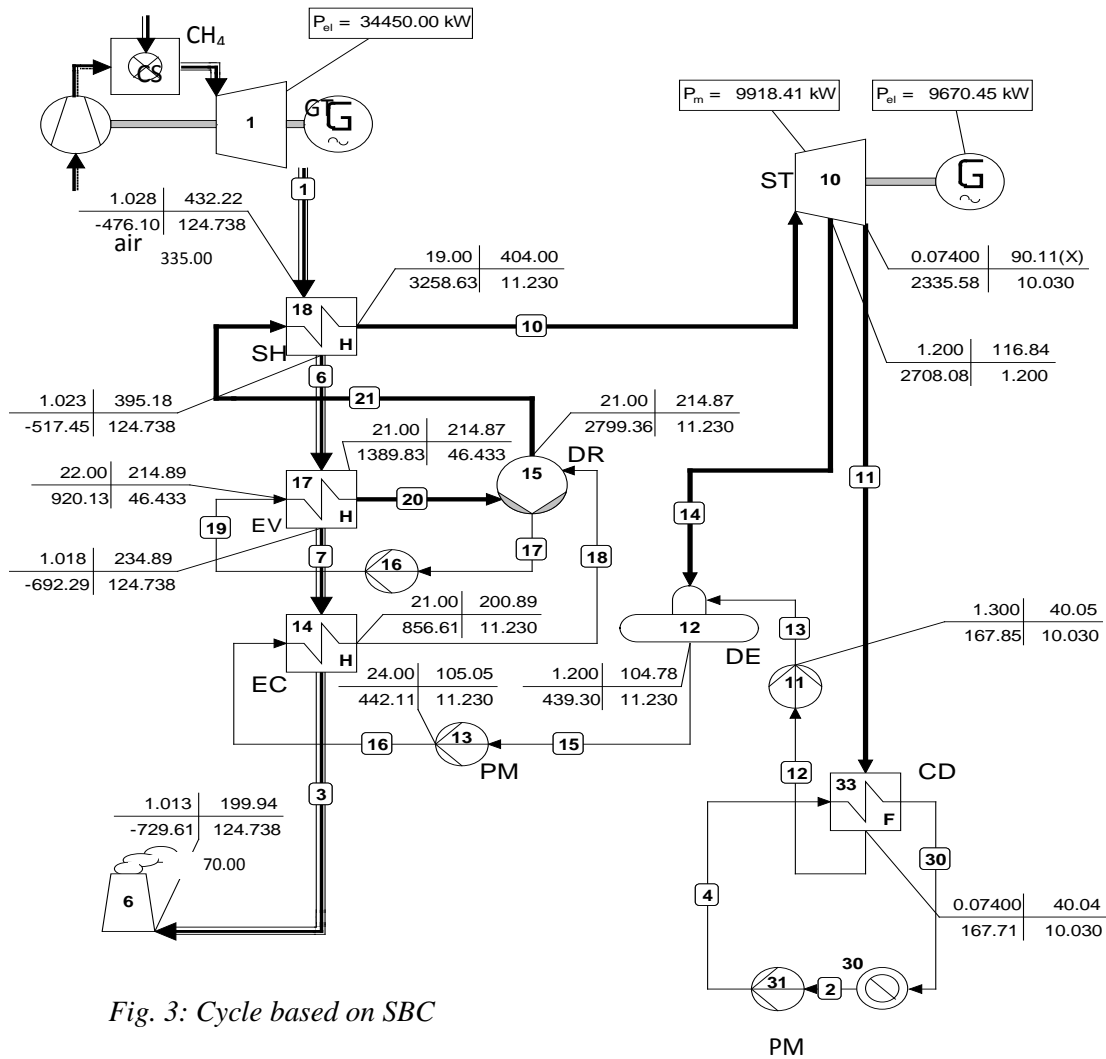


Fig. 3: Cycle based on SBC

3. Results and discussion

Main thermodynamic data related to the cycle performance, for the three examined bottoming cycles, are presented in Table 1. The S-ABC and SBC have nearly the same net output power; contributing to generate 44686 kW for the former and 44120 kW for the last, overtaking by far the C-ABC which delivers 41106 kW. However, the S-ABS is the less efficient cycle, with reference to the topping cycle, it augmented the cycle power by 28.07%, but it decreased the cycle efficiency from 36.56% to 31.87%. In contrary, the SBC is the more efficient cycle; with an energy efficiency of 46.78%, increasing then the topping cycle energy by 10.21 points. With energy efficiency of 41.60% the cycle based on the C-ABS improved the power generation by 19.32%. In term of exergy efficiency, relatively to the simple gas topping cycle the SBC and the C-ABC increase the cycle exergy efficiency from 34.36% (topping cycle), respectively, to 44.66% and 41.60%, the S-ABC decreased it slightly to 33.82%. Note that the cycle exergy efficiency associated to the S-ABC is greater than the energy efficiency.

The comparison between all the examined thermodynamic schemes depend on the relatively high number of thermodynamic parameters and combinations which can modify the performance of the cycle, i.e. turbines and compressors isentropic efficiency, heat exchangers effectiveness, pinch and approach temperature, condenser pressure, etc. The performance of the S-ABC can be improved by more cooling the air down in the intercooler, to less than 40°C, but this level of temperature is typical for cooling by dry air, adequate in regions poor in water resources. Further, at least one intercooler can be added, also an air to air recuperator

can be incorporated to recover some energy of the exhaust air bottoming cycle (143 kg/s at 231 °C). Eventually, the complexity degree of the cycle presents a constraint for any possible modification.

Even, if the S-ABC and the SBC have a comparable performance, potentially the S-ABC can offers 143 k/s of relatively hot air, 230°C, which can be adequate for heat processes requiring pure air.

Table 1. Performances of the three bottoming cycles, S-ABC, C-ABC and SBC.

	S-ABC	C-ABC	SBC
Net output power (kW)	44686	41106	44120
Energy efficiency (%)	31.87	43.63	46.78
Exergy efficiency (%)	33.82	41.60	44.66

4. Conclusion

A case study of solar-gas hybrid power plant has been analysed thermodynamically. The topping cycle of the plant was chosen to be of small size capacity gas turbine (35 MW). An air-bottoming cycle has been proposed instead the well recognized steam topping cycle. Its thermodynamic scheme was based on the combination of intercooling, reheating and gas to gas recuperation. The performance evaluation of the examined cycle was based on the comparison to two reference cases (without solar energy), steam bottoming cycle and conventional air bottoming cycle, in terms of net output power and energy and exergy efficiencies. It was found that the solar-air bottoming cycle and the steam bottoming cycle (without solar energy) had comparable net out powers; whereas the conventional air bottoming cycle (without solar energy) had the smaller capacity generation. However, the steam bottoming cycle is the most efficient cycle, followed by the conventional air-bottoming cycle and afterward by far the solar-air bottoming cycle. The difference in efficiency between the solar-air bottoming cycle and the steam bottoming cycle is due to the definition of energy and exergy efficiency related to the solar cycle. Since the solar heat is provided from the solar irradiation which is free and never depleted, it is may be more practical to don't consider the solar heat energy/exergy as an additional input energy/exergy in the calculation of the energy/exergy efficiency concerning the S-ABC. In that case, the S-ABC becomes the more efficient cycle, with cycle energy and exergy efficiency, respectively, 47.43% and 45.50%.

References

- [1] V. Quaschnig, Technical and economical system comparison of photovoltaic and concentrating solar thermal power systems depending on annual global irradiation, *Solar Energy* 44, 2004, pp. 171-178.
- [2] Commission de Regulation de l'Electricité et du Gaz (Electricity and gas authority of Algeria), www.creg.org.dz, Annual Report 2010 (in French).
- [3] Concentrated Solar Thermal Power-Now, European Commission, European Communities, 2005.

- [4] A. Poullikkas, Analysis of power generation from parabolic trough solar thermal plants for the Mediterranean Region- A case study for the Island of Cyprus, *Renewable and Sustainable Energy Reviews* 13, 2009, pp. 2474-2484.
- [5] M. A. H. El-Sayed, Solar supported steam production for power generation in Egypt, *Energy Policy* 33, 2005, pp. 1251-1259.
- [6] R. Hosseini, M. Soltani, G. Valizadeh, Technical and economic assessment of the integrated solar combined cycle power plants in Iran, *Renewable Energy* 30, 2005, pp. 1551-1555.
- [7] A. Baghernejad, M. Yaghoubi, Exergy analysis of an integrated solar combined cycle system, *Renewable Energy* 35, 2010, pp. 2157-2164.
- [8] M. S. Al-Soud, E. S. Hrayshat, A 50 MW concentrating solar power plant for Jordan, *Journal of Cleaner Production* 14, 2009, pp. 625-635.
- [9] Concentrating Solar Power-From research to implementation, European Commission, European Communities, 2007.
- [10] Energy Technology Perspectives-Scenarios&Strategies to 2050, www.iea.org, 2008.
- [11] A. Fernández-García, E. Zarza, L. Valenzuela, M. Pérez, Parabolic-trough solar collectors and their applications, *Renewable and Sustainable Energy Reviews* 14, 2010, pp. 1695–1721.
- [12] Y. S. H. Najjar, M. S. Zaaout, Performance analysis of gas turbine air-bottoming combined system, *Energy Convers. Mgmt.* 37(4), 1996, pp. 399-403.
- [13] M. Korobitsyn, Industrial application of the air bottoming cycle, *Energy Conversion and Management* 43, 2002, pp. 1311-1322.
- [14] Y. S. H. Najjar, Comparison of performance for cogeneration systems using single-for twin-shaft gas turbine engines, *Applied Thermal Engineering* 17(2), 1997, pp. 113-124.
- [15] Y. S. H. Najjar, Gas turbine cogeneration systems: a review of some novel cycles, *Applied Thermal Engineering* 20, 2000, pp. 179-197.
- [16] P. A. Pilavachi, Power generation with gas turbine systems and combined heat and power, *Applied Thermal Engineering* 20 (15-16), 2000, pp. 1421-1429.
- [17] Y. S. H. Najjar, Efficient use of energy by utilizing gas turbine combined systems, *Applied Thermal Engineering* 21, 2001, pp. 407-438.
- [18] L. Chen, Y. Li, F. Sun, C. Wu, Power optimization of open-cycle regenerator gas-turbine power-plants, *Applied Energy* 78, 2004, pp. 199-218.
- [19] A. Poullikkas, An overview of current and future sustainable gas turbine technologies, *Renewable and Sustainable Energy Reviews* 9, 2005, pp. 409-443.
- [20] C. Ruixian, J. Lixia, Analysis of the recuperation gas turbine cycle with a recuperator located between turbines, *Applied Thermal Engineering* 26, 2006, pp. 89-96.
- [21] A. L. Polyzakis, C. Koroneos, G. Xydis, Optimum gas turbine cycle for combined power plant, *Energy Conversion and Management* 49, 2008, pp. 551-563.
- [22] A. Franco, C. Casarosa, On some perspectives for increasing the efficiency of combined cycle power plants, *Applied Thermal Engineering* 22, 2002, pp. 1501-1518.

- [23] C. Carcasci, B. Facchini, Comparison between two gas turbine solutions to increase combined power plant efficiency, *Energy Conversion & Management* 41, 2000, pp. 757-773.
- [24] Cycle-Tempo Release 5.0, 2007, Delft University of Technology, The Netherlands.
- [25] G. Elsaket, Simulating the integrated solar combined cycle for power plants application in Libya, MSc Thesis, 2007, Cranfield University, UK.
- [26] M. J. Montes, A. Abánades, J. M. Martínez-Val, M. Valdés, Solar multiple optimization for a solar-only thermal power plant, using oil as heat transfer in the parabolic trough collectors, *Solar Energy* 83, 2009, pp. 2165-2176.
- [27] E. Hu, Y. Yang, A. Nishimura, F. Yilmaz, A. Kouzani, Solar thermal aided power generation, *Applied Energy* 87 (9), 2009, pp. 2881-2885.
- [28] M. V. J. J. Suresh, K. S. Reddy, A. K. Kolar, 4-E (Energy, Exergy, Environment, and Economic) analysis of solar thermal aided coal-fired power plants, *Energy for Sustainable Development*, 14 (4) 2010, pp. 267-279.

Economic Implications of Thermal Energy Storage for Concentrated Solar Thermal Power

Sharon J. Wagner^{1*}, Edward S. Rubin¹

¹ Carnegie Mellon University, Pittsburgh, PA, United States of America

* Corresponding author. Tel: +1 412 592 6986, E-mail: sjwagner@andrew.cmu.edu

Abstract: A 110-MW parabolic trough power plant operating in California was modeled to observe the effect of molten salt thermal energy storage capacity on plant performance, cost, and profitability. A plant with no storage (PT-NG) was modeled to match the hourly and annual electricity output of a comparable plant with storage (PT-TES). The solar field area for the PT-TES plant was selected to minimize the unsubsidized levelized cost of electricity (LCOE). For each storage capacity modeled here (1-12 hours), PT-NG resulted in a larger solar field area and higher O&M costs than the respective PT-TES option. PT-TES generally had higher capital costs than PT-NG, and the PT-NG levelized cost of electricity (LCOE) varied from 6% higher compared with smaller TES capacities to 6% less compared with larger TES capacities. The profitability of PT-NG compared to PT-TES followed a similar trend to the LCOE with larger margins of difference in select scenarios. These results were achieved with 3-22% of the net electric output from natural gas in the PT-NG plant. The 30% investment tax credit (ITC), currently in place for solar energy in the United States, lowered the capital costs and LCOE for each configuration. Electricity pricing through a power purchase agreement (PPA) of \$200/MWh was more profitable than hourly real-time electricity pricing, which resulted in a net annual loss for all configurations. Both the PPA and ITC were required to achieve a positive annual profit, and the maximum annual profit achieved was \$US 11 million per year with 0 hours of storage.

Keywords: concentrated solar power, thermal storage

Nomenclature

Q thermal energy..... MJ	h_e enthalpy at exit J/s
M mass kg	η efficiency or effectiveness.....
T temperature °C	h_{es} enthalpy of isentropic state at exit J/s
K piping thermal losses..... J/m ²	w work per unit mass J/kg•s
T_o ambient temperature..... °C	W power J/s
L length of pipe in solar field..... m	C_p specific heat J/kg
l_{gap} length of gap between solar collector assemblies (SCA)..... m	r density kg/m ³
w_{sca} SCA width..... m	CF plant capacity factor %
l_{br} length of space between SCA rows..... m	W_{design} design turbine output MJ
A_{SCA} SCA aperture area..... m ²	D_{htr} natural gas-fired heater heat duty..... MJ/hr
l_{sca} SCA length..... m	k loan interest rate %
n_{sca} number of SCAs per row.....	j loan lifetime years
θ incidence angle..... °	C cost \$US2009
η_{opt} SCA optical efficiency.....	i discount rate %
IAM incidence angle modifier.....	n plant lifetime years
F_s mirror soiling factor.....	F_{debt} debt portion of capital cost %
d_o outer diameter of solar field pipe m	F_{equity} equity portion of capital cost %
m mass flow rate kg/s	NPV net present value \$
Δh enthalpy change..... J/s	LAC levelized annual capital cost \$/yr
t hour of TES storage capacity hrs	C_{OM} annual operation and maintenance cost \$/yr
h_i enthalpy at inlet..... J/s	p price of electricity \$/MWh

1. Introduction

Solar energy is an attractive renewable energy source because the sun's energy is plentiful and carbon-free. Cost and intermittency issues have prevented widespread deployment of

solar power plants, but these issues may be partially mitigated with the addition of thermal energy storage (TES). Molten salt TES can be used in lieu of a natural gas boiler to provide backup energy for a parabolic trough concentrated solar thermal power (PT) plant during cloudy periods and nighttime. TES can enable a PT plant to provide reliable peak or baseload electricity without sacrificing carbon neutrality by relying on a natural gas backup system. However, the additional equipment associated with a TES system can add substantially to the already high capital cost of PT. An investor will only accept the additional cost of these components if the potential exists for an economic benefit that exceeds the extra cost. This study examines the economic implications of TES through an engineering-economic model. The model calculates the levelized cost of electricity and expected annual profit of a PT plant with varying TES capacities and compares these results to a similar PT plant with natural gas backup.

2. Methodology

An engineering-economic model was developed to simulate the hourly and annual performance and cost of a PT plant. A visual representation of the engineering portion of this model is presented in Figure 1. Typical meteorological year (TMY3) direct normal radiation (DNR) and ambient temperature data for Daggett, California [1] were used as inputs to a series of component-based mass and energy balances to simulate the thermodynamic operation of the system. Two separate and distinct engineering models were created: 1) PT-TES, which models a PT plant that uses a TES system, and 2) PT-NG, which models a plant that uses a natural gas-fired heat transfer fluid (HTF) heater in place of a TES system.

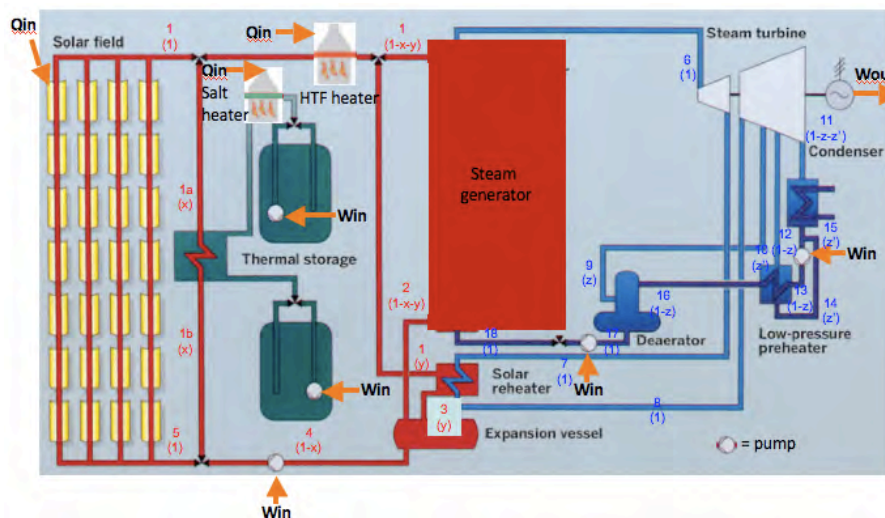


Fig. 1. Parabolic Trough Plant Schematic (adapted from [2]).

Hourly DNR enters the solar field and is concentrated on the heat transfer fluid (HTF) in the receiver tubes (red). The HTF is pumped to the power cycle where energy is transferred to steam (blue) via the steam generator and reheater. The heat from the steam drives the turbines to generate power (W_{out}) and the cooled HTF returns to the solar field. When the TES system is charging, some HTF flows to the heat exchanger to transfer energy to molten salt. Hot salt is stored in one tank and cold salt in the other. When the ambient temperature threatens to freeze the salt, the salt heater is activated to maintain the temperature above freezing. The HTF heater is used to maintain the HTF temperature above freezing when altering the HTF mass flow rate fails to prevent freezing. The HTF heater is used as an alternative to the TES system in the PT-NG plant. The heat energy input to the two heaters from natural gas combustion is represented as Q_{in} . Five pumps are used in the system, and the work required to operate them is shown as W_{in} . Red numbers refer to HTF states, blue numbers refer to steam states, and numbers in parentheses represent mass flow fractions.

The PT-TES model incorporates seven distinct operation modes, which are presented in Table 1. The hourly simulation selects operation modes based on whether all criteria are satisfied, following the hierarchy shown in Table 1. For example, if Day_TESC fails, the simulation will attempt to run Day_SOLAR. If Day_SOLAR fails, the simulation will attempt Day_TESD, and so on. The PT-NG model only uses Day_SOLAR, Night_SD, and Night_FP, and incorporates an additional mode similar to Day_TESD that uses the HTF heater in place of the TES system. The PT-NG model uses as inputs the T_1 , W_{net} , and W_{sold} results from the PT-TES model (see equations 30 and 31), and the solar field area for PT-NG is selected to minimize the difference between W_{sold} from each model, in order to simulate two different power plants that generate comparable amounts of hourly and annual electricity.

Table 1. Plant operation modes.

Mode ID	Description	Criteria
Day_TESC	Only the solar field delivers thermal energy to the power cycle; excess solar energy “charges” the TES system	$Q_{SF} > \min$ $M_{salt} < \max$
Day_SOLAR	Only the solar field delivers thermal energy to the power cycle; the TES system is idle	$0 < Q_{SF} \leq \min$ $M_{salt} \leq \min$
Day_TESD	The solar field and the TES system deliver thermal energy to the power cycle	$0 < Q_{SF} < \min$ $M_{salt} > \min$
Night_TESD	Only the TES system delivers thermal energy to the power cycle; HTF circulates through the solar field at a minimum mass flow rate to stay warm	$Q_{SF} \leq 0$ $M_{salt} > \min$
Night_SD	The power cycle is idle; HTF circulates through the solar field at a minimum mass flow rate to stay warm	$Q_{SF} \leq 0$ $M_{salt} \leq \min$
Night_TESFP	The power cycle is idle; HTF circulates through the solar field at a minimum mass flow rate, and the TES system protects the HTF from freezing	$Q_{SF} \leq 0$ $M_{salt} > \min$ $T_{HTF} \leq \min$
Night_FP	The power cycle is idle; HTF circulates through the solar field at a minimum mass flow rate, and the natural gas-fired heater protects the HTF from freezing	$Q_{SF} \leq 0$ $M_{salt} \leq \min$ $T_{HTF} \leq \min$

The hourly simulation uses an iterative process that selects an operation mode based on the net energy captured by the solar field (Q_{SF}), the total mass of salt in the “hot” TES tank (M_{salt}), and the temperature of the HTF. The minimum Q_{SF} for the 110-megawatt (MW) system modeled here is 245 megawatt-hours (MWh). The hourly Q_{SF} value depends on hourly ambient conditions and HTF temperature, as shown in equations 1 through 3. The solar field area (A) is specified at the beginning of each simulation and varied to achieve the lowest levelized cost of electricity (LCOE). Equation 2 is a simplified version of the calculation used to determine the length of pipe in the solar field, which is a required input to equation 3.

$$K = a + b \cdot (T_{HTF} - T_o) + c \cdot (T_{HTF} - T_o)^2 \quad (1)$$

where a , b , and c are empirical thermal loss coefficients [3]

$$L = l_{gap} + 2 \cdot w_{sca} + 2 \cdot l_{br} + (A \div A_{SCA}) \cdot ((l_{sca} \cdot w_{sca} - A_{SCA}) \div w_{sca} + l_{sca} + l_{br} \div (A_{SCA} \cdot n_{sca}) + (2 \cdot w_{sca} + 2 \cdot l_{br}) \div n_{sca} - (2 \cdot A_{SCA} \cdot (w_{sca} + l_{br})) / A) \quad (2)$$

$$Q_{SF} = A \cdot DNR \cdot \cos(\theta) \cdot \eta_{opt} \cdot IAM \cdot F_s - K \cdot \pi \cdot d_o \cdot L \cdot (T_{HTF} - T_o) \quad (3)$$

where $l_{gap}=1m$, $w_{sca}=5.77m$, $l_{br}=15m$, $A_{SCA}=817.5m^2$, $l_{sca}=149m$, $n_{sca}=4$, $d_o=0.07m$, and $\eta_{opt}=82\%$ [3]

Equation 4 shows how the model calculates the total amount of M_{salt} using the design values presented in [4]. The HTF factor (F_{HTF}) was selected as 1.5 after several iterations of the model indicated that the hourly m_{HTF} rarely exceeded 1.5 times the design value. The number of hours of TES capacity refers to the number of hours the turbine could operate at full rated capacity using only the thermal energy from the storage system. The extra salt factor (F_{salt}) represents the amount of salt that must remain in the TES tanks at all times. In this study, the nominal value for F_{salt} was 1.14 [4].

$$M_{\text{salt}} = -((3600 \cdot (m_{\text{HTF}} - m_{\text{HTF}0}) \cdot F_{\text{HTF}} \cdot (\Delta h_{\text{HTF}})) \cdot t \cdot F_{\text{salt}}) / (\Delta h_{\text{salt}}) \quad (4)$$

where $m_{\text{HTF}} = 1,206 \text{ kg/s}$, $m_{\text{HTF}0} = 121 \text{ kg/s}$, $F_{\text{HTF}} = 1.5$, $F_{\text{salt}} = 1.14$

The model calculates the design states and mass flow rates of all fluids in the system shown in Figure 1 through a series of component mass and energy balance equations based on the First Law of Thermodynamics, assuming steady-state conditions and zero kinetic or potential energy flows (equations 5-29). The key design inputs to these equations include: $T_1 = 393^\circ\text{C}$, $T_3 = 225^\circ\text{C}$, $T_5 = 293^\circ\text{C}$, $T_6 = 373^\circ\text{C}$, pressure (p) $_4 = 110 \text{ kPa}$, $p_5 = 620 \text{ kPa}$, $p_6 = 10,001 \text{ kPa}$, $p_7 = 1,900 \text{ kPa}$, $p_8 = 1,700 \text{ kPa}$, $p_9 = 700 \text{ kPa}$, $p_{11} = 8 \text{ kPa}$, $p_{12} = 200 \text{ kPa}$, $p_{18} = 10,200 \text{ kPa}$, $\eta_{\text{turbine}} = 85\%$, $\eta_{\text{pump}} = 80\%$, $\eta_{\text{preheater}} = 80\%$, TES heat exchanger effectiveness of heating and cooling = 88%. The hourly simulation also uses equations 5-29 to set the hourly states, beginning with a starting T_5 value of 100°C .

Heat exchangers (steam generator/ reheater, condenser, LP preheater, TES heat exchanger, salt & HTF heaters):

$$h_i = (\eta \cdot h_{\text{es}} - h_e) \div (\eta - 1) \quad (5)$$

$$h_e = h_i + \eta \cdot (h_{\text{es}} - h_i) \quad (6)$$

$$h_e = h_i + (m_{\text{steam}} \cdot (h_{i_{\text{steam}}} - h_{e_{\text{steam}}})) \div m_{\text{HTFadj}} \quad (7)$$

$$Q = m \cdot (\Delta h) \cdot 3600 \quad (8)$$

where, η = heat exchanger effectiveness, adj = mass flow rate adjusted with fractions shown in Fig. 1

Turbines:

$$w = \eta \cdot (h_i - h_{\text{es}}) \quad (9)$$

$$h_e = h_i - w \quad (10)$$

$$W = w \cdot m_{\text{steam}} \quad (11)$$

Rankine cycle pumps:

$$w = (h_i - h_{\text{es}}) \div \eta \quad (12)$$

$$h_e = h_i - w \quad (13)$$

$$W = w \cdot m_{\text{steam}} \quad (14)$$

Expansion vessel:

$$h_4 = (1-y) \cdot h_2 + y \cdot h_3 \quad (15)$$

Solar field pump:

$$W = m_{\text{HTF}} \cdot (r_4^{-1} \cdot (p_4 - p_5) \div \eta) \quad (16)$$

$$h_5 = h_4 - w \quad (17)$$

Mass flow rates and fractions:

$$z = (h_{17} - h_{16}) \div (h_9 - h_{16}) \quad (18)$$

$$z^2 = (z \cdot (h_{16} - h_{14}) + h_{14} - h_{16}) \div (h_{14} - h_{12}) \quad (19)$$

$$m_{\text{steam}} = W_e \div (h_6 + h_8 - h_7 - z \cdot h_9 - z^2 \cdot h_{12} - (1 - z - z^2) \cdot h_{11}) \quad (20)$$

$$m_{\text{HTF}} = (Q_{\text{SF}} \cdot 1000000) \div (h_1 - h_8) \quad (21)$$

$$y = (m_{\text{steam}} \cdot (h_7 - h_8)) \div (m_{\text{HTF}} \cdot (h_1 - h_3)) \quad (22)$$

$$x = (h_1 - h_{1a} \cdot m_{\text{HTF}}) \div (h_{1b} - h_1) \quad (23)$$

$$m_{\text{salt}} = -(x \cdot m_{\text{HTF}} \cdot (\Delta h_{\text{HTF}}) \div (\Delta h_{\text{salt}})) \quad (24)$$

Therminol VP-1 (HTF) and nitrate salt properties [5]:

$$C_{p\text{HTF}} = 7.888e-4 \cdot T^2 + 2.496 \cdot T + 1.509e3 \quad (25)$$

$$C_{p\text{salt}} = 1.72e-1 \cdot T + 1.443e3 \quad (26)$$

$$h_{\text{HTF}} = 1.377 \cdot T^2 + 1.498e3 \cdot T - 1.834e4 \quad (27)$$

$$h_{\text{salt}} = 8.6e-2 \cdot T^2 + 1.443e3 \cdot T \quad (28)$$

$$r_{\text{HTF}} = -7.762e-4 \cdot T^2 - 6.367e-1 \cdot T + 1.0740e3 \quad (29)$$

The net electricity generated by the system is calculated using equation 30, and then separated into electricity sold and bought (equations 31 and 32) for the cost model. The power losses due to auxiliary equipment such as electronic motors, drives, computers, etc (W_{aux}) are calculated using the series of equations described in [6]. Equation 33 calculates the capacity factor based on electricity sold, while equation 34 calculates capacity factor based on net electricity generated (after subtracting electricity used by pumps during nighttime hours).

$$W_{\text{net}} = W_{\text{turbines}} - W_{\text{pumps}} - W_{\text{aux}} \quad (30)$$

$$W_{\text{sold}} = W_{\text{net}} \text{ when } W_{\text{net}} > 0 \quad (31)$$

$$W_{\text{bought}} = \text{abs}(W_{\text{net}}) \text{ when } W_{\text{net}} < 0 \quad (32)$$

$$CF = W_{\text{sold}} \div (W_{\text{tdesign}} \cdot 8760) \quad (33)$$

$$CF_{\text{net}} = W_{\text{net}} \div (W_{\text{tdesign}} \cdot 8760) \quad (34)$$

where W_{aux} refers to power losses through auxiliary loads

The economic model calculates the total capital cost of the plant and the annual operation and maintenance (O&M) costs using a slightly adapted version of the National Renewable Energy Laboratory's (NREL) Solar Advisor Model (SAM) cost model [7], which was developed for a plant with a solar field area of 854,000 m². In order to apply this model to a variety of solar field sizes, a scaling factor (the ratio of the solar field area to the reference solar field area) is used for area-dependent O&M cost items. Calculations were added for the capital cost of the HTF and salt heaters as well (equations 35 and 36).

$$D_{\text{hr}} = (\max(Q_{\text{hr}}) \cdot 0.00094781712) \div 1000000 \quad (35)$$

$$C_{\text{hr}} = 13402 \cdot D_{\text{hr}} + 367158 \quad (36)$$

The levelized cost of electricity (LCOE) is calculated using equations 37-40. An alternative, subsidized levelized annual capital cost (LAC) is also calculated with the current United States federal investment tax credit (ITC) for solar energy investments. This ITC is applied as a cash grant, i.e., a deduction, of 30% of the total plant capital cost.

$$C_{\text{loan}} = (k \div (1 - (1+k)^{-j})) \cdot C_{\text{cap}} \cdot F_{\text{debt}} \quad (37)$$

$$\text{NPV}_{\text{loan}} = \sum (C_{\text{loan}} \div ((1+i)^{\text{year}})) \quad (38)$$

$$\text{LAC} = (i \div (1 - (1+i)^{-n})) \cdot (\text{NPV}_{\text{loan}} + C_{\text{cap}} \cdot F_{\text{equity}}) \quad (39)$$

$$\text{LCOE} = (\text{LAC} + C_{\text{OM}}) \div W_{\text{sold}} \quad (40)$$

The expected annual profit (P) is calculated using equation 41 and hourly historic electricity pricing data from the California Independent System Operator (CAISO) from 2008 [8]. This calculation assumes that the power plant receives the real-time price of electricity from the

CAISO. An alternative P is calculated under the assumption that the plant owner enters into a power purchase agreement (PPA), and this calculation is shown as equation 42.

$$P = \Sigma (W_{\text{sold}} \cdot (p - \text{LCOE})) \quad (41)$$

$$P_{\text{PPA}} = \Sigma (W_{\text{sold}} \cdot (p_{\text{PPA}} - \text{LCOE})) \quad (42)$$

3. Results

The solar field area for PT-TES was selected to minimize the LCOE, while the solar field area for PT-NG was selected to minimize the difference between W_{sold} in the two models. Figure 2 shows that the solar field area increased with increasing storage capacities in order to capture enough energy for the TES system. The solar field area for the PT-NG plant increased even more because it was required to meet the hourly solar-generated electricity output of the PT-TES plant without being able to store excess solar energy during high DNR hours. The capacity factor for each plant was almost identical since PT-NG was designed to match PT-TES. The net capacity factor for each system was smaller because it subtracts nighttime pump energy from the annual electricity generation. Overall, capacity factor increased with storage capacity as the plants operated for more annual hours. The PT-NG plant generated 3-22% of its annual electricity with the NG heater.

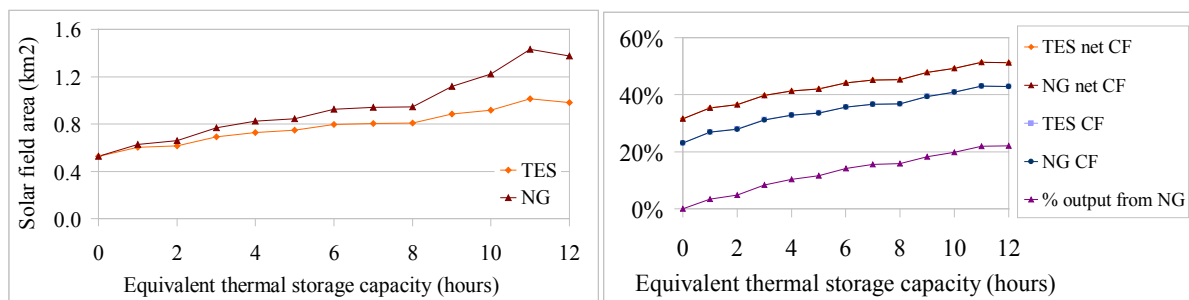


Fig. 2. Solar Field Area (left) and Plant Capacity Factor (right).
The first graph shows the solar field area selected for PT-TES to minimize LCOE and the area selected for PT-NG to match PT-TES electricity output. The second graph shows the corresponding plant capacity factors and the percent of output from natural gas in the PT-NG plant.

Figure 3 shows that the capital costs increased for both plants with increasing equivalent storage capacity, as a larger solar field was required. PT-TES with 1 hr TES had slightly lower capital costs than PT-NG as the latter required a slightly larger solar field. PT-TES with 3-12 hrs TES had higher capital costs than PT-NG as the cost of the TES system outweighed the larger solar field area required by PT-NG. O&M costs increased with storage capacity, as a larger solar field required more workers and maintenance. The O&M costs were higher for PT-NG because of the additional annual fuel purchase.

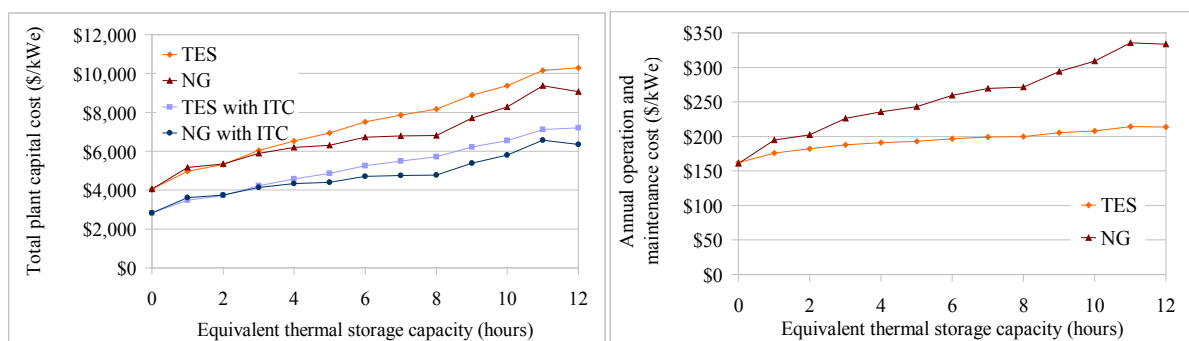


Fig. 3. Total Plant Capital Cost (left) and Annual Operation and Maintenance Cost (right).

The first graph shows the total plant capital cost for each plant with and without the 30% investment tax credit (cash grant). The second graph shows the annual O&M costs for each plant. Assumptions: natural gas = \$US 5.92/MMBtu, auxiliary electricity = \$US 135.15/MWh.

In Figure 4, the LCOE generally increased with storage capacity, and the LCOE of PT-NG varied +/- 6% from the LCOE of PT- TES. With smaller storage capacities, higher PT-NG O&M costs outweigh higher PT-TES capital costs to result in lower PT-TES LCOE. With higher storage capacities, higher PT-TES capital costs outweigh higher PT-NG O&M costs to result in higher PT-TES LCOE. This second effect was lessened with the ITC as the high PT-TES capital cost decreased, but the high PT-NG O&M cost remained unchanged. Based on these costs, a carbon price of \$US 153-\$383/tonne CO₂eq would be required for PT to be competitive with coal, depending on plant specifications.

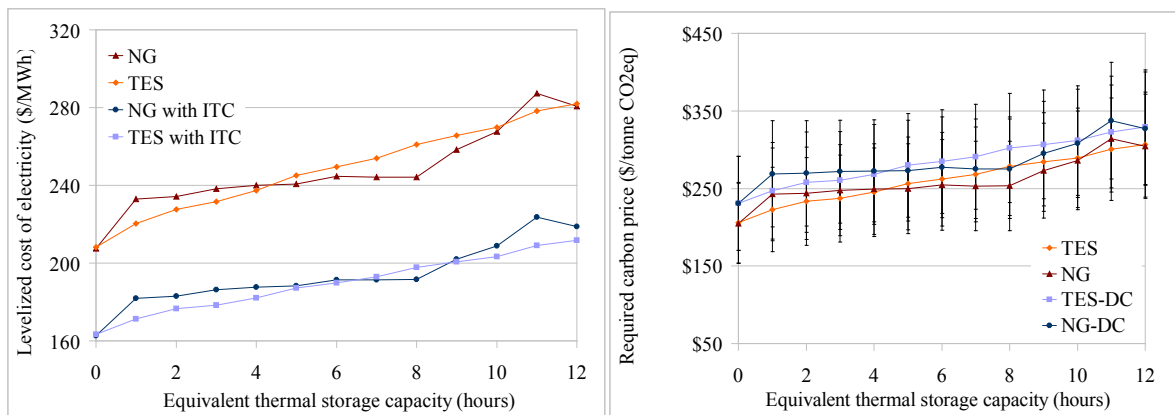


Fig. 4. Levelized Cost of Electricity (left) and Required Carbon Price (right). The first graph shows the LCOE of each plant with and without the ITC. Assumptions: $k=7\%$, $j=20$ years, $F_{debt}=60\%$, $F_{equity}=40\%$, $i=12\%$, $n=30$ years. The second graph shows the carbon price that would be required for these plants to be competitive with coal electricity generation in the United States. Assumptions: coal LCOE=\$US 64-74/MWh [9], coal greenhouse gas (GHG) emissions = 0.84-0.88 tonnes/MWh [10], and PT GHG emissions = 0.01-0.185 tonnes/MWh [11]. The bars represent the range of results associated with GHG emission and coal cost bounds.

Figure 5 shows that expected annual profit decreased with increasing storage capacity, and the only scenario that achieved positive annual profit was PPA/ITC with 0-8 hrs TES equivalent, highlighting the importance of guaranteed pricing and financial incentives. Hourly CAISO pricing with no ITC resulted in the largest annual loss, and similar trends were observed across storage capacities as those seen in the LCOE results: PT-TES was more profitable than PT-NG at storage capacities of 1-4 & 11 hr with no ITC, and 1-6 & 9-12 hr with the ITC. At the extremes, the profit of PT-NG with PPA/ITC was 4 times greater than 8 hr PT-TES and three times less than 11 hr PT-TES.

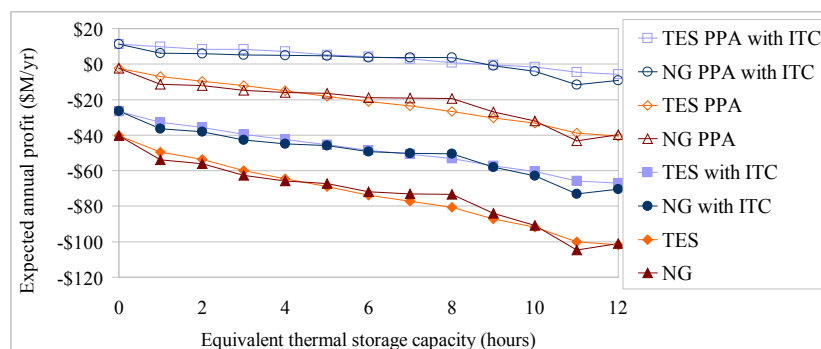


Fig. 5. Expected Annual Profit.

This graph shows the expected annual profit for each plant, using the unsubsidized LCOE, the subsidized LCOE (with ITC), hourly electricity pricing, and power purchase agreement pricing (PPA of \$US 200/MWh).

4. Discussion and Conclusions

The results of this analysis are subject to the specific assumptions and calculations outlined above. The uncertainty inherent in these assumptions and the sensitivity of results to changes in nominal values has not yet been explored, but is the subject of future analysis. Nonetheless, the limited scope presented here offers some insights for solar energy policy. Encouraging PT power plants to serve as baseload generators could result in cost increases and profit decreases, whether the additional generation is met by NG or TES. However, a small amount of TES (1-4 hours) is likely to be slightly more profitable and less costly than attempting to achieve similar annual generation with NG backup. If the policy goal is to encourage the deployment of PT power plants as baseload generators, incentives such as the U.S. federal 30% investment tax credit (ITC) or a generous power purchase agreement (PPA) are necessary to reduce the LCOE and result in a positive expected annual profit. The ITC favors TES compared to NG because it reduces the high TES capital cost but does not affect the high NG O&M costs. A price of \$US 153 per tonne CO₂eq or higher could make PT competitive with coal electricity generation.

References

- [1] Wilcox, S. and W. Marion. 2008. User's Manual for TMY3 Data Sets, NREL/TP-581-43156. April 2008. Golden, Colorado: National Renewable Energy Laboratory.
- [2] Price, H., ed. Assessment of Parabolic Trough and Power Tower Solar Technology Cost and Performance Forecasts. Rep.No. SL 5641. Sargent & Lundy LLC Consulting Group. Chicago, IL: NREL, 2003.
- [3] Kreith, Frank, and D. Yogi Goswami, eds. Handbook of Energy Efficiency and Renewable Energy. New York: C R C LLC, 2007
- [4] Estimated value from: Kelly, B. and Kearney, D. Thermal Storage Commercial Plant Design Study for a 2-tank Indirect Molten Salt System. Final Report, May 13, 2002 - December 31, 2004. Golden, CO.: National Renewable Energy Laboratory (2006).
- [5] National Renewable Energy Laboratory, Solar Advisor Model User Manual, 2009
- [6] National Renewable Energy Laboratory, Solar Advisor Model Reference Manual for CSP Trough Systems, 2009
- [7] Turchi, C. Parabolic Trough Reference Plant for Cost Modeling with the Solar Advisor Model (SAM), National Renewable Energy Laboratory Technical Report No. NREL/TP-550-47605, July 2010.
- [8] California ISO, version 5.7.7, <http://oasis.caiso.com>, accessed October 15, 2010.
- [9] Integrated Environmental Control Model 6.2.4 (with advanced features selected), <http://www.netl.doe.gov/technologies/coalpower/ewr/pubs/cmu-iecm.html>.
- [10] Jaramillo, P., W.M. Griffin, and H.S. Matthews. 2007. Comparative life cycle air emissions of coal, domestic natural gas, and SNG for electricity generation. Environmental Science & Technology. 41(17):6290-6296.

- [11] Lechón, Y., C. de la Rúa, and R. Sáez. 2008. Life cycle environmental impacts of electricity production by solarthermal power plants in Spain. *Journal of Solar Energy Engineering*. 130. 021012-1-7.

Social and technical aspects in solar system design

Dorota Wójcicka-Migasiuk^{1,*}, Andrzej Chochowski²

¹ Lublin University of Technology, Faculty of Fundamental Engineering, Lublin, Poland

² Warsaw University of Life Sciences, Warsaw, Poland

* Tel: +48 81 5384453, Fax: +48 81 5384706, E-mail: d.wojcicka-migasiuk@pollub.pl

Abstract: The paper defines and describes factors that should be considered when hybrid energy supply systems that incorporate solar systems in particular are planned. In the first point, the author establishes the hierarchy of criteria to apply at subsequent phases of the decision processes carried out when renewable energy systems are to be used. To do this, the authors take the advantage of shortly described case studies: a solar hot water system in an elderly house and an integrated system of steam boilers together with heat recovery from a cooling system in connection with solar heating in a food production plant, etc. Then, the paper indicates the necessity of energy simulations prior to taking up the decisions of localization and to final verification of the project. The example of the simulation method called equivalent thermal network is mentioned in the comparison to the advantages and disadvantages of the other software described. Some forms of promotion are presented, which can be applied to positively stimulate the sustainable development of the use of renewable sources in the European central eastern region on the background of a short comparison.

Keywords: local availability, hybrid systems, sustainable development

1. Introduction

Hybrid systems in relation to energy supply are the systems that incorporate different media such as electric current, flowing fluids or solid massive elements to carry out different forms of energy from various sources either renewable or conventional. They are also called integrated systems and can combine a traditional boiler gas fired, a heat pump transferring ground heat or the heat from solar thermal collectors, a usually small photovoltaic system supplying electrical energy for circulation pumps and somehow integrated a passive system such as e.g. solar walls. The particular composition is determined by operational conditions, energy source localization, availability and its form, and by other factors that influence the rational use of energy. The decisions can be taken up after thorough consideration of:

- local climatic conditions,
- social aspects that influence the cycle of energy demand,
- object character,
- technological aspects resulting from selected devices designed for the system,
- economical factors that determine investment capabilities in the frame of the analyzed enterprise and
- the cost of operation of the whole hybrid system.

The paper presents the description of the influence of selected factors on design and decision processes related to appropriate energy supply system and on the realization of objects that use solar energy. There is a vast diversity of social aspects and problems of matching between the demand and solar energy availability in a perspective characteristic for mid-severe climate, characteristic for central - eastern Poland. The procedure of careful analysis describes the most important contracting factors such as:

- high solar gain and low ambient temperature,
- high social acceptance and cost exaggerating investment capabilities in the region,
- standard regulations characteristic for the country and the region and availability of simulation tools, and with special attention
- the applicability of available simulation tools.

2. Methodology

The selection and decisive criteria can be divided in some hierarchy. It is obvious for engineers that the good will of having a system to supply renewable energy cannot be decisive for selection of components for the particular object. It is questionable, however, if the negative will (quite common in some societies) can be decisive for the resignation and if the decision should not be taken by local authority on the basis of justified technical reasons and natural conditions, having in mind the rational use of energy and environment protection. It is a distant goal to reach the situation when such justification is obligatory to potential investors. On this distant way to reach this goal either social mentality must undergo its process of evolution towards higher responsibility for the environment or legislation and standards must be established to rule new attempt to the selection of energy sources. The widely understood education drawing the attention to all mentioned determinants could be very helpful on this way to assume proper hierarchy in the processes of investment, design, realization, maintenance of systems and exploitation of resources to reach the final result established as sustainable development.

Usually, attempting the design process for a particular object, its localization and character is already established, but sometimes, we have a chance to adjust the localization for better exposition to solar radiation or for advantageous distribution of ground collectors and slightly adjust the waveform of load to the cycle of energy availability through some change of habits or technology. The principal idea of hybrid systems is not the most extensive use of all renewable energy sources (res) in one system but the most reasonable integration of those that are convenient for the localization and the object character. Country regions are comparatively flexible in fitting the localization to the needs of effective heating systems and this meets another fact that the systems that are used there are usually outdated and contain low effective boilers fuelled with coal or are expensive such as boilers fuelled with liquid gas or gasoil because of the cost of these fuels. In the first phase of design the availability and economics of resources is considered. The paper is focused on solar energy thermal conversion integrated within hybrid systems because widely understood conversion of solar energy has its special conditions and restrictions worth analyses.

The systems that use direct and dispersed beam require south oriented exposition with possible adjustment to horizontal plane, and thus should be placed on the ground or tilted roofs. They need the coincidence of load waveform and the cycle of availability as much as possible to avoid damage resulting from overheating of elements or heat loss because of extended accumulation. These systems are used:

- for hot water systems: in food industry, for sanitary and living purposes in permanently occupied buildings (SDHW) and to contribute low temperature heating systems, especially
- floor heating systems,
- to heat process water: in fish breeding ponds, to water glasshouse plants and to heat the ground,
- in drying processes of many purposes to contribute technological halls (air collectors and passive solar systems), especially biomass drying for solid biofuels,

Systems that cooperate with heat pumps in heating systems either in central heating or hot water systems require additional supply from electric grid and providing cooling power from the bottom source of so called bottom energetic potential i.e. from the ground, for example.

They can have the form of:

- ground water wells, which require proper soil absorption to receive water from absorption wells, proper localization in a distance to each other and good quality of soil to protect durability of drilled objects,

- horizontal and vertical heat exchangers that require big undeveloped land area. One should remember that undeveloped does not mean unused. The terrain with ground collectors underneath can serve as a parking place, sports yard, nice flower bed or grass and only big root trees must be avoided.

Boilers can be fuelled with biofuels but each case must be considered if the particular localization is economically justified in the aspect of transport cost. It is difficult to describe biofuels as one source of energy because they are diversified as much as biomaterials and processes used for their generation. Shortly describing, the generation can also be understood as origin and is the classifying factor for biofuels. The first generation biofuels are produced directly from eatable plants in fermentation and trans-esterification processes and have similar limitations as food raw material. The second generation biofuels are produced from biomass or non eatable seeds having in mind that waste material is its origin. The third generation biofuels use the same material as the second one but after additional treatment, processing and modifications. The fourth generation biofuels are rather a perspective target employing such advanced technologies as in photo bioreactors and the use of intermediary organisms, e.g. algae, during production processes. In Poland, the second generation biofuels will soon have the dominant role over the first one which is positive and desired tendency.

Heat recovery systems from production processes of many types, e.g. from ventilation, from cooling, quite frequent in food industry and rarely from air conditioning as it is not very popular in Poland, or heat recovery from litter in animal farmhouses.

Photovoltaic systems, usually recognized as expensive, become reasonable when traditional connection to grid is more expensive than standards, especially when increased power demand in a farm or a household requires additional investment from regional distribution company which in turn is transferred to a user. They are treated as additional support to supply devices of low demand in complex hybrid systems (e.g. PV panels for circulation pumps in solar domestic hot water – SDHW - systems). Environmental protection aspects can be sometimes decisive if the localization is situated in nature parks. The most famous localization of this type in our country is the mountain shelter in the Valley of Five Polish Tarns. Moreover, it is also practical to install PV panels in periodically occupied small objects such as forest shelters, guest rooms and shepherd's huts but there is a need to provide an energy store system and protection in the period of no use by e.g. spare duty lighting. The potential of photovoltaics is recognized as capable to reach 12% share in total production of energy in Europe by 2020 year. Unfortunately, in Poland, there are no favorable circumstances to promote PV systems [1].

Solar walls in our climate should be completed with TIM (Transparent Insulation Material) modules besides typical massive elements and air gaps because this additional insulation protects the building envelope during fall-winter seasons against thermal losses at low ambient temperatures. It is necessary that the whole insulation of these buildings is of best quality ranging u value between 0.1 and 0.3 at maximum and that the terrain around is properly adapted. Several case studies can be mentioned on the basis of the author's research [5, 7] and the other reference [1]. Particular conclusions can be derived in relation to the application of such passive structures as Trombe-Mitchell's walls in eastern mid-European regions [7]. This typical construction cannot be successfully used for the whole year because:

- insulation even by two glass panels is insufficient for winter and
- solar radiation in summer often exceeds the needs.

In the intermediary season of fall (spring/autumn), solar walls prove their usefulness and thus make possible to reduce heating period and energy demand in total thanks to the solar gain in several weeks within the range of the whole heating period. There is also a very useful solution to the problem of insulation, i.e. transparent panels. Thanks to the capillary structure they let radiation in and prevent from thermal losses because of air trapped within capillary and its material – organic glass - of insulation properties. Moreover, the shading can be realized by means of insulated folded blinds and with the help of leaf trees.

Because of low intensity of heat flux coming from renewable sources such as ground or solar radiation, the renewable systems have comparatively long pipelines and this is one of the reasons of thermal loss from active elements. That is also why designs should strictly reduce collective pipeline length placing collectors as close as possible to the receivers. Moreover, in comparison to traditional heating, the effectiveness of renewable systems depends more on the cycle of load. In particular, the systems that work at loads lower than calculated in the design, have much lower energy effectiveness which influences directly the cost-effectiveness. The research carried out by Chochowski A. and Czekalski D. [1] prove that energy parameters outstand the predicted ones on the basis of static characteristics. Unequal load of the system in subsequent days leads to the reduction of conversion efficiency even of 50%.

3. Results

At first, the exemplary case study of an elderly house for women in a village can be shortly described. The design of this system avoids long pipelines because the boiler room is on the ground floor directly under the roof where collectors are to be installed with proper exposition on south oriented tilted roof. The design process of this hybrid system was carried out when the total modernization of the whole object was considered, including the change of fuel from liquid gas stored in tanks on the backyard to natural gas from local network. The designed solar system was to contribute to the main supply. The designed system consists of the battery of twelve flat plate thermal collectors and nine collectors have been planned on the south tilted roof and the other three on the west roof surface with additional construction for southwest exposition. Optional expansion of the battery into another eight collectors could be possible after removal of gas tanks. The condition of source availability is fulfilled this way. Another criterion for consideration was matching the load waveform to the cycle of heat production. In this aspect there is an ideal phase coincidence either in annual cycle or daily use of hot water and heat production from the solar system. This is possible because of special care that must be carried for the residents, i.e. – because the residents are of advanced age and through this debilitated and less resistant to temperature changes, their bathing in winter must be limited to the necessitate minimum. In summer, when there is a lot of sun radiation there are no such threats as low temperature, cold draughts etc., the balneological care can be more frequently applied. There is also some good coincidence in daily treatment because the baths are taken in the afternoon hours when the house service staff have managed with cleaning and cooking and the water storage tank is full of water heated from collectors at the maximum for the day. In the evening hours, the water storage starts slowly cooling off and the staff except for the person on duty, goes home. Moreover, the residents in elderly houses do not go for holidays as housing estate inhabitants or do not go home in the afternoon as people working in offices. It is only a pity that at so many favourable circumstances, this design has been abandoned.

Czekalski D. [1] points out also some other solutions of good coincidence: a seminary with boarding house, a monastery or a convent with retreat centers, a school with a swimming

pool, etc. Academic centers are especially vulnerable to the pressure of educative aspects of renewable energy applications and they should extremely thoroughly consider the matter of coincidence. The good solution could be a guest room house combined with a sports center containing a swimming pool available for usage during holidays. It seems not justified to supply lecture buildings from solar energy because the largest amount of energy is to be used potentially when the real use drops to zero. Then it is necessary to employ this energy somehow to avoid the destruction of the whole system. Overheated collectors are damaged and hot water stored for too long than a few days is the environment for bacteria growth. This problem has to be solved also for single family houses. In this aspect municipal applications in blocks of flats are advantageous because the part of inhabitants stays at home for the whole year and it is not a problem if this is not the same group when hot water is prepared centrally. The remaining usage is usually sufficient to ensure continuous medium flow through collectors.

Another attempt to the problem of coincidence is the consideration of the integration of an individual system with municipal grids and networks, however at the present state of formal regulations and technical practice, it is an extremely difficult enterprise in our country, available rather to bigger energy producers than just families or single farms. So far, the connection of geothermal source with the heat distribution network and the integration of boilers fuelled by biofuels with gas boilers supplied from gas distribution network or with the heat distribution network has had the best practical experience. In the case of the integration with gas boilers, the network does not receive the energy from the renewable system, only gives the possibility to reduce the amount of supplied fuel. The connection together with the receipt of energy is especially desired in the case of photovoltaic systems and the grid. The two aspect can be covered there: one of autonomous operation of a renewable system and the regular profile of power supply.

The next example of good coincidence could be the idea of integration between the production processes and solar thermal collectors studied for the case of meat production plant. Because of the meat processing, hot water of 80 °C is used to wash production rooms (intensive use at about 3 p.m.) and water of 60 °C for hygienic purposes and another processing continuously during two shifts. Hot water is supplied from cooling system recovery and steam boilers that provide also central heating in the object. The hybrid system concept suggests the integration between cooling system heat recovery and solar collectors where load cycle fits the solar daily availability waveform and conventional support from steam gas boilers.

4. Discussion

Some evaluation if the selected modules of a composed hybrid system is possible in advance by means of simulations. The most advanced simulation techniques are useful for designers, who in the case of not standard objects can verify their effectiveness. It is worth mentioning that RES systems are mostly unique because of the local applications, sometimes differing even between neighbor farms or buildings.

The most representative is the following software that is available in European location but with some limitations:

ESOP [4] developed by Viessman – very well prepared software, intended for use by designers but suitable also for local authority representatives. It provides calculation for some typical SDHW systems with the possibility to calculate carbon dioxide emissions and comparisons among different fuels, available in Polish version.

TRNSYS [2] developed by University of Wisconsin – advanced software to calculate transient states in the variety of systems, with the reference to geographic and climatic conditions, very useful also for advanced use such as scientific analysis and for designers, however comparatively expensive and Polish version is not available. It is worth mentioning that the university provides some possibilities for free download from internet and even these limited versions are very educative and thus very useful for didactics. The software is grouped in packages for different media and RES and enables cost calculation on the basis of design system and selected devices from USA market.

WUFI [3] developed by Fraunhofer Institute – software suitable for passive systems such as multi-layer wall structures, available in Polish version also for free download for the purpose of didactics but with limitations, provides some information to know particular producers of the used materials and thus can be useful to calculate the cost of the system.

Moreover, the authors can also mention simulation algorithms based on equivalent thermal network developed in cooperation by Lublin Technical University and the University of Life Science in Warsaw [5, 6]. These algorithms at the current state are suitable for advanced users, perform calculations also for transient states and have not been commercialized yet. The use of these algorithms is undoubtedly more time consuming but the user can decide on all simplifications introduced to the system model and to the calculations. The method enables modeling of energy flow by means of different media and thus is suitable for integrated systems, provides results of calculated energy flux, flows and temperature reached in the system units in time for different days of a year in the form of graphs and matrices. The other algorithms have been developed for solar walls by means of FEM analysis.

What is even more important the ease of simulation analysis can add the value to the planned refurbishments and all purpose modernizations in many municipal sectors in the phase prior to the design instead of time consuming and expensive existing building inventorying in situ. This should be particularly taken into account when numerous objects are to be rebuild in the regions where older technology have been applied so far.

References

- [1] D. Chwieduk, R. Domański, et al., Renewable Energy. Innovative Technology and New Ideas., Chwieduk D., Domański R., Jaworski M. (editors) Warsaw 2008, p. 476.
- [2] <http://sel.me.wisc.edu/trnsys> Oct.'10.
- [3] <http://www.wufi.de> Oct.'10.
- [4] Viessmann, ESOP v.2.0 CD, 23.03.2003
- [5] Wójcicka-Migasiuk D., Modelling hybrid systems in rural regions, (in Polish) Inżynieria Rolnicza 1(89)/24, KTR PAN PTIR, Kraków 2007, p. 120.
- [6] Wójcicka-Migasiuk D., Nodal potential simulation for the analysis and design of SDHW systems. (in Polish) Acta Agrophysica No. 39/2001, Inst. Agrofizyki PAN, Lublin 2001, p. 106.
- [7] Wójcicka-Migasiuk D., Heat transfer through solar walls, (in Polish) LTN, Lublin 2008, p. 112.

On the Significance of Concentrated Solar Power R&D in Sweden

Torsten Strand^{1*}, James Spelling¹, Björn Laumert¹, Torsten Fransson¹

¹Department of Energy Technology, KTH Royal Institute of Technology, Stockholm, Sweden

*Corresponding Author. Tel : +46 70 268 4024, E-mail : torsten.strand@punkt.se

Abstract: Concentrated Solar Power (CSP) is an emerging renewable energy technology that has the potential to provide a major part of European energy needs at competitive cost levels. Swedish industry is strongly involved in CSP-based energy production either in the form of growing providers on the European energy market or as developers and producers of key components for CSP power plants. The growing industrial interest is reflected and accompanied by state of the art research in this field at the Department of Energy Technology at KTH. In the present paper the main challenges and opportunities for CSP R&D are presented and linked to the industrial environment and interests in Sweden. Related to these challenges, an overview of the latest research activities and results at the Department of Energy Technology is given with examples concerning CSP plant operation and optimisation, techno-economic cycle studies and high temperature solar receiver development.

Keywords: solar thermal power, Sweden, research and development

Nomenclature

<i>A</i>	area..... [m ²]	<i>I_o</i>	incident solar flux..... [W/m ²]
<i>C</i>	cost..... [€]	<i>LEC</i>	Levelised Electricity Cost..... [€/kWh _e]
<i>DNI</i>	Direct Normal Irradiation	<i>n</i>	payback time..... [years]
<i>E</i>	electrical energy..... [kWh _e]	<i>a</i>	annualisation factor [-]
<i>i</i>	interest rate..... [-]	<i>ε</i>	efficiency..... [-]

1. Introduction

At first glance, concentrated solar power (CSP) may not seem of great interest to Sweden, which receives only weak solar irradiation with few sunny days in winter when power is needed most. However, seen from the wider perspective of a sustainable energy system, with input from many different energy sources (such as hydro, wind and biomass) across Europe, North Africa and parts of Middle East, CSP could form a dominating part of the solution to future energy shortages and the problem of rising CO₂ emissions [1].

Sweden is today increasingly integrated in the European energy grid and major Swedish providers (e.g. Vattenfall, Fortum, E.ON) are growing on the continental energy market. Furthermore, many Swedish companies (e.g. Siemens Industrial Turbomachinery, ABB) are actively involved in the production of components for CSP plants such as steam turbines, mirrors for the collector fields and many more. As such, Sweden's interest in CSP is due not only to its wider environmental credentials, but also its direct economic importance to the country. There is thus good reason for Swedish energy institutions, authorities, industry and universities to actively take part in development to further strengthen the established position in this field.

2. Concentrated Solar Power Technology

In its most basic form, a CSP plant consists of solar collector field with mirrors that concentrate the solar radiation to one or more receivers where this radiation is converted to high temperature heat [2]. This high temperature heat source can be used to drive conventional power generation

equipment (such as steam cycles, Stirling engines, micro gas-turbines, etc.) to produce electricity. Significant amounts of waste heat are also available which are currently wasted but could be used to drive other processes.

The levelised cost of electricity (LEC) of CSP-based power plants has been shown to be amongst the most competitive of all renewable energy technologies [3], with a significant cost advantage over PV when deployed on a large scale. However, CSP technology has not yet matured to the point of grid-parity with conventional power generation systems, although this is predicted to occur within the next 15 years [4]. Rapid reductions in the LEC of CSP-based systems are expected, as shown in Table 1, whereas the cost of fossil-fuel based power is expected to rise with increased fuel prices and the introduction of CO₂ cap-and-trade schemes.

Table 1. Current and Predicted LEC of Selected Power Generation Technologies [4], [5]

LEC [€cts/kWh _e]	Parabolic Trough	Solar Power Tower	Dish Stirling	Solar PV	Coal
Current (2010)	17.2	24.1	28.1	28.4	8.4
Future (2025)	12.8	9.7	14.0	14.8	10.8

Direct solar irradiation is an abundant renewable energy source [1] but is available only at low flux densities: large areas must be used to collect enough energy. Even so, the area necessary to satisfy all of Europe’s electricity needs using currently available CSP technology would be only a small fraction of the North African deserts [1]. The most suitable areas for CSP deployment are within the tropics, where irradiation is good, almost all days are cloudless and the land is of desert type with low population [3]. Suitable areas for CSP are shown in Fig. 1.

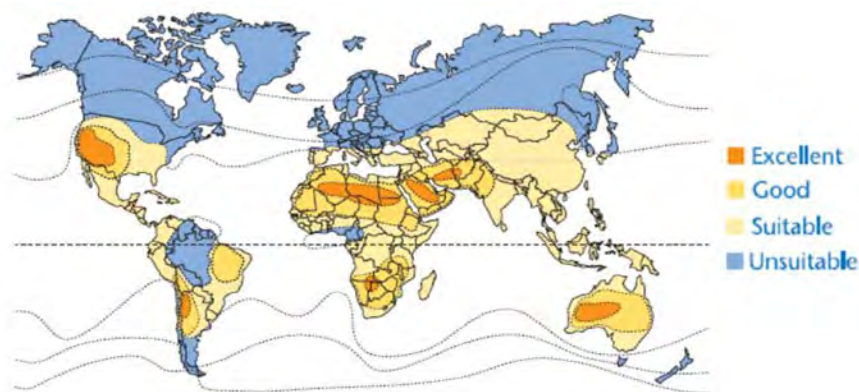


Fig. 1. Distribution of Sites Suitable for Solar Thermal Power Production
Source: German Aerospace Centre (DLR)

In Europe the requirements for economic electricity production with CSP are fulfilled for a number of countries around the Mediterranean Sea but the real “European Sun-belt” is in North Africa. A group of leading European industries have established the DESERTEC foundation [1] for promoting the deployment of CSP-technology in the North-African deserts, with the stated aim of providing 15% of the European electricity requirements [1], as well as meeting local demand. The total investment in CSP plants and transmission lines is expected to be in the region of €400 billion, to be realised by 2050.

2.1 Conventional CSP Technology

The dominating CSP technology: linear parabolic trough mirrors with collectors producing steam for conventional steam turbine plants, as shown to the left of Fig. 2, has been commercial for about 30 years [4]. The power range for these systems has been 30-80 MW_e with solar-electric efficiency around 15-20% [2]. A high number of 50 MW_e plants of that type are presently being put into operation in Spain [5]. Plants in the power range of 400 MW_e are built in the USA and planned for North Africa. Currently almost all steam turbines for solar thermal power plants are delivered from Sweden by Siemens Industrial Turbomachinery.

The technology is well proven and the present development trends are:

- Higher turbine inlet temperatures by developing heat transfer media with the ability to withstand higher temperatures
- Extension of operating time by hybrid operation, energy storage and shorter start-up times
- Efficiency improvements on mirrors and receiver pipes by optimised glass qualities and surface coatings

The cost break down of such a plant shows that the solar field is the most costly part, around 50% and that the thermal conversion unit is only around 24% [4].

2.2 Solar Towers: the Emerging Technology

Solar towers surrounded by heliostats, as shown to the right of Fig. 2, have higher solar concentration factors than parabolic troughs and can thus reach higher temperatures [2]. The size of the heliostat field around a tower has an optimum determined mainly by the height of the tower and the losses from the most distant mirrors. Today the optimal thermal power from a tower seems to be around 100 MW_{th} with a 160 m tower and some 830 heliostats with a 121 m² mirror area per unit [5]. Larger systems can be expected considering possible advancement in mirror and receiver efficiencies and control system precision.



Fig. 2. Conventional (left) and Emerging (right) CSP Technology
Source: Solar Millennium/Abengoa Solar

Presently the receivers are placed on top of the tower, which means the heat has to be transported by some means to the power block on the ground down the height of the tower. For small size units (up to around 6 MW_e) the power generation unit could be placed at the top of the tower, close to the receivers. The tower arrangement can be used with steam turbines, providing higher

live steam temperatures than the parabolic trough solar fields. More interesting is that gas-turbines can also be considered for the conversion of heat to electricity. Gas-turbines are cheaper, simpler to install, potentially more efficient and do not need water.

3. Challenges and Opportunities in CSP R&D

CSP remains an emerging technology, with an active R&D community working to improve the viability and effectiveness of the concept. On-going research activities at the Department of Energy Technology (EGI) of the Royal Institute of Technology, Stockholm have highlighted what the authors believe to be some key challenges in the development and deployment of CSP technology at the current time.

3.1 Increasing Economic Competitiveness

Solar thermal power technology cannot yet be considered to be directly competitive with conventional power generation technology (such as those based on the combustion of coal or natural gas) but later most probably with new nuclear power. In the current energy market, deployment of CSP technology is supported by government incentives such as feed-in tariffs and loan guarantees. Increasing the competitiveness of CSP technology is a key challenge in solar R&D and will go hand-in-hand with increased CSP deployment [2]. As such, any reduction in the cost of this technology represents a major opportunity for the industry.

Since the incident solar radiation is free, the cost of the electricity from a CSP plant is dependently solely on the depreciation of the initial investment cost C_{inv} and the annual plant maintenance cost $C_{O\&M}$. The standard definition of levelised electricity cost (LEC) used in solar thermal calculations [4] is based on the net electrical output E_{net} and an annualisation factor α , assuming a rate of interest i , a payback time n in years and an annual insurance rate k_{ins} . The net electrical output is a function of the total collector area A_{col} , the incident solar flux I_o and three efficiency factors ε_{col} , ε_{rec} , and ε_{cyc} for the collector field, solar receiver and power generation cycle respectively.

$$LEC = \frac{\alpha \cdot C_{inv} + C_{O\&M}}{E_{net}} \quad \text{with} \quad \alpha = \frac{i \cdot (1+i)^n}{(1+i)^n - 1} + k_{ins} \quad \text{and} \quad E_{net} = A_{col} \int_{year} \varepsilon_{col} \varepsilon_{rec} \varepsilon_{cyc} I_o dt \quad (1)$$

Any reduction in the LEC will increase the economic competitiveness of the technology and equation (1) brings to light key ways in which reductions can be made:

- The first focus can be placed on reducing the cost of the power plant components (both in term of initial investment C_{inv} , as well as the maintenance $C_{O\&M}$). As the solar field components represent over 50% of the total investment cost, priority should be placed on reducing the cost of these components. Fortunately, these components are still in the early stages of their learning curve and costs are dropping rapidly.
- A second focus can be placed on increasing the net electrical output E_{net} for a given power plant. This can involve optimizing plant design, reducing parasitic consumption as well as improving operational strategy, all of which serve to increase the integrated annual value of ε_{cyc} .

- The final focus can be placed on new power plant concepts. This can involve moving to more efficient thermodynamic cycles (generally requiring higher temperatures), new receiver designs and improved collector field layouts with the aim of increasing the three efficiencies ϵ_{col} , ϵ_{rec} , and ϵ_{cyc} and thus E_{net} . This can result in lower values of LEC for the plant, as long as the increase in E_{net} compensates for any increase in the cost.

3.2 Reducing Water Consumption

The deployment of CSP technology is most effective in areas with high direct normal irradiation (DNI). This fact, coupled with the large land requirements for CSP plants would seem to make desert locations very attractive for deployment [1]. However, the high DNI of desert regions comes with a significant draw-back, in that these regions suffer from a severe scarcity of water resources [6] which will place a limit on the number sites found suitable for deployment of this technology.

The current generation of solar thermal power plants, based on conventional steam-cycles, require water for a number of purposes:

- For the cooling of the condenser, with especially large volumes for evaporative cooling
- To replace that lost from the cycle during steam drum blowdown
- To maintain a high efficiency of the solar field: the mirrors need to be kept clean to ensure a high reflectivity

In order to facilitate the increased deployment of solar thermal power in water-scarce areas it will become necessary to reduce the water footprint of CSP plants, shown for a number of contemporary plants in Table 2. A number of options for achieving this have been highlighted:

- Replacing evaporative or once-through cooling systems in steam-cycle power plants with dry or indirect cooling systems, including options for cold-water storage
- Moving towards higher-temperature solar receivers, allowing the use of gas-turbine cycles, eliminating the use of water as a working fluid as well as the need for cooling
- Moving towards high-efficiency power generation cycles, reducing the size of the collector field per unit electrical output, reducing the water use due to mirror washing

Table 2. Water Consumption of contemporary Rankine CSP Plants [8]

Power Plant Type	Water Consumption [m^3/MWh_e]		
	Evaporative	Hybrid Dry/Wet	Air Cooling
Parabolic Trough	3.0	0.4 – 1.7	0.3
Solar Power Tower	1.9 – 2.8	0.4 – 1.0	0.4

3.3 Increasing Availability/Dispatchability of CSP Plants

The output from a solar thermal power plant is strongly dependent on the available solar flux, which varies due to both the predictable daily evolution of the Sun's position as well as the more unpredictable variations in local weather conditions. This raises two key issues for CSP plants:

- In order to maintain an acceptable lifetime for the power plant components (turbine, steam generators, etc.) the duration of transient operation should be minimized. To improve the dispatchability of CSP plants, it is also of interest to accelerate the start-up of the turbines in order to bring power rapidly onto the grid once solar energy is available
- In order to increase the flexibility and economic viability of a solar power plant in a liberalised electricity market, it is advantageous for the plant to be able to produce power during times of peak demand, which are not necessarily in phase with times when the solar flux is available.

Both these issues require a decoupling of the energy supplied to the power generation cycle from the incident solar radiation. Over a short time period, thermal energy storage can ensure a constant power output to the cycle during solar transients resulting from cloud cover or other meteorological phenomena [2]. Larger storage volumes can also allow dephasing of the electrical output, permitting increased operational flexibility.

At the current time, certain conventional CSP units are built as hybrid plants, using natural gas fired boilers or gas-turbine waste heat recovery boilers for additional steam production when solar radiation is insufficient or absent. With a gas-turbine in the cycle, power production becomes very flexible with the possibility not only to meet peak power demand and to operate at night, but also to reduce the size of the mirror field.

4. Opportunities for CSP R&D in Sweden

Swedish industry is heavily involved in the supply of steam turbines for solar thermal power applications (through Siemens Industrial Turbomachinery) and it can be seen that many of the key opportunities for solar R&D lie in the field of turbomachinery. As all commercial CSP plants are based on the use of steam-cycle technology, improvements in steam-turbine operational strategy present attractive opportunities for R&D. Swedish companies such as ABB are involved in supplying tracking systems and others such as Cleanergy supply Stirling engines for solar dish systems.

The challenges presented in §3 highlight the potential advantages in moving towards gas-turbine-based CSP plants. Use of gas-turbines reduces water consumption and opens the possibility for the use of more flexible hybrid plants as well as higher efficiency combined-cycle systems. Swedish industrial companies are ideally placed to provide gas-turbines in the power ranges suitable for solar thermal applications.

5. Research focuses at the Department of Energy Technology

On-going research activities at EGI are focused on responding to the key challenges identified in §3 as well as supporting Swedish industrial partners in addressing the opportunities created. The following sections present key current projects.

5.1 Solar Steam Turbine Operation

Due to the variable nature of the solar supply and the daily operating cycle of solar power plants, the number of turbine starts per year for solar steam turbines is an order of magnitude higher than for base-load turbines. As a result, the speed with which the turbines can be started assumes a

greater importance in CSP plants and modifications allowing turbines to start faster are examined as part of on-going research.

The speed at which the turbines can reach full load is based on the lowest metal temperature measured before start-up begins. As such, if the steam turbine can be kept hot during idle periods, the duration of the next start-up can be reduced without impacting negatively on the lifetime. A number of modifications that can be made to the turbines to maintain their temperature during idle periods have been evaluated. Heat blankets were shown to be the most effective measure for keeping the turbine casing warm, whereas increasing the gland steam temperature was most effective in maintaining the temperature of the rotor [7]. By applying a combination of these measures the dispatchability of the turbine can be improved significantly: electrical output can be increased by above 9% for both long and short cool-downs, as is shown in Fig. 3.

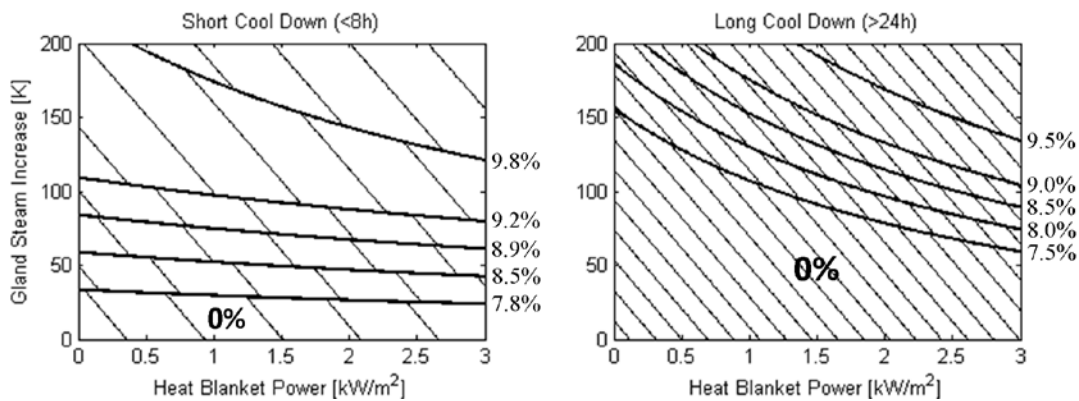


Fig. 3. Impact of applying a combination of heat blankets and gland steam temperature increase on the daily output of the plant on the day following the cool-down period [7]

5.2 Solar Power Plant Thermo-Economics

All operational commercial solar thermal power plants are based on the use of Rankine cycles, which are limited in the efficiencies they can achieve by the relatively low temperatures at the receiver. However, developments in the field of high temperature receivers [8] have opened up the possibility to use more advanced thermodynamic cycles, especially the use of gas-turbines. In order to evaluate the potential of new power plant concepts, thermo-economic models are used to predict investment and levelised electricity costs, as well as other important factors such as annual electricity production, water consumption, exergy efficiency, land use and many more [9]. Coupled with a multi-objective optimisation routine, Pareto-optimal power plant designs can be established and the trade-off between economic and environmental objectives analysed. Polygeneration concepts, mainly using waste heat for production of e.g. clean water, cooling or biogas for local consumption can also be positive factors both for acceptance and economy.

5.3 Solar Receiver Design and Testing for Gas-Turbine Integration

In order to support on-going solar gas-turbine research at EGI, small-scale but high temperature receivers are being design and tested for use with micro gas-turbines. Availability in Sweden of sunlight strong enough for testing is very limited and therefore a small indoor solar lab has been built, shown schematically in Fig 4. An artificial Sun consisting of strong Xenon lamps produces 11 kW of radiation which is directed to a parabolic dish of 1.8 m diameter and used to test small receivers of different innovative designs. Presently two receivers are being investigated:

- A medium temperature receiver in which materials with high thermal conductivity and coatings for good solar absorption are essential for high efficiency
- A generic high temperature volumetric receiver in which different types of heat exchange materials can be tested both for overall heat transfer data and detailed information on solar penetration depth, temperature gradients, pressure drops, etc.

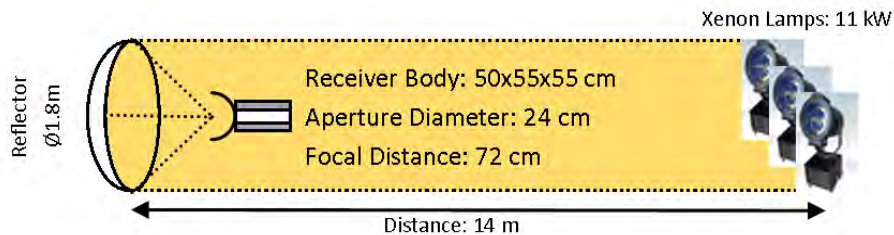


Fig. 4. Basic Layout of EGI's Receiver Test Facility

6. Conclusion

Amongst the plethora of renewable energy technologies on offer, CSP emerges as a promising option for sustainable power generation in the Sun-belt regions of the world. A diverse R&D community supports the refinement of the technology and commercial CSP plants are beginning to appear worldwide. Swedish industry is well-placed in the market, providing almost the entirety of the steam turbines for conventional CSP plants, as well as a number of ancillary components. Within Sweden, the nurturing of active R&D is essential to maintain this dominant position. EGI is actively pursuing key issues on different CSP systems such as techno-economic optimization, polygeneration arrangements, receiver components and their integration with the conversion unit.

References

- [1] G. Knies, U. Möller, and M. Straub, "Clean Power from Deserts: The DESERTEC Concept for Energy, Water and Climate Security", Hamburg, 2007
- [2] C. Philibert, "The Present and Future Use of Solar Thermal Energy as a Primary Source of Energy", International Energy Agency, Paris, 2005
- [3] K. Ummel and D. Wheeler, *Desert Power: the Economics of Solar Thermal Electricity for Europe, North Africa, and the Middle East*, Center for Global Development, 2008.
- [4] R. Pitz-Paal, J. Dersch, and B. Milow, "ECOSTAR: European Concentrated Solar Thermal Road-Mapping", Deutsches Zentrum für Luft- und Raumfahrt, 2004
- [5] C. Richter (Editor), "Solar Power and Chemical Energy Systems: Annual Report", Deutsches Zentrum für Luft- und Raumfahrt, Köln, 2008
- [6] US Department of Energy, "Reducing Water Consumption of CSP Electricity Generation", Report to Congress, 2001
- [7] J. Spelling, M. Jöcker and A. Martin, "Thermal Modeling of a Solar Steam Turbine with a focus on Start-Up Time Reduction", ASME TurboExpo, Vancouver, 2011
- [8] B. Hoffschmidt, F. Tellez, J. Fernandez., "Performance Evaluation of the 200kWth HiTRec-11 Open Volumetric Receiver", Solar Energy Engineering, vol. 125 (2003), pp. 87-97
- [9] J. Spelling, D. Favrat, A. Martin et al., "Thermo-Economic Optimisation of Solar Tower Thermal Power Plants", International ECOS Conference, Lausanne, 2010.

Experimental heat transfer research in enhanced flat-plate solar collectors

R. Herrero Martín¹, A. García Pinar¹, J. Pérez García*¹

¹ Technical University of Cartagena, Cartagena, Spain

* Corresponding author. Tel: +34-968-32.59.85, Fax: +34-968-32.59.99, E-mail: pepe.perez@upct.es

Abstract: Enhancement techniques can be applied to flat-plate liquid solar collectors towards more compact and efficient designs. Tube-side enhancement passive techniques can consist of adding additional devices which are incorporated into a smooth round tube (twisted tapes, wire coils), modifying the surface of a smooth tube (corrugated and dimpled tubes) or making special tube geometries (internally finned tubes). For the typical operating flow rates in flat-plate solar collectors, the most suitable technique is inserted devices. Based on previous studies from the authors, wire coils were selected for enhancing heat transfer. This type of inserted device provides better results in laminar, transitional and low turbulence fluid flow regimes.

To test the enhanced solar collector and compare with a standard one, an experimental side-by-side solar collector test bed was designed and constructed. The testing set up was fully designed following the requirements of EN12975-2 and allow us to accomplish performance tests under the same operating conditions (mass flow rate, inlet fluid temperature and weather conditions). In this work the preliminary results obtained are presented and the standardized efficiency curve is shown for both tested solar collectors. A relevant improvement of the efficiency has been reported and quantified through the useful power ratio between enhanced and standard solar collectors.

Keywords: heat transfer enhancement, wire-coil inserts, liquid flat plate solar collector

Nomenclature

A_A	Absorber area.....	m^2	ρ	Fluid density.....	kg/m^3
α_{AI}	Thermal losses coefficient.....	W/m^2K	t_a	Ambient temperature.....	$^{\circ}C$
c_p	Specific heat of working fluid.....	J/kgK	t_{in}	Inlet temperature.....	$^{\circ}C$
Q_{useful}	Useful power.....	W	t_{out}	Outlet temperature.....	$^{\circ}C$
Q	Flow rate.....	m^3/s	t_m	Mean temperature $t_m = t_{in} + \Delta t/2$	$^{\circ}C$
G	Global irradiance.....	W/m^2	T_m^*	Nondimensional temp. $T_m^* = (t_m - t_a)/G$	
η	Thermal efficiency		τ	Transparent cover transmittance	
η_A	Thermal efficiency based on absorber area		α	Absorptance of absorber plate	
η_O	Optical efficiency coefficient		F_R	Heat removal factor	
η_{OA}	Optical efficiency coefficient				

1. Introduction

In industrial applications, a set of enhancement techniques are widely used to improve the performance of heat exchangers. Enhanced surfaces can be used to increase heat exchange, reduce the size of equipments or save pumping power. Thermal liquid solar collectors are potential candidates for enhanced heat transfer, but not many studies have focused on this aspect. The vast majority of works carried out applying enhancement techniques to improve solar collector performance deal with air collectors, mainly inserting artificial roughness within the exchange surfaces [1, 2, 3].

Regarding liquid solar collectors just a few studies have focused on enhancement techniques. Kumar and Prasad [4] presented a remarkable work inserting twisted tapes in a serpentine solar collector. They investigated the effect of the twisted-tape geometry, different mass flow rates and intensity of solar radiation on thermal performance. The authors observed that heat losses were reduced (due to the lower value of the plate temperature) and consequently an increase on the thermal efficiency was observed.

Recently, Jaisankar et al [5] performed an experimental investigation of heat transfer, friction factor and thermal performance on a tube-on-sheet solar panel with twisted-tape insert devices. They also investigated the effect of the twisted-tape geometry for different Reynolds and intensity of solar radiation. They concluded that when twist ratio is increased, the swirl generation is decreased and both heat transfer and friction factor are minimized. Jaisankar et al also carried out several experimental investigations of heat transfer, friction factor and thermal performance of thermosyphon solar water heater systems fitted with twisted-tape insert devices. [6, 7, 8] The authors found that the heat transfer enhancement in the twisted tape collector was higher than in the standard collector.

Also Hobbi and Siddiqui [9] conducted an indoor experimental study to investigate the impact of several insert devices on the thermal performance of a flat-plate solar collector. They studied different passive heat enhancement devices: twisted strips, coil-spring wires and conical ridges. They observed no appreciable difference in the heat transfer to the collector fluid and concluded that the applied passive methods based on the enhancement of shear-produced turbulence were ineffective in augmenting heat transfer to the collector fluid.

In spite of the fact that many of the previous works within liquid collectors employed twisted tapes as inserted devices, basically due to the existence of well known design correlations [10, 11, 12], the use of other passive tube-side techniques such as wire coils still unexplored. Regarding the aforementioned fact, Webb and Kim [13] also pointed out that the existence of design correlations does not mean, however, that the twisted tape insert is the best insert device. As Garcia mentions [14, 15], wire coils are especially suitable for enhancing heat transfer in laminar, transition and low turbulent flow regimes. In a previous work from the authors, a numerical simulation methodology to study the heat transfer enhancement in a tube-on-sheet solar panel with wire-coil inserts, using TRNSYS as the simulating tool was developed. A parametric study was also performed to relate the fluid and flow characteristics with the heat transfer enhancement by wire-coil inserts. It was shown that the enhanced collector increased useful power in the whole range of mass flow rate when using water as the working fluid [16].

The purpose of the present work is then to characterize a flat-plate solar panel with wire-coil insert devices in terms of heat transfer, friction losses and thermal performance and compare this enhanced collector with a standard collector under the same operating and weather conditions. To test the enhanced solar collector and compare with a standard one, an experimental side-by-side solar collector test bed was designed and constructed. The testing set up was fully designed following the requirements of EN 12975-2 [17]. A relevant improvement of the standardized efficiency curve has been reported. Furthermore, the ratio of useful power and pressure drop between the enhanced and the standard solar collector for different flow rates and operating conditions were computed.

2. Experimental set-up

The experimental setup was designed to carry out simultaneously the thermo-hydraulic characterization of two solar collectors (an enhanced collector with wire-coil inserts and a standard collector) under the same operating (mass flow rate, inlet fluid temperature) and weather conditions. It is located in Cartagena, southeastern Spain (Latitude N'3736, Longitude W'00059). Furthermore, this facility was built in agreement with the requirements of standard EN 12975-2 [17]. A schematic layout of the test bed constructed is shown in Figure 1.

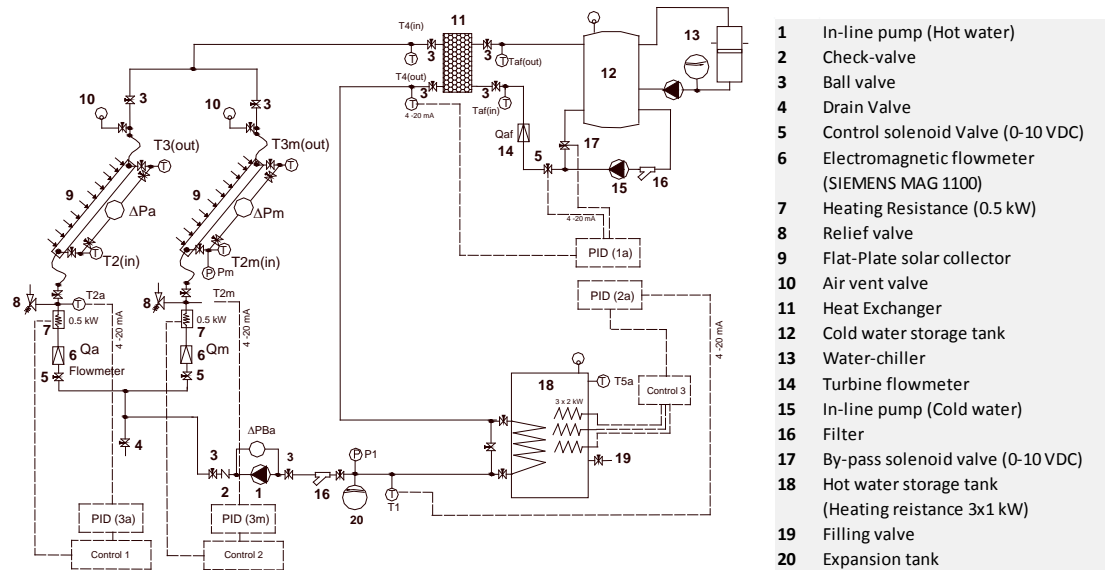


Fig. 1. Experimental set-up

The main components of the experimental setup are the two sheet-and-tube flat-plate solar water heaters with 9 parallel tubes (risers) on the back of the absorber plate, as it is detailed in Fig. 2. The risers are connected at the top and bottom by headers to homogenize flow distribution and static pressure at inlet and outlet sections. Both collectors have a single glass cover; their technical specifications are summarized in Table 1.

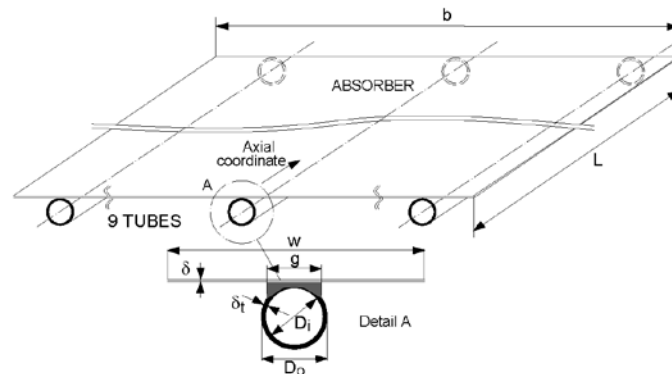


Fig. 2. Sheet-and-tube tested solar collector configuration

Table 1. Main characteristics of the flat-plate solar collectors

Material properties		Geometrical data			
k_{abs}	209.3 W/mK (Aluminum)	D_i	0.007 m	N_G	1
k_{tube}	372.1 W/mK (Copper)	w	0.1227 m	N_{tubes}	9
ϵ_g	0.88 (Glass)	g	0.0035 m	A_C	2.022 m ²
τ_g	0.93 (Glass)	δ_{abs}	0.0005 m	A_{edge}	0.2348 m ²
k_{ins}	0.05 W/mK	δ_{tube}	0.0005 m	L_t	1.83 m
ϵ_{abs}	0.05 (Miro-Therm)	δ_{ins}	0.025 m	β	45°
		α_{abs}	0.95 (Miro-Therm)		

One of the solar collectors was modified inserting wire-coils within their risers. A wire coil of dimensionless pitch $p/D=1$ and wire-diameter $e/D=0.0717$ was chosen (Fig. 3). This geometry showed good overall thermohydraulic behaviour for the operating conditions in solar collectors according to Garcia [15] work.

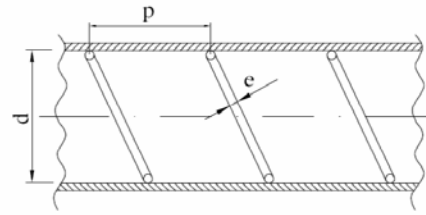


Fig. 3. Sketch of the helical-wire-coil fitted in the raisers of the modified solar collector.

2.1 Instrumentation

The instrumentation was selected and mounted according to the standard EN 12975–2 requirements. Thermoresistance Pt100 class 1/10 DIN A were used to measure the inlet and outlet fluid flow temperatures. To measure the flow rate and the pressure drop through the collectors, electromagnetic flowmeters (Siemens MAG1100 DN 3) and differential pressure transmitters (SMAR) with different configurable ranges were used. Regarding the weather conditions: 3 PSP class I thermoelectric pyranometers were employed to measure the solar irradiance (global irradiance in the aperture plane, global irradiance on the horizontal plane and the other one has a shading band to measure diffuse horizontal solar irradiance). Velocity and wind direction were measured with an ultrasonic anemometer (Windsonic from Gill Instruments Ltd). Ambient temperature, humidity and pressure were also measured. In Table 2 the main characteristics of the selected instrumentation are summarized.

2.2 Uncertainty propagation

We follow the criteria of ISO GUM (Guide to the expression of Uncertainty in Measurement) [18] to derive the equation for thermal efficiency proposed in EN 12975-2 and uncertainty propagation assessment. When the tests are accomplished in steady state, the thermal efficiency can be expressed as Eq. (1).

$$\eta_A = \frac{\dot{Q}_{\text{useful}}}{GA_A} = \frac{Q\rho_{(t)}c_{p(t)}(t_{\text{out}} - t_{\text{in}})}{GA_A} \quad (1)$$

The standard uncertainty of each magnitude is shown in Table 2. The uncertainty of each magnitude is a combination of the uncertainties of Type A evaluation, associated to the standard deviation of the mean of the repeated observations, and of Type B, evaluated from scientific statement based on the calibration available information. According to the uncertainty propagation study carried out, it can be concluded that the initial uncertainties are slightly amplified and the expanded uncertainty at a 95% confidence level are $\pm 0.1\%$ for non-dimensional temperature T_m^* and $\pm 0.9\%$ for thermal efficiency η .

3. Thermal performance calculations according to standard EN 12975-2

The useful power is calculated according to Eq. (2).

$$\dot{Q}_{\text{useful}} = Q\rho_{(t)}c_{p(t)}(t_{\text{out}} - t_{\text{in}}) \quad (2)$$

where, the fluid density and the specific heat are evaluated at the mean fluid temperature $t_m = t_{\text{in}} + \Delta t/2$, and the thermal efficiency can also be expressed according to Eq. (3) as a function of global irradiance intercepted, absorber area and useful power.

$$\eta = \frac{\dot{Q}_{\text{useful}}}{GA_A} \quad (3)$$

Table 2 . Instrumentation description and uncertainty.

Magnitude	Sensors	Instrumentation	Uncertainty
Solar Irradiation	3	1 st Class Kipp&Zonnen CMP6 Pyranometer Shadow band (Diffuse Irradiation)	±0.,1%
Ambient Temperature	1	Pt100 3w	±0.1°C
Ambient Pressure	1	Piezoresistive barometer	± 0,4 mbar a 20°C
Humidity	1	Capacitive sensor	±2%
Wind velocity and direction	1	WindSonic Gill Instrument (Vel. interval 0-60 m/s) (Vel. Direction 0-359°)	± 2% Velocity ± 3% Direction
Inlet and Outlet Fluid Temperature	4	Pt100 4w Class 1/10 DIN A	± 0,03 °C
Flow Rate	2	Electromagnetic Flowmeter Siemens MAG 1100 Transmitter MAG 6000	± 0,25 %
Differential Pressure	2	Differential pressure transmitter SMAR D0 type (-4 to +4 inch H ₂ O) Standard collector D1 type (0-20 inch H ₂ O) Enhanced collector	± 0,1 % of Span
Absolute pressure	1	Piezoresistive transducer	± 0,5 %

The thermal efficiency η can be correlated with the reduced temperature, $T_m^*=(t_m-t_a)/G$ using linear $\eta = \eta_0 - a_1 T_m^*$ or quadratic regressions $\eta = \eta_0 - a_1 T_m^* - a_2 G T_m^{*2}$, based on absorber or aperture area. The experimental data obtained show a good linear correlation ($R^2=0.9874$ for the standard solar collector, and $R^2=0.9282$ for the enhanced solar collector). These linear correlations are simpler and more useful in engineering applications. Additionally, their coefficients are independent of global irradiance.

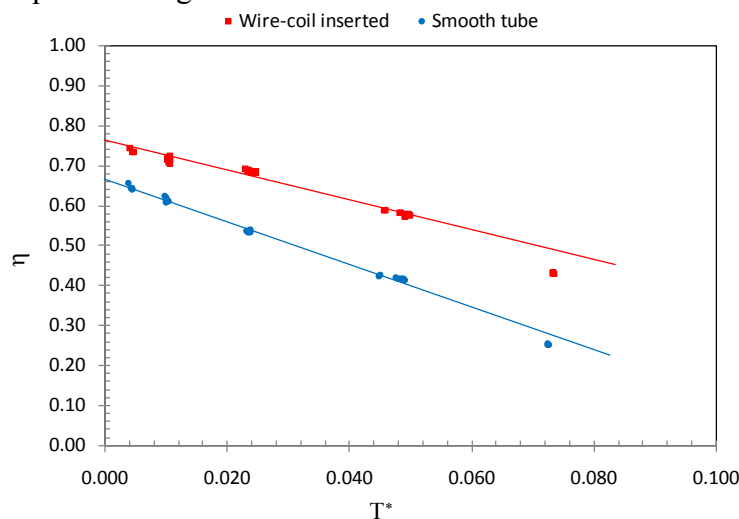


Fig. 4. Thermal efficiency curves for standard and enhanced flat-plate solar collectors (0.04 kg/s)

In Fig. 4 the standardized thermal efficiency curves for both standard and enhanced flat-plate solar collectors are shown. It can be observed that a significant improvement in the thermal efficiency of the solar collector with wire-coil inserts is achieved. Note that in the enhanced solar collector the optical efficiency coefficient η_{OA} is about 15% higher and the thermal losses coefficient α_{A1} is lower than in the standard one (Table 4). This effect can be due to the enhancement of heat transfer between the absorber plate and the working fluid which reduces its temperature and as a consequence, the thermal losses decrease. The uncertainty of the regression coefficients have also been assessed according to the methodology proposed by Coleman and Steele [19].

Table 4. Linear correlation coefficients and their uncertainties (95% I.C)

	Standard collector		Enhanced collector	
	Coefficient	Uncertainty	Coefficient	Uncertainty
η_{0A}	0.6670	0.44 %	0.7654	3.97 %
a_{1A}	-5.3410	1.71 %	-3.7640	0.52 %

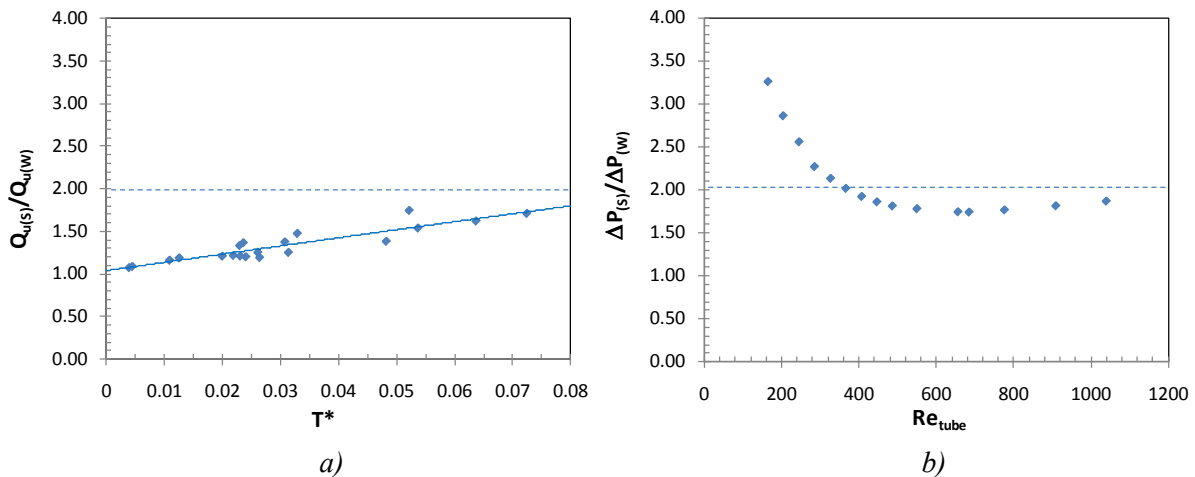


Fig. 5. Ratios between standard and enhanced solar collectors a) Useful power versus non-dimensional temperature, and b) Loss pressure versus Reynolds number inside raisers

In Fig. 5 a) the useful power ratio between the enhanced and the standard solar collector is showed for different flow rates (0.016÷0.04 kg/s) and operating conditions ($520 \leq Re_{tube} \leq 2340$). It can be observed that there is a linear dependence between the useful power ratio and the non-dimensional temperature. For increasing values of T^* the ratio of useful power is higher. This is due to the fact that the wire-coil insert lowers the absorber temperature reducing the thermal losses. This confirms the results from the previous numerical simulations carried out by the authors. [16] In Fig. 5 b) the pressure loss ratio between both collectors is represented. For Reynolds numbers higher than 500, inside the raisers, the pressure loss ratio remains constant at about 1.8. This increase in pumping power is compensated with an improvement in thermal efficiency, which would be especially suitable for large installations in which several solar collectors are connected in parallel. In this type of configuration an accumulative increase in thermal power is obtained, while the pressure loss remains the same in all the solar collectors, and thus, this configuration would enable optimum operation and would be the best-practice approach.

Nevertheless, in order to establish the optimum operating range within enhanced solar collectors with wire-coil inserts, a heat exchangers performance evaluation criterion has to be employed. A modified criterion (R3m) was proposed by the authors [16]. This criterion stands for the increasing useful power obtained in the enhanced and the standard collector at equivalent operating regimes to satisfy the constraint of equal pumping power. To compute this parameter further efficiency and friction factor tests are being carried out.

4. Conclusions

An experimental side-by-side solar collector test bed was designed and constructed to characterize the thermo-hydraulic behaviour of a standard and an enhanced solar collector under the same testing conditions (operating parameters and radiant conditions). The facility

was built in agreement with the requirements of standard EN 12975 to carry out thermal performance and pressure drop tests.

The thermal efficiency curves of two solar collectors, a standard and an enhanced collector were obtained. The enhanced collector was modified inserting spiral wire coils of dimensionless pitch $p/D=1$ and wire-diameter $e/D=0.0717$ within each riser. The thermal efficiency increments depend on the operating flow rates. For a flow rate of 144 l/h (0.04 kg/s) the efficiency optical factor was found to increase by 15%. The collector with wire-coil inserts enhances heat transfer and as a consequence the absorber temperature is reduced. This means a reduction in the thermal losses as well as a decrease of the loss coefficient by 30%. However, an increase in terms of friction losses is observed and thus pumping power rises. In order to account for the overall enhancement (thermo-hydraulic performance) that wire-coil inserts promote in the solar collector, the ratio of useful power and pressure loss between both solar collectors were computed. For increasing values of T^* the ratio of useful power is higher and reaches values up to 1.8. For Reynolds numbers higher than 500, inside the risers, the pressure loss ratio remains constant at about 1.8. The increase in pumping power is compensated with an improvement in thermal efficiency, which would be especially suitable for collectors connected in parallel. This configuration would enable optimum operation and would be the best-practice approach.

As a final conclusion, according to the present work, wire-coil devices can be successfully inserted within the flow tubes in solar water heaters for enhancing heat transfer rate.

Acknowledgements

This research is supported by the Spanish Regional Agency “ARGEM” (Agencia de Gestión de la Energía de la Región de Murcia) and by the “Fundación Séneca” in the frame of the research project “Design and development of an enhanced flat plate solar collector. Thermal efficiency evaluation and thermohydraulic characterization” Reference number: 08731/PI/08.

References

- [1] A. Kumar, J.L. Bhagoria, R.M. Sarviya, Heat transfer and friction correlations for artificially roughened solar air heater duct with discrete W-shaped ribs. *Energy Conversion and Management*, 50 (8), 2009, pp. 2106-2117.
- [2] S. B. Bopche, M. S. Tandale. Experimental investigations on heat transfer and frictional characteristics of a turbulator roughened solar air heater duct. *International Journal of Heat and Mass Transfer*, 52 (11-12), 2009, pp. 2834-2848.
- [3] K.R. Aharwal, B. K. Gandhi, J.S. Saini. Heat transfer and friction characteristics of solar air heater ducts having integral inclined discrete ribs on a absorber plate. *International Journal of Heat and Mass Transfer*, 52, (25-26), 2009, pp. 5970-5977.
- [4] A. Kumar, B. N. Prasad. Investigation of twisted tape inserted solar water heaters—heat transfer, friction factor and thermal performance results. *Renewable Energy*, 19 (3), 2000, pp. 379-398.
- [5] S. Jaisankar, T.K. Radhakrishnan, K.N. Sheeba. Experimental studies on heat transfer and friction factor characteristics of forced circulation solar water heater system fitted with helical twisted tapes. *Solar Energy*, 83 (11), 2009 , pp. 1943-1952.

- [6] S. Jaisankar, T.K. Radhakrishnan, K.N. Sheeba. Studies on heat transfer and friction factor characteristics of thermosyphon solar water heating system with helical twisted tapes. *Energy* 34, 2009, pp. 1054–1064.
- [7] S. Jaisankar, TK. Radhakrishnan, KN. Sheeba. Experimental studies on heat transfer and friction factor characteristics of thermosyphon solar water heater system fitted with spacer at the trailing edge of twisted tapes. *Applied Thermal Engineering*, 29(5–6), 2009, pp. 1224–31.
- [8] S. Jaisankar, T.K. Radhakrishnan, K.N. Sheeba, S. Suresh. Experimental investigation of heat transfer and friction factor characteristics of thermosyphon solar water heater system fitted with spacer at the trailing edge of Left–Right twisted tapes. *Energy Conversion and Management*, 50 (10), 2009, pp. 2638-2649.
- [9] A. Hobbi, K. Siddiqui. Experimental study on the effect of heat transfer enhancement devices in flat-plate solar collectors. *Int. J. of Heat and Mass Transfer* 52, 2009, pp. 4650–4658.
- [10] P.S. Bandyopadhyay, U.N. Gaitonde, S.P. Sukhatme. Influence of free convection on heat transfer during laminar flow in tubes with twisted tapes. *Exp. Therm. Fluid Sci.* 45, 1991, pp. 577–586.
- [11] R.M. Manglik, A.E. Bergles. Heat transfer and pressure drop correlations for twisted-tape inserts in isothermal tubes: Part II –transition and turbulent, *J. Heat Transfer*, 115, 1993, pp.890–896.
- [12] R.M. Manglik, S. Maramraju, A.E. Bergles. The scaling and correlation of low Reynolds number swirl flows and friction factors in circular tubes with twisted tape inserts, *J. Enhanced Heat Transfer*, 8, 2001, pp. 383–395.
- [13] R. L. Webb , N-H. Kim. *Principles of Enhanced Heat Transfer*, 2nd ed., Taylor & Francis, New York, 2005.
- [14] A. García, P.G. Vicente, A. Viedma. Experimental study of heat transfer enhancement with wire coil inserts in laminar-transition-turbulent regimes at different Prandtl numbers. *International Journal of Heat and Mass Transfer*, 48 (21-22), 2005, pp. 4640-4651.
- [15] A. García, J. P. Solano, P. G. Vicente, A. Viedma. Enhancement of laminar and transitional flow heat transfer in tubes by means of wire coil inserts. *International Journal of Heat and Mass Transfer*, 50, (15-16), 2007, pp. 3176-3189.
- [16] R. Herrero Martín, J. Pérez-García, A. García, F. J. García-Soto, E. López-Galiana. Simulation of an Enhanced Flat-Plate Solar Liquid Collector with wire-coil insert devices. Manuscript accepted for publication in *Solar Energy*.
- [17] EN 12975-2:2006 “Thermal Solar Systems and Components –Solar Collectors – Part 2 test methods”.
- [18] ISO/IEC Guide 98, Guide to the Expression of Uncertainty in Measurement (GUM), International Organization for Standardization (ISO), Geneva, Switzerland, 1995, pp. 9–78.
- [19] Coleman, H.W, Steele, W. *Experimentation and Uncertainty Analysis for Engineers*, John Wiley & Sons. 1999, 2nd Ed., New York. ISBN 0-471-12146-0, pp 202-235

Closed Environment Design of Solar Collector Trough using Lenses and Reflectors

Kazy Fayeem Shariar^{1,*}, Enaiyat Ghani Ovy², Tabassum Aziz Hossainy²

¹ Department of Electrical & Electronic Engineering
Islamic University of Technology, Board Bazar, Gazipur-1704, BANGLADESH

² Department of Mechanical & Chemical Engineering
Islamic University of Technology, Board Bazar, Gazipur-1704, BANGLADESH

* Corresponding author. Tel: +8801713083079, Fax: 880-2-9291260, E-mail: eshankonerbau@yahoo.com

Abstract: Concentrated sunlight has been used to perform useful tasks from ancient time. There are number of varieties of collector trough being used to perform these tasks. Each Variety comes with advantages as well as disadvantages. The aim of this research project is to improve the design of collector trough in terms of efficiency, lessen the heat declination, and eliminate the sun tracker mechanism. Most of the existing solar concentrators use open type trough which cause the rapid heat declination. The design attempted in this paper is to lessen this rapid declination and improve the efficiency by introducing Closed Environment Collector Trough (CECT). The CECT consists of spherical collector trough having a reflective bottom surface, five evenly distributed lenses, 30° apart from each other, on the upper half of the sphere to eliminate the sun tracker and hexagonal glasses to make the environment closed and impose greenhouse effect on the system. The CECT acts like a heat trap and keeps the heat inside the chamber for a longer period of time which basically lessens the heat declination. The reflective surface and lenses concentrate the sun light directly on the fluid pipe. In this paper novel design has been proposed to improve the overall performance of solar collector troughs.

Keywords: Solar Thermal Collector, Concentrated Solar Power, Closed Environment Collector Trough.

Nomenclature

A_a = absorber area..... (m^2)	T_a = ambient temperature..... (K)
A_f = collector geometric factor	T_r = receiver temperature..... (K)
A_r = receiver area..... (m^2)	t_i = inside design temperature..... (K)
D_s = direct irradiation..... (W/m^2)	t_o = outside design temperature..... (K)
f_w = wind or exposure factor	U_L = heat loss coefficient
f_c = construction type or quality factor	α = absorptivity
n_o = collector optical efficiency	\bar{d} = average bond thickness (m)
Q_u = rate of useful energy delivered by collector (W)	ρ = mirror reflectance
	τ = absorber transmittance

1. Introduction

Researches have been carried out to utilize the concentrated solar power in various fields. To utilize the solar energy different patterns of the collectors have been designed previously considering advantages as well as disadvantages [4]. From the previous literature survey it was found that parabolic concentrating collectors were developed to use the solar energy in an efficient way. Non tracking concentrator was also designed to avoid the handling of a tracking device [1, 3]. To increase the performance innovative design was also proposed and modeled with reflectors without increasing the system cost. In that research work aluminum-polymer-laminated steel reflector for use in solar concentrators was evaluated with respect to its optical properties, durability, and reflector performance in solar thermal and photovoltaic systems [2]. In this paper a novel and innovative design of a solar collector which is basically Closed Environment Collector Trough (CECT) has been proposed. This novel CECT system lessens

the rapid heat declination and improves the system overall efficiency. This paper mainly focuses the detail designing of the collector with accurate explanation.

2. Methodology

2.1. Description of the system

This paper proposes a new design of compound solar collector trough. The collector effectively combines Lenses, Reflectors and Closed Environment. The general structure of the trough is sphere shaped with two halves consisting a pipe at the center (Fig: 1). Different parts of the trough are labeled on the figure. A detailed description of different parts of the collector trough is given below.

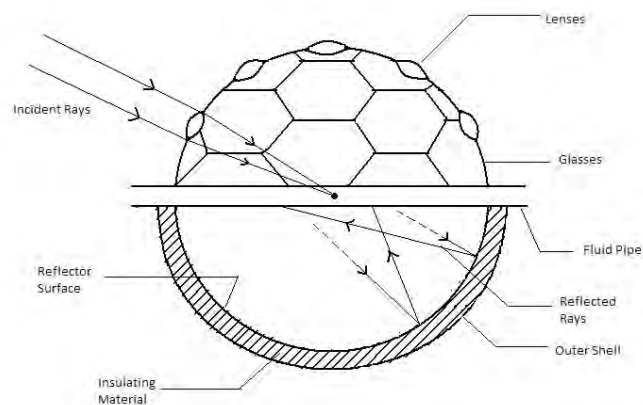


Figure 1: Closed Environment Collector Trough

The whole sphere shaped is main constructional shell of the system. It consists of two parts: Upper Shell and Lower Shell.

Lower Shell: Lower shell of the system is made of glazing metal (i.e. Aluminum). The outer surface is blackened and the inner surface is a reflector. There is another half sphere outside of this surface which is made of non-heat conductor material (i.e. asbestos). The inner diameter of the sphere is 40 c.m and outer diameter is 50 c.m. The space between the two surfaces is filled with cotton or rubber type materials (Fig: 2)

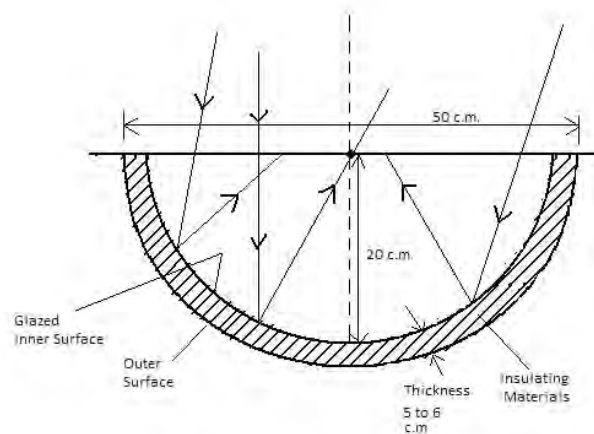


Figure 2: Lower shell

Upper Shell: The upper shell of the system is made of metal three dimensional lattice of hexagonal shape (Fig: 3). These shapes will accommodate small pieces of mirrors, which will allow the visible light to enter into the chamber but will trap the longer wavelengths of the infrared re-radiation from the heated objects are unable to pass through the glasses. The trapping of the long wavelength radiation leads to more heating and a higher resultant temperature.

There will be five lenses, evenly distributed on the upper surface of the mirror section. The lenses will be 30° apart from each other (Fig.4). The center lens will be at 90° angle. These lenses will concentrate the sunlight in to center line (for the lenses the center line will be the focus plane) of the sphere.

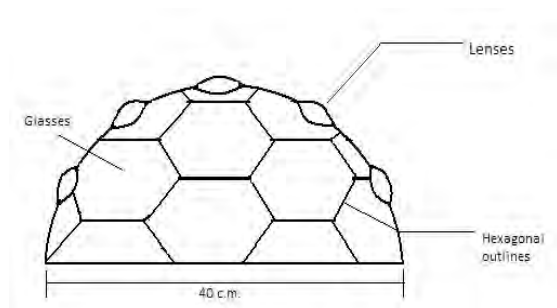


Figure 3: Upper Shell

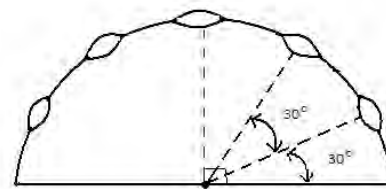


Figure 4: Arrangement of Lenses

Fluid Pipe: At the center of the sphere there will be a fluid carrying pipe. The fluid pipe will be consisted of two concentric pipes (Fig.5). The material of the outer pipe will be of transparent material (i.e. glass).The inner pipe will be metallic (i.e. Aluminum). The space between these two pipes will be evacuated. The inner pipe will carry the Heat Transfer fluid.

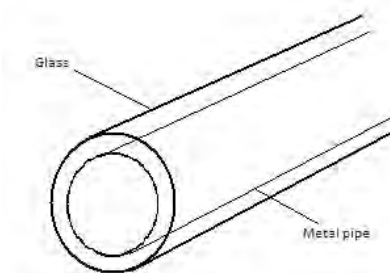


Figure 5: Fluid pipe

2.2. Calculation of Sun's Position in Bangladesh

To eliminate solar tracking mechanism effectively we have to calculate the sun's position throughout the year. Sun's position depends on local solar, elevation and azimuth angles. The equation to find the elevation and azimuth angles are given below:

$$\text{Elevation} = \sin^{-1} [\sin \gamma \sin \phi + \cos \gamma \cos \phi \cos HRA] \quad (1)$$

$$\text{Azimuth} = \cos^{-1} \left[\frac{\sin \gamma \cos \phi - \cos \gamma \sin \phi \cos \text{HRA}}{\cos \alpha} \right] \quad (2)$$

Where HRA is the Hour Angle

Sun's position throughout a year is given in Fig.6

As from the figure we can see that sun follows a specific path throughout the year, the solar tracking mechanism can be effectively eliminated by preparing a solar chart at a specific interval. The solar trough can be setup as shown in the Fig.7 and can be manually tracked daily basis [5].

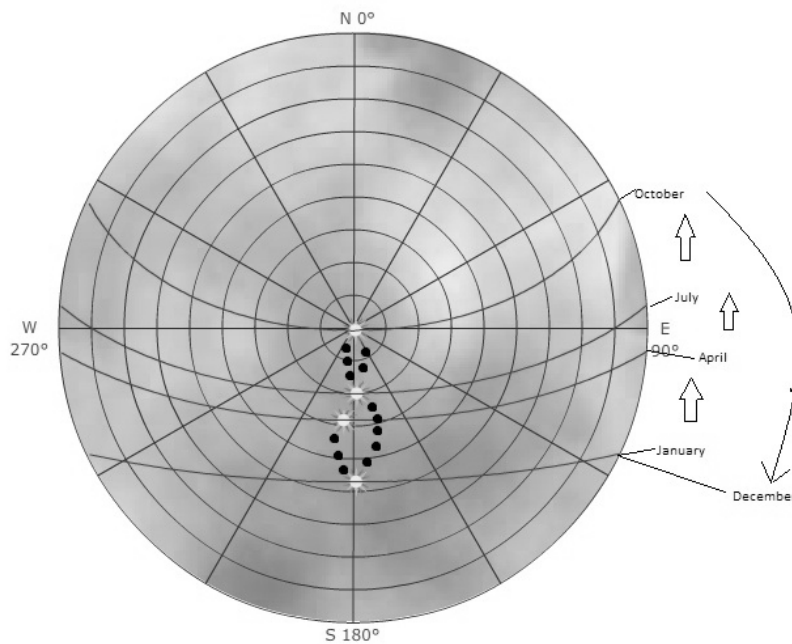


Figure 6: Sun's Position at 3 months interval. Dots represent the solar path

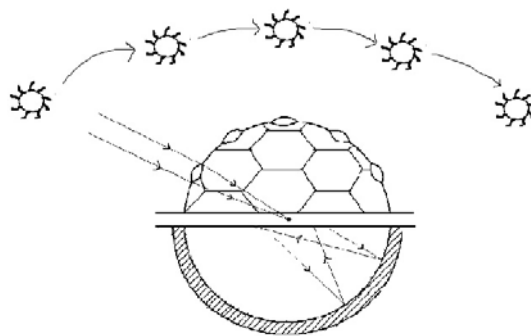


Figure 7: Collector position with respect to sun

2.3. Calculation of Solar Insolation in Bangladesh

Bangladesh is situated at 24° 00' North latitude and 90° 00' East longitude. At this position the amount of hours of sunlight each day throughout a year is shown in the following graph (Fig.8). The highest and the lowest intensity of direct radiation in W/m² are also shown in the

Fig.9. This data shows that using solar collector for high temperature is feasible in Bangladesh.

3. Calculation of useful energy delivered by the Collector

The generation of heat inside the chamber will occur in three different methods:

Lens concentrator: The lenses placed on the surface of the upper half of the heat chamber will concentrate the sunlight directly in to the focus plane of the lenses which in this case is the center of the heat chamber where the fluid pipe will be placed Fig 10. This will directly heat up the heat transfer fluid.

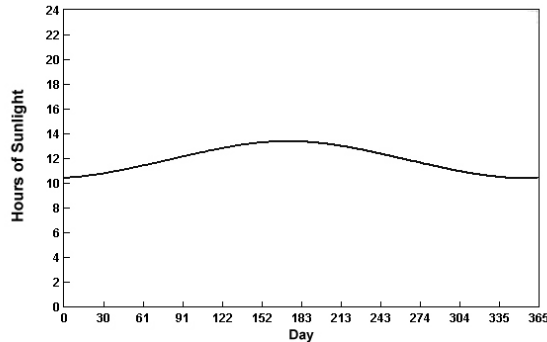


Figure 8: The amount of hours of sunlight in Bangladesh

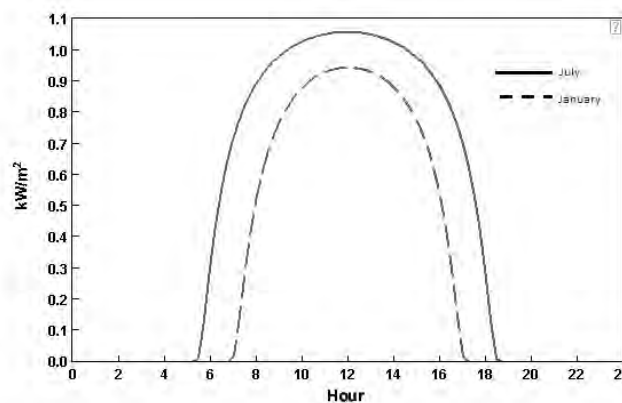


Figure 9: The highest and the lowest intensity of direct radiation in W/m²

The heat (in joules) generated by the lenses could be found by the following equation:

$$Q = ms (T_i - T_f) \quad (3)$$

Where Q is generated heat in joules, m is mass of fluid in KG, T_i is initial temperature of fluid in Kelvin and T_f final temperature of fluid.

Reflector concentrator: This method will heat both the fluid pipe and the inner environment of the heat chamber. The concave bottom surface will act like a reflector mirror and most of the sunlight will be again concentrated on the pipe. This will result a thorough pipe heating (Fig. 11).

The Green House: The hexagonal glasses of the upper half of the heat chamber will allow entering the visible light, but will trap the longer wavelengths of the infrared re-radiation from the heated objects. The trapping of the long wavelength radiation leads to more heating and a higher resultant temperature. This will keep the temperature of the chamber high.

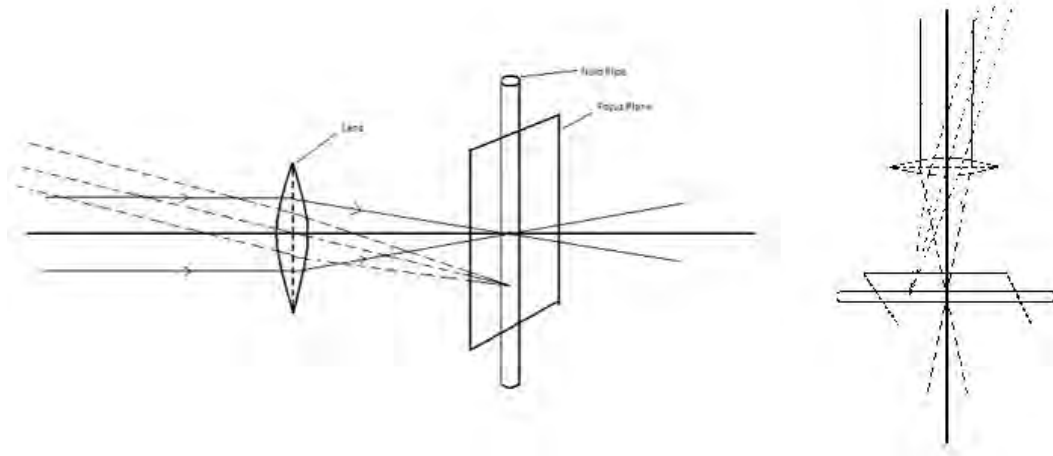


Figure 10: Lens and fluid pipe position

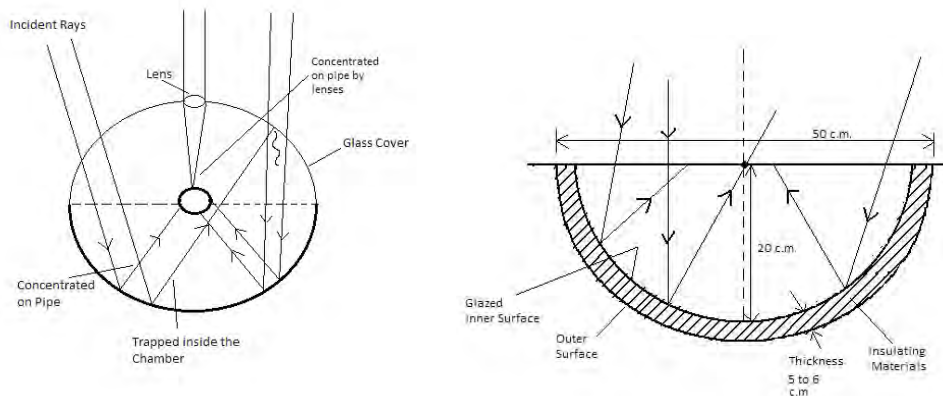


Figure 11: Front view and Section view of the collector

3.1. Overall energy calculation

The rate of useful energy delivered by the collector is governed by the following equation:

$$Q_u = D_s n_o A_a - A_r U_L (T_r - T_a) \quad (4)$$

As the system is a combination of Parabolic Collector Trough (PCT) the optical efficiency can be found from the PCT optical efficiency from the following equation:

$$n_o = \rho \tau \varepsilon \delta [(1 - A_f \tan(\varphi)) \cos(\varphi)] \quad (5)$$

As the system use a green house the heat loss coefficient is determined by the following equation:

$$U_L = \left[\frac{A1}{R1} + \frac{A2}{R2} \right] (t_i - t_o) f_w f_c \quad (6)$$

4. Results

A preliminary screening of the CECT is conducted in order to identify the best match of the load. The result is shown on a plot of efficiency as a function of the heat loss parameter in the following graph.

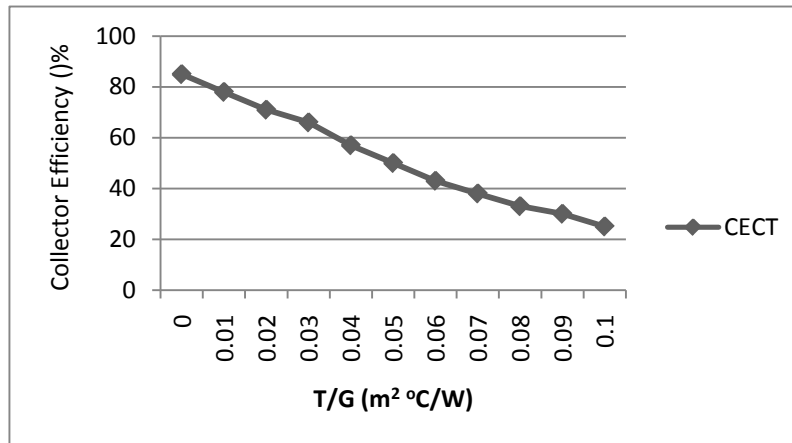


Figure 12: Collector efficiency

5. Discussion

Although Closed Environment Collector Trough is relatively a new concept, the system was expected to be more efficient than that of preliminary screening data. The future work should be based on the improvement of current design and optical as well as thermal optimization.

References

- [1] H. E. Imadojemu, Concentrating parabolic collectors: A patent survey Energy Conversion and Management, Volume 36, Issue 4, April 1995, Pages 225-237
- [2] Maria Brogren, Anna Helgesson, Björn Karlsson, Johan Nilsson, Arne Roos, Optical properties, durability, and system aspects of a new aluminium-polymer-laminated steel reflector for solar concentrators, Solar Energy Materials and Solar Cells, Volume 82, Issue 3, 15 May 2004, Pages 387-412
- [3] A. Thomas, Solar steam generating systems using parabolic trough concentrators Energy Conversion and Management, Volume 37, Issue 2, February 1996, Pages 215-245
- [4] Soteris A. Kalogirou, Solar thermal collectors and applications Progress in Energy and Combustion Science, Volume 30, Issue 3, 2004, Pages 231-295
- [5] <http://pvcfrom.pveducation.org/SUNLIGHT/SUNCALC.HTM>

Optimum integration of a large size collector to a solar thermal power plant

M. Yaghoubi^{1,*}, S. Zarrini¹, S. Mirhadi²

¹ Engineering School, Shiraz University, Shiraz, Iran

² Renewable Energy Organization of Iran, Tehran, Iran

* Corresponding author. Tel: +98 7116133028, Fax: +98 7112301672, E-mail: yaghoubi@shirazu.ac.ir

Abstract: In this paper the problem of increasing the capacity of an already constructed solar thermal power plant has been studied through the concept of lost available work. The required increased capacity has been proposed to be achieved by means of a new large size collector and an auxiliary boiler. Two different schemes along with an extra scheme for night operation of the power plant have been considered in the present work. For each scheme, three different operating conditions have been assumed, resulting in a total of nine operating options. For these options, results of analysis based on the second law of thermodynamics have been presented. These results might then be used to choose the optimum solar hybrid power plant configuration.

Keywords: Renewable energy, Solar thermal power plant, Parabolic trough, Exergy, Entropy generation

Nomenclature

\dot{W}	work interaction	kW	\dot{S}_{gen}	entropy generation rate	kW.K ⁻¹
\dot{Q}	heat interaction	kW	P	pressure	bara
\dot{m}	mass flow rate	kg/s	s	specific entropy	kJ.kg ⁻¹ .K ⁻¹
T	absolute temperature	K	h	specific enthalpy	kJ.kg ⁻¹
T_0	dead state temperature	K	v	specific volume	m ³ .kg ⁻¹
C_p	constant pressure specific heat ..	kJ.kg ⁻¹ .K ⁻¹			

1. Introduction

1.1. Problem description

Renewable energies play the key role in sustainable development and are the most promising remedy to the problem of air pollution worldwide. Among various sources of renewable energy, the usage of solar thermal energy in generating electricity can be regarded as the most reliable and developed one in the path of commercialization [1].

In Shiraz, Iran, the first solar thermal power plant (STPP) has been designed and constructed for 250 kW power generation [2]. For the first phase of development, this plant has been constructed and tested only to produce high pressure and high temperature steam (21 bar, and 250 °C). This steam is then fed into the steam turbine of a conventional Rankine cycle. Based on the new feasibility study, it has been decided to increase the nominal capacity of this plant to 500 kW by adding a new large size (100 meters long) parabolic trough collector and employing an auxiliary boiler to provide the deficiency of steam as well as running the system during night periods (or day periods in which the solar radiation is insufficient).

Various schemes are possible to integrate the new collector to the field of available collectors. In this paper, two different cases (A, B) along with a night case are considered to be suitable for the new system. Assuming three different operating conditions (by setting the turbine outlet pressure) for each case, a total of nine configurations have been analyzed. The three outlet pressures considered are 10, 25 and 100 kPa.

In the present article, these options are studied based on the first and second laws of thermodynamics. Each configuration has some advantages and disadvantages regarding

overall thermal performance, installation and operating costs. To assess the overall performance of various configurations in a comparative manner, exergy method has been applied to the corresponding cycles (as a representative of the second law analysis). Exergy and exergoeconomic methods have received considerable attention during the past decade in the analysis and optimization of power plant cycles to achieve higher efficiencies and to reduce the operating cost of the corresponding power plants [3,5].

For each case of the aforementioned cycles, results of exergy analysis are presented and exergetic losses due to various components (e.g. turbine, boiler, condenser etc) have been calculated. Finally the system with the best exergy efficiency to combine the new collector and increase the power rate of the plant is suggested for construction and operation.

1.2. Current Configuration

Shiraz solar thermal power plant consists of two separate cycles namely the oil cycle and the steam cycle. The oil cycle absorbs the solar radiation through collector field and transmits the harvested thermal energy to the steam cycle which is a classic Rankine cycle. The energy transfer between the two cycles takes place at three heat exchangers in series (E-201, E-202 and E-203). The collector field is composed of 8 parallel loops, each consisting of 6 collectors in series. The current configuration is able to produce 0.671 kg/s of steam at 21 bar and 250°C. This steam will be termed "field generated steam" as opposed to "boiler generated steam" which is the steam that is expected to be generated by the auxiliary boiler. A schematic of the plant is shown in Fig 1.

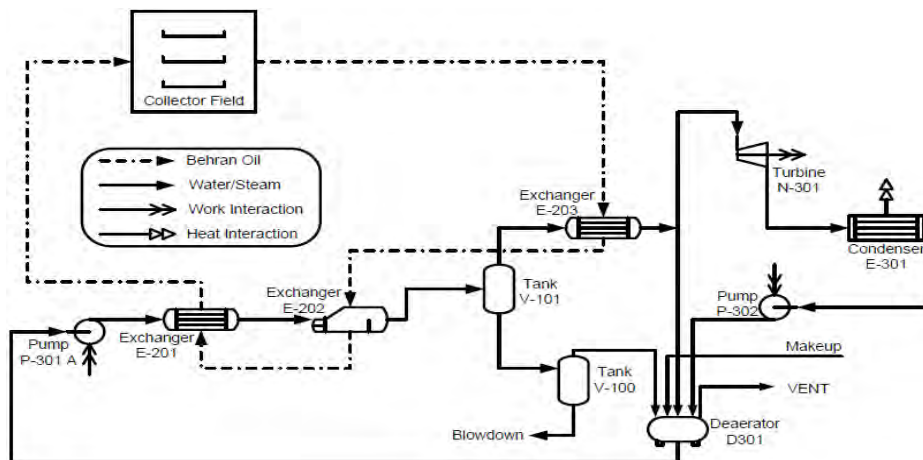


Fig. 1. Schematic of the current solar power plant.

1.3. Integration of the new collector

The new collector has been designed to bring Therminol VP-1 from 294°C to 313°C, supplying 200 kW of energy to the system. This energy can be introduced into the current configuration in a variety of ways. Two different approaches have been considered in the present work namely case A and case B. In case A the boiler provides steam at 21 bar 250°C. This steam is then mixed with the field generated steam and the mixture is then becomes more superheated (to 294°C) using available extra energy from the new collector in an extra heat exchanger (E-204). However, in case B, the boiler produces steam at 21 bar 294°C and in exchanger E-204, only the field generated steam becomes more superheated. The remaining energy from the new collector is then used to make the outlet oil from the field warmer, thus, increasing the amount of field generated steam. Therefore another extra exchanger is needed

in case B to bring the VP-1 oil from the new collector and the Behran oil from the existing farm into thermal contact. Simplified depictions of cases A & B are shown in Fig 2 and Fig 3.

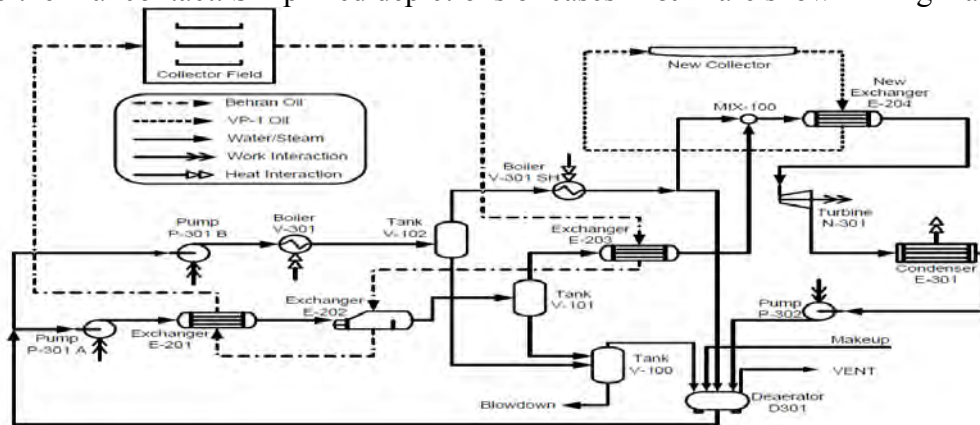


Fig. 2. Schematic of the proposed case A.

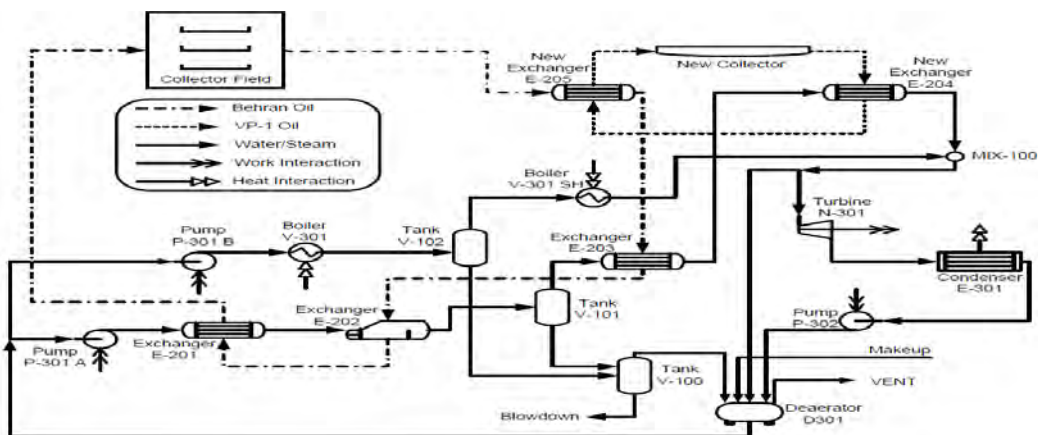


Fig. 3. Schematic of the proposed case B.

2. Methodology

As shortly explained in the preceding section, the problem at hand is a sort of semi-fixed system in which very few parameters are allowed to be altered. This is a direct consequence of the fact that we are dealing with a designed and constructed system and our attempt is to integrate a device into such a system which was not considered before. Thus we're not dealing with an ordinary optimization process in which particular parameters are allowed to vary in order to find the optimum set of parameters. Rather we are investigating the optimum case among a predefined set of choices. In other words, instead of optimizing the cycle, various predefined cases are compared based on the second law and the best can be chosen. The assessment of available options is done based on the destructed exergy associated with various components in each option. The destructed exergy (lost available work) is closely related to the rate of entropy generation through the following equation [4]:

$$\dot{W}_{lost} = T_0 \dot{S}_{gen} \quad (1)$$

where T_0 is the lowest temperature available for the system to reach theoretically (dead state). In this work the dead state has been assumed to be at 25°C and atmospheric pressure. Thus by calculating the rate of entropy generation for each component, the contribution to lost available work due to that component can be determined. The rate of entropy generation for

each component is readily derived from the general statement of the second law for open systems [4]:

$$\dot{S}_{gen} = \frac{dS_{cv}}{dt} - \sum_{i=0}^n \frac{\dot{Q}_i}{T_i} + \sum_{out} \dot{m}s - \sum_{in} \dot{m}s \quad (2)$$

where \dot{Q}_i is the i^{th} heat interaction of the corresponding component with the surrounding (positive when heat transfer takes place from surrounding to the control volume) and T_i is the temperature of that portion of the control surface through which the i^{th} heat interaction occurs. In calculating last two terms on the right hand side of Equation (2) one may frequently encounter the case of calculating Δs terms for steam and oil. For steam the corresponding terms are read from standard thermodynamic tables while for oil (both the collector field oil and the new collector oil) the Δs terms are determined using their specific heats as a function of temperature. Starting from the well-known first law relation [4] and treating oil as an incompressible liquid the Δs term associated with oil can be written as:

$$Tds = dh - vdP \xrightarrow{dP=0} ds = \frac{dh}{T} \xrightarrow{dh=C_p dT} ds = C_p \frac{dT}{T} \quad (3)$$

$$\Delta s = \int_{T_{in}}^{T_{out}} \frac{C_p}{T} dT \quad (4)$$

It should be noted that in the use of equation (4), the temperatures should be considered in an absolute temperature scale (Kelvin in this work). Having the complete set of states for the current configuration and assuming that the states of steam cycle remain unchanged (which seems reasonable) the new intermediate temperatures have been determined by applying energy balance using an available solver code.

3. Results

After satisfying energy balance for the whole system in every configuration, the state at each node becomes fixed. Knowing the fixed states, the values of entropy generation and subsequently the values of lost available work can be readily determined. In the following four tables the values of \dot{W}_{lost} for the main components in each configuration have been presented.

Example calculation 1:

The lost available work for exchanger E201 in case B for a turbine outlet pressure of 10kPa:

$$\dot{m}_h = 14 \text{ kg/s}, \dot{m}_c = 0.7525 \text{ kg/s}, T_{h,i} = 231.6^\circ \text{C}, T_{h,o} = 221.1^\circ \text{C}, T_{c,i} = 98.53^\circ \text{C}, T_{c,o} = 217.9^\circ \text{C}$$

$$P_c = 22.3 \text{ bara} \Rightarrow s_{c,i} = 1.28866 \text{ kJ/kg.K}, s_{c,o} = 2.49896 \text{ kJ/kg.K} \Rightarrow \Delta s_c = 1.2103 \text{ kJ/kg.K}$$

$$\text{For hot fluid (Behran Oil): } C_p = 0.8132 + 3.706 \times 10^{-3} (T + 273) \Rightarrow \Delta s_h = -0.05601 \text{ kJ/kg.K}$$

$$\dot{Q}_{c.v.} = 0 \Rightarrow \dot{S}_{gen} = \dot{m}_h \Delta s_h + \dot{m}_c \Delta s_c = 0.1266 \text{ kW/K}$$

$$T_0 = 25^\circ \text{C} = 298 \text{ K} \Rightarrow W_{lost} = 37.72 \text{ kW}$$

Table 1. Values of lost available work for cases A & B with turbine outlet pressure of 10 kPa.

case A			case B		
Component Type	Component Name	\dot{W}_{lost} (kW)	\dot{W}_{lost} (kW)	Component Name	Component Type
Exchanger	E201	35.30	37.72	E201	Exchanger
	E202	45.02	48.44	E202	
	E203	3.14	3.67	E203	
	E 204	5.90	3.39	E 204	
	-	-	2.82	E205	
Boiler	V301	143.81	237.47	V301	Boiler
	V301 SH	0.69	15.53	V301 SH	
Deaerator	D301	63.32	64.14	D301	Deaerator
Condenser	E301	146.75	150.01	E301	Condenser
Turbine	N301	321.59	318.58	N301	Turbine
Pump	P301A	0.42	0.46	P301A	Pump
	P301B	0.25	0.22	P301B	
	P302	0.96	0.89	P302	
Tank	V-100	3.30	4.43	V-100	Tank
	V-101	0.00	0.01	V-101	
	V-102	0.08	0.16	V-102	
Mixer	MIX-100	0.43	0.71	MIX-100	Mixer

Table 2. Values of lost available work for cases A & B with turbine outlet pressure of 25 kPa.

case A			case B		
Component Type	Component Name	\dot{W}_{lost} (kW)	\dot{W}_{lost} (kW)	Component Name	Component Type
Exchanger	E201	34.69	39.85	E201	Exchanger
	E202	44.94	48.14	E202	
	E203	2.35	1.49	E203	
	E 204	7.12	3.93	E 204	
	-	-	4.45	E205	
Boiler	V301	348.17	320.46	V301	Boiler
	V301 SH	0.92	21.22	V301 SH	
Deaerator	D301	43.01	43.74	D301	Deaerator
Condenser	E301	311.02	310.46	E301	Condenser
Turbine	N301	300.20	300.27	N301	Turbine
Pump	P301A	0.41	0.43	P301A	Pump
	P301B	0.33	0.29	P301B	
	P302	0.12	0.10	P302	
Tank	V-100	3.53	3.59	V-100	Tank
	V-101	0.12	0.21	V-101	
	V-102	0.00	0.16	V-102	
Mixer	MIX-100	0.53	0.00	MIX-100	Mixer

Example calculation 2:

The lost available work for condenser E301 in case A for a turbine outlet pressure of 25kPa:

$$\dot{m}_h = 1.1375 \text{ kg/s}, P_{h,i} = 0.25 \text{ bara}, T_{h,i} = 65.0^\circ \text{C}, P_{h,o} = 0.2 \text{ bara}, T_{h,o} = 60.09^\circ \text{C}, x_{h,o} = 0.967$$

$$\Rightarrow s_{h,i} = 7.59958 \text{ kJ/kg.K}, h_{h,i} = 2540 \text{ kJ/kg}, s_{h,o} = 0.83217 \text{ kJ/kg.K}, h_{h,o} = 250 \text{ kJ/kg}$$

$$\Rightarrow \Delta s_h = -6.76741 \text{ kJ/kg.K}$$

$$\dot{Q}_{c.v.} = \dot{m}\Delta h_h = -2605 \text{ kW} \Rightarrow \dot{S}_{gen} = -\frac{-2605}{298} + 1.1375(-6.76741) = 1.04368 \text{ kW/K}$$

$$T_0 = 25^\circ \text{C} = 298 \text{ K} \Rightarrow W_{lost} = 311.02 \text{ kW}$$

In the above calculation, the dryness fraction at the turbine outlet has been determined by considering an isentropic efficiency of 60% for the turbine which is a reasonable value for a turbine of this capacity.

Table 3. Values of lost available work for cases A & B with turbine outlet pressure of 100 kPa.

case A			case B		
Component Type	Component Name	\dot{W}_{lost} (kW)	\dot{W}_{lost} (kW)	Component Name	Component Type
Exchanger	E201	35.34	37.72	E201	Exchanger
	E202	44.32	48.44	E202	
	E203	1.75	3.67	E203	
	E 204	8.33	3.39	E 204	
	-	-	2.82	E205	
Boiler	V301	555.16	517.80	V301	Boiler
	V301 SH	13.49	33.84	V301 SH	
Deaerator	D301	4.23	3.84	D301	Deaerator
Condenser	E301	689.24	684.55	E301	Condenser
Turbine	N301	273.29	273.37	N301	Turbine
Pump	P301A	0.41	0.46	P301A	Pump
	P301B	0.53	0.49	P301B	
	P302	0.00	0.00	P302	
Tank	V-100	4.43	4.62	V-100	Tank
	V-101	0.16	0.01	V-101	
	V-102	0.00	0.00	V-102	
Mixer	MIX-100	0.17	1.47	MIX-100	Mixer

Table 4. Values of lost available work for Night case with turbine outlet pressures of 10,25 and 100 kPa.

Component Type	Component Name	\dot{W}_{lost} (kW)		
		10 kPa	25 kPa	100 kPa
Boiler	V301	707.79	780.60	985.28
	V301 SH	46.90	51.68	65.26
Deaerator	D301	73.33	43.76	3.96
Condenser	E301	151.74	310.46	689.24
Turbine	N301	318.96	300.27	273.29
Pump	P301B	0.65	0.71	0.90
	P302	0.09	0.10	0.00
Tank	V-100	3.27	3.59	4.54
	V-102	0.17	0.00	0.00

It is worth mentioning that, generally in solar thermal power plants the major fraction of total exergy loss takes places in the collector field (mainly due to the ultra high temperature of the

sun)[5]. However, in the present work, the operating conditions of the collector field are the same in all configurations. Thus the exergy loss due to the collector field is not reported for comparison. It should also be noted that the night cycle is essentially either cases A or B in which no collector is at service and boilers are the only suppliers of thermal energy to the system. A quick study of tables 1-4 reveals the fact that, generally by decreasing the turbine outlet pressure, the value of lost work decreases in the corresponding devices. Moreover reducing the turbine outlet pressure increases the amount of power which can be extracted from the turbine. But, as expected, these advantages have their own counterparts; the need for creating vacuum condition for condenser, the need to change the condenser type from air-cooled to water-cooled, etc. Another implication is that in each configuration the dominant sources of lost work are boilers, condensers and turbines and that the contribution made by pumps, mixers and tanks are negligible.

From another point of view, comparing the values of lost available work for same devices, one may conclude that, in the same operating conditions, case A is thermodynamically superior to case B.

4. Conclusions

- The concept of lost available work has been utilized to select the best choice of integration of a hybrid solar power plant.
- Regarding various cases, it is found that case A is thermodynamically the preferred case for integration.
- Case A has the advantage of requiring one less extra heat exchanger to be integrated into the current configuration.
- For optimum integration, one must also take into account the economic aspect of each case. In other words, a thorough thermo-economic analysis might be proper to further assess these two proposed cases.
- Moreover one should also consider water consumption rate for each case. Water is rarely available especially for regions where solar energy is considerable and such limitation might sacrifice higher efficiencies or lower available lost work for the final decision.

References

- [1] R. Shinnar, F. Citro, Solar thermal energy: The forgotten energy source, *Journal of Technology in Society* 29, 2007, pp.261-270
- [2] K. Azizian, M. Yaghoubi, R. Heasmi, S. Mirhadi, Shiraz pilot solar thermal power plant design, construction, installation and commissioning procedure, *Proceedings of 7th International Conference on Heat transfer, Fluid mechanics and Thermodynamics*, 2010
- [3] A. Baghernejad, M. Yaghoubi, Multi-objective exergoeconomic optimization of an integrated solar combined cycle system using evolutionary algorithms, *International Journal of Energy Research*, 2010
- [4] A. Bejan, *Advanced Engineering Thermodynamics*, Wiley, 2nd Edition, 1997
- [5] M.K. Gupta, S.C. Kaushik, Exergy analysis and investigation for various feed water heaters of direct steam generation solar thermal power plant, *Journal of Renewable Energy* 35, 2010, pp.1228-1235

Theoretical Modelling of a Dynamic Solar Thermal Desalination Unit with a Fluid Piston Engine

B. Belgasim and K Mahkamov*

*School of Computing, Engineering and Information Sciences, Northumbria University,
Newcastle upon Tyne, NE1 8ST, UK**

**Corresponding author. Tel: +44 191 2274739, Fax: +44 191 2437630,
Email: khamid.mahkamov@northumbria.ac.uk*

Abstract: Results of theoretical simulations of the steady-state operation of the dynamic solar thermal desalination unit with a fluid piston are presented in this paper. A laboratory prototype of a dynamic thermal water distillation unit was developed and it was built around an engine with fluid pistons. In the calculation scheme, the internal circuit of the desalination unit was split into several control volumes, namely the evaporator, the condenser and the cylinder. The lumped parameter mathematical model was derived based on the differential energy and mass conservation equations written for each of the control volumes and describing heat and mass transfer processes taking place during water evaporation and condensation under the cyclic variation of the pressure and temperature inside the system when the engine operates. The solution of the set of governing equations produces information on the variation of temperatures and pressure inside the system over the thermodynamic cycle and on the water desalination capacity of the unit.

Keywords: Solar water desalination, mathematical modelling

1. Introduction

The shortage in clean drinkable water supply has become one of the most important problems due to the continued growth in the world's population. Kalogirou [1] states that the fresh water represents only about 3% of all water on the earth. Approximately 0.25% of fresh water can be directly used from lakes and rivers and the rest is in the ice form or deep ground water which is difficult to reach. As a result, novel drinkable water production technologies are being continuously developed to resolve this important problem.

Desalination techniques are among feasible solutions to produce fresh water from saline water but such technologies require significant amount of energy. Using fossil fuels for water desalination results in high plant running costs and causes a considerable negative environmental impact. As a consequence, numerous studies are being performed on utilisation of an alternative energy source, namely renewable energy, for running desalination plants. The aim of the above research studies is to make the process of water desalination with the use of renewable energy safer for the environment and sustainable.

The literature review performed in this subject demonstrates that the majority of research carried out has been focused on the static solar stills in which the saturation pressure and temperature remain constant during the desalination process. Shatat and Mahkamov presented theoretical and experimental study of a static solar thermal distillation unit in [2]. The effect of the design parameters on the performance of the unit was investigated and an optimization of unit's design parameters have been conducted. Mahkamov and Belgasim described in [3] the concept of the dynamic solar distillation system in which an evacuated tube solar collector was coupled with a fluid piston thermal engine. The laboratory prototype of the proposed system was built and tested to demonstrate its functionality and preliminary experimental results were very encouraging. Furthermore, a comparative study between static and dynamic solar distillation systems was performed in the same study which demonstrates considerably higher fresh water production capacity of the dynamic system.

2. Model Description

The dynamic solar thermal desalination unit integrated with fluid piston engine is described in *fig.1*. This unit operates under a cyclic change in the pressure and temperature during the operation of the unit due to the expansion and the compression of the volume of the fluid piston engine. Such working conditions considerably intensify the desalination processes and fresh water production.

The plant's operation can be described as follows. Saline water is heated up and evaporated in the solar collector (1) causing pressure rise in the system. The initial increase of the pressure initiates oscillations of water columns (3) and (4) of the fluid piston engine and the whole system operates as a dynamic thermal oscillation system, in which the water evaporation is intensified by volume and pressure variations in the internal circuit. In its turn, this sustains oscillations of water columns. In this particular design, the distilled water is formed in the condenser (2) surrounded by the water jacket with the saline water and the condensate is collected in the distilled water vessel (6). The heated saline water from the water jacket of the condenser is pumped to the water storage tank.

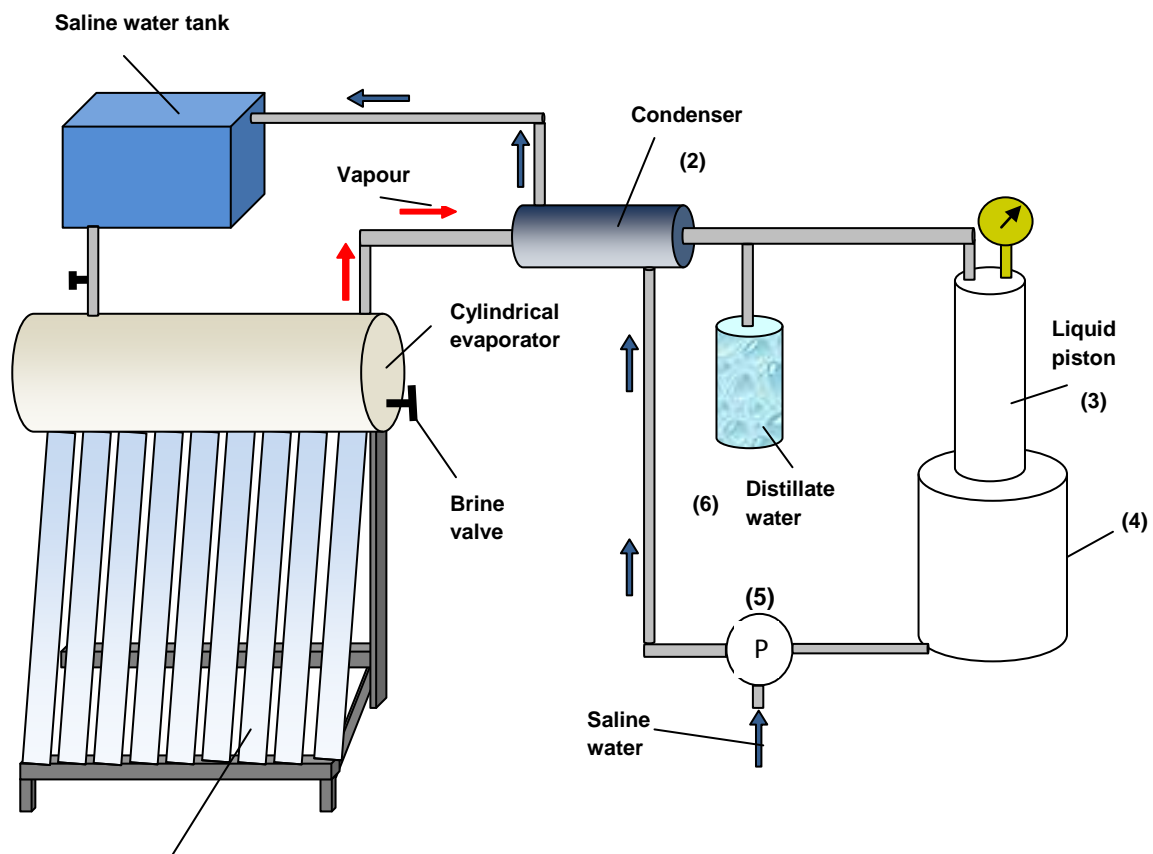


Fig. 1. (1) Evacuated tube solar collector

The above system was tested under a number of constant heat flux conditions created with application of a sun simulator: an array of 110 halogen floodlights placed above evacuated tubes. The heat flux magnitude is set using a three-phase transformer which controls the voltage of the electrical current supplied to the floodlights. Preliminary results obtained clearly show that such dynamic system has a considerable advantage in fresh water production capacity over conventional static systems. Currently the unit is being equipped with sensors to record oscillations of the liquid piston, temperature and pressure variations in components of the installation.

3. Theoretical Modelling

In order to perform the theoretical analysis, the unit was divided into three separate control volumes, namely the evaporator, the condenser and the fluid piston cylinder. The lumped mathematical model was derived based on energy and mass conservation differential equations written for each control volume taking into accounts the cyclic variation of the pressure and temperature inside the system during its operation.

3.1. Evaporator

The mathematical model of the system consists of the mass and energy balance equations written for each component. The mass conservation equation could be written as

$$\frac{d}{dt}(\rho V) = (\rho \dot{v})_{sw} - (\rho \dot{v})_v - (\rho \dot{v})_b \quad (1)$$

where t is time, V is volume, ρ is density and \dot{v} is volume flow rat.

The initial condition for the above equation is the amount $(\rho V)_0$ of the seawater at the beginning of the operation. Two assumptions are made: the amount of saline water inside the evaporator is constant; all the vapour produced in the evaporator will be then condensed in the condenser.

The salt concentration conservation equation is

$$\frac{d}{dt}(\rho V c) = (\rho \dot{v} c)_{sw} - (\rho \dot{v} c)_b \quad (2)$$

where c is salt concentration.

The initial amount of salt is $(\rho V c)_0$

Finally, the energy conservation equation can be derived by applying the energy balance principle for the same control volume.

$$\frac{d}{dt}(\rho V c_p T) = Q_{in} + (\rho \dot{v} c_p T)_{sw} - (\rho \dot{v} h_{fg})_v - (\rho \dot{v} c_p T)_b - Q_{loss} \quad (3)$$

where Q is the heat flow, T is temperature h is enthalpy and c_p is heat capacity at constant pressure.

The energy $(\rho V c_p T)_0$ is at the starting time. In this equation the heat capacity of the system material has been neglected so no heat storage is considered in the evaporator substance.

3.2. Condenser

It was assumed in the simulation process that all the produced vapour is converted into fresh water. The condenser design represents the counter flow tube-in-tube heat exchanger in which the condensation process takes place on the internal surface of the inner tube while the cooling water passes through the outer tube. In order to enhance the productivity and the thermal efficiency of the system, the seawater fed to the evaporator is first used as cooling water in the condenser's water jacket to gain the latent heat of condensation.

The mathematical description of the condensation process depends on a number of factors including the condenser shape, the flow pattern and the condensation rate. The inner heat transfer coefficient in the case when the condensation rate is low and the vapour has a low velocity in a short condenser, can be calculated as [4]

$$h_i = 0.555 \left[\frac{g \rho_l (\rho_l - \rho_v) k_l^3 h'_{fg}}{\mu_l (T_{sat} - T_s) D} \right]^{1/4}$$

where the modified condensation heat is $h'_{fg} = h_{fg} + \frac{3}{8} c_{p,l} (T_{sat} - T_s)$

The outer heat transfer coefficient is mainly effected by Nusselt Nu number which is a function of the flow pattern and depends on the Reynolds number Re . If $Re < 2300$ the flow is laminar and if $Re > 2300$ then the flow is turbulent. The outer heat transfer coefficient can be calculated as $h_o = \frac{k_l}{D_h} Nu_i$ [5]. Therefore, the overall heat transfer coefficient is $U = \frac{h_o h_i}{h_o + h_i}$

The condenser is considered as a control volume and using the mean temperature difference technique, the governing energy equation for the condenser can be written as:

$$Q = UA_s \frac{\Delta T_2 - \Delta T_1}{\ln(\Delta T_2 / \Delta T_1)} = \dot{m} c_{p,sw} (T_{c,in} - T_{c,out}) \quad (4)$$

where U is the overall heat transfer coefficient, A surface area, \dot{m} is mass flow rate, $\Delta T_1 = T_{sat} - T_{c,out}$ and $\Delta T_2 = T_{sat} - T_{c,in}$

In the above equation, the produced fresh water is assumed to be condensed at the saturation temperature.

3.3. Fluid piston engine

The fluid piston engine consists of two concentric cylinders attached to the collector at the top of the inner cylinder. The two cylinders are filled with water to work as a piston in both cylinders. After the solar collector starts to heat up the saline water, its temperature gradually increases leading to the rise in the pressure in the system. The pressure continue to rise until the inner cylinder piston, which is at the top position in the beginning of heating process, is pushed down. This results in expanding the volume of the system. The expansion process continues until the air pressure at the top of the outer cylinder balances the system pressure and then the system returns to the original position under the effect of the water weight and air pressure leading the cycle to be repeated again.

The expansion and compression processes are repeated continually allowing the unit to work under variable volume and pressure conditions. The change in the volume is important to estimate the change in pressure and in this study, the volume has been assumed to vary harmonically:

$$V_{tot} = V_{dead} + \pi A \frac{D^2}{8} [1 - \cos(\omega t)] \quad (5)$$

where V_{dead} is the dead volume of the system, A is the amplitude of the fluid piston oscillations; D is the diameter of the piston and f is the frequency of oscillations.

The relationship between the change in volume and in the pressure is calculated as

$$\Delta P = P_{sat} \left[\left(\frac{V_{tot(z)}}{V_{tot(x)}} \right)^k - 1 \right] \quad (6)$$

where ΔP is the pressure change due to the variation in the total volume of the system.

It was assumed that the expansion and the compression processes are isentropic processes.

4. Results and Discussion

The governing equations of the theoretical model are the set of ordinary differential equations with the time being the independent variable. The input parameters of the system include the initial conditions, the properties of water, the value of constant solar radiation and dimensions of the unit. In order to simulate the operation of the system, a MATLAB program has been written which uses Euler technique to solve the differential equations with a time step $\Delta t = 0.01 \text{ sec}$.

The theoretical simulations have been carried as set of a number cases with constant heat flux values, which are typical for different hours of the mid-summer day in the Middle East region.

The theoretical results on pressure and temperature variations inside the system for the heat flux corresponding to 12 noon are illustrated in *fig. 2* and *fig. 3*, respectively. During the expansion in the cylinder, the pressure drops to approximately 0.7 bar (minimum pressure) and rises to 1.15 bar (maximum pressure) during the compression stroke. These values are also close to experimental values of the minimum and maximum pressures in the cycle, measured using a manometer. The temperature during the cycle varies between 92 and 105 degrees C.

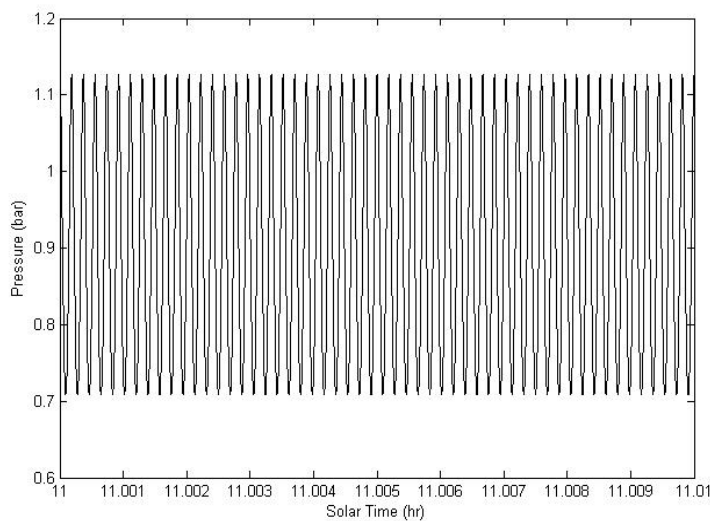


Fig. 2 The saturation pressure oscillation.

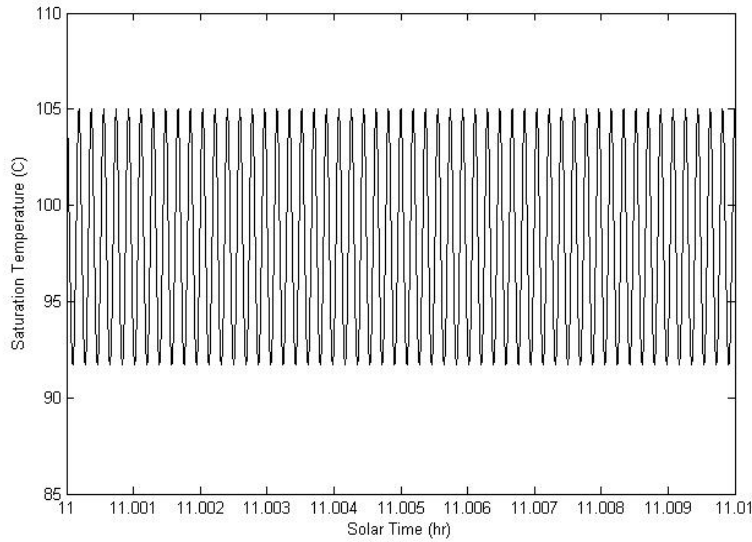


Fig. 3 The saturation temperature oscillation.

Theoretical results on the fresh water production capacity obtained by using the above mathematical model for a number of constant heat fluxes typical for different periods of the mid-summer day were used to produce the variation of the fresh water production capacity over the day, as shown in fig 4.

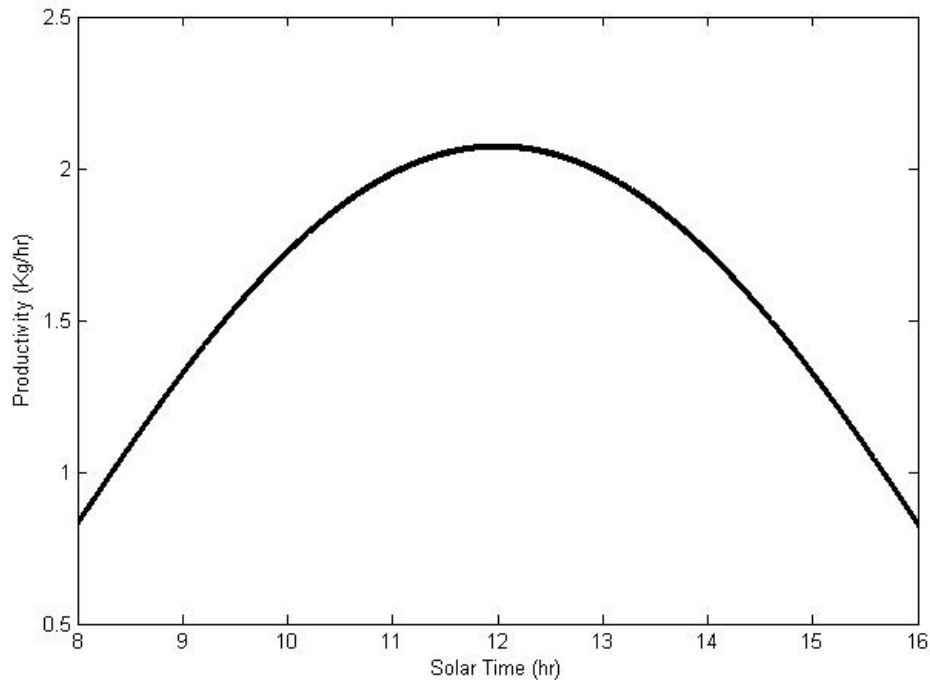


Fig.4 The productivity variation during the mid-summer day

The theoretical value for the daily fresh water production capacity is obtained by integration water production capacity curve in *fig. 4* and it is about 9 litres, which is greater than 6 litres for the conventional static solar stills. During preliminary experiments at the same heat flux value the fresh water production capacity was about 8.2 litres.

5. Conclusions

The paper presents results of theoretical modelling of the steady-state operation of the proposed dynamic water desalination system with a number of constant heat flux values upon the evacuated tubes of the solar collector. The heat flux values used are typical for a different periods of the mid-summer in the Middle East region. The fresh water production, obtained from this study, was found to be about 9 litres/day which is greater than the most of conventional static solar distillation designs. The theoretical data obtained on the fresh water production capacity is in a good agreement with data obtained on the test rig which was run simulating variation of insolation over the summer day.

Currently the unit is being equipped with sensors to record oscillations of the liquid piston, temperature and pressure variations in components of the installation. Such experimental information can be used for calibration of the mathematical model.

It is planned to conduct modelling of unsteady operation with at variable heat flux conditions in the future. The unsteady model also will describe processes taking place in the evaporator and condenser in more details making it possible to take into account the effect of the insolation variation on the levels of the saturated pressure and temperature.

The further development of the mathematical model will also include an optimization procedure for design parameters of the unit.

References

- [1] S. Kalogirou, Seawater desalination using renewable energy sources, *Progress in Energy and Combustion Science* 31, 2005, pp. 242-281.
- [2] M. Shata and K. Mahkamov, Determination of rational design parameters of a multi-stage solar water desalination still using transient mathematical modelling, *Renewable Energy* 35, 2010, pp. 52-61
- [3] K. Mahkamov and B. Belgasim, Experimental study of the performance of a dynamic water desalination system with a fluid piston engine, In: *The 14th international Stirling engine conference*, November 16-18, 2009, Groningen, The Netherlands.
- [4] S. Maroo and D. Goswami, Theoretical analysis of a single-stage and two-stage solar driven flash desalination system based on passive vacuum generation, *Desalination* 249, 2009, pp. 635-646.
- [5] F. Incropera and D. De Witt, *Fundamentals of heat and mass transfer*, New York: John Wiley&Sons, 3rd edition.

Theoretical study of the aspect ratio of a solar still with double slopes

A.Madhlopa^{1,*}, J.A. Clarke¹

¹ Energy Systems Research Unit, University of Strathclyde, James Weir Building, 75 Montrose Street, Glasgow G1 1XJ, United Kingdom.

* Corresponding author. Tel: +44 1415483204, Fax: +44 141548, E-mail: a.madhlopa@strath.ac.uk

Abstract: Clean water is essential for good health which influences the social and economic development of any nation. However, there is limited access to safe water on a global scale. This challenge can be overcome through a multi-faceted approach, including the development of appropriate technologies for water treatment and decision-making tools. Solar distillation is one of the commonest non-conventional methods for improving the quality of water. In this vein, the most widely-exploited solar distillation system is a conventional solar still, which has a thin layer of saline water in a shallow basin with a transparent cover over the water and one or two slopes. The productivity of a solar distillation system is influenced by design, climatic and operational factors, with solar radiation being the most influential meteorological parameter. It is therefore necessary to optimize solar radiation that effectively reaches the base of the solar still. Previous attempts have sought to improve the design characteristics of conventional solar stills through the consideration of system geometry and optical properties of construction materials. One of the important geometric parameters is the ratio (R) of length to width (aspect ratio) of the still base. For a single-slope solar still (SSS), R has been examined in preceding studies. Nevertheless, there is a paucity of information on the aspect ratio of a double-slope solar still. In this study, a state-of-the-art software (ESP-r) was used to simulate the variation of effective insolation with R for a double-slope solar still (DSS) in the east-west and north-south orientations and a SSS facing south. Meteorological data captured at the University of Strathclyde (55° 52' N, 4° 15' W) and Guantanamo Bay (19° 54' N, 14° 51' E) was employed in this analysis. Simulation results show that the optical performance of a DSS was lower (in both orientations) than that of a SSS at both sites. The DSS collected more solar energy in the east-west than north-south orientation, for a given value of R. In addition, effective insolation increased with R to an optimum level for both the DSS and SSS. Approximate optimum values of R were 3.0 and 2.0 for the University of Strathclyde and Guantanamo Bay respectively. However, the optimum value of R was not sensitive to the orientation of the DSS at the two sites. Further, the DSS and SSS exhibited the same optimal value of R at a specific site. It appears that R significantly affects solar collection in a DSS.

Keywords: Aspect ratio, Effective insolation.

Nomenclature

<i>A</i>	area of still base m^2	ϕ	latitude.....degree
<i>B</i>	width of still base..... m	θ	zenith angledegree
<i>G</i>	irradiance Wm^{-2}	ρ	reflectance dimensionless
<i>H</i>	mean annual daily effective insolation Jm^{-2}	τ	solar direct transmittance ... dimensionless
<i>I</i>	hourly effective insolation Jm^{-2}		
<i>L</i>	length of still base..... m		
<i>Q</i>	solar gain (%)		
<i>R</i>	aspect ratio dimensionless		
<i>x</i>	distance along x-axis (m)		
<i>y</i>	distance along y-axis (m)		
<i>z</i>	distance along z-axis (m)		
α	absorptance dimensionless		
β	tilt angle..... degree		

Subscripts

1	transparent cover 1
2	transparent cover 2
<i>b</i>	basin liner
<i>g</i>	ground
<i>w</i>	wall

1. Introduction

Clean water is essential for good health which influences the social and economic development of any nation. However, a large proportion of the available water on the earth's surface is saline [1]. This problem is exacerbated by environmental pollution predominantly

caused by anthropogenic activities. Consequently, there is limited access to clean water, especially in developing countries [2]. Solar distillation is one method of producing fresh water from salty water.

A conventional solar still is the most-widely exploited solar distillation system. It has a thin layer of water in a horizontal basin, transparent cover over the water with one or two slopes (Fig.1). The single-slope solar still (SSS) has a back wall which acts as an internal reflector while the double-slope solar still (DSS) has no back wall. Transparent covers in a DSS may be symmetrical ($\beta_1=\beta_2$) or asymmetrical ($\beta_1\neq\beta_2$), with a gable along each breadth. In both the SSS and DSS, saline water in the basin is heated by solar radiation passing through the transparent cover and absorbed by the water and bottom part of the still basin. Vapour flows upwards from the hot water and condenses when it comes into contact with the cooler inner surface of the transparent cover. The condensate (clean water) is collected in a channel fitted along the lower edge of the transparent cover. For a given set of system design parameters, the distillate output from the system is influenced by climatic and operational factors, and a SSS intercepts a higher proportion of solar radiation than a DSS at locations with both high and low latitudes [3]. Moreover, solar radiation is the most influential environmental parameter [4], and the DSS is economically more viable than the SSS [5]. So, it is necessary to optimize the design of the DSS in order to maximize its capability of solar collection.

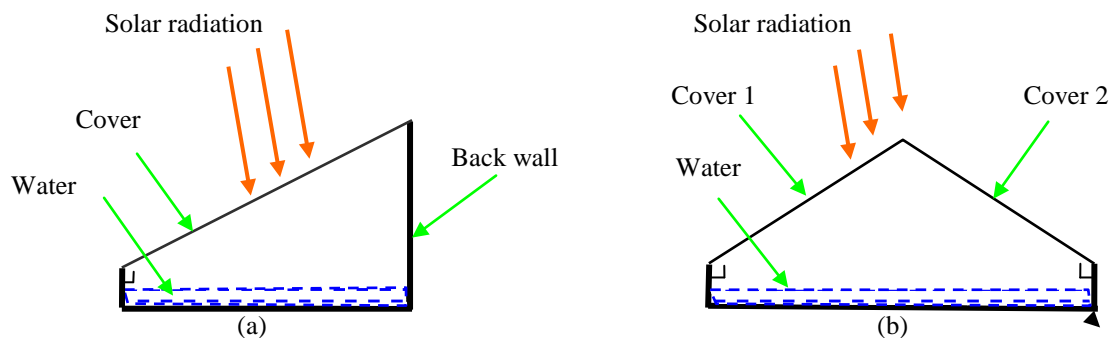


Fig.1: Cross-section of a basic solar still with a) single slope and b) double slopes.

Attempts have been made to establish materials with suitable optical properties of various components of a basin-type solar still. The cover absorbs and reflects part of the incoming solar radiation, with the remaining fraction being transmitted onto the still walls, the surface of saline water and basin liner. So, transmittance is the most important optical property of the cover layer, which may be plastic or glass. Different cover materials for solar stills have been investigated in previous work [6, 7]. It was found that solar stills with glass covers perform better than those with plastic covers. In addition, the internal surfaces of the walls of the still absorb and reflect part of the received solar radiation onto the surface of water. The reflectance of the walls of a solar still influences the effective insolation on saline water in the basin [8]. The basin liner also absorbs part of the solar radiation intercepted by the transparent cover. Consequently, the absorptance of the basin liner is an essential optical property. The various still components are assembled into a structure with specific geometry which affects the optical performance of the distillation system.

A solar still may be mounted on a tracker or fixed plane. A tracking solar still follows the sun on daily (one-axis) or daily and seasonal (two-axis) basis to maintain a low angle of incidence and thereby increase the transmission of solar radiation through the transparent cover. However, tracking solar systems are costly and unsuitable for large-scale production of

distilled water. In contrast, there is no cost associated with tracking in stationary solar stills. So, this variety of solar stills is more feasible for practical applications. The transparent cover of a fixed solar still is inclined at an angle (β) to the horizontal plane. It is reported that the optimum value of β is 10° which just enables the distillate to flow downwards on the inner surface of the cover without dropping back into the basin [3, 9]. Nevertheless, β also affects the transmission of solar radiation through the cover [10]. So, $\beta > 10^\circ$ is sometimes used depending on the latitude (ϕ) of the site [4]. Generally, $\beta = \phi - 10^\circ$ for summer season ($\phi > 10^\circ$), $\beta = \phi$ for annual performance and $\beta = \phi + 10^\circ$ for winter season [11]. In addition, a stationary DSS is oriented with the covers facing the east and west directions to optimize solar collection [12, 13]. On the other hand, a stationary SSS is commonly mounted facing the Equator for optimum performance. Capture of solar energy is also affected by the ratio of the length to width of the still base (R). Optimization of R is reported for a SSS [14] but there is a paucity of information on the aspect ratio of a DSS. The objective of this study was therefore to overcome this limitation

$$R=L/B \tag{1}$$

2. Methodology

2.1. System description and computational tool

Solar collection in a DSS with symmetrical slopes and a SSS has been studied theoretically. The major components of the systems were a) a horizontal basin, b) transparent covers and c) opaque walls and base (Fig.1). The basin liner was constructed from a steel material (0.001 m thick) while the covers were constructed from clear float glass (0.004 m thick) to allow solar radiation reach the internal surfaces of the still. Each cover was inclined at 55.9° to the horizontal at the University of Strathclyde ($55^\circ 52' N$, $4^\circ 15' W$) and 19.9° to the horizontal at Guantanamo Bay ($19^\circ 54' N$, $14^\circ 51' E$) to optimize solar collection on annual basis. The same slope was used for the DSS and SSS at a given site. Each wall was triple-layered with expanded polystyrene (0.05m thick) sandwiched between two plywood layers (0.005 m thick, each layer). Similarly, the base of each still was also triple-layered with plywood external (0.005 m thick), expanded polystyrene middle (0.05 m thick) and steel internal layers. The surface area of the base remained constant for different values of the aspect ratio. In addition, the height of the lower vertical sides was fixed at 0.05 m above the still base while the height of the higher vertical sides varied with R. Other design parameters are presented in Table 1.

Table 1. Design parameters of a double-slope solar still.

Parameter	Unit	Value
A	m^2	1.00
α_b	dimensionless	0.90
ρ_g	dimensionless	0.2
ρ_w	dimensionless	0.2
τ_1, τ_2	dimensionless	0.837

A state-of-the-art software (ESP-r, version 11.9) was used to compute hourly irradiance on the basin liners of the DSS and SSS. This software has a robust algorithm for computation of insolation and shading effects [15]. Beam and diffuse components of solar radiation are treated separately, and optical view factors and multiple reflections are taken into consideration. A geometric construction of each solar distillation system was made in ESP-r with the origin at $x=0$, $y=0$ and $z=1$ m to simulate the system in a mounted mode (the x-, y- and z-axes are mutually perpendicular, z-axis is vertical and x-y plane is horizontal). The still

base was in the x-y plane, with the diagonals of the base intersecting at the origin. The orientation of the DSS was varied by rotating the system about the vertical axis through the origin ($x=0$ and $y=0$). For each system configuration, view factors were calculated by using the ray tracing technique, and the computed optical view factors were used in the computation of effective irradiance on the base of the solar still in any given hour. The DSS was simulated with the covers oriented in the east-west and north-south directions while the SSS faced south at both sites. Effective hourly insolation (I_i) was computed from irradiance on each still base. The total annual effective insolation (E) was determined by summing up the hourly insolation for a given value of the aspect ratio (R). Then, the mean annual daily insolation (H) was computed from E . In addition, the area of the still base remained constant as R was varied from 0.5 to 4.0. At successive increments in R , the percentage solar gain (Q) was calculated. Equations for these calculations were as follows:

$$I_i = 3600G_i \quad \text{for } i=1, 2, 3, \dots, m \quad (2)$$

where m =number of hours in a year.

$$E = \sum_{i=1}^{i=m} I_i \quad (3)$$

$$H = E/j \quad (4)$$

where j =number of days in a year.

$$Q_k = 100(H_k - H_{k-1})/H_i, \text{ for } k=1, 2, 3, \dots \quad (5)$$

Mean hourly normal-incident beam and diffuse irradiance data, captured at the University of Strathclyde and Guantanamo Bay, was used in this study. This data covered the periods from 1 January to 31 December 2001 at the University of Strathclyde and 1 January to 31 December 1971 Guantanamo Bay. It should be noted that the University of Strathclyde and Guantanamo Bay are at high and low latitudes respectively.

2.2. Some assumptions

The following assumptions were made:

- a) the distribution of incoming diffuse radiation was anisotropic. So, an anisotropic model was employed in calculating the amount of diffuse radiation received by a given surface. It should be mentioned that anisotropic models are more accurate in estimation of diffuse radiation than isotropic models [16],
- b) the ground reflected diffusely because it is rough and so the reflected radiation is scattered,
- c) the basin liner was black on the interior surface to optimize solar absorption on the still base, and
- d) the solar still was not obstructed by other structures within the vicinity to reduce the effect of shading from these structures.

3. Results and discussion

The variation of mean annual daily effective insolation (H) on the base of the DSS and SSS simulated at the University of Strathclyde is shown in Fig.2. It is observed that the DSS collects less solar radiation than the SSS for a given value of the aspect ratio (R). This observation is attributed to the presence of a back wall in the SSS. The back wall reflects part of the incoming solar radiation onto the still base [8]. Garg and Mann [3] also found that the

DSS was optically less efficient than the SSS. In addition, the DSS captures more solar radiation in the east-west orientation than the north-south orientation, probably due to the effect of shading from the gables. For the east-west orientation, the gables are on the north and south of the still. So, one of these gables would cast a shadow on the still base when the sun is due north or south of the solar still, except when the sun traverses the sky over the local latitude. The sun traverses the sky to the south of the University of Strathclyde throughout the year. In this case, the southern gable would cast a shadow on the still base. However, solar radiation would be able to directly reach the still base even at low solar altitudes in the morning or afternoon. For the north-west orientation, the gables are on the east and west of the still. Thus, one of the gables would cast a shadow on the still base in the morning or afternoon times, except at local solar noon. The effect of shading is significant at low solar altitudes in the morning or afternoon, which accounts for the observed effect of orientation on the optical efficiency of the DSS [12, 13].

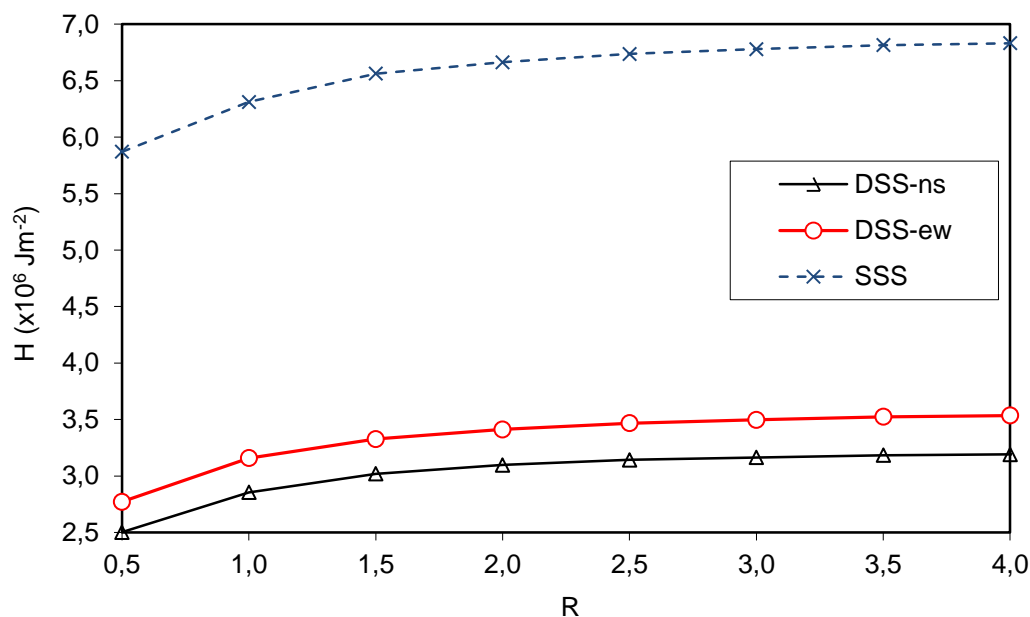


Fig. 2. Variation of mean annual daily effective insolation (H) with aspect ratio (R) for the DSS oriented east-west (DSS-ew) and north-south (DSS-ns), and the SSS facing south at the University of Strathclyde.

Fig.2 also shows that H increases with the aspect ratio (R) of the still base to an optimum level for both the DSS and SSS. This observation is ascribed to a reduction in self-shading arising from the wall along the breadth of the stills. It should be mentioned that R increases as the width (B) of the still decreases, leading to a decrease in the height and area of the slanted wall of the still (for a constant slope) and its shading effect on the internal part of the still base in both the DSS and SSS. Under the prevailing meteorological conditions, the optimum value of R (when $Q < 1.0\%$) was approximately 3.0 for the DSS (in both the east-west and north-south orientations) and SSS. For the SSS, El-Swify et al. [14] reported an approximate optimum value of $R=2.0$ for climate data from Cairo ($30^{\circ} 3' N$, $31^{\circ} 10' E$), which is lower than the present optimum value probably due to variations in site parameters. The latitude and longitude of a site affect solar angles and the distribution of solar radiation in a still.

Fig.3 shows the variation of H on the base of the DSS and SSS for the climate data from Guantanamo Bay. It is again observed that the DSS collects less solar energy than the SSS for a given value of R . In addition, the DSS captures more solar radiation in the east-west

orientation than the north-south orientation, in agreement with results for the climate data from the University of Strathclyde. For the east-west orientation, one of the gables would cast a shadow on the still base when the sun is due north or south of the solar still, except when the sun traverses the sky over the local latitude. It should nevertheless be noted that the sun traverses the sky over head, to the south and north of Guantanamo Bay during certain times of the year. In this case, a gable would cast a shadow on the still base when the sun is not crossing the sky over head but beam radiation would be able to directly reach the still base even at low solar altitudes in the morning or afternoon. For the north-west orientation, one of the gables would cast a shadow on the still base in the morning or afternoon times, except at local solar noon. Solar radiation would be unable to directly reach the still base at low solar altitudes during certain times in the morning or afternoon, which accounts for the observed effect of orientation on the optical efficiency of the DSS.

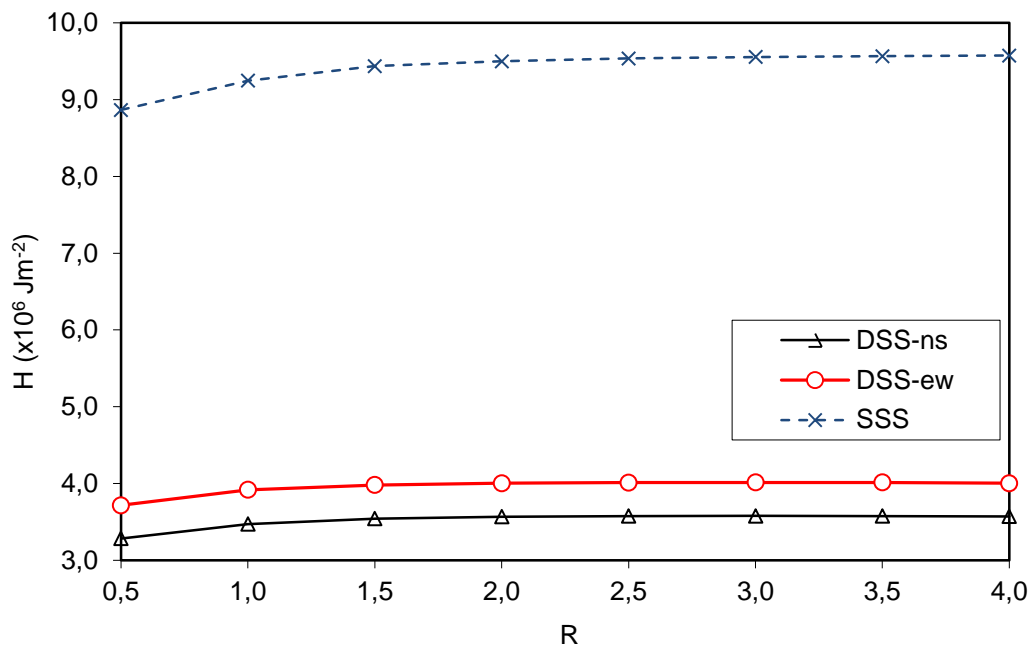


Fig.3. Variation of mean annual daily effective insolation (H) with aspect ratio (R) for the DSS oriented east-west (DSS-ew) and north-south (DSS-ns), and the SSS facing south at Guantanamo Bay.

It is also observed from Fig.3 that H increases with R to an optimum level for both the DSS and SSS. This observation is again attributed to a reduction in self-shading arising from the walls along the width of the stills. Under the prevailing meteorological conditions, the optimum value of R (when $Q < 1.0\%$) was approximately 2.0 for the DSS (in both the east-west and north-south orientations) and SSS, which is in close conformity with findings of El-Swify et al. [14]. This observation is probably because of the influence of site parameters. The latitude of Guantanamo ($19^{\circ} 54' N$) is closer to that of Cairo ($30^{\circ} 3' N$). It should be mentioned that the zenith angle (θ) is low around solar noon during most of the days at low latitude, with $\theta=0$ at solar noon during some days of the year. Low values of θ would tend to reduce the effect of shading and optimal values of R . In contrast, θ is relatively high around solar noon during most of the days at high latitude, with $\theta > 0$ at solar noon throughout the year. High values of θ would tend to increase the effect of shading and optimal values of R . These findings show that site parameters influence the optimum value of R .

4. Concluding remarks

The effect of aspect ratio (R) on solar collection in a double-slope solar still (DSS) has been simulated by using ESP-r software. Optical performances of the DSS and single-slope solar still (SSS) were compared under the same meteorological conditions. The DSS was studied with its transparent covers facing the east-west and north-south directions while the SSS faced south. Meteorological data captured at the University of Strathclyde (high latitude) and Guantanamo Bay (low latitude) was employed in this analysis. Simulation results show that the optical performance of a DSS (in both orientations) was lower than that of a SSS at these sites. The DSS collected more solar energy in the east-west than north-south orientation, for a given value of R. In addition, effective insolation increased with R but the increase was insignificant for values of $R > 3.0$ for both the DSS and SSS at a high latitude. Similarly, effective insolation increased with R but the increase was insignificant for values of $R > 2.0$ for both the DSS and SSS at a low latitude. It is therefore concluded that a) R significantly affects the collection of solar energy by a DSS, b) the approximate optimum value of R is sensitive to site parameters, c) the orientation of the DSS does not affect the optimum value of R, and d) the optimum value of R is approximately the same for the DSS and SSS at a given site.

Acknowledgements

Authors are grateful to Newton International Fellowships Scheme for the financial support.

References

- [1] G.N. Tiwari, H.N. Singh, R. Tripathi, Present status of solar distillation, *Solar Energy* 75, 2003, pp.367-373.
- [2] WHO, World Health Statistics 2008, World Health Organization, 2008.
- [3] H.P. Garg, H.S. Mann, Effect of climatic, operational and design parameters on the year round performance of single-sloped and double-sloped solar still, under Indian arid zone conditions. *Solar Energy* 18, 1976, pp.159-164.
- [4] A.S. Nafey, M. Abdelkader, A. Abdelmotalip, A.A. Mabrouk, Parameters affecting solar still productivity. *Energy Conversion and Management* 41, 2000, pp.1797-1809.
- [5] K. Mukherjee, G.N. Tiwari, Economic analysis of various designs of. conventional solar stills. *Energy Conversion and Management* 26, 1986, pp.155-157.
- [6] B.W. Tleimat, E.D. Howe. Comparison of plastic and glass condensing covers for solar stills. *Solar Energy* 12, 1969, pp.293-304.
- [7] H.M. Qiblawey, M. Banat, Solar thermal desalination technologies. *Desalination* 220, 2008, pp.633-644.
- [8] R. Tripathi, G.N. Tiwari, Performance evaluation of solar still by using the concept of solar fraction. *Desalination* 169, pp.2004, 69-80.
- [9] P.I. Cooper, W.R.W. Read, Design philosophy and operating experience for Australian stills. *Solar Energy* 16, 1974, pp.1-8.
- [10] P.I. Cooper, The absorption of radiation in solar stills, *Solar Energy* 12, 1969, pp.333-346.
- [11] M.A. Samee, U.K. Mirza, T. Majeed, N. Ahmad. Design and performance of a simple solar still. *Renewable and Sustainable Energy Reviews* 11, 2007, pp.543-549.

- [12] A.K. Singh, G.N. Tiwari, P.B. Sharma, E. Khan, Optimization of orientation for higher yield solar still for a given location, *Energy Conversion and Management* 36, 1995, pp.175-187.
- [13] V.K. Dwivedi , G.N. Tiwari, Experimental validation of thermal model of a double slope active solar still under natural circulation mode, *Desalination* 250, 2010, pp.49-55
- [14] M.E. El-Swify, M.Z. Metias, Performance of double exposure still, *Renewable Energy* 26, 2002, pp.531-547.
- [15] J.A. Clarke, *Energy simulation in building design*, Butterworth-Heinemann, 2nd edition, 2001, pp.212-255.
- [16] R. Perez, P. Ineichen, R. Seals, J. Michalsky, R. Stewart, Modelling daylight availability and irradiance components from direct and global irradiance, *Solar Energy* 44, 1990, pp.271-289.

Concentrating solar power plants for electricity and desalinated water production

Soteris A. Kalogirou^{1,*}

¹ Department of Mechanical Engineering and Materials Science and Engineering,
Cyprus University of Technology, P. O. Box 50329, 3603 Limassol, Cyprus

* Corresponding author. Tel: +357 2500 2621, Fax: +357 2500 2637, E-mail: Soteris.kalogirou@cut.ac.cy

Abstract: Electricity and water are two commodities which are usually both required in arid countries having a high solar insolation. A number of technologies exists for both systems, which are briefly reviewed in this paper. Among the most matured and suitable concentrated solar power (CSP) plants for electricity generation are the solar tower (ST) and the parabolic trough collector (PTC) systems, whereas for desalination these are the multiple effects distillation (MED) type evaporator and the reverse osmosis (RO). The paper shows also the possibilities that exist and the ways that these technologies can be combined in order to produce simultaneously electricity and water. The equipment required to be used for these systems (steam cycle components, MED or RO) is usually very expensive therefore, the system is required to operate continuously without complete shut down during the night. Such a system would be very suitable for arid countries, which due to the water shortage problem they face, locate power plants in coastal areas in order to use the seawater for the cooling needs of the steam cycle system (condenser). Therefore, in this case it would be comparatively easy to combine the power system with desalination as the resource for such a system, i.e., seawater would be readily available.

Keywords: Parabolic trough collectors, power tower, multiple effect boiling, reverse osmosis, desalination

1. Introduction

Cyprus does not have at the moment any sources of energy and depends exclusively on imported oil for its energy needs. The only inexhaustible natural source of energy that Cyprus possesses abundantly, is solar energy. It is well known that other forms of renewable energy, like the wind energy, wave energy and biomass have limited potential in Cyprus. Cyprus Government decided to erect a solar thermoelectric power generation station with a capacity of about 50 MW. The characteristics that need to be considered when selecting the right type of thermoelectric system are the cost of electricity produced and the land area that would be required to install the solar plant. The latter is very important as Cyprus has no desert land near the sea but on the contrary seaside areas are very expensive as they are used for touristic development. It should be noted that all existing power stations are located near the sea so the solar power station should also be located near to one of those stations to ease access to the grid and for the use of the seawater for the condenser.

2. Concentrating solar power

Concentrating solar power plants, use mirrors to generate high temperature heat that drives steam turbines traditionally powered from conventional fossil fuels. Some of these systems incorporate also heat storage which allows them to operate during cloudy weather and night-time. The main systems that are operational today in various countries are the parabolic trough collector (PTC) system and the central receiver or power tower system. More details about these systems can be found in [1].

2.1. Parabolic trough collector system

From the technologies available the most industrially matured is the parabolic trough system. This is mainly due to the nine large systems installed and operating in California, USA since 1985, which have a total installed capacity equal to 354 MWe. Mainly due to the plants

operating in California for more than 20 years, parabolic trough is the most proven technology and today they produce electricity at about US\$ 0.10/kWh. The success and durability of these plants has demonstrated the robustness and reliability of the parabolic trough technology. Compared to other technologies, this system has a high solar-to-electrical efficiency and low area per MWh requirement.

Parabolic trough collectors are the most mature solar technology to generate heat at temperatures up to 400°C for solar thermal electricity generation or process heat applications. Parabolic trough technology proved to be tough, dependable and proven. Today the second-generation parabolic troughs have more precise mirror curvature and alignment, which enables them to have higher efficiency than the first plants erected in California. Other improvements include the use of a small mirror on the backside of the receiver to capture and reflect any scattered sun rays back onto the receiver, the direct steam generation into the receiver tube to simplify the energy conversion and reduce heat losses, and the use of more advanced materials for the reflectors and selective coatings of the receiver.

2.2. Power tower systems

Power towers or central receiver systems use thousands of individual sun-tracking mirrors called "heliostats" to reflect solar energy onto a receiver located on top of a tall tower. The receiver collects the sun's heat in a heat-transfer fluid (molten salt) that flows through the receiver. This is then passed optionally to storage and finally to a power-conversion system which converts the thermal energy into electricity and supply it to the grid. In many solar power studies it has been observed that the collector represents the largest cost in the system, therefore, an efficient engine is justified to obtain maximum useful conversion of the collected energy. The power tower plants are quite large, generally 10 MWe or more, while the optimum sizes lie between 50-400 MW. It is estimated that power towers could generate electricity at around US\$ 0.04/kWh by 2020 [2].

The heliostats should reflect solar radiation to the receiver at the desired flux density at minimum cost. A variety of receiver shapes has been considered, including cylindrical receivers and cavity receivers. The optimum shape of the receiver is a function of radiation intercepted and absorbed, thermal losses, cost and design of the heliostat field. For a large heliostat field a cylindrical receiver is best suited to be used with Rankine cycle engines. Another possibility is to use Brayton cycle turbines which require higher temperatures (of about 1000°C) for their operation and in this case cavity receivers with larger tower height to heliostat field area ratios are more suitable. For gas turbine operation, the air to be heated must pass through a pressurized receiver with a solar window. Combined cycle power plants using this method could require 30% less collector area than the equivalent steam cycles. Rankine cycle engines driven from steam generated in the receiver operate at 500 to 550°C.

2.3. Heat storage and hybridization

An interesting feature of parabolic troughs and power tower systems is that it is possible to store heat, which enables them to continue producing electricity during the night or cloudy days. For this purpose, concrete, molten salts, ceramics or phase-change media can be used. The parabolic trough and the power tower systems produce superheated steam which is used to drive the turbines of a conventional Rankine type power station or an Integrated Solar Combined Cycle System, i.e., they replace the conventional steam boiler with the solar collection system. It has been proved in a previous publication that a system with four hours of storage is the optimum for Cyprus [3]. Both systems can also be operated with fossil fuel (usually natural gas) so as to continue the production of electricity at low irradiation hours and

during the night. This is due to the fact that the equipment involved is expensive and it is not viable to leave the systems to cool down and stay idle for a long time.

All existing power stations in Cyprus are located near the sea. Such a solar power system should also be located near the sea close to an existing power station to ease access to the grid and for the use of the seawater for the condenser. The erection of such a system inland is not possible due to the lack of water required for the condensation of the steam. This is because Cyprus suffers from a water shortage problem, so it has no adequate water supply inland and the proximity of the solar to an existing station means it will also be close to existing power lines and maintenance personnel from the station. Moreover, the location of the solar plant near the sea will enable it to be combined with solar desalination, for the production of fresh water which is also a required commodity for the island.

3. Desalination processes

Desalination can be achieved by using a number of techniques. Industrial desalination technologies use either phase change or thermal processes, or involve semipermeable membranes or single-phase processes to separate the salts from the seawater. All processes require a chemical pre-treatment of raw seawater to avoid scaling, foaming, corrosion, biological growth, and fouling and also require a chemical post-treatment. Here only two desalination methods are considered the multiple effect boiling system, falling in the first category, and the reverse osmosis system, falling in the second. These are the most suitable for the application considered as will be presented in the following sections.

3.1. The MED process

The multiple effect distillation (MED) process is composed of a number of elements, which are called effects. The steam from one effect is used as heating fluid in another effect, which while condensing, causes evaporation of a part of the salty solution. The produced steam goes through the following effect, where, while condensing, makes some of the other solution evaporate and so on. For this procedure to be possible, the heated effect must be kept at a pressure lower than that of the effect from which the heating steam originates. The solutions condensed by all effects are used to preheat the feed [4]. In this process, vapour is produced by flashing and by boiling, but the majority of the distillate is produced by boiling. The MED process usually operates as a once through system without a large mass of brine recirculating around the plant. This design reduces both pumping requirements and scaling tendencies [5].

Early plants were of the submerged tube design and used only two to three effects. In modern systems, the problem of low evaporation rate has been resolved by making use of the thin film designs with the feed liquid distributed on the heating surface in the form of a thin film instead of a deep pool of water. Such plants may have vertical or horizontal tubes.

Another type of MED evaporator is the Multiple Effect Stack (MES) type. This is the most appropriate type for solar energy application. It has a number of advantages, the most important of which are its stable operation between virtually zero and 100% output even when sudden changes are made and its ability to follow a varying steam supply without upset [4]. In Fig. 1, a four-effect MES evaporator is shown. Seawater is sprayed into the top of the evaporator and descends as a thin film over the horizontally arranged tube bundle in each effect. In the top (hottest) effect, steam from a steam boiler or from a solar collector system condenses inside the tubes. Because of the low pressure created in the plant by the vent-ejector system, the thin seawater film boils simultaneously on the outside of the tubes, thus creating new vapour at a lower temperature than the condensing steam.

applied to the salty solution, fresh water will pass from the brine into the water compartment. Theoretically, the only energy requirement is to pump the feed water at a pressure above the osmotic pressure. In practice, higher pressures must be used, typically 50-80 atm, in order to have a sufficient amount of water pass through a unit area of membrane [4]. With reference to Fig. 2, the feed is pressurised by a high-pressure pump and made to flow across the membrane surface. Part of this feed passes through the membrane where the majority of the dissolved solids are removed. The remainder, together with the remaining salts, is rejected at high pressure. In larger plants, it is economically viable to recover the rejected brine energy with a suitable brine turbine. Such systems are called energy recovery reverse osmosis (ER-RO) systems.

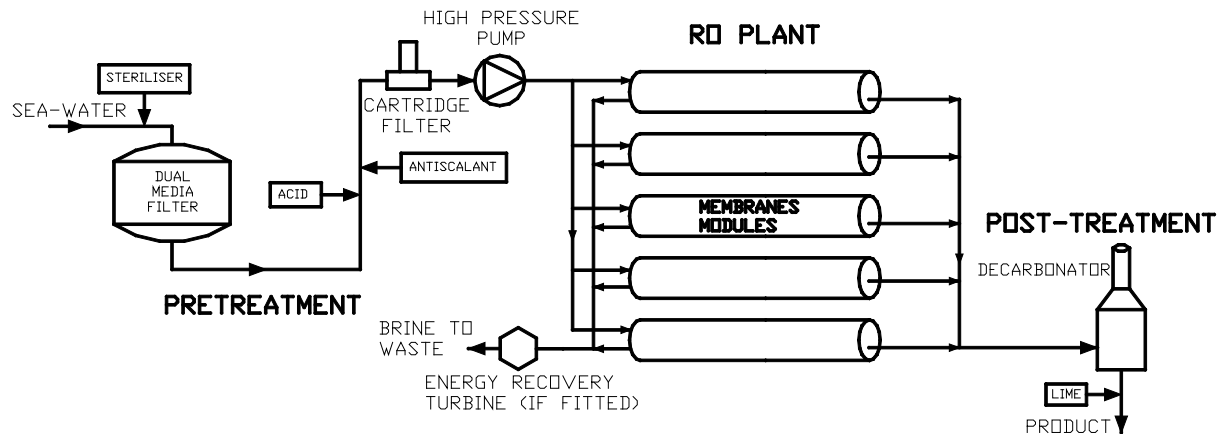


Fig. 2. Principle of operation of a reverse osmosis (RO) system.

Solar energy can be used with RO systems as a prime mover source driving the pumps or with the direct production of electricity through the use of photovoltaic panels. As the unit cost of the electricity produced from photovoltaic cells is high, photovoltaic-powered RO plants are not considered here. The membranes are in effect very fine filters, and are very sensitive to both biological and non-biological fouling. To avoid fouling, careful pre-treatment of the feed is necessary before it is allowed to come in contact with the membrane surface.

3.3. Characteristics of both processes

The identification and evaluation of the renewable energy resources (RES) in an area, is the primary step to be performed when designing a RES-driven desalination system. Such systems should be characterized by robustness, simplicity of operation, low maintenance, compact size, easy transportation to site, and simple pre-treatment and intake system [6].

The energy required for the two desalination processes considered, as obtained from a survey of manufacturers' data, is shown in Table 1 [4]. It can be seen from Table 1 that the process with the smallest energy requirement is RO-ER followed by RO and the MED.

Table 1. Energy consumption of desalination systems.

Process	Heat input (kJ/kg of product)	Mechanical power input (kWh/m ³ of product)	Prime energy consumption (kJ/kg of product) ¹
MED	123	2.2	149.4
RO	-	5-13 (10)	120
ER-RO	-	4-6 (5)	60

Notes: 1. Assumed conversion efficiency of electricity generation of 30%

2. Figure used for the prime energy consumption estimation shown in last column

A comparison of the desalination equipment cost and the seawater treatment requirement, as obtained from a survey of manufacturers' data, is shown in Table 2. The MED is the cheapest of all the indirect collection systems and also requires the simplest seawater treatment. RO although requiring a smaller amount of energy is expensive and requires a complex seawater treatment.

Table 2. Comparison of desalination plants.

ITEM	MED	RO
Scale of application	Small-medium	Small-large
Seawater treatment	Scale Inhibitor	Sterilizer, Coagulant Acid, Deoxidiser
Equipment price (Euro/m ³)	900-1700	900-2500
		Membrane replacement every 5-6 yrs

Note: Low figures in equipment price refer to bigger size in range indicated and vice versa.

4. Options considered

In this section, various options are considered to combine CSP with desalination. The first option considered is a thermal desalination system shown schematically in Fig. 3. In this option a solar field is used which provides thermal energy to a MED evaporator to produce fresh water. This solar heat can be given directly to the MED unit or in days with good irradiation the excess energy can be stored for use in periods of low sunshine and during the night. The system can also be hybridized using conventional fuel to run the desalination subsystem during the night. A very small quantity of electrical energy (compared to thermal) is required by the MED unit to drive the pumps. As the present RES system is thermal only, this quantity of electricity can be produced either from a PV system or obtained from the grid.

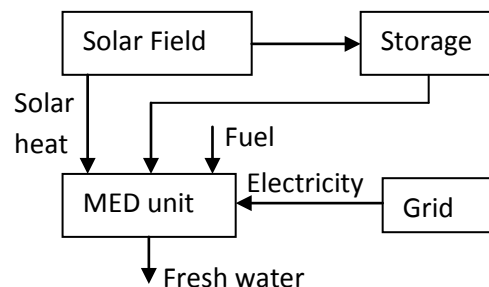


Fig. 3. Combination of a solar thermal system with MED for desalinated water production only.

The second option, shown in Fig. 4, concerns a solar thermoelectric system producing electricity with a CSP system. In this case some of the electricity produced can be used to drive a RO desalination system and the rest is supplied to the grid. This system has the advantage that the operators can decide according to the demand to produced either both, fresh water and electricity, or one of the two only. Any form of hybridization can go directly to the power plant as is normal to all such systems, when the storage is depleted a few hours after sunset, according to the size of the storage used.

The third option, shown in Fig. 5, is a combination of a normal solar thermoelectric power system with a MED unit to produce both electricity and fresh water. The MED requires thermal energy to operate in the form of high temperature hot water (>100°C) or low temperature steam. Therefore, this energy can be supplied either directly from the CSP system or from the waste heat of the power plant system, in the form of condensation heat. For this purpose the MED evaporator can be an integral part of the steam condenser of the Rankine

power plant cycle. In this option the hybridization is done directly on the power plant as is normal to all CSP power systems. The small quantity of electricity required by the MED is taken from the power plant.

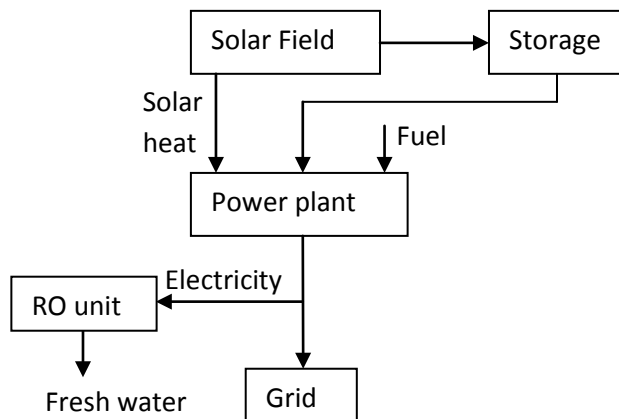


Fig. 4. Combination of a solar thermoelectric power system with RO to produce both electricity and fresh water.

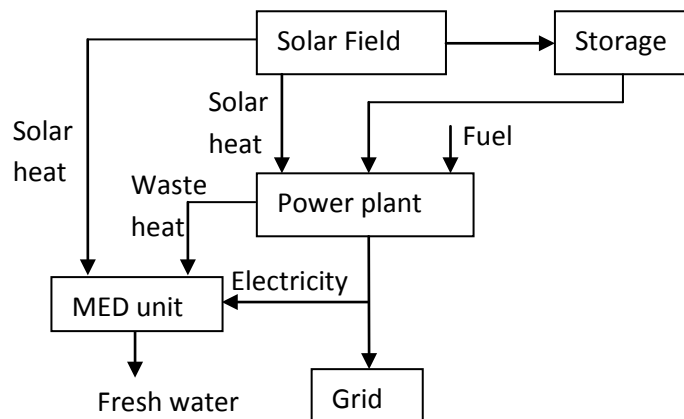


Fig. 5. Combination of a solar thermoelectric power system with MED, operated from solar and waste heat, to produce both electricity and fresh water.

The fourth option, shown in Fig. 6, is a combination of a solar thermoelectric power system with MED and RO systems for fresh water production. The RO unit operates as in the second option with the electricity produced by the CSP system, whereas the MED subsystem, which requires thermal energy to operate, can use either some of the thermal energy produced by the CSP system or the waste heat from the power plant, therefore the MED is part of the condensation system of the power plant. Again here the hybridization is done directly on the power plant as is normal to all CSP power systems. This option gives a larger number of operation options concerning the production of electricity and water according to the demand of each commodity however, it is a more expensive system as both MED and RO need to be purchased and installed.

All CSP systems shown in the above figures can use either a parabolic trough collector or a power tower system. As can be seen from the configurations presented above, there are a number of options to be considered when either only desalinated water or both electricity and fresh water are required. The choice of which system to apply for a particular case should depend on the particular requirements of each commodity and the characteristics of the load and water demand. Due to the high cost of the required equipment however, all systems needs

to be hybridized so as to operate the plants round the clock to reduce the idle time, the energy required to bring the systems to their operating limit and the problems associated with the frequent starts and stops of the equipment and thermal cycling. Before considering any hybridization though, the optimum size of storage needs to be used to minimize the adverse effects of the burning of fossil fuels on the environment. For this purpose a less polluting fuel needs to be employed, like the natural gas.

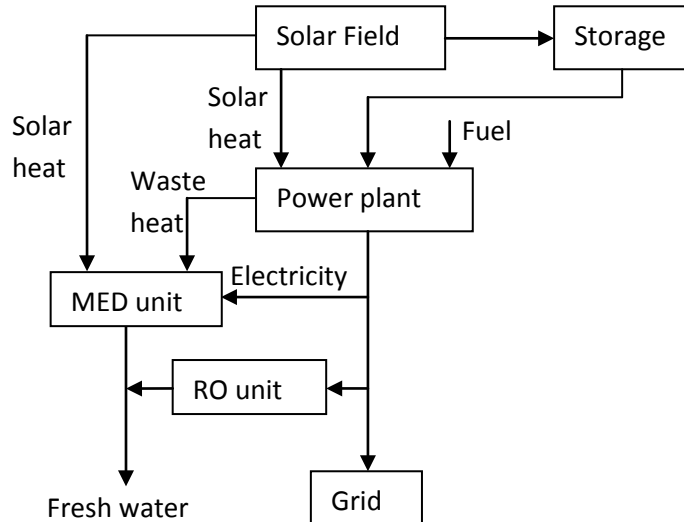


Fig. 6 Combination of a solar thermoelectric power system with RO and MED to produce both electricity and fresh water.

5. Conclusions

The parabolic trough and the power tower systems produce superheated steam which can be used to drive the turbines of the common Rankine cycle. Both systems can be supplied with conventional fuel (usually natural gas) so as to operate during hours of low irradiation and during night-time. For the reasons explained above such a solar plant need to be located near the sea. In such a case the solar plant can be combined with solar desalination to produce fresh water from seawater which is also a precious commodity for Cyprus. As shown in this paper a number of options exist for the combination of a CSP system with a desalination one to produce both electricity and water.

References

- [1] S.A. Kalogirou, *Solar Energy Engineering: Processes and Systems*, Academic Press, New York, 2009, pp. 521-552.
- [2] S. Taggart, Hot stuff: CSP and the power tower, *Renewable Energy Focus*, May/June issue, 2008, pp. 51-54.
- [3] S.A. Kalogirou, Solar Thermoelectric Power Generation in Cyprus, Selection of the Best System, *Proceedings of the World Renewable Energy Congress XI on CD ROM*, Abu Dhabi, UAE, 2010.
- [4] S.A. Kalogirou, Seawater Desalination Using Renewable Energy Sources, *Progress in Energy and Combustion Science*, 2005, Vol. 31, No. 3, pp. 242-281.
- [5] S.A. Kalogirou, Survey of solar desalination systems and system selection, *Energy-The International Journal*, 1997, Vol. 22, No. 1, pp. 69-81.
- [6] E. Tzen, R. Morris, Renewable Energy sources for desalination, *Solar Energy*, 2003 Vol. 75, No. 5, pp. 375-379.

Analysis of solar lithium bromide-water absorption cooling system with heat pipe solar collector

Amir Falahatkar^{1,*}, M. Khalaji Assadi¹

¹Department of Energy Engineering, Science & Research Branch, Islamic Azad University, Tehran, Iran

*Corresponding Author. Tel: +98 912 2506923, Email: eng.falahatkar@srbiau.ac.ir

Abstract: Solar energy applications in Iran for supplying domestic hot water, space heating and cooling have been considered severely in last decade. The purpose of this research is to analysis of solar single effect lithium bromide-water absorption cooling system in a typical office building in Tehran. The solar energy is absorbed by heat pipes and stored in an insulated storage tank. This system has been designed to supply the cooling load of mentioned typical office building where the cooling load is 35.17KW (10 tons of refrigerant) which events in July. Results demonstrate that depending on the Tehran climate and the specification of the building by means of optimized design of solar heat pipe collectors, up to 2400 m³/year Natural Gas energy saving can be reached by use of solar absorption cooling system. Achieving this purpose requires utilizing 16 collectors which everyone compromises 30 tubes with total absorber area of 45 m² which is the optimum collector area for this plant in Tehran. According to this replacement the investment payback rate would be 13 years which would be much shorter than the payback time of a solar cooling system combined with conventional all air systems.

Keywords: Absorption cooling, Heat pipe collector, Solar energy

Nomenclature

\dot{m} mass flow rate..... $kg.s^{-1}$	β slopedegree
Q thermal capacity.....w	ρ_g diffuse reflectance of the ground.....degree
c_p specific heat..... $j.kg^{-1}.c^{-1}$	δ deviation angledegree
ΔT temperature difference..... $^{\circ}c$	C capital cost\$
q_u useful energy..... $j.m^{-2}$	E energy saving..... \$.year ⁻¹
η thermal efficiency%	PB payback time.....year
\overline{H} monthly average daily total solar radiation on a horizontal surface..... $j.m^{-2}$	i energy inflation.....%
ϕdegree	ω_s sunset hour angle.....degree

1. Introduction

The energy demand for refrigeration and air-conditioning appliances has been increased continuously in last decades. World energy demand-and CO₂ emissions- is expected to rise by some 60% by 2030 respect to the beginning of this century [1]. The cooling load in summer is associated with high solar energy, which offers a suitable opportunity to utilize solar energy for cooling. Conventional vapor compression chillers require high quality energy, electricity which is produced from initial energy resources. Furthermore, vapor compression cooling systems use chlorofluorocarbons (CFCs) and hydrochlorofluorocarbons (HCFCs) as working fluids. These materials will lead to global warming and ozone depletion. Thermal-driven air-conditioning systems are using heat as motive energy to provide cold energy. These systems can be categorized on absorption systems, adsorption systems, duplex rankine, desiccant cooling and ejector refrigeration systems. The heat could be obtained from waste heat sources, combined heat and power technologies (CHP), and solar energy. Lithium Bromide (LiBr)-water absorption cooling systems are conventional in thermal-driven air-conditioning systems and have too many benefits in comparison with other cooling

systems; because their performance is good and cost is low. The single effect LiBr-water absorption systems operate at a generator temperature range 70 to 95 °C and the coefficient of performance (COP) of these systems are between 0.6 to 0.8, which are higher than NH₃-H₂O absorption cooling systems [2].

Sparber et al [3] reported that till 2007 there were 81 installed large scale solar cooling systems, eventually including systems which are currently not in operation. 73 installations are located in Europe, 7 in Asia, China in particular, and 1 in America (Mexico). 60% of these installations are dedicated to office buildings, 10% to factories, 15% to laboratories and education centers, 6% to hotels and the left percentage to buildings with different final use (hospitals, canteen, sport center, etc). They also cited that 56 installations are belong to absorption systems and the overall cooling capacity of the thermally driven chillers amounts to 9 MW 31% of it is installed in Spain, 18% in Germany and 12 % in Greece.

Bong et al [4] designed and installed solar absorption chiller in Singapore. The system included 7KW absorption chiller, heat pipe collectors with a total area of 32 m², a hot water storage tank, an auxiliary heater and a 17.5 KW cooling tower. They cited that the overall average cooling capacity provided was 4KW, solar fraction of 39% and COP of 0.58.

Balghouthi et al [5] accomplished a simulation using TRNSYS program in order to select and size different components of solar absorption chiller. They reported that solar absorption cooling systems were suitable for Tunisian's condition.

Alizadeh et al [6] simulated and optimized a solar LiBr-water absorption cooling system that has been design for Malaysia using evacuated tube solar collectors. The modeling of the solar absorption chiller was accomplished with TRNSYS program.

Yeung et al [7] designed and installed a solar driven absorption chiller at the University of Hong Kong. This system included 4.7KW absorption chiller, flat plate collectors with a total area of 38.2m², a cooling tower, a 2.75m³ hot water storage tank and the other equipments. They reported that the collector efficiency was estimated at 37.5%, the annual system efficiency at 7.8% and an average solar fraction at 55%, respectively.

The objective of this work is to evaluate and investigate the energy conservation capacity of a sample office building in Tehran, using solar LiBr-water absorption chiller and heat pipe solar collector. Furthermore, the payback time for initial investments of the system has been calculated.

2. Methodology

A cooling system possessing solar-operated absorption chiller provides the cooling demands for the typical office building in Tehran-Iran. Tehran is located at 35.68°N and 51.32°E. Figure 1 demonstrates both the variability of ambient temperature and relative humidity and in figure 2 the monthly solar radiation on horizontal surface is demonstrated. The office has a single storey and its floor area is 280m². The daily occupancy schedule is from 8:00 to 17:00, totally 9hours and the daily cooling system schedule is considered during June 1 to September 22. The daily average of global solar radiation of Tehran is about $23 \frac{Mj}{m^2}$ for the summer months [8]. The major components of the plant are heat pipe solar collectors, a 35.17KW (10 RT) single effect LiBr-water absorption chiller, a hot water storage tank, a cooling tower, a control system and some other auxiliary equipments.

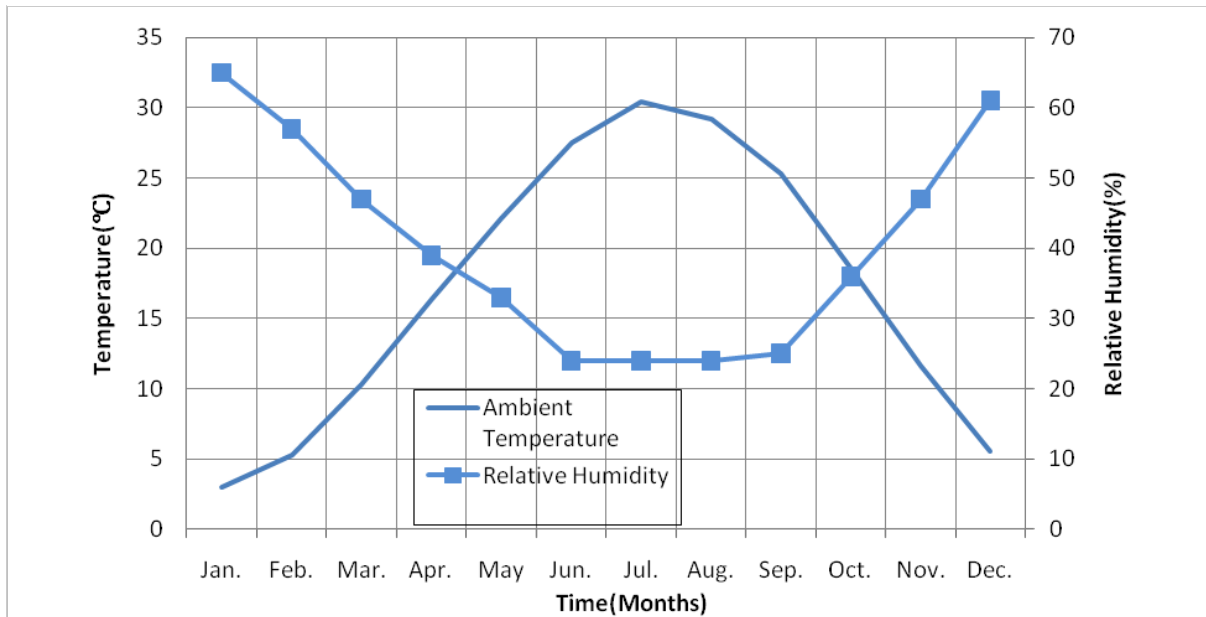


Fig. 1. Variability of ambient monthly temperature and monthly relative humidity for Tehran.

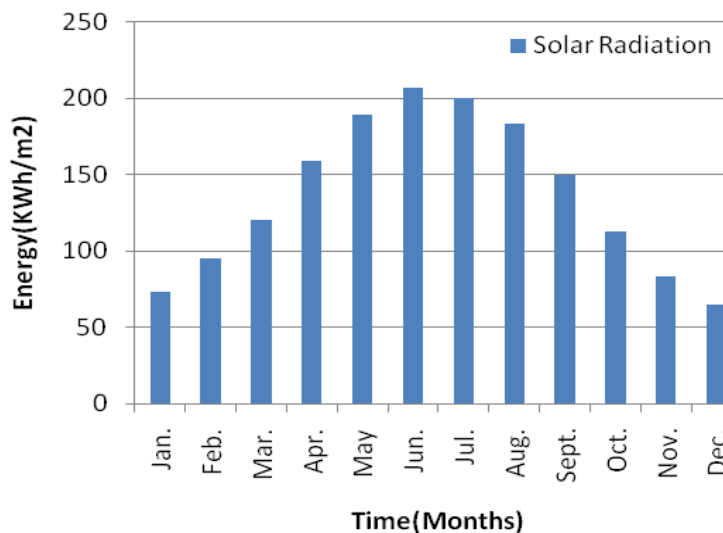


Fig. 2. Monthly solar radiation on horizontal surface in Tehran.

2.1. Solar Energy

The plant primary energy source is the solar energy, which is absorbed by heat pipe solar collector and stored in an insulated storage tank. Heat pipes are widely used for heat recovery and energy saving in various ranges of applications because of their simple structure, special flexibility, high efficiency, good compactness and excellent reversibility [9]. The heat pipe vacuum tube collects heat from the sun at high efficiency. It is important that heat pipe solar collectors must be installed with a tilt of at least 25°. They operate like a thermal diode where the flow of heat is in one direction only [10]. This type of collector commonly filled with alcohol or water in a vacuum and operates in two versions, one with a dry and one with a wet connection [11]. The most important difference between evacuated tube solar collectors and heat pipe solar collectors is that the heat carrier fluid inside of the copper heat pipe is not connected to the solar loop. The heat pipe collectors are mounted on a roof and tilted by 25° with the roof to utilize more radiation in summer and it is produced by APRICUS.

2.2. Absorption chiller

A water fired chiller (WFC) with a related capacity of 35.17KW cooling (10RT) produced by YAZAKI when it is operating at a hot water driving temperature of 88°C, coolant water temperature of 31°C and output chilled water at 7°C. The coefficient of performance (COP) of this chiller is 0.7 as reported by the manufacture.

2.3. Presentation of parameters

The thermal capacity of the equipments is determined by Eq. (1):

$$Q = \dot{m} \cdot c_p \cdot \Delta T, \quad (1)$$

Where \dot{m} is the mass flow rate, c_p is the specific heat at constant pressure and ΔT is the temperature difference.

The energy during a fixed period is determined by Eq. (2):

$$E = \int_{t_i}^{t_o} Q dt, \quad (2)$$

Where t_i is initial time and t_o is final time. Afterwards, the efficiency of solar collectors is obtained by Eq. (3) [2]:

$$\eta = \frac{q_u}{R \cdot H}, \quad (3)$$

Where q_u is the useful energy output of a collector per square meter, \bar{H} is monthly average daily total solar radiation on a horizontal surface. It should be noted that the efficiency of solar heat pipe collector is about 63% as reported by the manufacture. \bar{R} is the proportion of monthly average total radiation on tilted surface on the monthly average total radiation on horizontal surface which is determined by Eq. (4) [2]:

$$\bar{R} = \left(1 - \frac{\bar{H}_d}{\bar{H}}\right) \bar{R}_b + \frac{\bar{H}_d}{\bar{H}} \left(\frac{1 + \cos \beta}{2}\right) + \rho_g \left(\frac{1 - \cos \beta}{2}\right), \quad (4)$$

Where \bar{H}_b is monthly average daily beam solar radiation on a horizontal surface, \bar{H}_d is monthly average daily diffuse solar radiation on a horizontal surface, ρ_g is the diffuse reflectance of the ground and β is the slope of the collector, \bar{R}_b is the ratio of the average daily beam radiation on the tilted surface on that on a horizontal surface which is determined by Eq. (5) [2]:

$$\overline{R_b} = \frac{\cos(\phi - \beta)\cos\delta\sin\omega'_s + \left(\frac{\pi}{180}\right)\omega'_s\sin(\phi - \beta)\sin\delta}{\cos\phi\cos\delta\sin\omega_s + \left(\frac{\pi}{180}\right)\omega_s\sin\phi\sin\delta} \quad (5)$$

Where ω'_s is the sunset hour angle for the tilted surface for the mean day of the month and ω_s is the sunset hour angle, which are obtained by Eq. (6) and Eq. (7) [2]:

$$\omega'_s = \text{Min} \left[\begin{array}{l} \cos^{-1}(-\tan\phi\tan\delta) \\ \cos^{-1}(-\tan(\phi - \beta)\tan\delta) \end{array} \right] \quad (6)$$

Where ϕ is the latitude and δ is the solar deviation angle.

$$\omega_s = \cos^{-1}(-\tan\phi\tan\delta) \quad (7)$$

3. Results

3.1. Determining the optimum solar collector area

With calculating \overline{R} through equations 4 to 7, the useful energy output of a collector is determined. Figure 4 demonstrates the monthly energy derived from one square meter of collector in Tehran. The surface area for the heat pipe collector is determined by the proportion of the required energy for cooling the environment on the useful energy output of the collector.

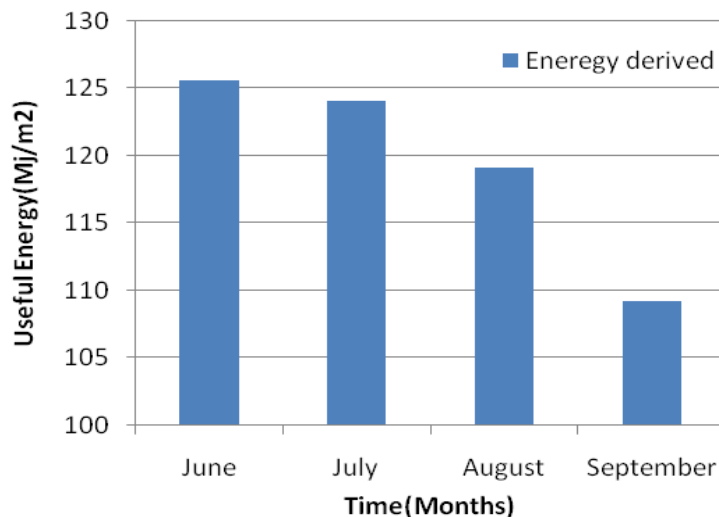


Fig. 3. Monthly energy derived from one square meter of collector in Tehran from June to September

Optimized solar collector area depends on some important factors such as: Solar radiation, intensity, cost increasing and amount of consumption [12]. To estimate the optimal surface of heat pipe solar collector, we should determine the solar cooling fraction (SCF). The solar cooling fraction is described as the ratio of solar heat yield to the total energy required to drive solar absorption chiller.

Finally, the optimum surface of heat pipe collectors for typical office building in Tehran is determined in each situation as presented as figure.4.

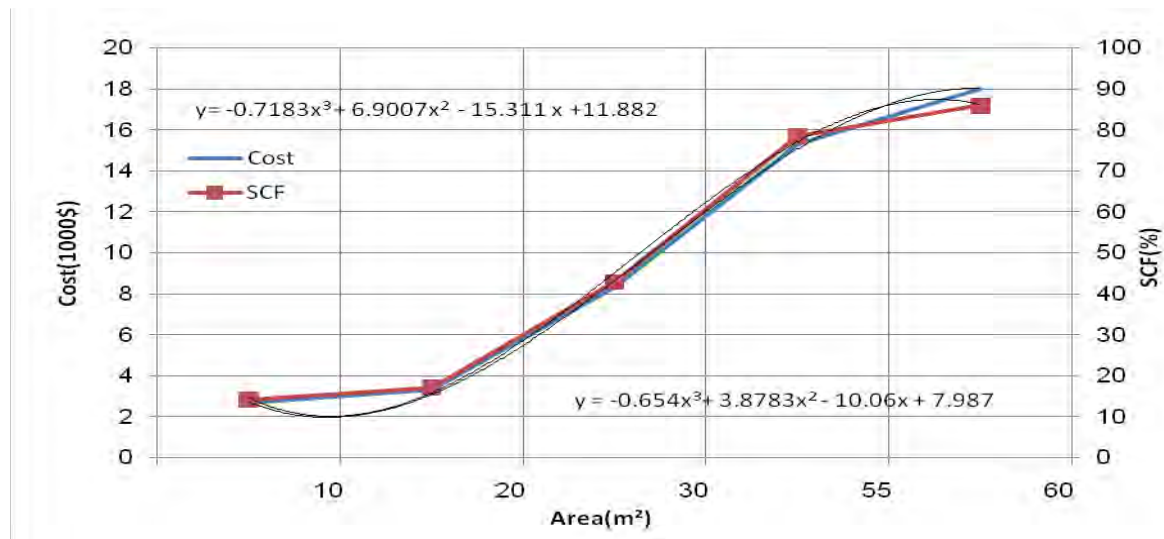


Fig. 4. Estimation of optimum solar heat pipe collectors for typical office building in Tehran

3.2. Economic analysis

Solar systems are commonly known by high investment and low operating cost. In order to estimate the payback time, total annual energy saving must be determined.

The payback time is determined by Eq. (8) [13]:

$$PB = \frac{\log\left[\frac{C}{E} \cdot \frac{i}{100} + 1\right]}{\log\left[1 + \frac{i}{100}\right]} \quad (8)$$

Where C is the capital cost of installed solar cooling equipment, E is the energy saving, i is the energy inflation and PB is the payback time.

The cost of equipments are summarized in table 1 and the cost of energy is shown in table 2.

Table 1. Cost of equipments

Equipment	Cost
LiBr-H ₂ O Absorption chiller	500 \$/KW
Heat pipe solar collector	278 \$/m ² absorber area
Auxiliary heater	50 \$/KW
Storage tank	790 \$/m ³
Cooling tower	65 \$/KW

Table 2. Cost of Energy

Energy	Cost
Electricity	0.330 \$/KWh
Oil	1.580 \$/t
Natural Gas	0.40 \$/m ³ (2010)

Furthermore, during the economic analysis some basic assumptions are needed, such as maintenance costs, installation costs, the energy inflation and natural gas heating value. The maintenance costs are 1% of investments cost [13], installation costs are 12% of the equipment costs [14], the energy inflation is about 2% [5] and natural gas heating value is about $38376 \frac{\text{Kj}}{\text{m}^3}$.

Consequently, the total energy and money saving are shown in table 3.

Table 3. total energy and money saving

Annual energy saving (MWh)	Annual money saving (\$)	Annual natural gas saving (m ³)
25.5	960	2400

Thus, with calculating *PB* through equation 8, the payback time is estimated approximately 13 years which would be reasonable for solar cooling systems.

4. Conclusions

In this investigation the technical and economical analysis for single effect LiBr-water solar absorption system was done. The analysis was accomplished for a typical office building in Tehran. The plant provided air conditioning for a floor space of 280m². Furthermore, the plant included an auxiliary fossil system and its capacity was about 13KW. The most important advantage of this system is that it offers the highest environmental benefits. The other advantage is that we utilize the highest total energy saving.

It was shown that the solar cooling fraction for mentioned office building was 64.3% and the optimum solar heat pipe collector area was 45m². It means that this plant utilizes 16 collectors which everyone compromises 30 tubes. Finally, the payback time of this plant was estimated about 13 years.

References

- [1] P. Bermejo, F. Javier Pino, F. Rosa, Solar absorption cooling plant in Seville, Solar Energy 84, 2010, pp. 1503-1512.
- [2] JA. Duffie, WA. Beckman, Solar engineering of thermal processes, Wiley, Third edition, 2006, pp. 579-587
- [3] W. Sparber, A. Napolitano, P. Melograno, Overview on worldwide installed solar cooling systems, Proceedings of 2nd international conference on Solar air conditioning, 2007, Spain
- [4] T.Y. Bong, K.C. NG, A.O. Tay, Performance study of a solar powered air conditioning system, Solar Energy 39, 1987, pp. 173-182.
- [5] M. Balghouthi, M. Hachemi Chahbani, A. Guizani, Solar powered air conditioning as a solution to reduce environmental pollution in Tunisia, Desalination 185, 2005, 105-10.
- [6] F. Assilzadeh, SA. Kalogirou, Y. Ali, K. Sopian, Simulation and optimization of a Libr solar absorption cooling system with evacuated tube collectors, Renewable Energy 30, 2005, pp. 1143-1159.

- [7] M.R. Yeung, P.K. Yuen, A. Dunn, L.S. Cornish, Performance of a solar powered air conditioning system in Hong Kong, *Solar Energy* 48, 1992, pp. 309-319.
- [8] B. Safaie, M. Khalaji Aassadi, H. Taghizadeh, A. Jilavi, G. Taleghani, M. Danesh, The evaluation of solar radiation potential in Iran, *Proceeding of 19th international conference on Power System*, 2004, Iran.
- [9] R. Parand, B. Rashidian, A. Ataei, KH. Shakibi, Modeling the transient response of the thermosyphon heat pipes, *Journal of Applied Sciences* 9(8), 2009, pp. 1531-1537.
- [10] J. Facao, A.C. Oliveira, Analysis of a plate heat pipe solar collector, *International Journal of low carbon technologies*.
- [11] The German solar energy society, *Planning and installing solar thermal systems*, Earthscan, Second edition, 2010, pp. 30-33
- [12] A. Ataei, M. Khalaji Assadi, R. Parand, N. Sharee, M. Raoufinia, A.H Kani, Solar combi-systems a new solution for space heating in buildings, *Journal of Applied Sciences* 9(8), 2009, pp.1458-1465.
- [13] G. Zidianakis, Th. Tsoutsos, N. Zografakis, Simulation of a solar absorption cooling system, *proceeding of 28th conference on building low energy cooling and advanced ventilation technologies in the 21st century*, 2007, 1187-1194
- [14] M. Peters, K. Timmerhaus, R. West, *Plant design and economic for chemical engineers*, McGraw-Hill, Forth edition, 1991.

Design analysis for expansion of Shiraz solar power plant to 500 kW power generation capacity

K. Azizian^{1,*}, M. Yaghoubi¹, R. Hesami¹, P. Kanan²

¹ Mechanical Engineering School, Shiraz University, Shiraz, Iran

² SUNA, Iran Renewable Energy Organization, Tehran, Iran

* Corresponding author. Tel: +989173029791 Fax: +987112301672, E-mail: kian_azizian@yahoo.com

Abstract: Various projects have been developed to use solar energy and some of them are in the course of developing all around the world. In Iran a 250 kW pilot solar power plant is constructed using parabolic trough collectors from 2001 to 2006. Results of thermal tests of the plant leads to the generation of steam with 250 °C temperature and 2 MPa pressure. Based on several years of experiments (from 2006-2010) it is decided to expand the solar thermal power rate to produce 500 kW electricity by combining the present system with a larger size collector and an auxiliary boiler. This article, explains the thermal design of the new collector and then various design options for combination of the new collector to the present plant have been studied and the most practical method of producing 500 kW is selected applying first law of thermodynamics utilizing a hybrid system.

Keywords: Solar power plant, Shiraz solar Thermal Power Plant (STPP), solar parabolic collector, plant expansion

1. Introduction

One of the most important problems for industrial countries in the upcoming decades is the replacement of fossil fuel energy sources with renewable energy technologies. Environmental pollutions, increasing price rate of fossil fuels and their limited sources has led to the development of new design and concepts for their replacement with cheap and available environmental friendly energy sources. Among them solar energy is one of the most important and available source of renewable energy all around the world and especially in Iran. The use of solar energy is daily growing in different fields such as generation of electricity [1]. In Iran several projects are defined to use this source of energy along with other countries of the world [2]. Among them, Shiraz solar Thermal Power Plant (STPP) is the first parabolic trough solar power plant constructed and tested successfully at Fars province at south of Iran. After the basic design and simulations [3-4], construction, installation and start-up of this power plant has been done to produce superheated vapor. For this plant different studies and simulations are made to find the overall performance of the plant [5-11]. Table 1 shows general specifications of the 250 kW STPP(Refer to [12] for more information on existing system operation).

After the successful testing of this parabolic solar power plant (from 2006-2010), it is decided to promote the system with advanced technologies and use an advanced parabolic trough collector for steam generation. This is made by beginning the constructing and installing a new parabolic trough collector with larger dimension and combining it with the existing system while increasing the power rate to 500 kW. The existing 250 kW Shiraz solar power plant, having been successfully tested for steam generation, uses old design, small parabolic trough collectors. Achieving the technology of parabolic trough collectors in the 250 kW power plant the following decisions were made:

- 1- Design and construction of a new collector, in the same dimensions as used in the new solar power plants of the world (such as Andasol plants).
- 2-Electricity generation

Table 1. Specification of 250kW Shiraz solar thermal power plant

Capacity	250 kW	Electricity generation System	Turbine+ Generator
Collectors Type	Parabolic Trough	Collector's Field Inlet Oil Temperature	231 °C
No. of Collectors	48	Collectors Field Outlet Oil Temperature	265 °C
Collector's Dimension	25×3.4 m ²	Oil Mass Flow Rate	13.7 Kg/s
Collectors' Driven System	Hydraulic	Steam Mass Flow Rate	0.673 Kg/s
Collector's Structure	Truss with Torsion Bar	Generated Steam Temperature	250 °C
Heat Transfer Fluid	Thermal Oil	Generated Steam Pressure	2 MPa

These steps would lead to an increase in power plant capacity from 250 kW to 500 kW and at the same time design and construction of a new collector in length of 94 m and aperture width of 5.27 m. The main problem in the way of developing the power plant (except for the cost increase due to low capacity of turbo-generator system and high price of electricity generated) is the method of combining the new collector with the existing system. Due to the high operating temperature of the new collector compared to the existing system, optimal usage of the absorbed heat is the most important issue in the process of combining the two systems of heating the old cycle primary fluid (oil) or its secondary fluid (superheated steam) or a combination of the two above. In addition to the above mentioned issue, the next step would be the selection of the appropriate turbo-generator considering the efficiency and price at the same time. Some explanations in this regard will follow. The most important equipment in the existing plant include the parabolic trough collectors field, heat storage and expansion tanks, three heat exchangers, deaerator and etc. To achieve the 500 kW power generation the equipment that shall be added to the system would be the new 100m collector, turbo-generator, storage and expansion tanks, fossil fuel boiler and condenser. In the following sections further explanation and results of thermodynamic analysis of the new design system are presented.

2. Design of new parabolic trough collector

After preliminary assessments [12] it was decided to construct and install a new collector and increase the capacity of the plant from 250kW to 500 kW. Based on these available technologies the design of the new collector of Shiraz solar power plant is made by following steps:

- 1-Thermal and thermodynamic design of collector
- 2-Design of structure and hydraulic system
- 3-Design of control and tracking system

2.1. Thermal design of Shiraz thermal solar power plant (STPP) with new collector

For thermal design and simulation of the new collector a program has been developed with Matlab software [13]. This program takes some primary data into account such as collector rim angle, optical properties of the mirror like its thickness and reflectance coefficient, errors in construction and installation of the collector, temperature of inlet and outlet of oil from the collector, temperature rise in the collector, date and day of design and its relevant data such as cloud factor, wind speed and ambient temperature, geographical location of the design point

and length of the collector. Some other information for the receiver tube such as absorbtivity coefficient of the tube, transmisivity coefficient of the glass tube, thickness of the glass cover tube and its diameter would be considered as input data to this program. The input data screen of software is shown in Fig.1.

INPUT PARAMETERS			
Calculation number:	1		
You can change data only in the last calculation page number ,then push "compute" pushbotton			
<input type="radio"/> Non Evacuated		<input checked="" type="radio"/> Evacuated	
Flim Angle(45.60.75.105)	90	Collector Length(m)	100
		Mirror Dia(cm)	500
		Absorber Thk(cm)	0.2
Glass Thk(cm)	0.3	Absorber Emmitance	0.25
		Absorber Conductance	58
		Glass Emmitnce	0.9
Reflectivity	0.9	Transmissivity	0.9
		Absorbtivity	0.9
		Sigmacontour(mRad)	2.2
Sigmacontour2	2.2	Sigmaspecular	2.2
		Sigmaspecular2	2.2
		Sigmatracking	2.2
Sigmadisplacement	2.2	Sigmasunnoonaverage	4.1
		Landa	0.1
		Tambient(K)	303
Tinlet(K)	503	Temp Diff(K)	40
		Design Day(1-365)	266
		LatitudeAngle	29.5
Cloud Factor	0.13	Wind velocity(m/s)	7
<input type="button" value="Calculate"/>			

Fig. 1. Data input of developed collector design software

The output of this simulation program include the total optical error, concentrating ratio, direct radiation (based on Daneshyar model[5]) effective length , oil mass flow rate, optical and thermal efficiency, heat loss and heat absorbed in each m^2 of the receiver tube surface. The allowable total error for the design of collector is calculated based on [14].

Collector design is based on Rabl et al. [15] procedure. The details of calculation procedure are explained in [13]. The thermal design of the collector is made for September 23rd at in the noon time for Shiraz (with latitude of 29.53°). Solar radiation is modeled from [5] relations, wind speed is assumed to be 7 m/s and ambient temperature is considered 30°C. Regarding the limitation of construction of collector structures hydraulic system and etc it is decided to construct a new collector parallel to the existing field of collectors, therefore the length of new collector is considered to be 100 m equal to the available space in the field. Results of calculation and specifications of the new collector of Shiraz solar power plant is presented in Table 2.

3. Combining the new collector with present system

The next step after designing the collector is to combine the collector to the present system showing in Fig 2. Regarding the differences between the oil used in the present collectors field (Behran thermal oil) and the new collector (VP1) and also the higher oil temperature of fluid in the new collector, combining the new collector to the present system need some considerations such as the transferring the absorbed heat in new collector to the secondary

fluid (the oil in the present cycle or produced steam), selection of turbine type, new control philosophy, etc. Therefore it was decided to study the two important issues of the new cycle:

- 1- The way of using the absorbed heat (either transmitting the absorbed heat to the steam in order to superheat it or to heat the oil or a combination of these two).
- 2- Selecting the exhaust pressure of steam turbine.

Table 2. Specifications of the new collector of Shiraz solar power plant

Input Parameters			
Rim Angle(Degree):82	Length (m): 94	Absorber Tube Dia. (m): 0.07	Absorber Emittance: 0.15
Absorber Absorbance: 0.94	Mirror Reflectance:0.90	Glass Transmittance: 0.9	σ - contour (mrad): 2.5
σ - specular (mrad): 2.5	σ - tracking (mrad): 3	σ - displacement (mrad): 3	T-ambient (K): 303
T-inlet (K): 567	T-rise (K): 19	Design Day: 23rd Sep.	Latitude Angle: 29.53
Output Parameters			
Avg. direct radiation (W/m2): 647.3	Avg. diffuse Radiation (W/m2): 84	Noon. Direct radiation (W/m2): 817.4	Noon diffuse Radiation (W/m2): 145.4
Concentrating ratio: 23.97	Mass flow rate (kg/s): 4.53	σ - total (mrad): 4.1	Mirror aperture width (m): 5.27

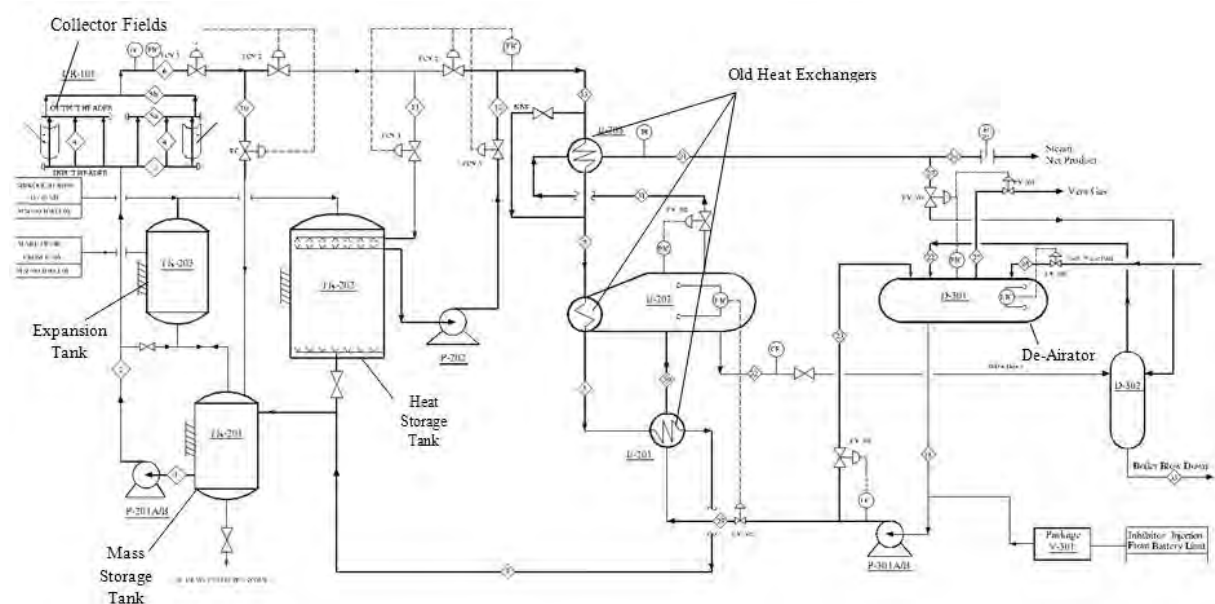


Fig. 2. The present PFD (Process & Flow Diagram) of STPP

Regarding the above objects, thermal design of the integration is made for two cases A and B. In case A, it is assumed that all the heat absorbed by the new collector would be transferred by an exchanger to heat generated steam in the present cycle and generated steam in the boiler, that leads to temperature rise of operating fluid in the new cycle. The heat absorbed will consequently lead to increasing steam temperature which leads to producing more electricity. In case B, the assumption is that a part of the heat absorbed in the new collector would be used to increase the temperature of superheated steam from the existing system and the rest of absorbed heat is used for heating up the outlet oil of existing collector field in order to increase the steam mass flow rate and consequently increasing the electricity generation. In this case 120 kW of the absorbed heat in the new collector is transferred to raise oil temperature and the rest (about 80 kW) will be used for superheating the generated superheated steam in the present cycle.

For each of the above cases 3 turbine outlet steam pressures of 100 kPa , 25kPa (using back pressure type turbine) and 10 kPa (using condensing type turbine) has been considered and the thermodynamic analysis for each case is carried out separately.

Considering the goal to produce 500 kW electricity power from the combination of the present plant and the new system, it is decided to add an auxiliary boiler to the system in order to compensate the superheat steam for generating 500 kW electricity and to provide possibility of using the power plant at night time. Fig. 3 shows results of thermodynamic analysis and condition for various cases studied. The estimated capacity for each equipment in each condition are provided in this table.

CASES	Farm Generated Steam				Boiler				Considered Shaft Power (kW)	Turbine			Condenser		
	Temp (°C)	Press (kPa)	Flow rate (kg/h)	Working Capacity (kg/h)	Installed Capacity (kg/h)	Boiler load (%)	Press. (kPa)	Temp. (°C)		Inlet Press. (kPa)	Inlet Temp. (°C)	Exhaust Pressure (kPa)	estimated steam consumption (kg/h)	Duty (kW)	
CASE A	100 kPa	250	2130	2389	3112	6000	52	2130	237	532	2100	294	100	5490	3429
	25 kPa	250	2130	2437	1951	5000	39	2130	215	532	2100	294	25	4095	2605
	10 kPa	250	2130	2486	1466	4500	33	2130	215	532	2100	294	10	3566	2286
CASE B	100 kPa	294	2130	2573	2912	6000	49	2130	294	532	2100	294	100	5467	3409
	25 kPa	294	2130	2573	1792	5000	36	2130	294	532	2100	294	25	4096	2605
	10k Pa	294	2130	2573	1336	4500	30	2130	294	532	2100	294	10	3558	2279

Fig.3. Results of calculators for the 6 primary plans cases

4. Selection of the appropriate plan

After considering the primary plans and the economical evaluation, one of the plans should be selected as the design plan. Each plan has some advantages and disadvantages. A list of the most important ones are summarized in Table 3.

The next step to choose a proper plan based on cost and other parameters. The most expensive equipments are condenser, turbine and boiler. Price quotations are gathered from local and international manufacturer for these three equipments. The relative cost with respect to case A of 100 kPa turbine outlet pressure is presented in Table 4.

Table 3. Results Advantage and disadvantages of case A and B

Case	Advantages	Disadvantages
A	Higher thermodynamic efficiency for exhaust pressure of 10 kpa	Dependency of electricity generation on the solar part
	Lower expenses due to use of a single heat exchanger	Impossibility of complete heat absorption of the new collector in the system
	Shutting down of present collectors there will be a possibility of using the heat absorbed by the new collector	Impossibility of separating contribution of solar part & fossil fuel part power generation
	Boiler working at a lower temperature	Un-available of the new collector, steam for turbine would not be at design condition
	Lower boiler loss for lower exhaust pressures.	Lower performance of one exchanger compared to two exchangers Impossibility of the new collector operation without boiler for produce power
B	Possibility of performance tests of new collector without boiler	Two heat exchangers needed Complicated control system
	Equal importance of solar part and fossil fuel part	With shutting down of present collectors field the new collector can be used to heat the oil in collectors field
	Independency of solar and fossil fuel parts	
	Possibility of electricity generation in case of an availability of solar part	
	Possibility of electricity generation with lower capacity in case that new collector is out of service	
	Better performance of two exchangers compared to one exchanger	
Lower capacity of boiler in the exhaust pressure of 25 Kpa		

Table 4. The relative cost of the new cycle for various cases

Case	Boiler	Turbine	Condenser	Total
A (Pout=100 kPa)	1	1	1	1
A (Pout=25 kPa)	0.8704	2.5129	2.0218	1.8140
A (Pout=10 kPa)	0.8055	2.5086	0.5523	1.4142
B (Pout=100 kPa)	1	1	1	1
B (Pout=25 kPa)	0.8704	2.5129	2.0218	1.8140
B (Pout=10 kPa)	0.8055	2.5086	0.5523	1.4142

One of the most important issue to be addressed before selection of a proper case is the type of condenser needed for the 3 exhaust pressures of the steam turbine. According to the estimations and calculations for turbine with 100 kPa and 25 kPa exhaust pressure the condenser needed could be air cooled type condenser, whereas for 10 kPa exhaust pressure, the condenser should be water cooled type. In case of using water cooled type condenser water a significant amounts of will be vaporized in the cooling tower.

According to Table 5, for the 3 items (turbine condenser and boiler) for each case A and B the final cost. A direct function of turbine price and consequently the boiler and condenser. Therefore it is observed that for both cases A and B for the different exhaust steam pressure the final cost is equal but regarding Fig. 3 the load of boiler in case of 10 kPa exhaust pressure is less than the case of 25 kPa exhaust pressure. In the same manner less than 100 kPa steam exhaust pressure, which would lead to lower fuel consumption and less fuel cost in the long term. But it must be mentioned that the weakness of 10 kPa exhaust pressure in comparison to the two other exhaust pressures is the requirement of water to cool the exhaust steam from turbine. Calculations show that the consumption of water in the power plant with capacity of 500 kW would be approximately 6.8 m³/hr. Due to the great limitations of water in the present plant location and for most part of Iran the case B with an exhaust steam pressure of 25 kPa has been selected as the final plan. This is due to relatively higher efficiency, lower water consumption and lower risk with air cooled condenser in spite of higher final cost. Fig. 4 shows the PFD (Process Flow Diagram) of the selected plan.

5. Conclusion

For Expansion of STPP the case B with exhaust turbine of 25 kPa is selected based on following advantages:

- 1-The selected power plant configuration has lower water consumption, which is critical for the arid region of Iran. This will be more economical to install large plant in the semi-arid region of Iran with no available water sources.
- 2-In the selected configuration, lower fossil fuel needed for generating 500 kW electricity energy (because of lower boiler load).
- 3-Solar and fossil part of the plant can operate and be assessed separately.
- 4-Performance of new designed collector can be measured during normal operation of the plant or individually.

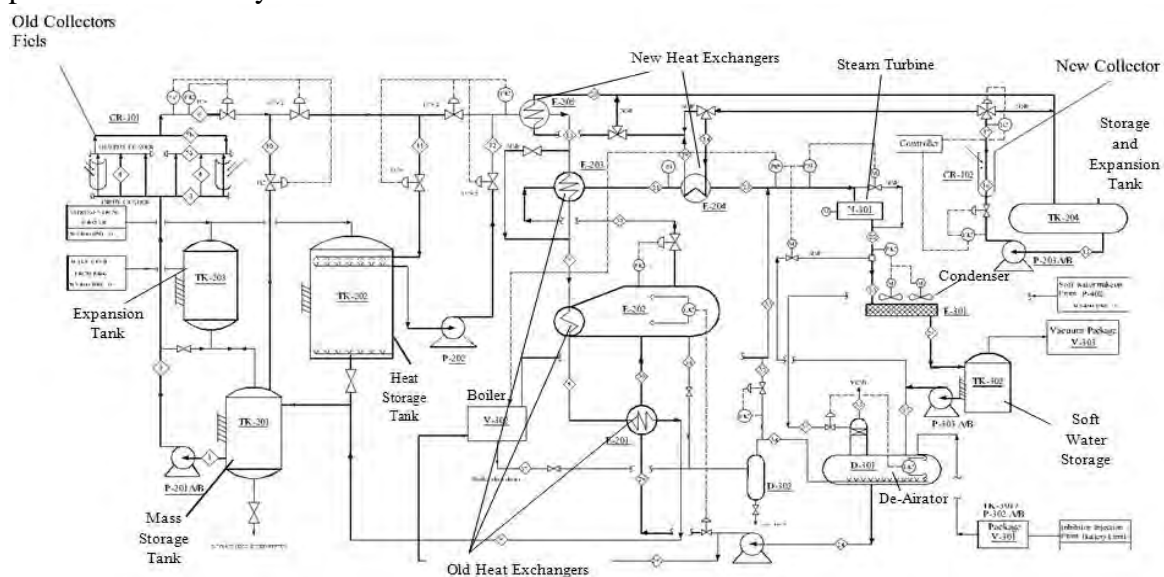


Fig. 3. PFD of the integrated 500 kW Shiraz parabolic trough solar power plant

Reference

- [1] C. Ramos, R. Ramirez, J. Laguns, Potential assessment of concentrating solar technologies for electricity generation in Mexico, Proceeding of SolarPACES 2009, Berlin, Germany, September 2009.
- [2] N. Supersberger, Energy scenario analysis of the Iranian energy system: role of renewable energy, Proceeding of SolarPACES 2009, Berlin, Germany, September 2009.
- [3] M. Yaghoubi, R. Mehryar, Design and Performance simulation of a 250 kW solar Thermal power plant for Shiraz, Iranian Journal of Energy, Vol. 3, 1999.
- [4] A. Kenary, M. Yaghoubi, F. Doroodgar, Experimental and numerical studies of a solar parabolic trough collector of 250 kW pilot solar power plant in Iran. Sharjeh Solar Energy Conference, Sharjeh, UAE, February 2001.
- [5] M. Yaghoubi, K. Azizian, A. Kenary, Simulation of Shiraz solar power plant for optimal assessment, Renewable Energy, Vol.28, 2003.
- [6] M. Yaghoubi, K. Azizian M. Salim, Shiraz solar power plant simulation with variable heat exchanger performance, Proceeding of ESDA04, 7th Biennial Conference on Engineering Systems Design and Analysis, Manchester, United Kingdom, July 2004.
- [7] N. Naeeni, M. Yaghoubi, Analysis of wind flow around a parabolic collector (1) fluid flow, Renewable Energy, Vol.32, 2007.
- [8] N. Naeeni, M. Yaghoubi, Analysis of wind flow around a parabolic collector (2) heat transfer, Renewable Energy, Vol.32, 2007.
- [9] M. Yaghoubi, A. Mokhtari, R. Hesami Thermo-economic analysis of Shiraz solar thermal power plant, Proceedings of the Third International Conference on Thermal Engineering: Theory and Applications Amman, Jordan, May 2007.
- [10] K. Azizian, M. Yaghoubi, J. Ghadiri, Optimal performance of Shiraz solar thermal power plant by exergy analysis, Proceedings of the Fourth International Conference on Thermal Engineering: Theory and Applications, Abu Dhabi, UAE, January 2009.
- [11] I. Niknia, M. Yaghoubi, Transient analysis of integrated Shiraz hybrid solar thermal power plant, Proceeding of World Renewable Energy Congress, Abu Dhabi, UAE, September 2010.
- [12] K. Azizian, M. Yaghoubi, R. Hesami, S. Mirhadi, Shiraz pilot solar thermal power plant design, construction, installation and commissioning procedure, Proceeding of HEFAT2010, 7th International Conference on Heat Transfer, Fluid Mechanics and Thermodynamics, Antalya, Turkey, July 2010.
- [13] M. Yaghoubi, M. Vazin, A. Kenary, Optimal assessment of parabolic trough collectors design, Proceeding of 17th International electricity engineering conference of Iran PSC 2002, Tehran, Iran, May 2002.
- [14] A. Vadeei, M. Yaghoubi, R. Hesami, P. Kanan, Optical assessment of Shiraz solar power plant collectors, Proceeding of 15th International mechanical engineering annual conference of Iran ISME 2007, Tehran, Iran, May 2007.
- [15] A. Rabl, P. Bendt, H. W. Gual, Optimization of parabolic trough solar collectors, Solar Energy, Vol. 29, No.5, 1982.

Thermal regimes in solar-thermal linear collectors

Javier Muñoz*, José M. Martínez-Val, Rubén Abbas

Grupo de Investigaciones Termoenergéticas ETSII- Madrid Polytechnic University

* Corresponding author. Tel: +34 913363128, Fax: +34 913363079, E-mail: jamunoz@etsii.upm.es

Abstract: In this paper the physics of linear receivers is analyzed. This analysis is oriented to evaluate the dependence of the thermal performance of the receiver on the characteristics of the concentrated solar radiation. It will be seen that two thermal regimes can be distinguished in that dependence, what will point out the need of studying at depth the features of systems with moderate concentration factors.

A fundamental question can be formulated as follows: what is the concentration factor required for obtaining the best solar energy exploitation within a design window established by some technical constraints?

In this performance analysis it has been found that moderate concentration factors (about 20 to achieve 400°C) can be close to optimal in a cost benefit analysis, taking into account temperature constraints. Beyond these values, thermal and exergetic efficiency curves advice to limit the concentration factors to values that could be achievable by linear Fresnel reflecting collectors, avoiding mobile parts such as ball-joints or flexible joints that could be important leak-points, as well as metal-glass welds, which are another cause of failure in trough collectors

Keywords: Renewable energy, Concentrated solar energy, Linear receiver, Fresnel

Nomenclature

α	selective coating absorptivity	-	Q_{rad}	radiation thermal losses	W/m^2
C_f	concentration factor	-	Q_{sun}	available thermal power	W/m^2
DNI	direct normal radiation	W/m^2	Q_{use}	transferred power to the fluid	W/m^2
ε	selective coating emissivity	-	T_a	bulk temperature of the air	K
η	efficiency	-	T_c	absorbing surface temperature	K
η_{ex}	exergetic efficiency	-	T_{env}	environment temperature	K
η_{th}	thermal efficiency	-	T_f	heat carrier temperature	K
$\eta_{th \rightarrow e}$	thermo-electrical conversion efficiency	-	T_{grnd}	ground temperature	K
h	heat transfer coefficient	$W/m^2 \cdot K$	T_{sky}	high atmosphere temperature	K
Q_{conv}	convection thermal losses	W/m^2				

1. Introduction and background

One of the most critical decisions in the design of a solar thermal power unit is the choice of the radiation concentration geometry [1] [2], which is in turn connected with the thermal flux needed in the receiver for fulfilling the objectives of the plant. In this context, technical coherence is a major word. In particular, if a high value is chosen for the concentrated radiation thermal flux, the global heat transfer coefficient of the transfer from the receiver surface to the heat carrier fluid must have a similarly high value [1] [2]. Otherwise, the temperature difference between the receiver and the fluid would be very large, which would enhance thermal losses from the receiver. Besides that, large temperatures differences between different parts of the receiver will convey important differential dilation effects, which can be a major cause of concern in the durability of a solar power collector.

There are two main approaches for concentrating solar radiation [1] [2]:

- Parabolic troughs [3] and linear Fresnel concentrators [4], with one axis tracking.
- Revolution parabolic disks and central tower receivers [1], with a two axes tracking system.

The latter is out of the scope of this article, aimed at analysing the thermal features of linear technologies. The receivers involve a long pipe (or a set of parallel pipes, in a general approach) with a selective coating [5] covering its absorbing surface, i.e., the surface where the concentrated solar radiation impinge. This coating is chosen for having a high absorptivity to solar photons and a low emissivity for photons of the planckian spectrum at similar temperatures to the working ones in the receiver.

Inside the tube, the heat carrier fluid circulates from one end to the other. In most of the cases, collectors are placed in a parallel lay-out, with a high pressure header for distributing the fluid from the central block of the plant (the BOP) and a low pressure header that collects the streams of all the parallel solar receivers and sends the total hot stream into the BOP.

A third line of solar power plant configuration can be cited, the Solar Boiler [6], which is based on a central tower, but without a single central receiver in the top of the tower. The receiver is a bundle of tubes going up along the wall of the tower. This set of tubes can be considered as a linear receiver, although radiation would be concentrated by reflection from a field of heliostats very similar to the central receiver case.

The selective coating is the radiation absorbing element, and it is the component reaching the highest temperature. The useful heat is carried by the fluid and its actual exergy value will depend on the temperature achieved when it leaves from the collector. In some applications, boiling inside the receiver tube is considered, and the steam title will also be a relevant parameter. In general, the increase in specific enthalpy and the mass flow are the variables characterizing the heating of the fluid. In this context, two energy balances must be taken into account: the overall heating of the fluid, which is equal to the total energy transferred from the absorbing surface to the heat carrier fluid, and the detailed heat transfer balance, which depends on the temperature map attained in the collector due to the transmission processes among the components of the collector, with two main results:

- Heat transfer to the carrier fluid, which is the basis of the overall energy balance
- Losses to the environment, mainly through convection to air and radiation to the surroundings

Heat transfer to the carrier fluid depends on its velocity. The convection coefficient between the tube and the fluid can be increased by increasing its speed, but this fact has other effects, as an increase in pressure drop and pumping power [7] [8]. For liquids, this effect can be of second order as compared to the thermal problem. For gases, the mechanical problem can be as important as the thermal one, and the pumping power needed to keep the gas flow at the level required by the thermal requirement, can be as large as the power collected from the sun, what makes the plant useless.

Another important point in the design of the system is the actual limitations in the temperature of the different components. This is the case of the selective coating, which sets up a ceiling to the maximum temperature allowed in the collector. Coatings resisting 500 °C without degradation are commercially available, but this is not usually the binding limitation, because in current trough-collector power plants, the most popular heat carrier fluid is synthetic oil, such as Therminol VP1 and the maximum working temperature is below 400 °C.

Those limitations in temperature convey similar limitations in the maximum thermal flux impinging on the receiver, and therefore in the concentration factor. Nevertheless, those

limitations in the temperature of some materials have to be assessed in the full analysis of the system. If it is effective in transferring the heat to the carrier fluid, and the flow is large enough for guaranteeing a controlled heating, all temperatures will be within the corresponding limits. However, this guarantee relies on the proper circulation of fluid, and it embodies the afore-mentioned problem of the required pumping power.

This coupling of thermal and hydraulics constraints can be characterized in the case of linear collectors, to identify optimum solutions in some design windows, particularly aimed at reducing the cost of solar power plants. This optimization process will embody an exergy analysis of a system featured by the working temperature reached by the heat carrier fluid.

2. Methodology: A linear collector model

There are detailed physical and numerical models to calculate trough collectors and reflection Fresnel devices [6] [9] [10]. They are particularly useful to feature a power plant in nominal conditions, which include the set of variables to define the calculation of the collector for the reference conditions chosen as nominal ones, and they can also be used for integrating the performance along the year.

The model used for this study works in similar form to that used in Muñoz et al [6], but does not take into account neither the way used for concentrating the solar radiation, nor the natural aperture of the sun beams, which is an important factor when the concentration geometry involves large distances.

This model can be described as a lumped-parameters representation of the collector. It includes an expression for featuring the useful heat, which is associated with a temperature in the carrier fluid at the collector outlet. The model can be used for investigating the relative importance of some parameters, or equations coefficients, and for identifying relevant trends in the evolution of the system when the boundary conditions change, including the change in the concentration of solar radiation.

The simplicity of the model does not allow using it for designing purposes, or for optimizing a system, but the model is easily followed, unlike many computational codes, which are managed as black boxes. The model is based on the equations listed below, and it can be used to feature general trends in the behaviour of the linear receivers. It is obvious that some hypotheses can not be kept in detailed computations, which are needed for calculating a given design in specified conditions.

The model is an integrated energy balance where the impinging radiation on the receiver goes to useful heat or to thermal losses (convection through the air and radiation to the background). Both thermal phenomena involve several heat transfer mechanisms, but they can be lumped into a single step, expressed in terms of the difference between relevant temperatures, and they include a coefficient, to which an effective value must be assigned. Those values can be estimated from previous detailed calculations of similar systems or from the bibliography. Moreover, sensitivity calculations can easily be carried out by varying those values and other parameters characterizing the boundary conditions.

Four temperatures are sufficient to define the model:

- The temperature T_c of the absorbing surface (selective coating) where the concentrated radiation impinges. It represents an average value of the coating temperature

- The temperature of the heat carrier fluid as an average value as it is heated along the receiver, T_f
- The bulk temperature of the air, T_a
- The temperature of the background radiation or environment, T_{env} . It can represent either the temperature of the earth's surface, T_{grnd} , or the temperature of the high atmosphere [1][11], T_{sky} , each one being affected by their corresponding view factor from the receiver (detailed analysis of this matter demonstrates that for the considered values this dependence has no relevant effect on the results)

Additional parameters of the model are the following ones. (Values assumed for the first set of calculations are given within brackets.):

- DNI = direct normal irradiation (1 kW/m²)
- C_f = concentration factor (variable)
- ε = selective coating emissivity (0.1)
- α = selective coating absorptivity (0.9)
- U = global coefficient for convection losses (8 W/m²·K)
- h = global coefficient for heat transfer from the absorbing surface to the heat carrier fluid (2 kW/m²·K)

In general, for all calculations the boundary conditions temperatures are:

- $T_{air} = 25\text{ °C}$ (=298 K)
- $T_{grnd} = 25\text{ °C}$ (=298 K)
- $T_{sky} = 0.0552 \cdot T_{air}^{1.5}$ [K] [11]

The model is defined by the following equations:

$$Q_{sun} = Q_{conv} + Q_{rad} + Q_{use} \quad (1)$$

$$Q_{sun} = C_f \cdot \alpha \cdot DNI \quad (2)$$

$$Q_{conv} = U \cdot (T_c - T_{air}) \quad (3)$$

$$Q_{rad} = \varepsilon \cdot \sigma \cdot (T_c^4 - T_{env}^4) \quad (4)$$

$$Q_{use} = h \cdot (T_c - T_{use}) \quad (5)$$

The absorbed energy and losses that are produced by convection and radiation, adding the cooling effect of the heat transfer fluid (thermal oil) determines the temperature level and the energy efficiency in the receiver itself that can be given, in function of the enthalpy increase in the heat transfer fluid (Q_{use}) by:

$$\eta_{th} = \frac{Q_{use}}{Q_{sun}} \quad (6)$$

Thermal efficiency is not sufficient to characterize a system designed to yield useful work against the environment: we also use the exergetic efficiency (η_{ex}) that take into account the

required blower power (W_b) with $\eta_{th \rightarrow e}$ is the conversion efficiency from thermal to electrical energy, evaluated as 33% [6]:

$$\eta_{ex} = \frac{Q_{use} - W_b}{Q_{sun}} \cdot \eta_{th \rightarrow e} \cdot \left(1 - \frac{T_a}{T_{use}}\right) \quad (7)$$

3. Results

This physical model has been applied to some simplified cases with the coefficients already given (first series of calculations) and the results are depicted in Fig. 1 and Fig. 2. It is worth commenting on the shape of the efficiency curve (thermal and exergetic), with two branches that are associated to two thermal regimes: a first branch with rapid increase in efficiency, followed by an almost horizontal second branch, where the heat transfer process from the collector's absorbing surface to the heat carrier fluid is saturated, and the efficiency value reaches a maximum value. A threshold can be marked as the beginning of the second regime. This threshold can be featured by the value of the slope of the curve, or by the relative value to the asymptotic level of the efficiency. In the case 400°C of fluid temperature the threshold of the second regime can be marked around a concentration factor of 20. If the fluid temperature is 300 °C, the threshold in the concentration factor is about 15. With a fluid temperature of 1000 °C the threshold is at 70.

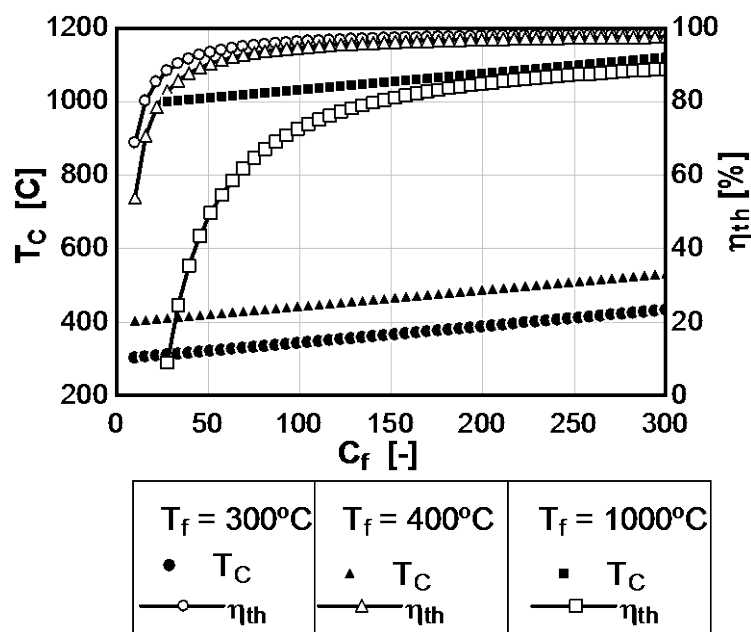


Fig. 1. Collector thermal efficiency and absorbing surface temperature Vs. concentration factor, for three values of T_f : 300 °C, 400 °C and 1000 °C. The global coefficient for heat transfer from the absorbing surface to the fluid, "h", has a value of 400 W/m²·K

It should be noted as well that the collector's absorbing surface temperature increases linearly with the concentration factor. This effect is influenced by some obvious limitations, because all materials, from the selective coating to the heat carrier fluid, have maximum operational temperatures (which can also depend on the mechanical stresses, in the case of structural materials).

As an initial advice from this analysis, it can be stated that linear collectors should be designed to operate in the saturated regime, limiting the concentration factor in order to limit

the temperatures. Moreover, the design point can be placed slightly above the threshold for that regime, if this option conveys a significant cost reduction because a lower concentration factor can be achieved with simpler and more robust collectors. Of course, this advice must be properly checked in a cost/benefit analysis, after reviewing in detail the thermo-physical features of collecting solar radiation in linear receivers.

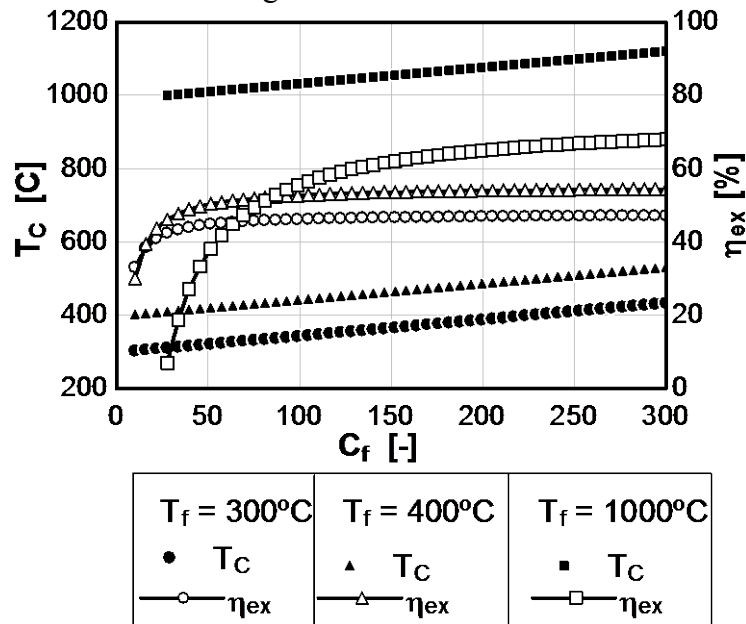


Fig. 2. Collector thermal efficiency and absorbing surface temperature Vs. concentration factor, for three values of T_f : 300 °C, 400 °C and 1000 °C. The global coefficient for heat transfer from the absorbing surface to the fluid, “ h ”, has a value of 400 W/m²·K

This finding opens a new way for Concentrated Solar Power, because a Fresnel of large size can be used for heating synthetic oil up to 390 °C, for activating a Rankine cycle similar to those of current power plants with parabolic trough collectors as Fig. 3 shows, with five Fresnel systems, each one of one total length, and all with the same impinging power: 2.5MW_{th}. The intensity goes from 5 to 25 kW/m², corresponding to lengths varying from 500 m from the former to 100 m for the latter.

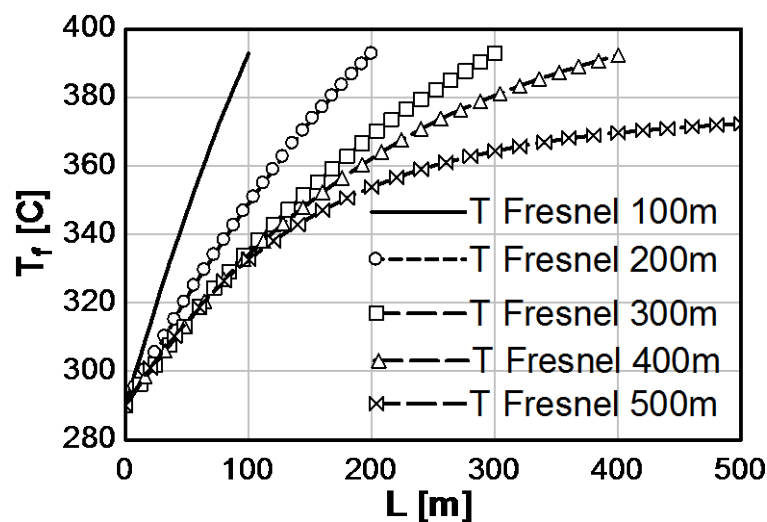


Fig. 3. Evolution of the fluid temperature along the collector length for a set of linear collectors receiving the same total power, with different radiation intensities and lengths.

It is seen that the case of 5 kW/m^2 does not reach the objective T ($392 \text{ }^\circ\text{C}$, corresponding to Therminol VP1 as heat transfer fluid), which implies that this case is below the threshold. Energy and exergy efficiencies are shown in Fig. 4, and it is seen how fast they decrease as the radiation intensity goes down. It must be said that this effect is produced, to a large extent, by the objective of achieving a final T of $392 \text{ }^\circ\text{C}$.

It is obvious that requiring higher temperatures in the fluid makes the receiver less efficient, because the temperature gap from the irradiated surface to the bulk of the fluid is shorter than the gap of less demanding collectors, and thermal losses to the surrounding materials increase, as it remains the same. So, if the fluid temperature required for a particular plant is much higher than 400°C , a Fresnel is not likely to be suitable, because its efficiency will be modest.

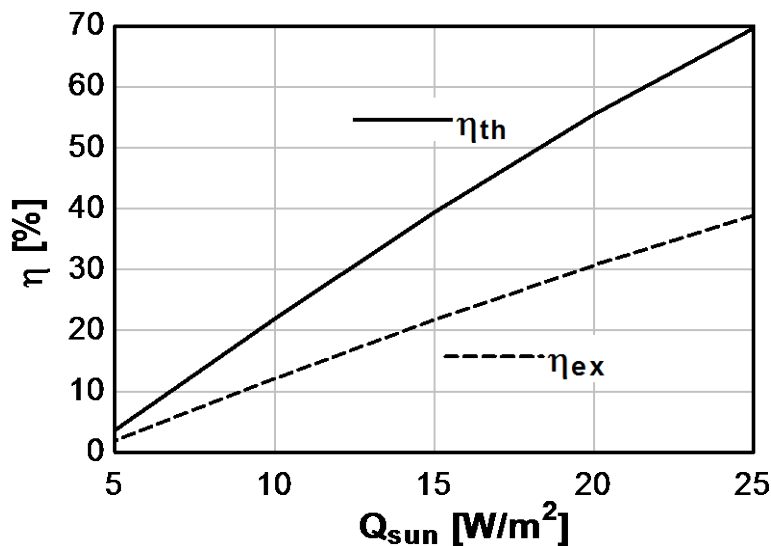


Fig. 4. Energy and exergy efficiencies of the collectors of the set introduced in the previous figure.

4. Conclusions

The analysis of thermal performance of linear collectors in the field of concentrated solar power shows the existence of two regimes: a lower regime, corresponding to small values of intensity impinging on the receiver and an upper regime, where the relevant thermal variable (notably, the efficiency) is almost saturated, opposite to the lower regime, where it increases very rapidly as radiation intensity does. The change from the lower to the upper regime is usually very well identified by a value, or a short range of values. It exists therefore a threshold for reaching the saturated regime. All these features depend on the temperature required in the heat-carrier fluid.

In this performance analysis it has been found that moderate concentration factors can be close to optimal values, due to temperature constraints. Thermal and exergetic efficiency curves show that beyond these values, i.e. increasing the concentration factor, the threshold is exceeded, and therefore efficiency increases slowly.

In the specific case of 400°C as objective temperature – usual in current solar thermal plants with through collectors that uses thermal oil – the concentration factor takes the value 20 approximately.

This observation must be properly exploited by identifying the simplest and most robust concentration scheme able to attain the upper regime of a given application, for feeding the

boiler of a Rankine cycle with given working temperatures. This is the case of linear Fresnel reflecting collectors, which avoid mobile parts such as ball-joints and flexible joints that could be important leak-points, as well as metal-glass welds, which are another cause of failure in trough collectors

References

- [1] J.A. Duffie & W.A. Beckman, *Solar Engineering of Thermal Processes*, John Wiley and Sons, New York, 2nd ed., 1991, pp. 330-378
- [2] D. Mills, *Advances in solar thermal electricity technology*, *Solar Energy*, vol. 76, no. 1-3, 2004, pp. 19-31
- [3] A. Fernández-García, E. Zarza, L. Valenzuela & M. Pérez, *Parabolic-trough solar collectors and their applications*, *Renewable and Sustainable Energy Reviews*, vol. 14, no. 7, 2010, pp. 1695-1721
- [4] D.R. Mills & G.L. Morrison, *Compact Linear Fresnel Reflector solar thermal powerplants*, *Solar Energy*, vol. 68, no. 3, 2000, pp. 263-283
- [5] M. Farooq & I.A. Raja, *Optimisation of metal sputtered and electroplated substrates for solar selective coatings*, *Renewable Energy*, vol. 33, no. 6, 2008, pp. 1275-1285
- [6] J. Muñoz, A. Abánades & J.M. Martínez-Val, *A conceptual design of solar boiler*, *Solar Energy*, vol. 83, no. 9, 2009, pp. 1713-1722
- [7] F.P. Incropera, *Fundamentals of heat and mass transfer*, John Wiley & Sons, Danvers, USA, 6th ed, 2007, pp 485-517
- [8] R.L. Mott, *Applied fluid mechanics*, 6th ed., Pearson Prentice Hall, Upper Saddle River, 2006, pp 226-245
- [9] R. Forristal, *Heat Transfer Analysis and Modelling of a Parabolic Trough Solar Receiver Implemented in Engineering Equation Solver*, NREL Technical Report, Golden, Colorado, USA, 2003
- [10] M.J. Montes, A. Abánades & J.M. Martínez-Val, *Performance of a direct steam generation solar thermal power plant for electricity production as a function of the solar multiple*, *Solar Energy*, vol. 83, no. 5, 2009, pp. 679-689
- [11] W.C. Swinbank, *Long-wave radiation from clear skies*, *Quarterly Journal of the Royal Meteorological Society*, vol. 89, no. 381, 1963, pp. 339-348
- [12] J.M. Martínez-Val, *Thermal solar energy collector*, Es 2 231 576, P CT/ES2009/000557, WO2010/076350 08 July 2010 (08.07.2010)

Surface temperature distribution and energy gain from semi-spherical solar collector

Ilze Pelece*, Imants Ziemelis, Uldis Iljins

Latvia University of Agriculture, Jelgava, Latvia
*Corresponding author: E-mail: ilze.pelece@llu.lv

Abstract: Usual constructions of solar energy receivers are not efficient enough in Latvia and others northern countries, and new constructions are required, that would be able to collect energy from all sides as well as to use the diffused radiation more efficiently.

The aim of the paper is to elaborate method for calculation of energy received by solar collector, usable for developing of new constructions of solar collectors, and to develop a new construction of solar collector using this method.

Such new construction can be a semi-spherical solar collector. Such collector has been made, and measurements of water heating have been carried out.

Method of calculations of received energy has been elaborated. Theoretical calculations of the energy gain from semi-spherical solar collector have been performed and verified by comparison of calculated daily energy sums with measured ones, and good coincidence has been obtained.

Method of calculations allows calculating not only integral received energy, but also distribution of the received energy along the surface. The measured distribution of surface temperature of the semi-spherical solar collector corresponds to the calculated one. There are no spot on the semi-spherical surface which would never get warm.

Such semi-spherical solar collector could be appropriate for use of solar energy in Latvia and other countries with similar geographical and climatic conditions.

Keywords: Solar collector, Semi-spherical, Distribution of surface temperature, Energy gain

Nomenclature

E_W	daily energy gain from solar collector J	I	intensity of the solar radiation $W m^{-2}$
E	daily energy sum at cloudy conditions..... J	I_D	intensity of the diffused radiation..... $W m^{-2}$
E_C	daily energy sum at clear sky conditions.. J	z	zenith angle of the sun..... rad
c	specific heat of water..... $J kg^{-1} K^{-1}$	δ	altitude of the sun rad
K	productivity of the water pump..... $kg h^{-1}$	Φ	azimuth of the sun..... rad
t_1	temperature of inlet water °C	S	solar constant..... $W m^{-2}$
t_2	temperature of outlet water °C	P	lucidity of the atmosphere r.u.
Δt	time between two measurements.....s	m	air mass r.u.
β	angle of incidence of solar raysrad	M	nebulositygrades

1. Introduction

Align with decrease of reserves of fossil fuel, as well as impact of use of fossil fuel on climate, in the world more attention has been paid to renewable sources of energy, including solar energy.

Also in Latvia the solar energy has been used, mostly in solar collectors for hot water production [1,2]. However in Latvia because of its geographical and climatic conditions there are some features in comparison with traditional solar energy using countries [3, 4]. Latvia is located at 57° northern latitude and 24° eastern longitude near the Baltic Sea. In Latvia at summer the length of day excides twelve and maximally reaches seventeen hours, accordingly is also long path of sun, but rather small altitude of sun (maximally 56 degrees above horizon) and therefore also small intensity of solar radiation. There is also frequently considerable nebulosity.

At winter the altitude of sun is very small (10°) and the length of day 7 h, therefore use of solar energy at winter in Latvia is not possible.

Because of mentioned above features traditional flat plate collector without tracking to sun is not appropriate enough for use in Latvia, but new collector constructions are required, that would be able to collect the energy from all sides as well as to use the diffused radiation more efficiently. To these requirements a collector with a semi-spherical absorber considered in this article could correspond [5]. Energy gain from such collector is similar to that from flat plate collector tracking to sun, but tracking device is complicated, expensive and hard to exploit, while semi-spherical collector is rather simple, with good appearance, durable against wind.

For a better elaboration and evaluation of new constructions of solar collectors, also new, more precise, complete and convenient methods for calculation and forecasting of the received energy are required, capable to calculate received solar energy of surface of any shape and orientation, taking into account also the nebulosity. Such method is proposed in this article. Calculations consist from three steps. At first, solar coordinates at every moment must be calculated. These calculations are based on astronomical considerations [6]. Second step is calculations of the energy received by some surface, depending on its shape and orientation. Third step is evaluation of impact of clouds. There is a new improved model of taking into account impact of the nebulosity used in these calculations.

The method has been verified by comparison of results of calculations with experimentally measured values. A collector with the semi-spherical absorber has been used in these measurements.

Method of calculations allows calculating not only integral received energy, but also distribution of the received energy along the surface. The measured distribution of surface temperature of the semi-spherical solar collector corresponds to the calculated one. There are no spot on the semi-spherical surface which would never get warm.

2. Methodology

Calculations and measurements of the solar radiation as well as the received energy of the solar collector have been performed in this article.

2.1. Measurements

Measurements of the global solar radiation have been performed using an ISO 1. class pyranometer from “Kipp&Zonen”. Measurements have been performed automatically, taking intensity of radiation after every 5 minutes and accumulating data in a logger. Thereafter from these data the daily energy density has been calculated. Measurements have been carried out from April 2008 till November 2010.

Data on the nebulosity from "Latvian Environment, Geology and Meteorology Centre" have been obtained. The nebulosity is evaluated visually in grades from 0 (clear sky) to 10 (entirely overcast) accordingly the World Meteorology Organization methodology after every 3 hours. Measurements of the received energy of the solar collector have been performed using a new construction – solar collector with a semi-spherical absorber, shown in Fig. 1.

The collector is made from a copper sheet shaped as semi-sphere and coloured black. Inside the dome is a copper tube shaped close to dome. Diameter of the tube is 10 mm, length 21 m. In this tube flows heat remover – water, transporting heat to the reservoir. The collector is covered with transparent polyethylene terephthalate (PET) dome. Radius of the collector is

1.12 m, what corresponds to 1 m² base area. In order to determine the received energy of collector temperatures of incoming and outgoing water have been measured after every 5 min. Water flow ensured a pump, which productivity was 30 l/h. Measurements with the semi-spherical solar collector have been carried out at 2009 from 1 August to 31 October and at 2010 from 1 Jun to 30 August.

Energy gain from solar collector has been calculated from Eq. (1)

$$E = \sum c \cdot K(t_2 - t_1) \cdot \Delta t \cdot 10^{-6} \quad (1)$$

where E is daily energy gain from solar collector (J), C is specific heat of water (4190 J kg⁻¹ K⁻¹), K is productivity of the water pump (kg/h), t₁ and t₂ are inlet and outlet water temperatures respectively (°C) and Δt is time between two measurements. All positive E values must be summed.



Fig. 1. Semi-spherical solar collector.

The distribution of the surface temperature of semi-spherical solar collector also has been investigated. For this investigation there are 30 thermocouples mounted onto surface of the semi-spherical solar collector at even distances from each other. Measurements of temperatures have been carried out using termologgers Pico TC08. Surface temperature investigations have been carried out with and without water flow in tubes.

2.2. Theoretical calculations

For the theoretical calculation of the received energy of some surface [7] at first solar coordinates (declination and azimuth) must be calculated at every moment (we used interval 15 min). From solar coordinates and the orientation of the surface (normal of the surface) the angle of incidence of solar rays β can be calculated. Then the intensity of the radiation received of a surface element can be calculated from Eq. (2).

$$I = SP^m \cos \beta + I_D \quad (2)$$

where S is solar constant (equal to 1367 W m^{-2}), P is lucidity of the atmosphere, r.u., m is air mass, r.u., and I_D is intensity of the diffused radiation, assumed to be constant and equal to 75 W m^{-2} .

The air mass m accordingly to literature [8] can be calculated from empirical expression Eq. (3).

$$m = \frac{1.002432 \cos^2 z + 0.148386 \cos z + 0.0096467}{\cos^3 z + 0.149864 \cos^2 z + 0.0102963 \cos z + 0.000303978} \quad (3)$$

where z is zenith angle of the sun.

In order to determine the daily energy sum received by some surface the intensity calculated from Eq. (1) have to be integrated (summed up) in time from sunrise to sunset as well as over all irradiated surface.

Calculation of the clear sky energy according to Eq. (2) and (3) has been explained in our previous works [3,4,7] and therefore is not considered here.

Impact of clouds has been taken into account using a new empirical model Eq. (4) with experimentally evaluated numerical coefficients A, B and C.

$$E = E_C (A - B \exp(CM)) \quad (4)$$

where E is daily energy sum at cloudy conditions (J), E_C is the same at clear sky conditions, and M is nebulosity (grades).

Comparison of calculated and measured values has been done using graphical method. The model can be evaluated from the scatter plot of calculated daily energy sums via measured ones. About correspondence of calculated values to measured ones indicate slope (must be close to one) and intercept (must be near to zero) of best-fit line, as well as coefficient of determination R^2 (must be close to one).

3. Results

3.1. Impact of clouds

Impact of clouds has been taken into account via Eq. (4). Coefficients A, B and C has been evaluated from comparison of calculated daily energy sums with those measured with pyranometer, then the model for calculating of daily energy sum at cloudy conditions is Eq. (5)

$$E = E_C (1.01 - 0.0425 \exp(0.295M)) \quad (5)$$

Such model gives good coincidence of calculated daily energy sums with measured ones, shown in Fig. 2.

The slope of the best-fit line in this case is 1.005, intercept 1.13, and coefficient of determination $R^2 = 0.88$.

3.2. Surface temperature distribution of semi-spherical solar collector

Energy received by semi-spherical solar collector surface element, which is determined with spherical coordinates θ and φ , can be calculated from Eq. (2), where β is angle of incidence of solar rays and can be expressed as scalar product of two vectors: surface normal \vec{n} and solar rays direction \vec{l} , Eq. (6).

$$\begin{aligned} \cos \beta &= \vec{n} \cdot \vec{l}_1 = \sin \theta \cos \varphi \cos \delta \cos \Phi + \sin \theta \sin \varphi \cos \delta \sin \Phi + \cos \theta \sin \delta \\ &= \sin \theta \cos \delta (\cos \varphi \cos \Phi + \sin \varphi \sin \Phi) + \cos \theta \sin \delta \end{aligned} \quad (6)$$

where δ is the altitude of the sun and Φ is the azimuth of the sun.

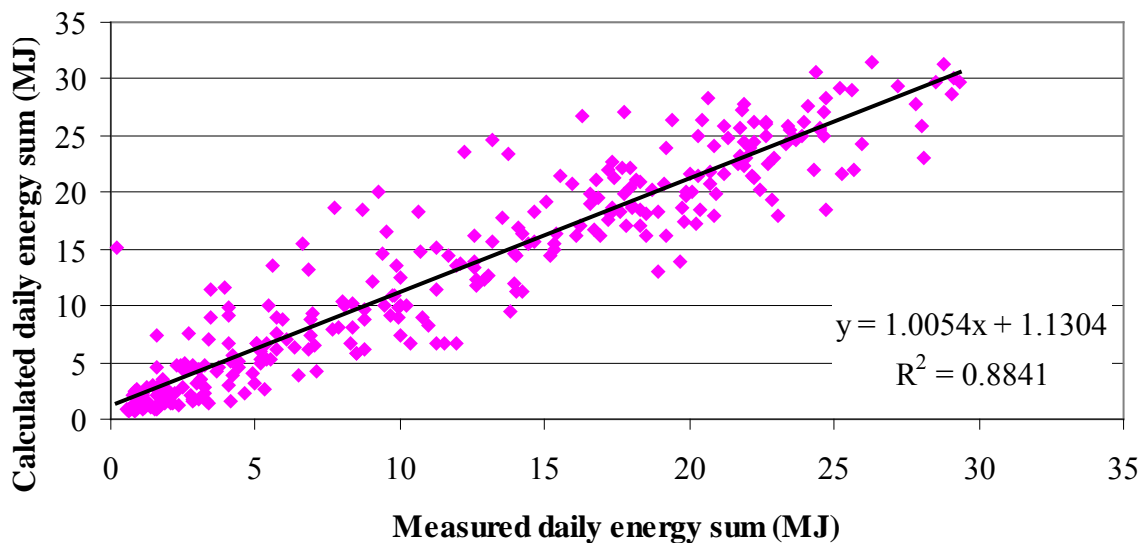


Fig. 2. Comparison of daily energy sums of solar energy, calculated from Eq. (5) with those measured with pyranometer from 1 January 2009 to 31 October 2009.

Results of these calculations in Fig. 3 b has been shown in comparison with measured distribution of surface temperature of semi-spherical solar collector Fig. 3 a.

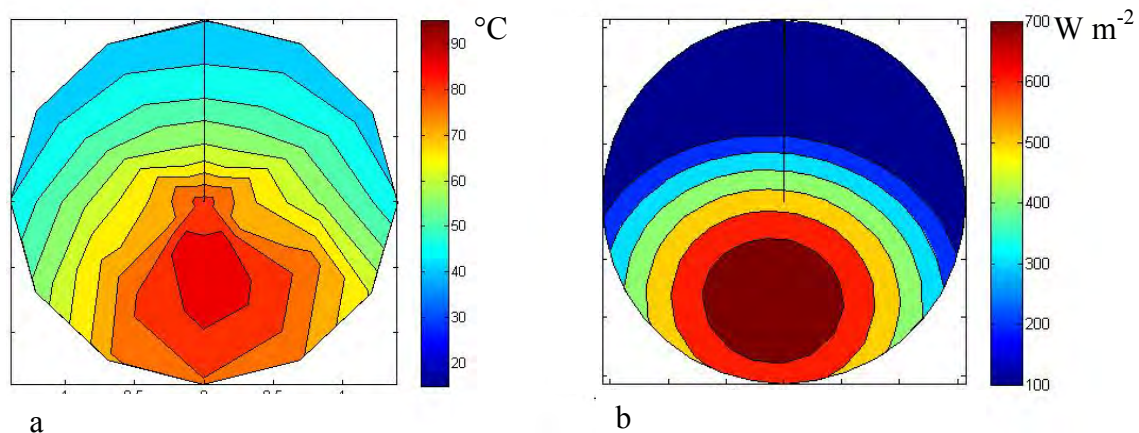


Fig. 3. Distribution of: (a) measured surface temperature and (b) calculated received energy of semi-spherical solar collector at 11 April 2010 at 13:00

Picture shows good correspondence between calculated and measured distributions. Measured distribution is more even because of heat conduction and convection in collector.

Fig. 4 s shows daily mean distribution of measured surface temperature (a) and calculated received energy (b). Also good correspondence has been obtained.

Fig. 5 shows daily course of mean temperature at eastern and western sides (arithmetical mean from measurements of 6 thermocouples mounted at corresponding side) of semi-spherical solar collector, but Fig. 6 of northern and southern sides. Of course, eastern side receives more energy at morning, but western side at evening. It is not explained yet why maximal temperature at eastern side is higher than that at western side. Temperature of southern side is certainly higher than that of northern side, with the exception early at morning at late at evening in the middle of summer, when sun rises at northeast and sets at northwest.

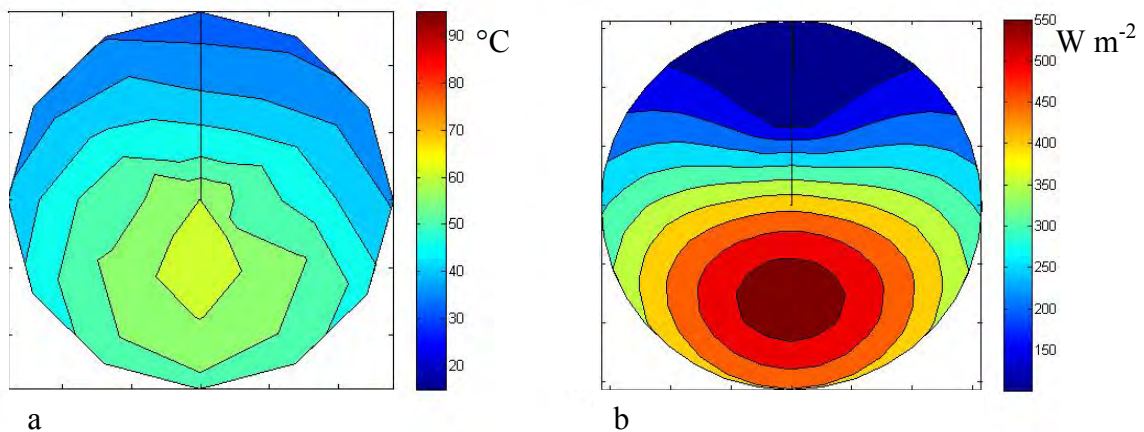


Fig. 4. Distribution of daily mean values of: (a) measured surface temperature and (b) calculated received energy of semi-spherical solar collector at 11 April 2010

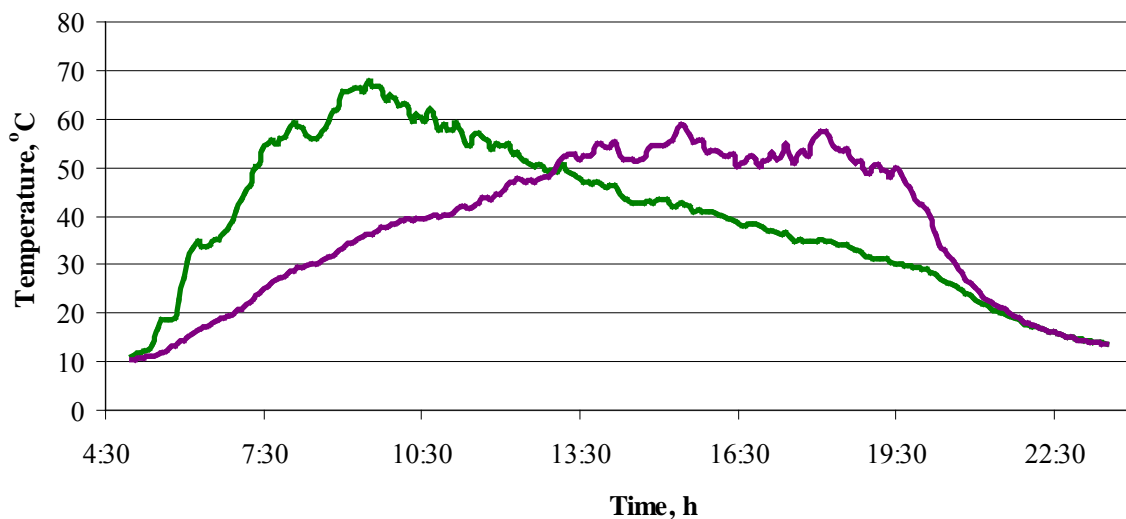


Fig. 5. Daily course of mean temperature at eastern (—) and western (—) sides of semi-spherical solar collector

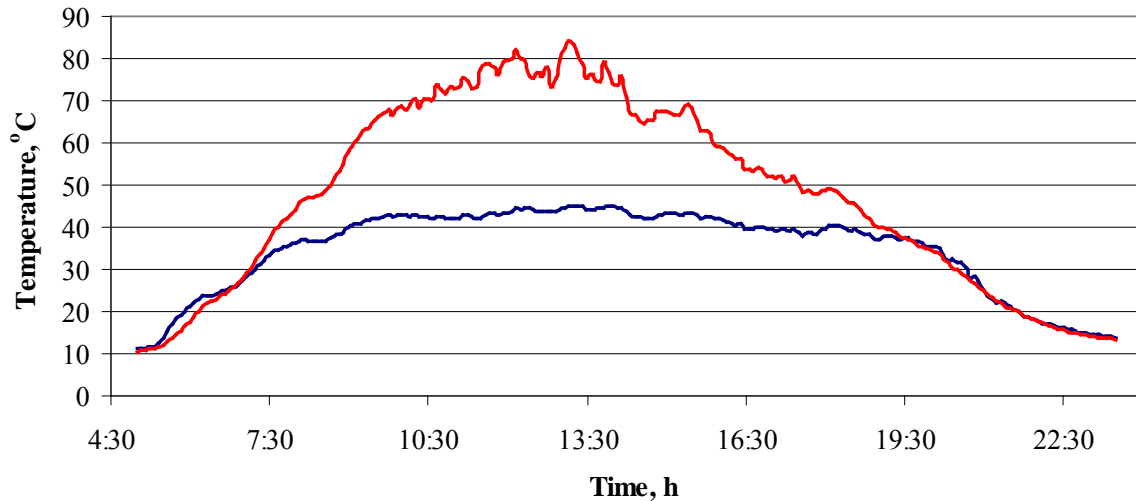


Fig. 6. Daily course of mean temperatures at northern (—) and southern (—) sides of semi-spherical solar collector

But at middle of day, when temperature of southern side reaches 80 °C, temperature of northern side reaches 40 °C. There is no spot on the surface of the semi-spherical solar collector, which never gets warm.

3.3. Energy gain from semi-spherical solar collector

Daily energy gain from semi-spherical solar collector has been calculated from Eq. (1). Results are shown in Fig. 7. There is daily energy gain from semi-spherical solar collector compared with daily sum of solar energy, measured with pyranometer. A linear coherence can be observed, with coefficient of determination $R^2 = 0.87$.

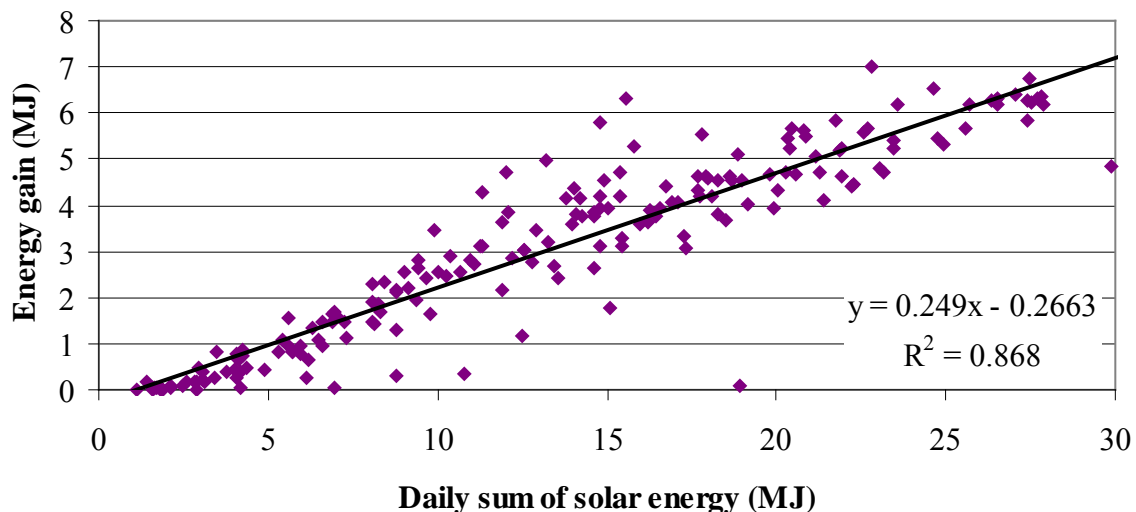


Fig. 7. Daily energy gain from semi-spherical solar collector via daily sum of solar energy, measured with pyranometer from 1 August to 31 October 2009 and from 1 Jun to 30 August 2010.

The slope of the best-fit line (0.25) in this case characterises efficiency of collector. It can be increased using up-to-date materials in the construction of the collector.

4. Discussion and conclusions

Obtained results suggest that semi-spherical solar collector can be appropriate for use of solar energy in Latvia and other countries with similar geographic and climatic conditions. Daily course of surface temperature suggests that semi-spherical solar collector better than common flat plate collector collects solar energy at morning and at evening.

The strong linear coherence between daily energy gain from solar collector and daily sum of solar energy can suggest on independence of work of semispherical solar collector on other circumstances. It can also be because the semi-spherical solar collector uses solar energy evenly all day. However this question needs to be studied additionally, as well as difference between maximal temperatures at eastern and western sides of semi-spherical solar collector.

Other result of this work is method of calculation of received energy of some surface, including impact of clouds. This method is rather simple, precise and not need many input data. This method is usable not only for solar collectors, but also for solar cells, also possible at several forms for better receiving of solar energy. Further study would be interesting on impact of several forms of clouds.

References

- [1] L. Kancevica, J. Navickas, E. Ziemelis, I. Ziemelis, Increase of the Efficiency of Solar Collectors, Proceedings of the Second International Scientific Conference “Biometrics and Information Technologies in Agriculture: Research and Development”, Lithuanian University of Agriculture, 2006, pp. 89-92.
- [2] I. Ziemelis, U. Iljins, J. Navickas, Economical Comparison of Some Parameters of Flat-Plate Solar Collectors, Proceedings of the International Research Conference “The Role of Chemistry and Physics in the Development of Agricultural Technologies”, Lithuanian University of Agriculture, 2004, pp. 23 – 25.
- [3] I. Pelece, Influence of nebulosity on use of solar energy in Latvia, Proceedings of the International Scientific Conference “Engineering for rural development”, 2008, Latvia University of Agriculture, pp. 28-33.
- [4] I. Pelece, U. Iljins, I. Ziemelis, Theoretical calculation of energy received by semi-spherical solar collector, Proceedings of the International Scientific Conference “Engineering of Agricultural Technologies”, Lithuanian University of Agriculture, 2008, Vol. 6. pp. 263-269.
- [5] U. Iljins, I. Ziemelis, I. Pelece, E. Ziemelis. Spherical solar collector. (In Latvian: Saules enerģijas kolektoriekārta ar sfērisko enerģijas kolektoru un tās pielietojumi) *Patent LV 13550 B* Riga: Patenti un precu zīmes 5/2007 p.637
- [6] J. Zagars, I. Vilks. Astronomy for high schools. (In Latvian: Astronomija augstskolām) Riga: LU 2005.
- [7] I. Pelece, U. Iljins, I. Ziemelis, Forecast of energy received by solar collectors, Proceedings of the International Scientific Conference „Applied Information and Communication Technologies”. - Jelgava: LLU, 2008. - lpp. 62-67.
- [8] A. T. Young, Air mass and refraction, *Applied Optics*, 1994, Vol. 33, pp. 1108–1110.
- [9] S. Younes, T. Muneer, Improvements in solar radiation models based on cloud data, *Building Serv. Eng. Res. Technol.*, 2006 Vol. 27, pp. 41-54.

The effectivity of a hybrid solar distillator directly combined with a solar cell

Kazuo Murase^{1,*}, Tin Yao¹, Toki Aoyagi¹, Keishi Okuyama¹

¹ Chuo University, 1-13-27, Kasuga, Bunkyo-ku, Tokyo, Japan

* Corresponding author. Tel : +81(3)3817-1912, Fax : +81(3)3817-1895; email: hmurase@kc.chuo-u.ac.jp

Abstract: Solar energy is one of the most promising natural and renewable energy resources. A solar membrane distillator hybridized with a photovoltaic cell supplies with both water and energy which are indispensable for human life and industry and contributes to effective utilization of renewable energy, especially solar energy. The effectivity of a hybrid solar membrane distillator was experimentally and numerically verified. The dependence of cell temperature on conversion efficiency was unrecognized in this work because of an amorphous Si module. However the hybrid solar distillator contributed to the stable standard conversion efficiency of a cell. Relationship between solar intensity and distillate productivity is almost identifiably approximated for the membrane distillator even if with or without a photovoltaic cell. This work indicated of the effectivity of a hybrid solar distillator with a photovoltaic cell.

Keywords: Hybrid solar distillator, Solar cell, Membrane distillation, PTFE membrane

Nomenclature

C_p : Specific heat	J/(kg·K)	R : Gas constant	Pa·m ³ /(mol·K)
D : Distillate productivity	kg/(m ² ·s)	T : Temperature	K
e : Porosity of PTFE membrane	[-]	u : Water velocity	m/s
FF : Fill Factor	[-]	U : Overall heat transfer coefficient	W/(m ² ·K)
I : Solar intensity	W/m ²	V_{OC} : Open Circuit Voltage	[V]
I_{SC} : Short Circuit Current	A	z : Interval	m
k : Thermal conductivity	W/(m·K)	Geek	
l : Thickness of partition	m	α : Absorptivity of partition	[-]
L : Length of hybrid distillator	m	Γ : Diffusion coefficient of vapor into air	m/s ²
P : Saturated vapor pressure	Pa	δ : Membrane thickness	m
P_{MAX} : Maximum Power	W	ε : Emissivity of partition	[-]
q_1 : Heat flux from solar energy	W/m ²	ρ : Density	kg/m ³
q_L : Latent heat flux	W/m ²	σ : Stefan-Boltzmann constant	W/(m ² ·K ⁴)
q_R : Radiative heat flux	W/m ²	η : Conversion efficiency	[%]
q_S : Sensitive heat flux	W/m ²		
q_U : Overall heat flux	W/m ²		

1. Introduction

Water and energy are indispensable for human life and our industry. However arid regions and demand for water sources have been year by year expanding in the world with drastic increases in industrialization. The consumption of natural resources, particularly fossil fuel, for generating the huge energy causes environmental problems such as global warming. Therefore we should aggressively utilize inexhaustible natural resources such as ocean for water and solar energy as one of renewable energy. Utilization of renewable energy for desalination is one of the promising technologies for simultaneously resolving energy and water problems and for the soft global process as reviewed in reference [1].

Desalination is one of chemical separation processes which remove salt from seawater or saline or brackish water. Practical desalination processes are classified in thermal and non-thermal processes. Thermal processes utilize phase-change process, evaporation and

condensation, to produce to distilled water such as Multi-stage flash, Vapor compression and solar still. Non-thermal processes are membrane separation processes such as Reverse osmosis and Electrodialysis. Only Membrane Distillation (MD) is classified into both thermal and membrane process. MD has the advantages of high selectivity of separation, lower temperature or pressure operation and the high-mass transfer rate as reviewed in reference [2]. A solar driven membrane distillation is suitable for the combination of desalination process and utilization of renewable energy [3].

On other hands solar energy is one of the most promising and all ranged renewable energy according to the rapid and diverse development of a solar cell. However the maximum conversion efficiency of a cell is below at most 35% in spite of the active research of a new type of solar cell. The low efficiency results from the independent reuse of solar energy that is solar ray or solar heat. Therefore several hybrid photovoltaic–thermal systems have been researched in order to improve the conversion efficiency due to the dependence of cell temperature [4] or recover waste heat [5-7].

We have been developing a flat type of solar distillator for environmental problem of the global warming by irrigation [8-10]. The flat type of a membrane distillator has the easy combination with other processes due to supporting the water surface with a membrane. In order to effectively utilize solar energy in both energy sources, solar ray and heat, a new solar membrane distillator directly hybridized with a solar cell was set up not in conventional desalination process [11] but in solar distillator unified with a solar cell. A double glass solar cell manufactured by KANEKA Co.Ltd and a wide PTFE membrane by NITTO DENKO were selected for the direct hybridization. The effectivity of our hybrid solar membrane distillator was experimentally and numerically investigated. .

2. Experimental set-up

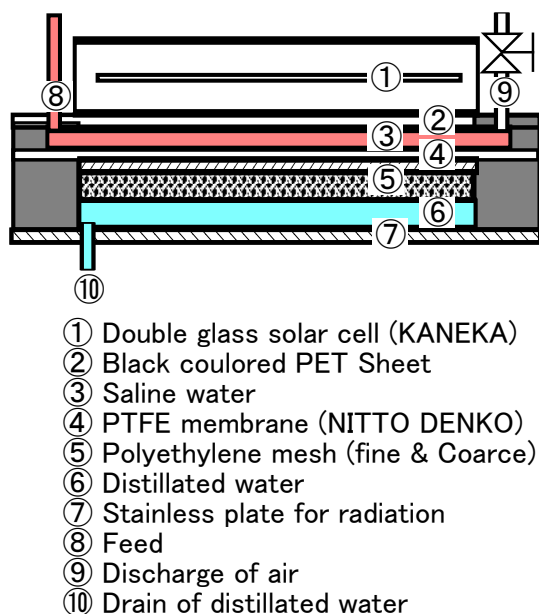


Figure 1. A schematic cross section hybrid solar distillator

composed of a solar absorber of black colored PET sheet (1.88mm in thickness), saline water (2mm in thickness), PTFE (Poly Tera Fluoro Ethylene) membrane (NITTO-DENKO Co.Ltd, NTF-5200, 1 μ m in pore diameter, 85 μ m in thickness and 80% in void fraction), diffusion gap of water vapor supported with fine and coarse types of polyethylene meshes (5mm in thickness) and radiator of stainless plate (2.2mm in thickness). The hybrid distillator was tilted at the lower angle, 2 deg., for the stable water flow and set up at the outdoor situation in JAPAN. The intensity of solar energy measured with a pyranometer (EKO Instruments Co. Ltd. Model MS-42). Distillate productivity and

partitions temperatures obtained with copper-constantan thermocouples were respectively recorded per one hour and one minute. The water volume heated through the cell was keeping at the constant value without the outlet of water. Each dynamic characteristics of separately solar cell, membrane distillator and the hybrid membrane distillator was independently measured in order to estimate the effectivity of the hybridization at the different weather conditions during the summer season in Japan

The Photovoltaic performance, particularly Conversion efficiency (η), was evaluated by I-V curve tracer (EKO Instruments Co. Ltd. Model MP-160) on the basis of experimental data of Open Circuit Voltage (V_{OC}), Short Circuit Current (I_{SC}), Maximum Power (P_{MAX}), Fill Factor (FF).

3. Numerical simulation

3.1. Heat and mass balances

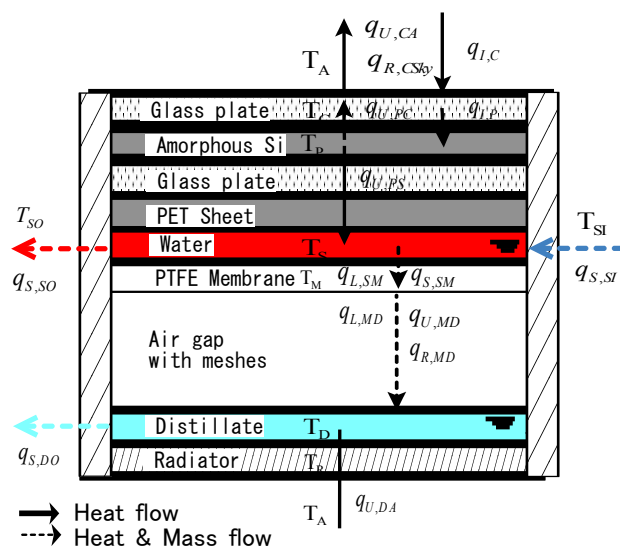


Figure 2. Heat and mass flow of a hybrid distillator

Figure 2 s shows flows of heat and mass transfer for the simulation model of a hybrid solar distillator. This model was constituted on the following assumptions ;

1. Temperature gradients in the flow direction are negligible.
2. Heat transfers with respect to PET sheet, PTFE membrane and radiator are approximated as overall heat transfer coefficients due to only heat conduction.
3. Temperature polarization across the PTFE membrane is negligible.

4. The mesh spacer within the air gap between the PTFE membrane and the radiator has no effect on the heat and mass transfer.

Energy balances for each partition are presented as follow:

$$\text{Glass cover [T}_C] \quad \therefore \rho_C C_{P,C} \ell_C \frac{dT_C}{dt} = q_{I,C} + q_{U,PC} - q_{U,CA} - q_{R,CSky} \quad (1)$$

$$\text{Amorphous Si [T}_P] \quad \therefore \rho_P C_{P,P} \ell_P \frac{dT_P}{dt} = q_{I,P} - q_{U,PC} - q_{U,PS} \quad (2)$$

$$\text{Saline Water [T}_S] \quad \therefore \rho_S C_{P,S} \ell_S \left(\frac{dT_S}{dt} + u_S \frac{dT_S}{dx} \right) = q_{U,PS} - q_{S,SM} + q_{S,SI} - q_{S,SO} \quad (3)$$

$$\text{PTFE Membrane [T}_M] \quad \therefore \rho_M C_{P,M} \ell_M \frac{dT_M}{dt} = q_{S,SM} - q_{L,MD} - q_{U,MD} - q_{R,MD} \quad (4)$$

$$\text{Distillated Water [T}_D] : \rho_D C_{P,D} \ell_D \left(\frac{dT_D}{dt} + u_D \frac{dT_D}{dx} \right) = q_{L,MD} + q_{U,MD} + q_{R,MD} - q_{U,DR} \quad (5)$$

$$\text{Radiator [T}_R] : \rho_R C_{P,R} \ell_R \frac{dT_R}{dt} = q_{U,MR} - q_{U,RA} \quad (6)$$

Distillate productivity is evaluated the following expression [12]

$$D = \Gamma \frac{\pi}{RT_{av}} \frac{1}{(\delta/e^{3.6} + z)} \frac{P_S - P_D}{P_{BM}}$$

3.2. Numerical analysis

Heat and mass transfer Equations.(1)-(7) were numerically simulated by Runge-Kutta method for estimating dynamic characteristics during one day and compared with experimental data in the open air situation. The temperature gradients along the flow direction may be negligible due to some partitions with high thermal conductivities. The initial or static conditions were estimated by simulated data at the steady state.

4. Results and discussion

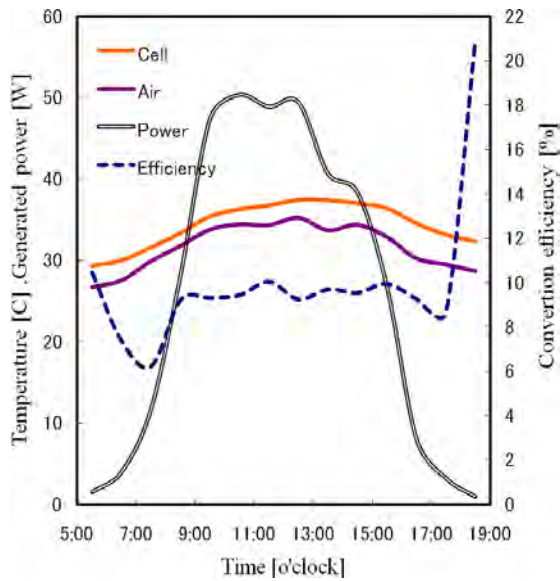
4.1. Dynamic characteristics of solar cell

4.1.1. Effect of hybridization on conversion efficiency (η)

Conversion efficiency of photovoltaic cell (η) can be estimated by the following expression.

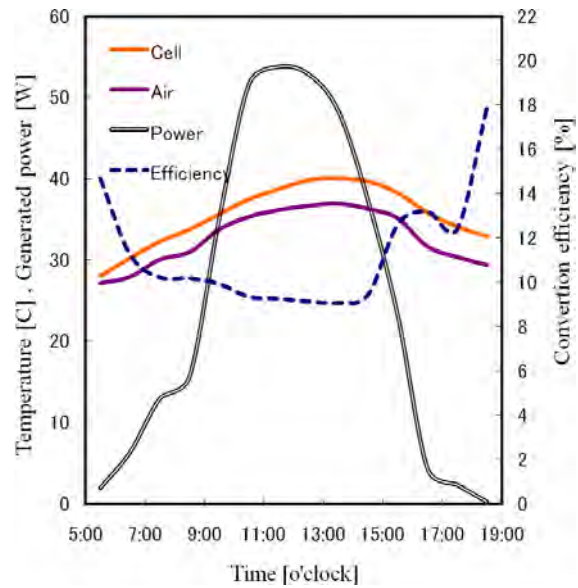
$$\eta = \frac{P_{\max}}{P_{in}} = \frac{V_{OC} I_{SC} FF}{P_{in}} \times 100[\%] \quad (8)$$

Figures 3-(a),(b) show profiles of generated power by a photovoltaic cell and conversion efficiency (η) averaged for one hour in case of (a) exclusive solar cell (11.Augus.2010) and (b) hybridized cell (26.August.2010). In spite of the lower solar intensity per a day Fig. 3(b) shows the higher peak power and average conversion efficiency as shown in Table 1, which is list up each averaged values from 7:00 to 18:00.



(a) Exclusive solar cell

[$I=20.4\text{MJ}/(\text{m}^2 \cdot \text{d})$, 11. August. 2010]



(b) Hybridized cell

[$I=19.0\text{MJ}/(\text{m}^2 \cdot \text{d})$, 26. August. 2010]

Figures 3. Profiles of generated power and conversion efficiency for one day

Table 1 Each characteristic value averaged for 10 hours from 7:00 to 18:00

	Efficiency(η)	Power(P)	$T_{\text{Cell-terminal}}$	T_{Air}
(a) Exclusive solar cell	9.13	32.13	35.36	32.76
(b) Hybridized cell	10.42	30.7	36.85	33.96

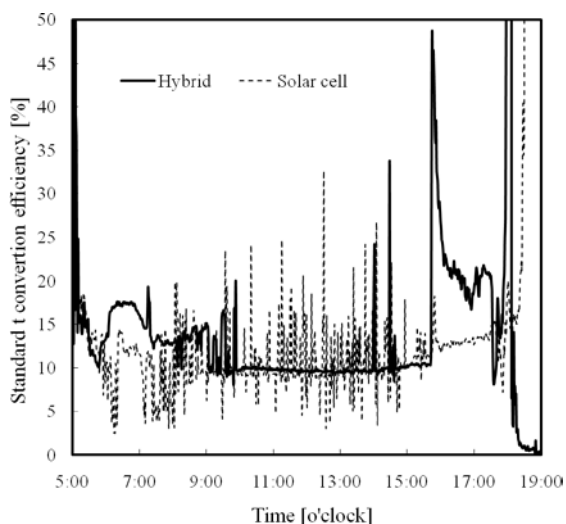


Figure 4. Detailed profiles of standard conversion efficiency

The conversion efficiency at the standard condition of solar irradiation ($1\text{kW}/\text{m}^2$) and of cell temperature (25C) is generally available for the public evaluation due to the free dependency of cell temperature. Figure 4 shows detailed profiles of standard conversion efficiency in two cases. Hybridization compresses fluctuation of standard conversion efficiency due to the steady water. In this work water has no flow along the PET sheet and was supplied only for the volume of evaporated water vapor due to the closed outlet of water. Solar intensity inherently has a fluctuated profile due to the presence of variable weather conditions such as cloud, indirect intensity, wind and so on.

4.2. Dynamic characteristics of membrane distillation

4.2.1. Effect of hybridization on temperature profiles of each partition

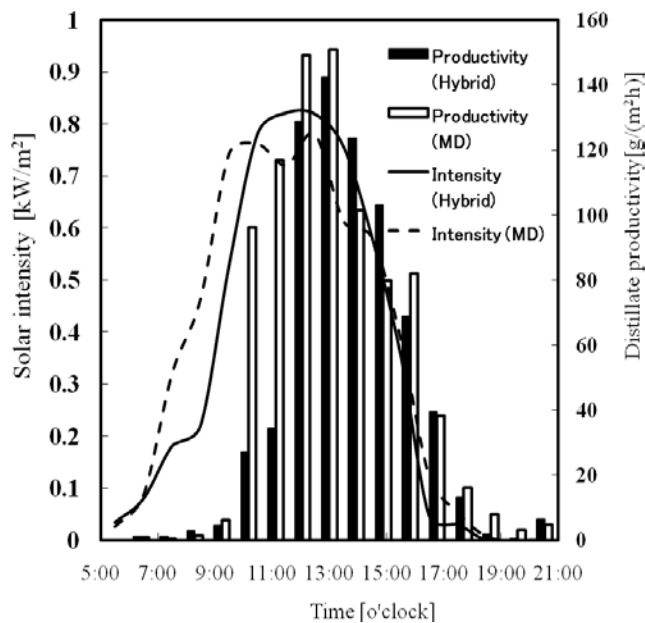


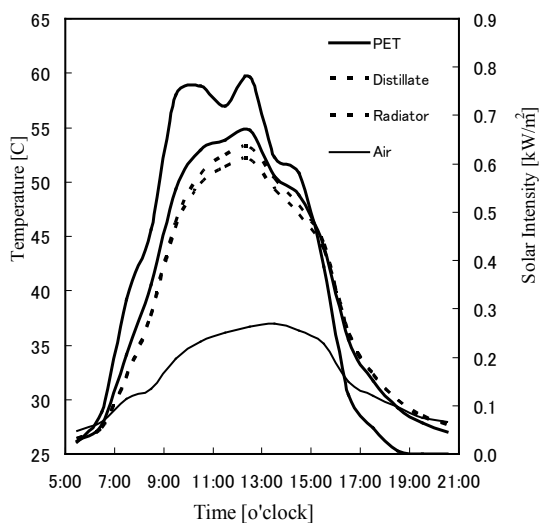
Figure 5. Effect of hybridization on distillate productivity for one hour

Figure 5 shows profiles of distillate productivity per one hour in two cases of hybrid distillator and membrane distillator without a photovoltaic cell. Table 2 lists up experimental data with total distillate productivity per a day in cases of MD with and without a cell. In spite of the less solar intensity by 20% i, the decrease of distillate productivity n case of the hybridized MD was settled within the less range of 7%.

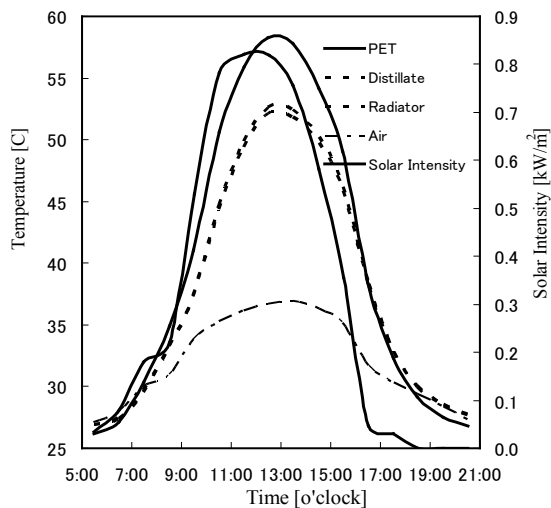
Figures 6-(a),(b) indicate that hybridization increases the temperature difference between PET sheet and distillate partition. The temperature on PET sheet almost equals to that of evaporated water. The distillate productivity only depends on t he temperature difference between evaporated vapor and condensed water .

Table 2 Total distillate productivity per a day in cases of MD with and without a cell

	Solar intensity [MJ/(m ² ·d)]	Distillate productivity[kg/(m ² ·d)]
MD without a cell	20.4	0.855
Hybridized cell	19.0	0.691



(a) MD without a cell

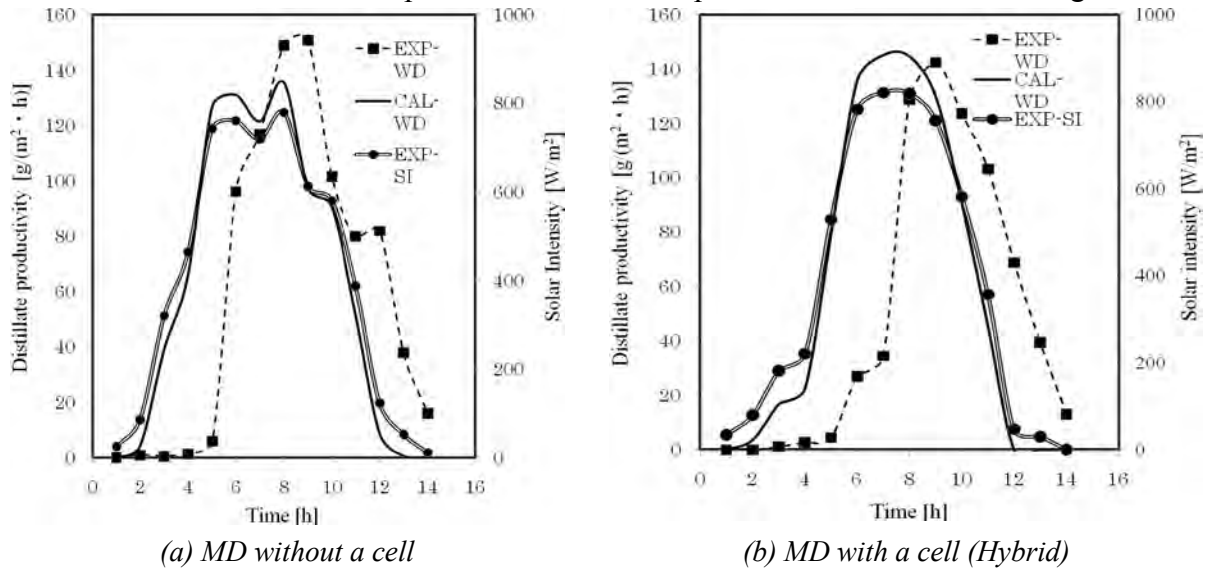


(b) MD with a cell (Hybrid)

Figures 6. Temperature distributions in two types of Membrane Distillators (MD)

4.2.2. Numerical results

Figures 7-(a),(b) show profiles of dynamic distillate productivity by numerical simulation in two cases of membrane distillator with and without a photovoltaic cell. Experimental solar intensity and air temperature were used as the weather parameters. The peak value of distillate productivity is underestimated because productivity in Fig.7-(a) was calculated by the hybrid simulation model. Both profiles of productivity in Figs.7-(a),(b) were correspondingly traced by the model. However experimental times at the peak productivity were shifted by two hours from that of solar intensity. The calculated productivity has a response of no time lags for solar intensity due to the negligible temperature gradient along the water flow. The assumption will be invalid in case of operational conditions of water flow. The larger specific heat of water and thickness of spacer mesh than other partitions result in the time lag.



Figures 7. Numerical prediction of distillate productivity

4.2.3. Effect of hybridization on distillate productivity

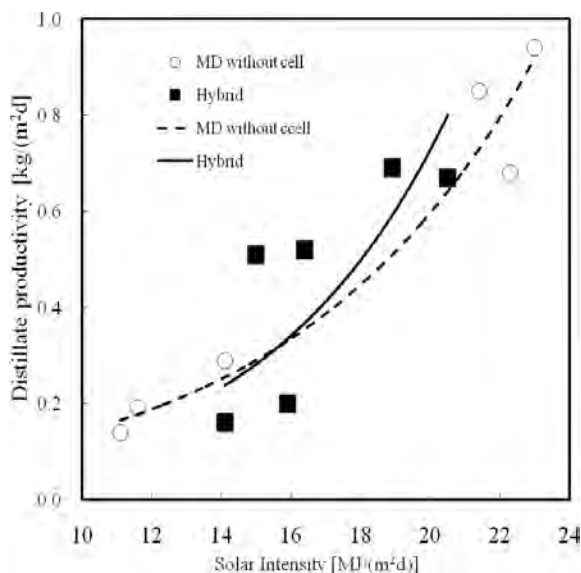


Figure 8. Effect of solar intensity on distillate productivity

Figure 8 shows the effect of solar intensity on distillate productivity for one day. Experimental data were intensively obtained at the summer season in Japan due to the less solar intensity than other arid lands. Approximated curves with experimental relationship between solar intensity and distillate productivity for membrane distillators even if with or without a photovoltaic cell were almost identifiable. The results indicate the effectivity of a hybrid solar membrane distillator directly with a photovoltaic cell even if for the increasing thermal resistances. The productivity is not necessarily desirable in comparison with our previous report [8]. The improvements of hybridization and process flow of water are required.

5. Conclusions

A solar membrane distillator hybridized with a photovoltaic cell supplies with both water and energy which are indispensable for human life and industry and contribute to effective utilization of renewable energy. The effectivity of a hybrid solar membrane distillator was experimentally and numerically verified.

The dependence of cell temperature on conversion efficiency was unrecognized in this work because of an amorphous Si module. However the hybrid solar distillator contributed to the stable standard conversion efficiency of a cell. An amorphous Si module is suitable for the comparatively higher temperature condition.

Relationship between solar intensity and distillate productivity is almost identifiably approximated for the membrane distillator even if with or without a photovoltaic cell. The performance of distillate productivity is not necessarily desirable. The improvements of hybridization and process flow of water should be required.

Acknowledgements

The authors would like to thank Mr. Takuji Nomura, KANEKA Co LTD, and Mr. Hajime Oya, NITTO DENKO CO.LTD, respectively for their support of a Photovoltaic cell and a PTFE membrane.

References

- [1] S.A.Kalogirou, Prog. Energy Combustion Sci.31, 2005, pp.242-281.
- [2] M.Khayet, Adv. Colloid Interface Sci., 2010.(in press)
- [3] H.Chang et al, Renewable energy 35, 2010 pp.2714-2722.
- [4] E.Skoplaki et al. , Solar Energy Materials & solar cells 92, 2008, pp.1393-1402
- [5] T.T.Chow et al. ,Solar energy 801, 2006, pp.298-306
- [6] R.M.da Silva and J.L.M.Fernandes, Solar energy 12, 2010 pp.1985-1996
- [7] A.Tiwari and M.S.Sodha, Renewable energy 31, 2006, pp.2460-2474
- [8] K.Murase et al., Bulletin Society of Sea Water Sci. Japan 54, 2000, pp. 30-36
- [9] K.Murase et al., Desalination and Water Treatment 9, 2009, pp. 96- 104
- [10] K.Murase et al., Proc. WC IDA (DB09-099), 2009, Dubai
- [11]S.Kumar and A.Tiwari, Energy Conversion and Management 51, 2010, pp.1219-1229
- [12] H.Kurokawa et al., Kagaku Kogaku Ronbunshu 14, 1988, pp.330-336

Comparative Energy and Exergy Analysis of Various Passive Solar Distillation Systems

Ragh Vendra Singh¹, Rahul Dev^{2,*}, M. M. Hasan¹, G. N. Tiwari²

¹Department of Mechanical Engineering, Jamia Milia Islamia, Jamia Nagar, New Delhi-110025, India.

²Centre for Energy Studies, Indian Institute of Technology, Delhi, Hauz khas, New Delhi-110016, India.

* Corresponding author. Tel: +91 9968344470, Fax: +91 11 26591251, E-mail: rahuldsurya@yahoo.com

Abstract: In this communication, a comparative energy and exergy analysis of various conventional solar distillation systems has been presented. The study includes passive solar distillation systems such as single and double slope solar stills. In a single slope solar still category, three solar stills with inclination angles 15°, 30° and 45° and a 15° inclined single slope multi wick solar still have been considered. Whereas one double slope solar stills and one double slope multi wick solar still, both inclined at 15° with east-west orientation, have been considered in double slope solar still category. The embodied energy is an important factor which depends on locally available materials and their manufacturing technologies. Materials like concrete, wood, steel etc are considered to calculate the embodied energy for the solar still equivalent to the fibre reinforced plastic after deriving the formulae. It has been found that the energy, exergy and embodied energy of single slope solar still are found higher than that of double slope solar still. Those materials which have lower thermal conductivity and low embodied energy than that of FRP such as concrete, PVC, wood can replace the FRP to save the embodied energy for similar performance. The metals have high embodied energy hence these can not be considered in terms of embodied energy despite the use of insulation.

Keywords: Solar distillation, Water purification, Energy, Exergy, Embodied energy.

Nomenclature

A_s area of solar still..... m^2	$l_{material}$ thickness of material..... m
$I(t)$ solar intensity..... W/m^2	l_{metal} thickness of metal..... m
$\dot{E}x_{evap}$ exergy output..... W/m^2	$l_{Styrofoam}$ thickness of Styrofoam..... m
$\dot{E}x_{in}$ exergy input..... W/m^2	\dot{m}_{ew} hourly distillate collected..... kg/m^2-h
$K_{material}$ thermal conductivity of material. W/mK	\dot{q}_{ew} heat utilized in evaporation of water... W/m^2
K_{metal} thermal conductivity of metal..... W/mK	T_a ambient temperature..... K
K_{FRP} thermal conductivity of FRP..... W/mK	T_s sun temperature..... K
L latent heat of vaporization..... $kJ/kg-K$	

1. Introduction

A solar distillation is a water purification technology. Saline/brackish water can be purified using solar energy. This technology works on the principles of greenhouse effect and hydrological cycle. The use of solar energy to produce potable water is a key factor in context of water & air pollution, global warming, energy security and climate change because most of other water purification technologies use conventional sources of energy such as coal, oil, gas etc [1]. A solar still is a device used for solar distillation in which impure or saline water is fed to obtain distilled water. It is a box type structure made of some materials such as fibre reinforced plastic (FRP), wood, concrete, or steel with insulation. It is covered with a simple window glass through which the solar radiation passes to incident on the water surface. A small amount of reflection heat losses and absorption take place at the glass cover and the water. A major part of incident solar radiation is absorbed by the basin liner. This heat is transferred to the saline water by convection as top heat loss and to the ambient as bottom heat loss. Heat transfer from the water to the glass cover take place by three mechanisms: evaporation, convection and radiation. Vapour leaves most of contaminants and microbes

through thermal diffusion on the basin liner. Further the vapour undergoes film type condensation at the inner surface of the glass cover because of inclination of glass cover, adhesion, cohesion between condensed water molecules, and gravity. The condensed water trickles down to a trough which guides it into a container placed outside [2]. Researchers have worked to improve the performances of solar stills by suggesting its various designs, materials and operating conditions for different weather conditions. Tiwari and Tiwari [3] have reported that the yield from a single slope passive solar still may vary from 0.5 to 1.2 kg/m²/day (in winter) and 1.0 to 2.5 kg/m²/day (in summer) for Delhi, India. Tiwari [4] has found the efficiency of the single slope solar still 25.8, 19.7, 22.8 % at glass cover inclinations 15°, 30° and 45° respectively for the summer climatic condition of Delhi, India. Malik et al. [2] have shown that overall efficiency of a passive solar still is achieved with least water mass in the basin.

Energy and exergy analysis of solar stills have been presented by various researcher such as Dunkle [5], Cooper [6], Tsilingiris [7], and Dwivedi [8, 9] etc. A group of improved heat and mass transfer correlations in basin type solar stills has been developed by Hongfei et. al. [10]. Torchia- Núñez et al. [11] have found that for same exergy input a basin, brine and passive solar still have exergy efficiencies of 12.9%, 6%, and 5% respectively. Dev and Tiwari [12, 13] developed the characteristic equation for single and double slope passive solar stills. In ideal solar still, the instantaneous loss efficiency is minimum (for zero depth of water mass) as analyzed by Cooper [6]. Rubio et al. [14, 15] have studied asymmetries in various temperatures and amount of distillate for a double slope passive solar still (DSPSS) and proposed mathematical models, one in terms of lumped parameters and another for controlled temperatures of glass cover and basin. Dwivedi and Tiwari [8, 9] have reported that the thermal efficiency for single and double slope solar still varies from 22.6% to 31.3% and 25.4% to 34.3% respectively at 0.01 m water depth. Similarly, the average exergy efficiency for single and double slope solar still is 0.65% and 0.82% respectively. The exergy efficiency of single and double slope solar still varies from 0.18 to 1.25% and 0.13 to 1.16% respectively. Tiwari and Yadav [16] have shown that a single slope distiller gives better performance than a double slope for cold climatic conditions whereas a double slope distiller gives better performance than a single slope for summer climatic conditions irrespective of either basin type or multi-wick type. It has also been reported that the concrete basin solar still gives better performance than the FRP single and double slope stills because of the probability of leakage of vapour in the FRP stills was more than for the concrete still. Sakthivel and Shanmugasundaram [17] have shown that the efficiency of single slope solar still using the black granite gravel reaches up to 52% maximum which is 8% higher than the conventional single slope solar still. Singh and Tiwari [18] have studied double effect multi-wick solar stills to increase the still efficiency by utilizing the latent heat released by the vapor at first effect. Kumar and Anand [19] have studied shown that a tubular multiwick solar still gives distillate output of about 8%, 13%, and 18% more than tubular, simple multi-wick and conventional basin type solar stills respectively.

The embodied energy is an important factor which depends on locally available materials and their manufacturing technologies. Hence, on the basis of literature survey the performance of the solar stills on the basis of energy, exergy and materials have been analyzed in this paper.

2. Solar distillation systems

Passive solar distillation systems such as single and double slope solar stills have been taken. In a single slope solar still category, three solar stills with inclination angles 15°, 30° and 45°

(Fig. 1a, 1b) and a 15° inclined single slope multi wick solar still have been considered. Whereas one double slope solar stills and one double slope multi wick solar still both inclined at 15° with east-west orientation, have been considered in double slope solar still category (Fig. 1c, 1d). All these experimental setup have been installed at Solar Energy Park, I.I.T. Delhi, New Delhi, India (28°35' N, 77°12' E, altitude 216 m from mean sea level). The single slope solar still works on same principle as given above.



Fig. 1 Various solar stills: (a) Single slope solar still inclined at 15° and 30° with orientation towards south, (b) Single slope solar still inclined at 45° with orientation towards south, (c) Double slope solar still inclined at 15° with orientation towards east-west, (d) Double slope multi-wick solar still inclined at 15° with orientation towards east-west.

A schematic diagram of double slope passive solar still has been shown in Fig. 1c. Two simple window glasses have been placed over the walls of the solar still at inclination angle 15° facing east and west directions. To absorb higher amount of solar radiation, an inside surface of the solar still has been painted black in color. An inlet through the rear wall has been provided to feed the brackish/underground water in to the basin of the solar still. And two troughs are provided at inside of each short wall of the solar still to collect the distilled water. The orientation of the solar still has been kept east-west to receive solar radiation for maximum hours of sunshine. When the sun lies in the east direction then higher temperature difference occur at west side due to low glass temperature which yield higher amount of distillate at this side and vice versa except at the time of noon when both the glass covers have almost the same temperature.

In the single and double slope multi-wick solar still, water is fed from water reservoir through the multiple porous absorbers (black jute cloth) at a slow rate for fast evaporation. The saline water goes upwards due to capillary action in the jute cloths and forms a thin water layer. The solar radiation, after transmission through the glass covers, strikes this water film and heats the water. The water evaporates and condenses at the inner surface of the glass cover by releasing latent heat of vaporization. The condensed water is collected through the drainages for distilled water. A double slope multi-wick solar still, as shown in Fig. 1d, is a

development over the single slope multi-wick solar still similar to double slope solar still, Malik et al. [2]. The specifications of these solar stills are given in Table 1.

Table 1. Design specifications of solar stills which are installed at Solar Energy Park, Centre for Energy Studies, IIT Delhi, New Delhi, India.

Sr. No.	Specifications	Single slope solar still			
		Conventional			Multi-wick
		Type 1	Type 2	Type 3	Type 4
1	Area of basin (m ²)	1 × 1	1 × 1	1 × 1	1.1 × 1.14
2	Height of south wall (m)	0.06	0.15	0.15	0.06
3	Height of north wall (m)	0.26	0.74	1.15	0.25
4	Angle of inclination (°)	15	30	45	15
5	Size of glass (m ²)	1.02 × 1	1.02 × 1.2	1.02 × 1.44	1.02 × 1.14
6	Quantity of glass	1	1	1	1
7	Putty (kg)	1	1	1.5	1
8	Paint (kg)	0.5	0.8	1	0.5
9	Iron stand (kg)	5	20	18	17
10	Metal (kg)	0.2	0.2	0.2	nil
11	Jute cloth (m ²)	4 × 1
		Double slope solar still			
		Conventional		Multi-wick	
Sr. No.	Specifications	Type 5		Type 6	
1	Area of basin (m ²)	2 × 1		2 × (1.1 × 1.14)	
2	Height at ends (m)	0.25		0.05	
3	Central height (m)	0.45		0.25	
4	Angle of inclination at both sides (°)	15		15	
5	Size of glass (m ²)	1.02 × 1.02		1.02 × 1.14	
6	Quantity of glass	2		2	
7	Putty (kg)	3		3	
8	Paint (kg)	1		1	
9	Iron stand (kg)	35		30	
10	Metal (kg)	0.2		0.5	
11	Black Jute cloth (m ²)	...		8 × 1	

3. Mathematical expressions

Following are the mathematical expression used for the analysis of energy and exergy of considered solar still systems.

The thermal efficiency of a passive solar still can be calculated by the following formula [1]:

$$\eta_i = \frac{\dot{m}_{ew} \times L}{A_s \times I(t) \times 3600} \times 100 \quad (1)$$

Exergy efficiency of a passive solar still can be calculated by the following formula [20]:

$$\eta_{EX} = \frac{\dot{E}x_{evap}}{\dot{E}x_{in}} \times 100 \quad (2)$$

where,

$$\dot{E}x_{evap} = \sum_{i=1}^{24} \left(1 - \frac{T_a}{T_w} \right) \times \dot{q}_{ew} \quad ; \quad \dot{q}_{ew} = A_s \cdot h_{ew} \cdot (T_w - T_{gi})$$

and

$$\dot{E}x_{in} = \dot{E}x_{sun} = A_s \times I(t) \times \left[1 - \frac{4}{3} \times \left(\frac{T_a}{T_s} \right) + \frac{1}{3} \times \left(\frac{T_a}{T_s} \right)^4 \right]$$

Equivalent thickness of materials for same performance as FRP has in case of solar still:

$$l_{material} = \frac{K_{material}}{K_{FRP}} \times l_{FRP} \quad (3)$$

Thickness of Styrofoam for insulation (when solar still is made of any metal and overall thermal conductivity is equivalent to FRP):

$$l_{Styrofoam} = \frac{K_{Styrofoam} \cdot (K_{Metal} \cdot l_{FRP} - K_{FRP} \cdot l_{Metal})}{K_{Metal} \cdot K_{FRP}} \quad (4)$$

4. Results and discussion

On the basis of literature survey and Eqs. (1, 2) it has been observed that energy, exergy efficiencies and embodied energy of single slope solar still remain higher in comparison to that of the double slope solar still. Dev and Tiwari [12,13] have found better performances at water depth 0.01 m and an inclination angle 30° for single slope passive solar still. They have also developed the characteristic equation of single and double slope passive solar still and suggested the sum of instantaneous gain and loss efficiencies ($\eta = \eta_i + \eta_{iL}$) remain lower than maximum efficiency under ideal i.e. 60%. Although, it can be seen that the energy efficiency can reach up to 60% maximum but because of several factor such as heat loss through vapor leakage and improper insulation, time lag in production, inclination angle, water depth etc, it does not attain such value. Similarly, the exergy efficiency which is measured for the source temperature i.e. sun temperature 6000 K, remain always very much lower than the energy efficiency because of the energy input by the sun is not fully utilized in evaporation process of the water in the solar still.

The design specifications (Table 1), properties of various materials (Table 2 which consists of probable materials for solar still), Eqs. (3) and (4) have been used to get total embodied energy for the solar still by considering metals, concrete, PVC, wood etc. equivalent to that of

FRP (i.e. to keep the productivity of the solar still same as of FRP). The metals have been found large thickness due to their conductivities but these metals (thickness 1 mm) can be considered with insulation of Styrofoam as shown in Table 2. One can see that steel which is very high energy intensive material can not be recommended as a material to make the solar still despite the use of insulation. The thicknesses of materials such as concrete, wood, and PVC have been found very near to the thickness of the FRP. Materials such as glass window and country fired bricks have more thickness which can not be considered.

Table 2. Various manufacturing materials of solar still, their thermal conductivities, embodied energy, density and thickness with and without insulation material.

Material	Conductivity at 25 °C (W/mK)	Embodied energy (MJ/kg) (In India)	Density (kg/m ³)	Thickness of material without insulation (m)	Thickness of insulation I _{styrofoam} (m) (for I _{metal} =1 mm)
Copper	401	112	8930	5.7	0.0005
Steel	16.3	42	7860	0.232	0.0005
G.I. sheet	80	50.8	7860	1.14	0.0005
Aluminium	250	260	2600	3.56	0.0005
Concrete	0.42	2.4	2200	0.006	-----
Country fired brick (22x10.5x6.5 cm ³ - delivered at 30 km)	1.31	7.9	286	0.018	-----
Simple window glass	0.96	15.9	2600	0.014	-----
Polystyrene expanded	0.03	117	640	0.001	-----
Wood	0.17	1.8	850	0.0025	-----
PVC	0.19	115	1410	0.003	-----
Styrofoam (for insulation only)	0.033	100	35	-----	-----
FRP	0.351	92.2	1800	0.005	-----
Paint	-----	90	6.1	-----	-----
Jute cloth	-----	55	-----	-----	-----

Note: Embodied energy values based on several international-local sources may vary.

The embodied energies of conventional single slope solar stills made of FRP, concrete, PVC, and wood are found and given in Table (3). The percentage increase in the embodied energy compared of other solar stills compared to that of single slope solar still inclined at 15°, with south wall height 0.06 m has also been given in same table which changes similarly irrespective of material used. The embodied energy double slope solar still, and double slope multi-wick solar still have been found to be 3070 MJ and 2323 MJ respectively when only FRP is considered. On the basis of this one can observe that the embodied energy of double slope solar stills including the multi-wick solar still are less energy intensive in comparisons to single slope solar stills (1361 MJ) and single multi-wick solar still (1495 MJ). One can see in Table 3, wood is found most suitable in terms of embodied energy but it degrades soon in comparison to other materials in terms of life. The PVC can be a better option over FRP in

terms of embodied energy and weight. According to previous studies [3, 4], single slope solar still inclined at 30° is suitable as per the latitude of Delhi. The total embodied energy for this solar still including glass, paint has been found 2587 MJ (FRP), 369 MJ (concrete), 1498 MJ (PVC), 292 MJ (wood). Similarly for double slope multi-wick solar still inclined at 15°, total embodied energy including glass, paint and fabric have been found 2875 MJ (FRP), 640 MJ (concrete), 1773 MJ (PVC), 562 MJ (wood).

Table 3. Embodied energy of single slope solar still for different materials such as FRP, Concrete, Steel, Wood.

Solar still	Specifications	Embodied energy (MJ)							
		FRP	Concrete	PVC	Wood	% increase	Glass	Paint	Fabric
Single slope	15°, with south wall height = 0.06 m	1361	52	718	6	----	168	28	----
	15°, with south wall height = 0.15 m	1776	68	937	8	30	168	45	----
	30°	2306	88	1217	11	70	208	73	----
	45°	2987	114	1576	14	120	245	90	----
Double slope	15°, Multi-wick	1495	57	790	6.6	10	226	45	27.5
	15°, Multi-wick	3070	117	1615	13.5	125	345	90	----
	15°, Multi-wick	2323	88	1221	10.2	70	407	90	55

5. Conclusions

1. On the basis of above analysis and literature survey, the energy, exergy and embodied energy of single slope solar still are found higher than that of double slope solar still.
2. Those materials which have lower thermal conductivity and low embodied energy than that of FRP such as concrete, PVC, wood can replace the FRP to save the embodied energy for similar performance.
3. The metals have high embodied energy hence these can not be considered in terms of embodied energy despite the use of insulation.
4. PVC material has been found to be better in terms of embodied energy in comparison to other materials.

On the basis of above study, the similar analysis can be recommended for other materials such as glass, steel, aluminum, copper, bricks, and other advance materials, as the research in the field of materials science is progressing, to have a material of less embodied energy, light in weight, good insulator and portable in comparison to FRP as well which should be easily available in less price.

References

- [1] G.N. Tiwari, A.K. Tiwari, Solar distillation practice for water desalination systems, Anshan Publication, UK Edition, 2008, pp. 1-40.
- [2] M.A.S. Malik, G.N. Tiwari, A. Kumar, M.S. Sodha, Solar Distillation, Pergamon Oxford, 1982, pp. 1-35.

- [3] A.K. Tiwari, G.N. Tiwari, Effect of the condensing cover's slope on internal heat and mass transfer in distillation: an indoor simulation, *Desalination* 180, 2005, pp. 73-88.
- [4] A.K. Tiwari, Annual performance of solar stills for different inclinations of condensing covers and water depths. PhD Thesis, Centre for Energy Studies, IIT Delhi, New Delhi, India, 2006.
- [5] R.V. Dunkle, Solar Water Distillation: The Roof Type Still and a Multiple Effect Diffusion Still, *Int. Development in Heat Transfer. ASME proceedings*, 1961(part5), pp. 895-902.
- [6] P.I. Cooper, The maximum efficiency of single-effect solar stills, *Solar Energy* 15, 1973, pp. 205-214.
- [7] P.T. Tsilingiris, Modeling heat and mass transport phenomena at higher temperatures in solar distillation systems – The Chilton–Colburn analogy , *Solar Energy* 84, 2010, pp. 308-317.
- [8] V.K. Dwivedi, G.N. Tiwari, Annual energy and exergy analysis of single and double slope passive solar stills, *Applied Science Research* 3(3), 2008, pp. 225-241.
- [9] V.K. Dwivedi, Performance study of various designs of solar still. PhD Thesis: Centre for Energy Studies, IIT Delhi, New Delhi, India: 2009.
- [10] Z. Hongfei, Z. Xiaoyan, Z. Jing, W. Yuyuan, A group of improved heat and mass transfer correlations in solar stills, *Energy Convers. Mgmt.* 43, 2002, pp. 2469-2478.
- [11] J. C. Torchia- Núñez, M. A. Porta-Gándara, J.G. Cervantes-de Gortari, Exergy analysis of a passive solar still, *Renewable energy* 33(4), 2008, pp. 608-616.
- [12] R. Dev, G.N. Tiwari, Characteristic equation of a passive solar still, *Desalination* 245, 2009, pp. 246-265.
- [13] R. Dev, H.N. Singh, G.N. Tiwari, Characteristic equation of double slope solar still, *Desalination* 267, 2011, pp. 261-266.
- [14] E. Rubio, M.A. Porta, J.L. Fernandez, Cavity geometry influence on mass flow rate for single and double slope solar stills. *Applied Thermal Engineering* 20, 2000, pp. 1105-1111.
- [15] E. Rubio, J.L. Fernandez, M.A. Porta-Gandara, Thermal performance of the condensing cover in a triangular solar still, *Renewable Energy* 29, 2004, pp. 895-906.
- [16] G.N. Tiwari, Y.P. Yadav, comparative designs and long term performance of various designs of solar distillery, *Energy Convers. Mgmt* 27(3), 1987, pp. 327-333.
- [17] M. Sathivel, S. Shanmugasundaram, Effect of energy storage medium (black granite gravel) on the performance of a solar still, *Int. J. of Energy Research* 32, 2008, pp. 68-92.
- [18] A.K. Singh, G.N. Tiwari, Performance study of double effect distillation in a multiwick solar still. *Energy Convers. Mgmt* 33 (3), 1992, pp. 207-214.
- [19] A. Kumar, J.D. Anand, Modelling and performance of a tubular multiwick solar still. *Energy* 17 (11), 1992, pp. 1067-1071.
- [20] A. Hepbasli, A key review on exergetic analysis and assessment of renewable energy resources for a sustainable future, *Renewable and Sustainable Energy Reviews* 12, 2008, pp. 593–661.

Simulation of a solar assisted combined heat pump- Organic Rankine Cycle-system

Stefan Schimpf^{1,*}, Karsten Uitz², Roland Span¹

¹ Ruhr-Universität Bochum, Thermodynamics, Bochum, Germany

² SIMAKA Energie- und Umwelttechnik GmbH, Argenbühl, Germany

* Corresponding author. Tel: +49 2343226390, Fax: +49 2343214163, E-mail: s.schimpf@thermo.rub.de

Abstract: In conventional collector systems for the supply of domestic hot water and space heating the collectors come to a standstill during summer whenever the maximum temperature in the storage tank is reached. The resulting excess heat can be harnessed by a combined heat pump-Organic Rankine Cycle-system. The aim of this work is to simulate such a system in order to determine the optimum operating conditions and impacts on power requirement and cost. For this purpose models for collector, storage tank, heat pump and geothermal heat exchanger are implemented. First results indicate that the isentropic efficiency of the scroll expander has the largest influence on the ORC-revenue. For a system consisting of 12 m² flat-plate collector area with an expansion efficiency of $\eta_{s,exp} = 0.7$ the power requirement for space heating and domestic hot water is reduced by 3.6%, whereas the costs decrease by 42 € or 12.3% respectively compared to a conventional system. The results suggest that an installation is more reasonable in larger dwelling units like hotels, senior citizens' homes and multiple family dwellings.

Keywords: Solar Heating, Organic Rankine Cycle, Heat pump.

Nomenclature

A_c	collector aperture area..... m ²	\dot{Q}_{DHW}	heat transferred to the generation of domestic hot water..... W
c	coefficients of the characteristic line of the collector	\dot{Q}_{Loss}	heat loss of a node..... W
$c_{p,CF}$	isobaric heat capacity of collector fluid..... kJ/kgK	\dot{Q}_λ	conductive heat flow across nodes... W
COP	coefficient of performance of the heat pump	t_{ORC}	operating time in ORC mode..... h
C_{tot}	total electricity costs..... €	T_a	ambient temperature..... °C
$E_{HP,DHW}$	electricity consumed by the heat pump for domestic hot water..... kWh	T_{ground}	temperature of the ground..... °C
$E_{HP,SH}$	electricity consumed by the heat pump for space heating..... kWh	T_{DHW}	temperature of domestic hot water. °C
E_{ORC}	electricity generated in the ORC. kWh	T_{SH}	space heating flow temperature..... °C
E_{tot}	total consumed electricity..... kWh	T_{in}	collector inlet temperature..... °C
F'	collector efficiency factor	T_m	mean collector temperature..... °C
G_b	beam radiation..... W/m ²	T_{ORC}	scroll expander inlet temperature.. °C
G_d	diffuse radiation..... W/m ²	T_{out}	collector outlet temperature..... °C
h	enthalpy..... kJ/kg	$w_{t,comp}$	specific work for compression.... kJ/kg
K_θ	incidence angle modifier.....	$w_{t,exp}$	specific work of expansion..... kJ/kg
\dot{m}_{ex}	external mass flow..... kg/s	\dot{V}	volume flow..... l/h
\dot{m}_{ex}	mass flow between nodes..... kg/s	\dot{V}_{str}	volume flow per collector string..... l/h
n_{ser}	number of collectors in series	β	collector slope
\dot{q}	specific heat flow..... W/m ²	$\eta_{s,c}$	isentropic compression efficiency
q_{cond}	specific heat of condensation..... kJ/kg	$\eta_{s,p}$	isentropic pump efficiency
q_{in}	supplied specific heat..... kJ/kg	$\eta_{s,exp}$	isentropic expansion efficiency
		ρ_{CF}	density of the collector fluid..... kg/m ³
		$(\tau_a)_n$	normal transmittance absorptance product

1. Introduction

The application of ground coupled heat pumps and solar combisystems providing both space heating and domestic hot water is a proven technology. In these conventional systems the collectors come to a standstill whenever the maximum temperature in the storage tank is

reached. However The resulting excess heat can be harnessed in an Organic Rankine Cycle (ORC). The domestic application of an ORC driven by solar heat has been a topic of interest in recent years [1]-[5]. In contrast in this study a scroll expander is applied as expansion device. Advantages of the use of a scroll expander are that no valves have to be used and that their low costs are low because of mass production. The performance of a scroll expander as the expansion device of a Rankine cycle has been investigated by [6]-[8]. In the ORC the working fluid of the heat pump is evaporated by solar heat and is afterwards expanded through the scroll compressor of the heat pump which in this case operates as a scroll expander. When the fluid condenses heat is recharged into the ground increasing the coefficient of performance of the heat pump and potentially reducing the necessary borehole depth. Upgraded controls and a pump for the ORC are the only additionally required investments compared to conventional systems. A schematic drawing of the combined heat pump-ORC system is given in Fig. 1.

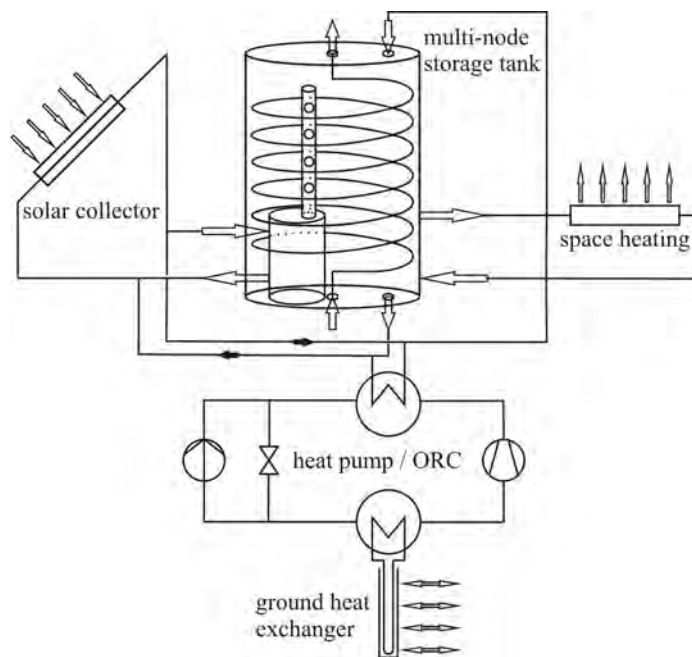


Fig. 1. Schematic drawing of the combined heat pump-ORC system.

2. Modelling of the components of the combined system

In order to simulate a combined system models for the solar collector, storage tank, heat pump, Organic Rankine Cycle and geothermal heat exchanger are required. The flat-plate collector has been modelled dynamically by use of a one-node model which is given in the European norm EN 12975 [9]. Dynamic modelling is necessary because the heat capacity of the collector strongly influences the ORC-revenues due to varying heating-up periods for different operating temperatures. The following differential equation Eq. (1) describes the thermal behaviour of a flat-plate collector.

$$\dot{q} = F'(\tau\alpha)_{en} K_{ob}(\theta)G_b + F'(\tau\alpha)_{en} K_{od}(\theta)G_d - c_1(T_m - T_a) - c_2(T_m - T_a)^2 - c_5 dT_m/dt \quad (1)$$

The beam and diffuse radiation on the sloped collector have been calculated by means of the algorithms of the European Solar Radiation Atlas [10]. If the collector is feeding the storage tank the volume flow is fixed to a constant value. However if it is operating in ORC mode the volume flow is adjusted to keep a constant temperature. In this case the differential term in

Eq. (1) is zero and for hourly irradiation data the process can be considered stationary. The resulting volume flow can be calculated by equating Eq. (1) and Eq. (2).

$$\dot{q} = \rho_{CF} \cdot c_{p,CF} \cdot \dot{V} \cdot (T_{out} - T_{in}) / A_C \quad (2)$$

The storage tank installed in the combined system is a multi-node storage tank with stratification device. The stratification system ensures the layering of solar heated water at different temperatures which allows for the use of low-temperature solar heat in a solar combisystem. For each time step a mass and an energy balance have to be solved. It has to be considered that a mass flow also accounts for an energy flow throughout via mixing. The mass and energy flows in a node are depicted in Fig. 2.

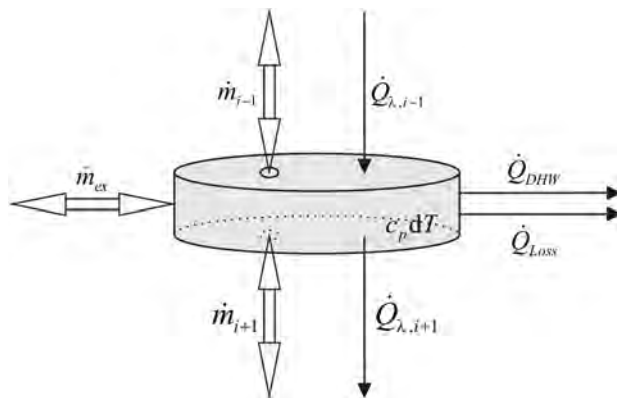


Fig. 2. Mass and energy flow in a node.

Mass flows between adjacent nodes ($\dot{m}_{i-1}, \dot{m}_{i+1}$) result from external flows (\dot{m}_{ex}) of the collector, heat pump or floor heating which are either supplied or removed. The terms $\dot{Q}_{\lambda,i-1}$ and $\dot{Q}_{\lambda,i+1}$ describe the heat conduction between adjacent nodes whereas \dot{Q}_{DHW} marks the heat flow from the node to the coiled tube heat exchanger in which the domestic hot water is generated. \dot{Q}_{Loss} indicates the heat loss from the storage tank to the ambient. The mass flows are first converted into equivalent heat flows, afterwards the set of differential equations is solved for each node.

All thermodynamic properties required for the simulation of the ORC and the heat pump are calculated with the software Refprop [11]. The terminal temperature differences in heat exchangers are set to 5 K. For the calculation of the COP of the heat pump the upper and lower pressure are the saturation pressures belonging to the temperatures T_{ground} and T_{SH} in case of floor heating or T_{DHW} in case of the generation of domestic hot water. The suction gas is overheated by 3 K (1a) and afterwards compressed (2a). The compression is assumed to be adiabatic with an isentropic efficiency of $\eta_{s,c} = 0.6$. Subsequently the refrigerant condenses (3a) and transfers heat to the floor or water heating system. The refrigerant leaves the condenser as saturated liquid so no subcooling is performed. To complete the cycle the pressure is relieved by an expansion valve (4a). The COP of the described process can be calculated with Eq. (3).

$$COP = \frac{q_{cond}}{w_{t,comp}} = \frac{|h_{3a} - h_{2a}|}{h_{2a} - h_{1a}} \quad (3)$$

For the calculation of the thermal efficiency of the ORC the pressure levels are given through the temperatures T_{ground} and T_{ORC} . The fluid is compressed by a pump with an isentropic

efficiency of $\eta_{s,p} = 0.6$ (2b). Afterwards the fluid is evaporated by heat transfer from the collector fluid (3b). The saturated vapour is expanded in the scroll expander (4b). By default the isentropic efficiency of the expansion is set to $\eta_{s,exp} = 0.5$ which is in good agreement with Peterson et al. [6]. Downstream of the expander the refrigerant is condensed and subcooled by 2 K (1b). The thermal efficiency of this cycle can be calculated as

$$\eta_{ORC} = \frac{w_{t,exp}}{q_{in}} = \frac{|h_{4b} - h_{3b}|}{h_{2b} - h_{1b}} \quad (4)$$

To model the ground heat exchanger a short time step model is required because the thermal response of the ground is critical for the description of condensation in ORC mode. With the analytical approach of Lamarche and Beauchamp [12] an hourly calculation, which is in good agreement with the short time-step g functions developed numerically by Yavuzturk and Spitler [13], is achieved.

3. Simulation and optimisation of the combined system

In this work a combined heat pump-ORC system has been simulated which is installed in a single family house. The house has a total floor space of 167 m² and a transmission heat loss of 148.2 W/K. Both values are characteristically for a low-energy consumption house fulfilling the German KfW 70 standard. For this type of building a heat pump with a heating output of 5 kW is sufficient. The simulations were carried out with the refrigerant R134a as working fluid of heat pump and ORC. The simulated system comprises a multi-node storage tank with a volume of 700 l. Six south orientated flat-plate collectors with an aperture area of 2 m² each are installed in the system. The working fluid of the collectors is a 20/80 propylene glycol-water mixture. The characteristics of both storage tank and collector represent those of commercially available products. Hourly data for the ambient temperature and solar radiation for the climatological station Weihenstephan (48° 24' N, 11° 42' E) are taken from the European Solar Radiation Atlas [10]. It is assumed that at 6:30, 7:30, 18:30 and 19:30 in each case 50 l of hot water with a temperature of 45 °C are generated in the coiled tube heat exchanger passing through the storage tank.

The aim of the simulation is to find the optimum configuration of the combined system. For the optimisation the number of collectors in series, the volume flow per string of collectors, the collector slope and the expander inlet temperature of the ORC are varied. The range of these parameters is given in Table 1.

Table 1. Modified parameters for the optimization of the combined system and their range of values.

Parameter	Range of simulated values
Number of collectors in series n_{ser}	1 – 3
Volume flow per string of collectors \dot{V}_{str}	20 – 80 l/h
Collector slope β	15 – 55 °
Expander inlet temperature T_{ORC}	60 – 90 °C

Chen et al. [5] simulated a small scale solar-driven carbon dioxide power system and mention the importance of the expansion efficiency as the power output decreases by 60% for an isentropic efficiency of 50% instead of 85%. Wang et al. [7] managed to increase the expansion efficiency from 50% to 70% by using a compliant expander instead of a kinematically constrained one. In this work it is therefore investigated in how far the efficiency of the expansion influences the ORC output and the overall performance of the

combined system. For this purpose additional simulations have been done with efficiencies of $\eta_{s,exp} = 0.6$ and $\eta_{s,exp} = 0.7$ instead of the default value of $\eta_{s,exp} = 0.5$.

The output values of the simulation are the electricity consumption of the heat pump for space heating and domestic hot water as well as the power generated in the scroll expander and the power consumption of the pump of the ground loop in the ORC. The power input of the ground loop pump is assumed to be 60 W and has to be subtracted from the power output of the scroll expander. For the financial evaluation electricity costs are set to 0.2 €/kWh whereas the generated power yields 0.3301 €/kWh under the current German feed-in tariff. All components have been simulated for one year with a time step of one minute except for the ground heat exchanger, which has been calculated on hourly basis. All simulations were performed using Microsoft Visual Basic for Applications scripts

4. Results

The results of the simulation show that the energetic optimum of the combined system is reached for collector slopes between 25° and 35°. The optimum is therefore found for slopes up to 23.4° lower than the rule of thumb of Duffie and Beckmann [14] proposing surface slopes equal to the latitude. This effect can be explained with the fact that in summer the total irradiation on slopes which are tilted to a lesser extent is higher. This relation which favours the ORC together with the influence of the volume flow on the power output of the ORC and the operating time in ORC mode are displayed in Fig. 3 for a connection of three collectors in series and an expander inlet temperature of 70 °C. The decrease of the ORC power output with increasing volume flow per collector string is due to the shorter operating time in ORC mode. With increasing volume flow lower collector outlet temperatures are achieved and thus the ORC starting temperature is reached less often.

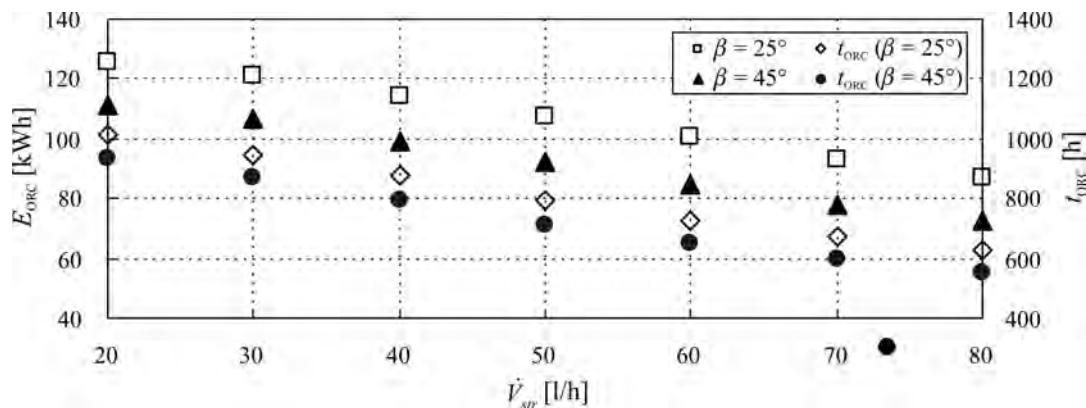


Fig. 3. Influence of the operating time in ORC mode t_{ORC} , the volume flow per collector string \dot{V}_{str} and the collector slope β on the ORC power output E_{ORC} for a connection of three collectors in series and an expander inlet temperature of 70 °C.

The influence of the array configuration, either parallel connection or connection in series, and the specific volume flow per m² aperture area on the system performance is outlined in Table 2 for a collector slope of 25° and an expander inlet temperature of 70 °C. Different array configurations (A, B, C) with the same specific volume yield similar output values. The ORC power output is an exception because it decreases with the number of collectors connected in series. The total electricity demand of the combined system however is almost constant. If the volume flow per collector string is held constant and the number of collectors in series is increased (A, D, E) the electricity consumption of the heat pump for space heating $E_{HP,SH}$ rises. To reach T_{SH} a rather low irradiance is required and the operating time in space

heating mode is quite high. As a consequence the operating time is rising to a lesser extent than the solar gain is dropping because of the lower volume flow. In contrast the electricity consumption of the heat pump for the generation of domestic hot water is reduced and the ORC power output is increased because higher operating temperatures are reached more often and faster for smaller specific volume flows.

Table 2. The effect of the array configuration and the specific volume flow per m^2 aperture area on the annual electricity consumption of the heat pump for space heating $E_{HP,SH}$ and domestic hot water $E_{HP,DHW}$ as well as the ORC power output E_{ORC} and the total power consumption E_{tot} for a collector slope of 25° and an expander inlet temperature of $70^\circ C$.

Case	n_{ser}	\dot{V}_{str} [l/h]	$\dot{V}_{str} / (n_{ser} \cdot A_c)$ [l/m ² h]	$E_{HP,SH}$ [kWh]	$E_{HP,DHW}$ [kWh]	E_{ORC} [kWh]	E_{tot} [kWh]
A	1	20	10	1261.6	611.2	113.4	1759.4
B	2	40	10	1260.1	612.4	102.8	1769.7
C	3	60	10	1258.7	599.2	100.3	1757.6
D	2	20	5	1303.6	598.0	123.5	1778.1
E	3	20	3.33	1354.1	536.5	125.9	1764.7

For the cases A, B and C given in Table 2 the influence of the isentropic expansion efficiency on the expander power output has been investigated. The results are illustrated in Fig. 4 together with the thermal efficiency of an Organic Rankine Cycle with the assumptions made in section 3, an evaporation temperature of $70^\circ C$ and a condensing temperature of $20^\circ C$. If the power consumed by the ground loop pump is subtracted from the values depicted in Fig. 4 the same values for the power output of the ORC as in Table 2 are obtained for $\eta_{s,exp} = 0.5$.

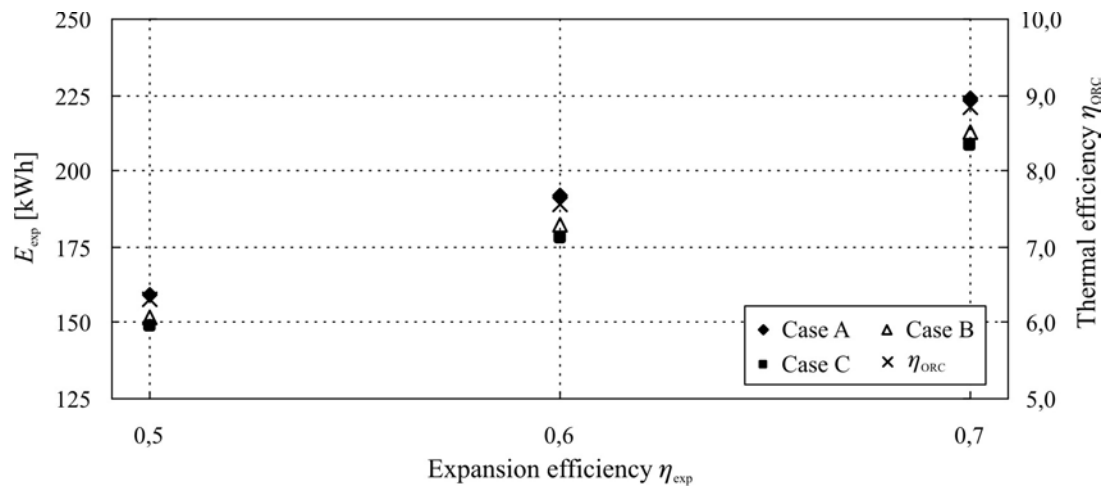


Fig. 4. Influence of the expansion efficiency $\eta_{s,exp}$ on the thermal efficiency of the ORC η_{ORC} and the expander power output E_{exp} for different array configurations with the same specific volume flow.

Fig. 4 shows that the thermal efficiency of the ORC η_{ORC} is the only variable influencing the expander output power. If the efficiency of the expansion is increased by ten percentage points the expander output power and η_{ORC} grow by about 20%. This result is in agreement with the course determined by Chen et al. [5]. With rising thermal efficiency a negligible lower amount of heat is recharged into the ground which would influence the electricity consumption of the heat pump. As the thermal efficiency has no effect on the operating time of the ORC, the power consumption of the ground loop pump remains constant. The results of the simulation reveal that all output values except for the power output remain almost unaffected by the expansion efficiency which has been expected.

Finally the optimised system configurations for each expander efficiency are compared with a conventional system from an energetic and financial point of view. The conventional system is simulated using the methods and assumptions presented in section 2 and section 3 just without the ORC mode. The simulation results for each optimised system and the conventional system are outlined in Table 3.

Table 3. Comparison of the electricity consumption and cost of a conventional solar combisystem and optimised system configurations of the combined heat pump-ORC system for different isentropic scroll expander efficiencies.

$\eta_{s,exp}$	n_{ser}	\dot{V}_{str} [l/h]	β [°]	T_{ORC} [°C]	E_{tot} [kWh]	ΔE_{tot} [%]	ORC-revenue [€]	Total costs C_{tot} [€]	ΔC_{tot} [%]
-	2	30	35	-	1729.3	-	-	346.1	-
0.5	1	40	35	60	1717.4	-0.7	30.2	328.6	-5.1
0.6	1	40	25	60	1693.0	-2.1	41.2	319.1	-7.8
0.7	1	30	25	60	1665.1	-3.6	53.7	308.6	-10.8
0.5	1	30	25	60	1719.5	-0.6	35.8	326.3	-5.7
0.6	3	20	25	70	1727.3	-0.1	61.9	316.3	-8.6
0.7	3	20	25	70	1689.9	-2.3	74.2	303.9	-12.3

The results indicate that the energetic and financial optima are reached for different system configurations. The relative cost savings exceed the energy savings which is due to the fact that 1 kWh generated electricity equals 1.65 kWh consumed electricity because of the feed-in tariff. The energetic optima are reached for a parallel connection of collectors. The rather low energy savings can be explained with the fact that in the combined system the storage tank is charged with less solar heat than in a conventional system. However the combined system is still superior in comparison. For higher expansion efficiencies the array configurations with the lowest specific volume flow become attractive from a financial standpoint as a consequence of the greater ORC revenues.

5. Conclusion

In this work annual simulations of a solar assisted combined heat-pump ORC system have been performed. The results indicate that this system is superior to a conventional solar combisystem from an energetic and financial standpoint. The annual savings strongly depend on the efficiency of the expansion. For a small combined system with a flat-plate collector area of 12 m² the relative energetic savings range from 0.7% ($\eta_{s,exp} = 0.5$) to 3.6% ($\eta_{s,exp} = 0.7$). The absolute monetary savings are about 20 € for $\eta_{s,exp} = 0.5$. They rise to 42 € for an increased efficiency of $\eta_{s,exp} = 0.7$. It therefore seems possible to cover the additional costs that arise from an ORC pump and advanced controls. As the costs for the controls are independent of the system size an application of the combined system is more reasonable in larger dwelling units like hotels, senior citizens' homes and multiple dwelling houses. Experimental studies to evaluate the efficiency of the scroll compressor in expansion mode are required. The results of this study concerning collector slope and volume flow can also be transferred to future works regarding solar-driven Organic Rankine Cycles.

Acknowledgements

The authors would like to thank the Federal Ministry of Economics and Technology for financially supporting this work.

References

- [1] J L. Wolpert; S. B. Riffat, Solar-powered Rankine system for domestic applications, *Applied Thermal Engineering* 16, 1996, pp. 281-289.
- [2] C.-H. Kuo; W.-J. Yang; N. Arai; K. Mori, Solar-powered organic Rankine system for domestic electric-power generation, *Energy and the environment: Proceedings of the Second Trabzon International Energy and Environment Symposium*, 1999, pp. 67-74.
- [3] A. Delgado-Torres; L. Garcia-Rodriguez, Analysis and optimization of the low-temperature solar organic Rankine cycle (ORC), *Energy Conversion and Management* 51, 2010, pp. 2846-2856.
- [4] X. R. Zhang; H. Yamaguchi; K. Fujima; M. Enomoto; N. Sawada, Theoretical analysis of a thermodynamic cycle for power and heat production using supercritical carbon dioxide, *Energy* 32, 2007, pp. 591-599.
- [5] Y. Chen; W. Pridasawas; P. Lundqvist, Dynamic simulation of a solar-driven carbon dioxide transcritical power system for small scale combined heat and power production, *Solar Energy* 84, 2010, pp. 1103-1110.
- [6] R. B. Peterson; H. Wang; T. Herron, Performance of a small-scale regenerative Rankine power cycle employing a scroll expander, *Proceedings of the Institution of Mechanical Engineers/ Part A, Journal of power and energy* 222, 2008, pp. 271-282.
- [7] H. Wang; R. B. Peterson; T. Herron, Experimental performance of a compliant scroll expander for an organic Rankine cycle, *Proceedings of the Institution of Mechanical Engineers/ Part A, Journal of power and energy* 223, 2009, pp. 863-872.
- [8] T. Saitoh; N. Yamada; S. Wakashima, Solar Rankine Cycle System Using Scroll Expander, *Journal of Environment and Engineering* 2, 2007, pp. 708-718.
- [9] EN 12975, Thermal solar systems and components - Solar collectors - Part 2: Test methods, 2006.
- [10] K. Scharmer; J. Greif, *The European solar radiation atlas*, Les Presses de L'École des Mines, 1st Edition, 2000.
- [11] E. W. Lemmon; M. O. McLinden; M. L. Huber, NIST Reference Fluid Thermodynamic and Transport Properties – REFPROP. NIST Standard Reference Database 23, Version 8, 2002.
- [12] L. Lamarche; B. Beauchamp, A fast algorithm for the simulation of GCHP systems, *ASHRAE Transactions* 113, 2007, 470-476.
- [13] C. Yavuzturk; J. D. Spitler, A short time step response factor model for vertical ground loop heat exchangers, *ASHRAE Transactions* 105, 1999, 475-485.
- [14] J. A. Duffie; W. A. Beckman, *Solar Engineering of Thermal Processes*, Jon Wiley & Sons, 2nd Edition, 1980, pp. 98-101.

Optimisation of Low Temperature Difference Solar Stirling Engines using Genetic Algorithm

Kwanchai Kraitong, Khamid Mahkamov*

School of Computing, Engineering and Information Sciences, Northumbria University,
Newcastle upon Tyne, NE1 8ST, UK*

*Corresponding author. Tel: +44 191 2274739, Fax: +44 191 2437630,

Email: khamid.mahkamov@northumbria.ac.uk

Abstract: This paper presents results of theoretical investigations on the determination of optimal design parameters of a Low Temperature Difference (LTD) Solar Stirling Engine using optimisation method based on Genetic algorithms. The developed thermodynamic mathematical model of the engine takes into account hydraulic and mechanical losses in the engine's working process and this model was coupled to the optimisation algorithm. A set of such design parameters as the stroke of the displacer and diameter and stroke of the power piston and the thickness of the regenerator placed in the displacer have been considered as variables. The engine's performance parameter such as the brake power is used as the objective function of the optimisation algorithm. The GA code is implemented in MATLAB. The accuracy of the optimal design engine's performance is examined using 3D CFD modelling of the working process of the engine. The set of design parameters obtained from the optimisation procedure provides the noticeable improvement of the engine's performance compared with the performance of the original LTD Solar Stirling engine with the same operating condition.

Keywords: LTD Stirling engine, Second-order mathematical model, Mechanical losses, CFD, Genetic algorithm.

Nomenclature

C_p specific heat at constant pressure... $J \cdot kg^{-1} K^{-1}$	V_c volume of the compression space..... m^3
C_v specific heat at constant volume ... $J \cdot kg^{-1} K^{-1}$	V_{c1} volume of the compression space in the displacer chamber..... m^3
D_p diameter of piston..... m	V_{c2} volume of the compression space in the piston cylinder..... m^3
D_D diameter of displacer..... m	V_{dc} dead volume of the compression space... m^3
f frequency..... Hz	V_{de} dead volume of the expansion space..... m^3
H_d thickness of regenerator..... m	V_e volume of the expansion space..... m^3
m mass of the gas in the control volume..... kg	V_{SP} swept volume of the piston
$maxvalue$ maximum fitness value in the value map m^3
\dot{m}_i inlet mass flow rate..... $kg \cdot s^{-1}$	V_{SD} swept volume of the displacer..... m^3
\dot{m}_o outlet mass flow rate..... $kg \cdot s^{-1}$	W work..... J
P_b brake power..... W	W_b cyclic brake work..... J
P_c pressure in the compression space..... Pa	W_c work of the compression space..... J
P_{c1} pressure in the compression space in the displacer chamber..... Pa	W_e work of the expansion space..... J
P_{c2} pressure in compression space in the piston cylinder..... Pa	x current displacement of the piston..... m
P_e pressure in the expansion space..... Pa	x_0 stroke of the piston..... m
P_i indicated power..... W	y current displacement of the displace..... m
Q heat transfer rate..... W	y_0 stroke of the displacer m
T total crank torque..... $N \cdot m$	Z_D stroke of displacer..... m
T_b frictional torque of the rolling bearing. $N \cdot m$	Z_p stroke of piston..... m
T_i inlet temperature..... K	θ piston crank angle..... rad
T_o outlet temperature..... K	φ displacement phase angle of the piston.. rad
T_p piston crank torque..... $N \cdot m$	k, ε turbulent kinetic energy and dissipation
t time..... sec	turbulent kinetic energy..... $m^2 \cdot s^{-2}$

Value..... fitness value

Table 1. Dimensions of the LTD Stirling engine manufactured by Kongtragool and Wongwisas [11]

The geometric data of a twin power piston LTD Stirling engine	Value
working piston stroke (m)	0.0826
working piston diameter(m)	0.083
working piston swept volume (m ³)	893.8x10 ⁻⁶
displacer piston stroke (m)	0.0795
displacer piston diameter (m)	0.32
displacer piston swept volume (m ³)	6393.8 x10 ⁻⁶
swept volume ratio	7.15
displacement phase angle of the pistons (°)	90

3. Modelling Procedure

3.1. Thermodynamic modelling

The second-order mathematical model taking into account the pressure drop and the mechanical losses developed by Kraitong and Mahkamov [10] was used for the performance prediction of the engine. This model is the modification of that developed by Timoumi et al. [7] and Urieli [12]. The equations of energy and mass conservation for each control volume are expressed as follows:

$$C_v \frac{d(mT)}{dt} = dQ - \frac{dW}{dt} - \dot{m}_o C_p T_o + \dot{m}_i C_p T_i \quad (1)$$

$$\frac{dm}{dt} = \dot{m}_o - \dot{m}_i \quad (2)$$

Work done by the working gas inside the compression space and the expansion space can be calculated as $\frac{dW_c}{dt} = P_c \frac{dV_c}{dt}$ and $\frac{dW_e}{dt} = P_e \frac{dV_e}{dt}$, respectively.

Volumes of the compression and expansion spaces are expressed as

$$V_c = V_{dc} + \frac{V_{SP}}{2}(1 + \cos(\theta - \varphi)) + \frac{V_{SD}}{2}(1 - \cos \theta) \quad (3)$$

$$V_e = V_{de} + \frac{V_{SD}}{2}(1 + \cos \theta) \quad (4)$$

where $V_{SP} = \pi \frac{D_p^2}{4} Z_p$ and $V_{SD} = \pi \frac{D_D^2}{4} Z_D$.

In order to determine the brake cyclic power, the kinetic motion equations of the mechanical transmission system of the reciprocating engine proposed by Guzzomi et al. [13,14] were used. The determination of the frictional forces in the sealing rings of the displacer rod is carried out using methodology described in [15]. These results were used to calculate the torque induced by the pistons (T_p). The brake cyclic work and the brake cyclic power, therefore, are calculated as

$$T = \Sigma T_p \tag{5}$$

$$W_b = \int \left(\frac{dW_b}{dt} \right) dt = \int_0^{\tau} \left((T - T_b) \frac{d\theta}{dt} \right) dt \tag{6}$$

$$P_b = W_b f \tag{7}$$

For numerical calculations, the cycle was split into 1000 time-steps and calculations were performed until the pressure and temperature curves converged and the overall heat balance in the system was reached.

3.2. CFD modelling

To achieve better understanding of the working process of the LTD Stirling engine and obtain more accuracy in the performance prediction, 3D CFD modeling using the standard $k-\epsilon$ turbulence model for a compressible flow was carried out to investigate the work of the engine. Commercial CFD software, FLUENT was used to perform CFD simulations of the working process of the engine. During the simulations the movement of pistons was taken into account and the regenerator of the engine was treated as a homogeneous porous medium. The subroutines describing displacements of the pistons and the displacer were written and then connected to the main body of the programme. The cycle was divided into equal 500 time-steps and calculations were performed using a high performance computer. The average gas temperature and pressure in each engine's working space were monitored during calculations in order to determine whether the steady-state condition was reached in the simulated operation of the engine.

3.3. Optimisation modelling

Genetics algorithm is a stochastic optimisation method based on the mechanism of natural selection for survival as the procedure in order to obtain optimal results [16]. The real-valued GA or the continuous GA is applied in this work for the quantitative limitation and the reduction of the computing time [17]. The structure of the continuous GA of the LTD Stirling engine is represented in Fig. 2.

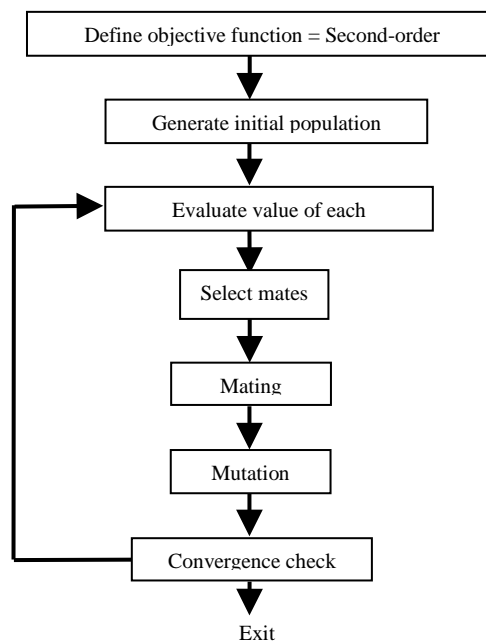


Fig. 2. The structure of the continuous GA of the LTD Stirling engine.

Several original engine design and operational parameters, namely the diameter of the displacer of 0.32 m, the engine speed of 46.5 rpm, the solar irradiation of 5097 W/m² created using a solar simulator and the cooler surface temperature of 307 K, are accepted to be fixed as constant values in this work. There are only four engine design parameters are defined as variables. These are the diameter and the stroke of the power piston, the stroke the displacer and the thickness of the regenerator:

$$\text{Chromosome} = (D_p; Z_p; Z_D; H_d) \quad (6)$$

The upper and the lower bound of each variable are as follows;

$$\begin{aligned} 0.02 < D_p < 0.13 & \quad ; D_p \text{ is diameter of piston (m)} \\ 0.04 < Z_p < 0.3 & \quad ; Z_p \text{ is stroke of piston (m)} \\ 0.04 < Z_D < 0.3 & \quad ; Z_D \text{ is stroke of displacer (m)} \\ 0.01 < H_d < 0.2 & \quad ; H_d \text{ is thickness of regenerator (m)} \end{aligned}$$

The above boundaries are defined based on the practical manufacturing and design considerations. The maximum diameter of the piston is limited by the diameter of the cold plate which is equal to the fixed displacer diameter. The range of the displacer stroke to be investigated is typical for displacers of LTD Stirling engines [18]. Only one of the engine's performances, namely the brake power, is defined to be the chromosome value because the heat source is solar energy which is assumed to be cost-free. The the brake power of the engine obtained using the developed second-order mathematical model is used as the objective function:

$$\text{Brakepower} = f(\text{chromosome}) = f(D_p; Z_p; Z_D; H_d) \quad (7)$$

In GA, there is no effect of the guessed initial chromosomes on the convergence of the solution, thus the initial population is created by using the absolutely random procedure. A generated initial population is in the matrix formation of various chromosomes. The size of the population effects the convergence in the optimization procedure. The number of chromosomes between 30 and 100 is the typical size to operate GA [19]. In this study, the number of chromosomes in a generation of 30 is used. The chromosome value which is the brake power is evaluated by the fitness function for locating in the value map of each generation [20]:

$$\text{Fitnessvalue} = \frac{1}{1 + \text{maxvalue} - \text{value}} \quad (8)$$

The fitness value of each chromosome is descending order to determine survival chromosomes for the next generation. The number of survival chromosomes is defined by the selection rate of 0.5 from the weighted random pairing selection and the rank weighting technique [17]. The single point crossover is used for the mating process that the parents are operated by the reproduction operator to produce some offsprings for the next generation. Fittest chromosomes of the ranking are randomly selected to be the parents for the reproduction operation. The second operator of the reproduction called the mutation is used as a tool to avoid finding only the local solution. The mutation rate of 0.2, though probably is high, results in the gradual convergence and ensures that the global maximum is not missed out in during simulations [17].

Finally, the new generation is produced and the population of new design parameters in this generation is then evaluated by the developed thermodynamic model and the fitness function is checked for the ranking until the solution found satisfying the termination condition. The maximum number of generation in the computing process of 80 is defined to obtain the convergence of this algorithm. The optimisation code was modified from [19] and implemented in MATLAB. In this case, the continuous GA was used to obtain the optimal design parameters for the performance's improvement of an original LTD Stirling engine. Simulations were, thus, conducted for the same operating condition. A set of optimal design parameters from the numerical simulations was then used to create the engine mesh for the 3D CFD simulation to more accurately predict the engine power.

4. Results from optimisation calculations

The modelling of the engine with the SM15-matrix regenerator was performed for the constant solar flux of 5097 W/m^2 , the cooler surface temperature of 307 K, the engine speed of 46.5 rpm with air at 1 bar pressure used as a working fluid. Figure 3 represents the best brake power for each generation. The best brake power first sharply increases and then gradually reaches the convergence with its value of 1.515 W. The design parameters of this generation are presented in Table 2. The corresponding indicated power is 1.668 W.

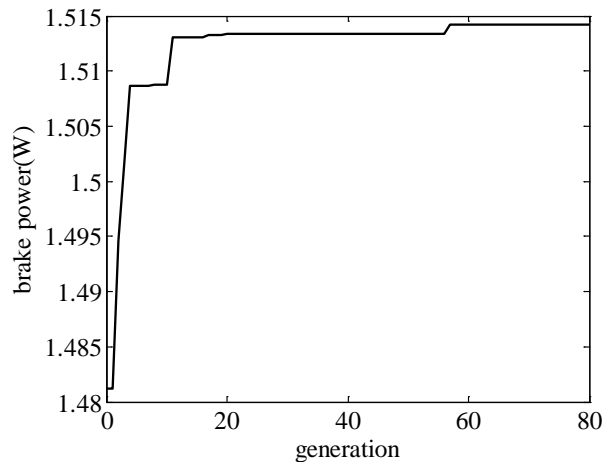


Fig. 3. The best brake power of each generation as the function of generations.

Table 2. The first set of optimal engine design parameters obtained from optimisation simulation.

Optimal engine design parameters	Value
working piston stroke (m)	0.228
working piston diameter(m)	0.065
displacer piston stroke (m)	0.074
displacer thickness (m)	0.056

However, it could be seen that the stroke of the power piston of 0.228 m which is much longer than the stroke of the displacer of 0.074 m. This may be unsuitable for the practical engine. Thus, the power piston and displacer strokes were fixed at 0.1 m and a new set the optimisation simulations with two variables were run. Optimal engine parameters from the second run are presented in Table 3 and the maximum brake and indicated power is 1.346 W and 1.47 W, respectively. There is only 11% reduction in power when compared with the results of the first optimization run.

Table 3. The second set of optimal engine design parameters is obtained from optimisation simulation.

Optimal engine design parameters	Value
working piston stroke (m)	0.1
working piston diameter(m)	0.1
displacer piston stroke (m)	0.095
displacer thickness (m)	0.058

Finally, two engines with optimal engine parameters shown in Tables 2 and 3 were modelled using 3D CFD simulation. The indicated power of the first and the second engine calculated from P-V diagrams which are shown in Fig. 4a and Fig. 4b are 1.427 W and 1.352 W, respectively. 3D CFD modelling results demonstrate that the second-order thermodynamic model used in optimisation procedure has an adequate accuracy in the prediction of the engine performance.

5. Conclusion

The developed second-order mathematical model of the LTD Stirling engine was developed which accounts for hydraulic and heat losses in the working process and mechanical losses in the engine. This model was used with GA optimisation code. As a result of optimization simulations a set of design parameters for the engine was obtained which provides a considerable improvement in the performance. Results obtained using the developed second-order thermodynamic model were calibrated using 3D CFD modeling technique. The optimisation procedure developed in his work can be applied to improve the design of a wide range of Stirling engines, including high temperature ones.

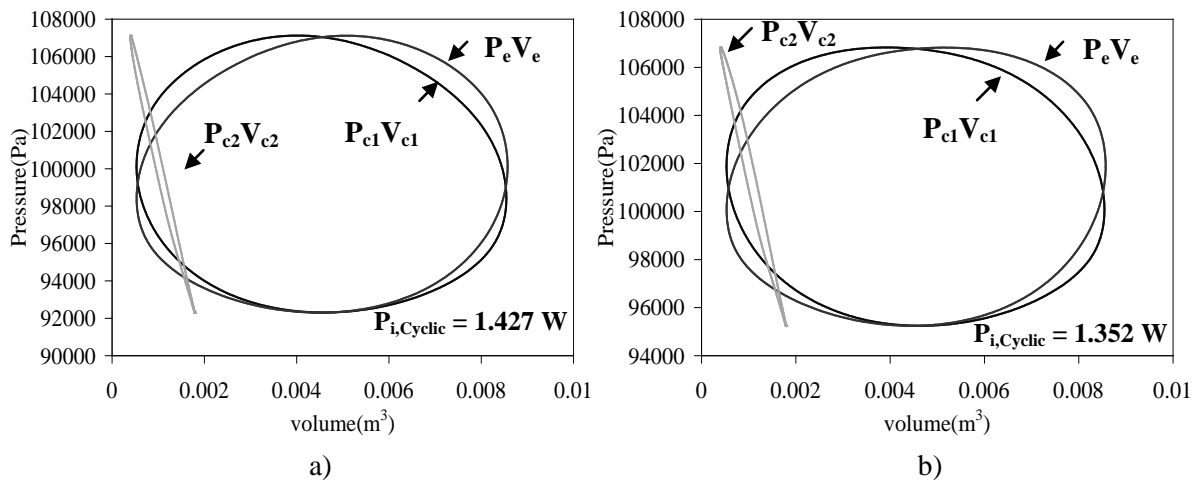


Fig. 4. 3D CFD modeling results: a) P-V diagrams for the first optimal parameters set obtained using and b) P-V diagrams for the second optimal parameters set

6. Acknowledgements

This work is a part of a PhD study which is supported by the Ministry of Science and Technology of the Royal Thai Government. Authors also would like to thank Professor Somchai Wongwises and Assistant Professor Bancha Kongtragool for providing data on their twin power piston LTD Stirling engine.

References

- [1] B. Kongtragool, S. Wongwises, A review of solar-powered Stirling engines and low temperature differential Stirling engines, *Renewable and Sustainable Energy Reviews*, 2003, pp. 131–154.
- [2] L. Erbay, H. Yavuz, Analysis of the Stirling heat engine at maximum power conditions, *Energy* 22, 1996, pp. 645–650.
- [3] S. Hsu, F. Lin, J. Chiou, Heat-transfer aspects of Stirling power generation using incinerator waste energy, *Renewable Energy* 28, 2003, pp. 59–69.
- [4] A. Tavakolpour, A. Zomorodian, A. Golneshan, Simulation, construction and testing of a two-cylinder solar Stirling engine powered by a flat-plate solar collector without regenerator, *Renewable Energy* 33, 2008, pp. 77–87.
- [5] N. Martaj, L. Grosu, P. Rochelle, Exergetical analysis and design optimisation of the Stirling engine, *Int. J. of Exergy* 3, 2006, pp. 45–46.
- [6] B. Orunov, V. T. Krykov, A. P. Korobkov, K. Mahkamov, D. Djumanov, The first stage of the development of a small Stirling tri-generation power unit, *Proceeding of 12th international Stirling engine conference*, 2005, pp. 416–423.
- [7] Y. Timoumi, I. Tlili, S. Nasrallah, Design and performance optimization of GPU 3 Stirling engines, *Energy* URL doi:10.1016/j.energy.2008.02.005.
- [8] Y. C. Hsieh, T. C. Hsu, J. S. Chiou, Integration of a free-piston Stirling engine and a moving grate incinerator, *Renewable Energy* 33, 2008, pp. 48–54.
- [9] A. Altman, SNAPpro: Stirling numerical analysis program, URL <http://home.comcast.net/snapburner/SNAPpro ISEC 2004.pdf>, 2004.
- [10] K. Kraitong, K. Mahkamov, Thermodynamic and CFD Modelling of Low Temperature Difference Stirling engines, *Proceeding of 14th international Stirling engine conference*, 2009.
- [11] B. Kongtragool, S. Wongwises, Performance of a twin power piston low temperature differential Stirling engine powered by a solar simulator, *Solar Energy* 81, 2007, pp. 884–895.
- [12] I. Urieli, Stirling Cycle Machine Analysis, URL <http://www.ent.ohiou.edu/urieli/stirling/me422.html>, 2008.
- [13] D. C. Hesterman, B. J. Stone, A systems approach to the torsional vibration of multi-cylinder reciprocating engines and pumps, *Proc. IMechE* 208, 1994, pp. 395–408.
- [14] A. L. Guzzomi, D. C. Hesterman, B. J. Stone, The effect of piston friction on engine block dynamics, *Proc. IMechE* 221, 2007, pp. 227–289.
- [15] K. Mahkamov, D. Ingham, Analysis of the Working Process and Mechanical Losses in a Stirling Engine for a Solar Power Unit, *J. of Solar Energy Engineering* 121, 1999, pp. 121–127.
- [16] D. E. Goldberg, *Genetic Algorithms in Search, Optimization & Machine Learning*, Addison-Wesley Publishing Company, USA, 1989, ISBN 0- 201-15767-5.
- [17] R. L. Haupt, S. E. Haupt, *Practical Genetic Algorithm*, John Wiley & Sons, USA, Edition 2nd, 2004, ISBN 0-471-45565-2.
- [18] J. R. Senft, *An Introduction to Low Temperature Differential Stirling Engines*, Moriya Press, USA, 2007, ISBN-13: 978-0965245517.
- [19] A. M. S. Zalzal, P. J. Fleming, *Genetic Algorithms in Engineering Systems*, The Institution of Electrical Engineers, UK, 1997, ISBN 0-85296- 902-3.
- [20] S. Elisaveta, B. Natasha, BASIC-A genetic algorithm for engineering problems solution, *Computers and Chemical Engineering* 30, 2006, pp. 1293–1309.

Performance Prediction and Experimental Analysis of a Solar Liquid Desiccant Air Conditioner

S. Alizadeh^{1,*}, H.R. Haghgou¹

¹Department of Energy, Materials & Energy Research Centre, P. O. Box 14155-4777, Tehran, Iran

*Corresponding author. Tel: +98 261 620 4131, Fax: +98261 6201888, E-mail: shahab_alizadeh@hotmail.com

Abstract: In a liquid desiccant air conditioner developed at Materials & Energy Research Centre (MERC), dehumidification of the outside air is achieved through a packed-bed heat and mass exchanger, using lithium chloride solution as the desiccant. The dry air thus obtained is evaporative cooled inside a cooling pad and directed into the conditioned space. The dilute solution from the dehumidification process is concentrated in a scavenger air regenerator using hot water from flat plate solar collectors. Carryover of the desiccant particles has been avoided by using eliminators, such as demister or filter.

In this paper the experimental results obtained from testing the prototype of the liquid desiccant absorber unit in a simulated Persian Gulf summer has been presented and compared with a previously developed model for the packed-bed. The comparison reveals that good agreement exists between the experiments and model predictions. The inaccuracies are well within the measuring errors of the temperature, humidity and the air and solution flow rates. The above tests further reveal that the unit would have a satisfactory performance in controlling the air temperature and humidity if installed on a commercial site of about 200 m² area in a hot and humid climate.

A commercialization study was performed for the solar operated liquid desiccant air conditioner (LDAC) and compared with the conventional vapour compression system. The study reveals that the operating cost of an LDAC is significantly lower than its conventional counterpart. The costs would further reduce if a storage system was used to store the concentrated solution of liquid desiccant. A simple payback of five years was determined for the solar components of the liquid desiccant system in this study.

Keywords: Liquid desiccant, Dehumidification, Packed-bed, Solar regeneration.

1. Introduction

Much work has so far been conducted in the area of air dehumidification using liquid desiccant and a cross-flow or a packed-bed type heat and mass exchanger, as the dehumidifier [1]. The use of the solar liquid desiccant air dehumidification / cooling system appears to be promising in hot and humid locations of Iran, such as the Persian Gulf region, due to high availability of solar energy. Figure 1 shows a schematic diagram of the solar air conditioner.

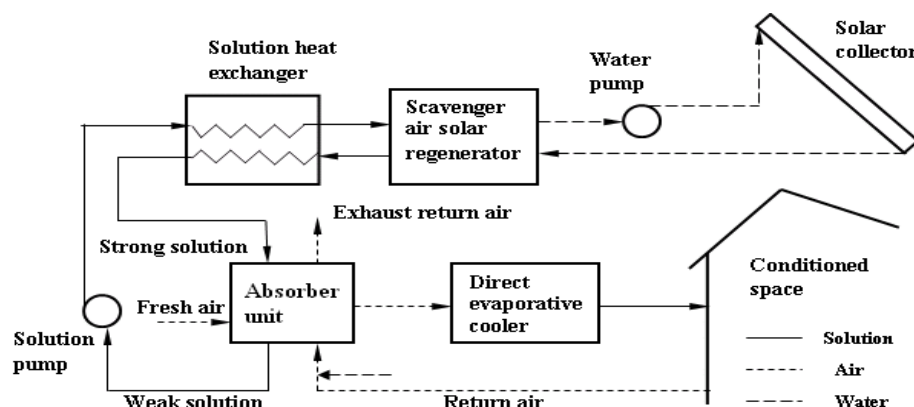


Figure 1. schematic diagram of a liquid desiccant solar air conditioner

Outside air is dehumidified in the absorber unit using a strong solution of lithium chloride and cooled within a direct evaporative cooler before it is introduced into the conditioned space. The dilute solution thus obtained is concentrated in a scavenger air solar regenerator using hot water from flat plate solar collectors. A solution heat exchanger, as indicated in the figure, is used for heat recovery between the strong and weak solutions. Return air from conditioned space has also been used to take some heat out of the outside air as shown in Figure 1.

Considerable laboratory experiments, computational analysis and design work has been carried out on a liquid desiccant system at the Sustainable Energy Centre of the University of South Australia [2-6], and the Queensland University of Technology [7, 8]. These involved modelling and experimental work on both cross flow and packed-bed dehumidifier as the absorber unit as well as the solar regenerator [9]. In the packed-bed system used in this study, different packing materials are considered, which include the polymer type usually used in cooling tower applications and the counter flow type with a layer of wick applied to the heat exchanger surfaces to reduce the carry over of the desiccant particles into the conditioned space, as well as to increase the dehumidification efficiency of the air conditioning unit.

In a solar liquid desiccant system the weak desiccant can be concentrated, stored and used at a later time; therefore, energy is stored as concentrated solution in the system rather than thermal. The system provides the options of using the solar LDAC either as a packaged roof top air conditioner for domestic or commercial use or as an air handler unit in commercial applications such as conditioning large volumes of ventilation air. The LDAC could also be used for space heating in winter due to the property of desiccants to provide heat when wetted and, thereby, indirectly heat the supply air.

2. Testing the conditioner prototype

In the experimental tests carried out on the developed LDAC, dehumidification and cooling are both achieved within the absorber unit by using liquid desiccant and the cool air from the conditioned space, respectively. A photograph of the absorber unit showing the system main components is demonstrated in Figure 2.



Figure 2. The LDAC packed-bed dehumidification unit as viewed from the MERC Energy Laboratory.

This 20 kW unit has an overall dimensions of approximately $1.3 \times 1.5 \times 1.8$ m. The conditioner casing is made from an insulating material to protect the system from heat transfer with the environment. The packing material is incorporated vertically inside the dehumidification tower with the weak solution container at the bottom. The conditioner prototype was optimized for the air and solution flow rates, further reducing electrical power consumed by the unit.

Preliminary tests have been carried out on the system with water to ensure a smooth operation of the unit. These involved running the air conditioner at variable fan speeds by reducing the applied voltage from 220 to 110 V. The air velocity on the supply and exhaust sides of the conditioner and on a face area of approximately 0.15 m^2 was measured. The power consumed by the fan during the system operation was also measured and recorded.

Two sets of experiments were carried out with liquid desiccant. In the first set of the experiments, the absorber unit was tested with desiccant only sprayed into the outside air, while the direct evaporative cooler was inactivated. The experiments were aimed to investigate the air temperature rise due to condensation of the air moisture content, and reduction in the air relative humidity. The process of dehumidification / cooling of the outside air for these two experiments are shown on the psychrometric chart in Figure 3. The dashed line on this figure represents the test with desiccant only.

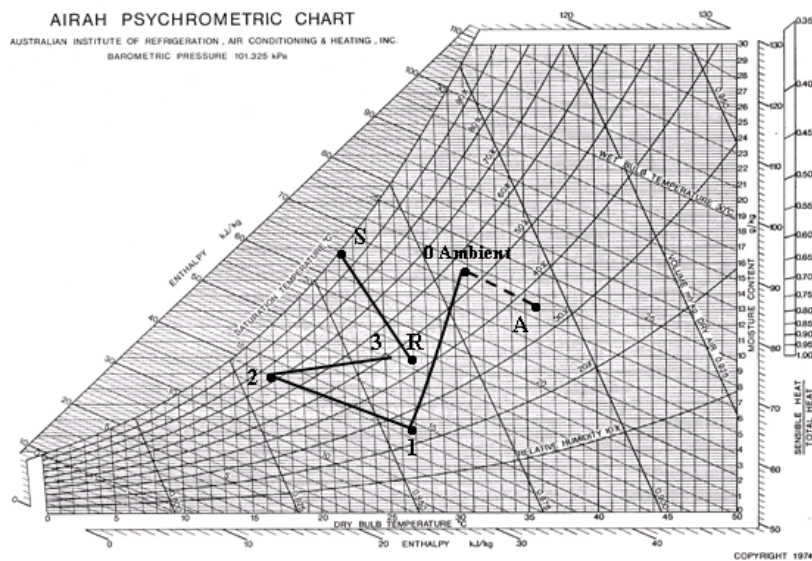


Figure 3. Psychrometric paths for the tests with: (a) desiccant only (dashed line); and (b) desiccant followed by evaporating cooling of the air. (Supply air: 0-1-2-3; Return air: R-S)

In the second set, the system was operated with the evaporative cooler activated, while lithium chloride solution was sprayed into the outside air. The test was to investigate the effect of dehumidification and direct evaporative cooling on the supply air. The process of dehumidification / cooling of the outside air for the above two experiments are shown on the psychrometric chart in Figure 3. The dashed line on this figure represents the test with desiccant only.

Following each set of experiments with liquid desiccant, the concentration of the dilute solution was measured, using a conductivity meter. A plot of conductivity-concentration as

indicated in Figure 4 was then produced for diluted samples and for several conductivity measurements. The plot was used to determine the subsequent values of concentration for new desiccant solutions, using a correction factor to be accounted for higher concentration values. The weak solution obtained from the dehumidification process in the above experiments was regenerated in a scavenger air solar regenerator. This will be described in section 4.

In Figure 5, the effect of air flow rate on the air temperature and relative humidity of the outside air has been studied. The air temperature and relative humidity on this figure are denoted by T_{bp} and H_{bp} , respectively, which are the air conditions before entering the packed-bed column. As seen from the figure a substantial reduction in the air relative humidity is achieved after it passes through the packed-bed column, which is due to the spray of the desiccant solution over the packing material. In Figure 5, values of the air temperature and relative humidity, following the dehumidification process, are denoted as T_{ap} and H_{ap} , respectively.

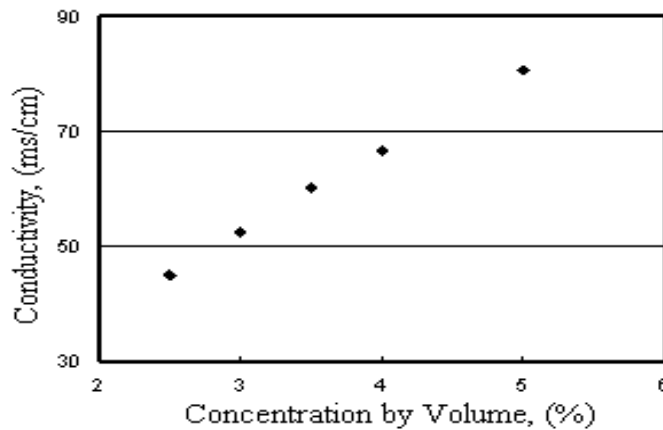


Figure 4. Conductivity-concentration chart for the lithium chloride solution.

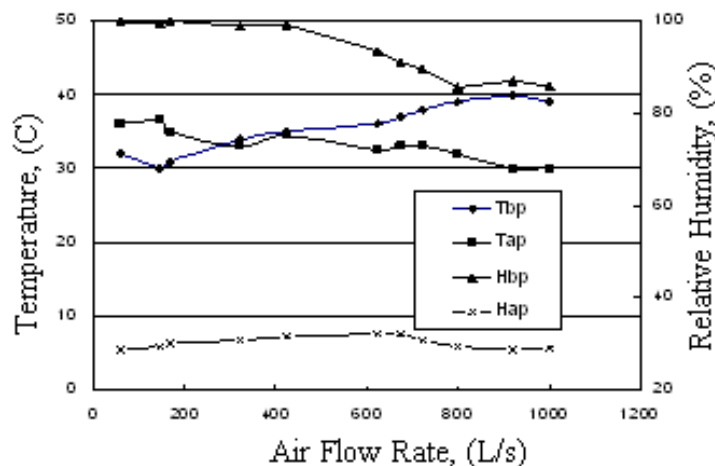


Figure 5. The effect of air flow rate on dehumidification process of the outside air.

In Figure 6 the experimental values of the temperature and humidity after the packing are compared with the predictions obtained from a developed model for the packed-bed. As can be seen from the figure there is good agreement between the data obtained from theory and experiment.

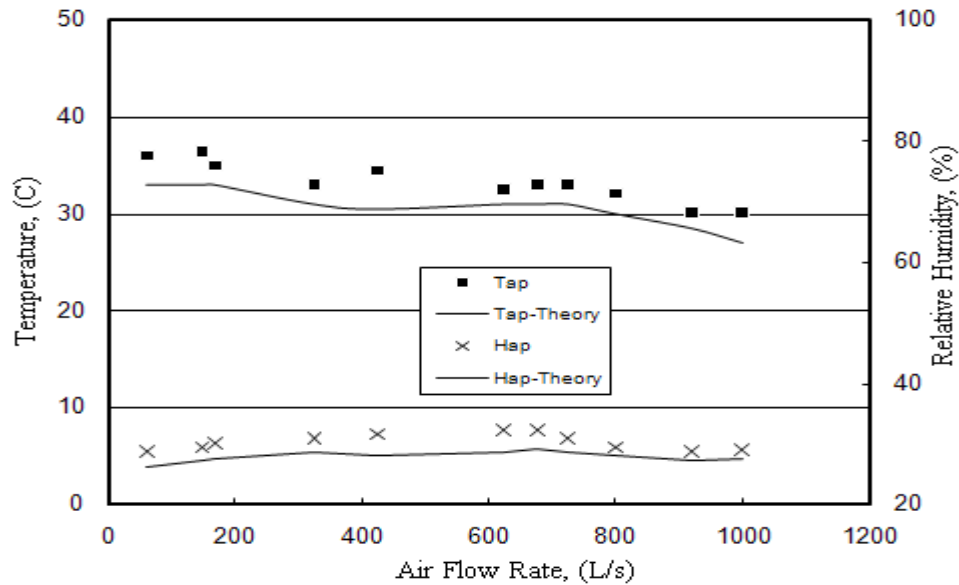


Figure 6. Comparison between the results obtained from the model and experiment.

3. Discussion of the test results

In the tests with desiccant only, the air dehumidification by liquid desiccant is an adiabatic (constant enthalpy) process; therefore, no heat is added or removed from the air during the process. However, according to Figure 3, for an adiabatic dehumidification the air dry bulb temperature increases as the relative humidity reduces. This is due to the heat generated in the process as a result of water vapour condensation in the air. The air wet bulb temperature as seen in Figure 3, remains constant.

The results from the tests with evaporative cooler and desiccant prove a satisfactory performance of the unit in a tightly control of the air temperature and humidity if installed on a commercial site of approximately 200 m² area in a hot and humid climate. This will maintain the building air conditions within the comfort zone (dry bulb temperature of about 25 °C and 50% relative humidity). The results of the tests further reveal that there are optimum values of air and solution flow rates, where the conditioner performance is enhanced.

To quantify the confidence level of the experimental data, the results of an uncertainty analysis are presented in Table 1 for the experimental values obtained from testing the conditioner prototype. In this analysis, the fixed errors are assumed to be calculated and accounted for via calibration against known standards. Hence, the remaining error is solely due to the precision error. The precision errors were determined by statistical means or from data provided by equipment manufacturers or by the best estimate based on experimental observations. Since the prototype testing of the absorber unit was under many uncontrolled environmental conditions, the results are quite acceptable.

The results obtained from the demonstration system in this study have been used in a solar liquid desiccant pilot plant project currently ongoing at MERC. The system was built and installed within the Fluid Mechanics Laboratory at Babol University of Technology, a hot and humid location on the Caspian Sea in the north of Iran. The system, which is also used for heating during the winter, is now being tested and monitored for a full year operation. Similar

equipment will also be installed and tested on the Persian Gulf region in southern part of the country, where the temperature and humidity are very high during most of the year.

Table 1. Experimental results obtained from the conditioner test and the uncertainty values.

Conditioner performance parameters	Measured values	Precision errors	Uncertainty values %
Supply and return air flow rates, L/s	1000	100	10
supply air temperature °C	15.2	1	6.7
supply air humidity ratio, kg/kg	0.0094	0.0005	5.3
Solution flow rate, L/min	3	0.2	6.8
Exit solution concentration, (wt %)	0.412	0.008	2
Effectiveness, %	82	5	6.1
Latent cooling, kW	16.7	0.5	3.3
Sensible cooling, kW	3.3	0.1	3.1
electrical energy used, kW	3	0.1	3.3
Total cooling, kW	20	0.6	3
Electrical COP	7	0.2	2.8

4. Performance of the solar regenerator

The concentration of dilute solution in this study is carried out in a scavenger air regenerator, using hot water from flat plate solar collectors. Both the scavenger air and the weak solution are preheated within the regenerator; however, solution regeneration will be more effective when preheating the air than preheating the solution [9]. It is notable that the lithium chloride desiccant can be concentrated using solar energy or other low grade heat at temperatures as low as 40 °C. The flat plate solar collectors used in this study can produce hot water at about 85 °C in summer.

In a scavenger air regenerator the weak solution is sprayed over a column of packed-bed (see Figure 7). Polymer pall rings, spheres or other polymer based materials are used as a packed-bed to increase the contact area between the solution and the scavenger air, which facilitates the regeneration process. A stream of outside air is passed through the column, using a fan, in a counter current operation to pick up the water evaporated from the solution, and the hot moist air is, subsequently, exhausted from top of the column. A mist eliminator, as shown in Figure 6, is used at the top of the regenerator column to prevent the carryover of the desiccant particles. Gas or electricity could be used as a back up for the regenerator during the peak cooling hours.

Eliminators, such as demister, are used to avoid carryover of desiccant into the environment. Alternative method in preventing the carryover is the use of indirect cooling, in which the supply air does not contact the desiccant [10]. The latter could also be used to produce potable water from the atmospheric air in remote areas when a cross flow plate heat exchanger is used. The water can either be used for human consumption or returned to the conditioner for evaporative cooling of the air.

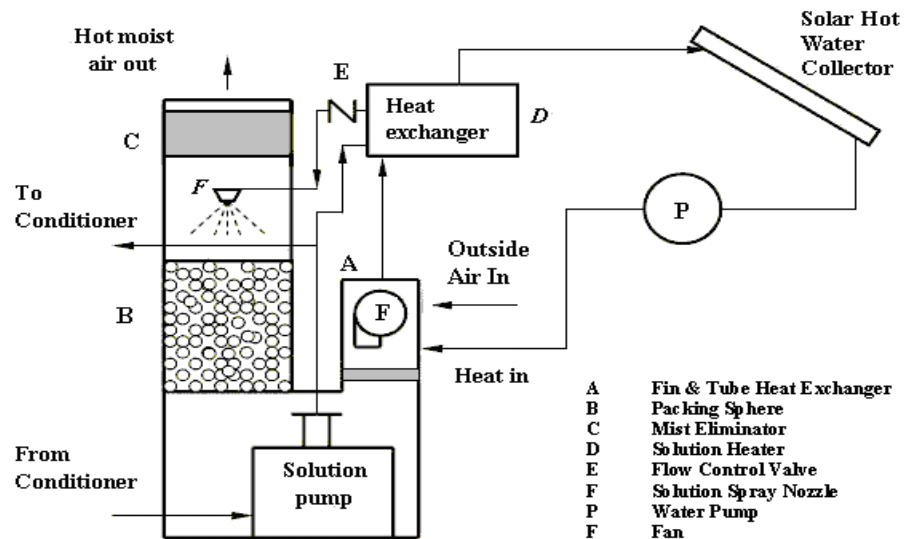


Figure 7. Schematic of the scavenger air solar regenerator.

5. Commercialization strategy for a solar LDAC

An LDAC, in which the carryover of the desiccant has been eliminated, creates new opportunities for solar cooling. A commercialization strategy has been proposed in this study for a solar operated LDAC and compared with conventional vapour compression systems. Based on the computer modelling results obtained from the system simulation for a building in the Persian Gulf region, the operating costs of an LDAC is significantly lower than its conventional counterpart. This study further reveals that using the solar operated LDAC with a storage system for the concentrated solution, will result in considerable savings in operating costs when compared with the equivalent gas-fired liquid desiccant system. A simple payback of five years was determined for solar components of the system in this study.

A 30 kW capacity, packaged roof-top LDAC delivering 1.5 m³/s of outside air could be used in domestic applications as well as the commercial. The unit uses a storage system and 100 m² of flat plate solar collector to dehumidify and cool 500 m² of a residential building in the Persian Gulf region. Compared with the conventional unit, an annual saving of \$2,500 with a payback of less than 5 years was determined for the solar LDAC in this application.

6. Conclusion

In this paper the performance of a solar LDAC developed at MERC, using packed-bed for air dehumidification, and a scavenger air regenerator was studied. It was found that the solar liquid desiccant system is an efficient and cost effective alternative to the conventional air conditioner. Elimination of carryover of the desiccant particles within the absorber unit in this study was performed through the cooling pad of the direct evaporative cooler, which acts as a filter, as well as evaporative cooling of the supply air. Using the indirect cooling technique, the unit could produce potable water from the atmospheric air in remote areas.

Experimental results obtained from prototype testing of the LDAC absorber unit indicates that the unit has a satisfactory performance in controlling the temperature and humidity when installed on a commercial site of about 200 m² area located on the Persian Gulf region. The tests further reveal that the experiments are in good agreement with a previously developed model for the packed-bed and that the conditioner unit can have an effectiveness of about 82% when used with liquid desiccant. The maximum electrical energy utilization of the unit,

which was determined through the above experiments, is 3 kW with an electrical COP of about 7.

For domestic roof-top applications, it was determined that a 30 kW capacity LDAC could dehumidify and cool 500 m² of a residential building on the Persian Gulf with an annual saving of \$2,500 and a payback of less than 5 years.

References

- [1] Y.J. Dai and H.F. Zhang, Numerical simulation and theoretical analysis of heat and mass transfer in a cross flow liquid desiccant air dehumidifier packed with honeycomb paper, *Energy Conversion and Management*, 2004, pp. 1343-1356.
- [2] W.Y. Saman and S. Alizadeh, Modelling and performance analysis of a cross-flow type plate heat exchanger for dehumidification / cooling, *Solar Energy*, 2001, pp. 361-372.
- [3] W.Y. Saman and S. Alizadeh, Design and Optimization of a Liquid Desiccant Solar Air Conditioner Using Cross Flow Type Plate Heat Exchanger, *ISES 2001 Solar World Congress*, 2001, Adelaide, Australia.
- [4] W.Y. Saman and S. Alizadeh, An experimental study of a cross-flow type plate heat exchanger for dehumidification / cooling. *Solar Energy*, 2002, pp. 59-71.
- [5] S. Alizadeh and W.Y. Saman, Modeling and performance analysis of a forced-flow solar collector / regenerator using liquid desiccant, *Solar Energy*, 2002, pp. 143-154.
- [6] S. Alizadeh and W.Y. Saman, An experimental study of a forced-flow solar collector / regenerator using liquid desiccant, *Solar Energy*, 2002, pp. 345-362.
- [7] S. Alizadeh, and K.Y. Khouzam, "A Study into the Potential of Using Liquid Desiccant Solar Air-Conditioner with Gas Backup in Brisbane – Queensland", *Proceedings of 42th Australian and New Zealand Solar Energy Society*, December 1-3, 2004, Perth, W.A.
- [8] S. Alizadeh and K. Khouzam, Economical and environmental study of a liquid desiccant solar air conditioner for Queensland, Australia, *Proceedings of the ISES Solar World Congress*, Orlando, Florida, U.S.A, 6-12 August, 2005.
- [9] S. Alizadeh, Development of a dehumidification/ indirect evaporative cooling system using liquid desiccant, PhD thesis, School of Advanced Manufacturing and Mechanical Engineering, the University of South Australia, Mawson Lakes Campus, S.A., 2002, Australia.
- [10] J. L. McNab and P. McGregor, Dual indirect cycle air conditioner uses heat concentrated desiccant and energy recovery in a polymer plate heat exchanger, *21st IIR International Congress of Refrigeration*, August 17-22, 2003, Washington DC, USA.

Investigation on radiative load ratio of chilled beams on performances of solar hybrid adsorption refrigeration system for radiant cooling in subtropical city

K.F. Fong*, C.K. Lee, T.T. Chow

Building Energy and Environmental Technology Research Unit, School of Energy and Environment & Division of Building Science and Technology, City University of Hong Kong, Hong Kong, China

** Corresponding author. Tel: +852 3442 8724, Fax: +852 3442 9716, E-mail: bssquare@cityu.edu.hk*

Abstract: The effectiveness of solar adsorption system for space conditioning would be enhanced through radiant ceiling cooling, since a higher chilled water temperature can be supplied. In such provision, desiccant dehumidification should be involved in order to cater for the latent cooling load. A solar hybrid adsorption refrigeration system is therefore formulated. In this study, the effect of radiative load ratio R of active chilled beams (ACB) and passive chilled beams (PCB) for the solar hybrid adsorption refrigeration system was investigated. Through the year-round dynamic simulation, it was found that the performances, like solar fraction and primary energy consumption, of the system with ACB or PCB would be improved along with the decrease of R from 0.3 to 0.1. At the same R , the system with PCB would have better performances than that with ACB. With suitable design and control, the solar hybrid adsorption refrigeration system with PCB at low R would be more technically feasible for office use in the subtropical climate.

Keywords: *Radiant cooling, Radiative load ratio, Adsorption refrigeration, Solar air-conditioning, High temperature cooling*

1. Introduction

To promote the low energy buildings in the hot and humid places, strategic use of renewable energy in air-conditioning would certainly contribute to sustainable design. Solar air-conditioning is getting popular in the European countries [1,2]. Through the approach of high temperature cooling, the energy performance of chiller can be enhanced by using higher chilled water supply temperature for radiant cooling. As the latent cooling load cannot be effectively handled in such provision, a separate desiccant dehumidification is necessary [3,4]. In fact, it would be effective to hybridize the adsorption refrigeration, radiant cooling and desiccant dehumidification, driven by solar energy for building space conditioning. In the previous study [5], this solar hybrid adsorption refrigeration system would have much less annual primary energy consumption than the conventional vapour compression air-conditioning system for office application. In this study, it is to investigate more deeply about the effect of chilled beams on the performances of the solar hybrid adsorption refrigeration system in the subtropical city.

The common chilled beams include the active chilled beams (ACB) and passive chilled beams (PCB), which are mounted at the ceiling level but not for structural purpose. ACB have finned coils, in which chilled water flows inside. ACB make use of forced convection for cooling through induction, so they are connected with a supply air stream that is mechanically driven. PCB also have finned coils inside, but they rely on natural convection rather than forced convection. Therefore, their performances would be affected by the radiative load ratio, which is the proportion of radiative to total (i.e. radiative and convective) cooling capacity of the chilled beams. In this study, the effect of the radiative load ratio R on the year-round performances of the solar hybrid adsorption refrigeration system was evaluated for the office application. Two types of offices were involved, a typical office and a high-tech

office, where the latter is featured with a much higher internal heat gains due to different electrical facilities of information technology and office automation.

Fig. 1 illustrates the design of solar hybrid adsorption refrigeration system with ACB serving an office. Solar energy is collected to supply to the adsorption refrigeration and the desiccant dehumidification through regenerative water and desiccant water respectively. Auxiliary heaters are involved whenever the required driving temperatures are not sufficient. The adsorption chiller provides chilled water to the chilled beams for sensible cooling, it also furnishes the chilled water to the supply air coil for supporting the desiccant dehumidification. The chilled beam valve and the supply air valve are used to control the required chilled water flow rate to the respective equipment. For the system with ACB, supply air fan is needed for induction of indoor air. However for PCB, no supply and return air fans, and the associated air ducts are required.

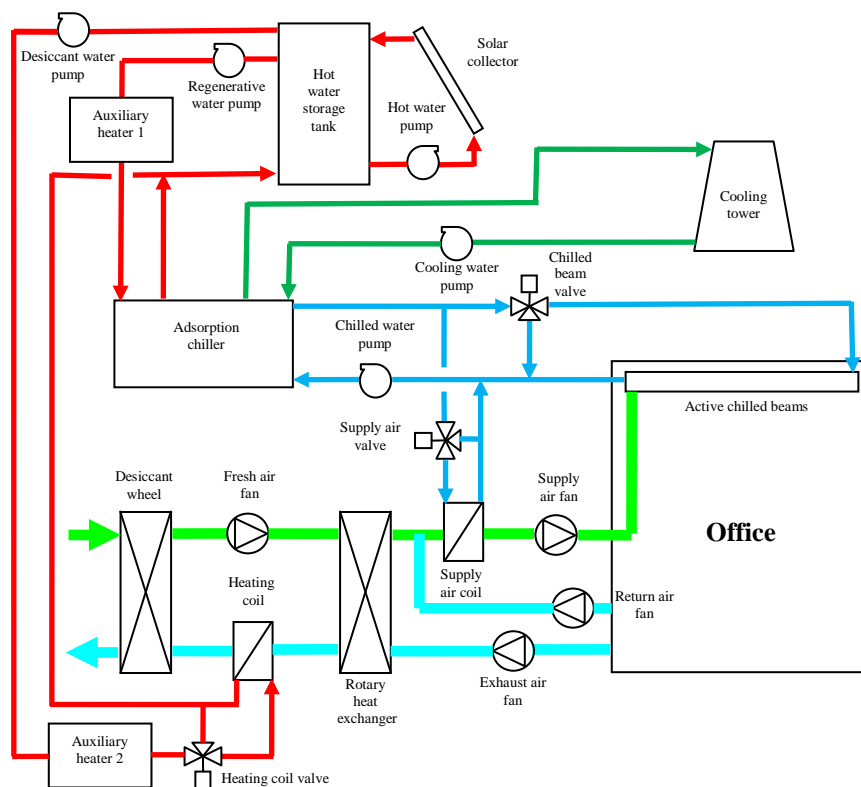


Fig. 1. Solar hybrid adsorption refrigeration system for active chilled beams.

2. Methodology

In this study, year-round dynamic simulation was applied for the solar hybrid adsorption refrigeration system. Generally the entire system model was built on the component-based simulation platform TRNSYS [6], and the validated component models of adsorption chiller [7] and desiccant wheel [8] were used. The models of ACB and PCB were developed from the empirical information of the manufacturers [9,10]. The other system components, including the office building zone, solar collector, storage tank, auxiliary heaters, rotary heat exchanger, water coils, cooling tower, pumps, fans and valves were based on those of TRNSYS and the component library TESS [11]. Different radiative load ratios were adjusted at the TRNSYS multizone building model. The indoor design conditions were set at 25.5°C and 60%RH. The floor area was 196 m² with 24 occupants and daily working schedule

between 08:00 to 18:00. The fresh air amount was based on 10 litres/s per occupant. The subtropical city Hong Kong (22.32°N and 114.17°E) was used, and the year-round dynamic simulation was carried out with the typical meteorological year for Hong Kong [12]. The major simulation parameters of the solar hybrid adsorption refrigeration system are summarized in Table 1.

Table 1. Values of major simulation parameters of solar hybrid absorption refrigeration system.

Fresh air stream		
Fresh air mass flow rate (kg·s ⁻¹)		0.288
Fresh air fan power (kW)		0.277
Exhaust air stream		
Exhaust air mass flow rate (kg·s ⁻¹)		0.259
Exhaust air fan power (kW)		0.166
Rotary heat exchanger		
Temperature effectiveness of rotary heat exchanger		0.8
Rotary heat exchanger power consumption (kW)		0.1
Desiccant wheel		
Mass per unit length of matrix material in desiccant wheel (kg·m ⁻¹)		0.003
Mass per unit length of silica gel in desiccant wheel (kg·m ⁻¹)		0.005
Half height or width of air channel (m)		0.0015
Outer diameter of desiccant wheel (m)		0.6
Effective area ratio of desiccant wheel		0.744
Fraction of wheel area for regeneration		0.5
Length of desiccant wheel (m)		0.2
Desiccant wheel speed (rph)		13
Number of discretization segments along the air channel length		20
Number of time steps for one revolution of the desiccant wheel		360
Desiccant wheel power consumption (kW)		0.1
Adsorption Chiller		
	Typical	High-tech
Number of stages per chiller		2
Mass of metal in adsorption/desorption chamber per stage (kg)	60	80
Mass of silica gel in adsorption/desorption chamber per stage (kg)	30	40
Mass of metal in condenser coil per stage (kg)	75	90
Mass of metal in evaporator coil per stage (kg)	75	90
Maximum adsorbate intake in Freundlich equation		0.552
Exponent in Freundlich equation		1.6
Ratio of initial adsorbate intake to maximum adsorbate intake		0.7
Adsorption/desorption period (s)		360

	Typical	High-tech
Cooling water system		
Cooling tower air volume flow rate (m ³ ·s ⁻¹)	2.640	3.333
Cooling tower fan power (kW)	0.812	1.026
Cooling water mass flow rate (kg·s ⁻¹)	0.7	0.8
Cooling water pump power (kW)	0.138	0.168
Chilled water system		
Chilled water mass flow rate (kg·s ⁻¹)	1.05	1.3
Chilled water pump power (kW)	0.207	0.277
Hot water system		
Hot water mass flow rate (kg·s ⁻¹)	2.55	3.15
Hot water pump power (kW)	0.200	0.294
Desiccant water pump flow rate (kg·s ⁻¹)		0.15
Desiccant water pump power (kW)		0.011
Regenerative water pump flow rate (k g·s ⁻¹)	1.2	1.5
Regenerative water pump power (kW)	0.145	0.184
Chilled beams		
Model of ACB used	DID600B-L-2-M/3000x3000 [9]	
Numbers of ACB used	24	32
Model of PCB used	36CBPB14 [10]	
Numbers of PCB used	42	54
Supply air stream (ACB only)		
Supply air mass flow rate (kg·s ⁻¹)	1.008	1.344
Supply air fan power (kW)	0.258	0.345
Return air stream (ACB only)		
Return air mass flow rate (kg·s ⁻¹)	0.72	1.056
Return air fan power (kW)	0.092	0.135

3. Results and discussion

3.1. Performance indicators

A number of performance indicators were used in this study, including solar fraction SF , coefficient of performance COP and primary energy consumption PE , as determined below.

$$SF = \frac{Q_{sol}}{Q_{sol} + (Q_{aux1} + Q_{aux2})} \quad (1)$$

where Q_{sol} is the solar thermal gain, Q_{aux1} and Q_{aux2} are the heat output from Auxiliary Heaters 1 and 2 respectively.

$$COP = \frac{Q_e}{Q_g} \quad (2)$$

where Q_e is the refrigeration effect of absorption chiller and Q_g is the heat input to generator of absorption chiller.

$$PE = PE_p + PE_f + PE_{aux} \quad (3)$$

where PE_p is the primary energy consumption of pumps, PE_f is the primary energy consumption of fans, cooling tower, desiccant wheel and rotary heat exchanger, PE_{aux} is the primary energy consumption of auxiliary heaters.

In addition, the annually averaged room conditions, including zone temperature T_z and zone humidity RH_z , were also examined.

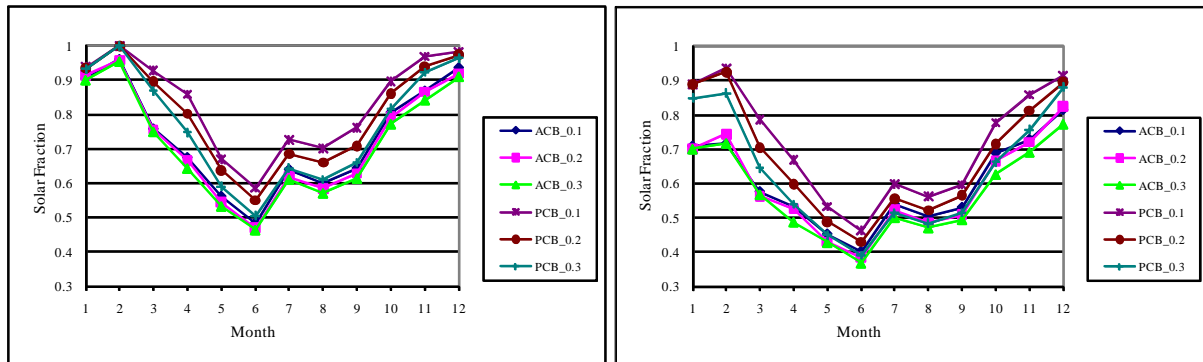
3.2. Solar fraction and coefficient of performance

Table 2 summarizes the annually averaged performances of the solar hybrid adsorption refrigeration system with different types of chilled beams for typical and high-tech offices. Generally the system could maintain satisfactory indoor conditions for both types of offices. The results of the typical office shows that the annually averaged SF of the system with PCB would become better, increased by 10.9% along with R decreased from 0.3 to 0.1, while that with ACB could be increased by 3.9%. Similarly for the high-tech office, the annually averaged SF of the system with PCB was raised by 15.6% for R from 0.3 to 0.1, and that with ACB by 6.4%. SF decreased with an increase of R , it was because the radiative load had less effect in reducing the zone air temperature. Hence, with a higher radiative load ratio, the zone air temperature would drop slower, meaning that the running hour of the chiller would increase. As such, the regenerative heat required was larger and resulted in a lower SF . For COP , although it was slightly increased with the rise of R , the change was minimal for both types of offices. At the same R , PCB had higher COP than ACB. The main reason was due to a higher chilled water supply temperature would be offered by the PCB, and the regenerative heat demand could be reduced.

Table 2. Annually averaged performance of solar hybrid adsorption refrigeration system.

Office	Chilled beams	R	SF	COP	T_z (°C)	RH_z (%)
Typical	ACB	0.1	0.689	0.548	25.02	53.12
	ACB	0.2	0.675	0.548	25.07	52.94
	ACB	0.3	0.663	0.548	25.13	52.80
	PCB	0.1	0.791	0.557	25.29	53.14
	PCB	0.2	0.754	0.558	25.39	53.09
	PCB	0.3	0.713	0.559	25.51	52.95
High-tech	ACB	0.1	0.568	0.546	25.19	52.51
	ACB	0.2	0.553	0.546	25.25	52.33
	ACB	0.3	0.534	0.547	25.33	52.07
	PCB	0.1	0.659	0.554	25.45	53.00
	PCB	0.2	0.616	0.554	25.56	52.87
	PCB	0.3	0.570	0.557	25.71	52.57

Fig. 2 illustrates the annual profiles of SF of the solar hybrid adsorption refrigeration system using ACB and PCB for both typical and high-tech offices at various R . The changing patterns were similar, with high SF from November to February and low SF from May to September. The former period was typical short autumn and winter in subtropical climate, while the latter was typical long summer. As compared between Fig. 2(a) and 2(b), the SF profiles of the typical office were generally higher than those of the high-tech offices, since the cooling demand of the typical office was lower and the involvement of auxiliary heaters would be less.

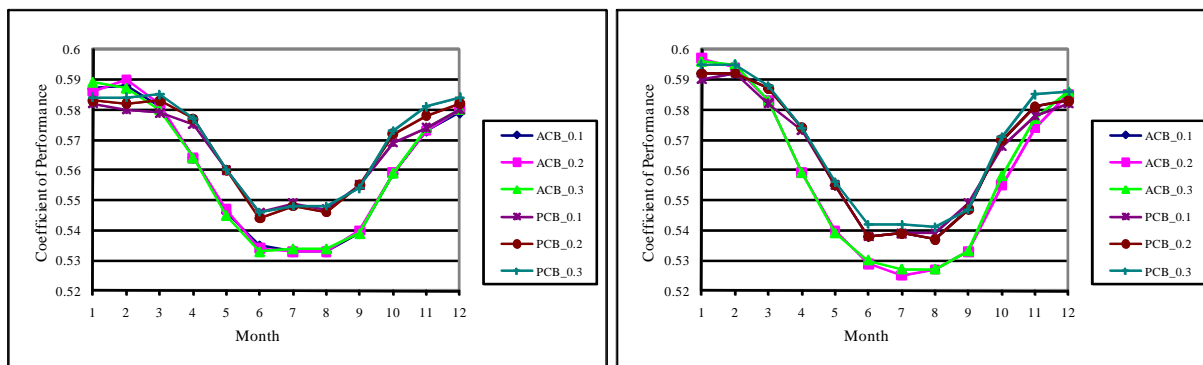


(a) Typical office

(b) High-tech office

Fig. 2. Annual SF profiles solar hybrid adsorption refrigeration system.

Fig. 3 presents the annual profiles of COP of the adsorption chiller for ACB and PCB for typical and high-tech offices at various R . Generally the COP was higher in the winter months, while lower in the summer months. However the variation range of COP was narrow and maintained within about 10% even for different scenarios, since the chiller was supported by auxiliary heating. As compared between the chiller for the typical office and that for the high-tech office, although the latter COP was higher in the winter months, it was lower in the summer months. As a whole, the adsorption chiller for the high-tech office had lower annually averaged COP already shown in Table 2.



(a) Typical office

(b) High-tech office

Fig. 3. Annual COP profiles of adsorption chiller of solar hybrid system.

3.3. Primary energy consumption

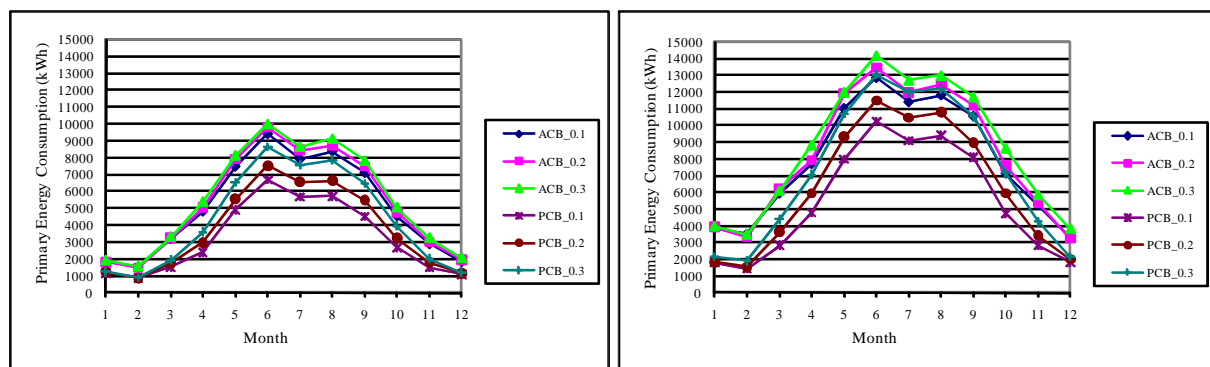
Table 3 summarizes the annual primary energy consumption of the solar hybrid adsorption refrigeration system with ACB and PCB for both typical and high-tech offices. The results of the typical office shows that the PE of the system with PCB would become less, reduced by 25.5% along with the decrease of R from 0.3 to 0.1, while that with ACB could be reduced by

8.0% only. Similarly for the high-tech office, the PE of the system with PCB was trimmed by 25.6% for R from 0.3 to 0.1, and that with ACB by 9.6%. These changing patterns were directly related to those of SF , since higher SF of the solar hybrid adsorption refrigeration system indicated less demand of auxiliary heating, thus leading to lower PE . At the same R , PCB could have less PE than ACB, up to 36.4% and 31.0% for typical office and high-tech office respectively. This was because the SF of the system with PCB was better than that with ACB, as discussed in Section 3.2, and the PE_{aux} of the system with PCB was less. In addition, the system with PCB did not have the additional supply and return air fans, so the PE_f of PCB was only about half of that of ACB.

Table 3. Annual energy performance of solar hybrid adsorption refrigeration system.

Office	Chilled beams	R	PE (kWh)	PE_p (kWh)	PE_f (kWh)	PE_{aux} (kWh)
Typical	ACB	0.1	60,943	19,466	8,232	33,247
	ACB	0.2	63,687	19,910	8,236	35,543
	ACB	0.3	66,212	20,155	8,238	37,820
	PCB	0.1	38,786	15,454	4,355	18,977
	PCB	0.2	44,764	16,588	4,361	23,815
	PCB	0.3	52,024	17,769	4,374	29,882
High-tech	ACB	0.1	94,371	26,124	9,670	58,578
	ACB	0.2	98,591	26,411	9,673	62,507
	ACB	0.3	104,398	26,971	9,676	67,751
	PCB	0.1	65,073	21,423	4,392	39,258
	PCB	0.2	75,309	22,871	4,402	48,036
	PCB	0.3	87,459	24,168	4,410	58,882

Fig. 4 presents the annual profiles of PE of the system with ACB and PCB for the two types of offices. Obviously the PE variation followed the seasonal change, and the system serving the high-tech office would demand higher PE . For the same type of chilled beams, higher R would require higher PE .



(a) Typical office

(b) High-tech office

Fig. 4. Annual PE profiles of solar hybrid adsorption refrigeration system.

4. Conclusion

Through the year-round study of the solar hybrid adsorption refrigeration system using the two types of chilled beams, the effect of R on the system performances was investigated,

particularly the *SF* and the *PE*. It was found that the system with either ACB or PCB could have higher *SF* and lower *PE* when *R* was decreased from 0.3 to 0.1. Although both ACB and PCB could provide satisfactory indoor conditions for the typical and high-tech offices, the PCB had better annually averaged *SF* and total *PE* at the same *R*. As the conventional *R* of ACB is 0.1 or less, and that of PCB is between 0.1 and 0.2, suitable equipment selection and control provision of the solar hybrid adsorption refrigeration system would be technically feasible for office use in the hot and humid city. Through appropriate system design and year-round evaluation of solar air-conditioning, this would certainly help to determine a solution for reduction of carbon footprint of buildings in the subtropical climate.

Acknowledgement

The work described in this paper was fully supported by a grant from City University of Hong Kong (Strategic Research Grant, Project No. 7008037).

References

- [1] H-M. Henning, Solar-Assisted Air-Conditioning in Buildings, A Handbook for Planners. Springer-Verlag Wien New York, 2004.
- [2] U. Eicker, Solar Technologies for Buildings. Chichester: Wiley, 2003.
- [3] D. Song, T. Kim, S. Song, S. Hwang, S. Leigh, Performance evaluation of a radiant floor cooling system integrated with dehumidified ventilation, Applied Thermal Engineering, 28, 2008, pp. 1299-1311.
- [4] J.L. Niu, L.Z. Zhang, H.G. Zuo, Energy savings potential of chilled-ceiling combined with desiccant cooling in hot and humid climates, Energy and Buildings, 34, 2002, pp. 487-495.
- [5] K.F. Fong, C.K. Lee, T.T. Chow, Z. Lin, L.S. Chan, Solar hybrid air-conditioning system for high temperature cooling in subtropical city. Renewable Energy, 35(11), 2010, pp. 2439-2451.
- [6] TRNSYS 16, a TRaNsient SYstem Simulation program. The Solar Energy Laboratory, University of Wisconsin-Madison, June 2006.
- [7] S.H. Cho and J.N. Kim, Modeling of a silica gel/water adsorption-cooling system, Energy, 17, 1992, pp. 829-839.
- [8] X.J. Zhang, Y.J. Dai and R.Z. Wang, A simulation study of heat and mass transfer in a honeycombed rotary desiccant dehumidifier, Applied Thermal Engineering, 23, 2003, pp. 989-1003.
- [9] TROX Active Chilled Beams, Type DID600B-L-2-M/3000x3000, TROX Technik, TROX GmbH, July 2006.
- [10] Carrier Product Data, Active and Passive Chilled Beams, model 36CBPB14, Carrier Corporation, 2008.
- [11] TESS Component Libraries – Version 2.0. The Thermal Energy System Specialists, Nov 2004.
- [12] A.L.S. Chan, T.T. Chow, S.K.F. Fong and J.Z. Lin, Generation of a typical meteorological year for Hong Kong, Energy Conversion and Management, 47, 2006, pp. 87-96.

A hybrid solar-gas air conditioning system based on adsorption and chilled water storage

Antonio P. F. Leite^{1,*}, Douglas B. Riffel², Celina M.C. Ribeiro¹, Francisco A. Belo¹, Paulo V.S.R. Domingos¹, Daniel Sarmento¹, Manoel B. Soares¹, Leonaldo J. L. Nascimento¹

¹ Solar Energy Laboratory, Federal University of Paraíba, Joao Pessoa-PB, Brazil

² Mechanical Engineering Department, Federal University of Sergipe, Aracaju-SE, Brazil

* Corresponding author. Tel: +55 83 32 16 71 27, Fax: +55 83 32 16 77 24, E-mail: antpralon@yahoo.com.br

Abstract: This paper presents constructive aspects and preliminary experimental results of an adsorptive chiller as part of a 20 kW central air conditioning unit for providing thermal comfort in a set of rooms that comprises an area of 110 m². Some simulation results of the air conditioner regeneration system are also presented. The cooling system is basically made up of a cold-water storage tank – supplied by an activated carbon-methanol chiller, and a hot-water storage tank – fed by a field of high efficient solar collectors with complementary heat by natural gas. The adsorber – a compact heat exchanger containing the activated carbon – was conceived and constructed in four modules, in order to allow heat and mass recovery. Other components are the same existing on conventional central air conditioners, as a condenser, an evaporator and a cooling tower. Constructive details of the collector's field, the adsorbers and the regenerating storage component are shown. The solar system is a 120 m² collection area field composed by 76 units of a flat plate collector covered with a high efficient transparent insulation. Results obtained from a multi-objective optimization based on a statistic modeling shown that – for a specific cooling power of 120 W/kg of adsorbent – the chiller's COP can reach 0.6. With this COP value, and considering the mean value of the total daily irradiation in João Pessoa (7°8'S, 34°50'WG), we can expect a solar energy cover fraction of 70%, for a typical summer day. This scenario is expected for the following operation temperatures: 30°C for the condenser, 7°C for the evaporator and 105°C at the start of the regeneration process. For an acclimatization period of 8 hours (9 to 17 h), the main dimensioning parameters were: 504 kg of activated carbon, 180 liters of methanol, 7,000 liters of hot water, 10,300 liters of chilled water with its temperature varying in the fan-coil from 1°C to 14°C.

Keywords: Solar-gas adsorptive chiller, Thermal storage, Numerical simulation.

1. Introduction

The simplicity of operation and minimal requires of maintenance of the adsorption chiller are certainly the major advantages compared to conventional liquid chiller (vapor compression) and to absorption chiller.

The scope of this technology involves besides the sectors of commerce and service, also the industrial, and it becomes possible the large-scale use of 'trigeneration' (combined heat, power and cooling).

The system consists basically of 3 components: an activated carbon-methanol adsorption chiller (water-cooling unit), a chilled water storage tank and an air-water heat exchanger (fan-coil). The schematic diagram of the system operation is shown in Fig.1.

The adsorption chiller is made up of the following main devices: four adsorbers (heat exchangers porous media/liquid), disposed in a parallel-series arrangement, one hot water storage tank supplied by solar energy and natural gas, two air condensers, one evaporator, and accessories such as valves and circulation pumps.

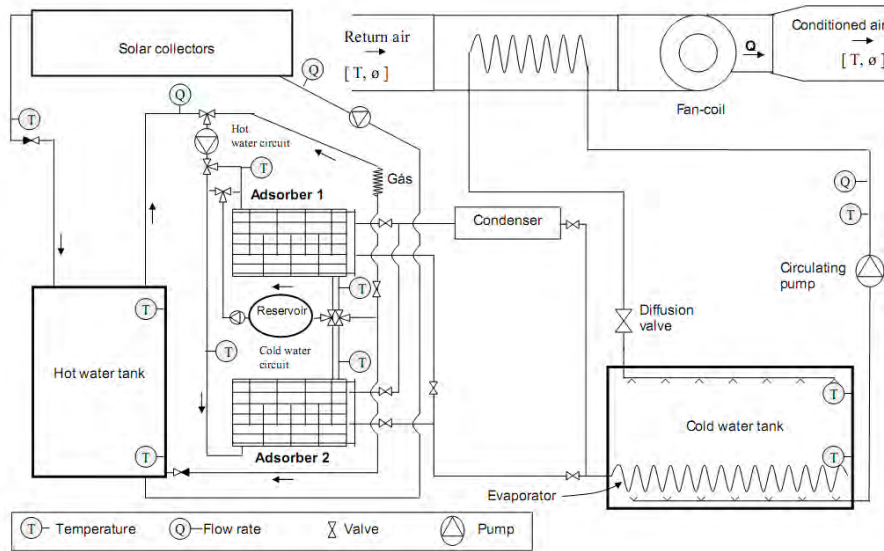


Fig.1. Scheme operation of the adsorption chiller fed by solar energy and natural gas, with thermal storage of chilled water (1).

2. Methodology

For dimensioning the adsorptive air conditioning system, we used a detailed study of individual components by means of a computer simulation program, using initially the analysis of each component and then the entire integrated system.

The computational simulation, called ADSOL, was carried out using the calculation program in the Simulink interface, with functions created in Matlab® to simulate the operation of the solar collectors field connected to the hot water storage tank and the adsorption chiller (2). For the collectors and the chiller, empirical correlations and simple methods of energy balance were used. For the storage tank, the function was based on the finite volume method.

The simulation of the complete system aims to determine the seasonal variations of different operating parameters such as the temperature, the efficiency of solar collectors, the coefficient of performance (COP) and the specific cooling power (SCP). With these data it is possible to adjust the operating times and other parameters of the system operation.

2.1. Solar collectors

For modeling the field of solar collectors it was used the quadratic efficiency collector Eq.(1) (3), which estimates the average efficiency of a solar collector at a given time, from the temperature difference between the collector (T) and the environment (T_{env}) and from the solar radiation (Rad) at that moment. The constants a_0 , a_1 and a_2 depend on the characteristics of the collector, as the overall coefficient of thermal loss to the environment and the relationship between the transparent and the total area. It also takes into account the arrangement of the collectors (parallel-series) that was disposed in two sets of 38 collectors each one.

$$\eta = a_0 - a_1 \frac{T - T_{env}}{Rad} - a_2 \frac{(T - T_{env})^2}{Rad} \quad (1)$$

The Eq.(2) represents a simple energy balance for each collector:

$$T_i = T_{i-1} + \frac{\eta A \cdot Rad}{\dot{V}_{col} c_p \rho} \quad (2)$$

Where, T_i is the temperature of the i -th collector in serie, A is the transparent area, \dot{V}_{col} is the water flow in each collector in parallel, c_p is the specific heat of the water and ρ is the density of the water (properties taken in the inlet temperature).

2.2. Adsorption chiller

The adsorption chiller operation was simulated using a model developed by Riffel et al. (4). It was investigated statistically the results of the dynamic model of the adsorber in order to obtain the optimum project parameters, taking into account the best operating points and the influence of seven variables (temperature and mass flow of hot water, cycle length, number of tubes, number of fins, fin thickness and material of manufacture) (5). The results showed that all variables are statistically significant and interdependent. In other words, a change in one variable affects directly the other one. This demonstrates the importance of using statistical modeling for this analysis. As a main result, we observed that the COP is highly dependent on the number of fins, the material and the cycle length. The inner surface of the adsorber, exchange heat with water from a hot or cold source, depending on the phase of the cycle. The adsorbent occupies the space delimited by the external wall of the tube and the corrugated fins. The adsorbent bed operates under vacuum for getting the required thermodynamic properties of the working fluid (the methanol). The micropores of the adsorbent medium has a diameter smaller than 2 nm. In the case of specific cooling power (SCP), the most important variables were the number of fins, the number of tubes and the hot water temperature.

The Eq.(3) represents an energy balance for the water that flows in the adsorber. Losses in the pipeline and the delayed response in thermal heat exchanger (adsorber) were not considered.

$$T_{out} = T_{in} - \frac{SCP}{COP} \cdot \frac{m_{ads}}{\dot{V}_{ad} c_p \rho} \quad (3)$$

Where, T_{out} and T_{in} are, respectively, the water temperatures at the exit and entry of the adsorbers, m_{ads} is the total mass of adsorbent (activated carbon), and \dot{V}_{ad} is the water flow in the adsorber.

2.2. Hot water tank

The geometry of the hot water storage tank is cylindrical, with is connected at the bottom and the top, with the solar collectors and the adsorbers. For calculating the heat exchanges in the tank the finite volume method was used and it was considered a stratified tank with one-dimensional heat transfer. The stratification occurs in layers of increasing density and decreasing temperature. This method presents a numerical solution that enables problem solving under any initial conditions and it consists in dividing the tank into a finite number of longitudinal nodes of same temperature and volume. Thus, we obtained the equations of the heat and mass transfers for each volume, applying the respective boundary conditions. The solution of the equations is performed by implicit formulation and the method of matrix inversion. The model of the hot water tank was developed by Riffel (2), by changing only the response of simulation to provide temperature values in both the base and on top of the tank.

3. Description of the central air conditioning unit

The air conditioning system is based on an adsorption cycle with heat recovery, in which the steps of regeneration and production of refrigeration effect occur simultaneously, i.e., the adsorbers (I and II, in Fig. 1) work in alternated way; when one is the adsorbing phase, the other is in the desorbing phase (1). The adsorber model takes into account the geometry of the finned-tube liquid-adsorbent heat exchanger. It is based on the activated carbon-methanol pair and is responsible for cooling the water that is accumulated in the tank. The working fluid is the methanol, which flows through a compact heat exchanger evaporator, where the water is cooled. The conditioned air is obtained by changing heat with the stored chilled water and the air process through a fan-coil, and then it is distributed in the set rooms by a pipelines network. The regeneration is made by solar thermal energy produced by a highly efficient solar collectors field that is stored in a water tank, and, from this main tank to the adsorptive chiller, an additional heat is supplied by the combustion of natural gas.

4. Constructive aspects of the central air conditioning unit

4.1. Regeneration system

The regeneration system comprises a field of flat solar collectors with high efficiency, coupled to a thermal storage tank. The water previously heated by the solar energy will get the process temperature of 105°C with the help of a small gas heater.

4.1.1. Solar collectors

The solar collectors are flat and static. The outer surface of the collectors is painted nonselective matte black, and a Teflon film is placed between the absorbing surface and the glass cover plate (Fig. 2) (6, 7).

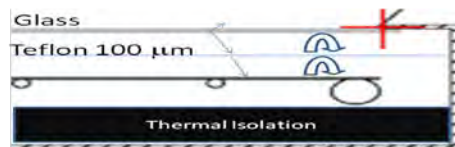


Fig. 2. Scheme of TIM cover.

The field of collectors was installed in a parallel-series arrangement, in two symmetrical blocks, each consisting of 38 units of a commercial flat collectors of 1.58 m² each, covering a total collection area of 120 m², installed on the roof titled 9° facing to the South (Fig. 3), which corresponds to the average value for the six hottest months in João Pessoa (7°8'S, 34°50'WG), whose climate is typically hot and humid (8).



Fig. 3. Field of flat plate collectors with TIM coverage installed on the LES/UFPB.

4.1.2. Hot-water storage tank

As showed in a previous article (9), the required cylindrical hot water tank for providing the minimum gas consumption was obtained from simulations to be around 7m³ of capacity, by comparing the volumes from 1m³ to 9m³ during 24 hours. It was built in steel, with 2.074m of diameter and 2.50m of height, insulated with 50mm thick polyurethane foam.

4.1.3. Adsorptive chiller

As result from simulations carried out by Riffel (4, 5), we have determined the characteristics of the adsorber, as shown in Table 1.

Table 1. Characteristics of the adsorber.

Dimensions	668mm x 330.2mm x 19mm
Number of flat tubes	27
Row number of fins	28
Tube external diameter	12.7mm
Tube internal diameter	10.9mm
Fin width	19mm
Fin thickness	0.3mm
Fin pitch	1.8mm
Heat transfer area (fin side)	4.175m ²

4.1.4. Condenser and evaporator

The equations related to the condenser and evaporator were widely described and experimentally validated on a previous paper (10). They are a finned-tube heat exchanger. From the simulation data, the evaporator must operate continuously (i.e., during the 24 hours a day) to ensure the storage of chilled water required by the heat exchanger air-water (fan-coil) and thus provide the design temperature for the inlet air of the rooms. For the evaporator we selected a compact plate heat exchanger, manufactured by CIAT (French), for a wide power range (2 to 200 kW) (11). The equipment will be adapted for the required operating conditions, to ensure that the outlet methanol is completely superheated.

4.1.5. Natural gas heater

The natural gas heater model GWH 300DE-GN - BOSCH, will heat the water from the hot water tank until the temperature of 105°C to ensure the regeneration. The simulation program calculates the total amount of natural gas need to be consumed in one day.

5. Results

For the simulation we have taken some considerations concerning some system parameters. The chilled water temperature is considered constant and equal to 7°C and the cold water temperature is taken 5°C above ambient temperature. The mass of the adsorbent (activated carbon) is considered equal to 116 kg for each adsorber, and the adsorber water flow is equal to 0.1L/s. The simulation results were obtained considering a typical summer day in Joao Pessoa, represented by the data of January 1, 2010 (10).

The water flow in each set of collectors in parallel arrangement was examined for different volumetric flows (0.1L/s, 0.2L/s, 0.3L/s, 0.4L/s and 0.5L/s) to verify which of them provides the lower gas consumption while the system reach a regeneration temperature. They are presented in different response curves generated for periods of 24 hours.

The volumetric rate flow through the solar collectors field was measured to compare this value with those obtained in the simulation. The measure was made with an ultrasonic flow meter, mark FMS, model UFM170. The volumetric flow rate is considered constant and the average of six measured values was about 0.71L/s.

5.1. Figures

The Fig. 5 shows the daily consumption of natural gas, for the water collector flow between 0.1L/s and 0.5L/s.

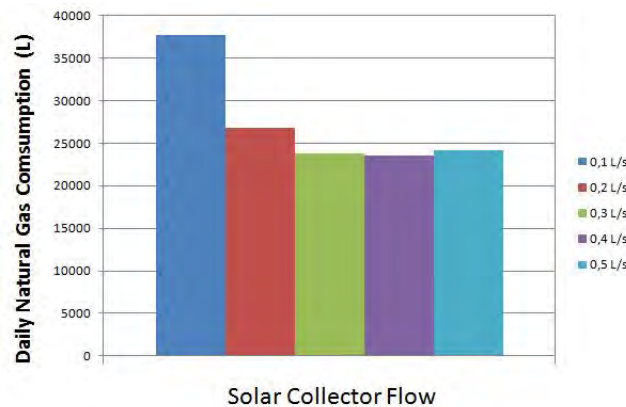


Fig. 5. Daily consumption of natural gas.

Taking into account the simulation results of Fig. 5, we can see that the solar collectors water flow of 0.4L/s gives the minimum consumption of natural gas. Thus, other results based on this flow rate are shown in Figs. 6 and 7.

The Fig. 6 shows the average water temperature in the hot water tank, during a whole day. The curves show that, at around 7am it was obtained the minimum temperature, of 58°C, corresponding to the maximum gas flow of 0.037L/s. The need of gas decreases with the temperature rise. Due to the thermal inertia, until the maximum temperature at 16:10h (86.2°C) the gas flow increases, and then it decreases following the same tendency of the temperature.

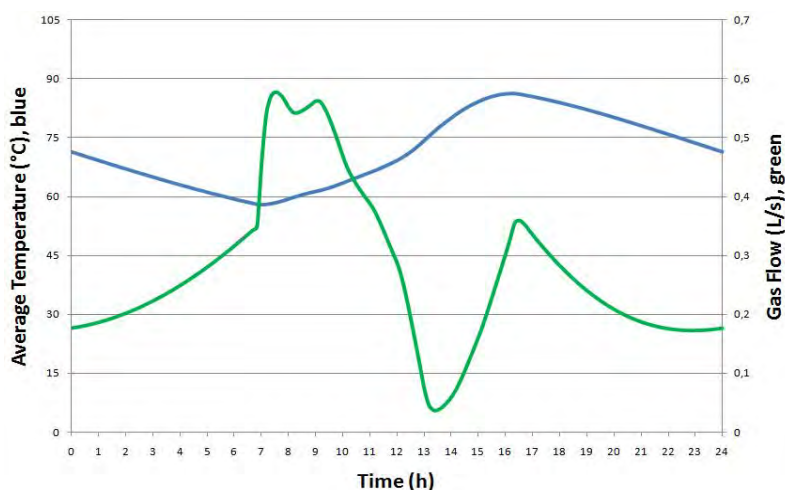


Fig.6 Average hot water temperature and the corresponding natural gas flow for the solar collector flow rate of 0.4L/s, during a day.

The Fig. 7 shows the solar collector temperatures (blue) and the temperatures of the bottom and the top (red and green) of the storage water tank, obtained with a water flow rate of 0.4L/s. We can see that there is an agreement between the temperature curves in the collectors

and on the top and the bottom of the storage tank. Due to the thermal inertia, the temperature at the bottom of the tank remains almost constant until around 8am, when it begins to increase, reaching its maximum at 16:20 and then starts to decrease.

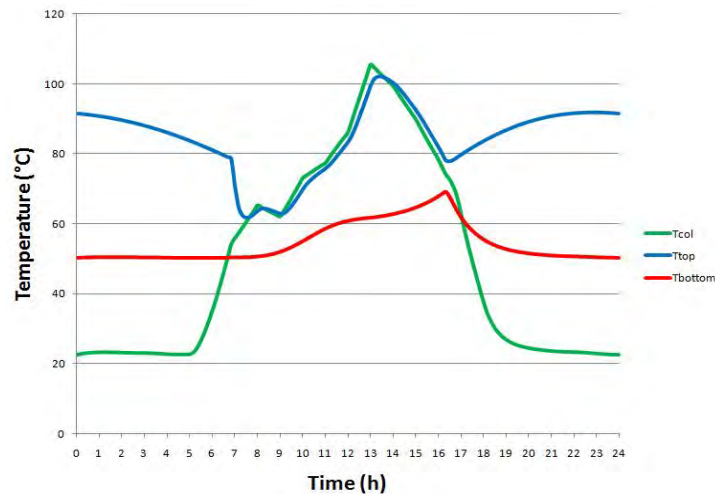


Fig.7. Thermal response of the system to the real situation, for a water flow rate of 0.4L/s, during a day.

6. Conclusion

We have presented the main parameters of a central air conditioning unit based on the adsorption of methanol in activated carbon and a hybrid regeneration system, projected to provide until 70% of the required heat by solar energy, the complementary heat by natural gas. A simulation program was developed and we have obtained from it an optimal volume of the storage hot water of 7,000 liters. It was found that 0.4L/s is the flow rate through the solar collectors field that gives the minimum consumption of gas, and the water pump should be regulated to obtain the ideal volumetric flow.

6.1. The current stage of the project

The solar collectors are installed and connected to the hot water storage tank; to compensate the thermal inertia of it a small tank of 500 liters was built and connected to the main one for providing the process regeneration temperature (105°C) with aid of the gas heater and. An equipment for analyzing the heat losses from the storage tank was also built.

The 4 adsorber modules were made, and a test bench is now under construction. The chilled water storage tanks were manufactured and their hydraulic connections installed. The air-water heat exchanger unit (fan-coil) and their pipelines network are already installed in a set of rooms.

Acknowledgements

The authors would like to thank CNPq (CT-Petro/CNPq 15/2007) and FAPITEC/SE (FUNTEC 02/2009) for the grant support, CNPq for the post-PhD scholarship to the third author and, CAPES for PhD scholarship to the first author and for post-PhD scholarship to the second author.

References

- [1] A.P.F. Leite, F.A. Belo, M.M. Martins, D.B. Riffel, Central air conditioning based on adsorption and solar energy, *Applied Thermal Engineering*, Volume 31, Issue 1, January 2011, Pages 50-58, ISSN 1359-4311.
- [2] D.B. Riffel, A.P.F. Leite, F.A. Belo, Simulação do aporte térmico de coletores solares planos em um tanque cilíndrico estratificado. In: *I Congresso Brasileiro de Energia Solar*, Fortaleza, CE, 2007.
- [3] J.A. Duffie and W.A. Beckman, *Solar Engineering of Thermal Processes*, J. Wiley & Sons, 1980.
- [4] D.B. Riffel, Estudo Teórico e Experimental da Dinâmica e da Otimização de Refrigeradores Térmicos por Adsorção, Tese de Doutorado (Eng. Mecânica), PPGEM/UFPB, 2008.
- [5] D.B. Riffel, U. Wittstadt, F.P. Schmidt, T. Nunez, F.A. Belo, A.P.F. Leite, F. Ziegler, Transient modeling of an adsorber using finned-tube heat exchanger, *International Journal of Heat and Mass Transfer*, Volume 53, Issues 7-8, March 2010, Pages 1473-1482, ISSN 0017-9310.
- [6] A.P.F. Leite, F.A. Belo, M.B. Grilo, R.R.D. Andrade, Avaliação experimental de um adsorvedor multitubular coberto com material isolante transparente, *Anais do V I Congresso Iberoamericano de Engenharia Mecânica (CIBEM6)*, Coimbra, Portugal, 15-18 Oct., 2003, Vol. I, pp. 253-258.
- [7] A.P.F. Leite, F.A. Belo, M.B. Grilo, R.R.D. Andrade, F. Meunier, An improved multi-tubular solar collector applied to adsorption refrigeration, *Proc. ISES Solar World Congress*, Orlando, Florida, USA, 6-12 Aug., 2005.
- [8] P.V.S. Domingos, D.B. Riffel, A.C.R. Veloso, C.M.C. Ribeiro, F.A. Belo, A.P.F. Leite, Simulação numérica do sistema de regeneração de um ar condicionado solar por adsorção baseado em um campo de coletores planos de alta eficiência, *IV Conferência Latino Americana de Energia Solar (IV ISES_CLA) y XVII Simposio Peruano de Energía Solar (XVII-SPES)*, Cuzco, Peru, 1-5.11.2010.
- [9] R.R.D. de Andrade, M.M. Machado, A. Lourenço, F.A. Belo, A.P.F. Leite, Avaliação experimental de uma cobertura isolante composta por material transparente para uso em coletor solar, *V Congresso Nacional de Engenharia Mecânica – COBEM 2008*, 25 a 28 de agosto, Salvador/Bahia, Brasil.
- [10] D.B. Riffel, F.A. Belo, A.P.F. Leite, Otimização de chiller adsorptivo solar por modelagem estatística, *Climatização & Refrigeração*, Abril de 2010, pags. 38 a 45.
- [11] D.B. Riffel, F.A. Belo, A.P.F. Leite, Heat and mass recovery in an activated carbon-methanol adsorptive chiller, *Proceedings of COBEM 2009 - 20th International Congress of Mechanical Engineering*, November 15-20, 2009, Gramado, RS, Brazil.

Performance analysis of the solar-thermal assisted air-conditioning system installed in an office building

Masaya Okumiya^{1,*}, Takuya Shinoda¹, Makiko Ukai¹, Hideki Tanaka², Mika Yoshinaga³, Kazuyuki Kato⁴, Toshiharu Shimizu⁴

¹ Nagoya University, Nagoya, Japan

² Chubu University, Kasugai, Japan

³ Meijyo University, Nagoya, Japan

⁴ Tohogas Co. Ltd., Nagoya, Japan

* Corresponding author. Tel: +81 527894653, Fax: +81 527893773,
E-mail: okumiya@davinci.nuac.nagoya-u.ac.jp

Abstract: In this study, performance of the solar-thermal assisted air-conditioning system installed in an office building is investigated. In this paper, firstly the results of field measurements in winter (heating) and summer (cooling) are presented. Efficiency and performance of equipments which constitutes a system are investigated. Also the utilization efficiency of solar energy and the solar fraction are estimated for winter/summer season. In addition to analysis of field measurement data, system simulation of performance was conducted in this paper. Simulation program using in this study was developed as the tool for Life Cycle Energy Management of HVAC system. In this paper mathematical model of each equipment are presented as well as how to model total system. Although there are some limitations of solar system simulation with 1 hour time step, the calculation result was well in agreement in an actual measurement.

Keywords: Solar-thermal assisted air-conditioning system, Field measurement, Simulation

Nomenclature

A_c area of collector..... m ²	$T_{1,in}$ inlet water temperature of heat exchanger in primary side..... C
C fluid thermal capacity rate ratio	$T_{1,out}$ outlet water temperature of heat exchanger in primary side..... C
C_{max} higher capacity rate of heat exchanger in two side..... kW/C	$T_{2,in}$ inlet water temperature of heat exchanger in secondary side
C_{min} lower thermal capacity rate of flow medium in two side	$T_{2,out}$ outlet water temperature of heat exchanger in secondary side
C_1 thermal capacity rate of fluid at primary side..... kW/C	U heat loss coefficient of collector.....kW/m ² ·s ⁻¹
C_2 thermal capacity rate of fluid at secondary side..... kW/C	UA overall heat transfer coefficient
FE water flow rate through collector..... kg/h	W_{max} higher flow rate of heat exchanger in two side.....kW/C
G gas consumption of absorption machine in cooling	W_{min} lower flow rate of heat exchanger in two side.....kW/C
J solar radiation	α absorption rate of collector.....
N number of transfer units	ε heat exchanger effectiveness
Q_c collected heat	η thermal efficiency of collector.....
Q_{hex} actual heat exchange rate	τ transmittance of collector cover glass.....
Q_{hexmax} ideal maximum heat exchange ratekW	ω specific dissipation of turbulent kinetic energy.....s ⁻¹
q load ratio of absorption machine in cooling	
T_a outdoor air temperature.....C	
$T_{c,out}$ collector outlet water temperature	
$T_{c,in}$ collector inlet water temperature	

1. Introduction

Practical use of renewable energy is necessary for CO₂ emissions reduction, especially, possibility of energy conversion by using solar thermal is high, and it is considered to be one of the effective means.

Although the solar-thermal-conversion air conditioning system combined with the absorption refrigerating machine was proposed at 1970's in Japan¹⁾²⁾, remarkable spread after that was not seen because of solar heat collection at high temperature having been difficult. Also there was not high performance thermal driven chiller (absorption machine) for effective use solar thermal energy.

In this paper, the actual proof examination of the air conditioning system which combined the solar collector and the gas absorption chiller/heater which can use solar heat is presented. The actual proof examination started from Jan. 2010 in Tsu City, Mie for the purpose to demonstrate effectiveness of solar HVAC system. Firstly the outline of building and system was described. Then performance of system in winter and summer season is presented and discussed. Furthermore the system simulation for solar system was introduced and possibility to represent the behavior of system is discussed.

2. Outline of Object Building and System

A building is 2,400m² of total area and 4 stories. The appearance is shown in Fig. 1. The layout of equipments on roof is shown in Fig. 2, and specification of equipments is shown in Table 1. The appearance of two type of collector is shown in Fig.3. The system flow of diagram and outline of control are shown in Fig. 4.

3. Result of Actual Proof Examination

3.1 Thermal efficiency of collector

Fig. 5 shows the change of amount of heat collection Q_c and thermal efficiency calculated by following equation.

$$Q_c = (T_{c,out} - T_{c,in}) * FE \quad (1)$$

$$\eta = Q_c / (J * A_c) \quad (2)$$



Fig.1 Appearance of building

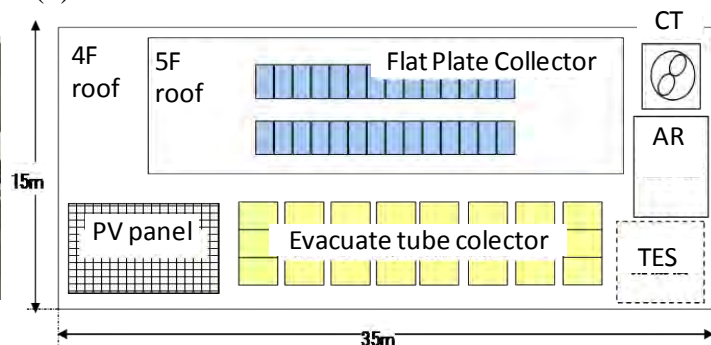


Fig.2 Layout of equipments on roof



Fig.3 Appearance of collectors

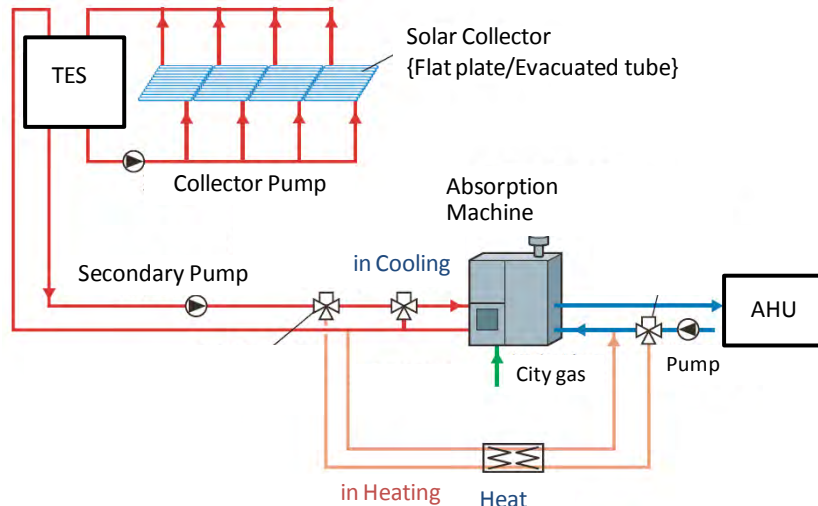


Fig. 4 System diagram of solar heating/cooling system

Table 1 Specification of equipments

Solar	Total are 139m ²	Flat plate
Collector	Medium : Water	2.0m ² x 28
	Tilted angle : 25°	Evacuated tube
	Angle of direcstion : SSW30°	4.1m ² x 20
Absorption	Three stage	
Machine	Cooling 527kW Heating 290kW	
TES	4.9m ³	

Fig. 6 shows daily solar irradiance and amount of heat collected in March 2010. Total amount of solar insolation was 16,800kWh and total amount of heat collected was 5,870kWh. Thermal efficiency of solar collector in March was 35%.

Thermal efficiency is plotted as a function of $\{(T_{c,out}+T_{c,in})/2-T_a\}/I$ in Fig.7. At the high collecting temperature (at large value of $(T_{c,out}+T_{c,in})/2-T_a$), efficiency of flat plate collector decrease while that of evacuate tube type heat pipe stable. It means evacuate tuyepe heat pipe collector is suitable for “Solar cooling” where absorption machine require relatively high temperature heat source water.

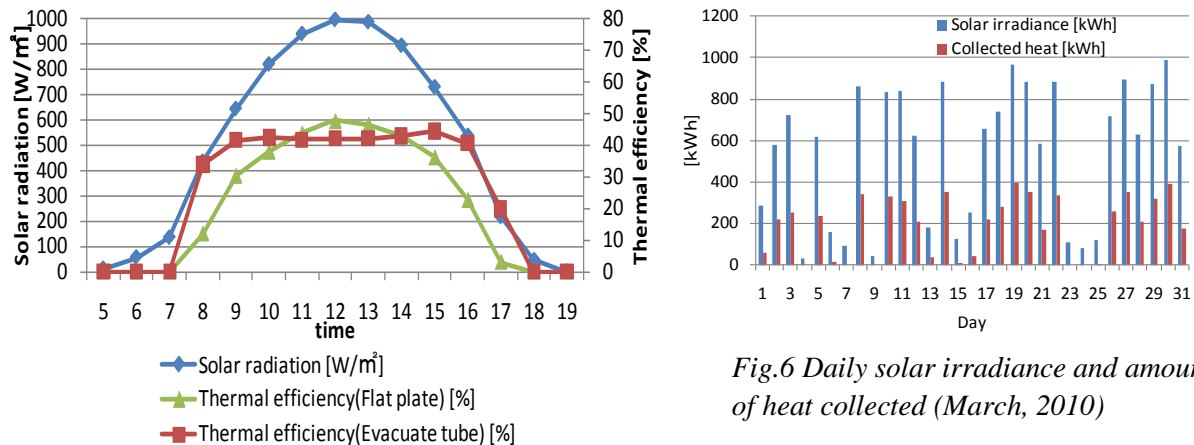


Fig.5 Collected heat and thermal efficiency of collector

Fig.6 Daily solar irradiance and amount of heat collected (March, 2010)

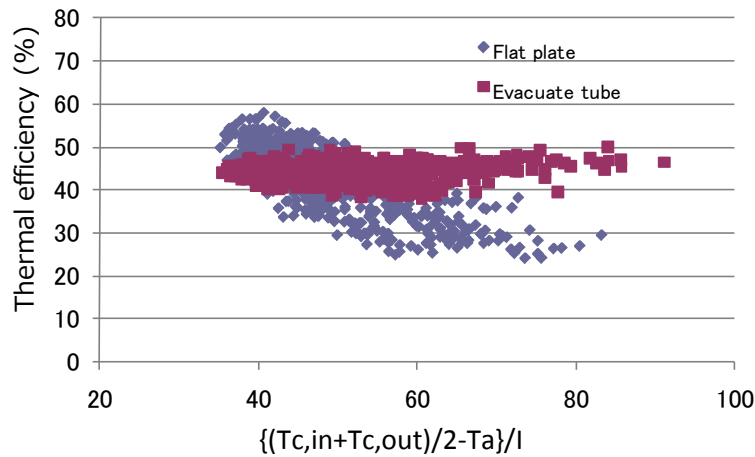


Fig.7 Plot of thermal efficiency as function of $\{(T_{c,in}+T_{c,out})/2-T_a\}/I$

3.2 System performance in winter (heating)

Fig. 8 shows daily amount of solar heat and gas energy consumed for heating. Monthly solar fraction calculated by following equation was 19%. Seasonal performance of the system is shown in Table 2. Solar heat utilization efficiency is 72% and solar fraction is 13.1 for heating season. Also ratio of pump energy to amount of collected heat is 12%.

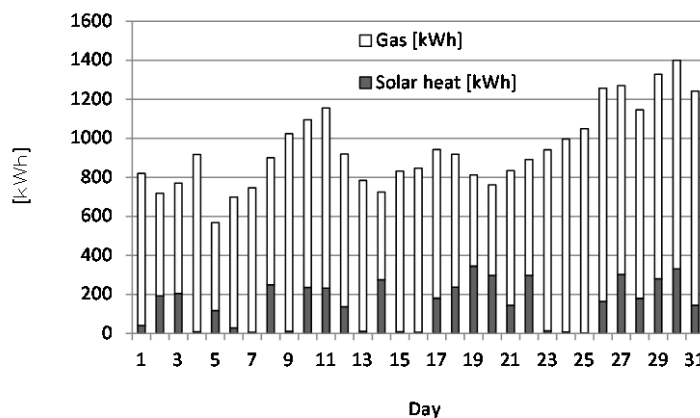


Fig.8 Daily amount of solar heat and gas energy consumed for heating

Table 2 Performance of system in heating season

		Feb.	Mar.	Apr.	Total
Collected heat	kWh	4,543	5,873	3,807	13,223
Heat delivered to heat exchanger	kWh	3,426	4,701	2,155	10,282
Heat loss	kWh	1,117	1,172	1,652	3,941
Pump energy (primary)	kWh	629	786	328	1,743
Solar fraction	%	8.3	16.0	25.5	13.1

3.3 System performance in summer (cooling)

Fig. 9 shows seasonal performance of the system for summer. Solar heat utilization efficiency changes among 78 to 89%. The highest heat utilization efficiency was seen in August. Fig. 10 shows . Monthly solar fraction calculated by following equation changes among 16 to 18%. In August, the coefficient of performance for system (System COP) and the saving rate of gas consumption were 1.4 and 0.1 respectively.

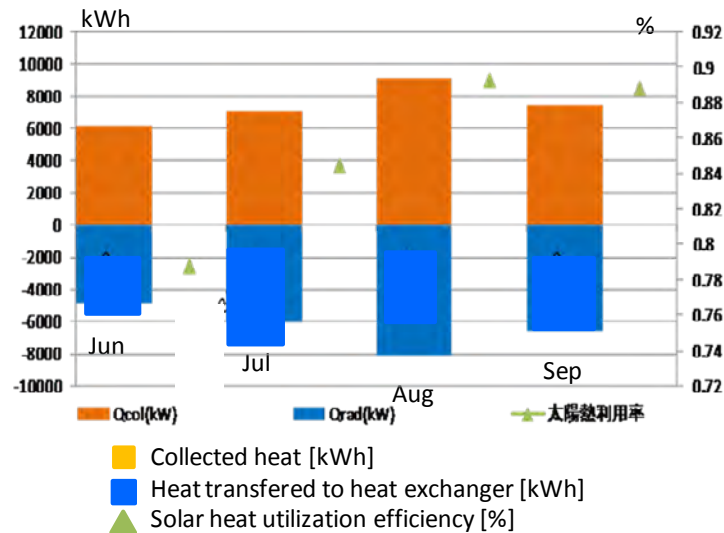


Fig. 9 Heat collected and transferred to absorption machine

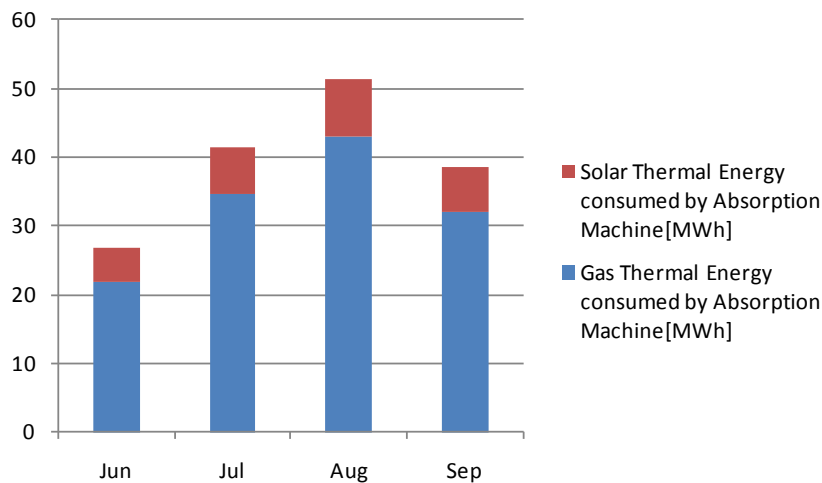


Fig. 10 Monthly amount of solar thermal energy and gas energy consumed for absorption machine

4. Simulation

In this paper, simulation of the performance of system in winter was conducted using LCEM tool. LCEM tool was developed by the basis of editorial supervision of Ministry of Land, Infrastructure and transportation, Japan for life cycle energy management of HVAC system.

4.1 Outline of Analysis Model

A part of LCEM tool Ver.3.02 was improved, and the simulation model was built. It consists of two models of the heat collection system shown in Fig. 11 and the air-conditioning system shown in Fig. 12. Two models are combined via interface.

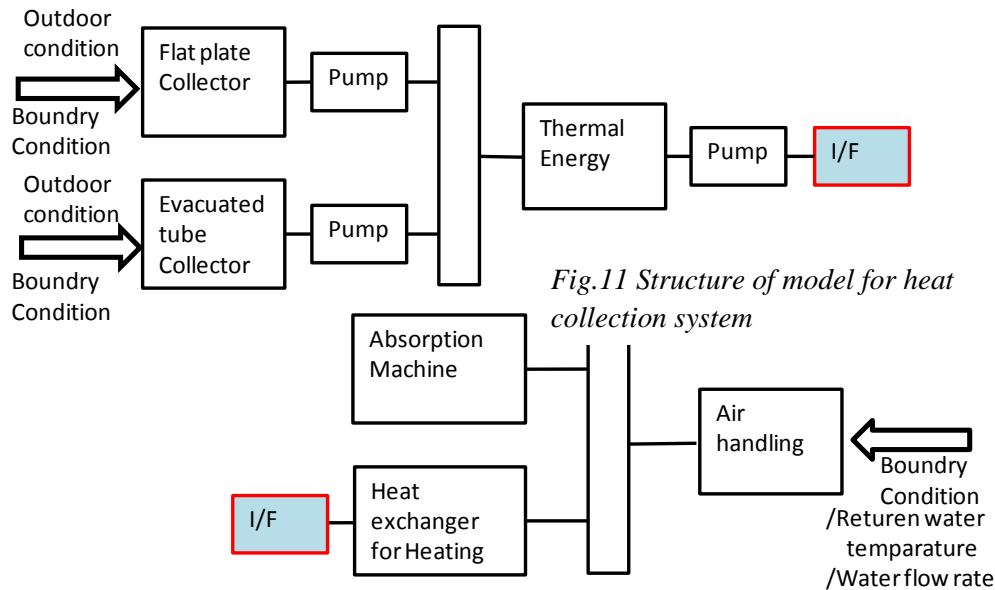


Fig.11 Structure of model for heat collection system

Fig.12 Structure of model for solar air-conditioning system

4.2 Collector Object

Heat collected by solar collector Q_c (kW) is calculated by the following equations.

$$Q_c = \eta * J * A_c \quad (3)$$

Moreover, thermal efficiency of solar collector is expressed with the following equations.

$$\eta = \tau * \alpha - U * \Delta t / J$$

$$\Delta t = (T_{c,in} + T_{c,out}) / 2 - T_a \quad (4)$$

The following characteristic were used in this simulation.

$$\text{Flat plate collector: } \eta = 0.578 - 0.00493 \Delta t / J \quad (5)$$

$$\text{Vacuum-tube type: } \eta = 0.496 - 0.00156 \Delta t / J \quad (6)$$

4.3 Thermal Storage Tank Object

The characteristic of thermal storage tank was assumed as complete mixed.

4.4 Pump Object

The energy consumed by pump is calculated using pump efficiency, water flow rate and head of piping system. Efficiency of pump is set constant in the object used in his paper. LCEM tool cannot make the model of the differential gap in the ON-OFF control of a pumps.

4.5 Heat Exchanger Object

The heat exchanger object used in this paper are as follows.

$$Q_{hex} = C1 * (T1_{in} - T1_{out}) = C2 * (T2_{out} - T2_{in}) = \epsilon * Q_{hexmax} \quad (7)$$

$$Q_{hexmax} = C_{min} * (T1_{in} - T2_{in}) \quad (8)$$

$$\epsilon = [1 - \exp \{-N(1-C)\}] / [1 - C \exp \{-N(1-C)\}] \quad (9)$$

$$N = UA/C_{min} \quad (10)$$

$$C = C_{min}/C_{max} \quad (11)$$

$$C_{min} = 4.186 * W_{min} / 60 \quad (12)$$

$$C_{max} = 4.186 * W_{max} / 60 \quad (13)$$

4.6 Absorption Chiller/Heater Object

The amount of gas consumption is assumed as the function of the load factor (q), and was modeled by the following formulas.

In case of $0\% < q < 25\%$

$$G = 1.2 * q / 100 * 25.8 \quad (14)$$

In case of $25\% < q < 40\%$

$$G = (-0.013 * q + 1.533) * q / 100 * 25.8 \quad (15)$$

In case of $40\% < q < 100\%$

$$G = q / 100 * 25.8 \quad (16)$$

The differential gap in ON-OFF of absorption machine can not be expressed by LCEM tool and the outlet temperature was set to constant value of 55 degrees C.

5. Simulation Result

In this section simulation results for heating operation are shown. Fig. 13 shows the comparison between measurement and simulation for flat plate collector and evacuated heat pipe. Fig. 14 shows the heat collected and delivered to heat exchanger. Also fig.14 shows temperature in thermal storage tank. Fig. 15 shows the change of output of absorption machine. From these figures, it can be concluded that simulation results using LCEM tool shows good agreement with an actual measurement. However there are limitations of simulation as follows.

Time interval of calculation

In this study, 1 hour of time interval for calculation is applied. The system is controlled by the shorter time interval. Therefore, calculation result of collected heat at end of operation (evening) is overestimated. Also output of absorption machine (operate as boiler in heating) is overestimated when heat load is small. In this situation, absorption machine repeats operation and stop at short time step. However, this action cannot be expressed by simulation.

Simplified model

In this study, components in the system are modeled simply, for example heat loss from storage tank was neglected. This kind of simplification effects on the accuracy of simulation.

6. Conclusion

The system performance for the 1st year has been grasped by field measurements. Also system simulation for heating season was conducted by using LCEM tool. The simulation for cooling season will be conducted from now on. Although the system demonstrated good performance, improvement of operation should be conducted based on the results of field

measurements and simulation. Also simulation program will be revised to reduce the limitation which was mentioned in this paper.

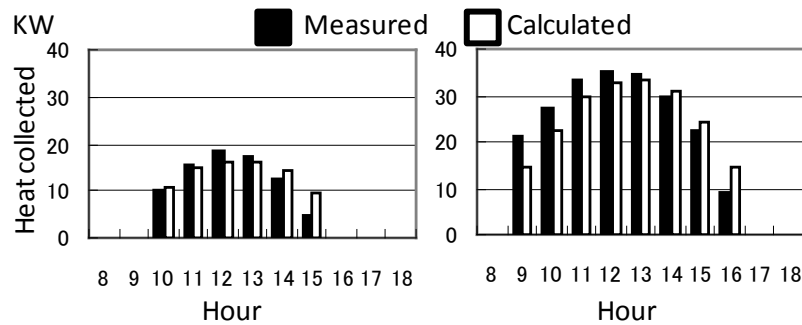


Fig. 13 Comparison collected heat by collector between measurement and simulation

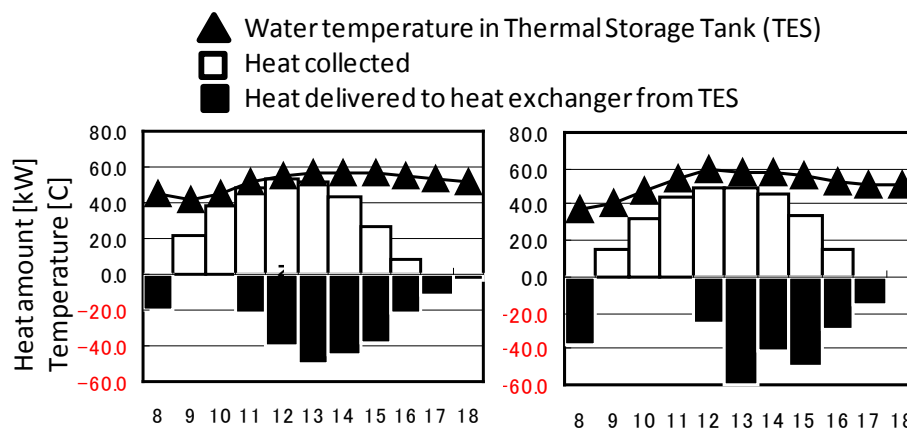


Fig.14 heat collected, heat delivered to heat exchanger and water temperature in thermal storage tank

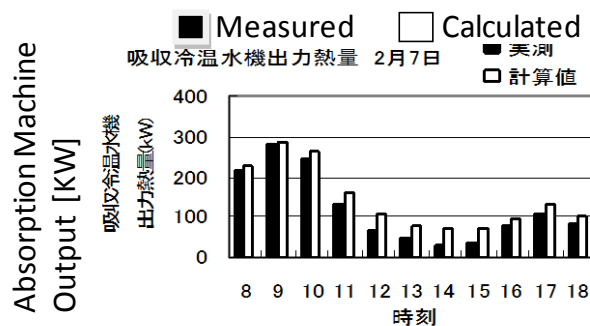


Fig. 15 Comparison of output of absorption between measurement and simulation

References

- [1] N.Nakahara, K.Okada, H.Niwa, Study on System Applications of CPC Solar Collectors Part 4-Actual Operating Results of Solar Facilities for Chita Citizen's Hospital, SHASE Transactoin, No.33, 1987,pp61-73 (in Japanese).
- [2] New Energy and Industrial Technology Development Organization, Japan, Design Guide for Solar Archiectyre, 2001 (in Japanese)

Characterization of nanostructure black nickel coatings for solar collectors

Z.Ghasempour, S.M. Rozati*

Physics Department, University of Guilan, Rasht, 41335.Iran

* Corresponding author. Tel: +98131220912 Fax: +98 1313220066, E-mail: smrozati@guilan.ac.ir

Abstract: In this research, black nickel coatings have been deposited on brass, copper and steel substrates by electrodeposition method. The physical properties of solar absorber black nickel coatings on different metallic surfaces have been investigated. The effect of different metallic substrates including brass, copper and steel with presence of bright nickel middle layer and without its presence on optical and structural properties of deposited layers have been studied. These coatings characterized by scanning electron microscopy (SEM), X-ray diffraction (XRD) and energy-dispersive X-ray analysis (EDAX). For investigation of optical properties of deposited layers, UV-VIS-NIR spectrophotometer was used.

Keywords: Electroplating, Black nickel, Bright nickel

1. Introduction

The use of selective coatings has been widely established as an industrial application which used to absorb solar thermal energy. Demands for design and construction of solar absorber plates to achieve reduced energy consumption and its applications in the areas of electrical energy, heating and cooling systems lead to the development of growing of black nickel coatings [1]. Fundamental properties of black nickel coatings are currently excessively studied because of their potential application in numerous fields such as electronic devices, opto-electronic, optics, biotechnology, human medicine, solar energy conversion and etc [2]. Black nickel is one of the most commonly used solar selective coatings in solar collector systems for the efficient conversion of solar energy into thermal energy [3]. Such coatings are identified by high solar absorptance ($\alpha > 95\%$) and low thermal emittance ($\epsilon < 40\%$). Considering all studied cases selected for selective solar absorber coating, black nickel plates due to lower consumption of requirement electrical energy also electroplating in large scale for production and development in the industry are considered as one of the most appropriate coatings [4]. There are different methods for the deposition of black nickel coatings, including Chemical vapor deposition (CVD), sputtering, spray pyrolysis[5], electroless[6], pulse plating[7] and electrodeposition [8,9]. Among these methods, because of simple setup, low cost process of coating in industrial scale, easy control of production processes and high speed production, the electroplating method attracted special attention.

Electroplating of metallic films is one of the appropriate techniques to obtaining absorber coatings with selective optical properties for solar collectors. Electrical current and reclamation agents that are used in this process are cheap and this good economic sense to develop this approach. By using this method, optical coatings with suitable properties for solar absorber plate's applications with large scale are provided.

Electroplating is a process in which by using electrical current, a thin layer of metal is deposited on the surface of another metal. Figure 1 shows the schematic of electroplating system in hull cell. The presence of the bright nickel middle layer causes changes in the optical properties, including absorptance and emittance, of the films.

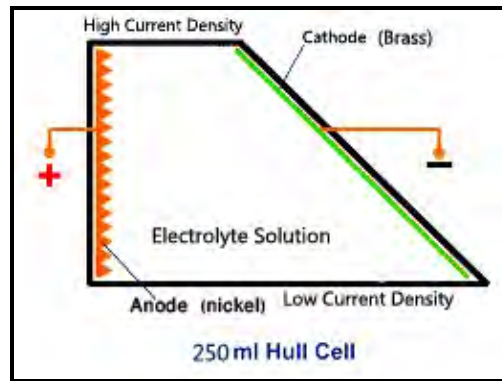


Fig. 1. The schematic of electroplating system in hull cell

2. Methodology

Black nickel coatings have been deposited on three different substrates namely brass, copper and stainless steel by electroplating method. Before deposition at first, the desired metal plates in dimensions of 7×10 cm perfectly polished and then thoroughly washed with distilled water. After that all substrates were degreased with a hot commercial alkaline solution followed by rinsing in distilled water. Finally they are placed in the chloride electrolyte solution for black nickel plating. All the coating process is carried out in hull cell. The Quality of black nickel coatings depend on the electrolyte solution composition and its concentration, electrodes, solution pH, bath temperature, current density and (deposition) duration (time). Therefore to obtain optimum optical properties for black nickel coatings, deposition parameters have to be optimized. In this type of coating, the soluble nickel metal used as a anode with 99% purity. Direct current passes between two electrodes in a conducting solution of nickel salts. The chemical bath for black nickel deposition consisted of a mixture of distilled water, nickel, zinc, tin and ammonium chloride with potassium thiocyanate. By flowing the current through the electrolyte, one of the electrodes (anode) is dissolved in the solution and the other electrode (cathode) is covered by a black nickel layer. In the electrolyte solution Ni positive ions (Ni^{++}) present so as the electrical current flows through the electrolyte, positive ions by absorbing two electrons on the surface of cathode are converted to nickel metal and deposited on the cathode surface. Reverse reaction occurs at the anode. So with the consumption of nickel in the cathode, the nickel ions are provided by anode. The concentrations of additives were varied to improve the optical performance. After numerous tests the best conditions for strongly adherent and durable black nickel coating, as mentioned in table 1, were obtained as follow: solution with pH 4.2, electrolyte bath temperature 65°C , plating time 10 min and current density 0.1 A/dm^2 .

The effect of different substrate metals including brass, copper and stainless steel without the presence of the middle bright nickel layer and with the presence of it, on the optical and structural properties of the black nickel coatings have been investigated. Changes in the physical as well as optical properties of black nickel coatings are measured. SEM and XRD analysis are carried out by Philips PW3710 and Philips XL 30; the absorption spectra of coatings and emittance spectra are measured by carry 500 and Jasco FTIR respectively.

Table 1: Optimum conditions of coating

Current density	Temperature	pH	anode	cathode	Deposition time
0.1 A/dm ²	65°C	4.2	Nickel metal	Brass plate	10 minute

3. Results

3.1. Evaluation of optical properties, absorption analysis

Absorption spectrum curves of the black nickel coatings for various wavelengths depending on the metal substrate; including brass, copper and steel with and without bright nickel middle layer are presented in Fig.1-a and Fig.1-b. As can be seen from the graphs below, the black nickel coating has high absorption coefficient. The results from Graphs show that by changing the substrate, the absorption spectrum will change. The highest absorption is related to the coating layer on brass substrate without bright nickel and lowest absorption is belonged to the coating layer on stainless steel substrate with present of bright nickel.

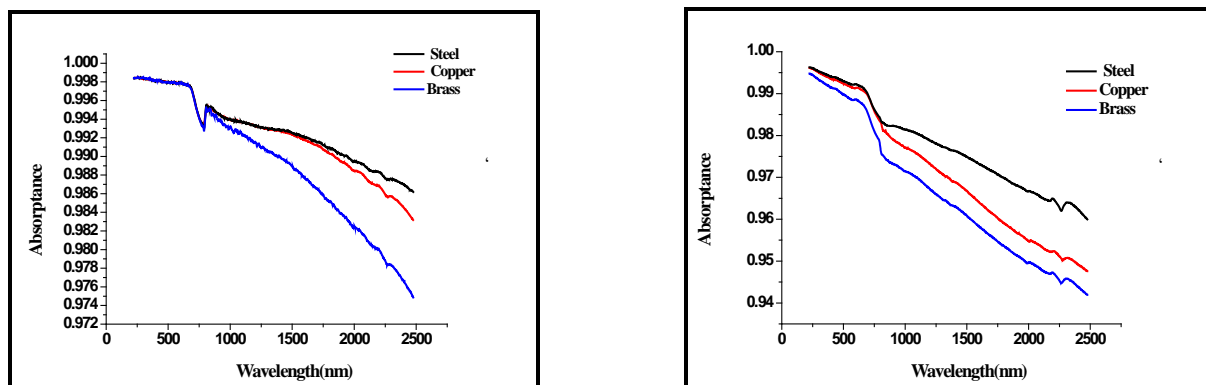


Figure (1 – a) absorption spectrum of black nickel on brass, copper and steel substrates without bright nickel, as a function of wavelength. Figure (1 – b) absorption spectrum of black nickel coating on copper, brass and steel substrates with bright nickel as a function of wavelength.

3.2. Emittance analysis

Below figure shows the result of emittance. By comparing the results the lowest emittance is belonged to the brass substrate and highest emittance is belonged to the steel substrate.

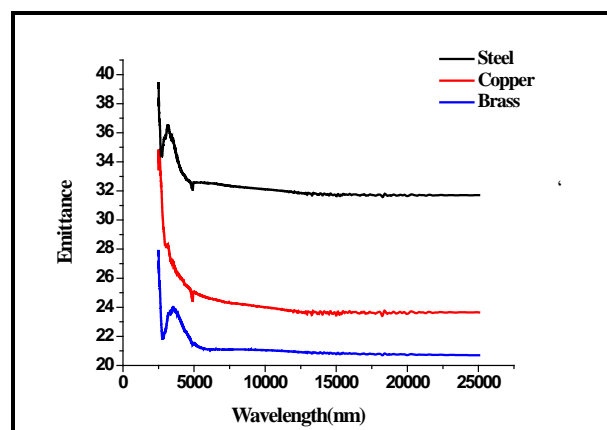


Figure (2) emittance spectrum of black nickel on brass, copper and steel substrates without bright nickel, as a function of wavelength.

3.3. SEM analysis

Scanning Electron Microscopy (SEM) Images of nano black nickel coatings prepared from nickel chloride bath with and without the presence of bright nickel middle layer. fig 3-a and 3-b shows the image of black nickel coating on brass substrate without and with bright nickel middle layer respectively.

By comparing the images of SEM it can be distinguished that layers with bright nickel have larger grains in comparison with layers without bright nickel. Since layers without bright nickel have a higher absorptance spectra so as result when grain size increase absorptance spectra decrees.

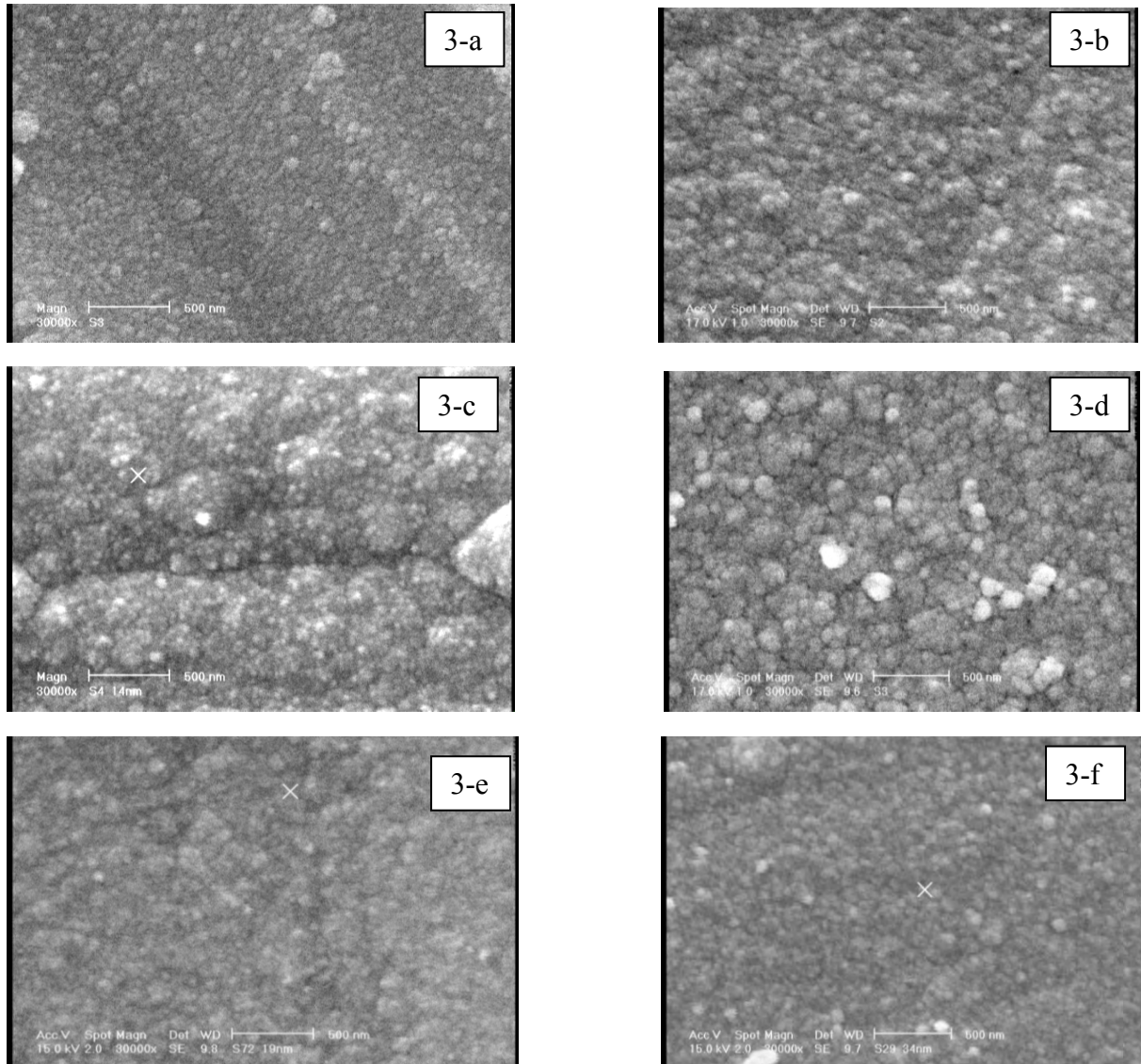


Figure 3: (SEM) Images of the black nickel coating
a) SEM image of a black nickel coating without bright nickel layer on the brass substrate b) SEM image of a black nickel coating on the brass substrate with bright nickel layer c) SEM image of a black nickel coating without nickel layer on the steel substrate d) SEM image of a black nickel coating With the bright nickel layer on stainless steel e) SEM image of a black nickel coating on copper without the bright nickel layer f) SEM image of a black nickel coating on copper with bright nickel layer

3.4. Results of X-ray diffraction and elemental analysis(EDAX)

Figure 4-a and 4-c show X-ray diffraction pattern of electrodeposited black nickel coatings on brass substrate. Two different structures clearly can be seen with and without the presence of bright nickel. Without presence of bright nickel there was no peak related to crystalline nickel and only the peaks belong to brass substrate have grown. While with regard to the 4-b, the presence of Ni element in the deposited films is provided by elemental analysis EDAX. The major difference between two structures can be recognized in fig 4-c. In XRD analysis of layer deposited in the presence of bright nickel the preferred orientations (111), (200) and (220) belong to nickel can be seen.

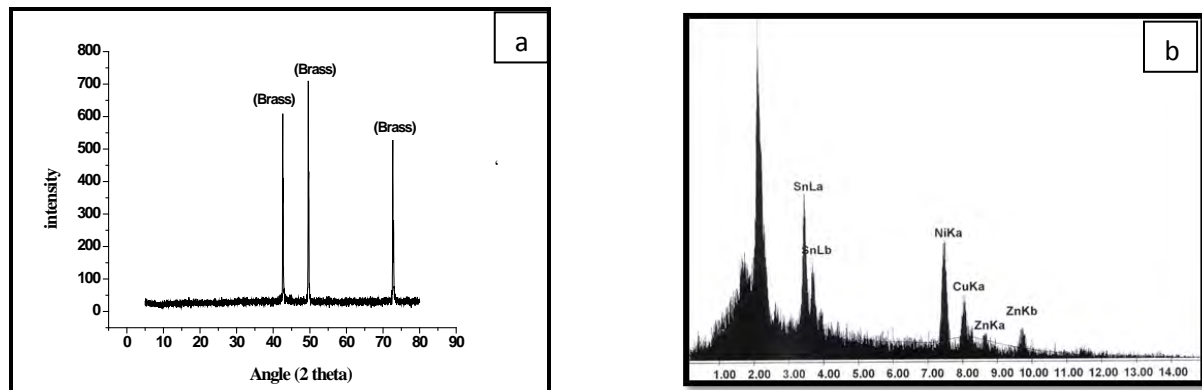


Figure 4– a, b X-ray diffraction pattern and elemental analysis black nickel coating without bright nickel

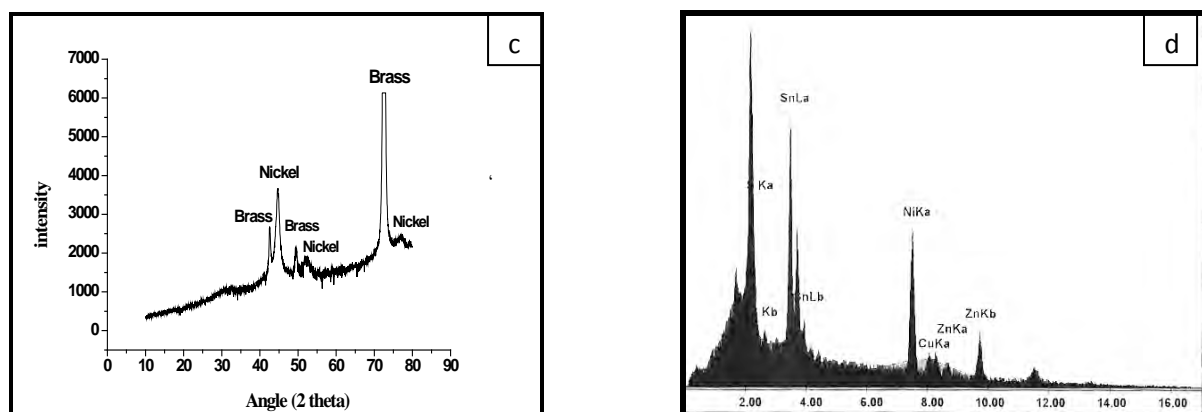


Figure 4–c, d X-ray diffraction pattern and elemental analysis black nickel coating with bright nickel

In order to identify the predominant nickel phase in the deposited films, it is necessary to investigate the coatings using X-ray diffractometer. Fig. shows the typical XRD pattern for the bright nickel substrate coated with black nickel films. This result is in good agreement with result of EDAX analysis.

4. Conclusion

The black nickel coatings with high absorption coefficient are suitable for solar applications. The coatings are very adhesive and have good thermal stability, with high absorption coefficient. SEM images show the relationship between absorption spectra with fine diameter of spherical particles, so that the layer of black nickel deposited on brass substrate without bright nickel coating have very small spherical particles and consequently optical properties of selected increases. Conversely, with the presence of bright nickel layer the particle size increases and absorption spectrum decreases. The highest absorption is for layer deposited on

brass without bright nickel and low absorption spectrum associated with the nickel coating on steel with bright nickel middle layer. EDAX analysis indicates presence of nickel on formed films. X-ray diffraction analyses show that electrodeposited films have polycrystalline structure and black nickel films were mainly consisting of metallic nickel. This result is matched with result of EDAX analysis. The presence of bright nickel middle layer cues the growth of nickel structure in orientation of (111), (200) and (220).

References

- [1] K. N. Srinivasan, N. V. Shanmugam, M. Selvam, S. John, B. A. Shenol, Nickel-black solar absorber coatings, *Energy Convers* 24, 1984, pp. 255-258.
- [2] S. R. Rajagopalan, K. S. Indari, K. S. G. Doss, An explanation for the black colour of black nickel, *Journal of Electroanalytical Chemistry*, 1965, pp. 465-472
- [3] P. K. Gogna, K. L. Chopra, Structure-dependent thermal and optical properties of black nickel coatings, *Thin Solid Films* 57, 1979, pp. 299-302.
- [4] M. Koltun, G. Gukhmen, A. Gavrilina, Stable selective coating black nickel for solar collector surfaces, *Solar Energy Materials and Solar Cells* 33, 1994, pp. 41-44
- [5] M. Madhusudana and H. K. Sehgal, Spray-deposited black nickel selective absorber surfaces for solar thermal conversion, *Applied Energy* 10, 1982, pp. 65-74.
- [6] S. John, N. V. Shanmugam, K. N. Srinivasan, M. Selvam and B. A. Shenoi, Blackening of electroless nickel deposits for solar energy applications, *Surface Technology* 20, 1983, pp. 331–338.
- [7] G. Devaraj and S. Guruviah, Pulse plating, *Materials Chemistry and Physics* 25, 1990, pp. 439-461
- [8] S. Shawki, S. Mikhail, Black nickel coatings for solar collectors, *Materials and Manufacturing Processes* 15, 2000, pp. 737-746.
- [9] S. N. Patel, O. T. Inal, A. J. Singh, A. Scherer, Optimization and thermal degradation study of black nickel solar collector coatings, *Solar Energy Materials* 11, 1985, pp. 381-399.

Investigations of heating process and absorber materials in air heating collector

Aivars Aboltins*, Janis Palabinskis

Institute of Agricultural Machinery, Latvia University of Agriculture, Cakstes bulv. 5, Jelgava, LV-3001, Latvia

**Corresponding author. Tel: +371 29134846, Fax: +371 46 13211001, E-mail: aivars.aboltins@llu.lv*

Abstract: The research had two aims-1 st. determine the airflow temperature distribution depending on the thickness of the collector air channel and collector length, where the absorber is a steel tinplate ; 2 nd. search non-traditional (utilized) materials (slices of black coloured beer cans, different size black colour seed boxes made of polypropylene) that could be used as absorbers of air heating solar collectors

0.1x0.5x1.0 meters long flat-plate collectors (FPC) for experimental research into the materials of solar air heating collector were built. The air velocity at the experiments was $v=0.9$ m/s, covered material - polystyrol plate. We used the sun following collectors, which guarantees perpendicular location of the plane of absorber from the flow of sun irradiance.

From the experimental data were obtained an analytical expressions that describe the solar radiation and collector air channel size influence to the flowing air temperature in FPC using steel tinplate absorber.

The panel of black colored slices of beer cans can be used for air heating solar collectors as absorber. The experimental data show the temperature difference in outlet of sun following collector reaches up to 10-11 degree with sun irradiance 1000 W/m^2 at different weather conditions. It is a little more better than the best seed boxes.

Keywords: Solar Collector, Air, Temperature, Absorber

1. Introduction

The greatest advantage of solar energy comparing with other forms of energy is that it is clean and can be supplied without environmental pollution. Over the past century, fossil fuels provided most of our energy, because it was much cheaper and more convenient than energy from alternative energy sources, and until recently, environmental pollution has been of little concern. The limited reserves of fossil fuels cause a situation in which the price of fuels will accelerate as the reserves are decreasing.

Solar energy is used to heat and cool buildings (both actively and passively), dry products, heat water for domestic and industry use, heat swimming pools, generate electricity, for chemistry applications and many more operations [1].

The application of solar energy is completely dependent on solar radiation, a low-grade and fluctuating energy source. An intrinsic difficulty in using solar energy is caused by the wide variation in the solar radiation intensity. The availability of solar irradiance depends not only on the location, but also on the season. Extreme differences are experienced between summer and winter, and from day to day.

In general, solar water and solar air heaters are flat-plate collectors (FPCs), consisting of an absorber, a transparent cover, and backward insulation. Despite the similarity in designs, the different modes of operations and different properties of the heat transfer medium greatly affect the thermal performance and electric energy consumption for forcing the heat transfer medium a through the collector. Solar water heaters are operated as a closed-loop system whereas, in most cases, solar air heaters are operated in the open-loop mode.

The performance of solar air heaters is mainly influenced by meteorological parameters (direct and diffuse radiation, ambient temperature, wind speed), design parameters (type of collector, collector materials) and flow parameters (air flow rate, mode of flow). The principal requirement of these designs is a large contact area between the absorbing surface and air.

The efficiency of solar collector depending on the collector covered materials (polyvinylchloride film, cell polycarbonate PC, translucent roofing slate) [2-5], absorbers (black colored wood, steel-thin plate etc.), with different air velocities in collector was investigated [6-9]. The main efficiency parameter of solar collector is the air heating degree and it we chose as a criterion of efficiency.

The plane of FPC absorber is perpendicular to the flow of sun irradiance at sun following collector therefore this type is more powerful than stationary collector. The sun rays fall under angle to collector plane (it means it falls under angle to covered material) and it gives more reflection.

For manufacturing of collectors it is important to know their thickness and its effect on the temperature distribution of heated air. As one of the best absorbers is a tin plate in the middle of collector, then it is interesting to know how heated air temperature changes above and below the plate.

There is a need to test the various, cheap, easily available materials in an absorbent material for manufacturing of solar collectors.

2. Methodology

In the laboratory a $0.1 \times 0.5 \times 1.0$ meters long experimental solar collectors were constructed for research into the properties of absorber materials. The air velocity at the experiments was $v=0.9$ m/s. Our investigations are devoted the sun following collectors, which guarantees perpendicular location of the plane of absorber from flow of the sun irradiance (Fig.1).

In the experiments, the collector covered material was a polystyrol plate. This material has gained immense popularity due to such properties as safety, mechanical crashworthiness, translucence and high UV radiation stability. The covered material - polystyrol plate reduced irradiance by 12-15 %.

The experimental data are recorded by means of an electronic metering and recording equipment of temperature, irradiance and lighting REG [10]. It is equipped with 16 temperature transducers and metering sensors of solar irradiance and lighting. The reading time of the data can be programmed from 1 to 99 minutes (1 minute in our case).

The recorded data are stored in the REG memory (there is a place for 16,384 records) and in case of need it is transferred to a computer for archiving with further processing. For evaluation and analysis of the results software REG – 01 has been developed, which is meant for transfer to the computer and processing of the recorded data. The information is stored in the form of a table and in case of need it is depicted as a graph.

The air heating experiments by this collector were made at different weather conditions. The solar irradiance measuring instrument is a pyranometer. The data of sun irradiance are dependent on clouds, shadows and we aligned the experimental data with the method of least squares using Eq. (1) [11].

$$\bar{y}_i = \frac{1}{35} [17y_i + 12(y_{i-1} + y_{i+1}) - 3(y_{i-2} + y_{i+2})] \quad (1)$$

where \bar{y}_i - aligned data, y_i - experimental data, i - index.



Fig. 1. Sun following collector at work

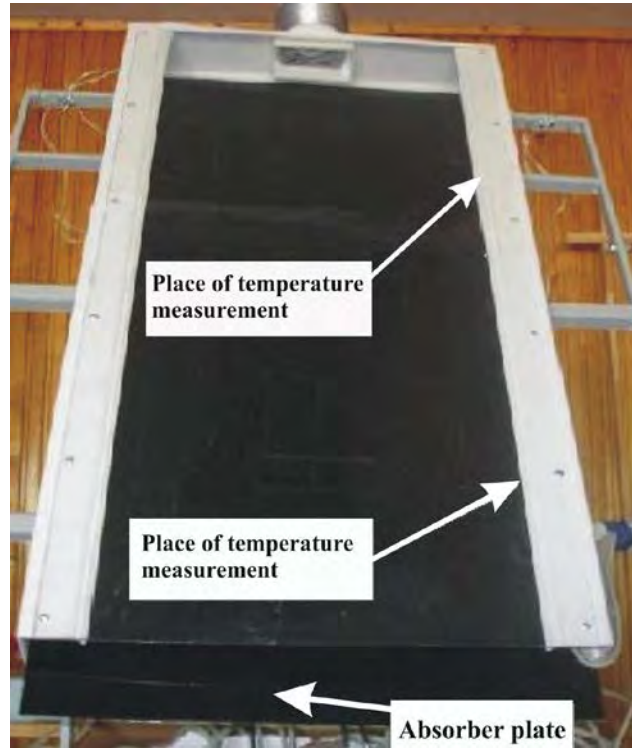


Fig. 2. View of solar collector with steel-tinplate absorber in middle.

3. Results

At first we researched a situation when the absorber (black coloured steel-thin plate) is put at the bottom and middle of the collector (Fig.2). Using the experimental results and statistical processing data we received correlation between the distance from absorber, sun irradiance to absorber plate and air temperature change in the collector. We got expressions for air temperature changing over steel-thin plate absorber in FPC at 35cm and 60cm from inlet.

The temperature change ΔT over absorber at 0.35 m distance from input can be expressed with Eq. (2);

$$\Delta T = 3.8 \cdot 10^{-3} \cdot R + 21.3 \cdot y - 318.5 \cdot y^2 - 4.6 \cdot 10^{-3} \cdot R \cdot y, \quad (2)$$

where y -distance from absorber,(m), R - sun radiation (W / m^2).

Close connection of this expression and the experimental data shows coefficient of determination $\eta^2 = 0.804$ in temperature increase domain $\Delta T \in (0; 3) ^\circ C$.

The temperature change ΔT over absorber at 0.60 m from inlet we can be expressed with Eq.(3);

$$\Delta T = 1.57 + 0.011 \cdot R - 4.15 \cdot 10^{-6} \cdot R^2 - 34.8 \cdot y + 369.8 \cdot y^2 - 0.021 \cdot R \cdot y \quad (3)$$

with coefficient of determination $\eta^2 = 0.855$.

The visual interpretation of expressions (2), (3) is shown in Fig.3-4.as contour plot .

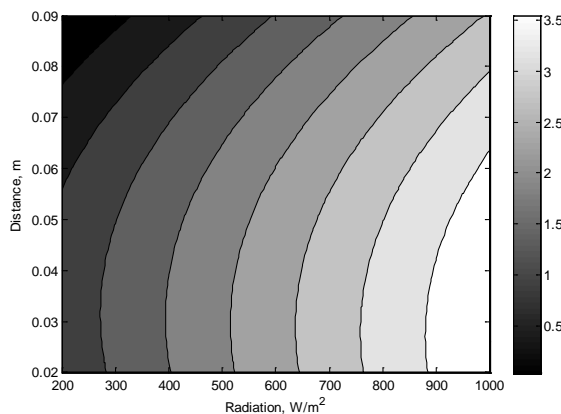


Fig. 3. Plot of air temperature increase ΔT depending on distance over absorber y (m) and radiation R (W / m^2) at 0.35 m from inlet

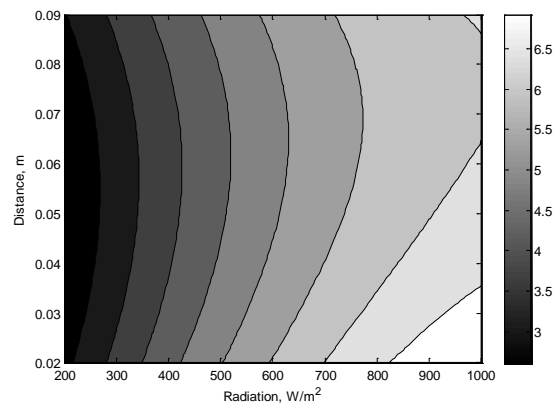


Fig. 4. Contour plot of air temperature increase ΔT depending on distance y (m) over absorber and radiation of sun R (W / m^2) at 0.6 m from inlet.

The temperature change ΔT in the collector length over absorber (steel-tinplate) put in the middle of the air channel can be expressed with Eq. (4);

$$\Delta T = 0.0073 \cdot R - 5.4 \times 10^{-6} R^2 + 17 \cdot x - 25.6 \cdot x^2 + 0.028 \cdot R \cdot x , \quad (4)$$

where x -length of collector,(m). Coefficient of determination $\eta^2 = 0.98$ in temperature increase domain $\Delta T \in (0; 18) ^\circ C$.

The temperature change ΔT in the collector under absorber can be expressed with Eq.(5) ($\Delta T \in (0; 10) ^\circ C$):

$$\Delta T = 4.2 \cdot x - 4.9 \cdot x^2 - 2.8 \times 10^{-3} \cdot R + 3.4 \times 10^{-6} R^2 + 0.012 \cdot R \cdot x , \quad (5)$$

with coefficient of determination $\eta^2 = 0.955$.

The graphical interpretation of these expressions is shown in Fig.5, Fig.6.

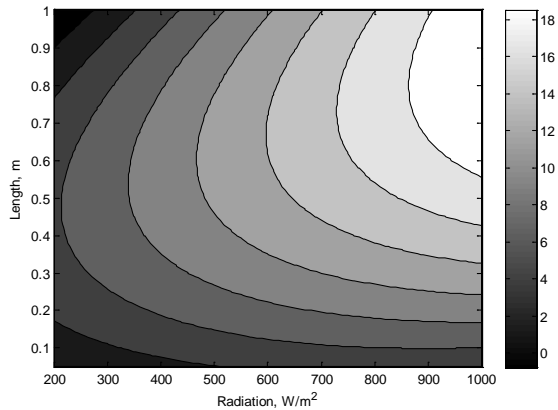


Fig. 5. Air temperature increase ΔT over steel-tinplate absorber depending on collector length x (m) and radiation R (W / m^2)

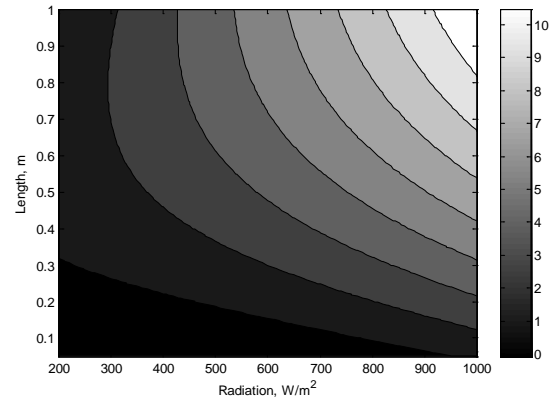


Fig. 6. Air temperature increase ΔT under steel-tinplate absorber depending on collector length x (m) and radiation R (W / m^2)

Second we tested new absorber materials which can be used in hand made air heated solar collectors. These materials must be cheap, light and simple use. We made panels with different size black seed boxes which were made of polypropylene (Fig.1, Fig.8) and a panel with coloured slices of beer cans (Fig.7, Fig.1) . These slices help to mix the air flow in the collector and rise the outlet air temperature.

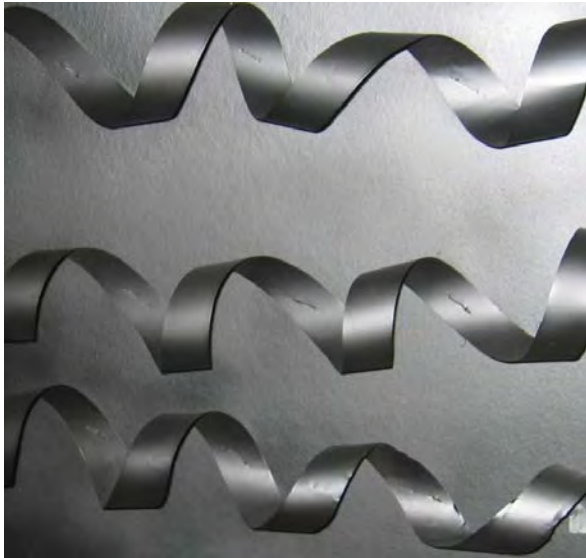


Fig.7 Black coloured slices of beer cans as absorbers of air collector



Fig.8 The panel of 13 seed boxes as absorbers of air collector

Air heating level is not highly dependent on ambient temperature. Much more it is influenced by solar radiation. Experimental results which was made in 7.September 2010. showed it (Fig.9).

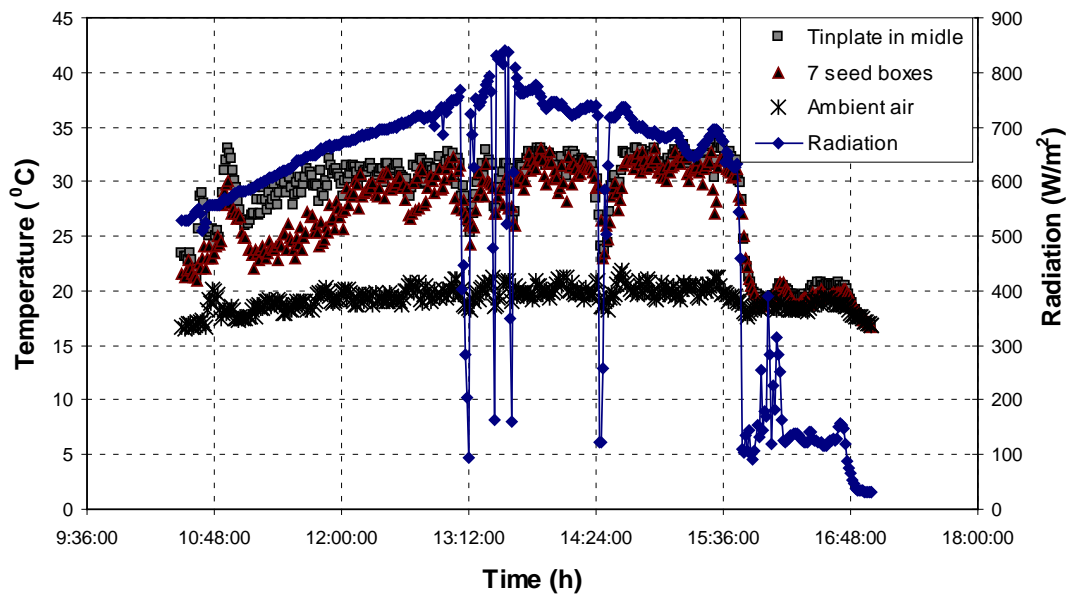


Fig.9 Ambient air, collectors(with tinplate, seed boxes absorbers) outlet temperatures and solar radiation changes (10:30 -17:00 o'clock).

Ambient air heating degree serves as the main effectiveness of collectors at the same size collectors with the same fan power. Comparing the absorbers with 7 seed boxes in line (the best variant of seed boxes [8]) and the absorber panel with slices at the same weather conditions we can see that the absorber panel with slices of cans gives little bit better results (temperature increases at the outlet of collector) than the variant of seed boxes Fig.10. The air inflow temperature equal with ambient air temperature and it changed from 17 °C to 25 °C during the experiment.

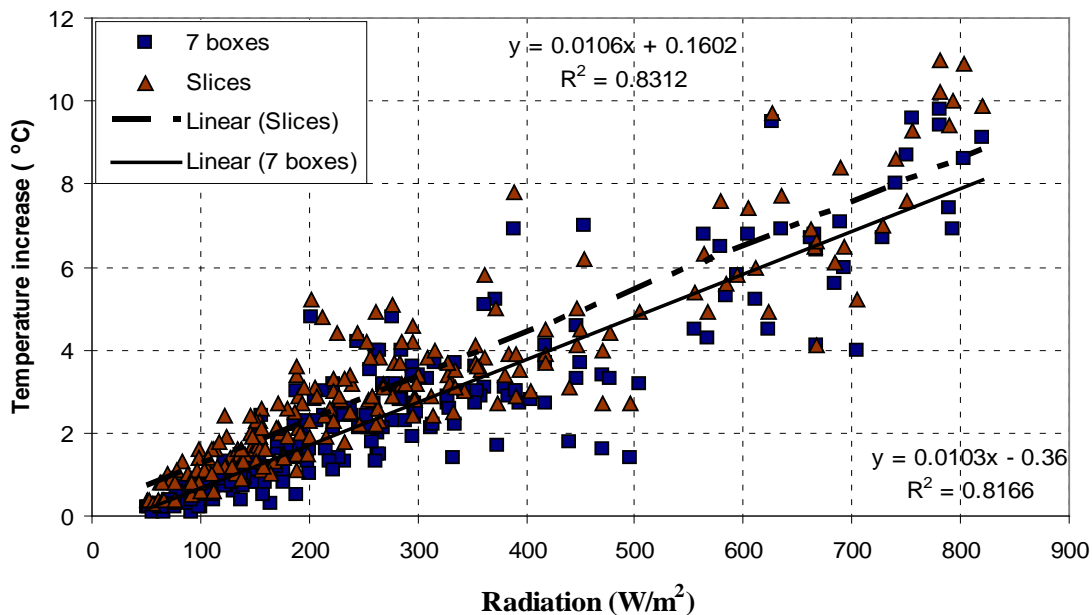


Fig.10 Air heating temperature difference with black coloured slices and 7 element seed boxes in line depending upon solar irradiance in sun following collector (11:00 -18:00 o'clock).

The experimental data show very good linear correlation between solar radiation and air-heating degree (correlation coefficient greater than 0.9).

The efficiency of solar air collectors is influenced both by the design and air circulation and by the properties of the material used for cover, absorber and insulation. The efficiency of this absorber material can be explained by the type of absorber which mix the air flow in thickness and width of the collector area. It is important because without air mix, air exchange at corners and near sides of the collector does not take place.

4. Conclusions

1. The theoretical expressions for air temperature which are changing over steel-thin plate absorber in FPC at 35cm and 60cm from inlet are obtained. These expressions show temperature distribution depending on the distance to the absorbent tin plate and radiation.
2. Using experimental data processing temperature distribution above and below the absorbent sheet according to the length of the collector and solar radiation was obtained.
3. Absorber black colored slices of beer cans can be used for air heating solar collectors. The experimental data show that the temperature difference in outlet of sun following collector reaches up to 9-11 degree with sun irradiance 1000 W/m^2 at different weather conditions.
4. Air solar collectors due to their physical and mechanical properties are suitable in Latvia for heating the air. At favorable weather conditions the heating degree of ambient air reaches more than 10 degrees at exit with the absorber length 1 m and air velocity $v=0.9 \text{ m/s}$.

References

- [1] S. Kalogirou Solar energy engineering: processes and systems, Academic Press Elsevier Inc. 2009.
- [2] A.Lauva, A. Aboltins, J. Palabinskis, N. Karpova-Sadigova Comparative studies of the solar material collector, Proceedings of the 5th International Scientific Conference “Engineering for Rural Development”, 2006, pp.90-94
- [3] A.Aboltins, J.Palabinskis, A.Lauva, J.Skujans, U.Iljins The material investigations of solar collector, Proceedings of the 6th International Scientific Conference “Engineering for Rural Development”, 2007, pp. 18-23
- [4] J. Palabinskis, A. Aboltins, A. Lauva, N. Karpova-Sadigova The comparative material investigations of solar collector, Agronomy Research, Vol. 6., Engineering of Agricultural Technologies”, 2008, pp.255-261
- [5] J. Palabinskis, A. Lauva, A. Āboltiņš, N. Karpova-Sadigova. Movable Air Solar Collector and its Efficiency, 7th International Scientific Conference „ Engineering for Rural Development”, 2008, pp 51 - 56

- [6] A. Aboltins, J. Palabinskis, A. Lauva, G. Rušķis The investigations of air solar collector efficiency, Proceedings of the 8th International Scientific Conference “Engineering for Rural Development “, 2009, pp.176-181
- [7] A. Aboltins, J. Palabinskis, A. Lauva, G. Rušķis The steel-thin plate absorbers investigations in air solar collector, Proceedings of the 8th International Scientific Conference “Engineering for Rural Development “, 2009, pp.182-187
- [8] A.Aboltins, J.Palabinskis, G. Rušķis Usage of different materials in air heated solar collectors, Proceedings of the 9th International Scientific Conference “Engineering for Rural Development “, 2010, pp.67-72
- [9] A. Aboltins, J. Palabinskis, G. Rušķis. The investigations of heating process in solar heating collector, Agronomy Research, Vol. 8 „Biosystems Engineering”, 2010, pp.5 - 11
- [10]REG Tehniskais apraksts un lietošanas pamācība (REG Technical description and using instruction), 2004, (in Latvian).
- [11]Веденяпин Г.В. Общая методика экспериментального исследования и обработки опытных данных (The general methology of experimental research and treatment of experimental data). Колос, М.,1967, (in Russian)

Characterization of black chrome films prepared by electroplating technique

S. Jafari, S. M. Rozati*

Physics Department, University of Guilan, Rasht 41335, Iran

* Corresponding author. Tel: +98 1313220912, Fax: +98 1313220066, E-mail: smrozati@guilan.ac.ir

Abstract: The surface and optical properties of black chrome films prepared by two different electrochemical baths were characterized. The black chrome films have been deposited on bright nickel substrates by electroplating technique. The surface morphology and phase structure of the films were investigated by using scanning electron microscopy (SEM) and X-ray diffraction (XRD), respectively. The chemical composition of prepared films was determined by energy-dispersive x-ray analysis (EDS). The spectral reflectance was also measured in the UV-Vis-NIR and IR regions. From the SEM analysis, it was found that prepared films by the first chemical bath is denser with nano size grains and by the second chemical bath they become porous, with micro sized grains. The XRD results show that in both cases chrome is the main chemical component in the films. The films prepared by second chemical bath have better optical properties than the films prepared by first chemical bath.

Keywords: Black chrome, Electroplating, Solar collector.

1. Introduction

The growing energy demand through out the world has attached great important to the study of renewable source [1]. The cost and effective utilization of solar energy and conversion of that into thermal energy requires an efficient solar coating as having high solar absorptance (>0.9) in the visible region and very low thermal emittance (<0.1) in the infrared to minimize the radiation heat loss [2, 3]. This property is named selectivity [4]. The higher the selectivity value, the better the thermodynamical efficiency of the solar energy collectors [1]. Other necessary properties of a practical solar selective coating are ease and availability of application, low cost and long-term durability under solar radiation [5]. Black chrome is one of the most commonly used solar selective coatings in solar collector systems for the efficient conversion of solar energy into thermal energy. A variety of deposition techniques such as chemical oxidation, CVD, spray, sputtering and electroplating are available for preparation of solar selective surfaces. Of the above techniques, electroplating is attractive due to its simplicity, low cost and large area involved [2]. Electroplating of metallic films is one the appropriate techniques for obtaining absorber coatings with selective optical properties for solar collectors. Electroplated black chrome is one of the most widely used solar absorber, mainly due to its high absorptance, good stability in a wide rang of oxidizing/reducing environments and high thermal resistance [3]. Coatings used as solar selective surface in solar collectors have low thicknesses, therefore these coatings cannot protect the substrate against atmospheric corrosion and thermal oxidation. For solving this problem bright nickel coating before black chrome deposition is recommended [6]. Nickel under coat before black chrome deposition decreases thermal emissivity and increases thermal resistance of black chrome coatings [3].

2. Experimental method

Electroplating is an electrodeposition process for producing a dense, uniform, and adherent coating, usually of a metal or an alloy, upon a conductive surface by the act of electric current. The core part of the electroplating process is the electrolytic cell (electroplating unit). In the electrolytic cell a current is passed through a bath containing electrolyte, the anode, and

the cathode. The workpiece to be plated is the cathode (negative terminal). The anode, however, can be one of the two types: sacrificial anode (dissolvable anode) and permanent anode (inert anode). The sacrificial anodes are made of the metal that is to be deposited. The permanent anodes can only complete the electrical circuit, but cannot provide a source of fresh metal to replace what has been removed from the solution by deposition at the cathode. Electrolyte is the electrical conductor in which current is carried by ions rather than by free electrons (as in a metal). Electrolyte completes an electric circuit between two electrodes. Upon application of electric current, the positive ions in the electrolyte will move toward the cathode and negatively charged ions toward the anode. This migration of ions through the electrolyte constitutes the electric current in that part of the circuit. The migration of electrons into the anode through the wiring and an electric generator and then back to the cathode constitutes the current in the external circuit. The metallic ions of the salt in the electrolyte carry a positive charge and are thus attracted to the cathode. When they reach the negatively charged workpiece, it provides electrons to reduce those positively charged ions to metallic form, and then the metal atoms will be deposited onto the surface of negatively charged workpiece [7].

Black chrome electroplates are obtained by replacing the sulphate ion in conventional chrome plating baths by fluoride, silicofluoride, acetate, borate, nitrate or sulphamate ions. Care should be taken to ensure complete removal of the sulphate ions; these are deleterious to the bath. The substances introduced in to the bath as catalysts can be divided into three groups, acetate baths, fluoride-catalysed baths and nitrates and other catalysts. In the fluoride or mixed catalyst plating baths a higher plating efficiency, a harder, more corrosion and wear-resistance deposit is obtained. The fluoride is commonly added as the SiF_6^{2-} ion in amount of 2-3g/l. this chemistry provides better substrate activation for plating on bright nickel [8].

The deposition of black chrome was carried out on bright nickel plated brass substrates in an electrochemical bath by electroplating technique. The brass substrates of 0.1 mm thickness were cut in strips of 5.5 cm × 6.5 cm for electroplating of bright nickel. The brass substrates were pretreated by different cleaning procedure. Mechanical polishing was done with a grinding paper No.2000, followed by rinsing in distilled water. Then substrates were cleaned in a hot commercial alkaline cleaner, followed by rinsing in distilled water and activated in an aqueous 10 vol% H_2SO_4 solution, followed by rinsing in distilled water. Then bright nickel deposited on prepared brass substrates by electroplating technique. The chemical bath for bright nickel deposition consists of nickel sulphate (NiSO_4), nickel chloride (NiCl_2) and boric acid (H_3BO_3). The bright nickel deposition carried out in $0.5\text{A}/\text{dm}^2$ current density for 5 min in 50 °C-60 °C temperatures. Nickel metal with 99.9% purity used as anode for bright nickel deposition and brass substrate was used as cathode. Prior to the deposition of black chrome, the prepared bright nickel substrates were cleaned in a hot commercial alkaline cleaner, followed by rinsing in distilled water and activated in an aqueous 10 vol% H_2SO_4 solution. Following activation the plates were thoroughly rinsed in distilled water to remove all trace sulphate. Then black chrome was deposited on bright nickel substrates. The deposition conditions to get black chrome were optimized by varying the chemical bath composition, current density and plating time. In this paper, two chemical baths were used for electroplating to comparison of surface and optical properties of these surfaces and selecting the better films.

The first bath for black chrome deposition consists of chromic acid, acetic acid and barium acetate (acetate bath). Electrodeposition carried out in $3\text{A}/\text{dm}^2$ current density for 180 seconds in 50 °C temperature. The second bath for black chrome deposition consists of chromic acid,

fluorosilicic acid and barium carbonate (fluoride-catalysed bath). Deposition carried out in 6A/dm² current density for 120 seconds in 25 °C temperature. Several experiments were done to prove the reproducibility of the samples.

Details of the optimized plating processes used in this study are given in table 1.

Table 1. Experimental electrodeposition parameters.

Bath	Composition	Temperature (°C)	Current density (A/dm ²)	Plating time (s)
First	Chromic acid (CrO ₃) Acetic acid (CH ₃ COOH) Barium acetate (Ba(CH ₃ COO) ₂)	50	3	180
Second	Chromic acid (CrO ₃) Fluorosilicic acid (H ₂ SiF ₆) Barium carbonate (BaCO ₃)	25	6	120

Barium compounds such as the carbonate, acetate or hydroxide are usually added to black chrome plating solutions. Their role is to precipitate any sulphate ions from solution, and apart from possible complexation of the carbonate ion with Cr (III), they are not expected to significantly affect black chrome electrochemistry [9].

For the black chrome deposition Pb-Sb alloy, which contains only 2-5% Sb, was used as the anode (the permanent anode) and bright nickel substrate used as cathode. After deposition the samples were cleaned in distilled water and air dried at room temperature. Surface morphology of the coatings was characterized with scanning electron microscopy (SEM), manufactured by Philips, XL30 model. The X-ray diffraction (XRD) analysis was done using a PW1840 diffractometer. The normal spectral reflectance of the electrodeposited black chrome coating in UV-Vis-NIR and IR regions was recorded using a Cary 500 Scan UV-Vis-NIR spectrophotometer and FTIR Jasco, respectively.

3. Results and discussion

3.1. SEM analysis

Fig. 1 gives the scanning electron microscopy (SEM) of magnification 15000× for black chrome films prepared from two different baths. Figure 1 shows that the surface morphology of films deposited from different bath composition are different. From the SEM analysis it was found that the black chrome films achieved from the first bath is denser with nano size grains but films deposited from the second bath they become porous, with micro sized grains.

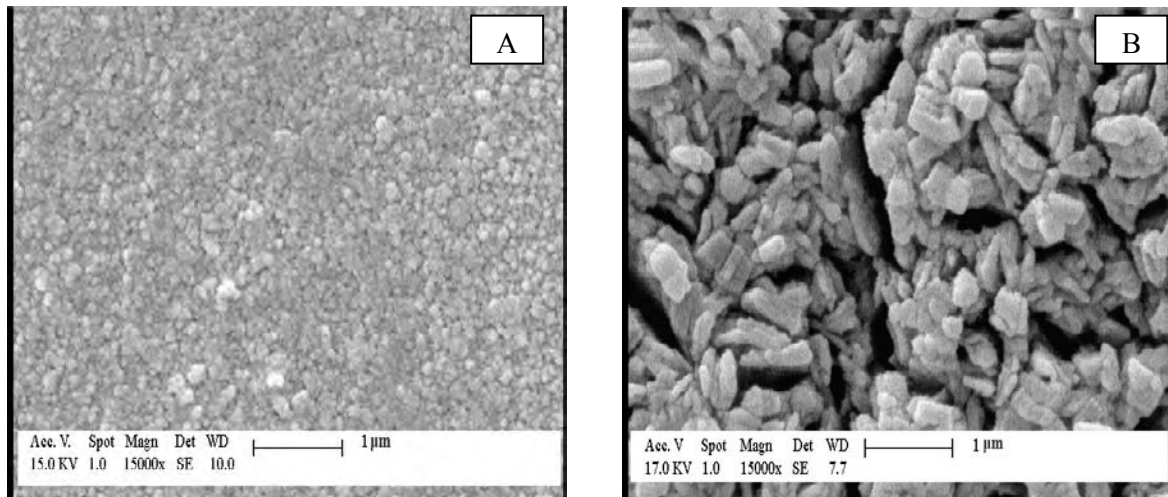


Fig. 1. The SEM images of black chrome films deposited on bright nickel substrates from two different baths. A: first bath, B: second bath.

3.2. EDS analysis

Fig. 2 and Table 2 show the chemical composition of black chrome deposited from two different baths. The data indicate that films prepared from both baths have contained chrome in their composition. Wight percentage of chrome in films prepared from the second bath is more than of the films prepared from the first bath.

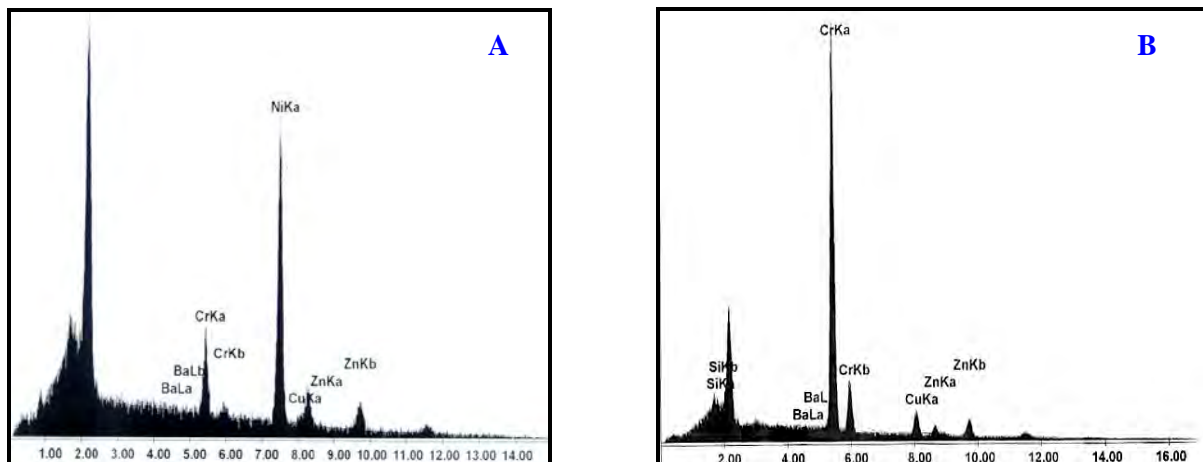


Fig. 2. The EDS spectrum for black chrome films deposited d on bright nickel substrate from two different baths. A: First bath, B: Second bath.

Table 2. The EDS analysis of black chrome deposited from two different baths.

Elements	Wt.% first bathe	Wt.% second bath
Cr	8.38	62.62
Ni	84.23	12.50
Cu	4.58	12.80
Zn	1.65	8.53
Si	-	1.92
Ba	1.16	1.63

3.3. XRD analysis

In order to identify the predominant chrome phase in the deposited films, it is necessary to investigate the coatings using X-ray diffractometer. Fig. 3 shows the XRD patterns for the bright nickel substrate coated with black chrome films. It is possible to detect that the bulk structure of the black chrome films were mainly consist of metallic chrome with the crystallographic plane (110) perpendicular to the substrate [6, 7]. As can be seen from Fig. 3, the different compositions of chrome are obtained in these two films prepared from two different baths.

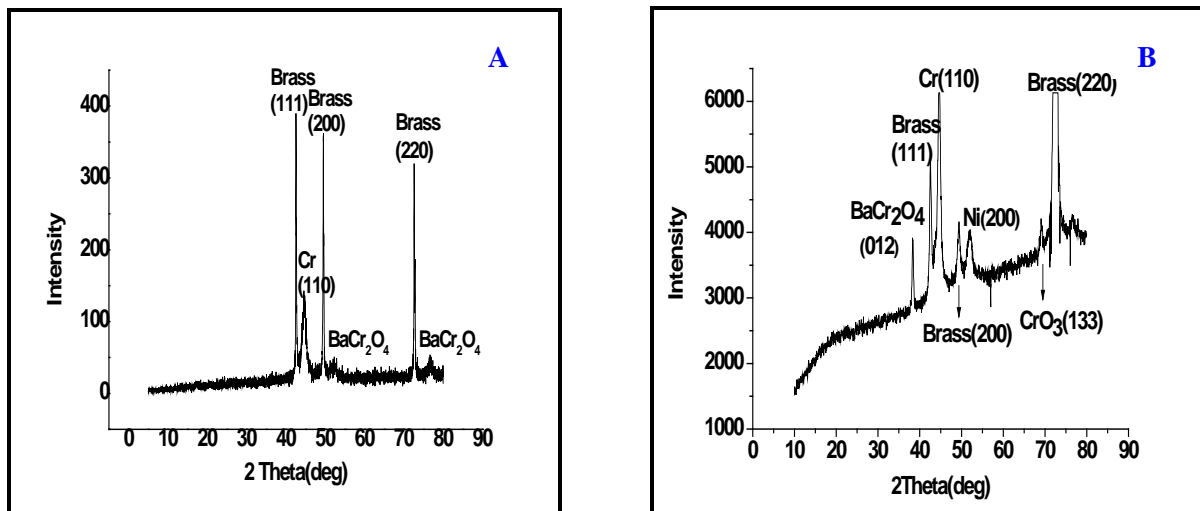


Fig. 3. The XRD patterns for black chrome films deposited on bright nickel substrate from two different baths. A: First bath, B: Second bath.

3.4. Spectral reflectance

The influence of two different electrochemical baths on the selective absorber properties of black chrome films are given in Figs. 4 and 5. Figs. 4 and 5 shows the spectral reflectance in the UV-Vis-NIR and IR regions for black chrome deposited on bright nickel substrates prepared from two different baths respectively. From figure 4 it is evident that the spectral reflectance in UV-Vis-NIR region is below 12% for black chrome films deposited on bright nickel prepared from both baths, indicating that in this spectral region the solar absorptance is quite high [2]. Spectral reflectance for black chrome films prepared from the second bath is less than of films prepared from the first bath, hence, its absorption is higher. This difference is probably due to the rougher surface and chemical composition of these samples which enhances the absorption of the radiation and can explain the high absorptance level of this material. Hence, using of second bath is recommended to get good solar selective black chrome coating in the UV-Vis-NIR region. Fig. 5 indicates that the spectral reflectance of black chrome films in the IR (2.5 μ m-20 μ m) region, and hence the emissivity of them. From Fig. 5 it is evident that films prepared from the second bath have lower thermal emittance. It can be seen in the figure 5 that by using of the first bath spectral reflectance is reduced and hence increases the thermal emittance of films will increase.

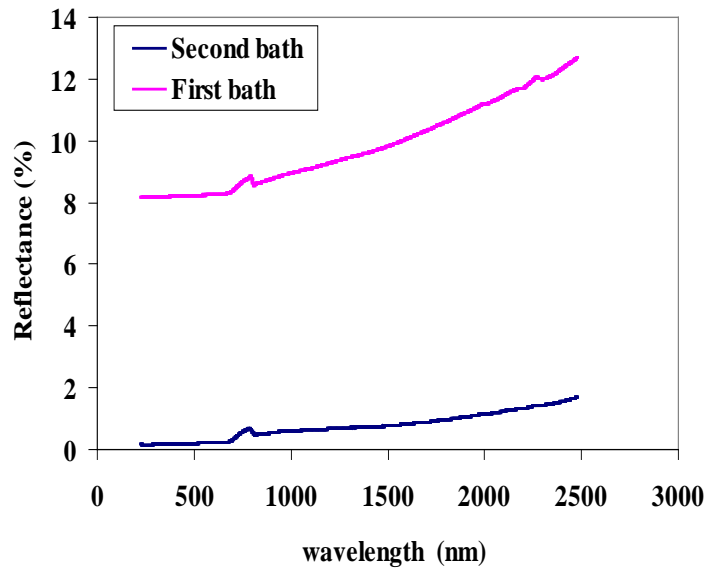


Fig. 4. The Spectral reflectance in the UV-Vis-NIR region for black chrome films deposited on bright nickel substrates from two different baths.

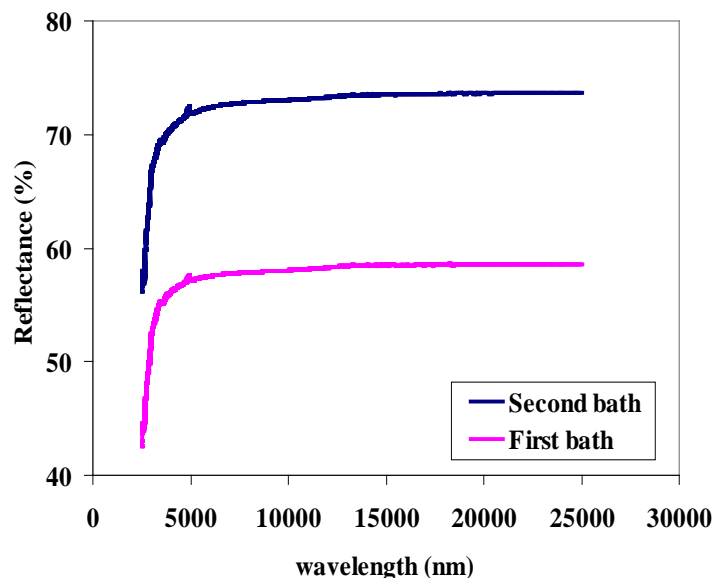


Fig. 5. The Spectral reflectance in the IR region for black chrome films deposited on bright nickel substrates from two different baths.

4. Conclusion

The black chrome films were prepared by electroplating technique from two different baths on bright nickel substrates. SEM analysis shows that films prepared from first bath is denser with nano size grains while films prepared from the second bath become porous, with micro sized grains. The EDS analysis results indicate the presence of chrome on films prepared from both baths. The chrome amount in the films prepared from second bath is higher than one. XRD analysis shows that structure of black chrome films from both baths were mainly consist of metallic chrome with (110) orientation. Black chrome films have good optical properties for solar energy absorption. The spectral reflectance in the UV-Vis-NIR and IR regions shows that films prepared from the second bath have higher absorption and lower emittance, Hence these films are better for using in solar collectors.

References

- [1] M. Aguilar, E. Barrera, M. Palomar-Pardave, L. Huerta, S. Muhl, Characterization of black and white chromium electrodeposition films: surface and optical properties, *Journal of Non-Crystalline Solids* 329, 2003, pp. 31-38.
- [2] J. Quintana, P. J. Sebastian, The influence of various substrate treatments on morphology and selective absorber characteristics of electrochemical black chrome, *Solar Energy Materials and Solar Cells* 33, 1994, pp. 465-474.
- [3] Z. Abdel Hamid, Electrodeposition of black chromium from environmentally electrolyte based on trivalent chromium salt, *Surface & Coating Technology* 203, 2009, pp. 3442-3449.
- [4] M. R. Bayati, M. H. Shariat, K. Janghorban, Design and chemical composition and optimum working conditions for trivalent black chromium electroplating bath used for solar thermal collectors, *Renewable Energy* 30, 2005, pp. 2163-2178.
- [5] G. E. McDonald, Spectral reflectance properties of black chrome for use as a solar selective coating, *Solar Energy* 17, 1975, pp. 119-122.
- [6] M. Daryabegy, A. R. Mahmoodpoor, Method of manufacturing absorbing layers on copper for solar applications (I), *Renewable Energy Organization of Iran* 2, 2006, pp. 35-39.
- [7] H. Lou, Y. Huang, Electroplating, *Encyclopedia of Chemical Processing*, DOI: 10.1081, pp. 1-10.
- [8] N. Vasudevan, V. K. William Grips and Indira Rajagopalan, The present status of black chromium plating, *Surface Technology* 14, 1981, pp. 119-132.
- [9] P. M. Driver, An electrochemical approach to the characterization of black chrome selective surfaces, *Solar Energy Materials* 14, 1981, pp. 179-202.

Selective solar absorber coating research at the CSIR (South Africa)

K.T. Roro^{1*}, N.Tile^{1,2}, B. Yalisi^{1,2}, M. De Gama¹, T. Wittes¹, T. Roberts¹, A. Forbes^{1,2}

¹CSIR-National Laser Centre, P.O. Box 395, Pretoria 0001, South Africa

²School of Physics, University of KwaZulu Natal, Private Bag X54001, Durban 5000, South Africa

* Corresponding author. Tel: +27128413794, Fax: +27128413152, E-mail: KRoro@csir.co.za

Abstract: A sol-gel technique has been established at a laboratory scale for low cost production of high efficient selective solar absorbers comprising a composite material of nano-structured carbon in a nickel oxide matrix. In order for these materials to be applied in real world scenarios it is necessary to extensively scale up the fabrication process to allow large area coatings. This can be done by adapting this sol-gel technique to large area deposition.

In this project, we are undertaking research and development activities for three-years to make a ‘Lab to Large scale’ transition in order to eventually integrate into existing solar collectors for low cost domestic water heating in a rural area for social good.

A spray coating technique has been used to deposit these C/NiO coatings on aluminum substrates. Preliminary optical results have shown absorptance of up to 90 %. The preparation and characterization as well as the process towards developing a large-area solar selective coating for low cost domestic heating will be discussed.

Keywords: Sol-gel, Carbon-nickel oxide, Selective solar absorbers, Large-area.

Nomenclature

α_{sol} normal solar absorptance

I_{sol} direct normal solar irradiance

ϵ_{ther} normal thermal emittance

I_P Plank black body distribution

R reflectance

1. Introduction

Hot water is required to maintain adequate sanitation and health. Often, water has to be boiled in order to make it safe for drinking. In rural Africa, the traditional fuel used for heating water is firewood, which produces smoke and is generally unsafe. Access to energy from fossil fuels such as oil, gas, and coal, by expanding grid electricity is either impractical or too expensive in these countries. There is therefore a clear need for low-cost and environmental friendly means of water heating.

Solar energy is a promising alternative energy source that can address these challenges. It is a resource readily available in every country around the world, and is not a threat to the environment through pollution or to the climate through greenhouse gas emission. As a matter of fact, most African countries have around 325 days of strong sunlight a year, on average, more than 6 kWh energy per square meter a day [1]. Solar thermal energy is a technology for harnessing solar energy for thermal energy (heat). Solar thermal collectors for water heating use a spectrally selective surface that absorb sunlight and convert it to heat. High performing selective surfaces already exist in the market, but most of these products are produced using complicated manufacturing process and are expensive. The spectral selective surfaces are the most costly component of a solar thermal collector [2]. This means that if one reduces the price of selective solar absorbers one can hopefully reduce the cost of a solar thermal collector.

A sol-gel technique has been established at a laboratory scale for low cost production of high efficient selective solar absorbers comprising a composite material of nano-structured carbon in a nickel oxide matrix [3,4]. These coatings were deposited using a spin coater. Some of the

advantages of this novel technique to fabricate carbon-metal oxide composite coatings are that it is simple and easy to control, utilizes readily available chemicals, does not require sophisticated equipments, the coatings can be deposited at ambient pressure conditions, and the process is low in material consumption. Therefore, the method is very promising for developing countries and could hopefully reduce the production costs for spectrally selective absorbers [5]. In order for these materials to be applied in real world scenarios it is necessary to extensively scale up the fabrication process to allow large area coatings. However, the spin coating process cannot be used for large area coatings. To succeed as a useful manufacturing technique, the specific deposition approach must be highly scalable while still producing films with the quality of laboratory deposition methods, e.g., spin coating. Spray deposition is historically scalable to large areas, and may also be applicable to deposit these C/NiO composite coatings. Thus, large area coating can be done by adapting this sol-gel technique to large area deposition.

In this study, we will demonstrate the preparation of sol-gel C/NiO nanocomposite coatings with reasonable optical properties on aluminum substrates by spray-coating technique and show the dependence of variation of the optical properties on different deposition process parameter.

2. Experimental

The absorbing films were coated on rough highly reflecting aluminum substrates. The substrates were cut into a $55 \times 55 \text{ mm}^2$ size and cleaned before deposition. The pre-cleaning process involved cleaning the substrates with aqueous detergent and distilled water in order to remove the grease. Due to poor adhesion to the aluminum surfaces (uncleaned or cleaned with soap and water), the substrates were etched. The pre-cleaned substrates were thoroughly rinsed and dipped in a phosphoric acid bath at $60 \text{ }^\circ\text{C}$ for about 30 minutes or in an HCl bath kept at room temperature to remove the protective oxide layer. They were then thoroughly rinsed using distilled water to remove the acid. Finally they were blown dry with a N_2 and coated immediately.

The preparation of the solution was adopted from a previous experiment [4]. The NiO precursor solution was prepared by dissolving an appropriate quantities of nickel acetate $[(\text{NiAc}_2), \text{Ni}(\text{CH}_3\text{COO})_2 \cdot 4\text{H}_2\text{O}]$ in 50 ml of absolute ethanol $[(\text{EtOH}), \text{CH}_3\text{CH}_2\text{OH}]$ followed by magnetic stirring at room temperature. An amount of diethanolamine $[(\text{DEA}), \text{NH}(\text{CH}_2\text{CH}_2\text{OH})_2]$ was added as a chelating agent. For the carbon precursor, sucrose was dissolved in doubly distilled water in the mass ratio 1:1 prior to mixing with the matrix precursor solutions. After a period of stirring appropriate quantity of polyethylene glycol $[(\text{PEG}), \text{HO}(\text{CH}_2\text{CH}_2\text{O})_n\text{H}]$, a structure directing template, was added to the NiO matrix precursor sol. The oxide and carbon precursor solutions were mixed and stirred again. The resultant solution was then further stirred until the formation of a sol. The final solution was poured into the spray gun and a conventional air compressor is used to eject the solution on top of the pre-cleaned aluminum substrates. The schematic representation of the spray deposition used during this study is shown in Fig. 1. A relatively low pressure (30-90 kpa) was used during deposition in order to ensure a fine atomization while preventing blowing off the droplets already deposited on the substrate. The distance of the spray gun from the substrate was kept at 50 cm. In order to vary the thickness of the coatings, number of passes of the spray gun across the substrate was varied.

Once the substrates were spray coated, the samples were put into a tube furnace for pyrolysis and crystallization. The furnace temperature was raised to $450 \text{ }^\circ\text{C}$ at a rate of

20 °C min⁻¹, maintained at that temperature for 60 minutes, and then left to cool to room temperature naturally. Nitrogen gas was continuously flown through the furnace throughout the heat treatment in order to maintain an inert atmosphere.

The near-normal spectral reflectance of the samples was measured in the 0.3-2.5 μm wavelength range with a Perkin Elmer Lambda 900 spectrophotometer. A spectralon sample was used for reference spectrum measurements. A Bruker Tensor 27 spectrophotometer with a gold mirror reference was used to measure near normal reflectance in the 2.5–20.0 μm wavelength range. The reflectance measurements were used to calculate solar absorptance, α , and the thermal emittance, ε , of the samples at 100 °C using Eqs (1) and (2), respectively [6]:

$$\alpha_{sol} = \frac{\int_{0.3}^{2.5} I_{sol}(\lambda)(1 - R(\lambda))d\lambda}{\int_{0.3}^{2.5} I_{sol}(\lambda)d\lambda} \quad (1)$$

$$\varepsilon_{ther} = \frac{\int_{2.5}^{20} I_p(\lambda)(1 - R(\lambda))d\lambda}{\int_{2.5}^{20} I_p(\lambda)d\lambda} \quad (2)$$

The thermo-gravimetric analysis (TGA) was done on Perkin-Elmer TGA 4000 thermo-gravimetric analyzer. Approximately 100 mg final mixture of C/NiO precursor solution was placed in open 190 μl alumina pan and heated from 25 °C to 980 °C at a heating rate of 5 °C min⁻¹ in N₂ atmosphere (flow rate 50 ml min⁻¹). The differential scanning calorimeter (DSC) results were collected on Mettler Toledo DSC 1 instrument. The surface morphology of the coatings was investigated using a ZEISS ULTRA plus FEG-SEM scanning electron microscopy. The Energy Dispersive Spectroscopy (EDS) analysis was done using a JEOL-JSM 7500F Scanning Electron Microscope. Raman spectra were collected using a Raman spectroscopy (Jobin-Yvon T64000 spectroscopy), equipped with an Olympus BX-40 microscope attachment. An Ar⁺ laser (514.5 nm) with energy setting 1.2 mW from a Coherent Innova Model 308 was used as an excitation source.

3. Results

In order to determine the optimal temperature of heat treatment, the C/NiO precursor solution was thermally analyzed by TGA and DSC techniques. Figure 2 displays a typical TGA and DSC curves for the C/NiO precursor solution. It can be seen from the figure that the DSC curve shows 1 endothermic peak at 83 °C and 4 exothermic peak at 210 °C, 262 °C, 342 °C and 436 °C. TGA curve exhibit four weight loss stages: 53 % the initial weight loss occurred

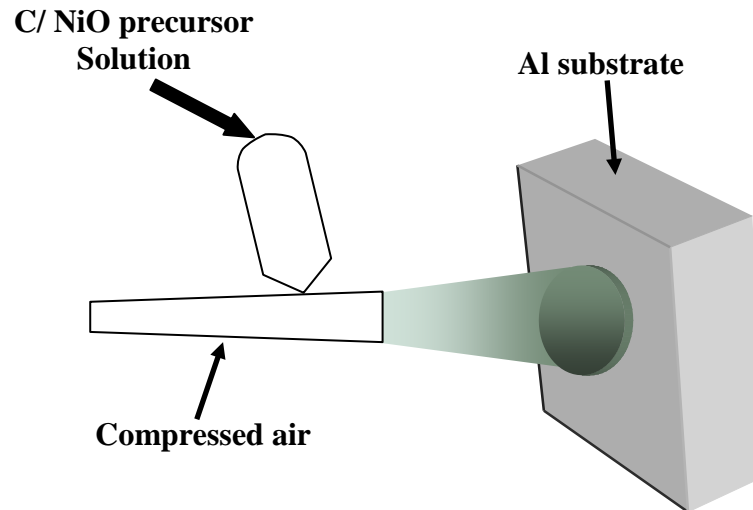


Fig. 1. A schematic diagram of the spray deposition technique used to deposit C/NiO nanocomposite coatings on Al surface.

31 and 57 °C, 10 % between 75 and 144 °C, 15 % between 144 and 295 and the final weight loss (13 %) between 295 and 341. The first weight loss was likely due to the evaporation of ethanol whereas the second and third was probably due to desorption of moisture and desorption of organic molecules, respectively. The fourth weight loss was most likely due to carbonization. Above 450 °C no noticeable weight loss has occurred. This stabilization of weight loss is accompanied by a distinct DSC exothermic peak at 437 °C which indicates the crystallization of the composite material. It is therefore decided to anneal the samples at temperatures between 450 °C to 550 °C. This choice has also been accompanied by the improvement of the optical absorption for samples heat treated in this temperature range (not shown).

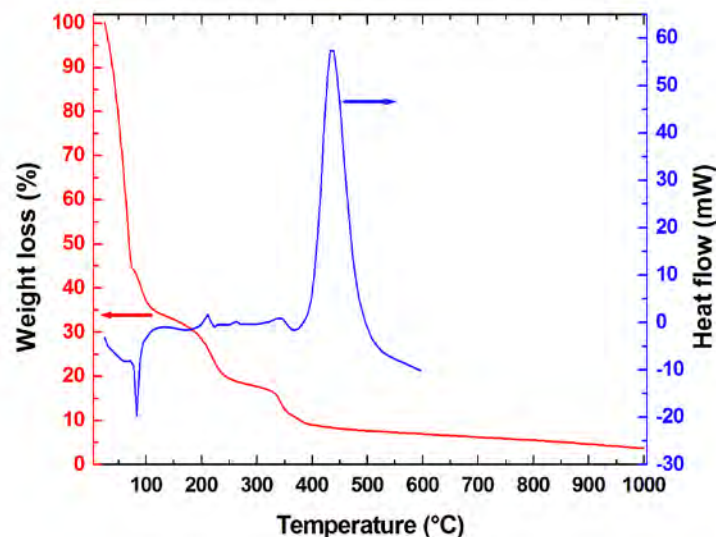


Fig. 2. Typical TGA and DSC spectra for C/NiO precursor solution.

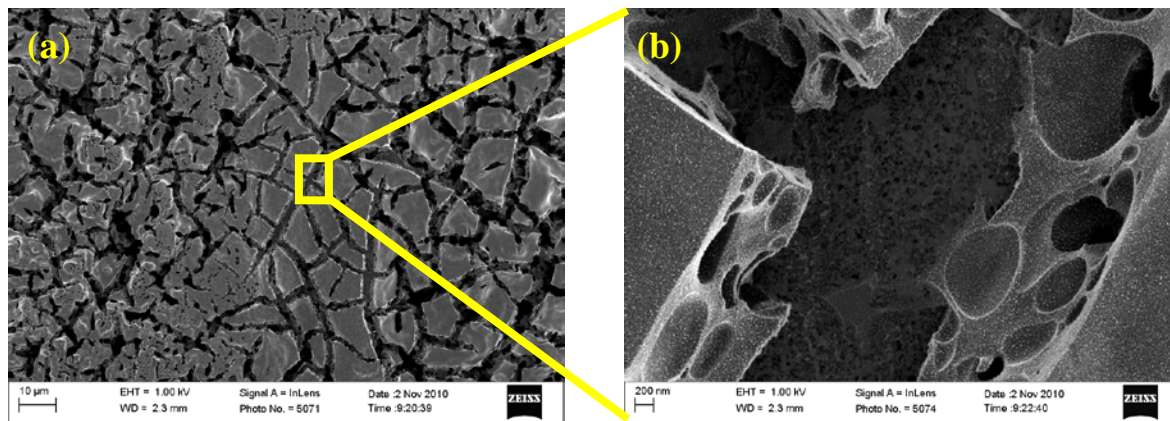


Fig. 3. (a) FE-SEM images of C/NiO nanocomposite coated on aluminum substrate, (b) enlarged image.

Figure 3 (a) depicts a typical SEM image of a C/NiO composite coating. The higher magnification image is shown in Fig. 3(b). As can be seen from Fig. 3 (a), the surface of the coating is uniform and cracked. The enlarged image (Fig 3(b)) shows that the coatings are porous. It is believed that the porosity of this film can produce high absorptance by multiple reflections [7]. The size distribution of the spherical particles in the coating is between 10 and 20 nm.

The composition of C/NiO composites was investigated using EDS (Fig. 4(a)). It reveals the presence of C, O, and Ni, which confirms the existence of NiO nanoparticles in the coating. The Al signal originates from the substrate used for coating. The presence of carbon in these films is further evidenced by Raman studies conducted on these coatings. Figure 4(b) shows a typical Raman spectrum of the C/NiO nanocomposite. The D band at $\sim 1350 \text{ cm}^{-1}$ originates from amorphous carbon and structural defects; the G band at $\sim 1580 \text{ cm}^{-1}$ is attributed to graphite structures, stems from tangential shearing mode of the carbon atoms [8-10]. The G' band at $\sim 2700 \text{ cm}^{-1}$ is an overtone of the D band which indicates the long range graphite ordering. Higher order Raman modes are also visible in the region $2920\text{-}3220 \text{ cm}^{-1}$.

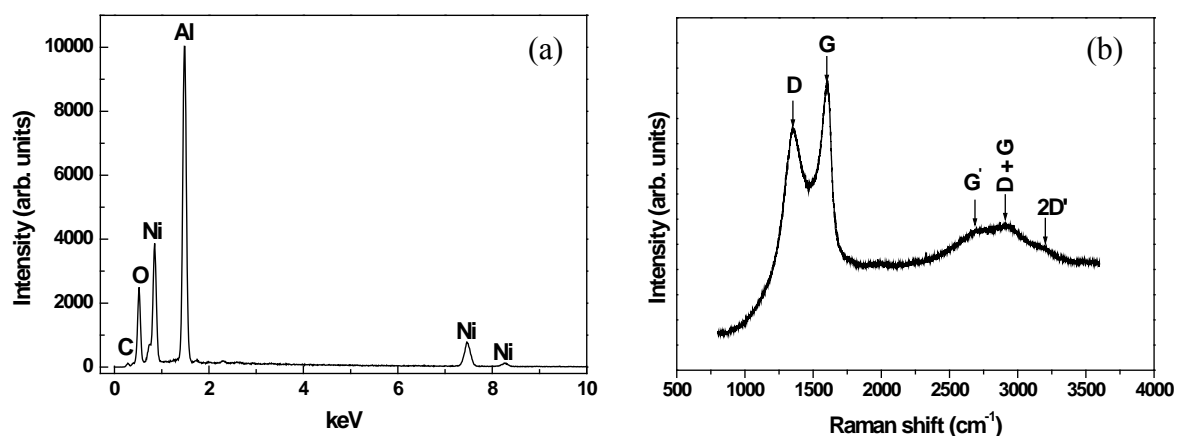


Fig. 4. (a) A typical EDS spectrum for C/NiO nanocomposite coated on aluminum substrate, (b) Raman spectra of the C/NiO nanocomposite coating.

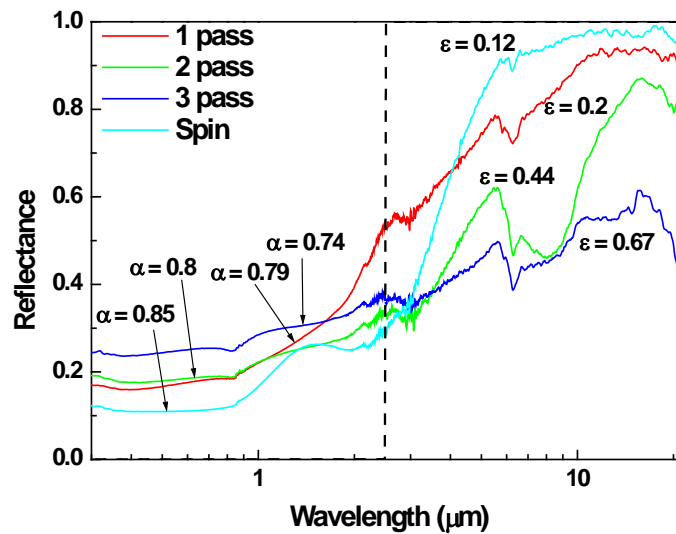


Fig. 5. The near normal reflectance spectra of C/NiO nanocomposite deposited with different passes on aluminum substrate etched with H_3PO_4 . The spectrum for spin coated samples is also included for comparison. The broken line represents the reflectance spectrum for an ideal selective solar absorber.

Figure 5 shows the reflectance spectra of spray deposited samples with different passes, together with a spin coated sample as a reference. The dips in the spectra at about $6.3 \mu\text{m}$ are due to water absorption (O–H bending vibrations at $1,600 \text{ cm}^{-1}$) [11,12]. The O–H bending vibrations for the spray deposited samples are much stronger than the spin coated samples. This implies that spray coated samples have higher emittance (lower reflectance) values.

The reflectance spectra of the C/NiO nanocomposite deposited on a luminum substrate cleaned with HCl are presented in Fig. 6. It can be seen from the figure that the O–H mode vibrations are also present in this C–NiO samples. Although the solar absorptance values for some of the samples cleaned using HCl are better than the spin coated sample, they are highly emitting.

4. Discussion

The main reason for film cracking is due to film shrinkage because of solvent out gassing during the heat treatment [13]. Although it is minor, the thermal expansion rate difference between the coatings and the aluminum substrate can also contribute to the cracking during the cooling process [13]. According to Borström *et al.* [14], film homogeneity and propensity of film cracking is very important for solar absorbing thin films. The durability of the coatings will be severely affected due to infiltration of water and subsequent degradation of aluminum substrates. This clearly suggests that further study is necessary in order to reduce these cracks.

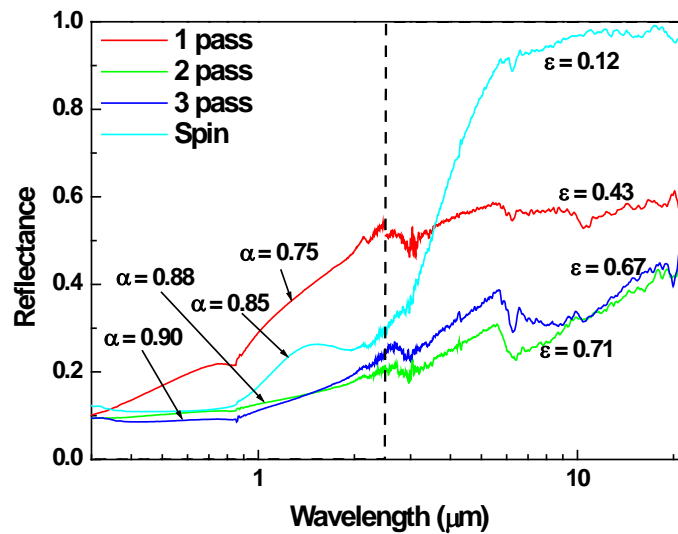


Fig. 6. The near normal reflectance spectra of C/NiO nanocomposite deposited with different passes on aluminum substrate etched with HCl. The spectrum for spin coated samples is also included for comparison. The broken line represents the reflectance spectrum for an ideal selective solar absorber.

In an effort to increase the absorptance of this single layer we have pretreated the substrate surface by etching with H_3PO_4 and HCl. It is well known that the solar absorptance of selective absorber coatings can be enhanced by producing a textured surface [13]. The surface texturing of the aluminum surface with HCl enhanced the absorptance of the coating considerably (Fig. 6). However, the emittance of these coatings becomes worse. The magnitude of the surface roughness accompanying the pretreatment has to be much smaller than the peak thermal radiation wave length and comparable to the solar wavelength [14].

The production cost for a 1 μm thick coating material for a lab scale is estimated to be R 0.35/ m^2 (\$ 0.05 / m^2). This price can change significantly if the precursor materials are purchased in bulk. All other additional production costs and heat treatment were not estimated. The price for aluminium substrate is R61.76/ m^2 (\$ 8.6/ m^2). This implies that the material cost for the coating is very small compared to the substrate price. The material cost for a 100 nm thick coating for Ni-Alumina coatings were estimated to be 0.14 $\text{€}/\text{m}^2$ (R 1.4 / m^2) [2]. It should be noted that the additional costs and heat treatment as well as transfer efficiency of the paint during spraying might slightly increase the cost.

Further research will focus on the optimization of the spray process parameters and the study of the durability of these coatings.

5. Conclusion

Spray deposition method was adapted for large-area deposition of sol-gel prepared C/NiO nanocomposite coatings on aluminum substrate for selective solar absorber application. The coatings were made possible by using conventional air compressor. The number of passes was varied in order to optimize the thickness of the coatings. The performance of the sprayed samples was compared with the spin coated. The preliminary results have shown that the sprayed samples have comparable solar absorption properties with the spin coated suggesting that the sol-gel synthesized and sprayed C/NiO composite films is very encouraging.

The properties of these coatings will, however, require further developments before it could be integrated into an existing solar collector for low cost domestic water heating in a rural area for social good.

References

- [1] G. Legros, I. Havet, N. Bruce, S. Bonjour, The energy access situation in developing countries, UNDP-WHO, 2009.
- [2] T. Boström, E. Wäckelgård, G. Westin, *Solar Energy* 74, 2003, 497-503.
- [3] G. Katumba, G. Makiwa, T. R. Baisitse, L. Olumekor, A. Forbes, and E. Wäckelgård, *phys. stat. sol. (c)* 5, No. 2, 2008, 549–551.
- [4] G. Katumba, L. Olumekor, A. Forbes, G. Makiwa, B. Mwakikunga, J. Lu, E. Wäckelgård, *Sol. Energy Mater. Sol. Cell.* 92, 2008, 1285– 1292.
- [5] T. Boström, G. Westin, E. Wäckelgård, *Sol. Energy Mater. Sol. Cell.* 91, 2007, 38-43.
- [6] J. A. Duffie and W. A. Beckman, *Solar Engineering of Thermal Processes*, JohnWiley & Sons, New York, NY, USA, 1980.
- [7] C. E. Kennedy, “Technical Report: Review of Mid-to-High-temperature Solar Selective Absorber Materials,” National Renewable Energy Laboratory, prepared under Task No. CP02.2000, NREL/TP-520-31267, 2002.
- [8] O. Lourie, H.D. Wagner, *J. Mater. Res.* 13, 2000, 2418.
- [9] A.M. Rao, A. Jorio, M.A. Pimenta, M.S.S. Dantas, R. Saito, G. Dresselhaus, and M.S. Dresselhaus, *Phys. Rev. Lett.* 84, 2000, 1820.
- [10] A. Jorio, G. Dresselhaus, M.S. Dresselhaus, M. Souza, M.S.S. Danatas, M.A. Pimenta, A.M. Rao, R. Saito, C. Liu, H.M. Cheng, *Phys. Rev. Lett.* 85, 2000, 2617.
- [11] G. Katumba, J. Lu, L. Olumekor, G. Westin, E. Wäckelgård, *J. Sol–Gel Sci. Technol.* 36, 2005, 33-43.
- [12] A.V. Rao, R.R. Kalesh, G.M. Pajonk, *J. Mater. Sci.* 38, 2003, 4407.
- [13] T. Boström, S. Valizadeh, J. Lu, J. Jensen, G. Westin, E. Wäckelgård, *J. Non-Cryst. Solids*, 2010, doi:10.106/j.jnoncrysol.2010.09.023
- [14] S. Sakka (Ed.), *Handbook of Sol-gel Science and Technology*, kluwer Academic Publishers, New York, 2005
- [15] W.F. Bogaerts and C.M. Lampert, *J. Mater. Sci.* 18, 1983, 2847.
- [16] F. Jahan, B.E. Smith, *J. Mater. Sci.* 5, 1986, 905-906.

Steel-Tinplate as a solar wall panel and its effectiveness

G. Ruskis*, A. Aboltins, J. Palabinskis

Institute of Agricultural Machinery, Latvia University of Agriculture, Cakstes blvd. 5, Jelgava, LV-3001, Latvia

* Corresponding author. Tel: +371 29490286, Fax: +371 63020762, E-mail: guntisruskis@inbox.lv

Abstract: The aims of the research, was to investigate black colored steel-tinplate use for absorber and covered material of collector and compare the efficiency of three types of air heating collectors. This heated air we can exploited for drying of agricultural produce, room ventilation and room heating and etc.

0.1*0.5*1.0 meters long flat-plate collector (FPC) for experimental research was built. Air velocity at the experiments was $v=0.9$ m/s. We used the sun following collectors. The experimental data were measured and recorded in the electronic equipment (REG). The experiments were carried out in September 2010 at the same weather conditions.

Collectors of insulated and un-insulated surfaces with steel-tinplate absorber as covering material warmed ambient air up to 10-12 and 5-6 degrees corresponding (at irradiance 800 W/m^2). This difference indicates the great importance of insulating the collector body. It can explain with intensify heat exchange between absorber and ambient air which reduce efficiency of collector. There was good correlation with irradiance and air heating degree.

Our investigations showed that more effective FPC was collector with absorber tinplate at middle of collector body. At favorable weather conditions the heating degree of ambient air at the outlet reaches 6-8 degrees more that at the outlet of insulated collector covered by steel-tinplate.

Keywords: Solar Energy, Air Heating, Collector, Solar Wall, Absorber.

1. Introduction

Under Kyoto targets, the European Commission member states and stakeholders identified and developed a range of cost-effective measures to reduce emissions. The new package sets a range of ambitious targets to be met by 2020, including improvement of energy efficiency by 20%, increasing the market share of renewable to 20%. In a renewable energy-intensive scenario, global consumption of renewable resources reaches a level equivalent to 318 EJ ($E = 10^{18}$) per annum of fossil fuels by 2050, but it is less than 0.01% of solar energy reaching the earth's surface each year [1].

Solar energy is used to heat and cool buildings (both actively and passively), drying production, heat water for domestic and industry use, heat swimming pools, generate electricity, for chemistry applications and many more operations [1].

One of the solar energy uses is a solar wall. Solar wall system is simple, effective, inexpensive, ecological, building integrated into any solution [2-3]. This system, raising the temperature of indoor air for 5 - 25 degrees above the outside air temperature, allowing to save 20 - 70% of fuel energy while supplying the area with fresh air.

This system successfully used around the world since 1977, when the Canadian government subsidized the eco-system tests. Solar wall missions are located in North America, Europe and Asia - a total of more than 25 countries worldwide.

There is no need for heat ventilation at the expense of the economy, because the system provides fresh air circulation, while the walls of the building do not overheat in the summer, because the system acts as a coolant. In many countries, is increasing interest in solar wall panels use. Solar wall panels use is discussed a lot in works of Italian climates [4].

Using solar collectors efficiency studies [5], the idea was to use steel-tinplate absorber as a solar panel on the wall. Steel-tinplate absorber can be used on the roof, thereby providing ventilation and heating in early spring and autumn, with the heat and fresh air, and drying the products with heated air in the summer.

Our aim was to find the collector's (the adsorbent is used as a coating material) efficiency of insulation using and warm-up stage of air.

2. Methodology

The aim of the research was to investigate black colored steel-tinplate use for absorber and covered material of collector and compare the efficiency of three types of air heating collectors: collectors with insulated and un-insulated surfaces with covered material - steel-tinplate and classical collector with covered material - polystyrol plate and absorber black colored steel-tinplate in middle. View of flat-plate collector (FPC) when the absorber (black colored steel-tinplate) is put in the middle of the collector is shown in Fig.1. In the second case, absorber placed collector coverage place, it means at the top of collector.

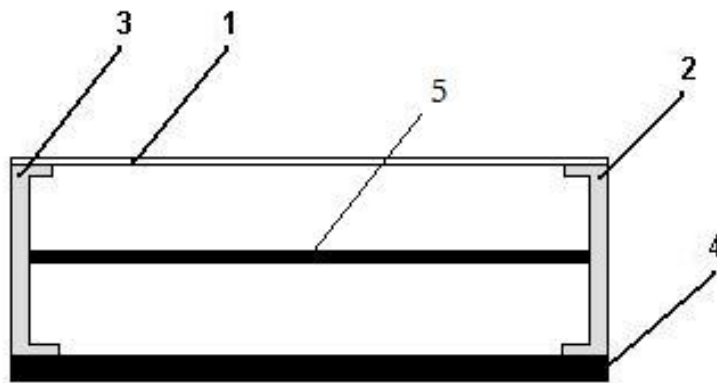


Fig. 1. Schema of solar collector frontal view: 1 – covered material; 2, 3 – side surface /plastic/; 4 – floor of collector; 5 – absorber (steel-tinplate)

In the experiments, the collector covered material was a polystyrol plate. This material has gained immense popularity due to such properties as safety, mechanical crashworthiness, translucence and high UV radiation stability.

In the laboratory a $0.1 \times 0.5 \times 1.0$ meters long experimental solar collector was constructed for research into the properties of absorber materials. Air velocity at the experiments was $v=0.9$ m/s. Our investigations devoted the sun following collectors, which guarantees perpendicular location of plane of absorber from flow of sun radiation.

Experimental data is recorded by means of an electronic metering and recording equipment of temperature, radiation and lighting (REG) [6]. It is equipped with 16 temperature transducers and metering sensors of solar radiation and lighting. Solar radiation measuring instrument was the pyranometer. The isolated collector was made by the collector surfaces faced with cellular plastic 2 cm plates.

We compare three equal sizes FPC: collectors of insulated and un-insulated surfaces with absorber steel-tinplate as a covering material and classic collector with the covering material polystyrene plate and absorber tinplate in the middle of collector. Experiments were made in

September 2010 in different weather conditions at different atmospheric air temperatures. To assess different absorbers influence was made comparatively research at similar weather conditions. Inflow air temperature in collector is equal to the ambient air temperature. Ambient air temperature was changing from 13°C to 18°C in our experiments.

The data of sun radiation are depended from clouds, shadows and we aligned experimental data with method of least squares using Eq. (1). [7]

$$\overline{y}_i = \frac{1}{35}[17y_i + 12(y_{i-1} + y_{i+1}) - 3(y_{i-2} + y_{i+2})] \quad (1)$$

Where \overline{y}_i - aligned data, y_i - experimental data, i - ordinal number.

3. Results

Using the experimental results and statistical processing data we received a relation between the length of the collector, sun radiation to absorber plate and air temperature exchange in the collector.

We research situation when absorber (steel-tinplate) puts at top of collector (Fig. 2). To compare insulated and un-insulated collectors with steel-tinplate as a covering material we can see that at the same weather conditions for insulated collector is warming up air to 3 degree up (at radiation 800 W/m²) than collector with un-insulated surfaces (Fig. 3).



Fig. 2. Sun collector comparatively research in experiment.

We can see that the solar radiation changes significantly affect the passing air temperature. This effect does not happen instantly, but with a delay of 3-5 minutes. It should be noted that the un-insulated collector efficiency is highly influenced by wind speed, which cools the surface of the collector body.

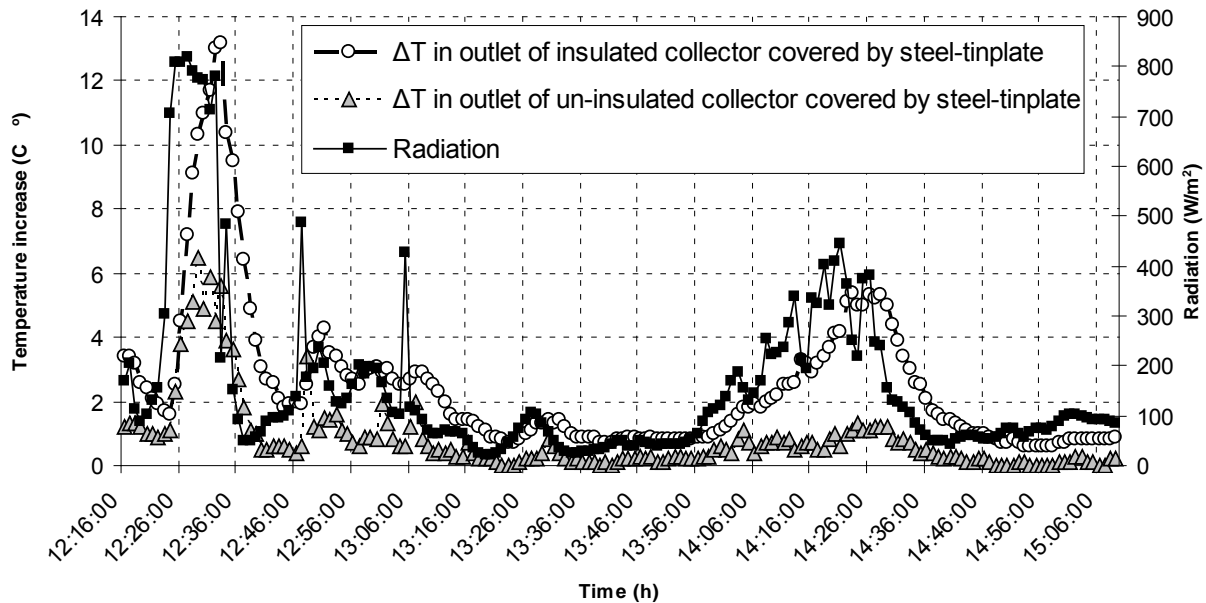


Fig. 3. Temperature difference in outlet of collector with steel-tinplate covering material for insulated and un-insulated surfaces comparing with sun radiation.

As you can see in Fig. 4, near little sun radiation are not visible constitutive air heating, but increasing sun radiation is growing air heating level and you can see that collector with absorber steel-tinplate at middle of collector body is more powerful than collector with steel-tinplate absorber as covering material. Air heating level is not highly dependent on ambient temperature. Much more it is influenced by solar radiation and insulation. If the collector is covered with the steel tinplate then this collector efficiency is highly influenced by environmental conditions, especially wind and ambient air temperature. These conditions reduces absorber own temperature. In the classic collectors whose effects are much smaller (Fig. 4)

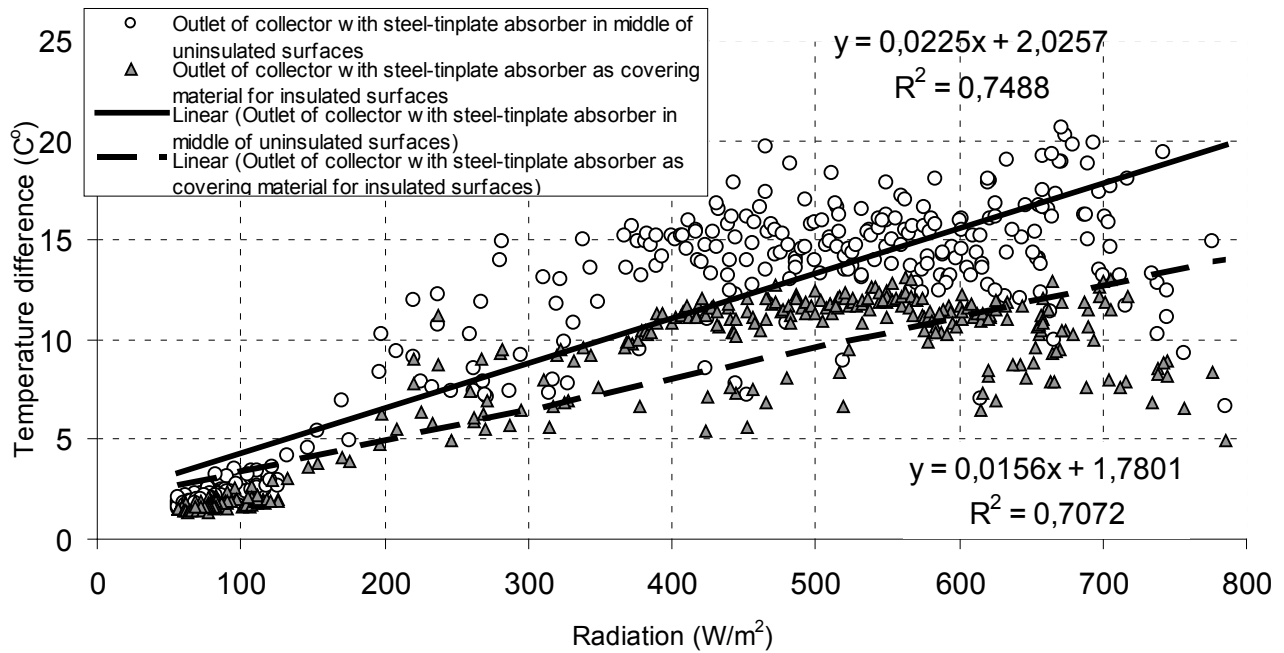


Fig. 4. Temperature difference in outlet of collector (with absorber tinplate at middle of collector body and with steel-tinplate absorber as covering material) comparing with sun radiation.

Near little sun radiation are not visible constitutive air heating, but increasing sun radiation is growing air heating level and you can see that collector with absorber steel-tinplate at middle of collector body is more powerful than collector with steel-tinplate absorber as covering material.

Using the experimental results and statistical processing data we received a relation between the air temperature exchange under the steel-thin plate absorber in the collector, length of the collector and sun radiation to absorber plate.

The temperature change ΔT under tinplate can be expressed with the Eq. (2).

$$\Delta T = 1.3 \cdot 10^{-2} x \cdot R - 4.8 \cdot 10^{-3} R - 1.9 \cdot 10^{-6} R^2 - 0.3x + 0.68x^2, \quad (2)$$

Where x – length of collector (m); R – sun radiation ($W \cdot m^{-2}$).

Coefficient of determination is $\eta^2 = 0.771$. The graphical interpretation of Eq. (2) is shown in Fig.3.

In Fig. 5. you can see contour plot of air temperature (under absorbent) increase dependence on length of collector and sun radiation for un-insulated collector with absorber with steel-tinplate as a covering material.

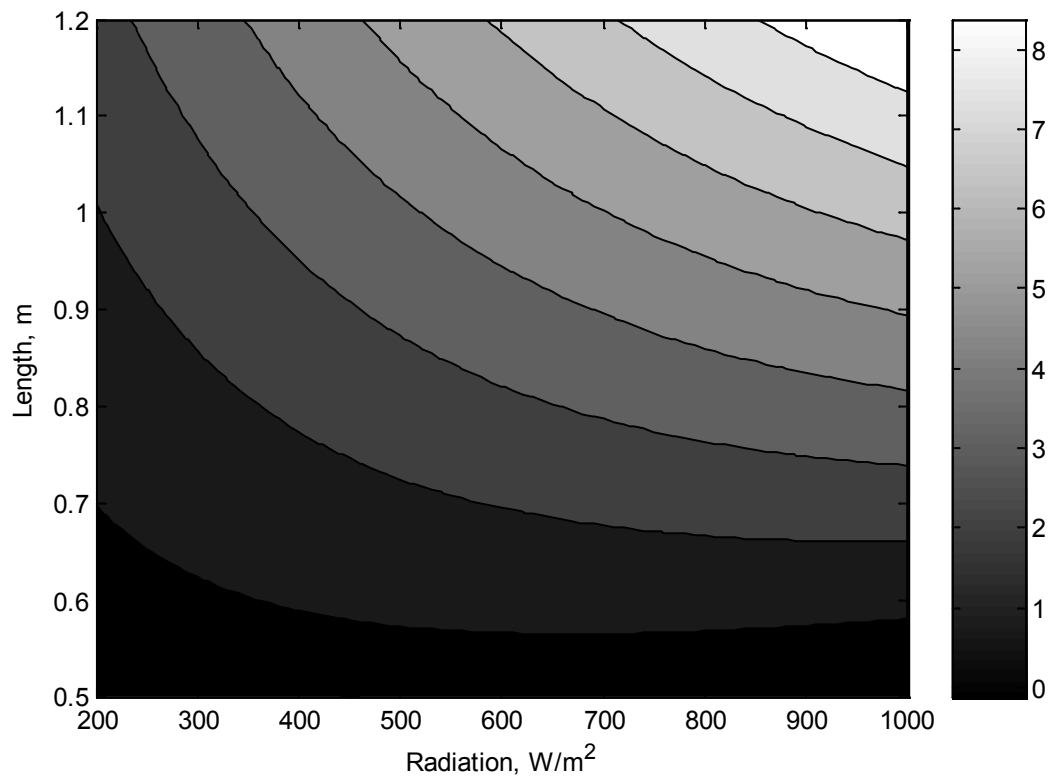


Fig. 5. Contour plot of air temperature (under tin plate) increase dependence on length of the collector and sun radiation.

4. Conclusions

1. Collectors of insulated and un-insulated surfaces with steel-tinplate absorber as covering material warmed ambient air up to 10-12 and 5-6 degrees corresponding (at irradiance 800 W/m^2). This difference indicates the great importance of insulating the collector body.
2. Use of isolation for collector construction dose not give inportant role if there is no wind to cool collector.
3. Using the experimental results and data statistical processing we received a relation between the air temperature exchange under the steel-thin plate absorber in the collector, length of the collector and sun radiation to absorber plate.
4. At favorable weather conditions the heating degree of ambient air at the outlet of collector with absorber tinplate at middle of collector body reaches 6-8 degrees more that at the outlet of insulated collector covered by steel-tinplate.
5. Our investigations showed that steel-tinplate absorber use as covered material of flat-plate collector for ventilated air heating is possible in Latvia.

References

- [1]. S. Kalogirou, *Solar energy engineering: processes and systems*, Academic Press Elsevier Inc., 2009.
- [2]. *Solar Buildings*: <http://www.nrel.gov/docs/fy99osti/24499.pdf>
- [3]. *Solar wall*: <http://solarwall.com/en/products/solarwall-air-heating/uses-and-applications/agriculture.php>
- [4]. F. Stazi, C. Di Perna, C. Filiaci, and A. Stazi, *The Solar Wall in the Italian Climates*, *World Academy of Science, Engineering and Technology* 37, 2008, pp. 31 – 39.
- [5]. A. Aboltins, J. Palabinskis, A. Lauva, G. Ruškis, *The steel–thin plate absorbers investigations in air solar collector*, *Proceedings of the 8th International Scientific Conference “Engineering for Rural Development”*, 2009, pp. 182 – 187.
- [6]. REG 2004 Tehniskais apraksts un lietošanas pamācība (Technical description and using instruction), pp. 11. (in Latvian)
- [7]. Веденяпин Г.В. *Общая методика экспериментального исследования и обработки опытных данных* (The general methodology of experimental research and treatment of experimental data). Колос, М., 1967. (in Russian)

Nano structure black cobalt coating for solar absorber

G.Toghdori¹, S.M.Rozati^{1*}, N. Memarian¹, M.Arvand², M.H.Bina³

¹Department of Physics, University of Guilan, Rasht42335, Iran

²Department of Chemistry, University of Guilan, Rasht42335, Iran

³Department of Materials Engineering, Esfahan University of Technology, Esfahan, Iran

* Corresponding author. Tel: +981313220912, Fax: +981313220066 E-mail: smrozati@guilan.ac.ir

Abstract: Black cobalt thin films on bright nickel plated on brass and copper substrates were prepared by the electrodeposition method. The Influence of substrate metal and heat treatment process on the surface morphology and absorptance of samples was investigated. Surface morphology and spectral reflectance of films were measured by scanning electron microscopy and spectrophotometer in the visible and near-IR region of spectrum respectively. Scanning electron microscopy images showed that the black cobalt films have porous structure. The absorptance of prepared films is over than 90%, which makes them suitable for using as solar absorbers.

Keywords: electroplating, black cobalt, solar absorber coating, black coating.

Nomenclature (Optional)

T Temperature °C
 t Time s
 α Solar Absorptance
 ε Thermal Emittance

1. Introduction

The preparative aspects of cobalt oxide thin films have been a subject of investigations by various workers because of their numerous applications in various fields of technology. They are attractive in application to solar thermal energy collectors as selective absorbing layers [1]. Spectrally selective surfaces exhibiting high values of solar absorptance α and low values of thermal emittance (ε) improve the thermal performance of solar collectors by reducing the radiative heat loss component [2]. Such surfaces are employed as receiver coatings in flat plate evacuated tube and concentrating collectors and may under stagnation conditions in the latter application, experience temperatures of 500°C. Many surface coating types have been developed which have potential for application as selective absorbers [3]. An attractive aim of selective surface research studies is the development of a single coating type which could be used for all solar collector designs. For successful industrial development such a coating would not only possess favourable optical properties but also would be readily reproducible, durable, thermally stable and inexpensive to produce. Selective solar absorber coating in solar thermal systems, working under moderate concentrations, experience operating temperatures in the rang 300-500°C. Cobalt oxide coatings [4] are proposed as potential candidates for this use. However, little is known about their stability and the modes of degradation when operated at high temperatures. It is well known that the metal substrate microstructure strongly influences the grain size and morphology of the in-situ grown film [5]. It is also well known that the microstructure of electrodeposits varies markedly with deposition parameters and that various impurities from the plating bath may be incorporated into the deposit [5].

A general class of absorber coatings is those formed by chemical “conversion” processes. The previous works on the electrochemical preparation of cobalt oxides can be divided in to two groups: direct and indirect. In the former, a solution is prepared by dissolution of the chemical components that allow the directly preparation of black cobalt on the substrate at the cathode in the electrolysis process [6]. On the latter the formation of cobalt oxide is

accomplished in two steps, i.e. first the metallic cobalt is deposited on the substrate and secondly, the cobalt is oxidized to black cobalt through chemical or thermal oxidation [6]. Because of its optical, semiconducting, magnetic and electrochemical properties, black cobalt is a promising material among transition metal oxides, which renders it attractive for solar photochemical applications and electrochemical devices as a counter electrode [7]. Today, although there are six physical mechanisms of solar absorptance [8]. It is recognized that one of the most efficient solar absorber films base their optical properties on its microstructural volume and superficial parameters. However, in spite of all the existing mechanisms, the textured surfaces are the most dependent of the surface morphology than whatever other material is. These materials show a high solar absorptance by multiple reflection of the incident radiation among dendrites that are approximately two microns apart, while the long-wavelength thermal emittance is rather unaffected by texture. Several techniques, such as chemical conversion and thermal oxidation of metallic films and electrodeposition, are currently used to achieve such spectrally selective, black-metal, solar absorber surfaces [9]. However, the desired characteristics of the metallic coating could be better controlled by directed electrodeposition. In this paper electrodeposition of cobalt photothermal material, suitable for using in solar energy collection, has been studied.

2. Experimental Details

Black cobalt thin films on bright nickel plated on brass and copper substrates were prepared by the electrodeposition method. The core part of the electroplating process is the electrolytic cell. In the electrolytic cell a current is passed through a bath containing electrolyte, the anode and the cathode. The workpiece to be plated is the cathode (substrate). The Anode is a metal which is coating on the cathode surface. Electrolyte is the electrical conductor in which current is carried by ions rather than by free electrons (as in a metal). When a direct electric current passes through an electrolyte, chemical reactions (Oxidation/Reduction) take place at the solution. Reduction takes place at the cathode, and oxidation takes place at the anode. Electrolyte completes an electric circuit between two electrodes. Upon application of electric current, the positive ions in the electrolyte will move toward the cathode and the negatively charged ions toward the anode. The metallic ions of the salt in the electrolyte carry a positive charge and are thus attracted to the cathode. When they reach the negatively charged workpiece, it provides electrons to reduce those positively charged ions to metallic form, and then the metal atoms will be deposited onto the surface of the negatively charged workpiece. Brass and copper plates were thoroughly degreased and cleaned, then subjected to a 1-min acid etch in 5% sulphuric acid prior to bright nickel deposition. According to watts bath [10] bright nickel deposition was carried out under the conditions mentioned in table 1. A piece of nickel metal with 99.9% purity was used as anode.

Table 1: Deposition condition and bath composition for deposition of bright nickel.

Composition bath		Current density	Temperature
Nickel sulphate	250 gl^{-1}	0.5 A/dm^2	70°C [11]
Nickel chloride	50 gl^{-1}		
Boric acid	50 gl^{-1}		

After bright nickel plating, the panels were rinsed with distilled water. Finally black cobalt deposition was carried out under the conditions described in table2 according to McDonald electrolyte bath [6]. The anode was cobalt metal with 99.9% purity and bright nickel plated brass and copper was used as cathode.

Table 2: Deposition condition and bath composition for deposition of black cobalt.

Composition bath	Current density	Temperature	pH
Cobalt sulphate 400 gl ⁻¹	3 A/dm ²	30°C	4
Cobalt chloride 50 gl ⁻¹			
Cobalt nitrate 4 gl ⁻¹			
Boric acid 40 gl ⁻¹			

The cobalt sulphate is the main source of cobalt ions, the cobalt chloride helps to improve the conductivity of electrolyte solution and the boric acid is a leveling agent. Cobalt nitrate was added to the bath to obtain a black layer on the sample.

The films deposited on brass substrate and bright nickel plated brass substrate annealed in the air environment at temperature 400 °C for 20 Min to study their physical properties after heat-treatment. The absorptance was calculated from the equation 1-R, in the visible region [12]. Where R is the room temperature reflectance measurement. Reflectance in the visible region was determined with a Carry 500 spectrophotometer. The morphology of the surfaces is detected by scanning electron microscope (SEM) model Philips XL30.

3. Results and Discussion

3.1. SEM Analysis

Figure 1 depicts the surface morphology of black cobalt films deposited on different bright nickel plated substrates. Fig.1.a is for a brass substrate and Fig.1.b belongs to a copper substrate. It is obvious that the crystal structure of black cobalt film deposited shows a porous structure. There is no evident difference between the morphology of films deposited on different substrates. While by changing the substrate metal the porous sizes have changed from micro, for copper substrate, to nano-sized porous structure for brass substrate. Figure 2 shows the surface morphology of black cobalt films deposited on brass substrate, (a) before heat-treatment and (b) after heat-treatment. From figures 1 and 2 it is clear that the films deposited on brass substrates after annealing had more cracks on the surface and the porosity of the structure was increased. By comparing fig.1a and fig.2a it is evidence that the presence of bright nickel middle layer causes a more uniform structure without any crack in the surface of electrodeposited black cobalt films on brass substrate. In addition by using the bright nickel middle layer the porosity of structure increased. This porous structure results enhanced the absorptance in coatings and makes these layers suitable for solar absorber application.

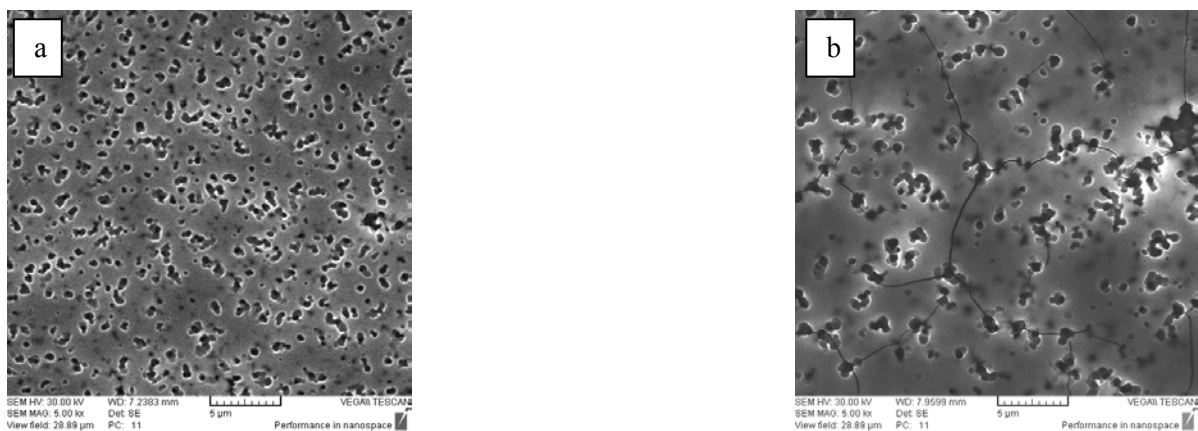


Fig. 1. The surface morphology of black cobalt film deposited on bright nickel-plated substrates (a) for brass substrate (b) for copper substrate.

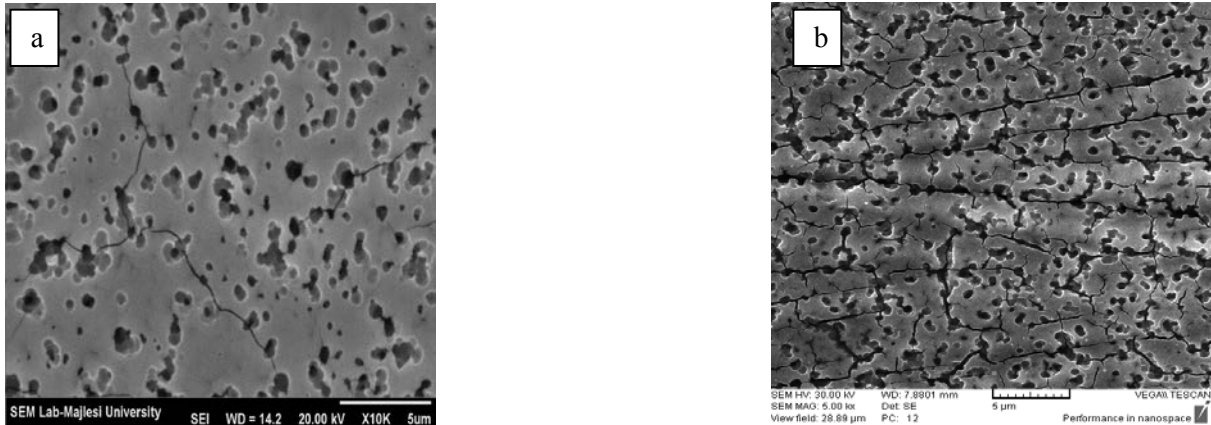


Fig. 2. The surface morphology of black cobalt films deposited on brass substrate (a) before annealing (b) after annealing.

3.2. EDAX Analysis

Figure 3 and table 3 show the elements in electrodeposited cobalt film on brass substrate by EDAX analysis. These Data expressed that the main elements in black cobalt coating, is cobalt metal.

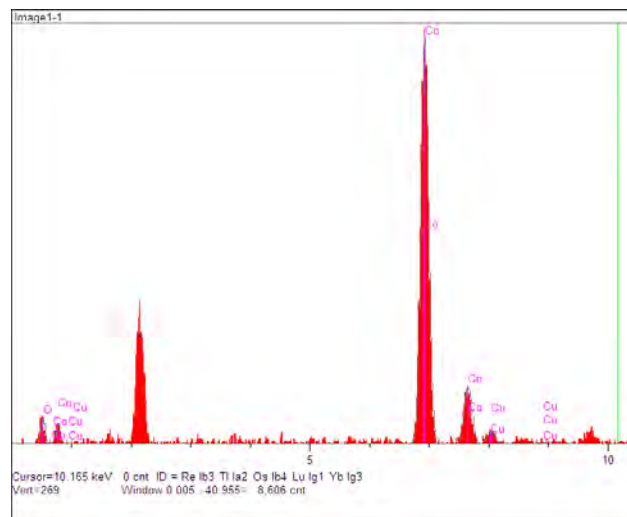


Fig. 3. EDAX of black cobalt as-deposited on brass substrate.

Table 3. The elemental concentration of black cobalt film deposited on brass substrate.

Intensity(c/s)	Conc. (Wt %)	Element
14.11	4.648	O
420.67	90.610	Co
13.34	4.742	Cu

3.3. Solar Absorptance Analysis

The changes in absorptance of layers by the wavelength for bright nickel-plated brass and copper substrates are shown in Fig.4. And the films absorptance of black cobalt films deposited on brass substrate before heat treatment and after heat treatment in visible region of wavelength are shown in Fig.5. The optimal solar absorptance was 98%-99.55% at wavelength range 400-1200 nm for the as-deposited films and films after heat treatment.

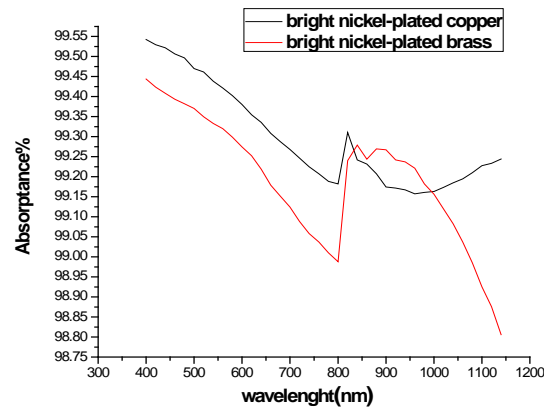


Fig. 4. The relationship between the absorbance and wavelength of black cobalt films deposited on different substrates.

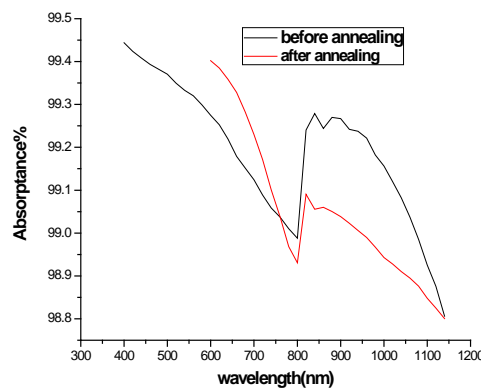


Fig. 5. The relationship between the absorbance and wavelength of black cobalt deposited on brass substrate (a) before heat treatment (b) after heat-treatment.

4. Conclusions

Black cobalt coatings on bright nickel plated on brass and copper substrate were prepared by the electrodeposition method. The influence of heat treatment on optical absorption and surface morphology of black cobalt films deposited on brass substrates has been studied. Heat treatment of black cobalt films deposited on brass substrates caused cracks in the surface structure. Heat treatment of black cobalt deposited on brass caused a slight decrease in an absorption in the near-IR region. Due to high absorption in visible region the best substrate for a black cobalt solar absorber coating is bright nickel-plated on copper substrate.

References

- [1] B. Pejova, A. Isahi, M. Najdoski and I. Grozdanov, Fabrication and characterization of nanocrystalline cobalt oxide thin films, *Material Research Bulletin* 36, 2001, pp. 161-170.
- [2] A.R. Shashikala, A.K. Sharma and D.R. Bhandari, Solar selective black nickel-cobalt coatings on aluminum alloys, *Solar energy materials & Solar cells* 91, 2007, pp. 629-635.
- [3] M. G. Hutchins, P.J. Wright and P.D. Grebenik, Coparision of different of black cobalt selective solar absorber surfaces, *Solar energy materials* 16, 1987, pp. 113-131.

- [4] C.Choudhury and H.K. Sehgal, High temperature degradation in cobalt oxide selective absorber, *Solar energy* 30, 1983, pp. 291-292.
- [5] S.C. Kwon, D.L. Douglass, The Selective Solar Properties of oxide films grown In-Situ on cobalt and cobalt alloys, *Solar Energy Materials* 11, 1984, pp.299-310.
- [6] E. Barrera, I. Gonzalez and T. Viveros, A new cobalt electrodeposit bath for solar absorber, *Solar energy materials and solar cells* 51, 1998, pp. 69-82.
- [7] Z. Abdel Hamid, A. Abdel Aal and P. Schmuki, Nanostructured black cobalt coating for solar absorbers, *Surf. Interface Anal* 40, 2008, pp. 1493-1499.
- [8] C. E. Barrera, L. Salgado, U. Morales and I. Gonzalez, Solar Absorptance of black cobalt and black cobalt-silver films and its relation with roughness coefficient, *Renewable Energy* 24, 2001, pp. 357-364.
- [9] E. Barrera, M. P. Pardave, N. Batina and I. Gonzalez, Formation Mechanisms and Characterization of black and white cobalt Electrodeposition onto Stainless Steel, *Journal of Electrochemical Society* 147, 2000, pp. 1787-1796.
- [10] T.M.Chang, M.Sone, A.Shibata, C.Ishiyama, Y.Higo, Bright nickel film deposited by supercritical carbon dioxide emulsion using additive-free watts bath, *Electrochimica Acta* 55, 2010, pp. 6469-6475.
- [11] B. Gaida, *Electroplating (Question and Answers)*, by La librairie de Traitements de Surface, first, 1983, pp.167-187.
- [12] G. McDonald, A Preliminary study of a solar selective coating system using a black cobalt oxide for high temperature solar collectors, *Thin Solid Films* 72, 1980, pp. 83-87.

Combining the radiative, conductive and convective heat flows in and around a skylight

Martin Fält*, Ron Zevenhoven

*Thermal and Flow Engineering, Department of Chemical Engineering, Åbo Akademi University,
Turku, 20500, Finland*

** Corresponding author. Tel: +358 2 215 4441, Fax: +358 2 215 4792, E-mail: martin.falt@abo.fi*

Abstract: Normal skylights bring light into the spaces located below them. By the use of infrared radiation (IR) transmissive polymer films and IR-emitting and absorbing gases, an advanced version of the skylight may supply cooling and thermal insulation to the room located below it. This novel radiative skylight can, in its cooling mode, lead heat from the room below, to the cool skies located above the skylight. When cooling is no longer needed or attainable this connection will be cut, thus providing the room with an optimal amount of thermal resistance. This article is a progress report on the modeling of the skylight. The main work is done to combine the different heat transfer methods into one single model by the use of the commercial program Comsol 4.1. The results show that a cooling effect of 100 W/m^2 is achievable when the skylight is compared to a similar skylight containing only air.

Keywords: Radiative cooling, heat transfer in participating media, skylight.

1. Introduction

Skylights are popular in building technology due to their ability to bring light into a space. However, as they light up a space, they also heat it up. This heat can be unwanted and therefore, has to be removed. This article will present the results from a numerical modeling of a skylight, which can function either as a radiative cooler or as a thermal insulator. Radiative cooling is a passive cooling method that connects a warm object located e.g. on top of a building to a lower sky temperature through heat radiation; one could describe it as an inverse solar collector [1].

The improved skylight contains a quantity of gas that is active in radiative heat transfer (i.e. a participating gas), and a cooling or insulating effect is achieved by controlling the circulating motion of this gas. The use of gases in the spaces between windows has been studied mainly with the goal of increasing thermal resistance by replacing air with a gas having lower conductive properties. Another option is to use gases that absorb and emit thermal radiation and thus decrease the radiative heat transfer through the window [2]. The use of such gases, which are active in radiative heat transfer, has also been studied for radiative cooling purposes; these studies show that cooling is also attainable during the day [3–5]. However, a window or a skylight that combines the three functions is a novel idea.

2. Methodology

The skylight model, whose design and function is described in [6], was designed at the authors' laboratory at Åbo Akademi University to determine its performance as a passive cooler and a thermal insulator. As shown in Figure 1, it consists of three windows. The outer and the inner window are made of an IR-transmitting polymer, $\tau=0.19$, and the middle window is made of silica glass, which is highly reflective to IR radiation at all wavelengths, $\rho=0.9$. The spaces between these windows contain a greenhouse gas that acts as the system's heat carrier. The walls are assumed to be thermally insulated and to have an absorptivity of $\alpha=0.9$. Heat that originates directly from the sun is not incorporated into this model as both

the windows and the gas are assumed not to absorb short wave heat radiation in the interval of 0.1–3 μm .

When the skylight is set in its cooling mode, heat is transferred to the gas through the lower window (Glass 1) by radiation, conduction, and convection from the room below. The heated gas rises to the upper compartment due to the decrease in the gases' density. In the upper space, the gas is cooled by radiative heat transfer through the upper polymer window (Glass 2) and the "atmospheric window" to the colder air masses in the upper atmosphere. There also exists a forced convective heat transfer between the upper part of the skylight and its surroundings. The effect of this heat transfer depends on the temperature of the surroundings; for the modeled cases, it is cooling.

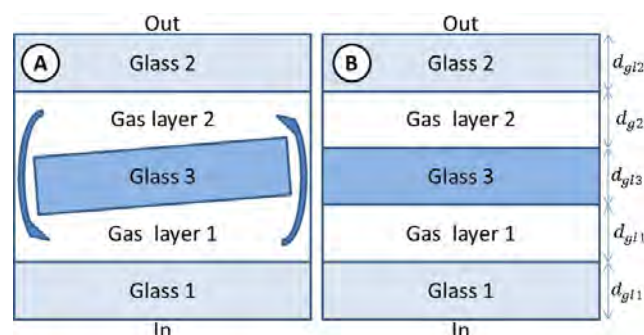


Fig. 1. Skylight in cooling mode "A" and in insulating mode "B"

When the greenhouse gas cools, its density increases, and it flows down to the lower part of the skylight. This convective heat flow is induced by the slightly tilted middle window. The angle of the tilt and the width of glass 3 has been chosen according to Fig. 2 so as to decrease the formation of hindering Bérnard cells (convective swirls).

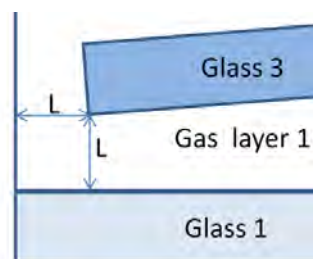


Fig. 2. Detail of the skylight in cooling mode

Then when no cooling is needed, the connection between the two gas spaces is cut, thus changing the task of the roof components from a passive radiative cooler to a thermal insulator. The weather parameters that are used in this modeling are average values for the months of February and July for year 2008 in Helsinki, Finland. The data for February is used to model when a skylight with a maximal amount of thermal resistance is needed and the data for July is used to model when cooling is needed. The data was procured from the Finnish meteorological institute, and it is presented in Table 1.

Table 1. Average weather data for two months in 2008 for Helsinki Finland.

Unit	February	July
$T_{\text{ambient}} [^{\circ}\text{C}]$	0.73	17.62
$T_{\text{sky}} [^{\circ}\text{C}]$	-7.51	3.67
$v_{\text{wind}} [\text{m/s}]$	4.13	3.20

Modeling natural convection induced by heat radiation is, however, somewhat tricky; an attempt to do this was made by the author in [6]. It has also been shown that the wavelength dependency is crucial for calculating radiative heat transfer in participating media [7].

The exponential wide-band method is used in this paper to calculate the gases absorptivity and emissivity, which are assumed to be equal [8]. The studied gas is chosen to be CO₂ which absorptivity is calculated to be, $\alpha=0.19$, as an isothermal and a gray value (no wave length dependency). In future work the gas absorptivity will be treated as temperature and wavelength dependent variable.

3. Results

The results from the modeling are given in Table 2 where the total heat transfers from the room to the skylight are presented. This data is calculated by the Comsol model in W/m as the model is 2 dimensional. These results are in turn squared to get them into a more comfortable unit of W/m². These results are from the last time step of a 1000 second long dynamic simulation. The reason for solving this problem as a time dependent instead of a stationary problem is to avoid unstable equilibrium points. The time of 1000 seconds was assumed to be a time period long enough for the heat flows to stabilize. However, some of the simulations seem not to have stabilized.

Table 2 shows that a cooling capacity 98 W/m² can be obtained during the summer by this design, when comparing the cooling case with CO₂ to the insulating case with air. The table also shows that if the skylight is set in its insulating mode for the winter an unnecessary heat loss of 80 W/m² would be achieved. This same effect is also achieved if the skylight is filled with air. A reason to this could be that the simulations were not simulated for a long enough time.

Table 2. Average heat transfer for two months in 2008 for Helsinki, Finland.

[W/m ²]	Summer Cooling	Winter Insulating	Summer Insulating	Winter Cooling
CO ₂	117	966	88	883
Air	15	983	19	655

Nonetheless, if the gas in the cooling skylight would be replaced with air instead of the greenhouse gas, CO₂ in this case, is it obvious that the cooling would drop by as much as 85%. The reason for this is that air does not absorb or emit heat radiation and cannot therefore be directly cooled down by the sky. If the winter insulating cases are then compared to each other is the skylight with the CO₂ at $\alpha=0.19$ a somewhat better thermal insulator than the skylight containing air. The reason for this is that CO₂ is a better conductive insulator than air; however, CO₂ is a better transfer medium for convective heat than air and therefore works better in the cooling mode.

So for the skylight to work as intended it is important to choose the thickness of the skylight correctly. The skylight should be thin enough to prevent convective air movement to form when the skylight is in the insulating mode but thick enough that a convective heat flow can occur between the two compartments when the skylight is in its cooling mode. The thickness of 10 cm has shown to give good results and is therefore used in this study; the width of the skylight is 0.5 m. While then observing Fig.3-a to Fig. 4-b it becomes obvious that the figures presented are not in scale; these distortions allow the figures to be more easily understood without taking too much space.

3.1. Skylight filled with CO₂

3.1.1. Cooling mode

The goal in the cooling mode is to get the gas inside the skylight to move from the lower compartment to the upper one. This movement should in turn transfer heat from the room to the sky. When observing the simulation results in Fig. 3-a and Fig. 3-b one can observe that this flow is taking place. Additionally, the gas that is moving around in the skylight, as pictured in Fig. 3-a, is clearly cooled down by radiative heat exchange between the sky and the skylight. This is certain as the temperature of this gas flow is lower than that of both the temperature of the room and the temperature of the ambient.

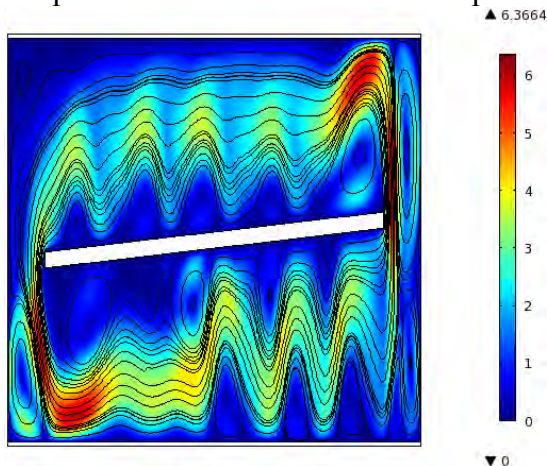


Fig. 3-a. Velocity profile in [cm/s] for cooling mode during summer*

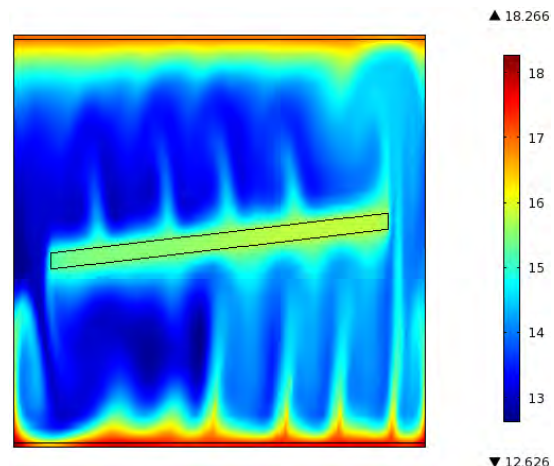


Fig. 3-b. Temperature profile in [°C] for cooling mode during summer*

3.1.2. Insulating mode

As mentioned above, for the insulating case to work optimally, the gas movement in the skylight should be kept to a minimum. This, however, is only partially achieved as clear Bénard cells can be seen in the lower part of the skylight, with also some minor circles in the upper compartment. This suggests that more work could be done to find an optimal depth for the skylight. An interesting phenomenon can be seen in Fig. 4-b where the lowest temperature is achieved in the lower part of the upper compartment. This has to do with the high reflectivity of the middle glass window.

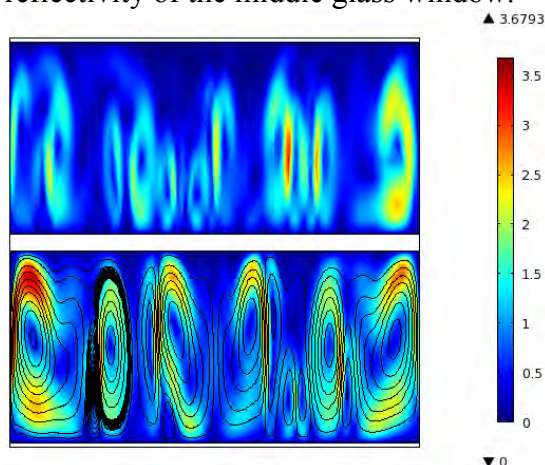


Fig. 4-a. Velocity profile in [cm/s] for insulating mode during winter*

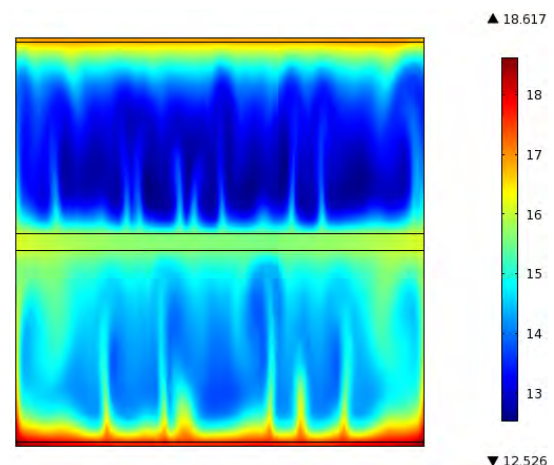


Fig. 4-b. Temperature profile in [°C] for insulating mode during winter*

* Note that the figures are not in scale.

3.2. Skylight filled with air

For comparison, the same analyses as presented in chapter 3.1, have also been made for a skylight filled with air.

3.2.1. Cooling mode

Even though the skylight is filled with air, a flow pattern is formed between the two compartments; this shown in Fig. 5-a. However, the flow velocities are somewhat slower in Fig. 5-a. than in Fig. 3-a. Furthermore, the temperature profile presented in Fig. 5-b shows that temperatures do not reach lower temperatures than that of the ambient and thus the air is not cooled by the sky.

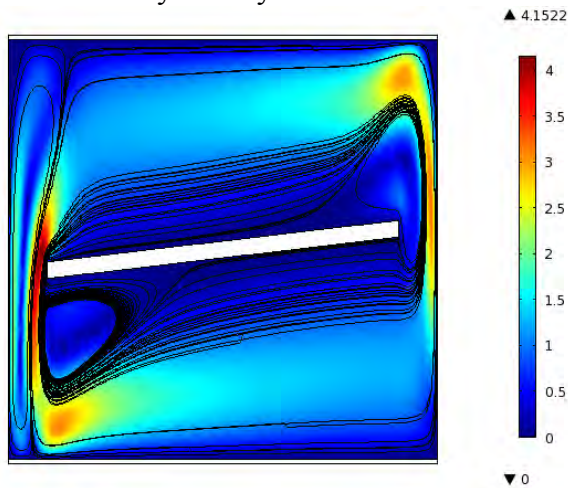


Fig. 5-a. Velocity profile in [cm/s] for cooling mode during summer[†]

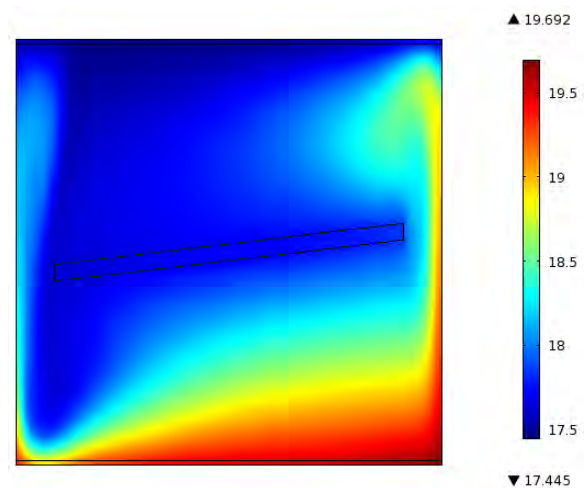


Fig. 5-b. Temperature profile in [°C] for cooling mode during summer[†]

3.2.2. Insulating mode

Interestingly the air filled skylight has the worst insulating properties. The main reason for this is the high air velocities that are presented in Fig. 6-a; another could one could be that the simulation time of 1000 seconds was too short. The temperature profile presented in Fig. 6-a reinforces that temperatures below the ambient are not achievable in a skylight filled with air.

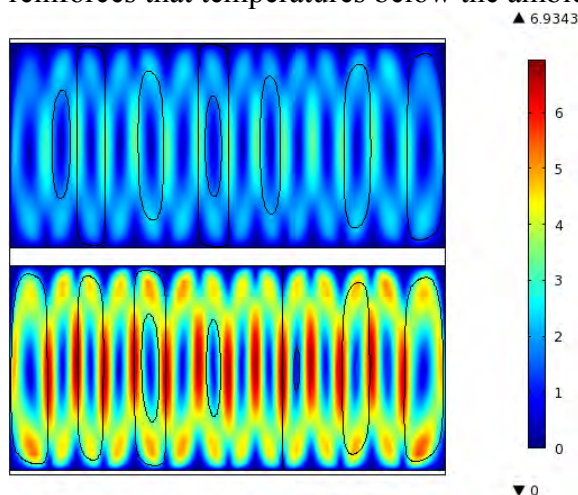


Fig. 6-a. Velocity profile in [cm/s] for insulating mode during winter[†]

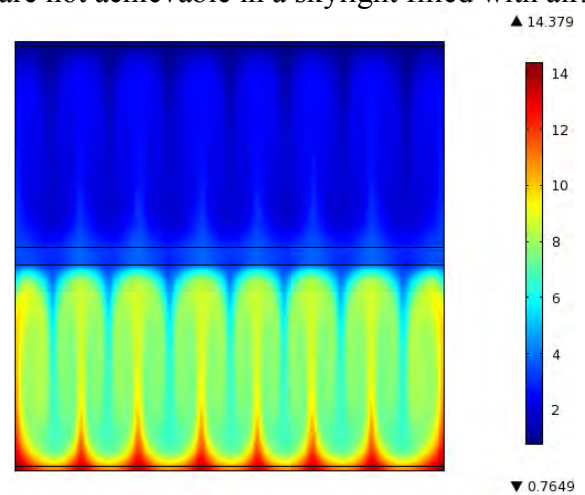


Fig. 6-b. Temperature profile in [°C] for insulating mode during winter[†]

[†] Note that the figures are not in scale.

4. Summary and Conclusions

This article presents an idea for using a regulated skylight to control heat flow in and out of a space located below. The concept was evaluated using a commercial multiphysics program Comsol.

This study shows that cooling effects of up to 100 W/m^2 are achievable under normal summertime conditions in southern Finland. However, improvements to the design could still be made and thus increase this cooling effect. These improvements would be a result from a careful analysis and optimization of the difference in heat transfer between the two skylight modes. Further improvements to the modeling would be to run Comsol parallel with Matlab so that wavelength dependency could be incorporated into the model, as it is an important factor for radiative heat exchange in participating media. The method chosen for calculating the wavelength dependency would be the exponential wide-band model.

If this system was successfully implemented, savings could be achieved by reducing the use of conventional cooling methods. Unfortunately, window materials that possess the necessary transmission properties typically have poor mechanical properties.

An experimental setup is being designed to assess the modeling results and to study different combinations of materials.

Acknowledgment

This work is funded by Maj and Tor Nessling Foundation projects 2009301, 2010362 and 2011285 “Solar heat engineering and carbon dioxide: energy recovery using a greenhouse gas”, and the Foundation for Åbo Akademi University.

References

- [1] E. Erell, Y. Etzion, Radiative cooling of buildings with flat-plate solar collectors, *Build. Environ.* 35, 2000, pp. 297 – 305.
- [2] M. Rubin, Calculating Heat Transfer Through Windows, *Int. J. Energy Res.* 6, 1982, pp. 341 – 349.
- [3] T.S. Eriksson, C.G. Granqvist, J. Karlsson, Transparent thermal insulation with infrared-absorbing gases, *Solar Energy Materials.* 16, 1987, pp. 243 – 253.
- [4] E.M. Lushiku, T.S. Eriksson, A. Hjortsberg, C.G. Granqvist, Radiative cooling to low temperatures with selectively infrared-emitting gases, *Solar & Wind Technology.* 1, 1984, pp. 115 – 121.
- [5] C.G. Granqvist, Radiative cooling to low temperatures general considerations and applications to selectively emitting SiO films, *J. Appl. Phys.* 52, 1981, pp. 4205 – 4220.
- [6] M. Fält, R. Zevenhoven, Radiative cooling in northern Europe using a roof window, *Proc. of ES2010*, Phoenix, AZ, May, 2010, paper 90192.
- [7] G. Rey Colomer, *Numerical methods for radiative heat transfer*, 2006, pp. 1–161.
- [8] R. Siegel, J.R. Howell, *Thermal Radiation Heat Transfer*, 3rd ed., Hemisphere Pub. Corp., Washington, D.C., 1992 pp. 562 – 567.

Development of a solar intermittent refrigeration system for ice production

G. Moreno-Quintanar, W. Rivera*, R. Best

Centro de Investigación en Energía, Universidad Nacional Autónoma de México
A.P.34, 62580 Temixco, Mor., México

* Corresponding author: Tel. +52 5556229740, E-mail address: wrgf@cie.unam.mx

Abstract: A solar powered intermittent absorption refrigeration system has been developed at the Centro de Investigación en Energía of the Universidad Nacional Autónoma de México. The system was evaluated with the ammonia/lithium nitrate/water (NH₃/LiNO₃/H₂O) mixture. The system was designed to produce up to 8 kg/day of ice. The system consists of a Compound Parabolic Concentrator (CPC) with a cylindrical receiver acting as the generator/absorber, a condenser, an evaporator and an expansion valve. The system operates exclusively with solar energy and no moving parts are required. Evaporator temperatures as low as - 11°C were obtained for a period of time up to 8 hours. Coefficients of performance as high as 0.098 were obtained. These coefficients were 24% higher than those obtained with the same system operating with the binary ammonia/lithium nitrate (NH₃/LiNO₃) mixture previously reported in the literature. The results showed that the developed system seems to be a good alternative for refrigeration in zones where electricity is not available.

Keywords: solar cooling, absorption systems, ice production, ammonia/lithium nitrate/water.

Nomenclature

A	concentrator aperture area	m^2	Q_R	heat received from solar radiation.....	MJ
C_p	heat capacity	$J\ kg^{-1}\ K^{-1}$	T	temperature	K
COP_s	solar coefficient of performance		t	time	s
G	solar radiation	$W\ m^{-2}$	ρ	density	$kg\ m^{-3}$
H	insolation	$MJ\ m^{-2}$	v	specific volume	$m^3\ kg^{-1}$
h_{fus}	heat of fusion of ice	$kJ\ kg^{-1}$	m	mass.....	kg
Q_{EV}	cooling capacity	MJ			

1. Introduction

Solar refrigeration is a useful application in areas of the world with high insolation levels where there is a demand for cooling and there is not electricity to supply conventional power systems.

Although the basic concepts of solar refrigeration appeared since about five decades, to date there are only a limited number of developed systems reported in the open literature, some of the most important works are the following. Erhard et al. [1] reported the performance of a solar refrigeration system operating with NH₃/SrCl₂. The main part of the device is an absorber/desorber unit which is mounted inside a concentrating solar collector in which the heat of absorption is transported out of the solar collector by means of two horizontally working heat pipes. The overall efficiency defined as the cooling capacity to the solar radiation received by the solar collectors of the cooling system varied from 0.05 to 0.08. Wang et al. [2] published the results of a combined adsorption heating and cooling system which operated with activated carbon/methanol. The system was tested with electric heating and it was found that with 61 MJ heating it was able produce up to 9 kg ice were made. The calculated Coefficient of Performance (COP) which is defined as the cooling capacity to the heat supplied to the generator of the system

was 0.0591. Li et al. [3] published the experimental study on dynamic performance of a flat-plate solar solid-adsorption refrigeration for ice maker operating with activated carbon/methanol. The experimental results showed that this machine can produce 4–5 kg of ice after receiving 14–16 MJ of radiation energy with a surface area of 0.75 m², while producing 7–10 kg of ice after receiving 28–30 MJ of radiation energy with 1.5 m². Hildbrand et al. [4] reported the results of the performance of an adsorptive solar refrigerator built in Yverdon-les-Bains, Switzerland operating with the adsorption pair silicagel + water. Cylindrical tubes function as both the adsorber system and the solar collector. The condenser is air-cooled and the evaporator contains 40 l of water that can freeze. The results showed that the gross solar coefficient of performance defined by the authors varied between 0.1 and 0.25 with a mean value of 0.16. Khattab [5] presented the description an operation of a novel solar-powered adsorption refrigeration system operating with activated carbon/methanol. The system consisted of a modified glass tube having a generator (sorption bed) at one end and a combined evaporator and condenser at the other end and a simple arrangement of plane reflectors to heat the generator. The daily ice production was 6.9 and 9.4 kg/m² and the net solar COP was 0.136 and 0.159 for cold and hot climate respectively. Li et al. [6] developed a no valve, flat plate solar ice maker on the basis of previous research achievements. The system operated again with activated carbon/methanol. The authors reported that the no valve solar ice maker prototype was approached to practical application of mass production from view of cost and techniques. Rivera et al [7] published a paper about the development of a solar intermittent system operating with the ammonia/lithium nitrate mixture. The authors reported that solar coefficients of performance as high as 0.08 can be obtained with the developed system

From the literature review it is clear that although there has been relevant research on developing solar refrigeration systems the most of them have been focused in adsorption systems which have in general low coefficients of performance. Because of this in the present paper the system developed previously by Rivera [7] was evaluated but using now the ternary mixture ammonia/lithium nitrate/water with the purpose to increase the mixture conductivity and to decrease the mixture viscosity trying to increase the system efficiency. Physical and thermodynamic properties of the ternary mixture were taken from Libotean et al [8,9].

2. System description

The system was designed to operate with the ammonia/lithium nitrate/water mixture for a maximum capacity of 8 kg of ice/day. It consists of a compound parabolic collector CPC with a cylindrical receiver acting as the generator/absorber, a condenser, a storage tank, an expansion valve, a capillary tube, an evaporator and a (see Fig. 1). The system operates exclusively with solar energy and no moving parts are required.

During the day, the ammonia/lithium nitrate/water mixture in the generator-absorber is heated by the solar radiation incident on the CPC until it reaches the saturation temperature. Then the ammonia is partially evaporated from the solution. Due to the increase of the temperature and consequently of the pressure of the solution in the cylindrical receiver of the CPC, the ammonia vapor goes to the condenser, where it is condensed by water and then it is stored in the tank. In the night, the temperature and pressure in the generator-absorber decreases because of the decreases of the ambient temperature and the ammonia liquid passes through the expansion valve (which is opened manually) decreasing its pressure and temperature, producing the refrigerant

effect in the evaporator. After the ammonia has absorbed heat from the water stored in the trays inside the evaporator, the pressure in this component increases. In this way, the pressures are inverted in the components in natural way, and the ammonia vapor returns to the generator-absorber where it is absorbed by the strong solution. About 7 o'clock in the morning, after the ice has been produced and the ammonia has been absorbed by the solution stayed in the cylindrical receiver of the CPC, the expansion valve is closed and the ice removed from the trays leaving the system ready for a new cycle.

The CPC is made out of an aluminum sheet with a reflectance of 0.85. The cylindrical receptor is covered with a selective black paint with a range of emittance from 0.25 to 0.49 and absorptance from 0.88 to 0.94; it resists temperatures higher than 300°C. The CPC's concentration ratio is 3.3, with a half-angle of 11.54° and an aperture area of 2.54 m². The condenser is a heat exchanger composed of a helicoidal aluminum coil, immersed in a water store. The water inside of the condenser is continuously recirculated by a pump that is connected to a cooling system. It is important to mention that the pump is used just in order to keep the condenser temperature fixed eliminating the system variability with regard to the ambient temperature, however, this pump it is not necessary in normal operating conditions. Furthermore the cooling system and the pump are used exclusively to control the temperature of cooling water for experimental purposes. The cylindrical storage tank has a capacity of 8.5 L; a tube to measure the level is connected to the tank. Leaving the tank, there are two expansion devices: the capillary tube and the needle valve. Only one of these expansion devices is used during the evaporation process. The capillary tube is recommended because it permits the automation of the evaporation process. The evaporator is a heat exchanger that consists of a coil inside an insulated metal container with a front door, in which the ice is produced. The coil is horizontally distributed along five levels, each one bearing an aluminum tray. Water to be frozen is contained in these trays. Fig. 2 shows a photograph of the developed system.

In order to evaluate the system, 14 thermistors, 7 wall thermocouples, 5 pressure transducers, 2 manometers, 1 level tube (placed in the storage tank) and 1 pyranometer were used (see Fig. 1).

3. Evaluation parameters

Five main parameters were used in order to evaluate the experimental system: (i) the amount of the ammonia produced in the generator, (ii) the insolation, (iii) the solar energy received by the CPC, (iv) the cooling capacity and (v) the solar coefficient of performance.

The amount of the ammonia produced in the generator can be obtained as:

$$m_{NH_3} = \rho v_{NH_3} \quad (1)$$

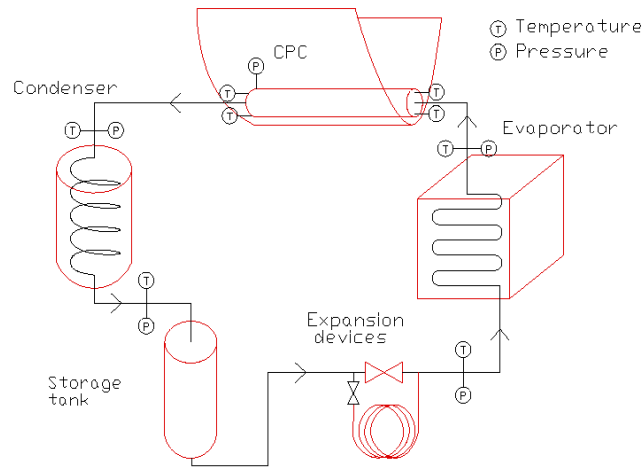


Fig. 1. Schematic diagram of the solar intermittent absorption refrigeration system.



Fig. 2. Photograph of the solar intermittent absorption refrigeration system developed.

The energy received from the solar radiation is calculated as the sum of the contributions of the product of the irradiation, the time and the aperture area.

$$Q_R = \sum_{i=1}^n G_i t A \quad (3)$$

The cooling capacity is the sum of the sensible heat to reduce the water temperature from ambient to 0°C plus the heat of fusion of ice

$$Q_{EV} = m_{H_2O} (h_{fus} + C_p \Delta T) \quad (4)$$

Finally, the solar coefficient of performance is defined as the cooling capacity in the evaporator to the energy received from the solar radiation.

$$COP_S = \frac{Q_{EV}}{Q_R} \quad (5)$$

4. Results

In order to experimentally evaluate the solar refrigeration system operating the two mixtures, more than 40 tests runs were carried out mainly during summer time, however, only 18 were taken in the analysis since in the others the solar radiation was considerably low (lower than 14MJ) because of long cloudy skies periods (normally higher than 2 hours).

During the experimental test runs, the main evaluating parameters such: temperatures, solar radiation and pressures were logged every 15 seconds.

Fig. 3 shows the maximum pressure reached in the cylindrical receiver against the maximum solution temperature reached during the generation stage. It can be observed that the pressure increases slightly with the increment of the solution temperature. The solution temperatures varied from 87°C to 112°C, meanwhile the pressures varied from 13 bar to 16.1 bar.

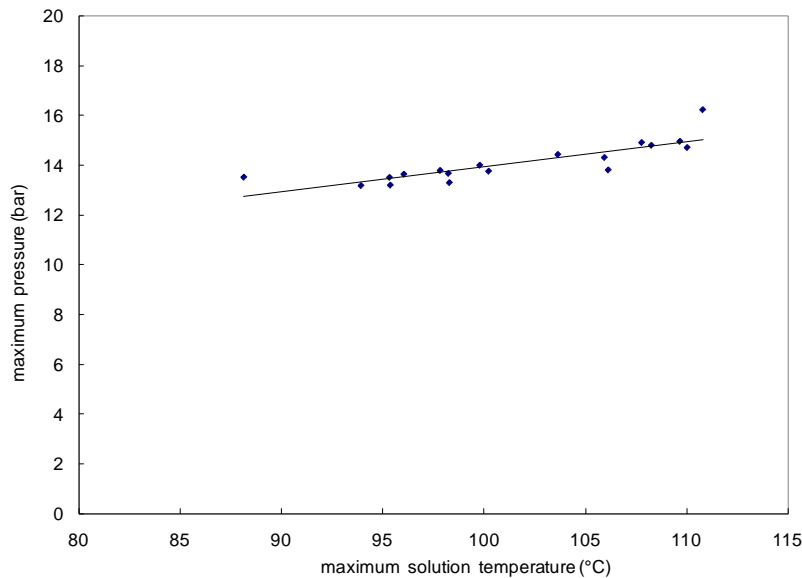


Fig. 3. Maximum pressure against maximum solution temperature for the solar system.

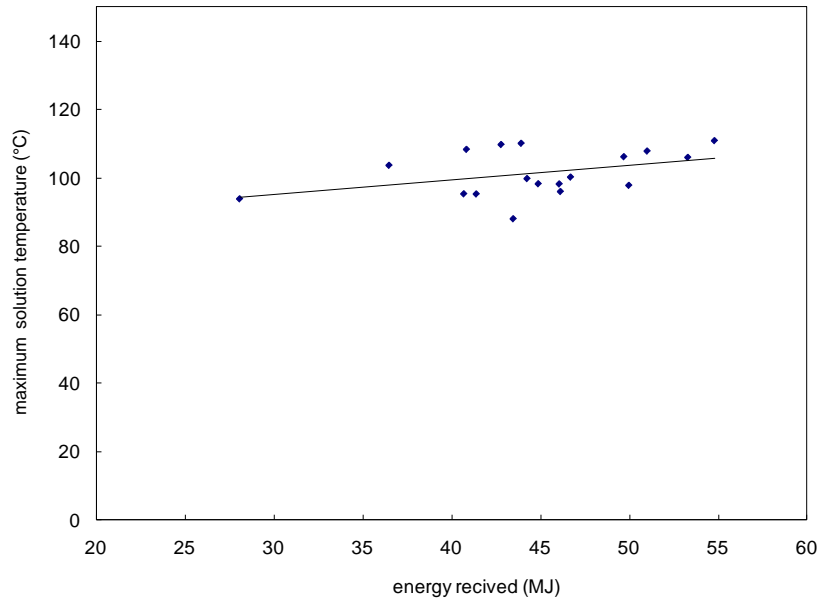


Fig. 4. Maximum solution temperature against the energy received by the CPC.

Fig. 4 shows the maximum temperature reached by the solution during the generation stage as function of the energy received by the CPC during the sunshine hours. In this figure it can be seen that there is a considerable data dispersion between these two parameters, however, it can be observed as it was expected that the solution temperature increases with the energy received by the CPC. It can be observed that the energy received by the CPC varied considerably from about 27 MJ to 56 MJ which is almost two times the minimum value. The high difference that exist among the energy received values is related with the cloudy of each day, since the solar radiation was almost the same since the most of the values (16 of the total) were obtained during the same season (summer).

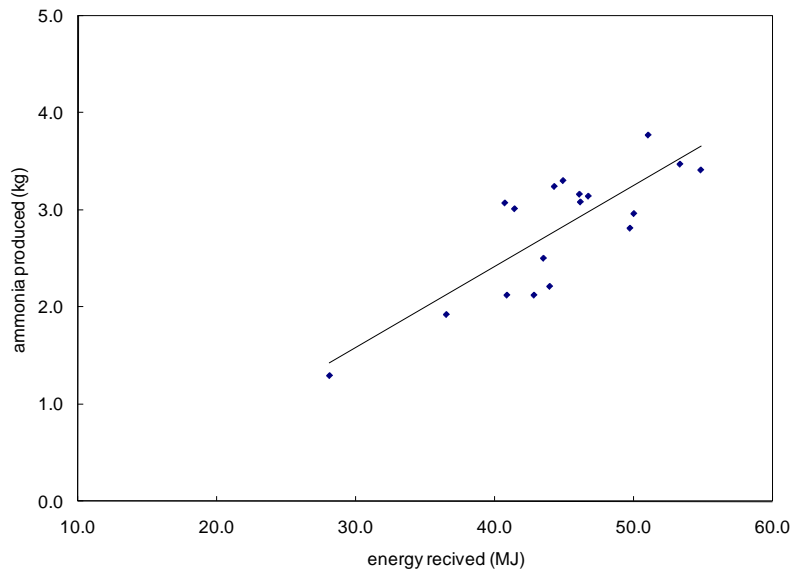


Fig. 5. Ammonia produced during the generation stage against the energy received.

In Fig. 5 it can be seen that the amount of ammonia produced (measured after the sunshine hours in the level tube placed in the condensate tank) increases considerably with the increase of the energy received by the CPC. The amount of ammonia produced varied from 1.3 kg at an energy received of 28.2 MJ to 3.8 kg at an energy received of 50 MJ. From this figure and from the explained in Fig. 4 that the amount of refrigerant produced (ammonia) is very dependent of the solar radiation received by the CPC.

In Fig. 6 it can be seen the solar coefficient of performance against the cooling capacity. It can be observed that the solar coefficient of performance increases considerably with and increases of the cooling capacity. The solar coefficient of performance varied from 0.06 at a cooling capacity of 1.7 MJ to a 0.098 at a cooling capacity of 4 MJ.

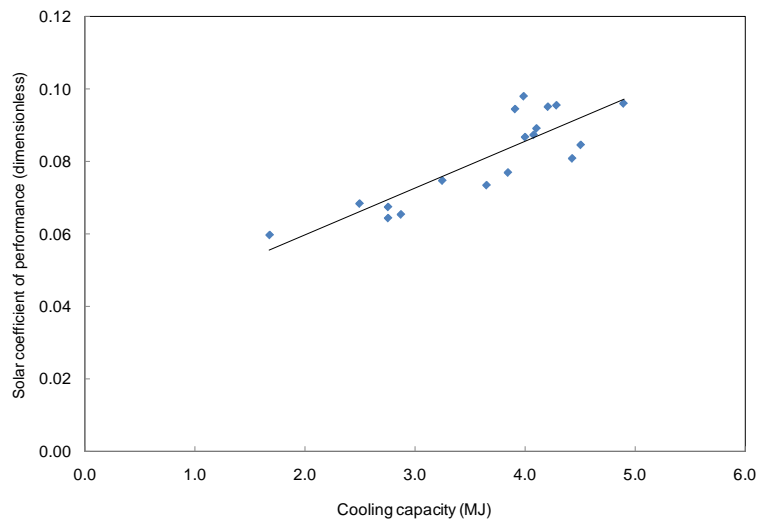


Fig. 6. Solar coefficient of performance against cooling capacity.

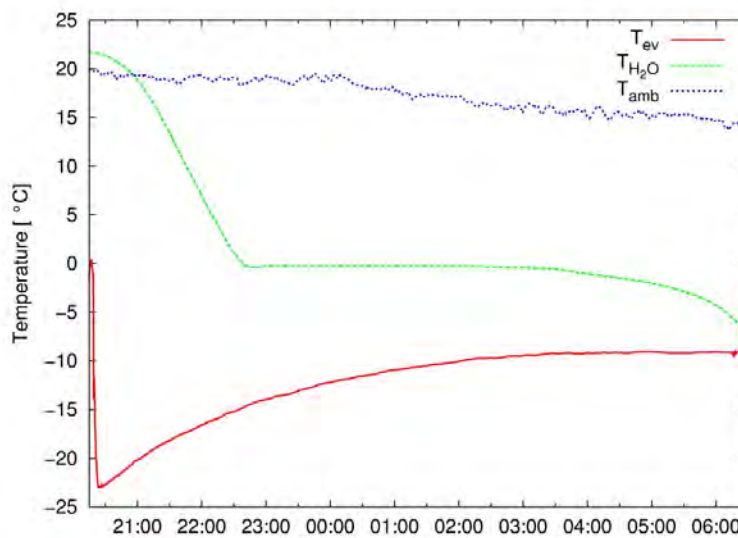


Fig. 7. Evaporator, water and ambient temperatures against time.

In Figure 7 it can be seen that the evaporator temperature was lower than -11°C for a period

higher than 8 hours. Also it can be seen how the water temperature decreases from the ambient temperature to 0°C and remains constant while the ice is been produced.

5. Conclusions

A solar intermittent refrigeration system for ice production has been evaluated with the ammonia/lithium nitrate/water mixtures at the Centro de Investigación en Energía of the UNAM. Evaporator temperatures as low as - 11°C were obtained for a period of time up to 8 hours. The solar coefficient of performance reached values up to 0.098, which is 24% higher than the maximum obtained previously by Rivera [7] operating the system with the ammonia/lithium nitrate mixture.

Acknowledgments

The authors would like to thank to PAPIIT-UNAM project number IN110706-2 to sponsor the present research and to Dr. Victor Hugo Gómez Espinoza for his invaluable help.

References

- [1] A. Erhard, K. Spindler, T. Hahne, Test and simulation of a solar powered solid sorption cooling machine, *Int. J. Refrigeration* 21(2), 1998, pp. 133-141.
- [2] R. Z. Wang, Y. X. Xu, J. Y. Wu, M. Li, H. B. Shou, Research on a combined adsorption heating and cooling system, *Applied Thermal Engineering* 22, 2002, pp. 603–617.
- [3] M. Li, R. Z. Wang, Y. X. Xu, J. Y. Wu, A.O. Dieng, Experimental study on dynamic performance analysis of a flat-plate solar solid-adsorption refrigeration for ice maker, *Renewable Energy* 27, 2002, pp. 211–221.
- [4] C.Hildbrand, P Dind, M. Pons, F. Buchter, A new solar powered adsorption refrigerator with high performance. *Solar Energy* 77, 2004, pp. 311–318.
- [5] N. M. Khattab, A novel solar-powered adsorption refrigeration module, *Applied Thermal Engineering* 24, 2004, pp. 2747–2760.
- [6] M. Li, C. J. Sun, R. Z Wang, W. D Cai, Development of no valve solar ice maker, *Applied Thermal Engineering* 2004;24:865–872.
- [7] W. Rivera, G. Moreno-Quintanar, C. O Rivera, R. Best, F. Martínez, Evaluation of a solar intermittent refrigeration system for ice production operating with ammonia/lithium nitrate, *Solar Energy* 85(1), 2011, pp. 38-45.
- [8] S. Libotean, D. Salavera, M. Valles, J. Esteve, A. Coronas, Vapor-liquid equilibrium of ammonia+lithium nitrate+water and ammonia+lithium nitrate solution from (293.15 to 353.15) K, *Journal Chemical and Engineering Data* 52, 2007, pp. 1050–1055.
- [9] S. Libotean, D. Salavera, M. Valles, J. Esteve, A. Coronas, Densities, viscosities, and heat capacities of ammonia + lithium nitrate and ammonia + lithium nitrate + water solutions between (293.15 to 353.15) K, *Journal Chemical and Engineering Data* 53, 2008, pp. 2383–2393.

Development of Model Solar Kitchen with Green Energy for Demonstration and Application in Rural Areas

Sanjib Kumar Rout

C.V. Raman College of Engineering, Bidyanagar, Mahura, Janla, Bhubaneswar-752054, India
*Telephone: 91-674 2460043/2460093, FAX- 91-674246009, Email-sanjibrou.1@gmail.com

Abstract: The paper demonstrates how effectively hoteliers and corporate can architect and utilize both solar thermal and green gas energy for the production of zero carbon foot print food products. It involves the usage of shefflers, solar parabolic reflectors, solar ovens, solar cookers, solar dryers, solar water heaters, biomass gasifiers, biogas plant, etc which have been suitably designed and placed architecturally in the green kitchen premises to harvest maximum solar thermal green energy for effective production of low and zero carbon foot print food products with minimal loss of nutritional value. Further, the digested slurry of biogas plant is used as humus rich fertilizer for spice garden spread around the green kitchen to beautify the ambient. Replacement of conventional energy partially by green and thermal energy reduces the energy cost substantially. It not only cuts down the cost of fuel but also maintains a clean environment in canteen area and its surroundings in addition to providing nutritious food. The methods developed in this project may also be implemented in vast rural mass and community centre for cost effective and hygienic food production.

Keywords: Fossil fuel, Carbon foot print, Green canteen, Solar energy, Biomass energy

1. Introduction:

Today, India is growing with an average GDP growth of 8.9% per annum, which signifies the tremendous growth of its economy. Massive investment are being laid out by the Government and private sectors for the development of small and large manufacturing software industries and in service sectors like education, healthcare, hotels and real estates. These are being constructed throughout the country and environment becomes a concern everywhere. Our Government is enforcing norms to ensure that all these projects remain as much greener as possible. In any corporate offices, hotels, schools and colleges, quantity kitchen is mandatory to support their employees, students and customers so that they can avail nutritional food [1]. A survey has been conducted with some hotels and schools located in the rural part of Odisha State of our Country about the greenery of their kitchen and about their waste disposal. Today most of these industries, corporate offices, hotels and motels are very much aware of the energy saving equipment but have least ideas to make their environment green by applying the cheapest and easiest methods of non-conventional energy [2]. We tried to collect the feedback to understand their knowledge about energy saving devices, carbon emission, carbon footprint products and application of non-conventional energy for quantity kitchen.

It is a matter of concern of rural hotels and schools where food is prepared for more than 500 people per day with all conventional fuel and equipment. Our survey found most of these organizations trying to project their awareness by using energy efficient electrical and ceramic appliances, low-cost wood and coal steamers and also by disposing the food waste in isolated places without making the assessment how much damage is made to the environment [3].

The aim of this project is to develop a model green kitchen to demonstrate an effective and cheaper prototype which shall

1. Reduce carbon dioxide emission to a substantial level by the application of solar thermal reflectors, ovens and driers [4].
2. Establish a convenient waste management system and through it produce methane in order to utilize it in the kitchen [5] and to generate bio-fertilizer for its easy utilization in the spice garden.
3. Produce zero carbon footprint food products with higher nutritional value.
4. Reduce the total operational cost by at least 40% of the conventional one.

2. Materials and Methodology

2.1. Materials for green kitchen and its layout

A green kitchen attached to a 500 person capacity quantity kitchen was established at C.V. Raman College of Engineering, Bhubaneswar, India as per the layout shown in Fig. 1.

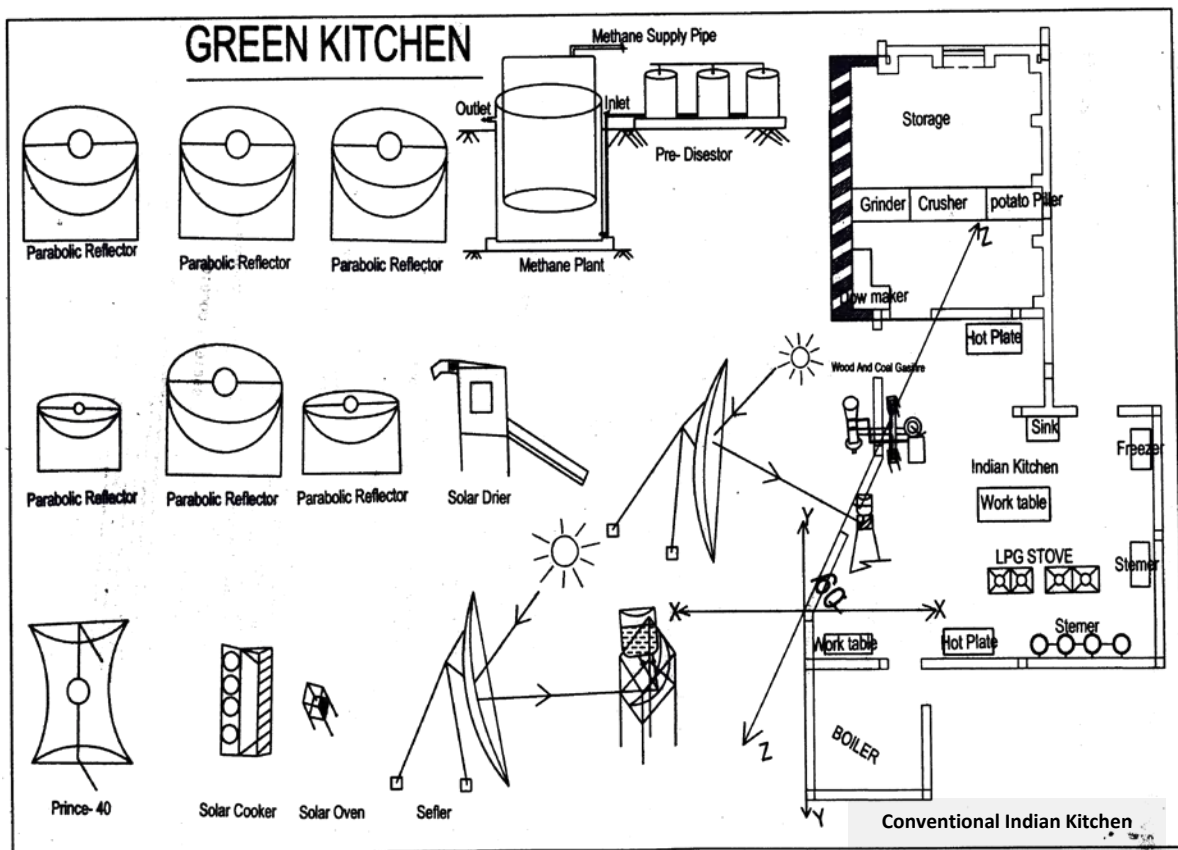


Fig. 1 Layout of green kitchen

Devices like solar reflectors of parabolic type, Schefflers, solar driers, solar oven [6], solar water heaters, biomass gasifier and a food waste digester methane plant were installed. All these equipments have been installed by taking the following points into consideration:

1. The conventional kitchen wall facing the Scheffler was in east-west direction
2. Scheffler foundation was done taking latitudinal angle into consideration[7]
3. Thermal reflectors were located where maximum sun-light is available [8]
4. Schefflers fixed focus concentrator
5. Methane plant was installed near the conventional kitchen wall with less sun-light

From the survey conducted, it was realized that the small, medium and large hotels and motels of the locality had expressed serious concern regarding the effective utilization of solar thermal equipments in quantity food preparation and found that the food waste disposal outside the kitchen boundary as the most easiest and cheapest way. By way of this disposal, they were ignorant about the emission of methane gas to the atmosphere which has more than 20 time green house effect than that of carbon dioxide gas. They were also very much doubtful to accept the concept of the reduction fuel consumption by the food waste.

The layout of solar and green energy devices as shown Fig. 1 was designed for the demonstration to hoteliers and corporate to observe as well as analysed how the green kitchen effective and convenient for the reduction of cost of food production. This project had taken all the observations and experiments considering 78,000 Lux intensity of sun light as a reference during the month of August to December, the winter season. In a sunny day of the period green kitchen was able to cook grains, vegetables, meats and produce hot water continuously for more than six hours in a day from 9 hour morning to 15 hour evening. During summer the Lux intensity of sun light might rise for the locality as per temperature weather relationship curve, shown in Fig. 2 [7].

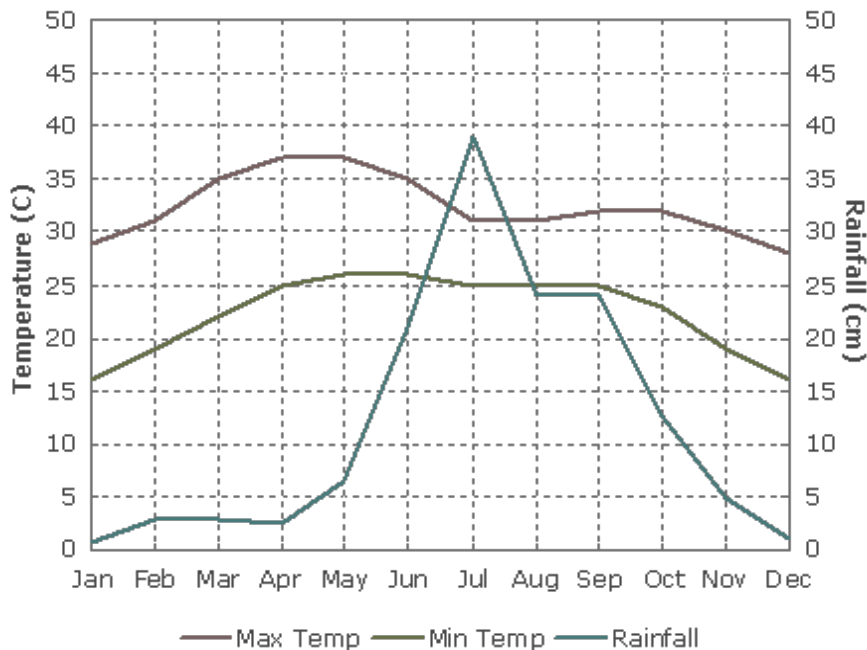


Fig. 2 Relationship of atmospheric temperature, average rain fall vs season

2.2. Methods adopted for the installation of green energy devices

The details of green energy devices are presented in Fig. 3 along with specification and cost.

Sl. No.	Name of equipment	Photograph	Cost of the equipment (in Indian Rupees)
01	Scheffler – 1		80,000
02	Scheffler – 2		1,20,000
03	Parabolic reflector-1		37,000
04	Parabolic reflector-2		32,000
05	Solar drier		10,000
06	Solar oven		3,000
07	Solar water heater		1,00,000
08	Methane plant		5,00,000
09	Biomass gassifier		10,000
			8,92,000

Fig. 3 The detailed specification and cost of green energy devices

2.3. Theoretical background for the installation of Scheffler

The installation of Scheffler-1 disc above the ground was taken as 5.2 m and the distance of the receiver from the disc centre as 3.8 m while the height of the receiver above the ground was evaluated using the equation 1.

$$Y = B - \{X \cdot \sin(A)\} \quad \text{-----} \quad (1)$$

where, Y = height of the receiver, B = height of the disc above the ground, X = distance of receiver from disc centre and, A = latitudinal angle at any place

In order to keep the focal line constant, orientation of scheffler was adjusted with a programmable motor fitted device as per the movement of the solar rays on earth.

2.4. Basic principles of the installation of other solar devices

2.4.1. Parabolic Reflector

Both parabolic reflectors shown in Fig. 3 (Sl. No. 1 & 2 - Schefflers) and (Sl. No. 3 & 4 – Prince-40) [9] were installed to receive full sun rays and get concentrated on fixed focal centre through reflection where the cooker was placed with blacken surface to absorb maximum thermal energy. Here also the orientation of reflectors were adjusted with a programmable motor fitted device as per the movement sun rays

2.4.2. Solar dryer

The solar dryer was designed on the principle of green house glass where high frequency solar radiation got absorbed through inclined glass surface by the food materials but longer wavelength radiations reflected out. Moisture content was continuously ventilated. The inclination angle was experimentally evaluated to receive maximum temperature.

2.5. Methane Plant

The cellulosic materials comprising both vegetable waste and food waste of the canteen are predigested aerobically. The digested slurry with high biological oxygen was an aerobically digested to methane rich biogas which was purified by the separation of carbon dioxide gas. The high calorific methane rich gas was found to produce $0.6 \times 10^{-3} \text{ m}^3$ of methane gas per kg of cellulosic waste on dry basis. The digested effluent was found to be rich in P_2O_5 with small quantity of K_2O and Nitrogen ingredients to act as ideal fertilizer for spice garden making the hotel environment greener, beautiful and profitable.

2.6. Biomass gasifier

Waste dry biomass collected by locals was fired in the special designed oven and thermal energy was fire through exhaust fan drive in a special designed energy efficient oven to utilize its maximum thermal energy by the cooking vessel.

3. Results and Discussion

3.1. Cost analysis of equipments

The cost of all equipments utilized in the project with respect to the cost in Indian market are worked out and compared with the conventional devices adopted by hoteliers, etc. on the basis of preparing food for 500 consumers as given in Table 1.

Table 1: Equipments used in a conventional kitchen to prepare food for 500 persons

<u>Sl. No.</u>	<u>Name of the equipment</u>
01	Cooking Range 4 Burner (LPG)
02	Cooking range High Pressure
03	Convection oven
04	Griddle
05	Stock Pot Burner
06	Deep fat fryer (2 Comp.) 5 Ltr.
07	Potato Peeler Heavy Duty
08	Dough mixer
09	Steamer compartment with boiler
10	Tandoor (Gas/coal)
11	Thawing tub
12	Vegetable slicer
13	Chapatti Puffer cum holplate
14	Aluminium steamer idli
15	Deep freezer
16	Vegetable steamer big
17	Hot dog roller

The conventional Indian quantity kitchen cost is around Rs. 25 Lakhs. This is three times the cost of the green kitchen. Making a simple comparison of the total cost of a green kitchen and a quantity kitchen we have found that the former is 30% less.

3.2. Cost saving analysis

In this exercise, we have tried to calculate the savings of fossil fuel per day by utilizing all these green equipments for preparing the following items:

a. Preparation of rice, b. Preparation of vegetables, c. Preparation of meat, d. Preparation of grains. In this total exercise (Table 2), it is calculated in a sunny day by utilizing this green kitchen. Fig. 2 shows the atmospheric temperature and rain fall profile in a year at the surveyed place.

Table 2: Saving of fossil fuel, its cost and environmental benefits by the implementation of solar thermal devices and methane gas plant for 500 people per meal

Sl. no.	Recipe	Quantity		Ambience of light (Lux)	Total time taken (Min.)	Quantity of savings of		
		Ingredient	Water (Lit.)			Fossil fuel(kg)	CO ₂ (kg)	Cost (Rs.)
01	Cooked rice	Raw rice (60 kg)	144	78,000	72	9.6	29	288
02	Vegetables	Vegetables (75 kg)	60	78,000	69	12	36	360
03	Grains	Dal (25 kg)	90	78,000	108	6.75	18	180
04	Meat	Chicken (70 kg)	252	78,000	108	16.8	50	504

To prepare two meals in a day for 500 people the employed boiler consumes about 40 kg fire woods. On the other hand, upon employing gasifier it reduces 50 % of fire wood (20 kg) consumption in addition to 20 kg equivalent of CO₂ emission.

Approximately 120 kg of food waste is produced daily from the canteen emitting CH₄ and CO₂ as green house gases to the environment. Methane (CH₄) has 21 times stronger green house effect than CO₂. By generating bio gas out of this food wastes and considering all losses into account about 4 lakhs Indian rupees is saved in compensation to LPG consumption.

3.3. Application in spice garden

In most of the hotels, motels and corporate we have seen they spent a substantial amount of money in manure to keep their garden attractive and flowering. In our project we have introduced a concept of organic spice garden which we have demonstrated by doing a beautiful green landscape and planting 63 varieties of spices in the garden as an alternative to traditional rock and flower garden. In this food waste plant which we have installed that contains digested effluent which is being utilized in this spice garden to grow healthy and produce organic spices which can be reutilize in kitchen by using all the food wastes in the system.

We are yet to calculate the total value of spices generated in 1.5 acres of land in one year which can be worked out in the next year.

3.4. Theoretical background for architect

Green kitchen can be installed very conveniently at low installation cost if it is planned during the construction of the project. Architect should have fundamental knowledge about the geographical location of the place for installation of thermal reflectors because they can adjust the floor level of the kitchen to an operational height which cannot be done with an established kitchen. We have given an example of 4 places and shown a calculation as per equation (1) conveying the idea of geographical location of the place is important to install the thermal reflectors as shown in Fig. 4.

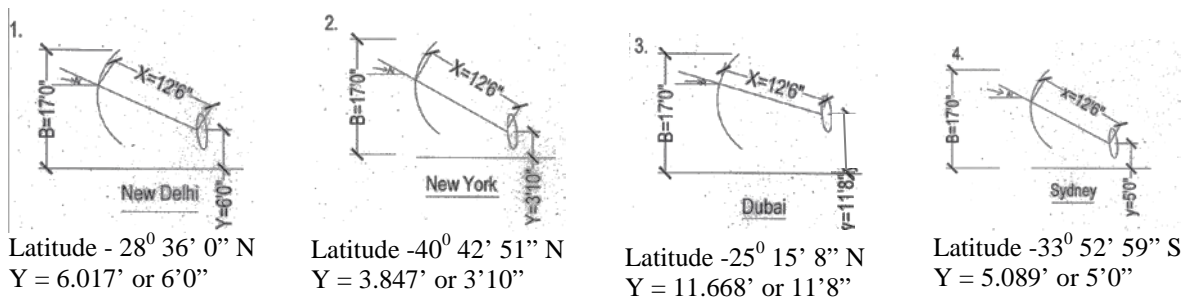


Fig. 4: Diagram showing the angle of incidence of solar ray on Scheffler and its height from the ground at different location

This study shows if the architect is aware of these factors then will keep in mind so that the reflector can be installed at a convenient height for operation. Apart from reflector the architecture should workout for disposal of waste from methane plant in such a way that it will not have any negative impact on the environment and kitchen surroundings, so that the waste can be easily pumped to the green kitchen site.

4. Conclusion

The C.V. Raman College of Engineering, Bhubaneswar, India has successfully installed a composite 500 students green kitchen project for demonstration to hoteliers, corporate that how effectively to produce low and zero carbon foot print food products and also to incorporate this concept during design stage. On total in a year (operation of 6 months) using this green kitchen, around 4.8 lakh Indian rupees is saved than the conventional method of cooking along with a reduction of about 48,000 kg of green house gas emission to the environment. 50 % utilization of green kitchen in an annum, it has been evaluated that the total investment is fully recovered in a year in addition to providing tremendous safety to the environment. The methods developed in this project may also be demonstrated to vast rural mass and community centre for cost effective and hygienic food production.

References

- [1] Blaine P. Friedlander Jr. Sweden, Researchers at school of Medicine, New York, Dr Vlassara, National Academy of Sciences, Proceedings from World Conference of Advances in Solar Cooking & The Times of India (14th Nov. 2002)
- [2] Suhatme S.P., Solar energy principles of thermal collection and storage, New Delhi: Tata McGraw-Hill; 1996
- [3] Parkin G.F., Own W.F., Fundamentals of anaerobic digestion of waste water sludge, J. Environ. Eng.-ASCE 112, 1986, pp. 867-920
- [4] Alexopoulos, S., Hoffschmidt, B Solar tower power plant in Germany and future perspectives of the development of the technology in Greece and Cyprus, Renewable Energy 35, 2010, pp. 1352-1356
- [5] Standard methods for the examination of water and wastewater. 19th ed. Washington, DC: APHA-AWWA-WEF; 1995
- [6] Mullick S.C., Kandpal T.C. and Subhod Kumar, Thermal test procedure for paraboloid concentrator solar cooker, Solar Energy 46, 1991, pp. 139-144
- [7] Chung T.M., A study of luminous efficacy of daylight in Hong Kong, Energy Buildings 19, 1992, 45
- [8] Temps R.C., Coulson KL. Solar radiation incident upon slopes of different orientations, Sol Energy 19, 1977, pp. 179-84
- [9] Ajay Chandak: Paraboloidal Solar Concentrator with Square / Rectangular Sections: Patent Application no. 581/MUM/2008 with Indian Patent Office.